STATE OF CALIFORNIA DEPARTMENT OF TRANSPORTATION

TECHNICAL REPORT DOCUMENTATION PAGE

TR0003 (REV. 10/98)

1. REPORT NUMBER	2. GOVERNMENT ASSOCIATION NUMBER	3. RECIPIENT'S CATALOG NUMBER
CA12-1775		

4. TITLE AND SUBTITLE	5. REPORT DATE
Feasibility Studies for Improving Caltrans Bridge Fragility Relationships	September, 2012
	6. PERFORMING ORGANIZATION CODE

7. AUTHOR(S)	8. PERFORMING ORGANIZATION REPORT NO.
Reginald DesRoches[1], Jamie Padgett[2], Karthik Ramanathan[1], Jazalyn Dukes[1]	na

9. PERFORMING ORGANIZATION NAME AND ADDRESS	10. WORK UNIT NUMBER
[1]School of Civil & Environmental Engineering Georgia Institute of Technology Mason Building, 790 Atlantic Drive Atlanta, GA 30332-0355 [2]Department of Civil & Environmental Engineering Rice University 6100 Main Street Houston, TX 77005	11. CONTRACT OR GRANT NUMBER DRISI Research Task No. 1775 DRISI Project No. P266 Contract No. 65A0322

12. SPONSORING AGENCY AND ADDRESS	13. TYPE OF REPORT AND PERIOD COVERED
California Department of Transportation Division of Research, Innovation and System Information, MS-83 1227 O Street Sacramento CA 95814	Final Report 14. SPONSORING AGENCY CODE 913

15. SUPPLEMENTAL NOTES

This document bundles five individual reports prepared during the course of a wide-ranging feasibility investigation exploring analytical methods to improve seismic fragility relationships for California bridges. The primary focus was to demonstrate that improved models could be developed for use in emergency-alerting applications such as ShakeCast. Part I is the Ph.D. thesis of Karthik Ramanathan which describes an initial end-to-end iteration through the entire model development process for a representative range of bridge classes. Parts IV and V provide post-thesis revisions and supplemental discussion by the PI's of key research findings. Part II presents parallel work by Jazalyn Dukes toward the secondary goal of piloting a bridge-design-support tool using comparable methods. Part III provides validation results.

Although preliminary fragility models are presented in this report, they are not intended for deployment. Planned subsequent project phases will complete validation work and adopt refined versions of both damage models and bridge taxonomy that are needed for deployable models.

16. ABSTRACT

Feasibility studies were completed as an initial phase of a larger research initiative focused on the development of a new generation of seismic fragility relationships tailored for the California bridge inventory. The new "Generation-2 Fragility (g2F)" models are designed to be compatible with California earthquake hazard levels, and leverage Caltrans' seismic design expertise and unique bridge-information assets. Primary applications are for incorporation into the ShakeCast earthquake-damage alerting system and to support seismic reliability evaluations. Simultaneously, the methods used in the
development of these g2F models are also being explored for their potential to support bridge-specific seismic design decisions. An initial end-to-end iteration through the entire model-development process was completed for a representative range of bridge classes. Results clearly demonstrate the feasibility of developing g2F models that yield distinct performance differences between bridge classes/subclasses that are not captured by earlier models. Fragility models presented in this report are preliminary, and are not intended for deployment.

17. KEY WORDS	18. DISTRIBUTION STATEMENT
Feasibility Study, Seismic Fragility, California Bridges, Design Era, Generation-2 Fragility (g2F), Bridge Damage Models, Stochastic Bridge Models, Probabilistic Seismic Demand Model, Nonlinear Time History Analysis	No restrictions. This document is available to the public through the National Technical Information Service, Springfield, VA 22161

19. SECURITY CLASSIFICATION (of this report)	20. NUMBER OF PAGES	21. PRICE
Unclassified	540	

Division of Research & Innovation

Feasibility Studies for Improving Caltrans' Bridge Fragility Relationships

Final Report

Damage State Criteria

Bridge system damage states	SS-1 MINOR	SS-2 MODERATE	SS-3 EXTENSIVE	SS-4 COMPLETE
ShakeCast Inspection Priority levels	Low	Medium	Medium-High	High
Likely Immediate Post-Event Traffic State	Open to normal public traffic – No Restrictions	Open to Limited public traffic – speed/weight/lane restrictions	Emergency vehicles only – speed/weight/lane restrictions	Closed (until shored/braced) – potential for collapse
Traffic Operations Closure/detour? Traffic restrictions?	Very unlikely Unlikely	Unlikely Likely	Likely Very Likely	Very likely Very Likely - Detour
Emergency Repairs Shoring/bracing? Roadway leveling?	Very unlikely Unlikely	Unlikely Likely	Likely Very Likely	Very likely Very Likely - Detour
Component Damage Range Primary component Secondary component	CDT-0 to 1 CDT-0 to 2	CDT-1 to 2 Above CDT-2	CDT-2 to 3 NA	Above CDT-3 NA

Bridge Taxonomy

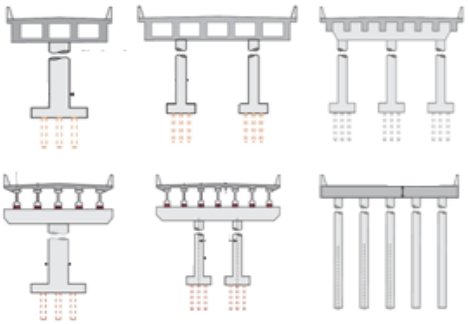

Component Capacity

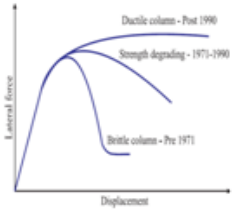

CA Shaking Hazard

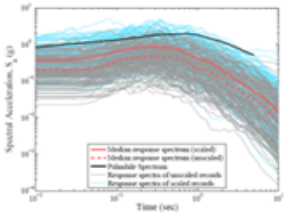

Stochastic Method

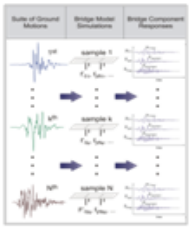

Nonlinear Analysis

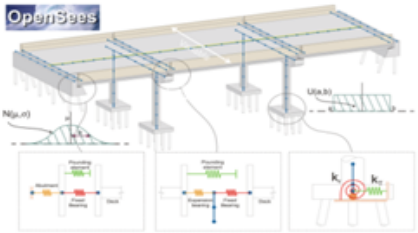

Probabilistic Demand Model

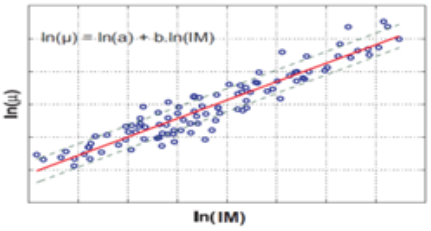

Component and System Fragility Models (Preliminary)

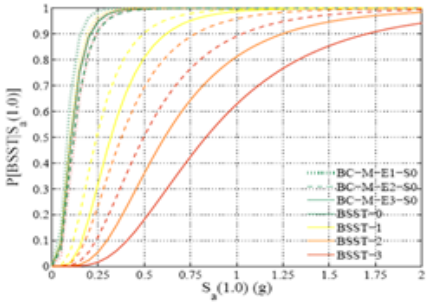

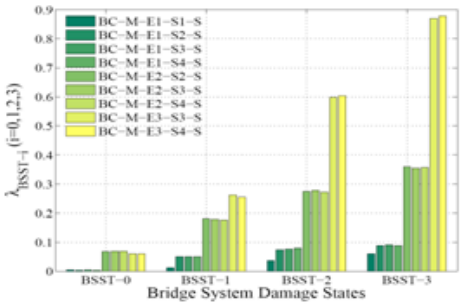

Report CA12-1775
September 2012

Feasibility Studies for Improving Caltrans' Bridge Fragility Relationships

Final Report

Report No. CA12-1775

September 2012

Prepared By:

School of Civil & Environmental Engineering
Georgia Institute of Technology
Mason Building, 790 Atlantic Drive
Atlanta, GA 30332-0355

Prepared For:

California Department of Transportation
Division of Research and Innovation, MS-83
1227 O Street
Sacramento, CA 95814

DISCLAIMER STATEMENT

This document is disseminated in the interest of information exchange. The contents of this report reflect the views of the authors who are responsible for the facts and accuracy of the data presented herein. The contents do not necessarily reflect the official views or policies of the State of California or the Federal Highway Administration. This publication does not constitute a standard, specification or regulation. This report does not constitute an endorsement by the Department of any product described herein.

For individuals with sensory disabilities, this document is available in Braille, large print, audiocassette, or compact disk. To obtain a copy of this document in one of these alternate formats, please contact: the Division of Research and Innovation, MS-83, California Department of Transportation, P.O. Box 942873, Sacramento, CA 94273-0001.

Feasibility Studies for Improving Caltrans' Bridge Fragility Relationships

Preface Comments by Caltrans Project Manager

This document reports on the first phase, Task 1775, of a multi-phase research initiative, Project P266, aimed at systematic development of "Generation-2 Fragility (g2F)" models tailored for the California bridge inventory. The project is structured to use advanced analytical methods to create fragility models compatible with California earthquake hazard levels, and which leverage Caltrans' seismic design expertise and unique bridge information assets. Primary applications envisioned for g2F models are for incorporation into the ShakeCast earthquake-damage alerting system and to support seismic reliability evaluations. Simultaneously, the methods used in the development of these g2F models are also being explored for their potential to support bridge-specific seismic design decisions.

This feasibility investigation involved concurrent work and substantial coordination between Caltrans' staff within both research and design units and the team of university researchers at the Georgia Institute of Technology and Rice University who prepared these reports. The overall methodology, along the potential impacts of incremental decisions made during application of the methodology, were new to Caltrans at the onset of the project. Recognizing the need to 'walk before running' with this new capability, Project P266 was structured to be an *iterative* development and optimization process. Within this larger project context, the Task 1775 feasibility investigations aimed to explore whether several emerging concepts could be seamlessly integrated into a methodology to yield a new generation of models tailored for Caltrans' applications. New concepts explored include:

- Development of a prototype set of bridge damage-state definitions having similar consequences for post-earthquake *functionality* expressed in terms of emergency repairs needed and traffic capacity retained;
- Definition of bridge damage models in terms of quantitative engineering metrics at the component level (e.g. column, joint, etc.) which could be logically combined to yield performance at the system level (i.e. overall bridge);
- Development of a prototype 2nd-generation bridge taxonomy that significantly extends the number of bridge classes/subclasses relative to older 1st-generation methods by considering additional attributes available through unique Caltrans' information assets;
- Prototype application of advanced numerical modeling strategies (i.e. parameterized stochastic bridge models) and techniques (i.e. non-linear dynamic finite-element analysis) coupled with extreme earthquake ground-motions representative of the full range of California hazard.

Within this exploratory context, the limited objectives of the Task 1775 feasibility studies were to complete an initial end-to-end iteration through the entire model-development process for a representative range of bridge classes so as to:

- Orient Caltrans seismic design practitioners to the overall methodology, and simultaneously orient the academic research team to practical design details and concerns;
- Demonstrate both the feasibility and potential utility of g2F models vis-a-vis earlier fragility models as having a greater number of distinct bridge performance classes/subclasses, as well as supplemental component-level information;
- Provide initial insight into those bridge-taxonomy factors having greatest influence on model results to support prioritization of Caltrans data-gathering efforts required to implement the emerging taxonomy;
- Provide initial insight into performance trends anticipated for selected bridge classes/subclasses and how they are distinct from earlier fragility models;
- Demonstrate the overall consequences on final g2F models of various incremental decisions made during the development process so as to guide future iterative refinement; and

- Provide example models to support concurrent development of new processes and interfaces within the ShakeCast emergency-alerting application.

During the course of this feasibility investigation, strong inter-dependencies within the methodology became apparent between damage state definitions, available bridge data, parameterized bridge models, and fragility results. While this was broadly understood at the onset of the work, the initial end-to-end application of the methodology provided important insight and specific lessons that will be used to guide future phases of the research. Lessons include:

- The limit-state definitions used in the component damage models were found to be generally too conservative. For example, the threshold for 'complete' column damage for a modern bridge was specified as a curvature ductility demand value of 12, but upon review of initial results and additional consideration, a more appropriate value may be on the order of 20 or more. This is discussed in more detail in Part V of this report. Similar conservatism occurred in both the specification of values adopted for lower component damage states as well as the selection of components to be incorporated into the system damage state. All damage models will be revisited in future research phases.
- The bridge taxonomy used in the feasibility study significantly extended the number of bridge classes/subclasses relative to 1st-generation methods. While some added attributes (e.g. design era, abutment type, interior-support type) were found to show great promise for creating *distinct* performance classes, other attributes were shown to be less significant and may be eliminated. Planned future research will include an extensive preliminary sensitivity analysis to aid the iterative process of determining the bridge attributes and combinations having the most significant impact on fragility models.
- Existing real bridge systems are incredibly varied and cannot always be neatly divided into classes/subclasses. For example, the taxonomy used in this feasibility study adopted two broad abutment types: seat and diaphragm. However, depending on field configuration, diaphragm abutments may involve strong or weak coupling to the backfill soil. This uncertainty could be accommodated either by defining additional abutment subclasses or analytically by incorporating a wider mixture of representative bridges into the definition of the parameterized abutment models. The challenge is to identify a manageable set of classes/subclasses based on this and other components where each class/subclass yields distinct performance with acceptable model dispersion. Future research phases will be guided by the sensitivity analysis, but will also require a significant degree of trial-and-error iteration to yield an optimal taxonomy that can be deployed.
- Additional methodological considerations identified as important to optimizing a deployable g2F bridge taxonomy include: a) whether available bridge information assets are, or can be made to be, capable of accurately assigning existing bridges to analytically-promising bridge classes, b) whether common bridge attributes such as skew and length can be reasonably treated as adjustment factors applied uniformly to all classes or must be treated separately for each bridge system, and c) whether the implied system of bridge classes based on an extensive hierarchy of component combinations might be meaningfully re-organized into a more manageable number of cross-hierarchy classes.

Key outcomes of this first phase of the multi-phase research project were: a) to have successfully completed an end-to-end application of the emerging g2F methodology for a representative range of California bridge types, b) that results revealed distinct performance differences between bridge classes/subclasses that are not captured by earlier 1st-generation methods, and c) that while iterative refinements to each element of the g2F methodology described herein are needed, the overall approach is indeed feasible and useful for Caltrans' applications.

Although the initial fragility models reported herein meet the limited objectives of this feasibility study, these models are *not intended for deployment*. Rather, they serve as a foundation and guide for continued development under future phases of Project P266 where models will be verified and the inter-dependencies noted above will be iteratively examined and optimized to yield final g2F models that are fully consistent with intended applications and policies.

Feasibility Studies for Improving Caltrans' Bridge Fragility Relationships

Final Report Organization

This document bundles five individual reports that were prepared during the course of a wide-ranging feasibility investigation exploring analytical methods to improve seismic fragility relationships for California bridges. The five reports are listed as Parts I through V below.

The primary focus of this feasibility investigation was to demonstrate that improved fragility models could be developed for use in emergency alerting applications such as ShakeCast. Part I of this report is the Ph.D. thesis of Karthik Ramanathan which forms the core of this effort. Its goal was to complete an initial end-to-end iteration through the entire model-development process for a representative range of bridge classes. Part IV provides amendments to Part I stemming from Caltrans revisions to damage state definitions which occurred after thesis defense. Part V provides supplemental discussion, by the project principal investigators, of initial key findings and impacts on future research.

A secondary, parallel, focus of this feasibility investigation was to explore the potential of using comparable methods to support the design of new bridges. Part II of this report presents work primarily by Jazalyn Dukes on the development of a pilot bridge-specific design-support tool to allow bridge engineers to examine risk implications of altering key design variables.

Finally, as purely analytical methods were employed throughout this study, an early feasibility task was to demonstrate that the computational methods employed herein could reasonably reproduce observations from instrumented bridges. Part III of this report summarizes model/method validation work.

Part I: **"Next Generation Seismic Fragility Curves for California Bridges Incorporating the Evolution in Seismic Design Philosophy",** Ph.D. Thesis of Karthik N. Ramanathan (Also see Part IV for amendments to Part I)

Part II: **"Bridge Specific Fragility Framework and Design Support Tool for Two-Span Integral Box Girder Bridges in California",** Technical Report by Jazalyn Dukes, Reginald DesRoches, and Jamie E. Padgett

Part III: **"Finite Element Model Validation",** Technical Report by Karthik N. Ramanathan, Jong-Su Jeon, Behzad Zakeri, Reginald DesRoches, and Jamie E. Padgett

Part IV: **"Amendments to Part I to Accommodate Caltrans Revisions to Damage State Definitions",** Supplemental Technical Report by Karthik N. Ramanathan

Part V: **"Additional Discussion of Phase-1 Findings and Impact on Future Research",** Supplemental Technical Report by Reginald DesRoches and Jamie E. Padgett

Table of Contents

(For Integrated 5-Part Final Report)

Feasibility Studies for Improving Caltrans' Bridge Fragility Relationships

Final Report

Part I

NEXT GENERATION SEISMIC FRAGILITY CURVES FOR CALIFORNIA BRIDGES INCORPORATING THE EVOLUTION IN SEISMIC DESIGN PHILOSOPHY *

Ph.D. Thesis of Karthik N. Ramanathan

*** NOTE: Also see Part IV for amendments to Part I**

TABLE OF CONTENTS

LIST OF TABLES

LIST OF FIGURES

SUMMARY

Quantitative and qualitative assessment of the seismic risk to highway bridges is crucial in pre-earthquake planning, and post-earthquake response of transportation systems. Such assessments provide valuable knowledge about a number of principal effects of earthquakes such as traffic disruption of the overall highway system, impact on the regions' economy and post-earthquake response and recovery, and more recently serve as measures to quantify resilience. Unlike previous work, this study captures unique bridge design attributes specific to California bridge classes along with their evolution over three significant design eras, separated by the historic 1971 San Fernando and 1989 Loma Prieta earthquakes (these events affected changes in bridge seismic design philosophy). This research developed next-generation fragility curves for four multispan concrete bridge classes by synthesizing new knowledge and emerging modeling capabilities, and by closely coordinating new and ongoing national research initiatives with expertise from bridge designers.

A multi-phase framework was developed for generating fragility curves, which provides decision makers with essential tools for emergency response, design, planning, policy support, and maximizing investments in bridge retrofit. This framework encompasses generational changes in bridge design and construction details. Parameterized high-fidelity three-dimensional nonlinear analytical models are developed for the portfolios of bridge classes within different design eras. These models incorporate a wide range of geometric and material uncertainties, and their responses are characterized under seismic loadings. Fragility curves were then developed considering

the vulnerability of multiple components and thereby help to quantify the performance of highway bridge networks and to study the impact of seismic design principles on the performance within a bridge class. This not only leads to the development of fragility relations that are unique and better suited for bridges in California, but also leads to the creation of better bridge classes and sub-bins that have more consistent performance characteristics than those currently provided by the National Bridge Inventory. Another important feature of this research is associated with the development of damage state definitions and grouping of bridge components in a way that they have similar consequences in terms of repair and traffic implications following a seismic event. These definitions are in alignment with the California Department of Transportation's design and operational experience, thereby enabling better performance assessment, emergency response, and management in the aftermath of a seismic event. The fragility curves developed as a part of this research will be employed in ShakeCast, a web-based post-earthquake situational awareness application that automatically retrieves earthquake shaking data and generates potential damage assessment notifications for emergency managers and responders.

CHAPTER 1

INTRODUCTION

1.1 Problem Description and Motivation

Quantitative and qualitative assessment of the seismic risk to highway bridges is crucial in pre-earthquake planning, and post-earthquake response of transportation systems. Assessing the consequences of natural hazards such as earthquakes on highway infrastructure systems has typically focused on economic losses and closure time (Basoz and Kiremidjian, 1997; Mackie and Stojadinovic, 2005; Liao and Yen, 2010; Padgett et al., 2010; Zhou et al., 2010; Luna et al., 2008). Such assessments provide valuable knowledge about a number of principal effects of earthquakes such as traffic disruption of the overall highway system, impact on the regions' economy and post earthquake response and recovery, and more recently serve as measures to quantify resilience (Bruneau et al. 2003). According to the Bureau of Transportation Statistics (BTS), U.S. Department of Transportation (US DOT), the nation's freight transported by all modes steadily increased between 1980 and 2009, rising at an average annual growth rate of about 1.4 percent per year (FHWA, 2010). Based on the composite estimates of commercial freight activity in the United States for 2009, trucks account for 9.8 trillion dollars of shipment thereby holding 91% of the relative share among all the other transportation modes and 97% of tonnage. Further, the estimates resulting from a combined BTS and Federal Highway Administration Authority (FHWA) effort to geocode bridges from the National Bridge Inventory (NBI) suggest that the state of California accounts for 28.3% of 159,859 structurally deficient and functionally obsolete bridges in the continental United States. Bridges are considered structurally deficient if significant load-carrying elements are found to be in a poor or worse condition due to

deterioration and/or damage, while functional obsolescence is a function of geometrics of the bridge in relation to those required based on current design standards (FHWA, 2006) and inability to meet traffic demands. The latter is directly related to the age of the bridge and the varied design, detailing and construction practices followed across decades adds to their functional obsolescence. Due to the major dependence of the nations' freight economy on highway infrastructure systems that have a large proportion of deficient bridges, coupled with the increased awareness of the seismic hazard in the region, a proper understanding of their seismic response and vulnerability is important for risk assessment.

Fragility curves, which are conditional probability statements that give the likelihood that a structure will meet or exceed a specified level of damage for a given ground motion intensity measure, have found widespread use in probabilistic seismic risk assessment of highway bridges. The conditioning parameter is typically a single intensity measure such as peak ground acceleration (PGA) or spectral acceleration at the geometric mean of the longitudinal and transverse periods. Fragility curves are a fundamental building block used in multiple (current and potential future) applications including:

- Emergency Response:
    - Optimize initial bridge inspection priorities (through ShakeCast near-real-time alerting system);
    - Rapid initial estimate of loss (for support of emergency declarations).
- Design Support - Performance-Based Earthquake Engineering:
    - Bridge-Specific: Develop bridge-specific fragility curves to serve as a design check and support design strategy decisions.
    - Bridge Classes: Evaluate classes of bridge systems to optimize design guidelines for safety, cost, and functionality.
- Planning Support:
    - Traffic impacts from scenario earthquakes (e.g. Golden Guardian);
    - Performance of specific transportation corridors (e.g. lifeline routes);

    - Cost-effectiveness of alternate bridge retrofit strategies;
    - Screening for additional seismic retrofit needs.
- Policy Support - Risk Nomenclature
    - Capacity for issuing scientifically-defensible (internal, interagency, or public) statements regarding anticipated transportation system performance that accounts for unavoidable uncertainties in earthquake shaking and variable bridge design/construction/age.

The intent of the present research is to develop fragility curves for predominant concrete bridge classes in California based on unique bridge inventory information which will enable the identification of significant features and creation of seismic performance sub-bins capturing the temporal evolution of design and detailing standards of bridges. The sub-bin fragilities can be used in a variety of current and future applications, mentioned previously, and more importantly emergency response and management in the context of the present study.

Most of the fragility curves developed for California bridges are structure specific (Mackie and Stojadinovic, 2005; Zhang and Huo, 2009). Structure specific fragility curves do not capture the uncertainty associated with the geometric parameters that describe a bridge class and other uncertainties associated with them. On the other hand, Nielson and DesRoches (2007), Padgett and DesRoches (2008), Ramanathan et al. (2010, 2012) developed fragility curves for as-built (seismically and non-seismically designed bridges) and retrofit bridge classes in central and south eastern United States (CSUS). These are not applicable for vulnerability assessment in California due to discrepancies in the composition of bridge classes and design details. Further, there is a significant evolution in the seismic design philosophy for bridges in California over the last few decades which is absent in the case of CSUS bridges, thereby preventing the adoption of CSUS bridge class fragilities for their California counterparts. Added discrepancies in the definition of damage states to support regional risk assessment and

decision-making needs, further add to the incompatibility between CSUS and California bridge class fragilities.

The only fragility curves that are remotely applicable to bridge classes in California were the ones developed by Mander and Basoz (1999) which are employed in HAZUS (HAZUS-MH, 2011) and ShakeCast (Lin and Wald, 2008). ShakeCast is an application developed by the United States Geological Survey (USGS) for automating ShakeMap delivery to critical users such as lifeline utilities. Critical users can receive automatic notifications within minutes of an earthquake indicating the level of shaking and the likelihood of impact to their own facilities. The HAZUS fragility relationships were developed for bridge classes based on a limited number of parameters available in the NBI, damage states based on limited sets of field damage observations and simplified two dimensional analysis techniques. Further details about the limitations of HAZUS fragilities and the need to move beyond them are discussed in the next chapter. Another significant drawback in the field of bridge seismic risk assessments is the mismatch between the damage state definitions used in fragility analysis and overall bridge functionality post a seismic event. This hampers the decision making needs by agencies like the California Department of Transportation (Caltrans) with regards to emergency response and management.

A gap currently exists in the literature and fragility models used in practice to support risk assessment of bridge classes representative of the California bridge inventory that align with decision making needs expressed by Caltrans. Exacerbating this situation is the lack of systematic organization of bridge design, retrofit, and maintenance data (beyond NBI parameters) required to make substantial improvements. Common California bridge classes have a broad range of differences and temporal variations in their geometric and design attributes and quantifying their vulnerability by not accounting for these features, as in the case of the existing HAZUS fragilities, could lead to serious errors in their vulnerability estimates. This necessitates the development of a

binning structure based on the design and detailing attributes and unique fragility functions associated with them.

1.2 Research Objectives

The limitations in the HAZUS fragilities and previous studies on fragilities of bridge classes in CSUS in general were identified in the preceding section. The main objective of this research is to make substantial improvements in fragility relationships for bridges typical of California by leveraging new knowledge and emerging modeling capabilities, and by closely coordinating new and ongoing national research initiatives with Caltrans design and user expertise. Specific endeavors which hold high potential for improving fragility relations include:

1. Identify the most common concrete bridge types in California and perform a detailed analysis to statistically describe their major geometric parameters using the NBI database.
2. Capture and understand the unique design and detailing aspects associated with the evolution of column design philosophy, seat widths, abutment types, superstructure to substructure connectivity, foundation types, to mention a few, based on extensive review of bridge plans and literature search. These details are gathered over three significant design eras, separated by the historic San Fernando (1971) and Loma Prieta (1989) earthquakes (these events affected changes in bridge seismic design philosophy).
3. Supplement the NBI information available about bridges with the aforementioned details and bridge design, retrofit and maintenance data made available through Caltrans in-house databases and expertise to extend and subdivide existing bridge classes into seismic performance sub-bins, primarily separated by the three significant design eras, to better account for the California bridge inventory.

4. Generate three dimensional non-linear finite element models of the chosen bridge classes using the advances in component modeling strategies. This also involves the identification and probabilistic modeling of potentially uncertain modeling parameters.
5. Refinement and development of the component and system level damage states and their mapping in such a way that they align with the design and operational experience of bridge owners to be effectively used in seismic risk assessment. In this way, the fragility curves developed in this study will have direct implications in terms of repair and operational consequences in the aftermath of an earthquake and will be tailored to the decision-making needs at the regional level.
6. Generate a refined set of component and system level fragility curves for the bridge classes along with their seismic performance sub-bins. This will help provide insight into the relative vulnerability of bridge classes and their seismic performance sub-bins, assess the effectiveness of seismic design philosophy currently adopted for the design of bridges, and guide future data collection that is presently absent in the NBI and the state databases.

1.3 Dissertation Outline

The dissertation is organized into seven chapters with the following contents:

Chapter 2 summarizes existing research in the area of seismic risk assessment and seismic bridge fragility curves.

Chapter 3 provides a detailed analysis of the California bridge inventory including statistical distributions for bridge geometric parameters. The general design details and potential vulnerabilities of bridges designed prior to 1971, those designed between 1971 and 1990 and post 1990 are identified based on an extensive review of bridge plans to supplement the information provided by the NBI. Detailed information pertinent to bridge components: superstructure, columns, foundations, abutments are gathered across

the design eras to aid in the development of stochastic finite element models for fragility analysis.

Chapter 4 provides extensive details about the modeling strategies for bridge components: superstructure, single and multi column bents, foundation systems, abutments including backfill soil and piles, restrainers and shear keys. Three dimensional analytical bridge models are developed and deterministic responses are presented to provide insight into the response of bridge components.

Chapter 5 outlines the framework that will be adopted in the development of analytical fragility curves for the bridge classes considered in this study. Details are provided regarding the different aspects of the multi-phase framework: ground motion suite, range of uncertainties considered including distributions, formulation of probabilistic seismic demand models and definition of capacity models.

Chapter 6 presents the results of component and system level fragility curves for the chosen multispan bridge classes and their seismic performance sub-bins. Insights are provided on the relative performance of bridge classes and their seismic performance sub-bins, the importance of sub-binning by design era and the influence of different design details on the vulnerability along with guiding future data collection currently absent in the NBI. Finally, comparisons between the results of the present study and the fragility curves presented in the risk assessment package, HAZUS are also presented.

Chapter 7 presents the conclusions from the present research, along with providing impacts of the work and suggestions for future research.

CHAPTER 2

EXISTING RESEARCH ON HIGHWAY BRIDGE FRAGILITY – A STATE OF THE ART SUMMARY

Probabilistic seismic risk assessment approaches, such as the Probabilistic Performance-based Earthquake Engineering (PBEE) framework (Cornell and Krawinkler, 2000; Mackie and Stojadinovic, 2001), have evolved to become central to risk mitigation decision making for structures and infrastructure systems. Such approaches aim to better understand the risk to engineered systems and apply this knowledge to design structures to achieve goals of life safety, reduced economic loss, or minimized recovery downtime in the aftermath of a seismic event. The central focus of numerous projects such as HAZUS (2011), REDARS (Werner et al., 2003), ShakeCast (Lin and Wald, 2008), and the Pacific Earthquake Engineering Research (PEER) Center highway demonstration project (Moore, 2000) has been on large-scale simulations of transportation networks to provide economic impact analyses in the aftermath of an earthquake. Bridges form a critical link in a highway network and are vulnerable to earthquake hazard, often with severe consequences in terms of economic loss and its effect on the regional economy.

With the advancement of the PBEE framework, the central focus is on metrics such as damage probability functions or fragility curves for describing the performance and vulnerability of highway bridges under seismic input. Fragility curves are conditional probability statements that give the likelihood that a structure will sustain or exceed a specified level of damage for a given ground motion intensity measure. These are expressions of performance at different levels of seismic input intensity unlike the description of performance as “safe” or “unsafe” which is typical of the deterministic design criteria. This is of particular relevance considering the inherent uncertainty in not

only the seismic hazard but also in the structural capacity and various other attributes associated with highway bridge networks. Probabilistic methods facilitate the definition of acceptable performance criteria under hazard levels and therefore have tremendous potential for a wide range of applications as stated in the previous chapter.

The most widely adopted probabilistic seismic risk assessment (PSRA) framework is the one presented by the Pacific Earthquake Engineering Research Center (PEER). The typical strategy employed in the PEER framework is to deconvolve the uncertainty in different parts of the seismic risk assessment problem such as the seismic hazard, structural performance (response and damage) and consequences (financial loss, interruption time) using the theorem of total probability, in an effort to achieve a consistent reliability-based approach for decision making (Cornell and Krawinkler, 2000; Mackie and Stojadinovic, 2005). Each of these assessment modules are essentially independent and are linked together by pinch point variables (Kaplan and Garrick, 1981), such as the intensity measure (*IM*), engineering demand parameter (*EDP*), and the damage measure (*DM*). The mean annual frequency, λ_{DV}, of a decision variable (*DV*) exceeding a limiting value (*dv*), is expressed in equation (2.1).

$$\lambda_{DV}(dv) = \int_{dm}\int_{edp}\int_{im} G(dv \mid dm)\cdot\left|dG(dm \mid edp)\right|\cdot\left|dG(edp \mid im)\right|\cdot\left|d\lambda(im)\right| \tag{2.1}$$

In equation (2.1), $G(DV|DM)$ represents the loss model describing the cumulative distribution function (CDF) of a decision variable conditioned on a damage measure such as repair cost or downtime, $G(DM|EDP)$ is the damage, capacity or the limit state model describing the CDF of a *DM* conditioned on a *EDP*, $G(EDP|IM)$ is the demand model describing the CDF of an *EDP* such as curvature ductility, abutment displacement etc., conditioned on an *IM*, and $\lambda(IM)$ is the seismic hazard model describing the mean annual frequency of exceeding an *IM*. It must be noted that the convolution of $G(DM|EDP)$ and $G(EDP|IM)$ yields fragility curves.

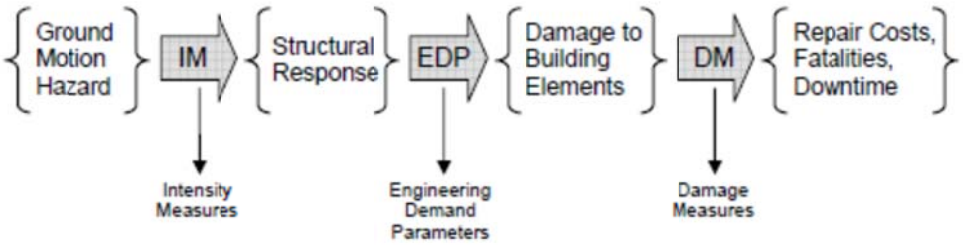

Figure 2.1: Schematic representation of seismic risk assessment (Baker et al, 2005)

2.1 Evolution in the Development of Fragility Curves

Fragility curves have found widespread use in risk assessment of bridges and highway systems and are the fundamental building block in multiple applications including emergency response, design, planning support, and policy recommendations. Over the years, fragility curves have evolved.

The earliest attempt to formalize seismic risk assessment procedures is found in the seminal work by Whitman et al. (1975). Since then several attempts have been made to quantify the risk to highway infrastructure systems. The Applied Technology Council (ATC, 1985) took the first step in performing seismic risk assessment of infrastructure for the state of California using damage probability matrices and restoration functions. Subsequently, several committees constituted by ATC have been solely devoted to the risk assessment of lifelines. The ATC 25 report (ATC, 1991) introduced the concept of continuous fragility functions for lifeline systems including bridges by performing regression on the discrete values of damage probability matrices. Further attempts to push forward the seismic risk assessment methods were made by the Federal Emergency Management Agency (FEMA) by the constitution of a committee of experts and introduction of a Geographic Information Systems (GIS) based risk assessment software, Hazards United States (HAZUS, 1997) in 1997. Since that time HAZUS has undergone several improvements and revisions and now includes models for estimating potential losses from a variety of natural disasters like earthquakes, floods, and hurricanes.

Over the years, structural fragilities have been determined in a variety of ways. The ATC 13 Report (ATC, 1985) documents risk assessment of the infrastructure stock in California essentially based on expert opinion. A panel of 42 experts was assembled to

develop damage probability matrices for bridge infrastructure based on their expertise. This technique has several major drawbacks since the procedure is totally subjective and depends on the number of experts queried and therefore is based on expertise and experience of the individuals with little correlation to actually observed earthquake damage. The 1989 Loma Prieta, 1994 Northridge and 1995 Kobe earthquakes were watersheds for fragility research. Several researchers (Basoz and Kiremidjian, 1997; Yamazaki et al., 1999; Der Kiureghian, 2002; Shinozuka et al., 2000, 2003; Elnashai et al., 2004) developed empirical fragility curves based on actual damage data observed in these earthquakes. Although the adopted procedure differed slightly among the researchers, the general essence was the same. Basoz and Kiremidjian (1997) assembled damage frequency matrices and performed a logistic regression analysis to develop fragility curves while Shinozuka et al. (2003) used the Maximum Likelihood Method to estimate the parameters of a lognormal probability distribution describing the fragility curves. Der Kiureghian (2002) employed a Bayesian approach in order to develop fragility curves. However, lack of sufficient damage data, discrepancies in the damage assessments in the aftermath of a seismic event, variation in the ground motion intensities at the damage sites depending on the earthquake source are some of the limitations of this technique for developing fragility curves.

Advances in modeling capabilities coupled with a lack of sufficient earthquake damage data motivated the development of fragility curves using analytical and simulation based methods. Several researchers have employed analysis techniques with different levels of sophistication to develop analytical fragility curves for bridges. Yu et al. (1991) used simple single-degree-of-freedom models and Elastic Response Spectrum Analysis (RSA) to develop fragility curves for highway bridges in Kentucky while Hwang et al. (2000) furthered this approach by quantifying uncertainties in seismic demand and capacity assessments. This was one of the earliest studies that looked at fragility curves for a class of highway bridges. Nonlinear static procedures (NSP) that use the force-deformation characteristics of structures stemming from pushover analyses started gaining wide acceptance and application. The Capacity Spectrum Method (CSM),

Coefficient Method (CM) and the N2 Method are all different types of nonlinear static procedures. CSM was first proposed by the ATC (1996) while CM was proposed by FEMA-273 (1997). Dutta (1999), Basoz and Mander (1999), Banerjee and Shinozuka (2007), Jeong and Elnashai (2007) used the CSM to develop fragilities for highway bridges in the United States. Currently, the fragilities proposed by Mander and Basoz (1999) are employed in HAZUS-MH for seismic risk assessment of highway infrastructure systems. Further details about the fundamental assumptions and limitations of the HAZUS fragilities are discussed in the next section. Fajfar (2000) proposed the N2 method as a special form of CSM in which pushover analysis of a multi-degree-of-freedom (MDoF) model is combined with the inelastic response spectrum analysis of an equivalent single-degree-of-freedom (SDoF) system in the acceleration-displacement format. Gardoni et al. (2003) and Zhong et al. (2008) proposed a modification to the N2 method to aid in the development of probabilistic seismic demand models (PSDMs) for reinforced concrete bridges with single and two column bents, respectively. Most of the studies employing CSM to develop fragility relationships were restricted to two dimensional analytical bridge models.

Several researchers resorted to more reliable yet computationally expensive techniques such as Nonlinear Time History Analysis (NLTHA) and Incremental Dynamic Analysis (IDA) to develop fragility curves. Kim and Shinozuka (2004) used NLTHA on two dimensional bridge models to study the effect of steel jacketed column retrofits on the performance of bridges. Mackie and Stojadinovic (2005) employed NLTHA and IDA to develop fragility curves. These formed the basis of a rational methodology to evaluate damage potential and to assess probable highway bridge losses for critical decision making regarding post earthquake safety and repairs to highway networks. Mander et al. (2007) used IDA in a performance-based earthquake engineering context to investigate the expected seismic damage and the associated financial loss from highway bridges. Zhang and Huo (2009) developed fragility curves for conventionally designed and base

isolated bridges using NLTHA and IDA to aid in assessing the effectiveness and optimum design parameters of isolation devices. Huang et al. (2010) used NLTHA coupled with a Bayesian updating procedure to develop PSDMs for typical California reinforced concrete bridges with single column bents considering the effect of near-field ground motions and effects from soil characteristics. Nielson et al. (2007), Padgett et al. (2008), Ramanathan et al. (2010, 2012) employed NLTHA to develop fragility curves for common bridges in Central and Southeastern United States (CSUS) in their as-built and retrofitted conditions, accounting for multiple component vulnerability, while Pan et al. (2010) developed fragility curves for as-built and retrofitted multispan simply supported steel girder bridges in New York state using NLTHA. Figure 2.2 summarizes the existing bridge fragilities for multi-span continuous concrete box-girder bridges with and without the consideration of seismic design principles. These curves were developed by various researchers by employing different techniques. Clearly, there is a well pronounced variability in the curves even for consistent damage states which deserves attention.

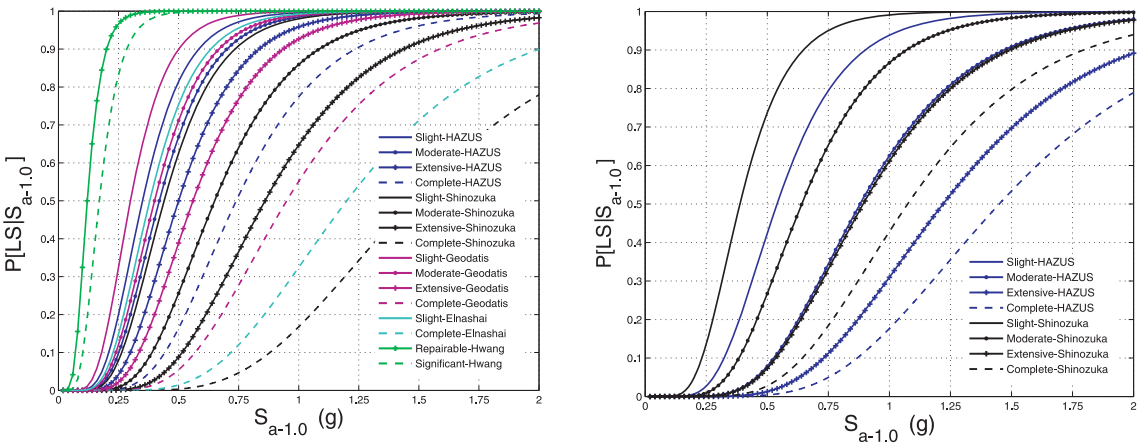

a) b)

Figure 2.2: Existing fragility curves for multispan continuous concrete box-girder bridges a) seismically designed, b) non-seismically designed

Fragility analysis techniques often differ based on two major aspects: mechanical analysis methods adopted to determine structural response and the reliability assessment

method. The former deals with the approach to simulate seismic loading, assess structural response, and consider geometric effects, while the latter is central to predictive response modeling, uncertainty treatment and system component analysis and combinations, which is discussed subsequently in this section. The mechanical analysis techniques considered in the past account for linear or nonlinear material responses, static, dynamic or spectral responses and the inclusion of geometric effects such as P-Δ or full nonlinear or large deformations. In the context of seismic performance evaluation of bridges, the distinction between analysis techniques can be made in terms of seismic load input to the structure. Therefore, the demand analysis tends to be the primary distinction in the methods. This section presents the details of the RSA, CSM, NLTHA and IDA techniques in an effort to categorize them based on the method formulation, fundamental assumptions and possible implications for their extension to three dimensional fragility analyses of highway bridges. The viability, scope, and application of the various analytical tools are also discussed.

2.1.1 Response Spectrum Analysis (RSA)

The elastic response spectrum analysis method (RSA) is one of the simplest and most efficient techniques used for demand analysis in the development of fragility curves (Yu et al., 1991; Hwang et al., 2000). This simplicity has resulted in the frequent use of RSA in the design field to serve as a quick reference calculation while designing critical components such as columns in a bridge. Typically, the response spectrum of the ground motion or design spectrum is used to obtain the maximum response quantities. The analytical models used are linear elastic models based on effective stiffness properties and assumed equivalent viscous damping ratios. This technique is most applicable for bridges that are expected to perform in the linear elastic range based on cracked section properties. It could also be used for determining inelastic response of bridges with equivalent linearization based on initial stiffness and appropriate modifications based on

energy principles or equal displacement principles. However, the method suffers from a few drawbacks. Where significant nonlinearity occurs, the method under-predicts the displacement demand and significantly over predicts the force. This technique only estimates the maximum modal responses which do not necessarily happen at the same time during earthquake excitation. The estimation of maximum modal responses is facilitated by the use of modal combination rules such as absolute sum (ABS) (Chopra, 2007), square-root-of-sum-of-squares (SRSS) (Rosenblueth, 1951), and complete quadratic combination (CQC) (Der Kiureghian, 1981). These methods are used based on the principle of superposition which is valid as long as the inelastic deformations are small. Typically, in the inelastic range, which is often of interest in fragility modeling, the displacements exceed the elastic range by many fold thereby undermining the validity of typical modal combination rules adopted in RSA.

2.1.2 Nonlinear Static Procedure (NSP) or Capacity Spectrum Method (CSM)

Capacity spectrum method is a simplified procedure for seismic response evaluation of structures. The capacity of the structure is evaluated by performing a nonlinear static pushover analysis of the structure with material as well as geometric nonlinearity included under load patterns which correspond to the dominant mode shapes of the structure. On the other hand, the demand on the structure is evaluated using a scaled down response spectrum derived for individual ground motions. The intersection of the demand and capacity spectrum indicates the estimated maximum response of the structure under the specified seismic ground motion. In order to construct the load pattern for pushover analysis for seismic capacity evaluation of the bridge, an eigenvalue analysis is performed and modal properties of the bridge are realized. Using the orthogonality property of the modes and extending it as an assumption to the realm of the nonlinear structure response, the overall maximum seismic response of the bridge can be estimated by evaluating the maximum response of the structure in two orthogonal

directions separately and combining the results using modal combination rules. The load pattern in pushover analysis for each horizontal direction corresponds to the associated fundamental mode shape.

A fundamental dilemma exists in the application of this method for bridges since the recommendations in ATC 40 (1996) are pertinent to building structures. Although researchers (Dutta, 1999; Basoz and Mander, 1999; Banerjee and Shinozuka, 2007; Jeong and Elnashai, 2007) have used the technique in the past, very little/no guidance is available for the choice of the bridge structural behavior type and the associated damping modification factor. Further, the fragility curves are sensitive to the damping modification factor and therefore the choice of a structure type plays a crucial role in determining the performance under seismic excitation.

2.1.3 Nonlinear Time History Analysis (NLTHA)

NLTHA technique has been exploited by several researchers (Mackie and Stojadinovic, 2001, 2005; Kim and Shinozuka, 2004; Zhang and Huo, 2009; Nielson, 2005; Padgett, 2007; Ramanathan et al., 2010, 2012) and has proven to give reliable estimates of system performance and seismic fragility relationships. It serves as the foundation for even more computationally intensive techniques such as IDA, which is discussed in the next section. NLTHA offers the flexibility to consider analytical models with linear or nonlinear cyclic material characteristics and geometric nonlinearities such as P-Δ or full nonlinear or large deformations. The distinguishing feature of NLTHA when compared to CSM or RSA is the ability to consider a temporal dimension in addition to two or three spatial dimensions defined by the geometry. This approach is the most rigorous, and often the response can be very sensitive to the characteristics of the individual ground motion used as seismic input. Therefore, several analyses are required using different ground motion records to achieve a reliable estimation of the probabilistic distribution of structural response. Since the properties of the seismic response depend on

the intensity, or severity, of the seismic shaking and characteristics of the record, a comprehensive assessment requires numerous NLTHA at various levels of intensity to represent different possible earthquake scenarios. This is typical of the "cloud" approach (Baker and Cornell, 2006) and is also commonly referred to as probabilistic seismic demand analysis (PSDA). This technique involves making an apriori assumption about the probabilistic distribution of seismic demand which tends to be a drawback. Yet another drawback of the technique is associated with the complexity of the approach in general, which limits its usage to a great extent.

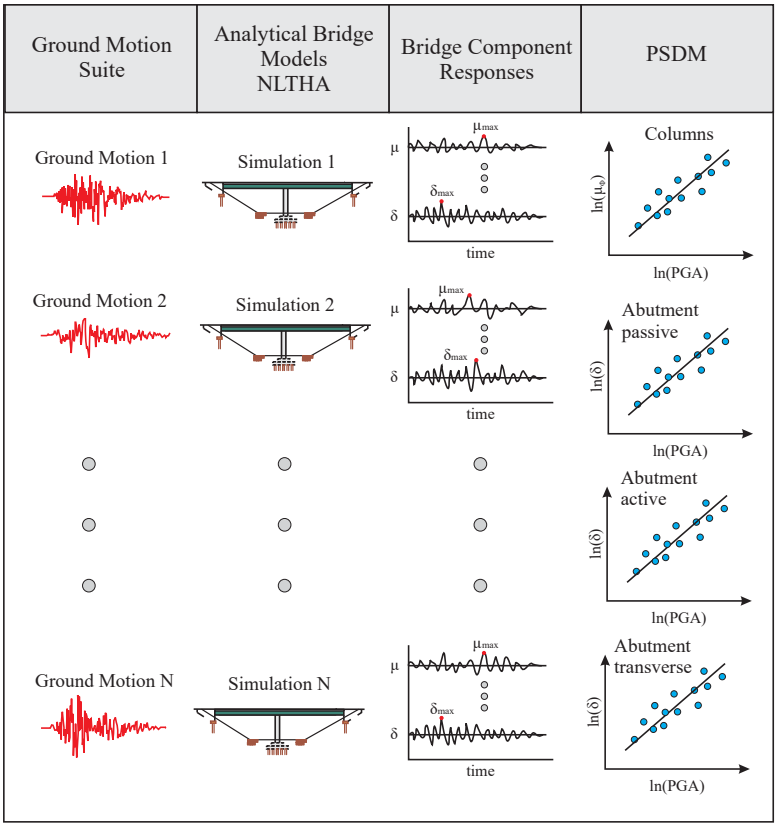

Figure 2.3: Schematic representation of the NLTHA procedure used to develop PSDMs

A schematic of the procedure for NLTHA is shown in Figure 2.3. Statistically significant yet nominally identical 3D analytical bridge models are typically created by sampling on the probability distributions for uncertain parameters. These are then

randomly paired with ground motions and in each case a NLTHA is performed to record peak component demands that are deemed to contribute to the vulnerability of the bridge system. Probabilistic seismic demand models (PSDMs) are developed and convolved with capacity models to obtain fragility curves. This study employs this method for generating fragility curves and extensive details are presented in Chapter 5.

2.1.4 Incremental Dynamic Analysis (IDA)

IDA is a special type of nonlinear dynamic analysis which facilitates seismic structural demand and capacity comparisons through a series of NLTHA for ground motions that are scaled successively until significant strength reduction (collapse) of the primary load bearing elements in the structural system. Unlike the previous technique, IDA may be classified as a "scaling" or "stripe" type technique (Baker and Cornell, 2006) where ground motions are incrementally scaled and analysis is performed at different hazard levels. This enables the structure to transition from linear elastic behavior to final global dynamic instability which marks the conclusion of the analysis and ground motion scaling. The method is analogous to the transition from a single static analysis to an incremental static pushover analysis. IDA was established as a state-of-the art method to determine the global collapse capacity by the FEMA guidelines (FEMA-350, 2000; FEMA-351, 2000). The overall formulation of the technique was proposed by Vamvatsikos and Cornell (2002) although it has been used in several forms in the work of many researchers (Bazzurro and Cornell, 1994; Luco and Cornell, 2000). IDA provides a thorough understanding of the changes in structural response with increasing ground motion intensities along with providing accurate and reliable estimates of the global collapse capacity of the structure. However, IDA does suffer similar drawbacks as NLTHA with respect to the computational difficulties involved in the approach. Another major drawback associated with the technique is that the process involves scaling the intensity without altering the frequency content of the ground motions. This could lead to

unrealistic time histories which might not be representative of the seismic hazard of the bridge site under consideration. Since the IDA technique is computationally expensive and involves scaling a single earthquake time history to increasing levels of intensity, a smaller subset of ground motions are typically selected to perform analyses.

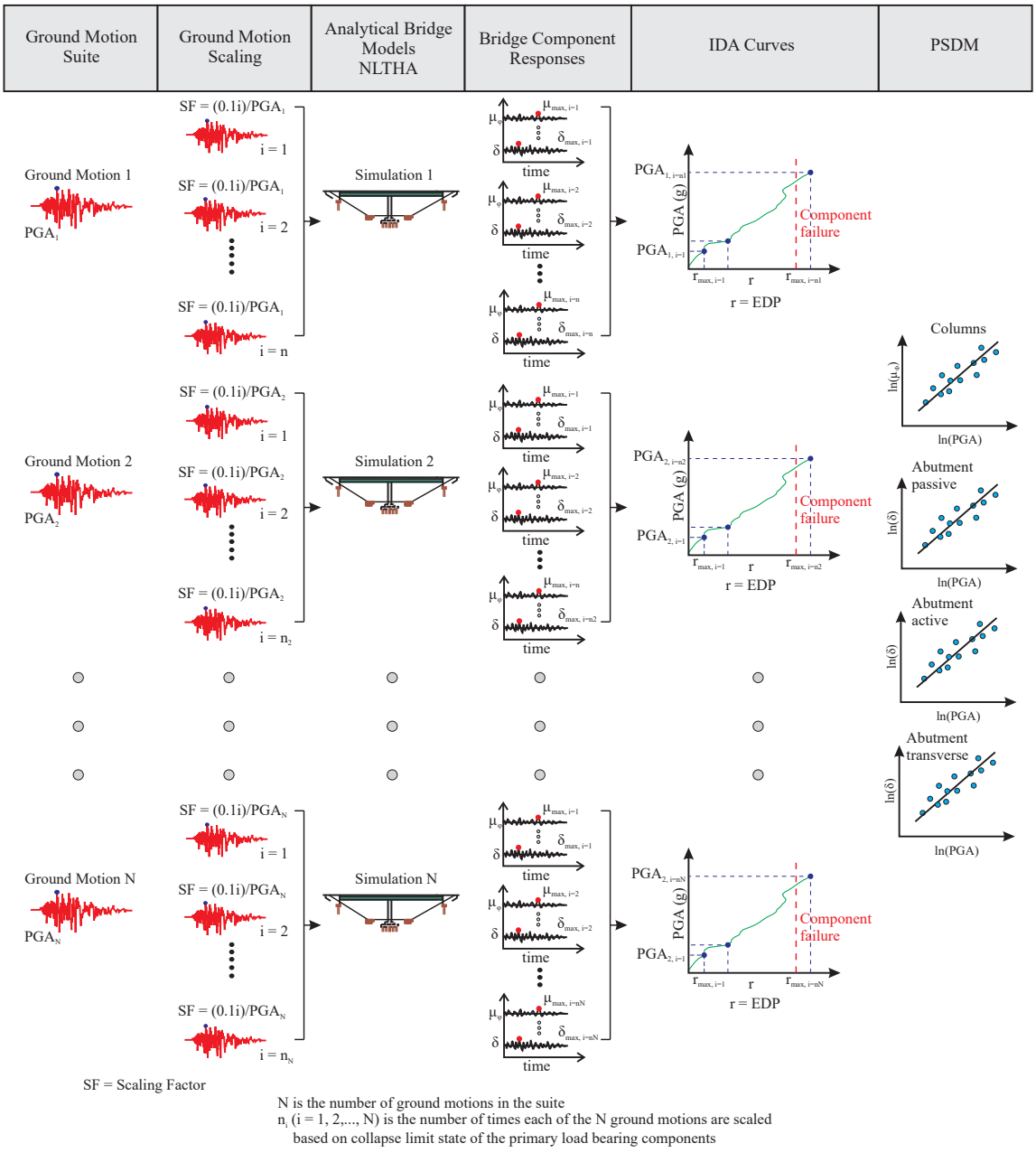

Figure 2.4: Schematic representation of the IDA procedure used to develop PSDMs

IDA curves describing the relation between peak *EDP*s and *IM* are then developed for every bridge-ground motion pair. For every scaling iteration of a ground motion, the component responses are obtained by performing NLTHA and are compared to the respective damage state prescriptive measures. The ground motion scaling is stopped when the prescriptive value associated with the complete damage state is exceeded by any one of the components considered in this study. As mentioned previously, some analysts directly derive fragility curves from IDA data either by deriving point estimates of the damage state exceedance probability at each ground motion level or by estimating the probability density function of the PGA for ground motions in which the damage state thresholds are exceeded. However, this approach requires a large sample size and subsequent number of simulations which is a common limitation of the approach. Alternatively PSDMs are derived for use in the fragility analysis using the same formulation presented for the other methods. Typically, the majority of the applications of IDA assess collapse level fragilities based on the excessive global strength or stiffness reductions revealed by the incremental analyses, which is the actual benefit of the method.

2.2 Structural Reliability Assessment Techniques for Bridges

The previous section described the different mechanical analysis procedure used in the estimation of bridge responses to imposed seismic demand. Likewise, researchers have adopted different techniques to probabilistically model the structural response, propagate and deal with uncertainty and develop fragility curves by the convolution of demand and capacity models. The derivation of component based fragility curves is straight forward and is a closed-form solution (equation (2.1)) basing that the demand and capacity (or resistance) are assumed to be lognormal (Mackie and Stojadinovic, 2001; Cornell et al., 2002; Bazzurro and Cornell, 2002; Ellingwood and Wen, 2005; Nielson and DesRoches, 2007; Padgett et al., 2008; Celik and Ellingwood, 2010). In equation

(2.1), D and C denote demand and capacity, S_D and S_C denote the median values of demand and capacity and $\beta_{D|IM}$ and β_C denote the dispersions (logarithmic standard deviation) of the demand and capacity, respectively. It must be noted that S_C and β_C are defined based on the limit state under consideration.

$$P[D > C \mid IM] = \Phi\left(\frac{\ln\left(S_D / S_C\right)}{\sqrt{\beta_{D|IM}^{\,2} + \beta_C^{\,2}}}\right) \tag{2.1}$$

Estimates of system reliability considering the vulnerability of multiple components can be obtained by convolving the individual PSDMs to develop a joint probabilistic seismic demand model (JPSDM) and then integrating it over all possible failure domains (prescribed limit states) to obtain the probability of failure at a particular IM. The process can be repeated at several IM levels to develop system level fragility curves. However, in situations where the system vulnerability is characterized by the vulnerability of multiple components, as will be in the current research, closed form integration over all possible failure domains tends to be extremely challenging and mathematically intense in formulation.

Several researchers have proposed techniques to develop fragility curves for the bridge as a system. Hwang and Huo (1998) used a logistic model to characterize the response and determine the system reliability of multispan simply supported bridges in Memphis, Tennessee. The parameters of the logistic model were determined from a logistic regression of a vector of Bernoulli random variables (zeros and ones), depending on whether the bridge sustains a particular damage state or not. Shinozuka et al. (2003) used the maximum likelihood estimators to determine parameters of the lognormal distribution (median and dispersion) describing the system fragility curves. As in the case of Hwang and Huo (1998), the event of the system exceeding user defined damage states were simulated using a Bernoulli random variable and the mean and dispersion of the

fragility curves were determined using a standard optimization algorithm. Mander and Basoz (1999) developed fragility curves using the CSM described in section 2.1.2 directly and assumed a value of the dispersion arbitrarily. Hwang et al. (2000a) proposed a simplified method to develop system fragility curves, where the median value of demand was expressed as a function of a ground motion intensity measure using a linear regression analysis, although the value of dispersion was arbitrarily assumed.

Mackie and Stojadinovic (2005) used a mean value, first order, second-moment analysis for each of the limit state functions describing the components that contribute to the system vulnerability. Having determined the mean and standard deviation for each of the response quantities (columns, abutments etc.), parametric first order reliability method (FORM) analysis was used to determine the probability of failure for each of the response measures. The series system assumption was then used to determine the system level fragility curves. Choi et al. (2004) developed first order bounds for system reliability assuming series systems, as one of the earliest attempts to account for some level of correlation among bridge components. Nielson and DesRoches (2007), Padgett and DesRoches (2008) and Ramanathan et al. (2010, 2012) used the joint probabilistic seismic demand model (JPSDM) and Monte Carlo Simulation to develop bridge system fragility curves. The JPSDM is first developed from the individual marginal PSDMs for the response measures realizing that the demands on various components have some level of correlation. A Monte Carlo simulation is then used to compare realizations of the demand (using the JPSDM defined by a conditional joint normal distribution in the transformed space) and component capacities to calculate the probability of system failure for a particular IM value, based on the assumption of a series system. The procedure is repeated for increasing values of the IM. Regression analysis is used to estimate the lognormal parameters, median and dispersion, which characterize the bridge system fragility.

Zhang and Huo (2009) adopted a weighting scheme of bridge component failures to preferentially establish bridge system level failure based on the components that contribute the most to the load carrying capacity or post event functionality criterion. Although the approach realizes that not all components contribute equally to system level damage states, the establishment of weights is particularly subjective and difficult as the number of components characterizing the system vulnerability increases. Kim et al. (2006), Lupoi et al. (2006), Zhang and Huo (2009) used other approaches to define system reliability such as parallel system, combination of series and parallel components, or adaptive systems that add components as damage accumulates.

Closed form solutions are recently emerging and these provide means to evaluate the system failure probability regardless of the system abstraction. Song and Kang (2009) used the matrix-based system reliability method to develop system level fragility curves by considering a wide range of component level failure events also accounting for bridge component correlations. Duenas-Osorio and Padgett (2011) proposed a closed form combinatorial method to develop system fragility curves by explicitly evaluating all possible ways in which bridge components can fail within and across limit states.

Singhal and Kiremidjian (1996), Der Kiureghian (2002), Gardoni et al. (2002, 2003), Koutsourelakis (2010) used a Bayesian framework to formulate system fragility relationships. While Der Kiureghian (2002) used the maximum likelihood method in conjunction with the Bayesian approach, Koutsourelakis (2002) used Markov Chain Monte Carlo techniques along with the Bayesian approach to develop multi dimensional fragility surfaces as a function of multiple ground motion characteristics. The fundamental advantage of the Bayesian formulation is the ability to yield a distribution of possible fragility curves which denote the epistemic uncertainty around them, which are also referred to as confidence bounds.

Statistical learning techniques, also known as surrogate models or metamodels have also been used to generate system level fragility relationships. Metamodels typically

help in replacing computationally expensive finite element models used in simulations for reliability assessment process. Response surface metamodels are the most commonly used due to its transparency and relative ease and have found wide spread use in the performance assessment of civil engineering structures (Bucher and Bourgund, 1990; Rajashekhar and Ellingwood, 1993; Guan and Melchers, 2001). Having developed the metamodels, a logistic regression is used to develop component and system level fragility relationships. Ghosh et al. (2012) extended the approach for the reliability assessment of highway bridges along with the application of several other surrogate models such as multiple adaptive regression splines, radial basis functions and artificial neural networks.

2.3 Fragilities for Bridge Classes, HAZUS and the Necessity to go Beyond HAZUS

The previous section detailed different techniques and mechanical analysis procedures to determine structural fragilities along with their limitations. It must be noted that researchers in the field must continue to investigate improvements in these methods. The aim is to develop more reliable fragility curves that can be used in a variety of ways ranging from damage assessments, retrofit prioritizations, risk assessments and more importantly emergency response in the context of the present study. The intent of the present research is to develop fragility curves for predominant bridge classes in California based on unique California bridge inventory information. Most of the fragility curves developed for California bridges are structure specific (Mackie and Stojadinovic, 2001, 2005; Zhang and Huo, 2009). Structure specific fragility curves are advantageous and useful for risk assessment of the specific bridge structure, but the approach is prohibitive for the performance assessment of regional bridge inventories. Hence, the trend towards performance and vulnerability assessment of bridge classes or portfolios that represent bridges with variable parameters require fragility curves that are generated by varying these parameters, which are not captured in the structure specific scenarios. These parameters can be broadly classified under two categories – geometrical and

material. Attributes such as span length, deck width, column height, number of spans, superstructure type, design details that are unique to a bridge class, fall under the category of geometrical parameters, while concrete compressive strength, reinforcing steel yield strength, stiffness of the bearing pads, soil stiffness fall under the purview of material parameters. Nielson and DesRoches (2007), Padgett and DesRoches (2008), Ramanathan et al. (2010, 2012) developed fragility curves for bridge classes in CSUS considering as-built and retrofit strategies. These fragility relationships cannot be applied for the vulnerability assessment elsewhere due to discrepancies in the bridge class compositions and design details. There has further been a significant evolution in the bride design philosophy in California, which is detailed in section 2.4.1, which is absent in the CSUS bridges, thereby preventing the adoption of CSUS bridge class fragilities for their California counterparts. Added discrepancies in the definition of damage states to support regional risk assessment and decision-making needs, further add to the incompatibility between CSUS and California bridge class fragilities.

The only fragility curves that are applicable to bridge classes in California were the ones developed by Basoz and Mander (1999) and are employed in HAZUS-MH (2011) and ShakeCast (Lin and Wald, 2008). ShakeCast is an application developed by the United States Geological Survey (USGS) for automating ShakeMap delivery to critical users such as lifeline utilities. Critical users can receive automatic notifications within minutes of an earthquake indicating the level of shaking and the likelihood of impact to their own facilities.

The HAZUS fragilities suffer a few major limitations and these are described henceforth. These fragility relationships were developed for bridge classes based on a limited number of parameters available in the NBI, damage states based on limited sets of field damage observations and simplified two dimensional analysis techniques such as the CSM. Bridge classes, defined beyond the parameters listed in NBI, were extended taking into account seismic design, number of spans (single versus multiple), span

continuity (continuous versus simply supported), and bent type (single versus multi). Particularly, separate fragilities are assigned based on seismic design and this is taken into account in terms of a spectrum modification factor, strength reduction factor due to cyclic motion, drift limits and the longitudinal reinforcement ratio (HAZUS, 2011). California bridges have a significant evolution of the seismic design philosophies, which is described in section 2.3.1, and not accounting for their factors in the stochastic modeling procedure for generating fragility curves can lead to significant errors in the vulnerability assessment. In any case, the stochastic analyses used in the generation of HAZUS fragilities did not consider the variability of the bridge class geometrical attributes such as the variation of number of spans, span length, deck width, column height, at the least. These fragilities included limited uncertainty characterized by material properties such as concrete compressive strength and reinforcing steel yield strength. Additional and specific information for bridges pertinent to a region might be difficult to obtain and hence the curves were developed with the intention that the information out of NBI is all that is required for seismic evaluation of bridge classes.

Another significant drawback of the NBI based fragility relationships employed in HAZUS and ShakeCast is that these curves were derived assuming that the vulnerability of the bridge is characterized by the vulnerability of the columns alone. However, the unseating potential of the bridge deck at the seat abutments or the bents, tearing of the elastomeric bearing pads, collapse of the shear keys etc. adds to the vulnerability of the bridge system and will need significant repairs in the aftermath of an earthquake, and these components are not accounted for the in the formulation of the HAZUS fragilities. Further, there is a mismatch between the damage state definitions used in fragility analysis and overall bridge functionality post a seismic event. This hampers the decision making needs by agencies like the California Department of Transportation (Caltrans) with regards to emergency response and management. Attempts have subsequently been made to account for some differences in California bridge design

by incorporating design specific parameters such as span length, span-to-column height ratio, column-to-superstructure dimension ratio, reinforcement nominal yield strength, concrete nominal strength, longitudinal and transverse reinforcement ratio, deck thickness, foundation soil dry unit weight and angle of internal friction (Mackie and Stojadinovic, 2005). These attempts, however, were mainly focused on deriving structure specific fragility relationships or fragility curves applicable for a smaller subset of bridges such as single frame multispan continuous box-girder bridges with a single column bent (Mackie and Stojadinovic, 2005). This research aims to address all of the drawbacks associated with the HAZUS fragilities along with a refinement of the bridge classes by the inclusion of seismic performance sub-bins (SPS) characterized by seismic design philosophy of bridge components and several unique attributes, details of which are provided extensively in Chapter 3.

2.3.1 Emergence of Seismic Design Provisions for Bridges in California

Early seismic design provisions in the United States were developed following the historic 1906 San Francisco earthquake (FEMA, 2006). However, the first design provisions for bridges were not incorporated until 1940. Early seismic design provisions were based on wind loads and static lateral force concepts rather than dynamic analyses principles. The 1940 design provisions involved design for a lateral seismic force equal to a certain percentage of the dead load determined by a design engineer, placed at the center of mass of the bridge. Specifications were made slightly more specific in 1941, where the dead load percentage was specified to be between 2% and 6% based on the foundation type, and subsequently found a place in the American Association of State Highway and Transportation Officials (AASHTO) specifications. Unique structural characteristics such as energy absorption capacity of the structure and natural period were incorporated into the design specifications in 1965 (Moehle et al., 1995). The minimum lateral force of 2% of the dead load of the structure was still retained and engineers were

instructed to pay special attention to bridge structures founded on soft soils and bridges with massive piers.

The 1971 San Fernando earthquake paved the way for a major change in the seismic design philosophy. The lateral design forces were increased by a factor of 2 or 2.5 and the designs had to take into account factors such as fault proximity, site conditions, dynamic structural response, ductile design philosophy and energy dissipation capabilities. All of these aspects were included in the 1971 Caltrans Seismic Design Code (Sahs et al., 2008). The prime focus was to drive damage to the columns while the remainder of the bridge structure remained elastic (Moehle et al., 1995). Despite the modifications in design, the 1989 Loma Prieta earthquake caused spectacular damage to bridge structures. This drove Caltrans to solicit the Applied Technology Council (ATC) to conduct a detailed study and provide design and detailing recommendations, which, however, were not incorporated until after the 1994 Northridge earthquake. The modern day Caltrans Seismic Design Criteria (SDC, 2010) incorporates all the recommendations of the ATC-32 report since its very first inception in 1996. Modern day design follows the capacity design philosophy which ensures flexural failure mode in the bridge columns (Sahs et al., 2008).

California has close to 29,000 bridges which vary in age based on their time of construction. As detailed previously, the seismic design incorporated and the performance depends on the era in which the bridge is constructed. In short, the 1971 San Fernando and 1989 Loma Prieta earthquakes provoked significant changes in the seismic bridge design philosophy. In order to obtain reliable estimates of the risk associated with the bridge classes, it is crucial to capture the design attributes and unique vulnerabilities associated with the bridges based on their time of construction, which is the intent of the present study. Significant details about the characteristics of the design eras, potential vulnerabilities and design attributes are presented in Chapter 3.

2.4 Closure

This chapter provided a detailed description of the seismic risk assessment framework including the different assessment modules that are essentially decoupled in their evaluation. Fragility curves, which form an integral part in the risk assessment framework, help in translating seismic demand (characterized by an intensity measure) into a performance metric (probabilities of exceeding user defined performance thresholds), which would help stakeholders and decision makers in a wide variety of ways, primarily risk mitigation and management. A detailed evolution along the fragility timeline was presented in terms of mechanical analysis approaches, such as response spectrum analysis, capacity spectrum method, incremental dynamic and nonlinear time history analyses (NLTHA), and the reliability assessment frameworks used in their generation and the drawbacks associated with them. Lack of empirical bridge damage data from past earthquakes and advances in computational tools have paved the way for sophisticated and reliable techniques such as NLTHA to be widely used. NLTHA with high fidelity three dimensional analytical models will be used in the current research to develop fragility curves for highway bridge classes.

Transportation risk assessment typically focuses on the performance and anticipated damage to highway bridge clusters in a potential future earthquake. A wide majority of the existing bridge fragilities are site specific and cannot be used to replicate the performance of bridge classes with variable attributes in geometry and material characteristics. The only fragilities that are applicable to bridge classes in California are the ones that are developed by Basoz and Mander (1999) and these are adopted in HAZUS (2011). The potential limitations of the HAZUS fragilities are identified and a case is made for improvement in these probabilistic relationships, which is the focus of the present study. Further, the California bridge inventory has a wide array of bridges varying in age, designed and constructed using unique design specifications and detailing aspects prevalent at that point in time. Therefore, analytical models capturing these

design philosophies and their evolution are needed in order to obtain sufficiently accurate estimates of the vulnerabilities and risk associated with the bridge classes.

CHAPTER 3

CALIFORNIA BRIDGE DESIGN ATTRIBUTES

Understanding and characterizing the highway bridge inventory in California is a critical aspect of seismic vulnerability assessment of highway bridge classes in the state. This chapter presents an in-depth study of the California bridge inventory utilizing the National Bridge Inventory (NBI) database (NBI, 2010). Furthermore, an in-depth review of bridge plans and use of in-house databases such as BIRIS obtained from the California Department of Transportation (Caltrans) is used to supplement the NBI data to capture design details such as column dimensions and reinforcement details, bent cap details, common superstructure and abutment configurations, pile classes, and seat widths, which are absent in the NBI data. This helps to create sub-bins within a bridge class and leads to better bridge classes that have more consistent performance, design and detailing characteristics. The initial sections in this chapter present results from a detailed analyses of the California bridge inventory made available through the NBI database. Subsequent sections are devoted to the issue of sub-binning bridge classes and characterizing bridge geometric information pertinent to these sub-bins utilizing Caltrans in-house databases and an extensive review of bridge plans.

3.1 Bridge Classification Based on National Bridge Inventory and HAZUS

The National Bridge Inventory (NBI, 2010) is a database compiled by the Federal Highway Administration with the purpose of having a unified database for bridges, including identification information, bridge types and specifications, operational conditions, geometric data and functional description, and inspection data. The data available through the NBI database includes state and local county bridges and was

developed primarily for maintenance purposes and not necessarily seismic risk assessment. Every bridge is identified by a unique code consisting of 116 fields and detailed descriptions of the fields are found in the *Recording and Coding Guide for the Structure Inventory and Appraisal of the Nation's Bridges* (NBI Coding Guide, 1995). Although the code does not provide a complete description of the bridge, it provides information sufficient for a broad and general classification of highway bridge classes. Field 43 (A and B) aids in a broad classification of highway bridge classes. Field 43 is composed of two subfields: 43A and 43B, associated with the material type and/or design and type of design and/or construction of the superstructure, as detailed in Table 3.1 and 3.2, respectively.

Table 3.1: Kind of material and/or design listed in NBI (NBI, 1995)

Field 43A	Kind of material and/or design
1	Concrete
2	Concrete continuous
3	Steel
4	Steel continuous
5	Prestressed and post-tensioned concrete
6	Prestressed and post-tensioned concrete continuous
7	Wood or timber
8	Masonry
9	Aluminum, wrought iron, or cast iron
0	Other

HAZUS (2011) provides yet another classification scheme for highway bridge classes. Bridges are classified into 28 classes (HWB1 through HWB28) with similar performance characteristics when compared to NBI in an attempt to obtain better fragility curves when data becomes available. Bridges are classified based on seismic design, number of spans and span continuity in addition to the material and type of construction that is provided by NBI. Complete description of the HAZUS bridge classes is documented in Table 7.2 of the HAZUS Technical Manual (HAZUS-MH, 2011).

Table 3.2: Type of design and/or construction listed in NBI (NBI, 1995)

Field 43B	Type of design and/or construction
01	Slab
02	Stringer/multi-beam or girder
03	Girder and floor beam systems
04	Tee beam
05	Box beam or girders – multiple
06	Box beam or girders – single or spread
07	Frame (except frame culverts)
08	Orthotropic
09	Truss – deck
10	Truss – thru
11	Arch – deck
12	Arch – thru
13	Suspension
14	Stayed girder
15	Movable – lift
16	Movable – Bascule
17	Movable – swing
18	Tunnel
19	Culvert (includes frame culverts)
20	Mixed types
21	Segmental box girder
22	Channel beam
00	Other

Bridge classes in California are classified under thirteen main types and their description based on NBI is listed in Table 3.3. Their equivalent HAZUS classifications are also noted to facilitate comparison later on. Upon examination of the results in Table 3.3, it is seen that the bridge classes indicated in bold account for about 65% of the concrete bridge inventory in the state and these are considered for fragility modeling in the present study. The single span concrete girder bridge class is not considered in this study as these historically tend to be resilient under seismic loading (Nielson, 2007) due to the absence of columns which tend to be the most vulnerable component in many other bridge classes.

As noted in Table 3.3, MSCBG bridges account for the bulk of the overall (state and local) inventory and this class of bridges is comprised of single and multiple frame bridges. Based on the analysis of an in-house database of state bridges assembled by Caltrans engineers, it was seen that MSCBG bridges account for about 37% of the state

bridge inventory and is the predominant bridge type. These consist of single and multiple frame bridges. Fifteen percent of the box-girder bridges have at least one in-span hinge and these are typically referred to as multiple frame (MSC-MBG) bridges. Further, multiple frame bridges were seen to be characterized with five spans or more and this was used as the cut-off number of spans to distinguish them from single frame (MSC-SBG) bridges in the present study.

Table 3.3: Bridge classes in California and their proportion in the overall inventory

Bridge class	Nomenclature	Classification			Number of bridges	
		NBI		HAZUS	Count	%
		43A	43B			
Multispan continuous concrete box-girder	**MSCBG**	2, 6	05	HWB8, 9, 20, 21	**5314**	**20.89**
Single span concrete girder	SSC girder	1, 2, 5, 6	01, 02, 03, 04, 05, 22	HWB3, 4	4582	18.02
Multispan continuous slab	**MSCSL**	2, 6	01	HWB10, 11, 22, 23	**4004**	**15.74**
Multispan continuous concrete girder	**MSCG**	2, 6	02, 03, 04, 22	HWB10, 11, 22, 23	**2164**	**8.51**
Multispan simply supported steel girder	MSSSSG	3	02, 03, 04, 22	HWB13, 14, 25	1085	4.27
Single span steel girder	SSSG	3, 4	01, 02, 03, 04, 05, 22	HWB3, 4	936	3.68
Multispan simply supported concrete girder	MSSSCG	1, 5	02, 03, 04, 22	HWB6, 7, 18, 19	900	3.54
Multispan simply supported concrete box-girder	MSSSCBG	1, 5	05	HWB6, 7, 18, 19	398	1.56
Multispan simply supported slab	MSSSSL	1, 5	01	HWB6, 7, 18, 19	391	1.54
Multispan continuous steel girder	MSCSG	4	02, 03, 04, 22	HWB15, 16, 26, 27	322	1.27
Multispan continuous concrete frame	MSCCF	2, 6	07	HWB10, 11, 22, 23	8	0.03
Multispan simply supported concrete frame	MSSSCF	1, 5	07	HWB6, 7, 18, 19	4	0.02
Other†	Other				5326	20.94
					25434	100

†Other bridge types include concrete and steel culverts, concrete tunnels, concrete and steel bridges with other structural systems, wood/timber, masonry, aluminum, cast/wrought iron bridges.

Bold face entries in the table are the bridge classes considered in this study.

MSCC slab bridges account for about 12% of the state inventory while the MSCC girder bridges account for roughly 11% of the state inventory. The proportion of slab and girder bridges in the state inventory is consistent with their proportions in the overall inventory. MSCG bridges can be further classified into two types depending on the type of girder in the superstructure and the ability to transfer moments from the superstructure to the substructure. MSCG bridges with Tee girders in the superstructure are generally cast monolithic with the deck slab and the bent and thereby transfer moment to the substructure while girder bridges with Standard I and Bulb Tee girders rest on bearing pads at the bent. These are non-integral with the bent and do not transfer any moment to the substructure. Further details are provided in the latter part of this chapter. It was seen that about 45% of the MSCC girder bridges have non-integral (MSCG-I) I- and Bulb-tee girders while 55% of them have integral (MSCG-T) tee girders in their superstructure. The bridge classes considered for fragility modeling in this research are listed in Table 3.4 and account for about 45% of the bridge inventory in the state.

Table 3.4: Bridge classes considered for fragility modeling

Bridge class	Nomenclature
Multispan continuous concrete single frame box girder bridges	MSC-SBG
Multispan continuous concrete slab bridges	MSCSL
Multispan continuous concrete Integral Tee girder bridges	MSCG-T
Multispan continuous concrete Non-integral I- and Bulb-tee girder bridges	MSCFG-I

3.2 Bridge Class Statistics

In addition to facilitating a broad classification of bridges, NBI provides information on several other geometrical parameters associated with bridges. Fields 45, 48, 52 and 54 provide information regarding number of spans, maximum span length, deck width, and minimum vertical underclearance, respectively. It must be noted that NBI does not list the individual span lengths in the case of multispan bridges and only provides information about the maximum span length. Field 34 provides information

regarding skew in the bridge superstructure, measured as the angle between the centerline of a pier and a line normal to the roadway centerline. A value of 99 corresponding to this field indicates variable skew in the bridge.

Parameter estimation and distribution testing (Ang and Tang, 1975) is a common technique adopted to capture the spread of parameters with smaller data sets. However, in the present scenario, with the abundance of data made available by NBI, more reliable techniques such as fitting empirical cumulative distribution functions (CDFs) to the geometric data is chosen. In this technique, the data set containing N data points is rank ordered, generally in ascending order, $x_1 \leq x_2 \leq x_3 \leq \cdots \leq x_N$. The probability of the i^{th} observation (or the CDF value) is then calculated by using the rank mean plotting position, given in equation (3.1), which is an unbiased estimator.

$$F_X(x_i) = \frac{i}{N+1} \tag{3.1}$$

Figure 3.1 shows empirical CDFs for maximum span length, deck width and minimum vertical underclearance for the bridge classes chosen in this study. Inspection of the span length distribution (Figure 3.1a) reveals that a majority of the MSCSL bridges have span lengths ranging from 16 ft to 50 ft, while the MSC-SBG have much longer span lengths up to 180 ft. In the case of MSCG-T girders, the range is between 30 and 80 ft, while the MSCG-I girders have span lengths ranging between 30 and 150 ft. These ranges are consistent with suitable span lengths for which these types of construction are generally chosen (BDA, 1988, 1989, 1995, 2004, 2009). Figure 3.1b shows the empirical CDF for deck width across all bridge classes chosen in this study. There is relatively small difference in the overall distribution of deck widths across bridge classes. It is intuitive since deck width is a function of number of traffic lanes on the bridge.

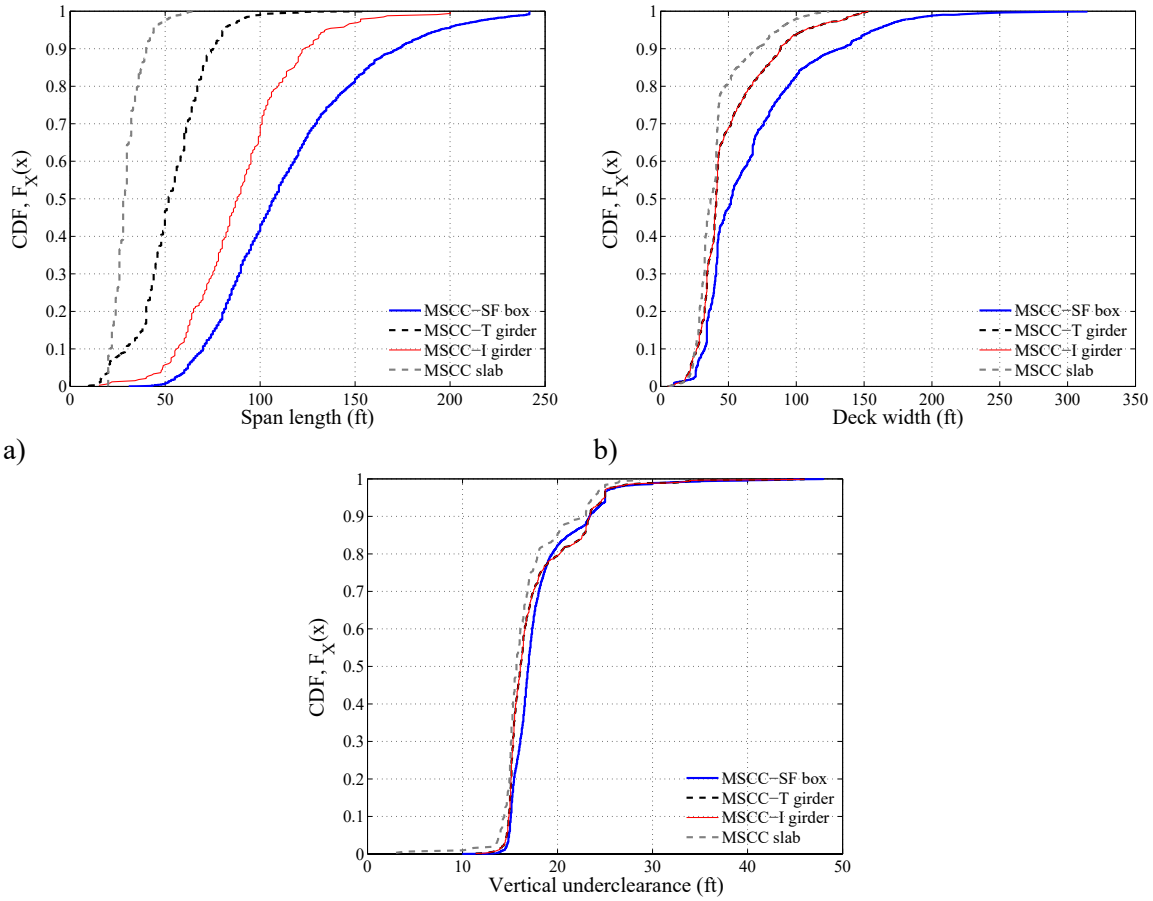

Figure 3.1: Empirical cumulative distribution functions for the chosen bridge classes for a) maximum span length, b) deck width, and c) minimum vertical underclearance

NBI does not explicitly record the height of bridge columns. In this study, column heights are inferred based on the vertical underclearance field in NBI, measured as the height between the underside of the bridge deck and the roadway surface. Based on permissible span-to-depth ratios, column height is obtained by deducting the superstructure depth (excluding the slab thickness) from the vertical underclearance. Empirical CDF for vertical underclearance across bridge classes is shown in Figure 3.1c. Similar to deck widths, the distribution for vertical underclearance is consistent across bridge classes chosen, with a range between 15 and 30 ft. Some basic statistics for these geometric features are provided in Table 3.5 to give an idea of the central tendency and

dispersion. The empirical CDFs completely describe the distributions and will be used in generating parameterized bridge models for fragility analyses.

Table 3.5: General statistics for bridge class geometrical parameters

Geometric parameter	Bridge class	Mean (ft)	Median (ft)	Std. Dev. (ft)
Span length	MSC-SBG	114.8	106.9	40.5
	MSCSL	30.1	27.9	7.61
	MSCG-T	53.1	51.8	17.9
	MSCG-I	89.5	87.9	27.9
Deck width	MSC-SBG	67.2	51.8	42.2
	MSCSL	41.9	37.1	19.1
	MSCG-T	53.0	41.0	33.5
	MSCG-I	53.0	41.0	33.5
Vertical underclearance	MSC-SBG	18.0	16.9	3.7
	MSCSL	16.7	15.7	3.2
	MSCG-T	17.7	16.1	4.2
	MSCG-I	17.7	16.1	4.2

Unlike the geometric parameters described previously, number of spans takes on discrete values and hence non-parametric probability mass functions (PMF) are generated for this parameter. The frequency of this data at each span number is determined and the count divided by the total number of bridges in a particular bridge class is defined as the respective probability of having that number of spans. Figure 3.2 shows PMFs for number of spans across bridge classes. Upon examination of the PMFs in Figure 3.2, it is seen that the most likely number of spans for MSCSL, MSCG-T and MSCG-I bridges is three while it is two for MSC-SBG bridges. This mode statistic for number of spans is used in generating parameterized bridge models for fragility analysis.

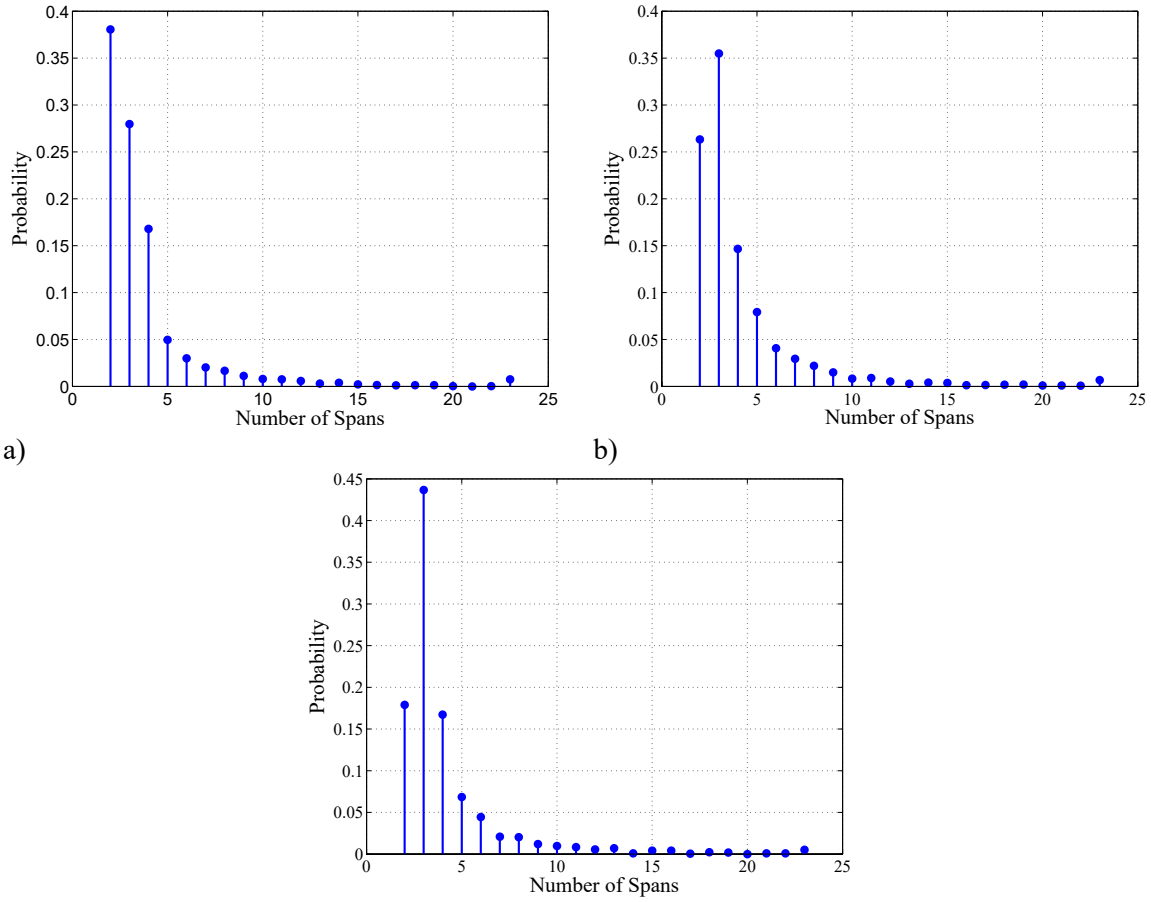

Figure 3.2: Probability mass function for number of spans for a) MSC-SBG, b) MSCSL, c) MSCG-T and MSCG-I bridge classes

As stated previously, NBI records skew in the bridge superstructure. Upon analysis of this parameter, it was seen that the average skew was 14.5°, 13°, and 14.4° for MSC-SBG, MSCSL, and MSCG-T and MSCG-I bridges, respectively and the mode statistic being zero in all cases. Since the majority of the bridges considered in this study have either zero skew or a value less than 15°, it is justified to neglect the effect of skew in this initial study. Further studies will determine the effect of skew on the vulnerability of bridges. At this point, it is recommended to use the modification factors for capturing the effect of number of spans and skew suggested in HAZUS-MH (2011), until more appropriate factors are determined.

3.3 Need for Sub-binning Beyond NBI

Seismic bridge design provisions in California have evolved significantly over the last few decades in response to the deficiencies exposed after significant seismic events (ATC, 1981, 1996; BDS, 1990; SDC, 1999, 2010). In order to develop reliable metrics such as fragility curves to quantify the seismic performance of bridges classes, it is imperative to understand the vulnerability associated with them as these design standards evolve. Geometric attributes captured in the NBI do not furnish any credible information regarding the potential vulnerabilities associated with the bridge classes. Bridge design details and physical characteristics help to capture the vulnerabilities associated with various components. Therefore, there is a need to sub-bin the bridge classes based on design eras with Caltrans bridge design, retrofit and maintenance data in addition to the information provided by NBI.

3.4 Bridge Design Eras and Typical Design Details

This section and the subsequent ones are devoted to identifying unique bridge design attributes and their evolution over three significant design eras, separated by the historic 1971 San Fernando and the 1989 Loma Prieta earthquakes. This is achieved by an in-depth review of bridge plans pertinent to the design eras for the chosen bridge classes, use of Caltrans in-house databases such as BIRIS and extensive input from design engineers and maintenance staff. Caltrans maintains a complete image archive of all bridge as-built plans, bridge inspection reports, photos, and other significant correspondence in the BIRIS database. It also contains completed maintenance activities, and minor and major rehabilitation projects.

The MSCC slab bridge class typically employs columns which are pile extensions above the ground. As will be demonstrated in this section and the subsequent ones, the major change in design philosophies across design eras is the details used in bridge

columns. Since, slab bridges are comprised of pile bents, there is not a major change in its design and performance across design eras (BDA, 1989, 1995, 2004, 2009).

3.4.1 Pre 1971 Design Era

Early Californian bridge seismic design codes dealt with the philosophy that seismic forces were proportional to the dead weight of the structure. Bridges were designed for a lateral seismic force equal to 6% of the structural dead weight until 1965, at which point structural period and amplification factors were considered (Duan and Li, 2003). The concept of ductility was absent and the detailing of reinforcement to achieve ductility by current standards was very poor.

3.4.1.1 Typical design details

The column shear reinforcement consisted of #4 transverse stirrups spaced at 12 in on center regardless of the column size or the size of the longitudinal reinforcing bars. Very short seat widths in the range of 6 to 8 in. were typical at the expansion joints. There was inadequate lap splice lengths of the column longitudinal bars near the footing and inadequate development of the column longitudinal bars into the footing without any standard hooks. Lap splicing of the column stirrups in the cover was also very common.

3.4.1.2 Vulnerabilities

The 1971 San Fernando earthquake revealed several vulnerabilities associated with bridges designed prior to that date. Column shear failure and pull-out of the longitudinal reinforcement was predominant due to the lack of ductility. Provision of short seat widths at the bents and the abutments increased the unseating potential. These were seen during the San Fernando, Loma Prieta and Northridge earthquakes (Yashinsky, 1995; Yashinsky and Karshenas, 2003; Caltrans, 2007; Priestley et al., 1996).

3.4.2 1971-1990 Design Era

The 1971 San Fernando earthquake emphasized the importance of detailing and ductility in the response of bridge structures with the introduction of capacity design principles in their design standards. The lateral load carrying capacity of the bridges was increased by a factor of 2 or 2.5 and the aspects of fault proximity, site conditions, dynamic structural response and ductile details (Yashinsky and Karshenas, 2003). These factors featured in the Caltrans design specifications in 1973. The Applied Technology Council (ATC) developed guidelines which were documented in the ATC-6 report (1981). These formed the basis for design of Caltrans bridges and primarily remained unchanged until the 1989 Loma Prieta earthquake. The standard practice was to design for plastic shear in the columns with the intention of failing the column in flexure while all the other components of the bridge remained elastic.

3.4.2.1 Typical design details

Some of the typical design details of this intermediate era are summarized below:

- The spacing of the transverse reinforcement in the columns was reduced with a typical spacing of 4 to 6 in. However, the confinement of the plastic hinge region was still absent
- Increase in the negative moment reinforcement in footing and pile caps without any shear reinforcement
- Splicing of column longitudinal bars was not permitted at locations of maximum moment
- Seat widths were slightly increased from 6-8 in in the Pre 1971 design era to about 12 in
- Prior to the occurrence of the Loma Prieta and 1994 Northridge earthquake, there seemed to be a common notion that column flares were typically non-structural components and would probably spall during an earthquake. However, it was seen

that the presence of a flare reduced the length of the column and increased the plastic shear demand. This design era was characterized with poor flare details which was improved in the following era

- Joint reinforcement between column and the bent cap and column and the footing was absent

3.4.2.2 Vulnerabilities

Column shear failure in the plastic hinge regions was typical due to the lack of confinement in this zone. Due to the poor flare details as explained in the previous sub-section, shear failure was seen in columns with flares. Unseating potential at the bents, abutments and in-span hinge locations continued to be high due to the provision of short seat widths.

3.4.2.3 Retrofit strategies

Caltrans began the Phase-I bridge seismic retrofit program after the 1971 San Fernando earthquake (Yashinsky, 1995). The main objective of this program was to prevent unseating of bridge decks by the inclusion of longitudinal restrainers and transverse shear keys at the bents, abutments and in-span hinge locations. Failure of longitudinal restrainers and shear keys was reported during the 1989 Loma Prieta earthquake (Yashinsky and Karshenas, 2003).

3.4.3 Post 1990 Design Era

With the occurrence of the Loma Prieta earthquake, Caltrans solicited the ATC to provide recommendations for design standards, performance criteria, and practices (Duan and Li, 2003) and concurrently, extensive research focused on the seismic design and retrofitting of bridges in the United States (Priestly et al., 1996). All the recommendations from the ATC described in ATC-32 (1996) were incorporated into the Caltrans Bridge Design Specifications (BDS, 1990), and several internal design manuals (MTD 20-4,

1995; BDA, 1995; MTD 20-1, 1999; SDC, 1999). The fundamental emphasis was on displacement-based or capacity design approach which ensures a ductile failure mode in the columns while the remainder of the bridge remained elastic. The 1994 Northridge earthquake stood testimony to the superior performance of the retrofit program, and is discussed in the later part of this section.

3.4.3.1 Typical design details

- In a general sense, bridges in this era had fewer number of expansion joints and more continuity in the superstructure, larger skews were avoided, and usage of column flares was very minimal
- Tight confinement reinforcement was provided in the column plastic hinge zones with spacing of less than 6 times the longitudinal bar diameter
- Large seat widths on the order of 24 in were provided
- Improvised flare details were provided by isolating the flare from the superstructure by the introduction of a 2 in to 4 in gap
- No lap splices were provided in the plastic hinge zones
- Shear reinforcement was provided in the footing and pile caps
- Joint reinforcement was provided between column and the bent cap and column and the footing

3.4.3.2 Retrofit strategies

With the occurrence of the Loma Prieta earthquake, Caltrans began a Phase-II bridge seismic retrofit program to address a wider range of problems associated with the Pre 1971 design era bridges and adopted a more sophisticated approach (Yashinsky, 1995). The fundamental focus was on the non-ductile Pre 1971 columns by retrofitting them with steel or fiber jackets. As mentioned previously, failure of a number of short hinge restrainers provided during the Phase-I retrofit program was observed during the

Loma Prieta earthquake. These were replaced by longer restrainers and further pipe seat extenders were provided to prevent unseating in the event of failure of the restrainers (Yashinsky and Karshenas, 2003). Footings were strengthened by increasing the height of the cap and providing additional piles. This would minimize the potential for the column longitudinal bars to pull out due to the availability of a greater length in the footing for their development.

3.5 Bridge Components and Typical Details

Having discussed the progression of seismic bridge design specifications and the potential vulnerabilities at the bridge system level over three significant design eras, this section provides details about individual bridge components for the bridge classes considered in this study. The details provided here are based on an extensive review of bridge plans pertinent to the chosen bridge classes in the three design eras.

3.5.1 Bridge Superstructure

Bridges are composed of two parts – superstructure and the substructure, as illustrated in Figure 3.3. Clearly, different bridge types have different load transfer mechanisms in the longitudinal and transverse directions. MSC-SBG and MSCG-T bridges are generally cast-in-place (CIP) and the deck and girders are monolithic over the bents (i.e. have integral bent caps). Longitudinal reinforcing bars or the post-tensioning (if applicable) ensures frame action in the superstructure. MSCSL bridges also fall under the same category where the deck slab is monolithic over the bents. Therefore, during an earthquake, the integral bent cap connection ensures that the columns move along with the superstructure and force transfer occurs by a combination of flexure and shear. On the other hand, the MSCG-I bridges are typically pre-cast (PC) or pre-manufactured at a factory location off-site and assembled at the bridge site. The girders are placed on top of dropped bent caps and are stabilized by the inclusion of end and intermediate

diaphragms. These form a critical part of the load path in transferring the dead loads and seismic forces from the deck and girder system down to the bearings and the bent cap. It must be noted that the presence of bearings allows for a relative rotation between the girders and the bent cap.

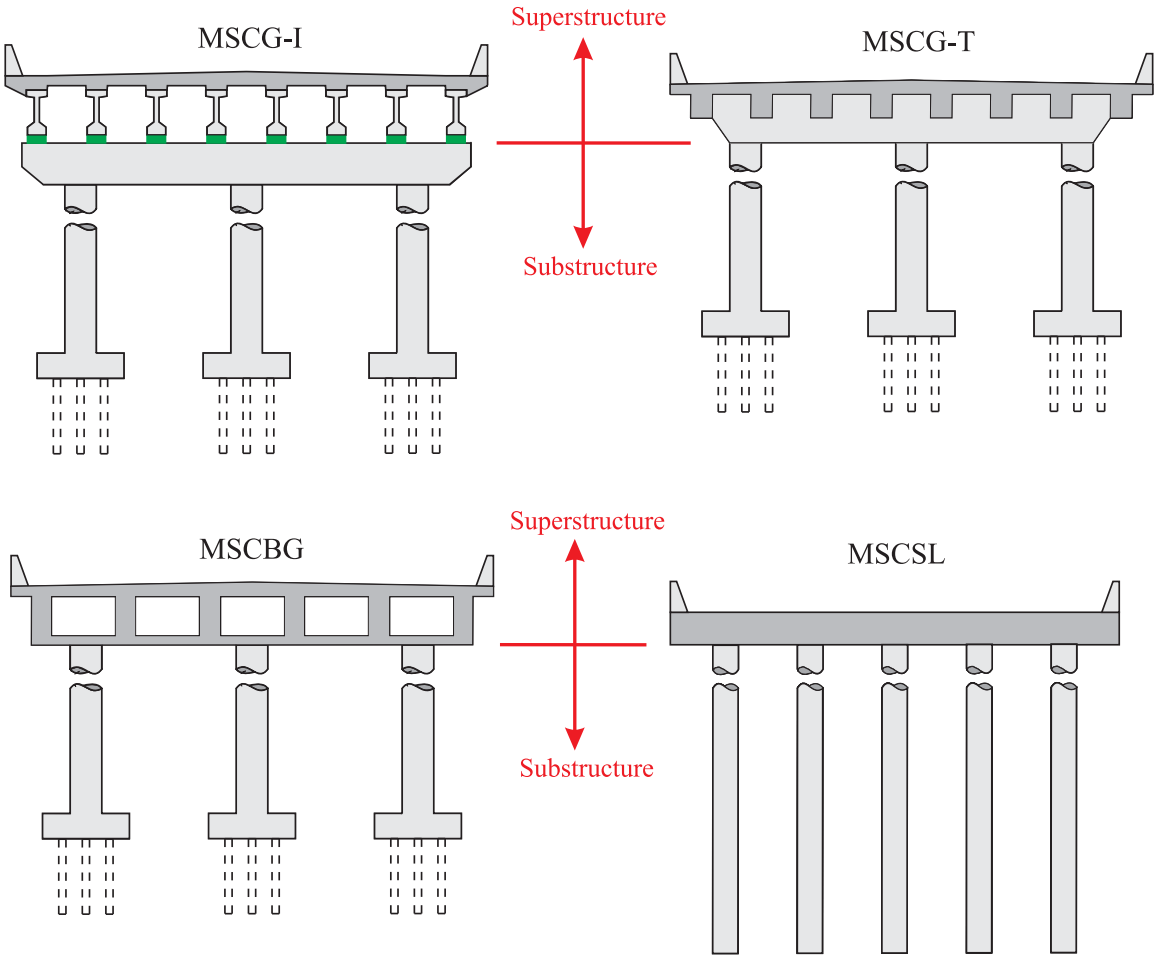

Figure 3.3: Superstructure and substructure classification for different bridge classes

Bridge superstructures have generally performed well during past earthquakes. This is typically because they tend to remain essentially elastic with very little or no non-linear effects. The general vulnerabilities associated with the superstructure are unseating at the seat abutments when large relative displacements between the deck and the abutment backwall exceeds the seat length. Figure 3.4a shows a depiction of excessive displacement between the deck and the abutment backwall during the 1994 Northridge

earthquake. Figures 3.4b and 3.4c shows total collapse of the Cypress Street Viaduct and the Interstate 5 Overpass during the Loma Prieta and Northridge earthquakes, respectively. Local spalling of concrete may also take place due to impact between the deck and the abutment backwall. Figure 3.4e shows pounding damage to a bridge in-span hinge during the 1994 Northridge earthquake.

MSCC-I girder bridges in the pre 1971 and 1971-1990 design eras have been made continuous over the bent for live load i.e., by making the deck continuous over the bents and the inclusion of diaphragm over the piers. This reduces the potential for collapse and typically leads to the girders falling the height of the bearings and then sliding on the bent cap. Figure 3.4d shows deck damage in the Bolu viaduct consisting of precast I girders, during the 1999 Duzce earthquake. In the case of CIP bridges, the columns might experience larger forces in comparison to PC bridges, due to the rigid connection between the superstructure and the substructure in the former case. In either case, the superstructures could develop large lateral forces causing failure of bearings and the connection to the substructure. Extensive details about superstructure configuration for the chosen bridge classes across design eras are documented in Appendix A.

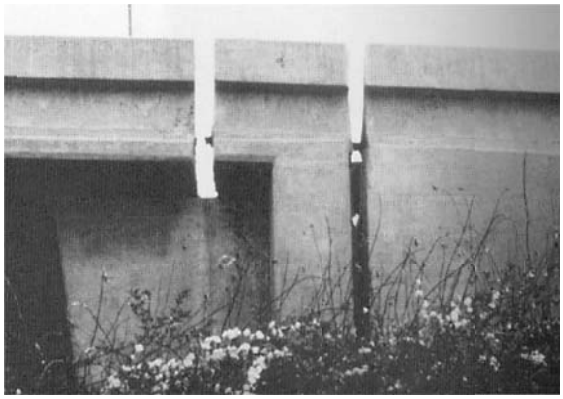

a)

b)

c)

d)

e)

Figure 3.1: a) Large relative displacements between deck and the abutment backwall during Northridge earthquake, b) span unseating in the Cypress Street Viaduct during the Loma Prieta earthquake, c) deck collapse in the Interstate 5 overpass during the Northridge earthquake, d) deck damage in the Bolu viaduct during the 1999 Duzce earthquake, and e) pounding damage in Santa Clara River bridge between the deck and abutment backwall during the Northridge earthquake

3.5.2 Columns

A majority of bridge seismic failures in the past are attributed to column failures. The failure mode (flexure versus shear) depends, in part, on the era in which the column

was designed. The flexural response of reinforced concrete (RC) bridge columns depends on a number of factors such as the longitudinal and transverse reinforcement ratios, reinforcement detailing, aspect ratio as well as the axial load ratio (Wight and MacGregor, 2011). The major contribution rests with the design details which vary based on the design era. The flexural failure mode is typically ductile in nature and is characterized by horizontal cracks and is the preferred mode of failure. On the other hand, the shear response of RC bridge columns is governed by four independent mechanisms: shear friction in compression zone, aggregate interlock, truss mechanism of the transverse reinforcement, and dowel action of the longitudinal reinforcement (Wight and MacGregor, 2011). Dowel action is typically minimal and can therefore be neglected in most cases. The relative contribution of the other three mechanisms to the shear response depends on the era in which the column is designed. Unlike the flexural failure mode, the shear failure mode is brittle in nature and is characterized by diagonal cracks.

3.5.2.1 Pre 1971 Columns

Columns designed prior to 1971 are predominantly characterized by shear response and as a result cannot fully develop their flexural capacity. A typical column in this era has transverse reinforcement consisting of #4 stirrups at 12 in on center irrespective of the column dimensions or the longitudinal reinforcement. The column relies on shear friction and aggregate interlock predominantly for strength and cracking is exacerbated since the aggregate interlock component declines rapidly leading to a brittle failure. However, even if the column yield moment is attained, the strength of the column degrades rapidly thereafter due to the poor confinement provided by the transverse reinforcement. The aforementioned behaviors are undesirable and typically results in total collapse of the bridge structure. Figures 3.5a and 3.5b show cases of shear failure in bridge columns during the San Fernando earthquake.

Another distinct detail associated with this design era was the embedment of the column longitudinal bars into the footing and bent cap without 90 degree hooks. Further, it was common practice to lap splice the column longitudinal bars just above the footing. In either case, the embedment or the lap splice length was too short (less than 20 longitudinal bar diameters) to develop the yield stress of the reinforcement. This caused pull out failures of columns from the footing during the San Fernando earthquake, as shown in Figure 3.6.

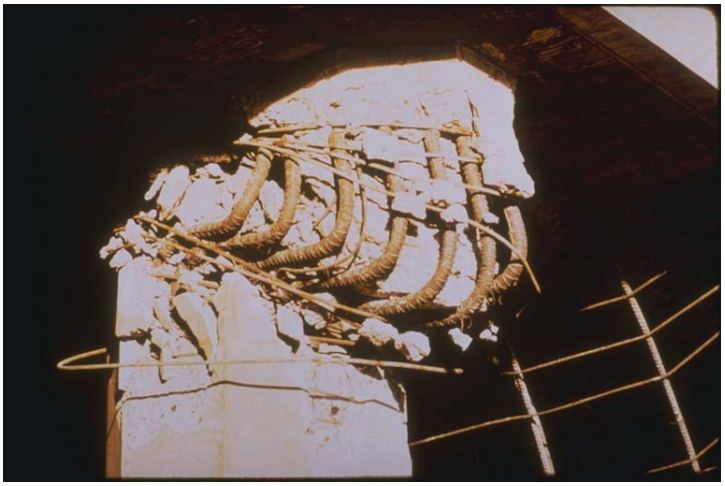

a)

b)

Figure 3.5: Shear failure in bridge columns a) at the intersection of Interstate 5 and 210, and b) of Foothills Freeway Overpass, during the San Fernando earthquake

Figure 3.6: Column pull out failures during the San Fernando earthquake

3.5.2.2 1971-1990 Columns

Columns in this design era were designed based on the capacity design process. Sufficient reinforcement was provided to develop the yield moment in the cross-section. However, the importance of cyclic degradation of shear strength and longitudinal bar buckling was not realized. Therefore, even if the yield moment of the cross-section was attained, the capacity degraded fairly quickly due to inadequate confinement of the plastic hinge region. This leads to fracture of the transverse reinforcement and buckling of the longitudinal reinforcement. Figure 3.7 depicts the aforementioned failures in bridge columns during the Northridge earthquake.

a)

b)

c)

Figure 3.7: Shear failure in the a) and c) plastic hinge region of column, and b) flared column, during the Northridge earthquake

3.5.2.3 Post 1990 Columns

The columns in the modern era are designed by giving complete consideration to the shortcomings of the previous eras. These are characterized by superior confinement of the plastic hinge region thereby preventing longitudinal bar buckling and shear failure. The columns have significant ductility and energy dissipation capacity. Therefore, in the event of an earthquake, they might experience significant nonlinearities, but manage to maintain the gravity load carrying capacity and thereby ensure collapse prevention. The capacity design process adopted in the modern era forces a flexural failure mode in columns prior to shear failure. If this does not occur, then the columns would experience a ductile shear failure primarily due to the truss mechanism of shear strength exhibited by

the transverse reinforcement. In such cases, yielding and eventual fracture of the transverse stirrups or hoops is likely.

Figure 3.8 shows the difference in performance of the columns based on their evolution across the design eras discussed in this section. Details about the column dimensions, longitudinal and transverse reinforcement ratio for the bridge classes is obtained by an extensive review of bridge plans and the details are presented in Appendix A. As stated previously, MSCSL bridges employ columns which are pile extensions and a major change in the pile cross-sections or details were not observed across the design eras considered in this study. Details about the pile cross-sections and the reinforcement layout are also documented in Appendix A.

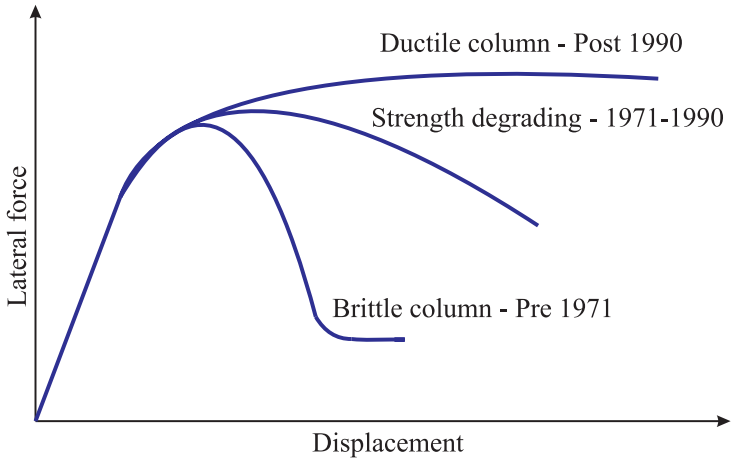

Figure 3.8: Lateral force deformation curves for typical bridge columns through the design eras

3.5.3 Superstructure to Substructure Connectivity

In the past, connections between the column and the superstructure and column and the foundations have proven to be vulnerable. This is particularly relevant in the case of MSC-SBG, MSCSL and MSCG-T bridge classes which have an integral bent cap and the column reinforcement frames into the superstructure. Connections should have the capability of resisting large shear forces, bending moments and axial forces. Often the connections have little room to develop reinforcement and provide confinement. Figure

3.9 shows a schematic of the possible connectivity types based on the bridge class and type. The connectivity types are referred to as Moment Frame Action (MFA) types drawing reference to their ability to transfer moments and shears. These further reinforce the continuity with respect to earthquake forces, more so with the moment frame kind of behavior rather than the continuity with regards to live load as in the case of NBI.

- MFA-0 depicts the case when the reinforcement over the bents is not continuous. The girders are essentially simply supported and the continuity is enforced by the presence of a continuous deck slab across the bent. There is no moment transfer from the superstructure to the substructure. MSCG-I bridges in the Pre 1971 and 1971-1990 design eras fall under this category.
- MFA-1 depicts the case when the girders and the deck slab are continuous across the bent. However, in this case there is also no moment transfer between the superstructure and the substructure. Both MFA-0 and MFA-1 are characterized typically by the presence of bearings. MSCG-I bridges in the Post 1990 design era fall under this category.
- MFA-2 is a moment resisting connection where there is a negative moment transfer between the superstructure and the substructure. This is enabled by the presence of continuous top reinforcement in the superstructure across the bents. However, the bottom reinforcement in the superstructure is terminated just before the bent. MSC-SBG, MSCSL and MSCG-T girder bridge classes in the Pre 1971 and 1971-1990 design era fall under this category.
- MFA-3 is a moment resisting connection where both positive and negative moments are transferred between the superstructure and the substructure. This is the premise of the capacity design process adopted in the modern era bridges. MSC-SBG, MSCSL and MSCG-T bridge classes in the Post 1990 design era fall under this category.

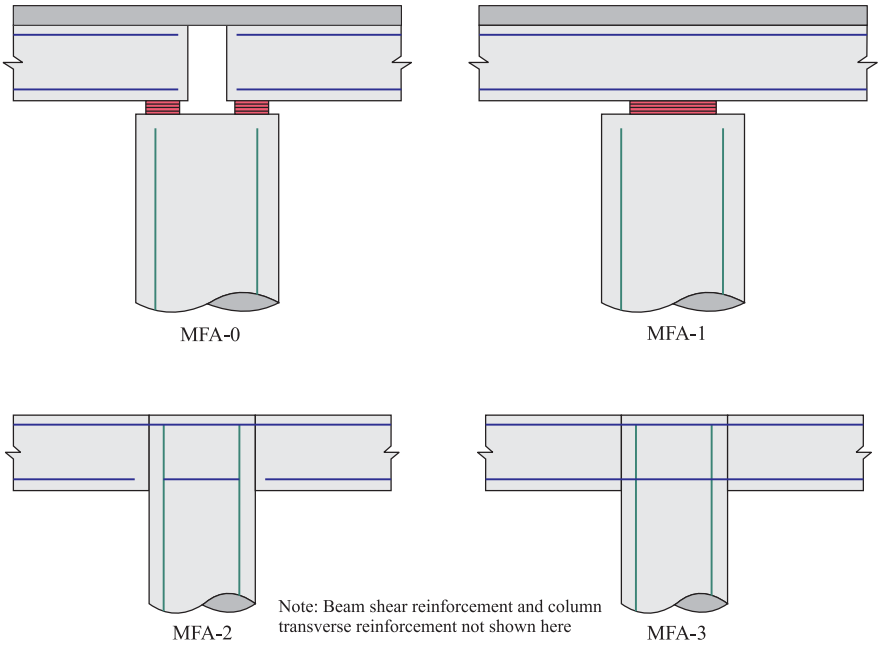

Figure 3.9: Schematic of superstructure to substructure connectivity types

The fundamental advantage of having connectivity types MFA-0 and MFA-1 in a bridge (as in the case of MSCG-I bridge class) is that the superstructure is not subjected to the seismic moments transferred by the column. This helps in achieving longer continuous spans in the superstructure (Priestley et al., 1996). For bridges with single column bents with a moment resisting connection at the base (this is typically the case), the column behaves like a vertical cantilever in both longitudinal and transverse directions and hence the response is independent of the direction. This provides for the design and usage of simple column circular cross-sections. However, the presence of MFA-0 and MFA-1 connectivities prohibits the use of pin connections at the column base in multi column bents.

On the other hand, bridges with connectivities MFA-2 and MFA-3 create the potential for additional redundancies in the seismic load path. Moment resisting connection between the superstructure and substructure provides a potential location of a plastic hinge at the column top thereby increasing the energy dissipation capacity. This

could be particularly beneficial in single column bents, where there is an additional location for energy dissipation complementing the plastic hinge at the column base. This connection type facilitates the provision of pinned connection at the base of multi column bents. However, if moment resisting connections are provided at the base of multi column bents similar to their connection with the superstructure, then it paves the way for adopting simple circular column cross-sections since the stiffnesses are equal in either directions and independent of the response (Priestley et al., 1996).

A main disadvantage associated with the connection of type MFA-2 or MFA-3 is the vulnerability associated with them based on when they were designed. Bridges with type MFA-2 were predominant in the Pre 1971 and 1971-1990 design era and these had inadequate longitudinal reinforcement at the top and no bottom reinforcement (as depicted in Figure 3.9). Seismic forces typically cause the joint to crack and in such cases stability is provided by the longitudinal reinforcement going through the crack and the crack is held intact by the transverse reinforcement. Failure of joints was reported during the Loma Prieta earthquake and is shown in Figure 3.10. Figure 3.11a shows a poorly detailed joint in a Pre 1971 MSC-SBG bridge. Integral connections of this type further might create a critical design condition where seismic moments will add to or subtract from the gravity load moments at the column face. Longitudinal reinforcement on the bottom face will have to be provided in order to carry the positive moment. As mentioned previously, the absence of bottom longitudinal reinforcement at the joint might lead to an increased vulnerability in the case of bridges with connectivity type MFA-2. This problem was however overcome in the Post 1990 era bridges where bottom reinforcement was provided at the joint and the top reinforcement was increased. Figure 3.11b shows a modern MFA-3 type joint that is well detailed and is the preferred type for MSC-SBG and MSCG-T bridge class. Figure 3.11c shows a MFA-3 type joint for MSCSL bridge class. Also shown in Figure 3.11d is connectivity type MFA-0 in an MSCG-I bridge.

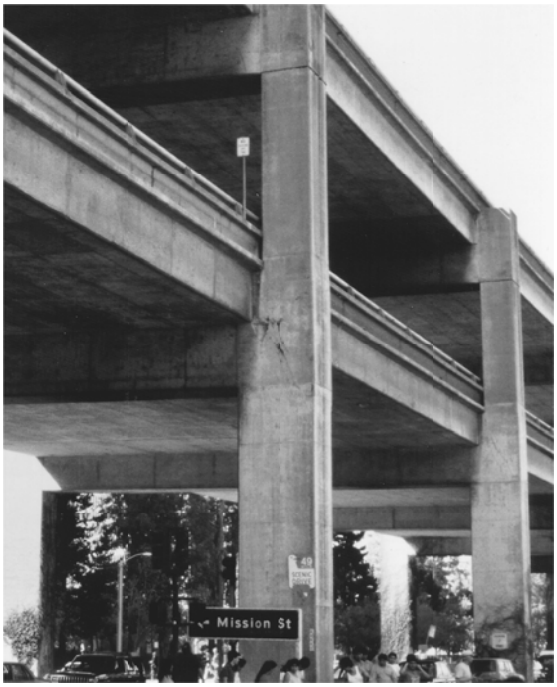

Figure 3.10: Joint damage to the Embarcadero viaduct during the Loma Prieta earthquake

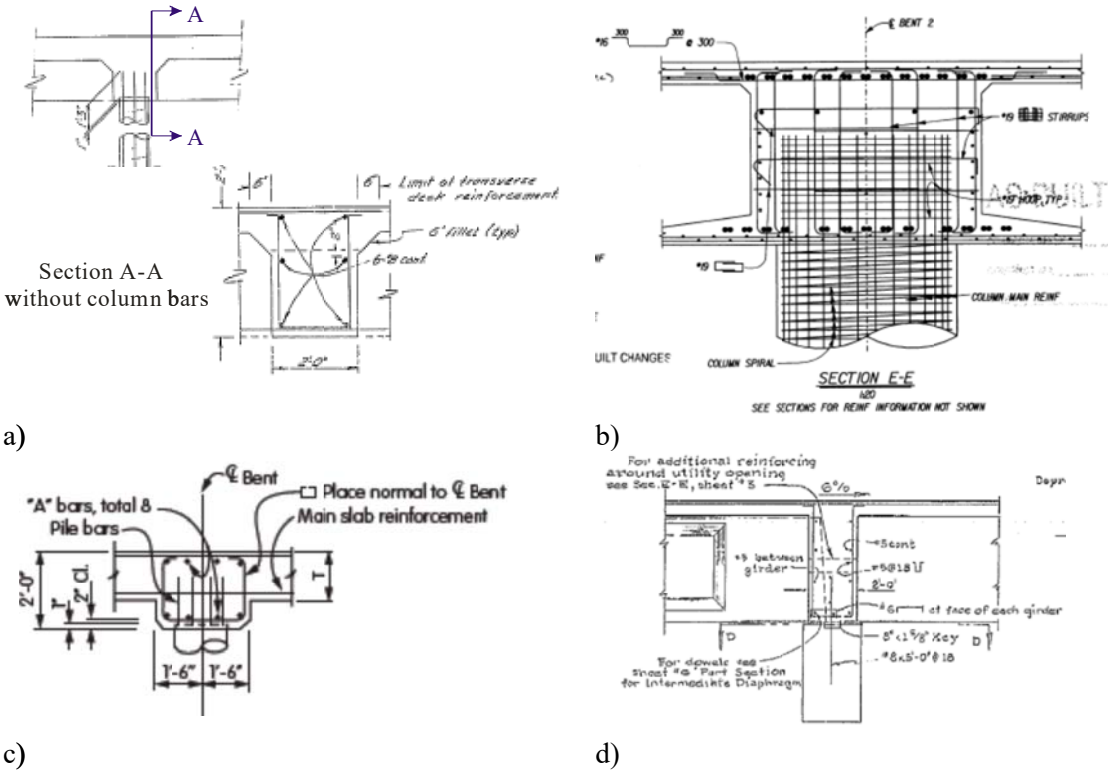

Figure 3.11: Typical joint details from a) Pre 1971 design era in MSCC-SBG, b) Post 1990 MSC-SBG, c) MSCSL, and d) MSCG-I girder bridge class

3.5.4 Abutments

Abutments can be classified into two basic types: open end and closed end. Diaphragm and seat type abutments fall under the category of open end abutments. These abutments are typically placed at the top of the approach embankment and have evolved from the desire to present an open appearance to traffic beneath the structure. The fundamental difference between the seat type and diaphragm abutments is that the former allows superstructure movement independent of the abutment while the latter does not. Closed end abutments present a closed appearance to approaching traffic by placing the structure support adjacent to traffic and are classified as below. Figure 3.12 shows a schematic of the different abutment types. Closed end abutments are used infrequently and better suited for bridge widenings and constrained urban locations. Abutments can be classified as follows:

a) Backfilled
    i. Cantilever abutment
    ii. Strutted abutment
    iii. Rigid frame
b) Cellular
    i. Bin
    ii. Closure wall

Open end abutments are more economical, adaptable and attractive when compared to the closed end abutments (BDA, 1989). These typically have lower height walls when compared to closed end abutments and therefore have a smaller settlement of the approach slab in bridges. Only open end abutments are considered as a part of this research.

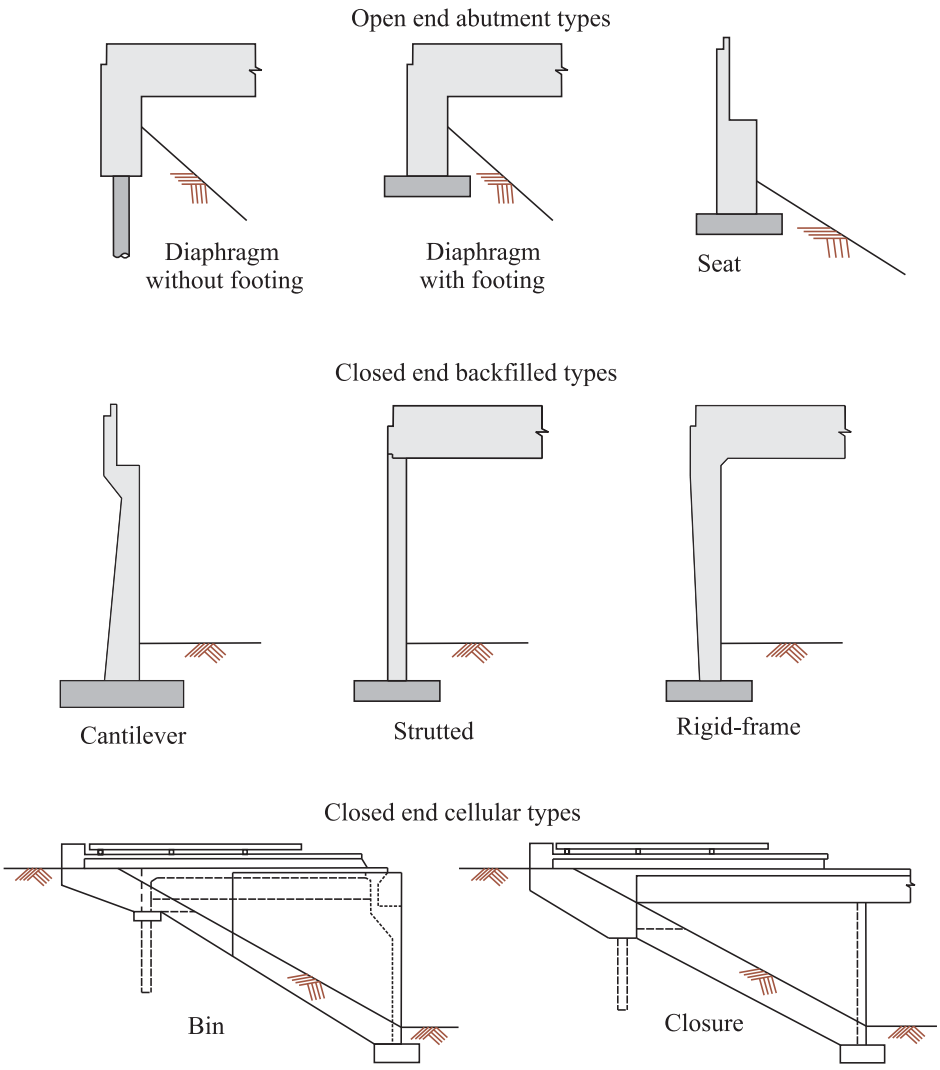

Figure 3.12: Schematic of abutment configurations

3.5.4.1 Diaphragm abutments

Diaphragm abutments are cast monolithic with the superstructure and readily engage the backfill soil and therefore provide a great source for seismic energy dissipation. This configuration is attractive because it reduces the likelihood of span unseating. The gravity loads are typically carried by the piles and the longitudinal resistance to seismic forces is provided jointly by the passive pressure in the backfill soil and the piles. Bridges with diaphragm abutments tend to be stiff and the abutments in particular are stiffer than the adjacent bents thereby attracting a larger proportion of the

imposed seismic force (Priestley et al., 1996). The longitudinal resistance provided by the backfill is based in mobilizing the backfill equal to the depth of the superstructure (SDC, 2010). Figures 3.13a and 3.13b show standard details for diaphragm abutments without and with foundations across bridge classes for all design eras (BDA, 2009). Details about the pile spacing are provided in Appendix A. The design recommendations and guidelines for these abutments are provided such that flexural failure of the backwall precedes shear failure. Typically, the large levels of resistance provided by the passive pressure of the backfill soil in the longitudinal direction is absent in the transverse direction, and the resistance is based on the piles and shear capacity of a wing wall (Priestley et al., 1996). Wing walls typically act as external shear keys and the ultimate force is restricted to 75% of the shear capacity of the adjacent bent (MTD 5-1, 1992).

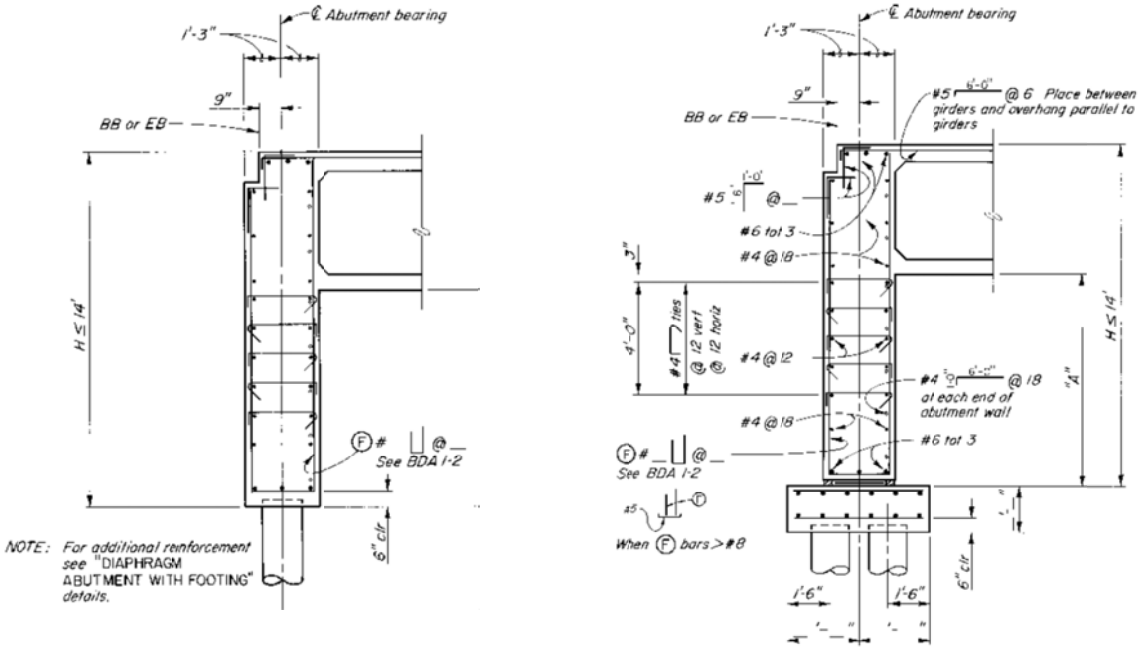

a) b)

Figure 3.13: Standard details for diaphragm abutments a) without footing, and b) with footing (Source: BDA, 2009)

Past experiences have shown that damage to the abutment during a major earthquake does not lead to the possibility of collapse in the superstructure in the case of diaphragm abutments (MTD 5-1, 1992). However, since the active response of the abutments is solely based on the piles, damage to the piles can take place when the superstructure displaces away from the abutment in the longitudinal direction. Figure 3.14 shows damage to abutment piles during the 1991 Costa Rica earthquake.

Figure 3.14: Abutment pile damage during the 1991 Costa Rice earthquake (Source: Moehle and Eberhard, 2003)

3.5.4.2 Seat type abutments

Seat type abutments provide a bearing support to the superstructure which is restrained longitudinally by the abutment backwall and transversely by the shear keys. The presence of gap between the end of the deck and the backwall increases the potential for unseating. High resistance and stiffness is provided when the initial gap is closed under longitudinal seismic response. However, when the superstructure moves away from the abutment, the resistance depends primarily on the bearing pads. The backwall in a seat type abutment is typically designed to fail under impact and passive response, before damaging forces are transmitted to the lower portion of the abutment (MTD 5-1, 1992).

As in the case of diaphragm abutments, the transverse resistance is provided by the piles and the shear keys. The shear keys are designed to resist shear forces equal to 75% of the shear capacity of the adjacent bent. Figure 3.15 shows standard details for a seat type abutment adopted in the bridge classes across design eras.

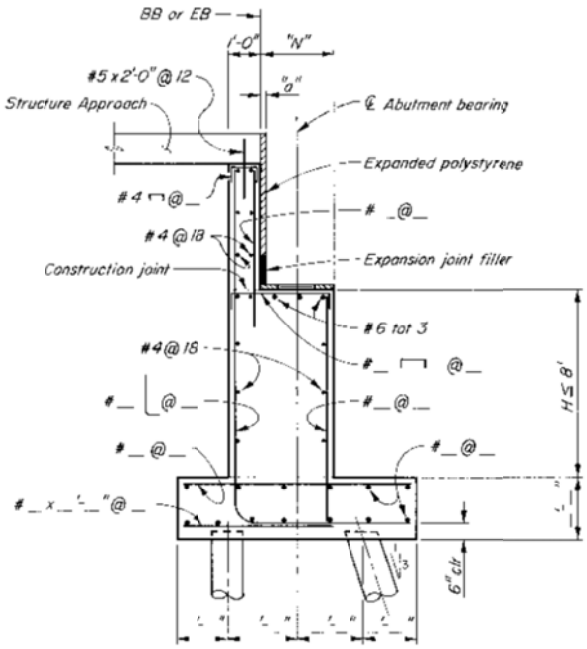

Figure 3.15: Standard details for seat type abutments (BDA, 1988)

The potential vulnerabilities associated with seat type abutments are superstructure span unseating and damage to the shear keys. Figure 3.16a shows damage to external shear key shear key in a seat type abutment during the Northridge earthquake while Figure 3.16b shows span unseating at the abutment. Details about the abutment configuration and pile spacing are provided in Appendix A.

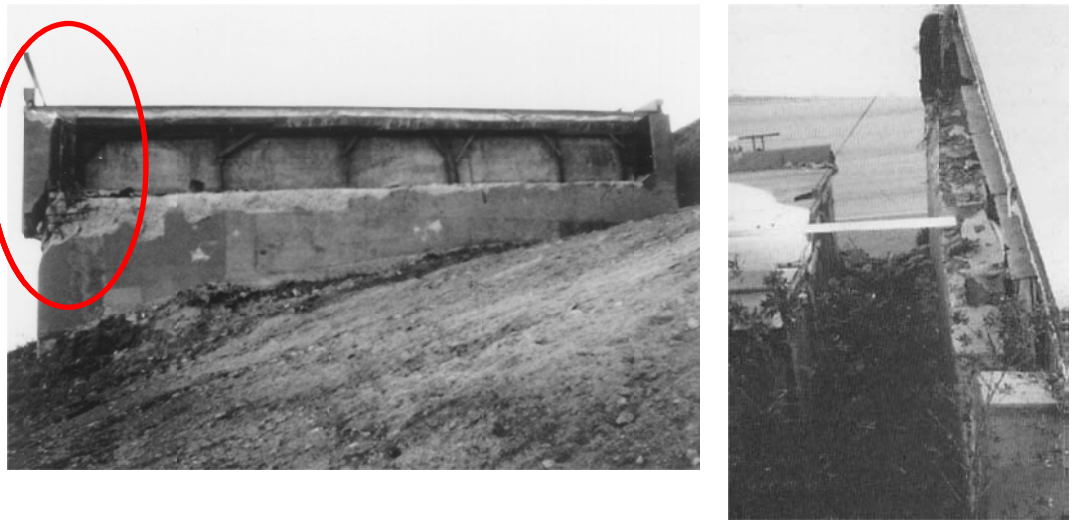

a) b)

Figure 3.16: a) Damage to external shear keys (Source: Moehle and Eberhard, 2003), b) span unseating (Source: Caltrans, 2007) during the Northridge earthquake

3.5.5 Foundation Systems

Foundations provide a means whereby service and ultimate loads are transmitted from the structure to the underlying soil. Bridge foundations have a number of alternatives such as spread footings, integral pile-shaft or columns and pile supported footings. The appropriateness of the different types are governed by the loading requirements, site specific soil conditions, overhead clearance, existing utilities and proximity of existing facilities such as buildings and railroads (Caltrans, 2008). The fundamental design criterion is to force the plastic hinge to form at the base of the column.

Figure 3.17 shows the possible footing types in bridges. Spread footings (Figure 3.17a) are used in cases where the underlying ground is firm and has rocky conditions. Review of bridge plans for different bridge classes across design eras revealed the prevalence of integral pile shafts and pile supported footings. These two types are considered in the present study. Integral pile shafts are used extensively in MSCG-T and MSC-SBG bridges across all design eras and are cast-in-drilled-hole (CIDH). Review of

bridge plans for MSCSL bridges also revealed the predominant presence of integral pile-columns where columns were pile extensions above the ground without a change in cross-sectional dimensions (shown in Figure 3.17c). These footing types are economical when compared to pile supported footings. In the case of integral pile-columns, the plastic hinge typically forms at a depth close to two pile diameters (Priestley et al., 1996). The length of plastic hinge is typically longer than that in pile supported footings and spalling of concrete is prone to occur with larger hinge rotations and this typically goes undetected in the aftermath of an earthquake unless inspectors focus on excavating sufficient depth underneath the column. Integral pile-column with oversize piles (Figure 3.17d) are common in the case of MSC-SBG bridges where the pile moment capacity is increased above that of the column to force the plastic hinging to occur at the column base. This facilitates easy inspection in the aftermath of an earthquake but the downside being early spalling of the cover concrete due to reduced plastic hinge lengths.

Pile supported footings, shown in Figures 3.17e and 3.17f, typically consist of precast (reinforced or prestressed concrete), driven, or CIDH piles with pile cap footings. In all cases, positive connection is provided between the pile and the pile cap to ensure proper force transfer. As in the case of integral pile shafts, the fundamental philosophy in this case is also to force the plastic hinging at the base of the column.

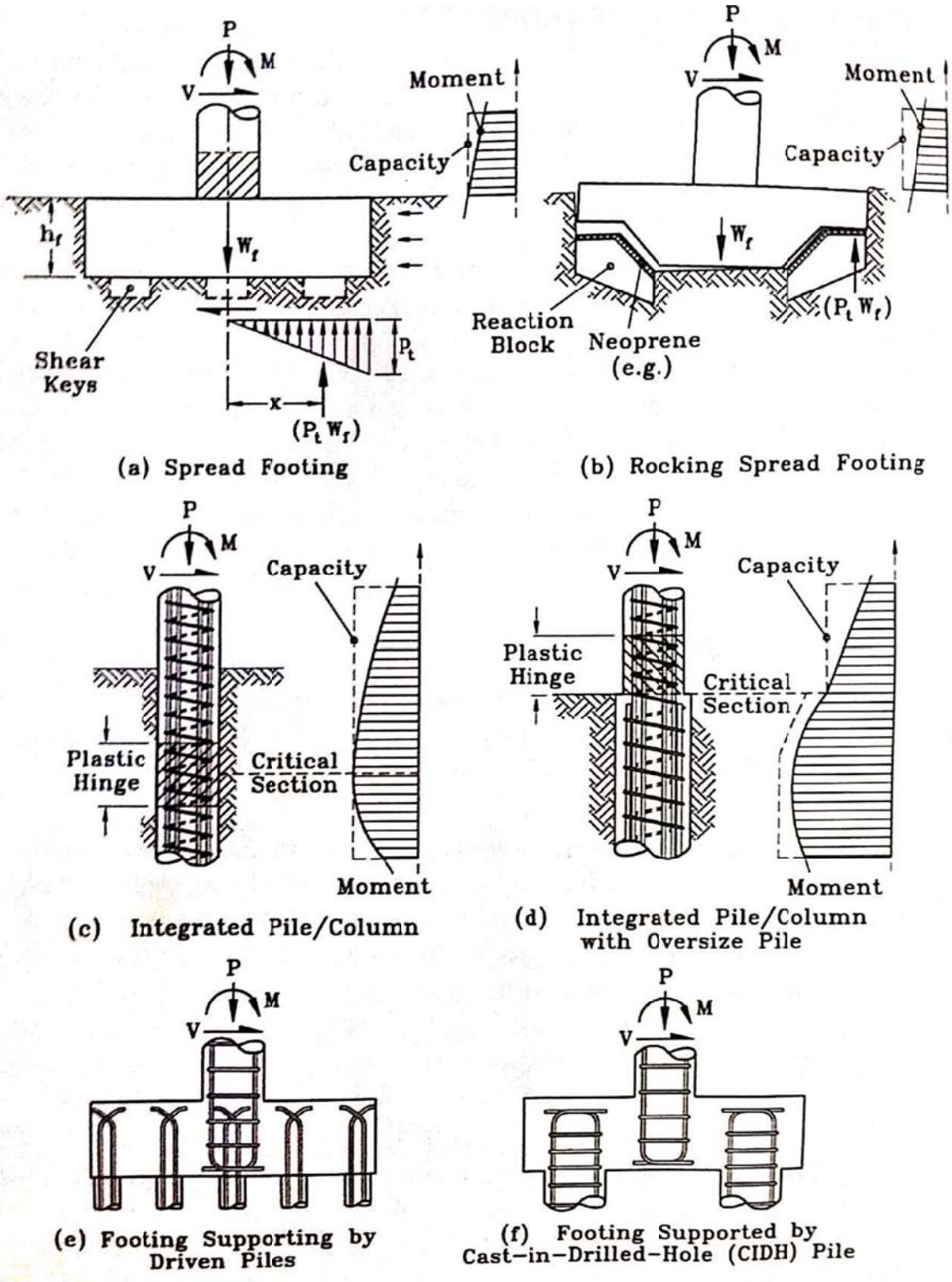

Figure 3.17: Bridge foundation types (Source: Priestley et al., 1996)

Bridge foundations have generally performed well during past earthquakes. Damage to foundations is reported to have taken place after extensive damage to the bridge columns at which point it is redundant. Foundations designed prior to 1971 were smaller in size compared to those designed after 1971 and comprised of positive moment reinforcement alone. This disables them from resisting the negative moment induced by soil overburden or tension piles. Further, the absence of shear reinforcement makes them susceptible to shear failure. Bridge foundations on liquefiable soil may be subjected to vertical settlement and/or lateral movement causing severe damage to them along with damage to the columns and superstructure. Post San Fernando earthquake, several foundations were retrofitted by the provision of negative moment reinforcement. However, post Northridge earthquake, the foundations were further retrofitted by the provision of shear reinforcement and additional piles. Figure 3.18 shows the retrofit strategy in a pile supported footing.

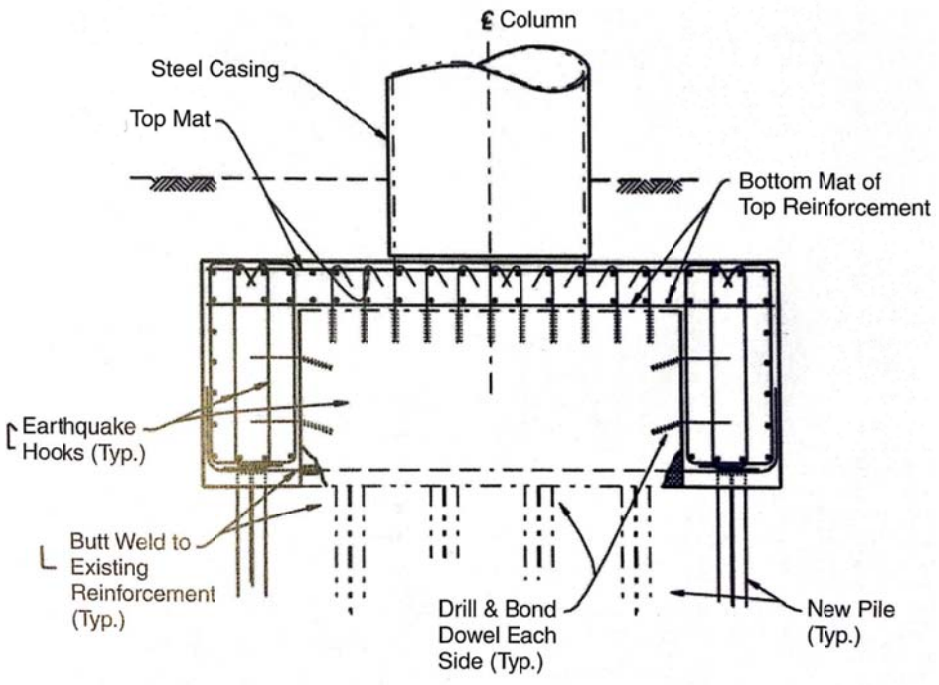

Figure 3.18: Pile supported footing retrofit (Source: Yashinsky and Karshinas, 2003)

Appendix A documents the different foundation systems and soil profiles for the bridge classes considered in this study. Also provided here are details of the pile cross-sections and reinforcement layout. The distributions encompass a wide range of soil profiles from soft soils to stiff clay for different foundation configurations.

3.5.6 Seat, Bearings, Restrainers and Shear Keys

As described in Section 3.4, a major consequence of the San Fernando earthquake was widespread unseating of bridge decks at the abutments, bents and expansion hinges. Majority of the subsequent efforts (Caltrans Phase-I and Phase-II retrofit programs) involved means to prevent unseating by increasing the seat width in new designs, provision of longitudinal restrainers and transverse shear keys to existing bridges. With the failure of a number of short hinge restrainers provided in the Phase-I retrofit program during the Loma Prieta earthquake, longer restrainers and pipe seat extenders were provided. This section presents details about the range of bridge seats, restrainers and shear keys considered across bridge classes and design eras based on the review of bridge plans.

Bridge seat and joint locations vary by the bridge class. Seat type abutments, as the name suggests, consists of a seat at the abutment where the bridge deck rests. A support seat at the bent cap exists for MSCG-I bridges while it is absent in the case of the other bridge classes considered in this study due to the presence of an integral bent cap. Bridge seat widths chronologically increased from the 4 – 12 in (S1) range in the Pre 1971 design era to 12 – 18 in (S2) range in the 1971-1990 design era and 18 – 24 in (S3) and greater than 24 in (S4) range in the Post 1990 design era. The Phase I and II retrofit programs addressed this issue by retrofitting the pre 1971 and 1971-1990 to the post 1990 seat categories by the provision of restrainers and pipe seat extenders. Bridge joints are typically sealed and the type of seal chosen for the purpose depends on the movement rating (MR). MR is the total anticipated movement from widest to narrowest opening of a

joint. This typically equals the total thermal movement plus any anticipated shortening. Typically, joint seals are the first components in a bridge joint to be damaged under a seismic event. The type of seal used generally depends on the movement rating and is tabulated in Table 3.6 (MTD 7-1, 1994). Figure 3.19a through c shows standard details for the joint seal types indicated in Table 3.6.

Table 3.6: Type of seals adopted in bridge joints

Movement rating (MR)	Type of seal
Less than or equal to 0.5 in	Type A (poured sealant)
1 in thru 2 in	Type B (neoprene compression sealant)
2 in thru 4 in	Joint seal assembly (strip seal)
Greater than 4 in	Joint seal assembly (modular unit)

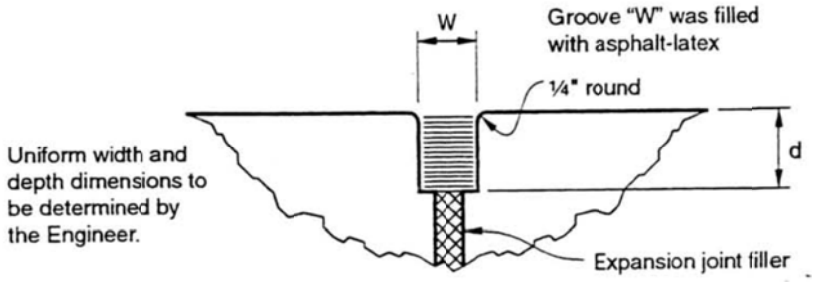

a)

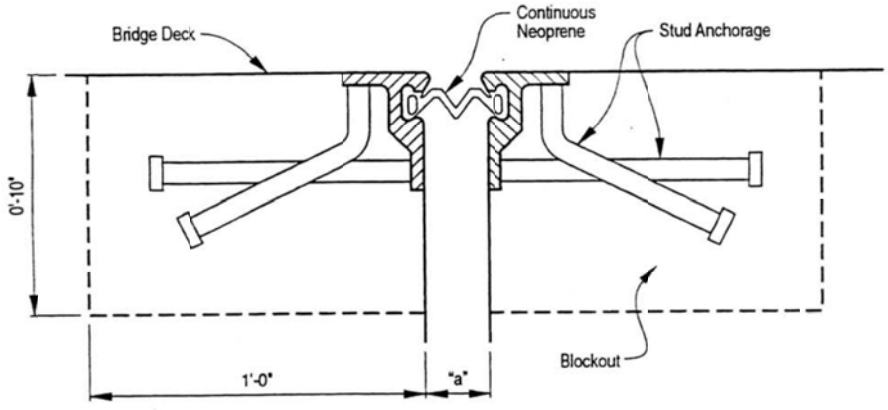

b)

c)

Figure 3.19: a) Type A and Type B joint seals, b) strip seal joint assembly and c) modular joint assembly (Source: MTD 7-1 and D. S. Brown Company)

Utilizing Caltrans's in house databases, MR values at bridge joints (in applicable cases) were catalogued and the statistics of MR values are shown in Table 3.7. Note that the tabulated values in Table 3.7 are pertinent to the entire inventory of state bridges in California. It is assumed that the small gap sizes exist in the case of MSCSL and MSCG-I bridge class joints while both small and large gap sizes exist in the case of MSCG-I and MSC-SBG bridge class joints. Note that the gap here refers to the gap between the bridge deck and the abutment backwall in the case of seat type abutments while it refers to the gap between the deck girders for MSCG-I at the bent. Due to the relatively small proportion of bridges with gaps larger than 6 in, the gaps in this study are restricted to two ranges: 0 to 2 in and 2 to 6 in.

Table 3.7: Distribution of gap sizes in the California state bridge inventory

Gap size	Abutment	Bent cap	In span hinge
0 to 2 in	88%	94%	75%
2 in to 6 in	11%	5%	19%
6 in to 12 in	0.7%	0.4%	5.1%
Greater than 12 in	0.3%	0.2%	0.9%

Restrainers provide yet another means to prevent unseating in bridges and these form an integral part of the as-built design in the 1971-1990 and post 1990 design eras. Large seat widths are the most effective means to prevent unseating and restrainers typical act as the second line of defense in modern day bridges. Restrainers are designed with adequate slack to allow thermal movement of the superstructure while restraining excessive relative movement at the joints. These are adopted in two basic types: cables and rods. The choice typically depends on a few factors such as the structure period, flexibility, strength of the diaphragm, and to some extent the geometry of the superstructure (Keady et al., 2003). Figure 3.20 shows a typical longitudinal restrainer that is used to prevent movement of a precast concrete girder that is continuous over the bent. Figure 3.21 shows a schematic describing the layout of restrainers at the seat type abutments for the bridge classes considered in this study.

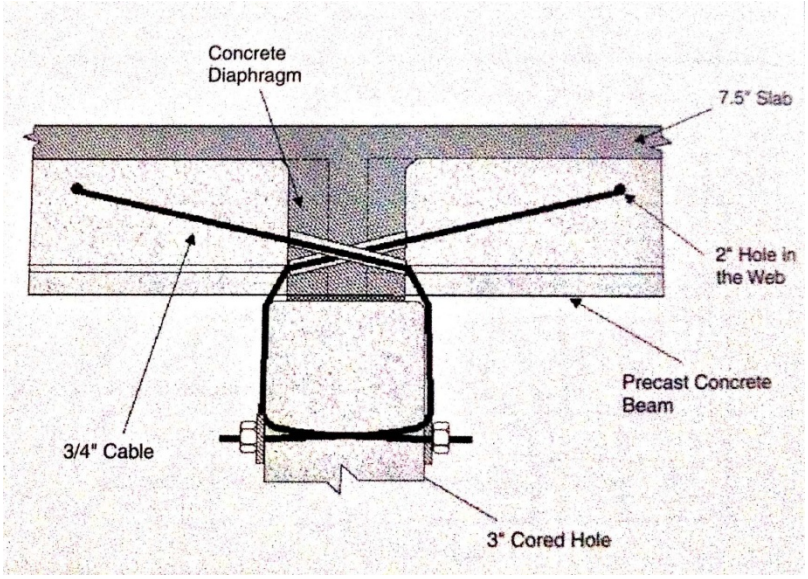

Figure 3.20: Precast girder and cap beam restrainer (Source: Yashinsky and Karshenas, 2003)

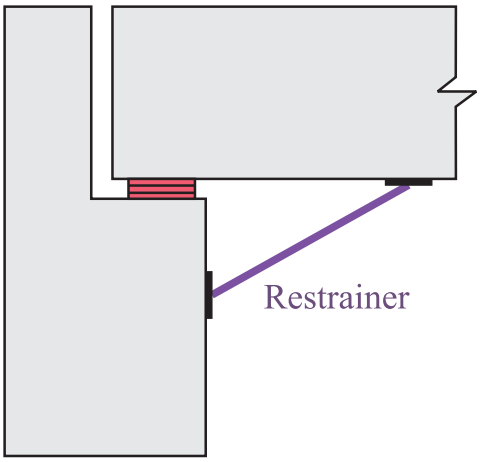

Figure 3.21: Schematic showing restrainer layout at a typical seat type abutment

Shear keys form an integral part of bridges with seat type abutments to facilitate the transfer of shear force between the superstructure and abutment in the transverse direction. These play a crucial role in restraining the transverse movement similar to the restrainers in the longitudinal direction. Shear keys are also located on the bent in the case of MSCG-I bridges to prevent their transverse movement. In the past, shear keys were commonly designed based on the assumption of constrained displacement at the abutments and acceptable failure criterion (Priestley et al., 1996). Damage to shear keys was reported in the past earthquakes and this lead to change in their design philosophy. It was realized that the design adopted previously was undesirable and there was a lot of uncertainty in the estimation of maximum shear key forces. Adoption of capacity design principles lead to better prediction of the shear key forces (SDC, 1999, 2010). Shear keys in the modern era bridges are expected to remain serviceable during earthquakes. In the present study, shear keys at the abutments are designed to resist 75% of the shear capacity of the bent while those at the bents are designed to resist 120% of the bent shear capacity. The fundamental idea is that significant damage would be inflicted in the columns before the failure of shear keys which is in line with the capacity design process

adopted by Caltrans. Figure 3.22 shows damage to abutment shear keys during the Loma Prieta earthquake.

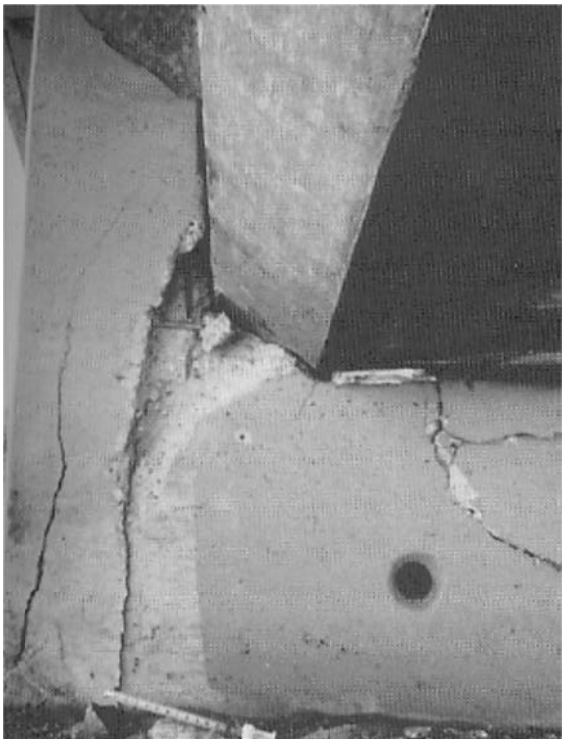

Figure 3.22: Damage to abutment shear keys during the Loma Prieta earthquake

3.6 Conventional Bridge Classes and Seismic Performance Sub-bins

This section details the bridge classes considered in this study along with the seismic performance sub-bins (SPS) separated by the historic 1971 San Fernando and 1989 Loma Prieta earthquakes. As stated in the preceding sections, bridge design and detailing aspects are captured for the bridge classes over the three design eras based on an extensive review of bridge plans, details of which are presented in Appendix A. The nomenclature associated with the bridge classes and the respective SPS are presented in Tables 3.8 and 3.9 and these will be used in the remainder of the thesis document here on. Fragility curves will be developed for each of the SPS in the bridge classes shown in

Table 3.8 as a part of this study. The BC and SPS codes put together completely describe sub-class and the primary bridge class. For example, MSCC-BG-M-E3-S4-L represents Post 1990 multispan continuous concrete box-girder bridge class with multi column bents and seat type abutments with seat width greater than 24 in and a large gap (2 – 6 in) between the girder and the abutment backwall.

Table 3.8: Conventional bridge class codes (BC) adopted in the present study

Spans	Continuity	Material	Superstructure	Bent type	Nomenclature
Multi (MS)	Continuous (C)	Concrete (C)	Box-Girder (BG)	Multi column bent (M)	MSCC-BG-M
				Single column bent (S)	MSCC-BG-S
Multi (MS)	Continuous (C)	Concrete (C)	Slab (SL)	Pile extensions (P)	MSCC-SL-P
Multi (MS)	Continuous (C)	Concrete (C)	T-Girder (TG)	Multi column bent (M)	MSCC-TG-M
				Pile extensions (P)	MSCC-TG-P
Multi (MS)	Continuous (C)	Concrete (C)	I-Girder (IG)	Multi column bent (M)	MSCC-IG-M
				Single column bent (S)	MSCC-IG-S

Table 3.9: Seismic performance sub-bins (SPS) in each bridge class

Design era	Abutment type	Seat width class	Gap size	Nomenclature
Pre 1971 (E1)	Diaphragm	NA (S0)	NA	E1-S0
	Seat	4 – 12 in (S1)	Small (S)	E1-S1-S
		12 – 18 in (S2)	Small (S)	E1-S2-S
		18 – 24 in (S3)	Small (S)	E1-S3-S
			Large (L)	E1-S3-L
		> 24 in (S4)	Small (S)	E1-S4-S
			Large (L)	E1-S4-L
1971 – 1990 (E2)	Diaphragm	NA (S0)	NA	E2-S0
	Seat	12 – 18 in (S2)	Small (S)	E2-S2-S
		18 – 24 in (S3)	Small (S)	E2-S3-S
			Large (L)	E2-S3-L
		> 24 in (S4)	Small (S)	E2-S4-S
			Large (L)	E2-S4-L
Post 1990 (E3)	Diaphragm	NA (S0)	NA	E3-S0
	Seat	18 – 24 in (S3)	Small (S)	E3-S3-S
			Large (L)	E3-S3-L
		> 24 in (S4)	Small (S)	E3-S4-S
			Large (L)	E3-S4-L

3.7 Closure

Four conventional bridge classes are identified for fragility analysis. These four bridge classes account for about 45% of the bridge inventory in California. Detailed review and analysis of the National Bridge Inventory is performed to develop empirical cumulative distribution functions for geometrical parameters such as span length, deck width, column height and number of spans. The conventional bridge classes chosen are divided into sub-bins separated by the 1971 San Fernando and 1989 Loma Prieta earthquakes. The general design details and potential vulnerabilities of bridges designed prior to 1971, those designed between 1971 and 1990 and post 1990 are identified based on an extensive review of bridge plans to supplement the information provided by the NBI. Detailed information pertinent to bridge components: superstructure, columns, foundations, abutments are gathered across the design eras to aid in the development of stochastic finite element models for fragility analysis. By the very nature of the inventory information along with the design details across the three significant eras obtained herein, the resulting fragility curves will be appropriate for suites of bridges across California.

CHAPTER 4

ANALYTICAL MODELING PROCEDURES AND DETERMINISTIC BRIDGE COMPONENT RESPONSES

Advances in modeling capabilities coupled with lack of damage data from past seismic events motivated the development of fragility curves using analytical methods. Fragility curves derived analytically often differ based on the level of detail and sophistication in the analytical models, the approach to simulate seismic loading, assessment of structural response, and considerations of geometric effects in addition to the various reliability assessment techniques (simulation versus closed form) to obtain estimates of component and system vulnerability. High fidelity three dimensional analytical models considering geometric and material nonlinearities are used in this study for fragility curve generation using Nonlinear Time History Analyses (NLTHA). The models are created in the finite element platform OpenSEES (McKenna et al., 2010). The results of NLTHA are used to develop predictive models of demand, and therefore the ability to capture the behavior of various components is dictated by the fidelity and robustness of the model.

This chapter presents a detailed description of the modeling strategies at the component level and their subsequent integration at the bridge system level. Details are provided about the typical layout of representative bridges from four multispan bridge classes with box-girders, slab, Tee and I-girders in the superstructure, across the three significant design eras considered in this study: pre 1971, 1971-1990 and post 1990 eras, drawing on the details provided in the previous chapter. Eigen value analyses and select deterministic component responses are presented and discussed in every case to provide insight into the relative response of various components and to use as a sanity check.

4.1 Bridge Component Modeling Strategies

This section presents details about modeling considerations for various bridge components.

4.1.1 Substructure – Single and Multi Column Concrete Bents

Californian bridges have different pier types such as pier walls, hammerhead piers, single and multi column rigid frame piers or bents. Single (SCB) and multi column bents (MCB) are the most common types based on an in-depth review of bridge plans for the bridge classes chosen in this study. Table 3.8 in Chapter 3 presented details about the bent types considered in the analytical models for various bridge classes across design eras. The bents are modeled using a combination of displacement based beam column elements and rigid links to cause moment and force transfer between the members of the bent. Figure 4.1 presents the finite element discretization of the bents for the bridge classes. Displacement based beam-column elements with fiber defined cross-sections are used to represent the columns and bent beams in the case of MSCC-IG bridge class. In the case of MSCC-BG, MSCC-SL and MSCC-TG bridges with monolithic solid diaphragms, transverse rigid elements are used to represent the diaphragm while displacement beam-column elements with fiber cross-sections are used to represent the columns. In either case, rigid links are used to connect the top of the column to the bent beam or the solid diaphragm. Translation and rotational springs representing the behavior of foundations are located at the base of the column. The details of the concrete and steel material models along with cross-section modeling attributes are presented in the sections that follow.

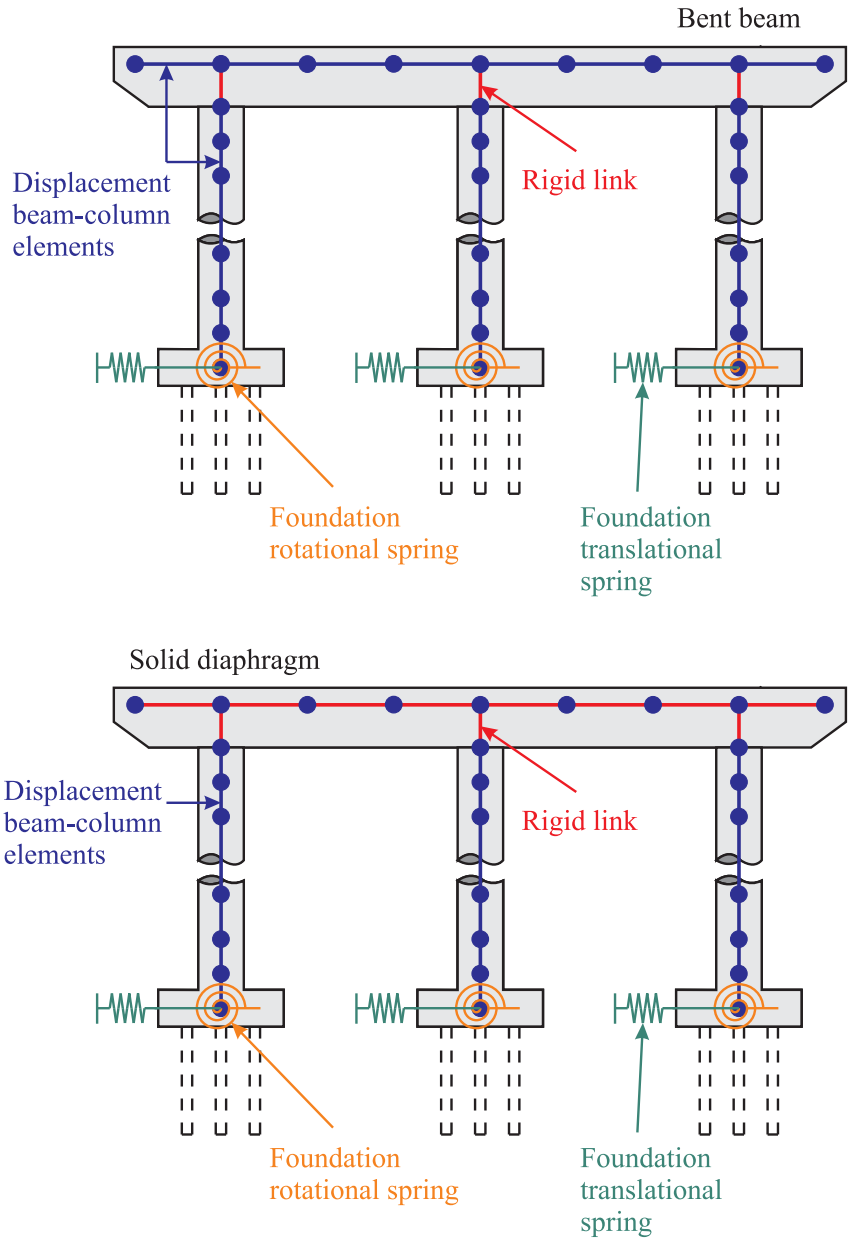

Figure 4.1: Finite element discretization of the bent

4.1.1.1 Concrete, Reinforcing and Prestressing Steel Material Models

Fiber defined cross-sections have the unique advantage of allowing the specification of material properties specific to different locations in a member cross-section. For instance, unconfined concrete properties are assigned to the cover concrete while confined concrete properties are assigned to the core fibers. Further, the precise

location of the longitudinal reinforcing bars and prestressing strands may be specified and material properties assigned to them.

Reinforced concrete behavior is modeled using the *Concrete 07* material provided in OpenSEES. This material used the Chang and Mander's model (1994) to define the monotonic stress strain curves for confined and unconfined concrete. The model was established based on statistical regression analysis on the experimental data from cyclic compression tests performed by a number of researchers. Figure 4.2 shows the stress strain curves for concrete with standard compressive strength, f'_c = 5000 psi and reinforcing steel yield strength, f_y = 60 ksi with varying degrees of confinement offered by #4 stirrups at 3 in, 6 in and 12 in on center, typical of post 1990, 1971-1990 and pre 1971 bridge columns of 3 ft diameter. It must be noted that the effect of confinement is pronounced on the peak compressive stress and ultimate strain in the confined concrete stress strain relationship as shown in the figure.

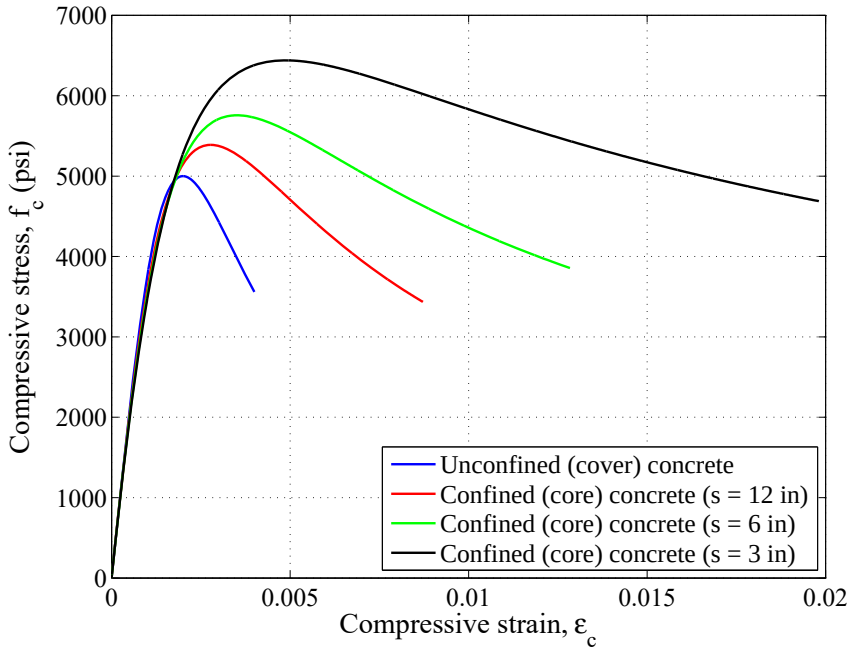

Figure 4.2: Concrete stress strain curves with varying transverse reinforcement confinement ratios

Reinforcing steel is modeled using the *Steel 02* material provided by OpenSEES which uses the Menegotto and Pinto model (1973) later modified by Filippou et al. (1983) to include isotropic strain hardening. The prestressing strands are modeled as an elastic perfectly plastic material. This is used in the case of prestressed and precast prestressed concrete piles which extend as columns above the ground in the case of MSCC-SL bridge class. The material models for reinforcing steel and prestressing strands are shown in Figure 4.3.

4.1.1.2 Fiber Cross-sections – Column and Bent Beam

The bridge columns are modeled using displacement based beam column elements for all the bridge classes across the design eras. The cross-section is modeled using fiber elements and this helps in capturing the spread of plasticity in the column elements. Details such as column diameter, longitudinal and transverse reinforcement ratio vary across bridge classes and further with the design era as presented in Appendix A. Figure 4.3 shows a discretized fiber section for a bridge column which consists of unconfined and confined concrete properties assigned to the fibers along with a precise location of the longitudinal reinforcement and prestressing strands (in the case of pile cross-sections). Also shown in Figure 4.3 is a discretized typical bent beam prevalent in MSCC-SL and MSCC-IG bridges.

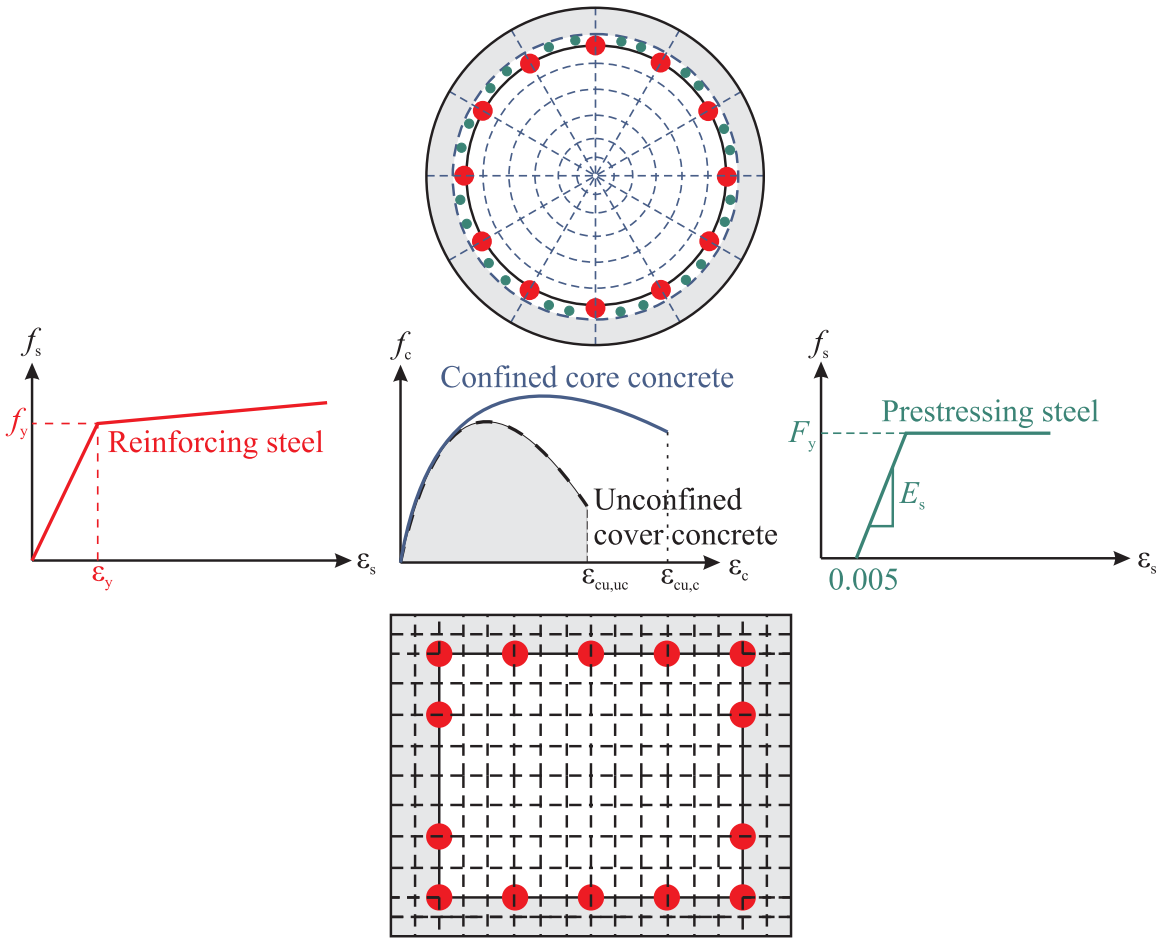

Figure 4.3: Fiber based discretization of a circular reinforced concrete column and bent beam

4.1.1.3 Foundation translation and rotational springs

As stated previously in section 3.5.5, different foundation systems are considered in this study based on the bridge class. These include integral pile shafts and pile supported footings consisting of precast (reinforced or prestressed concrete), driven or CIDH piles. Further, since this study aims at developing fragility curves that are applicable for bridge classes across a wide geographic area, a range of soil profiles from soft to medium and stiff are considered. The foundation systems and the different soil profiles were modeled in LPILE (2012) in order to determine the stiffness of translational and rotational springs that are then located at the base of the columns to represent the

behavior of foundation systems. It should be noted that MCBs founded on pile supported footings are pinned at the base and therefore have no rotational stiffness. On the other hand, MCBs consisting of integral pile columns, as in the case of MSCC-SL and MSCC-TG bridge classes, have translational and rotational stiffness. Further details about the soil profiles and the corresponding stiffness of the translational and rotational springs across bridge classes are provided in Appendix A.

The translational and rotational springs are modeled using simple linear springs and are assigned to zero length elements at the base of the columns as shown in Figure 4.1. In the case of abutment piles, trilinear response stemming from the recommendations of Choi (2002) is used to model their response in the longitudinal and transverse directions. Further details are presented in section 4.1.2.

4.1.2 Abutments

Observations from past earthquakes reveal the potential for great demands on bridge abutments due to seismic forces. Earth pressures on the abutment can result from longitudinal response of the bridge deck and these pressures are further increased due to the pounding of the deck against the abutment backwall in the case of seat abutments. Response of the abutments in the longitudinal direction is different when compared to the transverse direction. Further, the longitudinal response is composed of two types of resistance: passive resistance, which is developed when the abutment wall compresses the backfill soil, and active resistance, when the abutment backwall moves away from the backfill soil. The passive resistance is provided by the backfill soil and the piles while piles alone contribute to the active resistance. Caltrans SDC (2010) states that the effect of wing walls decreases as the width of the abutment increases (beyond 50 ft), and therefore, only piles are considered to contribute to the transverse resistance of the abutments.

Early research typically considered the effect of abutments by the addition of discrete linear springs to the bridge model. Caltrans SDC (1990) provided guidelines for the stiffness of the linear springs based on a passive soil resistance of 20 kip/in/ft for a standard 8 ft backwall. The effect of piles was accounted for by adding a resistance of 40 kips/in/pile in the longitudinal (active and passive) and transverse directions. A limiting value of 55 psi was suggested for the passive backfill soil pressure to limit the load taken by the abutment under cyclic seismic loading. Research conducted at the University of California, Davis (Maroney et al, 1993) on half scale abutment specimens to estimate the longitudinal stiffness concluded that the stiffness proposed by Caltrans SDC (1990) overestimated the passive soil resistance tremendously. Goel and Chopra (1997) developed abutment models and concluded that the transverse abutment modeling considerations suggested by Caltrans SDC (1990) produced good results consistent with experimental tests and field observations. Caltrans SDC (1999) revised its previous deterministic estimate of 20 kip/in/ft of passive soil resistance to fall within a range: 20 kip/in/ft to 50 kip/in/ft. However, in the work performed by Maroney et al. (1994), it was seen that the passive resistance of the abutment decreased as the displacement of the abutment increased and the passive stiffness reduced to zero before the ultimate soil pressure was mobilized. This reinforced the necessity to account for a non-linear soil model to accurately capture the abutment response. This was further reinforced in the work by Martin and Yan (1995) where the ultimate soil pressure was seen to be mobilized with displacements of 6 to 10% of the backwall height based on the type of backfill soil: cohesive vs. cohesionless.

The hyperbolic soil model proposed by Shamsabadi and Yan (2008) is used in the present study to capture the response of the abutment backwall soil in passive response. The model is based on experimental testing of bridge abutments with 5.5 ft. high backwalls and typical cohesionless and cohesive backfill soils conducted at the University of California Los Angeles (Shamsabadi and Yan, 2008). The test results were

then extended to develop closed form solutions for the abutment backfill soil response for a range of backwall heights based on a series of analyses using the limit-equilibrium method that implements mobilized logarithmic-spiral failure surfaces coupled with a modified hyperbolic soil stress strain behavior. Figure 4.4 shows a typical abutment force displacement backbone curve, where F_{ult} is the maximum abutment force developed at maximum displacement, y_{max}. y_{ave} is the displacement corresponding to half the maximum abutment force and K is the average soil stiffness.

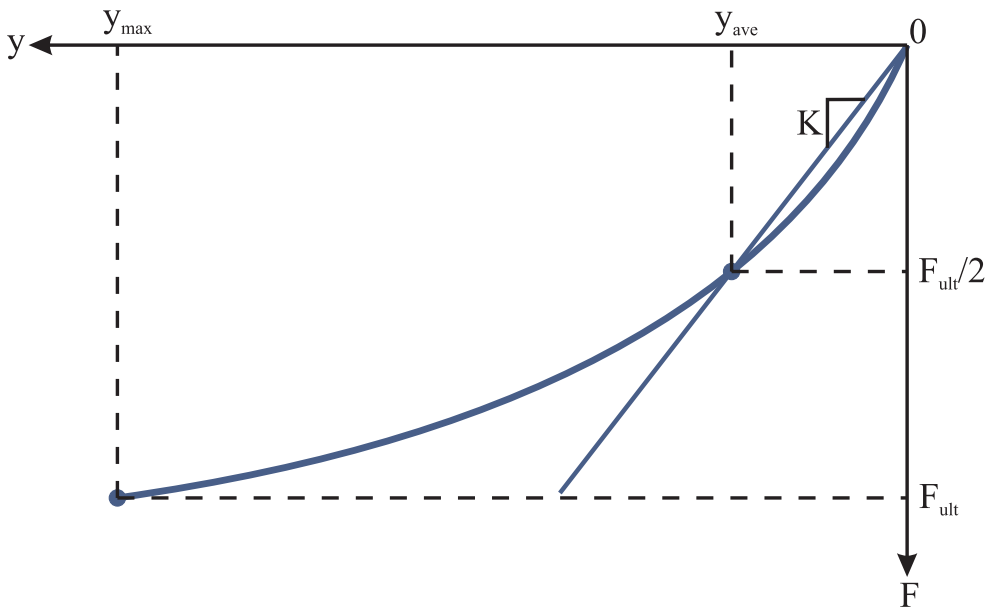

Figure 4.4: Force displacement response of the abutment backfill

Equation (4.1) presents the closed form solution for the force displacement response of the backfill soil, where F is the force expressed in kip/ft width of the backwall, y is the displacement expressed in inches, and H is the height of the backwall expressed in feet.

$$\begin{aligned} F(y) &= \frac{8y}{1+3y} H^{1.5} \qquad \textit{Granular backfills} \\ &= \frac{8y}{1+1.3y} H \qquad \textit{Cohesive backfills} \end{aligned} \tag{4.1}$$

Shamsabadi and Yan (2008) noted that the maximum displacement of the backwall is 0.05H and 0.1H (expressed in inches) for granular (sandy soils) and cohesive (clayey soils) backfills, respectively, and substitution of these values in equation (4.1) yields the ultimate force in the abutment. According to MTD 5-1 (1992), the longitudinal stiffness assumed for seismic analyses should be based on mobilizing the soil equal to the depth of the backwall. Zero length springs characterized by nonlinear soil behavior are used to capture the response of the abutment soil. The *HyperbolicGapMaterial* provided by OpenSEES is used to model the response of the backfill soil, which is based on the model proposed by Shamsabadi and Yan (2008). It must be noted that in the case of diaphragm abutments, the gap between the deck and abutment backwall is zero while a gap exists in the case of seat type abutments. The abutment dimensions: width and height of the backwall, and backfill soil type (sand vs. clay) are considered as random variables in this study and typical ranges of the values will be presented in the next chapter.

As stated previously, piles are considered to provide longitudinal and transverse stiffness to the abutments. For the passive longitudinal response, piles act in parallel with the backfill soil, while piles alone account for the active resistance. The transverse resistance just like the active resistance is also provided solely by the piles. Trilinear response stemming from the recommendations of Choi (2002) is used to model the response of the piles. The model assumes that piles become plastic at a deformation of 1 in and first yielding occurs at a displacement equal to 30% of the ultimate deformation. The initial stiffness is assumed to degrade with soil surface yielding. The force deformation response of the pile along with the model parameters are presented in Figure 4.5. The stiffness of the abutment pile depends on the type: CIDH, driven steel H section, driven steel pile, drilled shafts and is considered a random variable and these take on a range of values across all simulations, as detailed in Chapter 5 of this thesis.

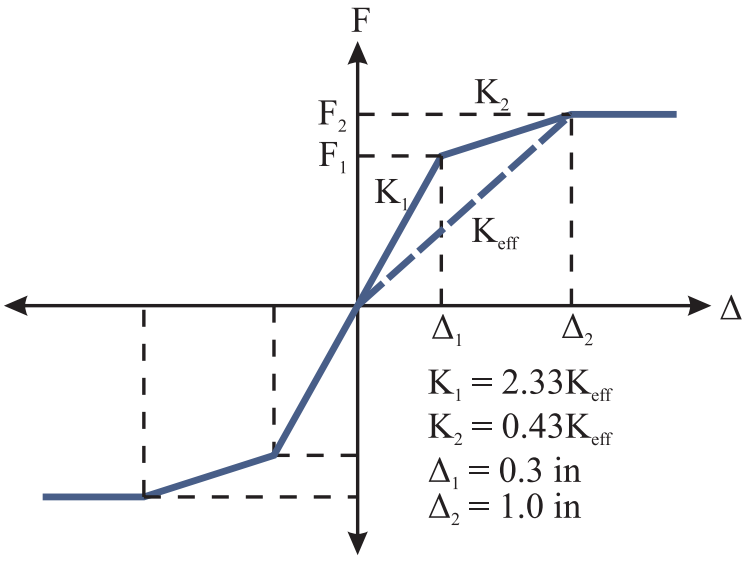

Figure 4.5: Force displacement response of the pile

4.1.3 Deck Elements

The deck elements are modeled using elastic beam column elements since the superstructure generally remains elastic during seismic events. The properties of the deck elements are calculated based on composite section properties wherever applicable (MSCC-BG, MSCC-IG, MSCC-TG). Effective width of the superstructure is considered in order to calculate cross-section properties that are assigned to the longitudinal deck elements. In the case of open soffit superstructures with I- and T-girders as in the case of MSCC-IG and MSCC-TG bridge classes, the girders offer less resistance to the torsional resistance of the bent cap and the effective width is reduced accordingly (SDC, 2010). In either case, the width of the superstructure is reduced for one-quarter span length on either side of the bent to calculate the cross-section properties to be assigned to the deck elements. The calculation of the effective deck width is illustrated in Figure 4.6. As will be demonstrated in the next chapter, the width of the bridge is a random variable and derivation of empirical CDFs for the same was demonstrated in Chapter 3. Other geometric parameters such as deck slab thickness, girder dimensions (in the case of MSCC-IG, MSCC-TG, MSCC-BG) are considered to vary across simulations.

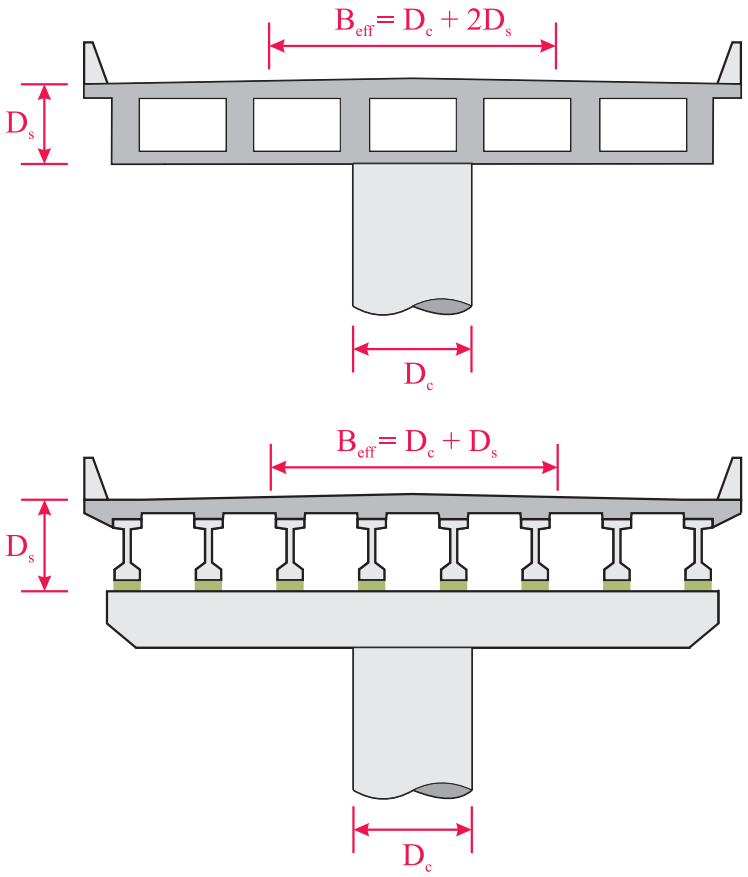

Figure 4.6: Effective width of the superstructure

4.1.4 Elastomeric Bearing Pads

Elastomeric bearings are the most commonly adopted bearing types in concrete bridges. These bearings typically transfer horizontal forces by friction and their behavior is characterized by sliding which in turn depends on the initial stiffness. Once the coefficient of friction is exceeded, the stiffness of the rubber pads drops to zero and therefore, their response can be characterized by elastic perfectly-plastic material. The initial stiffness, k_{pad}, of the bearing pad is calculated using equation (4.2), where, G is the shear modulus, A is the cross-sectional area, and h is the thickness of the bearing pad.

$$k_{pad} = \frac{GA}{h} \tag{4.2}$$

Figure 4.7 shows the force deformation response of the elastomeric bearing pad. The yield force, F_y, is calculated by multiplying the normal force, N, acting on the bearing with the coefficient of friction, μ, of the pad. Scharge (1981) presented an expression for the coefficient of friction, specific to elastomer on concrete, based on experimental tests and is a function of the normal stress, σ_n, as presented in equation (4.3). The response of the bearing pad is captured using the *Steel01* material provided by OpenSEES and is applied to a zero length element to capture its force deformation response.

$$\mu = 0.05 + \frac{0.4}{\sigma_n} \qquad \sigma_n \text{ in MPa} \tag{4.3}$$

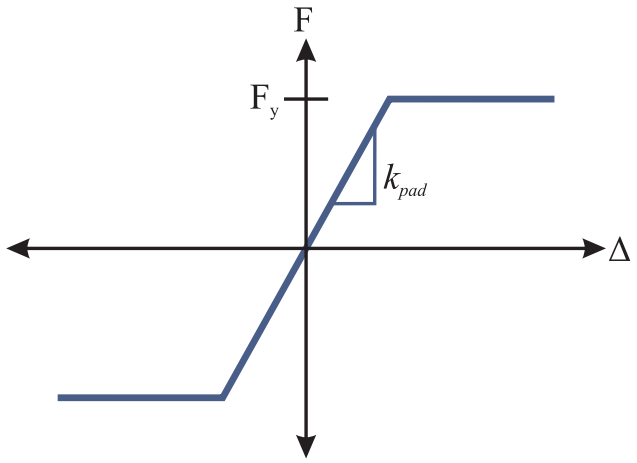

Figure 4.7: Force deformation response of an elastomeric bearing pad

As will be demonstrated in the next chapter, the dimensions of the bearing pad, coefficient of friction, and shear modulus are considered random variables and take on a range of values.

4.1.5 Shear Keys

Shear keys play an important role in constraining the relative transverse movement between the deck and the abutments in the case of continuous bridge

superstructures. Typically shear keys have the potential to fail through one of the four different mechanisms: shear friction, flexure, shear and bearing (Megally et al, 2002). Shear keys are located at the abutments and at the bents in the case of MSCC-IG bridges with seat type abutments, while they are located at the abutments alone for all the other bridge classes considered in this study with seat type abutments. No shear keys are used in bridges with integral bents and diaphragm abutments. MTD 5-1 (1992) indicates that transverse shear keys at the abutments should be designed to resist 75% of the adjacent bent capacity to prevent significant damage to the underlying piles. Based on personal communication with Caltrans design engineers (Caltrans, 2010-2012), the shear keys at the bents are designed to resist 120% of the bent shear capacity. These are inherently very strong components and provide complete transverse coupling of the bent beyond the point of formation of plastic hinge in the underlying columns.

Figure 4.8 shows the nonlinear force deformation response of the shear key that is adopted in the present study. P_{cap} denotes the capacity of the shear key and is calculated based on the expressions in equation (4.4).

$$P_{cap} = factor \times V_{bent} \tag{4.4}$$

where, $factor$ = 0.75 at bents, 1.2 at abutments, and V_{bent} is the shear capacity of the bent, calculated as in equation (4.5). The bent shear capacity is determined by adding the shear strength of concrete and that of steel reinforcement (ACI, 2008).

$$V_{bent} = n\left(3.5\sqrt{f'_c}\left(0.8D^2\right)\sqrt{1+\frac{N_u}{500A_g}}+\frac{A_v f_y\left(0.8D\right)}{s}\right) \tag{4.5}$$

where, n is the number of columns per bent, f'_c is the concrete compressive strength (psi), D is the column diameter (in), N_u is the column axial load (lbs), A_g is the gross cross-sectional area (in^2), A_v is the area of transverse reinforcement (in^2), f_y is the steel yield strength (psi), and, s is the transverse reinforcement spacing (in).

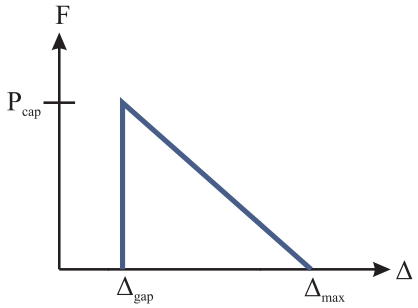

Figure 4.8: Force displacement model for the shear key

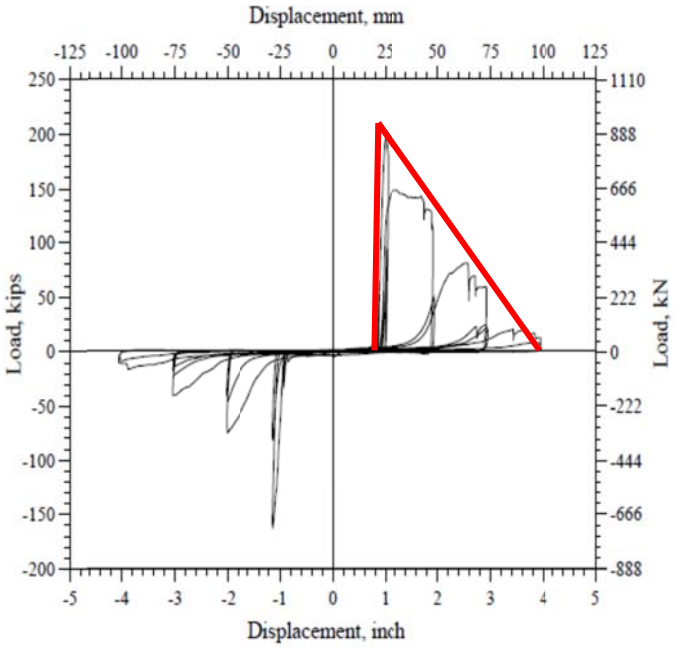

Figure 4.9: Load displacement curves from the experimental testing of abutment shear keys (Megally et al., 2002)

The model chosen in this study is based on the research by Megally et al. (2002) based on a series of experiments on external shear keys in bridge abutments. They found that shear keys undergo a maximum displacement of 3.5 in before their capacity reduces to zero. Figure 4.9 shows the load deformation response from the experiments conducted on abutment shear keys at the University of California San Diego (Megally et al., 2002). Zero length elements characterized by this nonlinear force deformation response are used to capture the response of shear keys.

4.1.6 Restrainers

Restrainers serve to limit relative longitudinal displacement between the spans and prevent unseating. These are often employed in bridges with insufficient seat widths which is typical in the pre San Fernando era. As mentioned previously, several bridges constructed prior to the San Fernando and Loma Prieta earthquakes have been retrofit with restrainer cables as a part of the Caltrans Phase I and II retrofit programs. Cable restrainers are considered in this study although it is realized that restrainers come in several forms including plates and rods. Restrainer cables, ¾ in in diameter (0.222 in^2 cross sectional area) are considered across design eras for MSCC-BG and MSCC-IG with seat type abutments.

Parameters associated with the restrainers are also considered variable in the simulations. Although ¾ in diameter restrainers are adopted, the length of the cables is assumed to vary across simulations and so is the initial slack in the cables, since these have shown to significantly affect the response of the bridge (Saiidi et al, 1996). Further details about the range of these parameters are provided in the next chapter. BDA 14-1A (2009) gives information about the restrainer properties and based on testing by Caltrans, the yield force, F_y, for ¾ in cables is reported as 46 kips and the specified modulus of elasticity, E, is 14,000 ksi. Figure 4.10 shows the typical stress strain curve for a ¾ in restrainer cable (BDA, 2009).

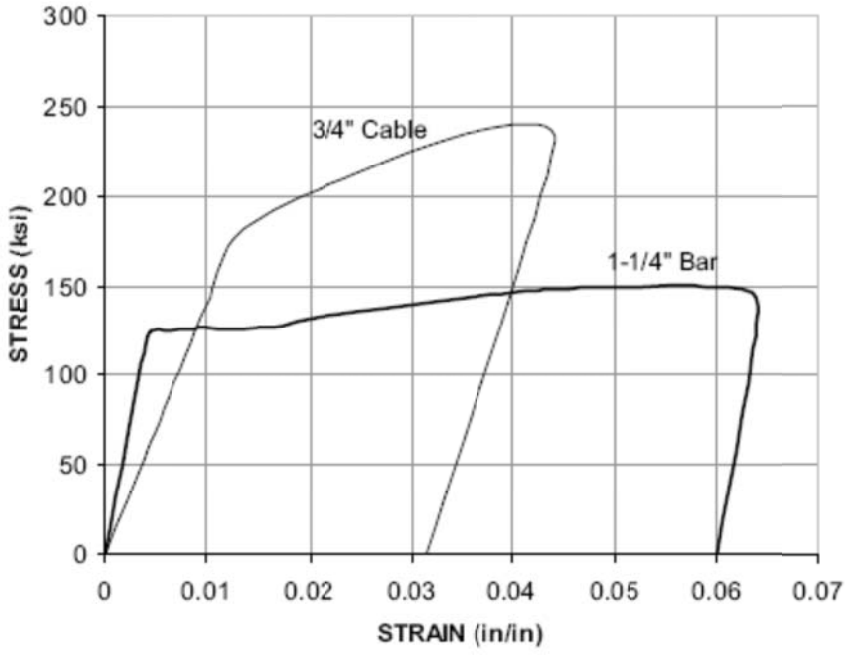

Figure 4.10: Stress strain curve for ¾ in restrainer cable (BDA, 2009)

The fundamental restrainer design philosophy is to limit the longitudinal movement of the bridge superstructure and to keep them tied together during an earthquake without yielding. Several restrainer design procedures are available, such as the one adopted by Caltrans, American Association of State Highway and Transportation Officials (AASHTO), W/2 method, equivalent linear static design for restrainers and modified Caltrans method, all with varying levels of complexity (Saiidi et al., 2001). In this study, the W/2 method is adopted for designing the restrainers which assumes that the bridge superstructure unseats during an earthquake and is supported by the restrainers alone. Therefore, the restrainers on each side of the span are designed to resist one-half of the weight of the span. The W/2 method was reported to perform well in most bridges (Saiidi et al, 2001).

Figure 4.11 shows the stress strain curve adopted for the restrainer cable in the present study. For a certain length, the yield displacement is calculated using equation (4.6). The number of restrainers are then determined using equation (4.7). A post yield

stiffness of 1% is used as shown in Figure 4.11, consistent with the observations in tests on restrainer cables. Zero length elements characterized by this force deformation response are used to capture the response of restrainer cables.

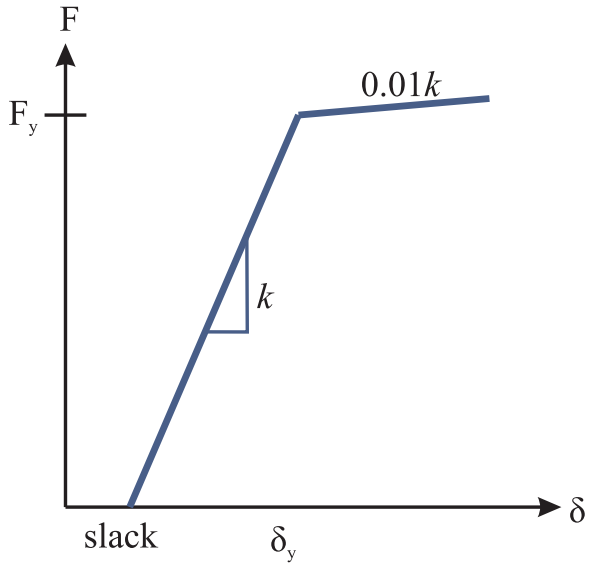

Figure 4.11: Force deformation response of the restrainer cable

$$\delta_y = \frac{F_y L}{A_s E} \tag{4.6}$$

$$n = \frac{\left(\frac{W/2}{F_y}\right)}{A_s} \tag{4.7}$$

4.1.7 Impact or Pounding Elements

The contact element approach proposed by Muthukumar (2003) is used in this study for modeling the impact between the deck and abutment backwall. A bilinear model that captures impact and energy dissipation is used and is shown in Figure 4.12. The stiffness parameters, K_{t1}, K_{t2}, yield displacement, δ_y, and maximum deformation, δ_m, are shown in the figure and are consistent with those presented in Nielson (2005).

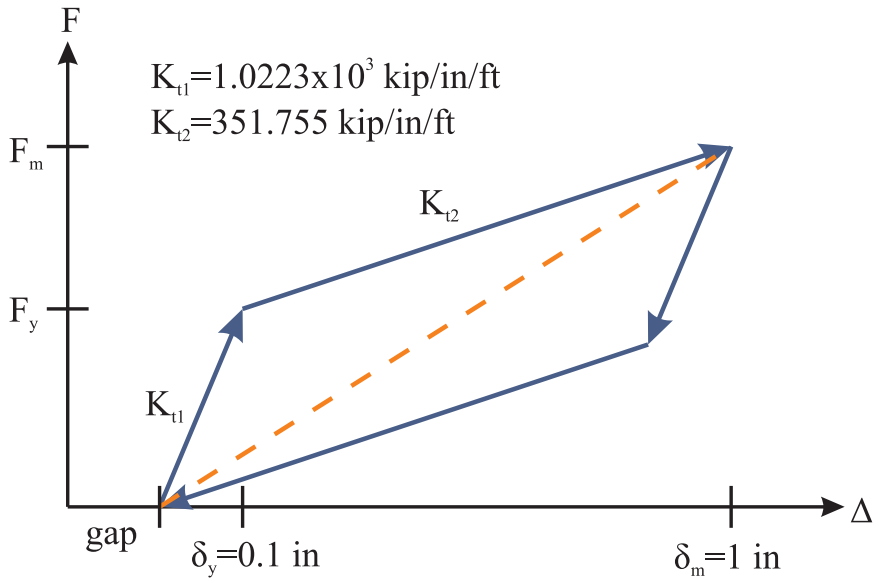

Figure 4.12: Analytical model for pounding between deck and abutment backwall (Muthukumar, 2003)

4.2 Global Bridge Finite Element Models

The preceding section provided extensive component modeling strategies adopted in the present study. This section presents the integration of various component level models to generate a global analytical model of the bridge to be used in fragility analyses. Elastic beam column elements with lumped mass representing the longitudinal deck elements are connected to rigid elements in the transverse direction. Displacement based nonlinear beam column elements with fiber defined cross sections are used to model the columns. Translational and rotational springs at the base of the columns are used to replicate the behavior of column footings. Zero length elements capturing the response of the abutment backfill soil and piles are connected in parallel and are connected to the transverse deck elements in the case of diaphragm abutments. In the case of seat type abutments, zero length elements describing the response of elastomeric bearing pads, restrainers and pounding between the deck and abutment backwall are connected in

parallel and are connected to the transverse rigid deck elements. These are then connected in series with the soil-pile springs to capture the response of the abutment system.

In the case of MSCC-BG, MSCC-SL and MSCC-TG bridges, where the superstructure is integral with the bent, rigid links are used to connect the column tops to the transverse rigid deck elements. These help in transferring all of the forces and moments and are typical of an MFA-3 type connection. In the case of an MFA-2 type connection, where only the negative moments are transferred between the superstructure and substructure, rigid links are used to transfer all forces and moments except the longitudinal moment. A tension only rigid link is used to transfer the longitudinal moment from the deck to the bent.

In the case of MSCC-IG bridge class with bearing supported superstructure, the column nodes are connected using rigid links to the bent beam. Nonlinear displacement based beam column elements with fiber defined cross-sections are used to model the bent beam. Zero length elements characterized by the force displacement response of elastomeric bearings are used to connect the bent beam with the transverse rigid deck elements. These are joined in parallel with the restrainer elements at the bent similar to the case at the seat type abutments.

4.3 Analytical Bridge Models and Deterministic Responses

In this section, select component responses from the chosen bridge classes are presented to provide insight into their response and criticality using NLTHA on deterministic bridge models. In all cases, the deterministic responses are illustrated using a single ground motion from the suite of ground motions developed for the PEER Transportation Systems Research Program (Baker et al., 2011). Further details about the ground motion suite are provided in Chapter 5. The chosen ground motion pertains to a rock site with an average shear wave velocity of 2180 ft/sec and is characterized by a moment magnitude of 7.62 and hypocentral distance of 16.27 km. The ground motion

time histories for the fault normal and fault parallel components are shown in Figure 4.13. Also shown as an inset in the figure is the response spectrum corresponding to the two orthogonal components.

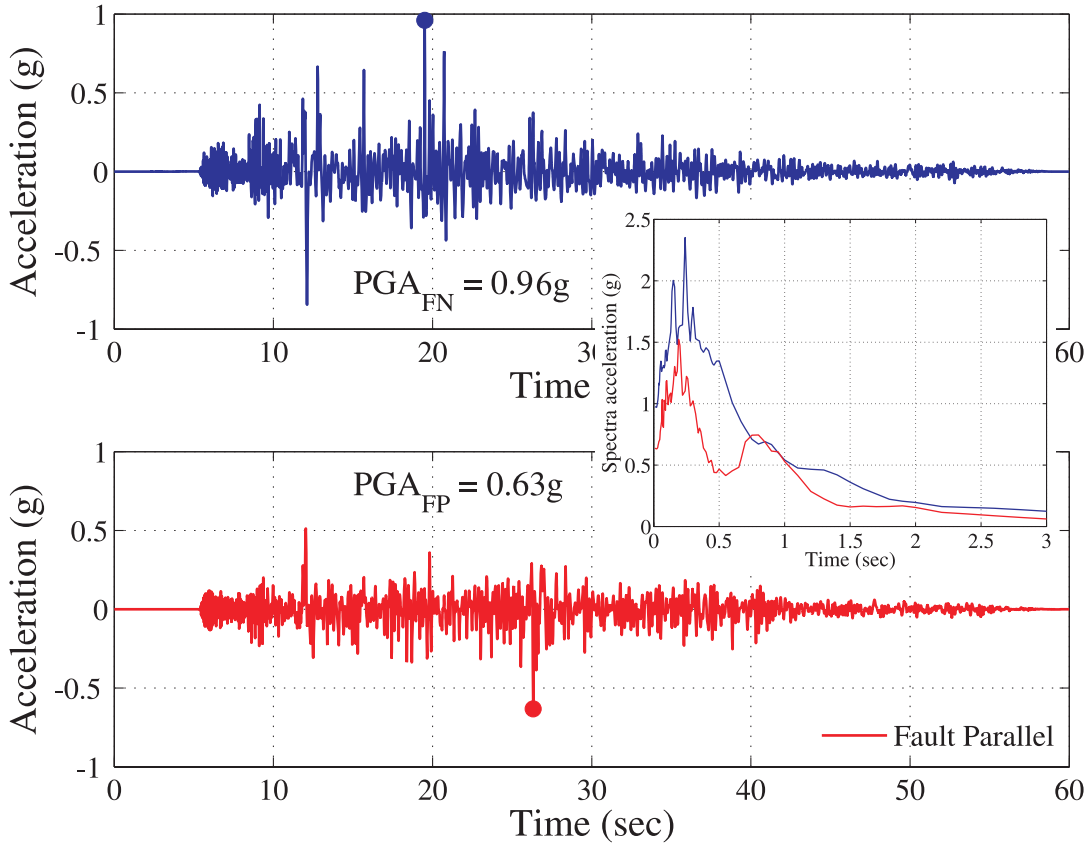

Figure 4.13: Fault normal and fault parallel components of ground motion used in deterministic analyses

The forthcoming sections present details and insight into the performance of bridges and their components. Bridge models with median values of geometric and material properties are developed and time history analyses is performed in each case. The following cases are considered:

- MSCC-BG bridges with single (MSCC-BG-S) and multi column (MSCC-BG-M) bents and seat and diaphragm abutments across all design eras (E1, E2, E3). Since this bridge class forms the bulk of the bridge inventory in the state of California,

an effort is made to contrast and compare the performance through deterministic analyses

- MSCC-SL with integral pile columns or pile extensions (MSCC-SL-P)
- MSCC-TG with multi column bents consisting of pile extensions (MSCC-TG-P) and circular columns (MSCC-TG-M) with seat and diaphragm abutments in the post 1990 design era (E3)
- MSCC-IG with single (MSCC-IG-S) and multi column (MSCC-IG-M) bents with seat and diaphragm abutments in the 1971-1990 design era (E2)

4.3.1 Multispan Continuous Concrete Single Frame Box Girder Bridges

4.3.1.1. General Layout

MSCC-BG bridges are typically used for longer spans and this class constitutes the bulk of the highway bridge inventory in California. Figure 4.14 shows the typical configuration of a two span continuous concrete box-girder bridge. Two span analytical finite element models are developed for this bridge class across design eras, consistent with the mode statistic for the number of spans, as discussed in section 3.2. The geometric parameters describing the bridge models used for deterministic analyses across design eras are documented in Table 4.1. It must be noted that all of the parameters reported in Table 4.1 are median values of the respective distributions that will be used in the generation of fragility curves. The number of columns per bent and the number of cells in the box-girder are a function of the width of the bridge. Further details about the geometric attributes obtained from the review of bridge plans are presented in Appendix A. Box-girder bridges are integral at the bent and this section typically is a solid diaphragm. As described in Chapter 3, the superstructure to substructure connectivity is type 2 in the case of Pre 1971 era bridges while it is type 3 in the other two design eras. Also shown in Table 4.1 are the box-girder dimensions, column size and reinforcement

details. MSCC-BG bridges employ circular columns and their diameter and reinforcement depends on the number of columns per bent, determined in this study based on an extensive review of bridge plans. Based on the design era and the associated longitudinal and transverse reinforcement ratio, the number of #11 longitudinal reinforcing bars and spacing of #4 stirrups are calculated and employed in the finite element models. The girders are typically proportioned based on acceptable depth-to-span ratios which are 0.055 and 0.04 for cast-in-place (CIP) reinforced concrete and CIP prestressed concrete boxes, respectively. The latter is considered to present results from the deterministic analyses. Both SCBs and MCBs are supported on a pile cap with a group of piles underneath it, as shown in Figure 4.14. SCBs are prevalent in all design eras, while the maximum number of columns in a MCB differ based on the design era and so is the individual column diameter. MCBs are pinned to the pile cap while SCBs have a moment transfer connection. The stiffness of the translational and rotational springs at the base of the column are also reported in Table 4.1. Both abutment types have a 6 ft tall backwall with Class 70 CIDH piles spaced at 7 ft on center. Concrete compressive strength of 4860 psi and reinforcing steel yield strength of 67.4 ksi are adopted.

The superstructure box-girder frames into the diaphragm abutment thereby transferring all forces and moments. In the case of seat type abutments, the box-girders rest on 14 in x 14 in x 2.5 in elastomeric bearing pads at the abutment seat. Two cases of seat type abutments are modeled: one where a small gap of 0.75 in exists between the deck and the abutment backwall and another where a larger gap of 3.75 in is considered between the deck and the backwall. 14 ft long, ¾ in diameter restrainer cables are considered at the seat type abutments with 0.625 in slack. The number of restrainers is determined based on the W/2 method discussed in the preceding section and the number of restrainers is indicated in Table 4.1. The mass of the deck is increased by 35% to account for any additional mass on the bridge such as railing, electrical poles etc.

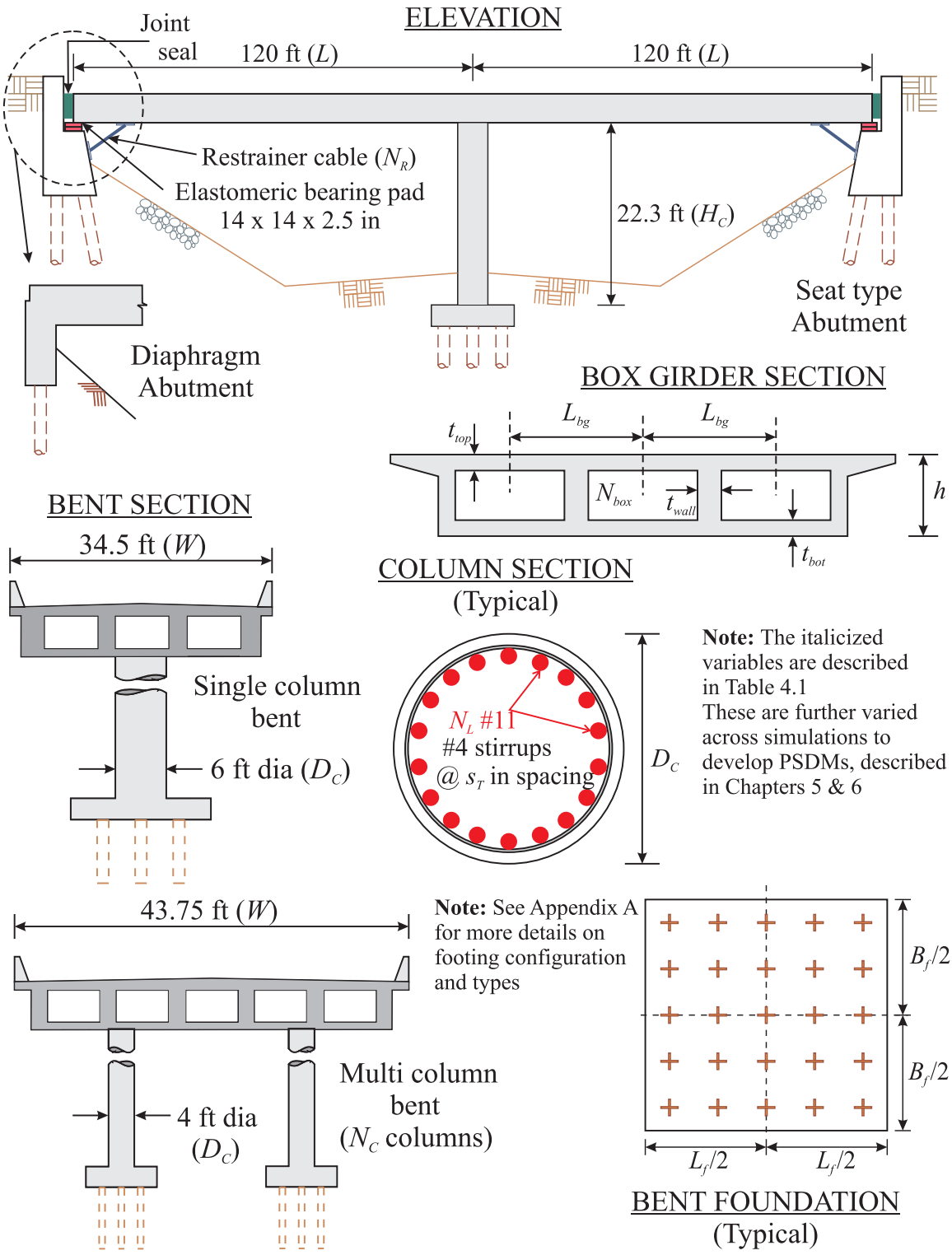

Figure 4.14: General layout of MSCC-BG bridges

Table 4.1: Deterministic bridge model attributes for MSCC single frame box-girder bridges

Attributes	Pre 1971		1971-1990				Post 1990				
	SCB	MCB	SCB	MCB			SCB	MCB			
Column details											
Number per bent (N_C)	1	2	1	2	3	4	1	2	3	4	5
Column height (ft) (H_C)	22.3	22.3	22.3	22.3	22.3	22.3	22.3	22.3	22.3	22.3	22.3
Diameter (ft) (D_C)	6	4	6	5	5	5	6	5	5	5	4
Longitudinal reinforcement (#11 bars) (N_L)	50	22	62	44	44	44	58	42	42	42	26
Transverse reinforcement spacing (in) (#4 stirrups) (s_T)	12.0	12.0	3.0	3.0	3.0	3.0	3.0	3.0	3.0	3.0	3.0
Superstructure details											
Span length (ft) (L)	120.0	120.0	120.0	120.0	120.0	120.0	120.0	120.0	120.0	120.0	120.0
Deck width (ft) (W)	34.5	43.75	35.25	43.75	90.0	110.0	35.25	43.75	70.0	90.0	127.5
Box-girder details											
Number of boxes (N_{box})	3	5	3	5	9	11	3	5	7	9	15
Total superstructure depth (in)* (h)	57.6	57.6	57.6	57.6	57.6	57.6	57.6	57.6	57.6	57.6	57.6
Top flange depth (in) (t_{top})	8.875	7.875	8.875	7.875	8.375	8.375	8.875	7.875	8.375	8.375	8.375
Bottom flange depth (in) (t_{bot})	6.0	6.0	6.5	6.5	6.5	6.5	7.0	7.0	7.0	7.0	7.0
Wall thickness (in) (t_{wall})	12.0	12.0	12.0	12.0	12.0	12.0	12.0	12.0	12.0	12.0	12.0
Cell center-to-center spacing (ft) (L_{bg})	11.5	8.75	11.75	8.75	10.0	10.0	11.75	8.75	10.0	10.0	8.5
Number of restrainers (N_R)	10	12	10	12	20	32	10	12	20	26	34
Column footing details – Spring stiffnesses											
Translational (kip/in)	1700	800	1400	1200	1200	1200	1400	1200	1200	1200	800
Rotational (kip-in/rad)	4.1×10^7	0	6.5×10^7	0	0	0	6.5×10^7	0	0	0	0

*Proportioned based on permissible depth-to-span ratio: 0.055 for CIP reinforced concrete and 0.04 for CIP prestressed concrete

4.3.1.2. Eigen Value and Time History Analysis

Eigen value analysis of the bridge models are performed in OpenSEES and the fundamental and second mode time periods are listed in Table 4.2. The fundamental mode shapes for different configurations of the post 1990 bridges with diaphragm and seat abutments is shown in Figure 4.15. In the case of seat type abutments, the fundamental mode is in the longitudinal direction. However, in the case of diaphragm abutments, the fundamental mode could either be longitudinal or transverse, as shown in Figure 4.15. In most of the cases, the second and higher modes invoke transverse and torsional responses of the bridges.

Table 4.2: First and second mode time periods for MSCC-BG bridges considered for deterministic analysis

Design era	No. of columns	Diaphragm abutments		Seat type abutments	
		First mode (sec)	Second mode (sec)	First mode (sec)	Second mode (sec)
Pre 1971	1	0.63	0.57	0.73	0.64
	2	0.77	0.63	1.23	1.07
1971-1990	1	0.57	0.53	0.78	0.73
	2	0.72	0.51	0.96	0.79
	3	0.77	0.38	0.99	0.83
	4	0.82	0.76	1.12	1.02
Post 1990	1	0.57	0.54	0.74	0.68
	2	0.64	0.37	1.01	0.91
	3	0.81	0.78	0.99	0.83
	4	0.71	0.38	1.02	0.93
	5	1.11	1.09	1.58	1.43

Diaphragm abutments

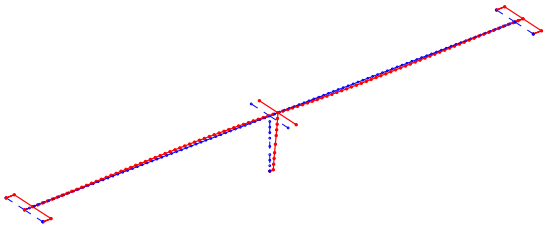

a) Single column bent

Seat type abutments

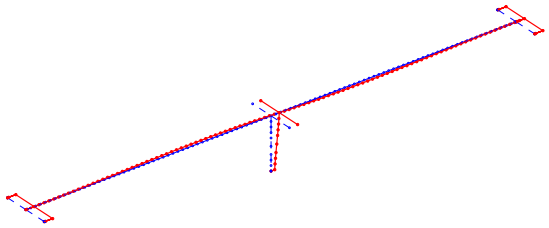

f) Single column bent

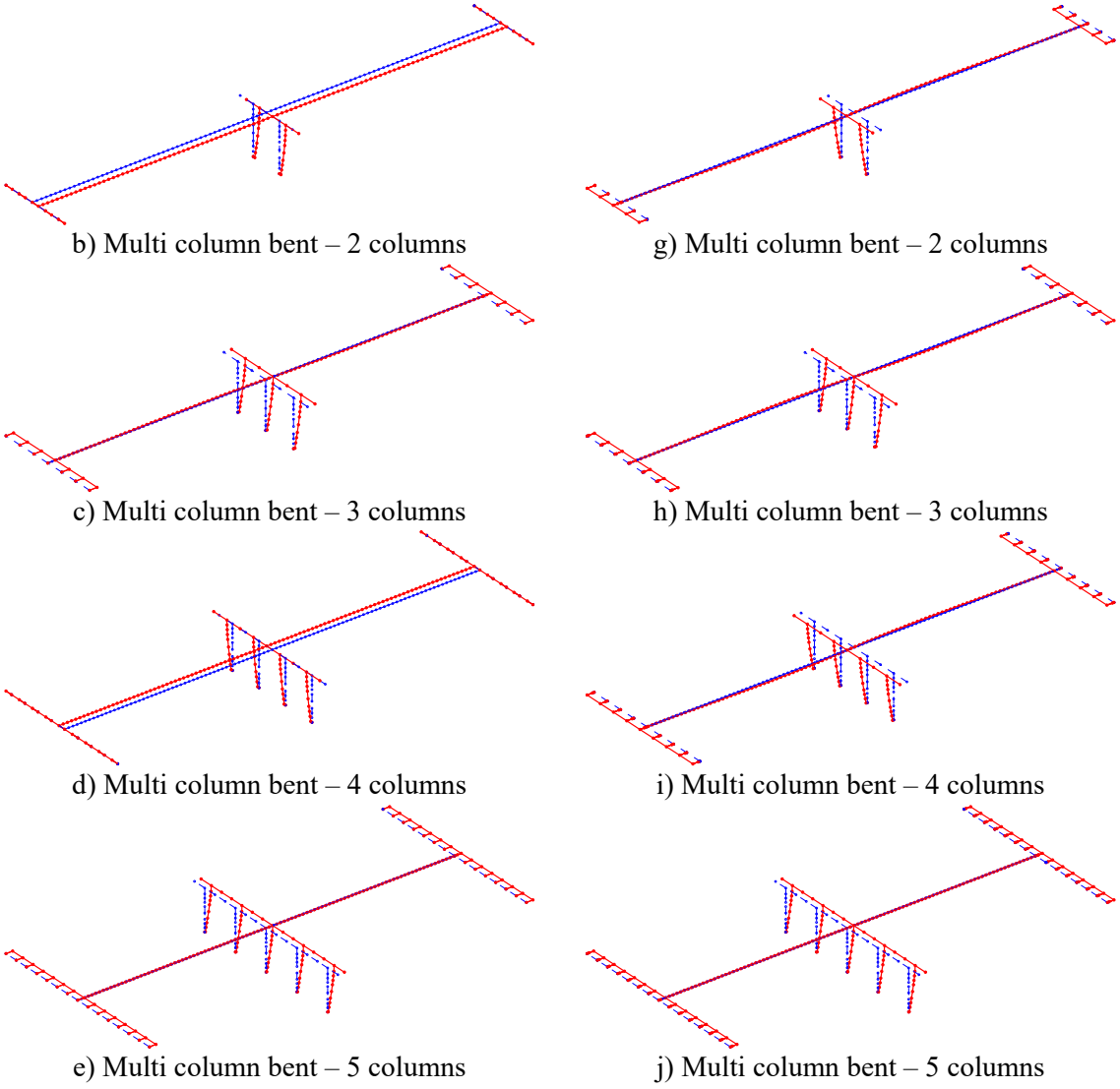

Figure 4.15: Fundamental mode shapes for Post 1990 MSCC-BG bridges with SCBs and MCBs

4.5% Rayleigh damping is used in the time history analysis performed on the bridge model subjection to a pair of ground motions records show in Figure 4.13. The ground motion records with a PGA of 0.96g is applied along the longitudinal axis of the bridge while the record with a PGA of 0.63g is applied in the transverse direction. Only the response of a few bridge components is presented below due to the large number of components and responses in each of the bridge models with different number of columns and abutment type.

Figure 4.16 shows the displacement response of the deck nodes in either spans in the longitudinal and transverse directions for a bridge with four columns designed in the 1971-1990 era with diaphragm and seat abutments. It can be seen that the response of both the spans match perfectly which is expected when the superstructure is continuous. It can be seen that the deck undergoes a longitudinal displacement of about 4 in for both the abutment types. The transverse displacement is slightly different based on the abutment type. Bridges with diaphragm abutments undergo a larger transverse displacement since in this case a monolithic connection exists between the deck and the abutments a larger mass is excited.

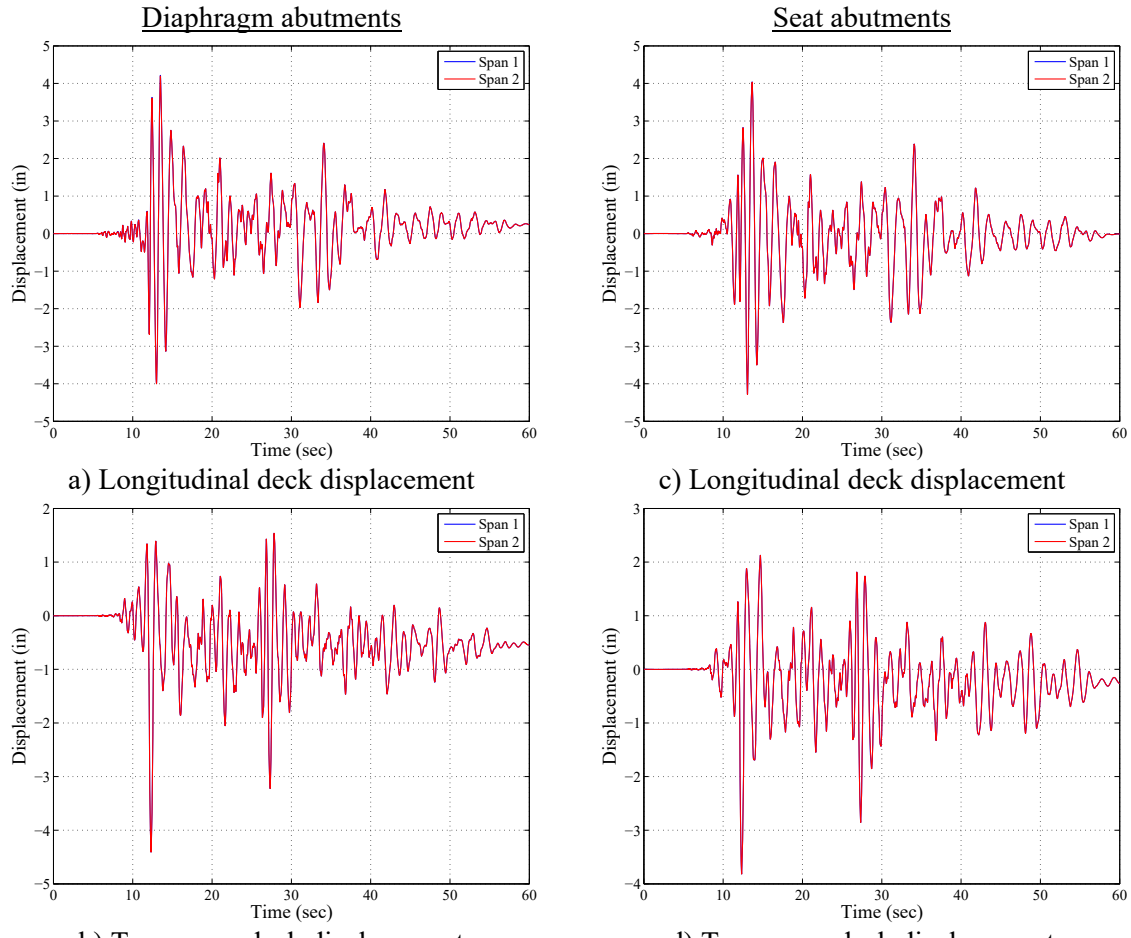

Figure 4.16: Displacement response of the deck for a MSCC-BG bridge with four columns in the 1971-1990 design era

In all the cases considered, moment curvature response of the column is monitored and a few of them are shown in Figure 4.17. Figures 4.17(a) and (b) show the seismic moment curvature response of a column in the longitudinal and transverse direction belonging to a pre 1971 designed MSCC-BG bridge with SCB and diaphragm abutments. It is seen that the columns are subjected to a larger longitudinal moment and curvature. Figure 4.17(c) shows the response of the column in transverse direction for a pre 1971 designed bridge with seat abutments and MCB, while Figure 4.17(d) shows the longitudinal response of a SCB of the same design era and seat abutments.

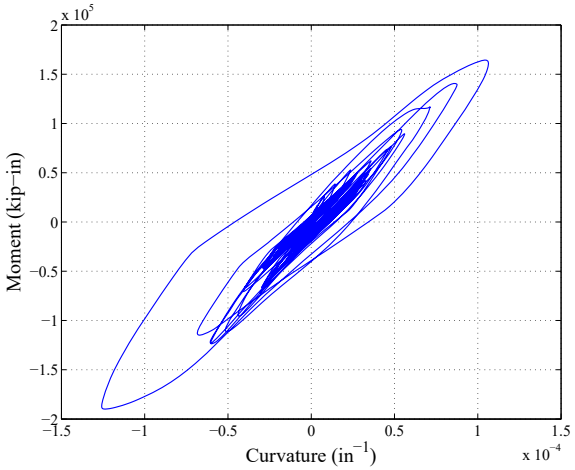

a) Longitudinal response – SCB – Diaphragm abutments

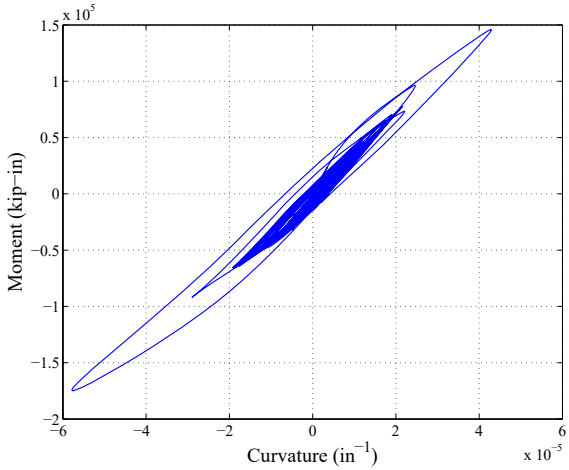

b) Transverse response – SCB – Diaphragm abutments

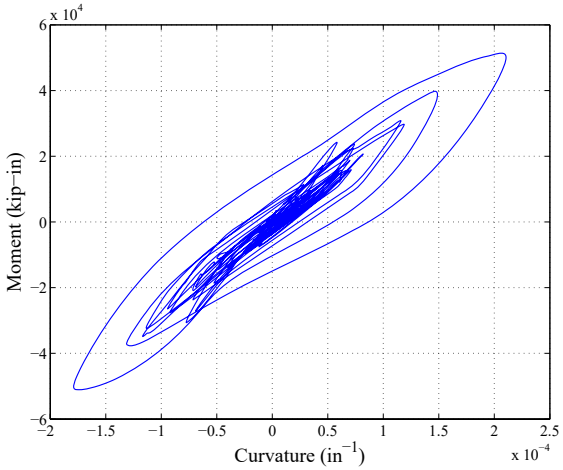

c) Transverse response – MCB – Seat abutments

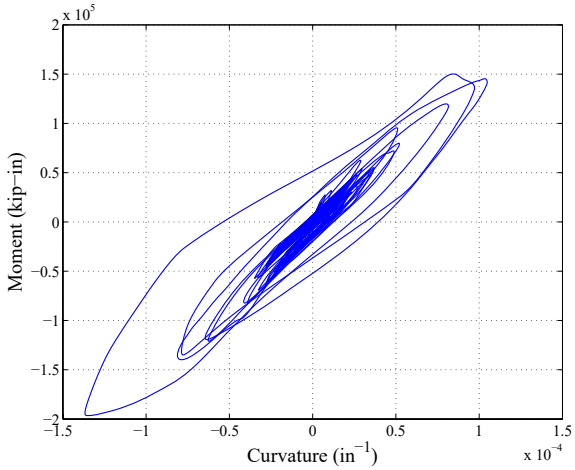

d) Longitudinal response – SCB – Seat abutments

Figure 4.17: Moment curvature response of columns

Curvature ductility, μ_ϕ, is a common way of interpreting the response of columns and is defined as the ratio of ultimate curvature and yield curvature. Moment curvature analysis of the section is used to determine the yield curvature by fitting a bilinear response to the original data. Figure 4.18 shows the moment curvature response across design eras for columns in SCBs and MCBs. Clearly, the evolution of column design philosophy is visible in Figures 4.18(a) and (b) as seen in the strength degradation and limited ductility in the case of Pre 1971 columns. These characteristics are enhanced in the columns in the other two design eras and this is consistent with the trends observed based on the review of bridge plans, as described in the previous chapter. Figure 4.18(c) shows the bilinear approximation to the moment curvature response of a column cross-section. The curvature at transition of the two linear segments is reported as the yield curvature signifying the curvature at the onset of the first yield of the outermost reinforcing bar.

As mentioned previously, SCBs have a connection at the column bases close to fixity while MCBs are pinned at the base. The plot of curvature over the height of the column is shown in Figure 4.19 for bridges designed post 1990. It is seen that the columns become significantly nonlinear during the ground motions excited. This further demonstrates the significant ductility capacity of modern columns in comparison to the ones designed prior to 1971. In the case of SCBs, it is seen that the regions of the column close to the superstructure have higher curvature ductility when compared to the regions close to the pile cap. This is mainly because of the heavy moment and shear transfer from the superstructure. Further, the heavy superstructure mass excites the sections of the column close to the superstructure (like a lumped mass) thereby causing significant yielding in the column sections in this region. Similar behavior is seen in the case of multi column bents which are in any case free to rotate at the base.

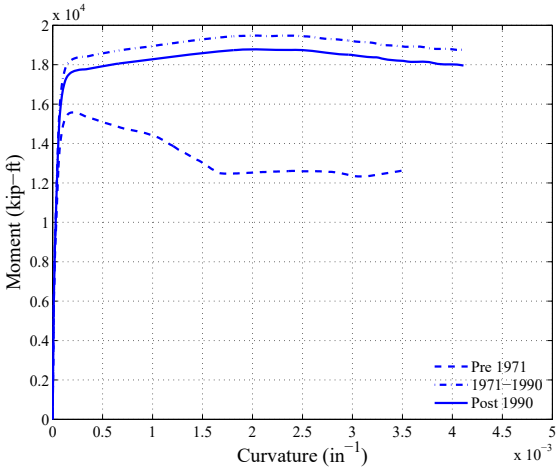

a) Columns in single column bent

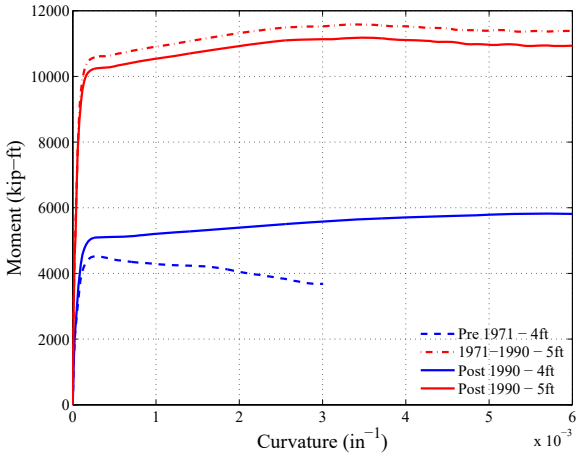

b) Columns in multi column bent

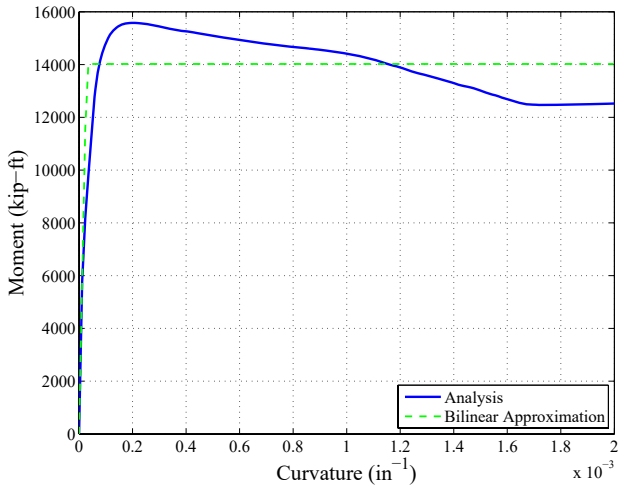

c) Bilinear approximation to determine yield curvature

Figure 4.18: Comparison of **c**olumn moment curvature responses

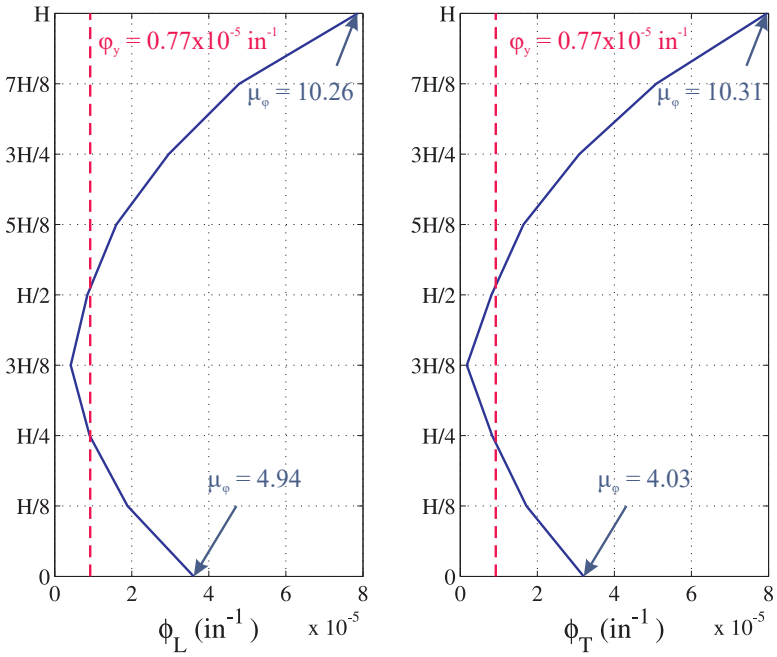

a) Single column bent

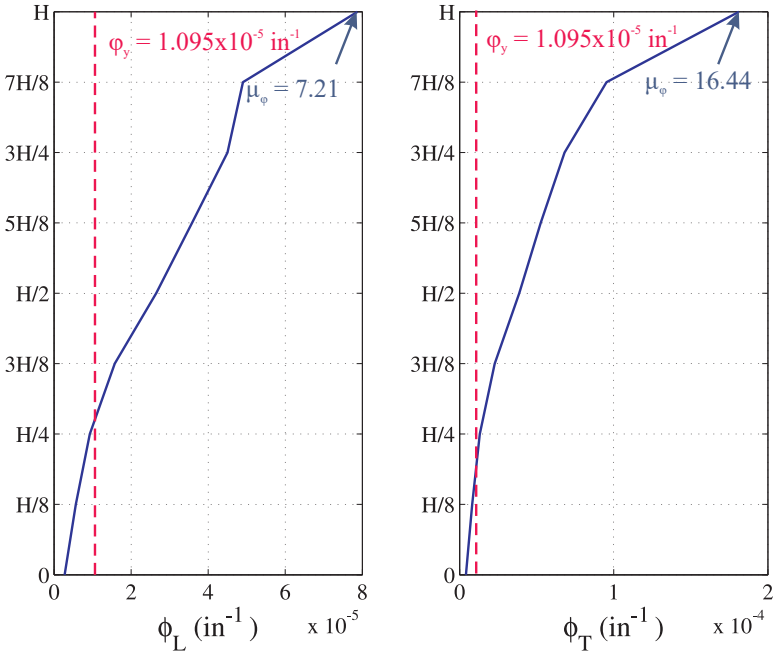

b) Multi column bent

Figure 4.19: Variation of curvature over the height of a column

Figure 4.20 shows the response of the abutment soil-pile system for diaphragm versus seat abutment in a MSCC-BG bridge with SCB designed in the 1971-1990 design era. The longitudinal response of the abutments is characterized by the contribution of

backfill soil and piles in the passive action and solely by the piles in active action. Piles alone account for the transverse response of the abutments. Note that in both the cases, the backfill soil is clay. In the case of diaphragm abutments, the abutments act monolithically with the superstructure while in the case of seat type abutments, the abutment engages when the gap between the deck and the backwall closes which is 0.75 in in this case. This is depicted in the response of the backfill soil shown in Figures 4.20(a) and (d). For the same reasons, the backfill soil experiences greater nonlinearity in the case of diaphragm abutments when compared to their seat type counterparts.

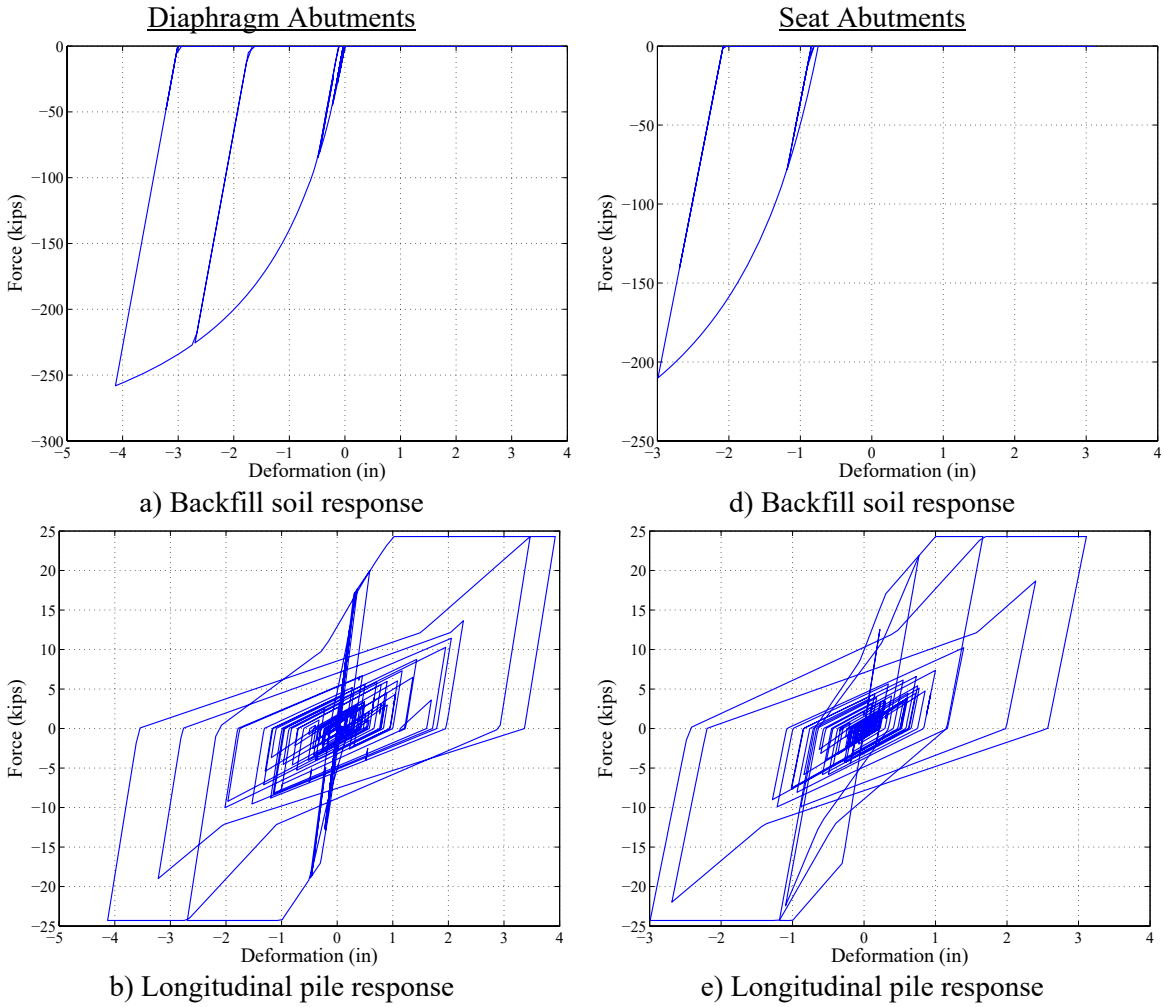

a) Backfill soil response

d) Backfill soil response

b) Longitudinal pile response

e) Longitudinal pile response

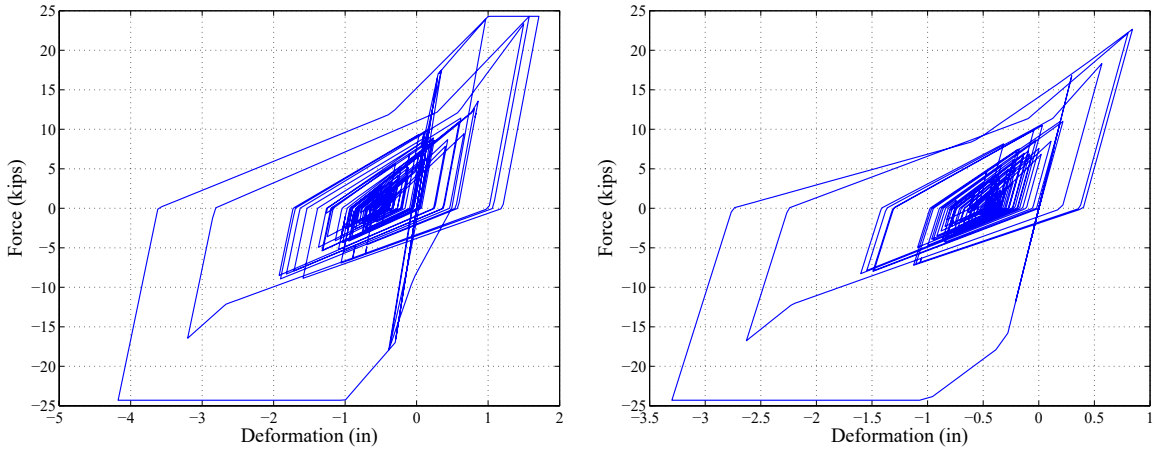

c) Transverse pile response f) Transverse pile response

Figure 4.20: Response of abutment backfill - pile systems in MSCC-BG bridges designed in the 1971-1990 design era

Similar to the case of backfill soils, the extent of nonlinearity in piles is greater in the case of diaphragm abutments when compared to seat type abutments in both longitudinal and transverse directions. The reduction in the case of seat type abutments may be attributed to the load being resisted by restrainers and bearings in the longitudinal directions and the bearings and shear keys in the transverse direction.

The next logical question that arises would be the impact of backfill soil type on the response of bridges. Figure 4.21 shows the response of a MSCC-BG bridge with a SCB and diaphragm abutments designed in the 1971-1990 design era: one with a clayey backfill and the other with a sandy backfill. Abutment backwalls with sandy backfills are stiffer than clayey backfills and thereby attract more force, as seen in Figure 4.21(a). The displacement of the backwall and piles are smaller for sandy backfills when compared to clayey backfills, as seen in Figures 4.21(b) and (c). It can be concluded that the backfill soil type affects the bridge dynamic characteristics. This is further substantiated by the column response shown in Figure 4.21(d). Unlike the lower displacement response of the abutment soil-pile system, the columns in a bridge with sandy backfills experience larger curvatures and moments when compared to their counterparts with clayey backfills. In

any case, the mode shapes are identical and there is a small change in the modal periods: 0.61 sec for clayey backfill versus 0.57 sec for sandy backfills.

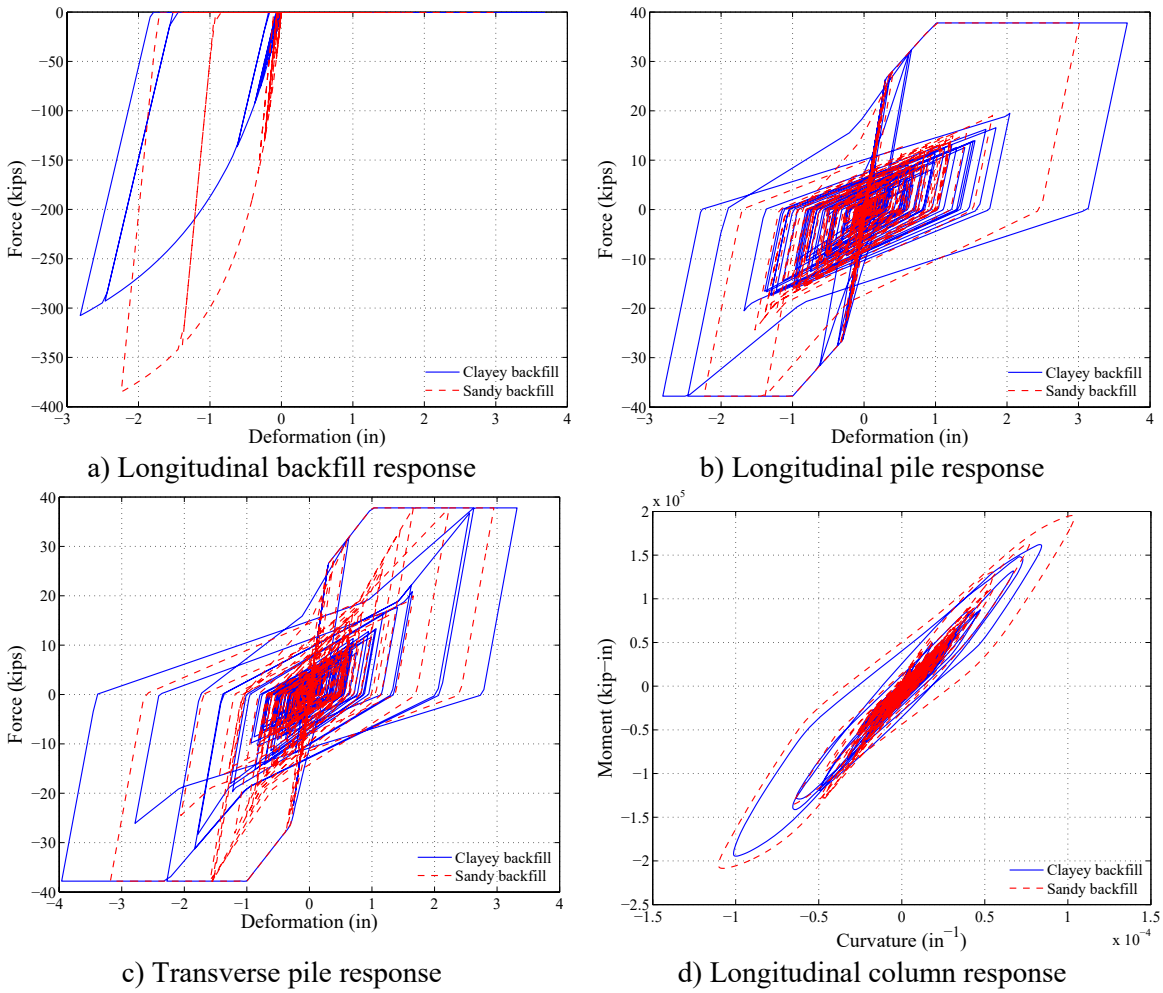

Figure 4.21: Influence of abutment backfill soil type on the response of bridge components

Figure 4.22 shows the response of restrainers and elastomeric bearing pads in a MSCC-BG bridge with seat type abutments designed in the post 1990 design era. As the superstructure moves towards and away from the abutment backwall, the elastomeric bearing pads and restrainer cables share the load transferred by the superstructure in proportion to their stiffness. When the bearing pads yield, restrainers pick up the additional forces transferred from the superstructure until the gap between the deck and

abutment backwall closes, at which point, the abutment soil-pile system engages in resisting the superstructure forces.

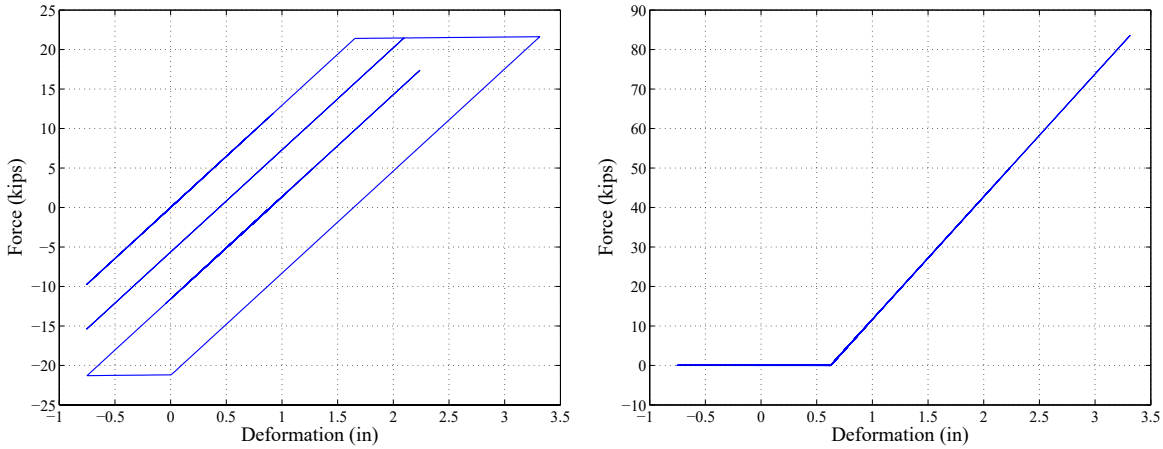

a) b)

Figure 4.22: Response of a) elastomeric bearing pads, and b) restrainer cables in the longitudinal direction

4.3.2 Multispan Continuous Concrete Slab Bridges

4.3.2.1. General Layout

Slab bridges typically employ standard piles as columns (or integral pile columns) and unlike the case of columns in MSCC-BG bridges described in the previous section, there is no evolution in the pile cross-section and reinforcement patterns across the three significant design eras considered in this study. Slab bridge construction is generally employed over shorter span lengths and the overall configuration is similar to that of the box-girder bridges. The general layout of MSCC-SL bridges is shown in Figure 4.23.

Three span slab bridges are most prevalent in the inventory and based on the review of bridge plans it was seen that the ratio of the maximum span length to the length of the approach spans is typically 1.2. As shown in Figure 4.23, for the sake of deterministic analyses, three span finite element models are developed with the center span considered as the longest measuring 28 ft and the two approach spans measuring 23

ft each. The deck measures 37 ft in width and the bridge consists of two multi column bents with 15 ft tall columns. Both diaphragm and seat type abutments with clayey and sandy backfills are considered and the height of the backwall is 6 ft in both the cases. A 0.75 in gap is considered between the deck and the abutment backwall in the case of seat type abutments. These parameters are median values of their respective ranges. A typical value of the depth-to-span ratio for slab bridges with continuous spans is 0.05 and therefore a 22 in thick deck slab is considered in model used to present deterministic analyses results.

Since slab bridges have shorter spans, the substructure for this class of bridges is smaller when compared to all the other bridge classes and hence these typically employ smaller integral pile columns. These typically measure 16 in in diameter and are of two fundamental types: precast concrete (PC) piles and precast prestressed concrete (PPC) piles. The details of the pile cross-sections are also shown in Figure 4.23. Based on a review of bridge plans and Caltrans standard drawings over the last four decades, it was seen that MSCC-SL used only 45 ton (90 kips) and 70 ton (140 kips) piles. These are generally referred to as Class 45 and Class 70 piles, where the class number denotes the design load or one-half the ultimate load in tons. This yields ultimate loads of 180 kips and 280 kips for Class 45 and Class 70 piles, respectively. As shown in Figure 4.23, the details of Class 45 and 70 PC and PPC piles are summarized below:

- Class 45 precast concrete piles: These measure 15 in in diameter and the longitudinal reinforcement consists of 8 #6 bars and transverse reinforcement comprised of #5 gauge wire spirals at 3 in on center
- Class 45 precast prestressed concrete piles: These measure 15 in in diameter and consist of 16-φ7/16 prestressing strands. 4 #6 reinforcing bars are present in the top 3.5 ft of the column and these frame into the superstructure. The transverse reinforcement consists of #5 gauge wire spirals at 3 in on center

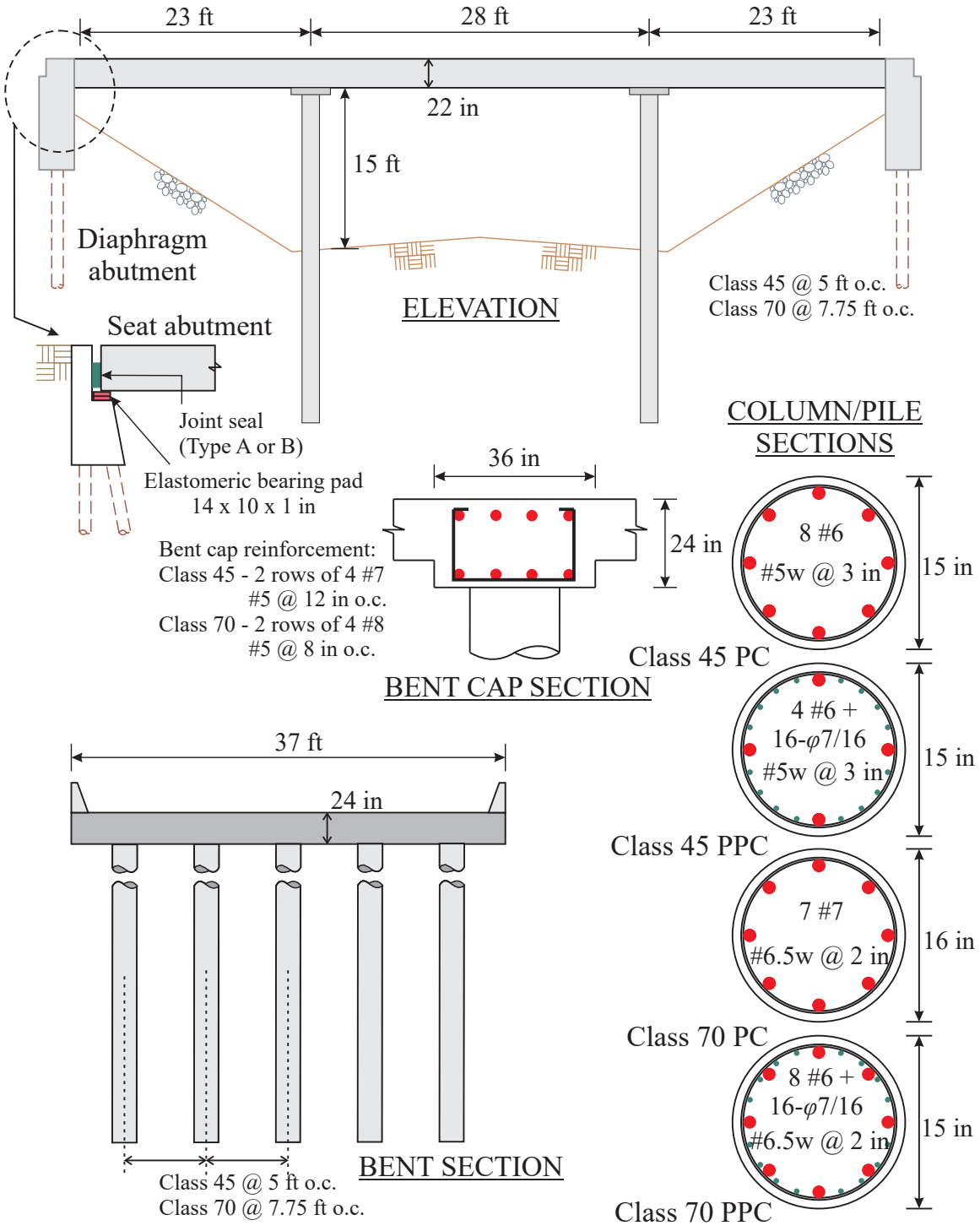

Figure 4.23: General layout of MSCC-SL bridge

- Class 70 precast concrete and cast-in-driven hole (CIDH) piles: These measure 16 in in diameter and the longitudinal reinforcement consists of 7 #7 bars. The transverse reinforcement is comprised of #6.5 gauge wire spirals at 2 in on center
- Class 70 precast prestressed concrete piles: These measure 15 in in diameter and consist of 16-φ7/16 prestressing strands. 8 #6 reinforcing bars are present in the top 3.5 ft of the column and these frame into the superstructure. The transverse reinforcement consists of #6.5 gauge wire spirals at 2 in on center

Akin to MSCC-BG bridges, MSCC-SL bridges are integral at the bent. As mentioned in Chapter 3, slab bridges have MCBs alone. However, it must be noted that the MCBs in this case are not pinned at the base since the columns extend below the ground surface as piles. The stiffness of the translational and rotational springs at the base of the column is 30 kip/in and 80,000 kip-in/rad, respectively. The center to center spacing of the integral pile columns at the bent and the spacing of abutment piles depends on the span length and the pile class. In the present case, the center-to-center spacing of the columns at the bent is 5 ft in the case of Class 45 piles and 7.75 ft in the case of Class 70 piles. The same applies to the spacing of abutment piles. The presence of a bent cap depends on the span length and detailed information regarding the dimensions and reinforcement layout is given in Appendix A in the form of design charts. In this case, the bridge has a 36 in × 24 in bent beam. The reinforcement consists of two rows of 4 #7 bars each at the top and bottom and #5 stirrups at 12 in on center in the case of Class 45 piles, and two rows of 4 #8 bars each at the top and bottom and #5 stirrups at 8 in on center in the case of Class 70 piles. The superstructure slab frames into the diaphragm abutment thereby creating a monolithic connection. However, in the case of seat type abutments, the deck slab rests on elastomeric bearing pads. In all cases, 14 in × 10 in × 1 in elastomeric bearing pads are used. The survey of bridge plans did not reveal the presence of restrainer cables and shear keys at the abutments and henceforth these are not considered in the analytical models for this bridge class.

4.3.2.2. Eigen Value and Time History Analysis

MSCC-SL bridges have shorter periods when compared to MSCC-BG bridges due to their relative stiff nature. Table 4.3 lists the first two modal periods for MSCC-SL bridges with diaphragm and seat abutments and the pile class. It must be noted that the pile class dictates the center-to-center spacing of the integral columns at the bent. This in turn drives the number of columns in a bent and therefore, the pile class can affect the period of the structure, as seen in Table 4.3. For both abutment types, the fundamental mode is in the longitudinal direction and the second mode is in the transverse direction. Higher modes are vertical and torsional. The first two mode shapes for slab bridges with both abutment types is shown in Figure 4.24.

Table 4.3: Modal time periods for MSCC-SL bridges

Abutment	Pile class	First mode (sec)	Second mode (sec)
Diaphragm	Class 45	0.47	0.44
	Class 70	0.57	0.54
Seat	Class 45	0.64	0.61
	Class 70	0.76	0.74

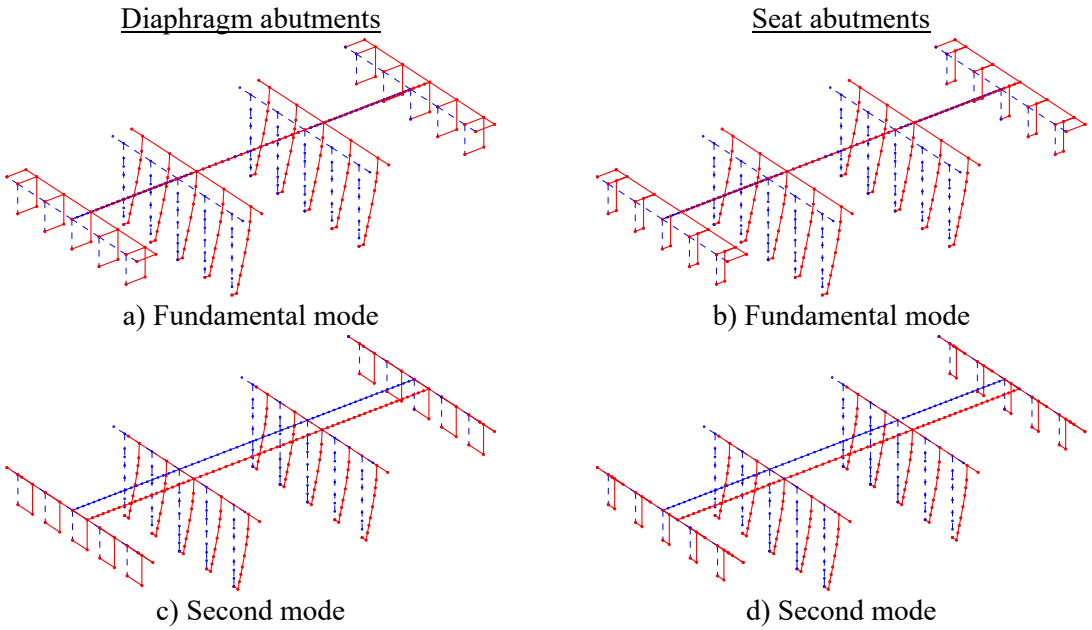

Figure 4.24: Mode shapes for MSCC-SL bridges with diaphragm and seat abutments

Time history analyses are conducted using the orthogonal pair of ground motions shown in Figure 4.13 and the response of deck, columns, abutment soil-pile system, and elastomeric bearings is recorded. Figure 4.25 shows the longitudinal and transverse displacement response of the mid span sections. The displacements of the three spans are equal owing to the continuity of the superstructure across the bents. The maximum longitudinal and transverse displacements are 2.4 in and 1.55 in, respectively for diaphragm abutments, while these values are 4.15 in and 3.95 in for seat type abutments. Bridges with seat type abutments are relatively flexible when compared to those with diaphragm abutments and the presence of the gap between the deck and backwall leads to an increased deck displacement, as seen in Figures 4.25(c) and (d). Further the absence of shear keys leads to an increased displacement in the transverse direction.

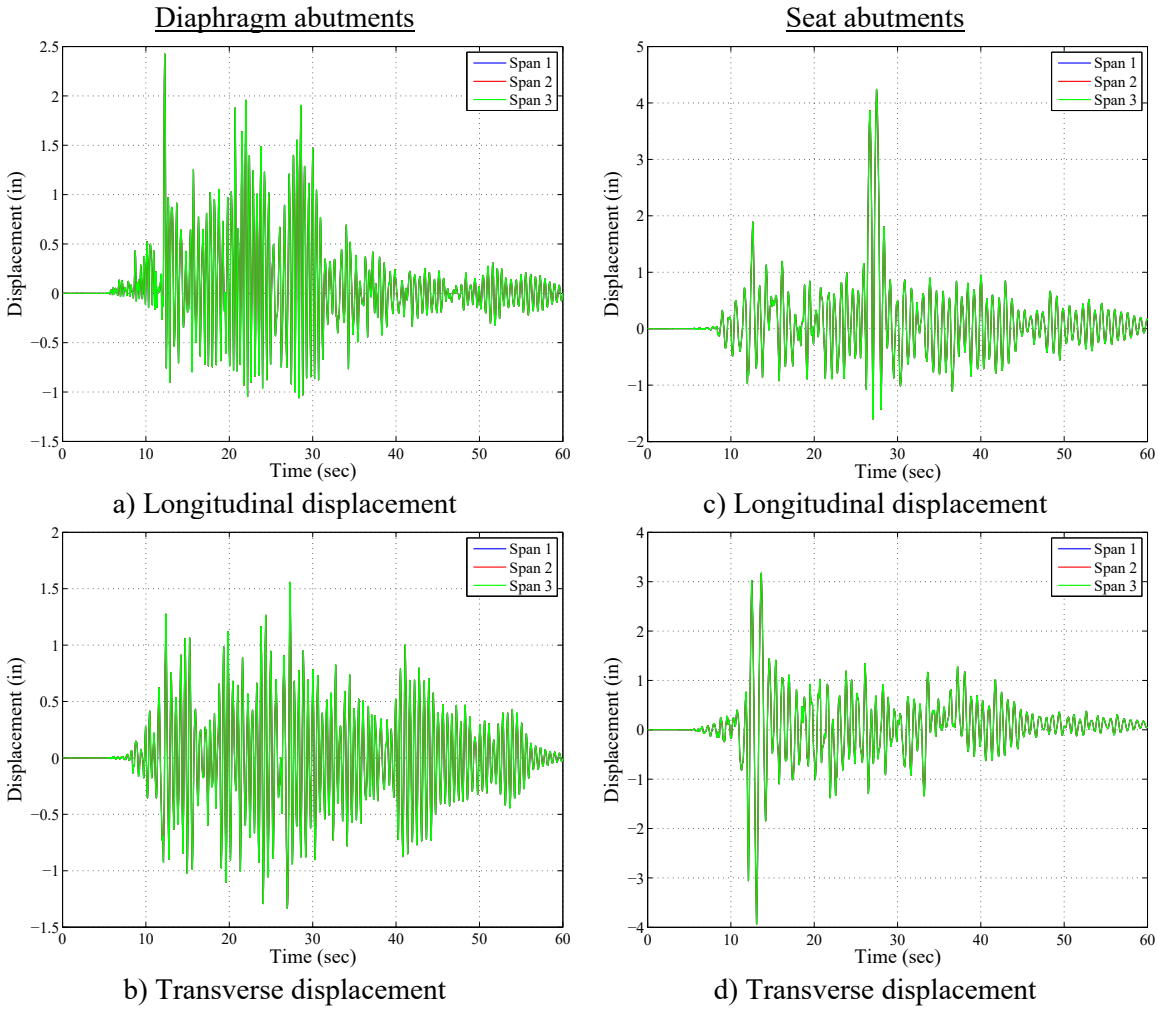

Figure 4.25: Longitudinal and transverse displacement of the individual spans in a MSCC-SL bridge with diaphragm and seat abutments

The response of the columns in the longitudinal and transverse directions for MSCC-SL bridges employing Class 70 PPC piles with diaphragm and seat abutments is shown in Figure 4.26. Figure 4.27 shows the moment curvature response of Class 45 and 70, PC and PPC pile cross-sections and the respective yield curvatures determined using a bilinear approximation, as described in the previous section. It is seen that the columns behave in their elastic range in both cases. This may be attributed to the fact that slab bridges have larger number of integral pile columns across the bent thereby offering more ways for the superstructure forces and moments to be distributed.

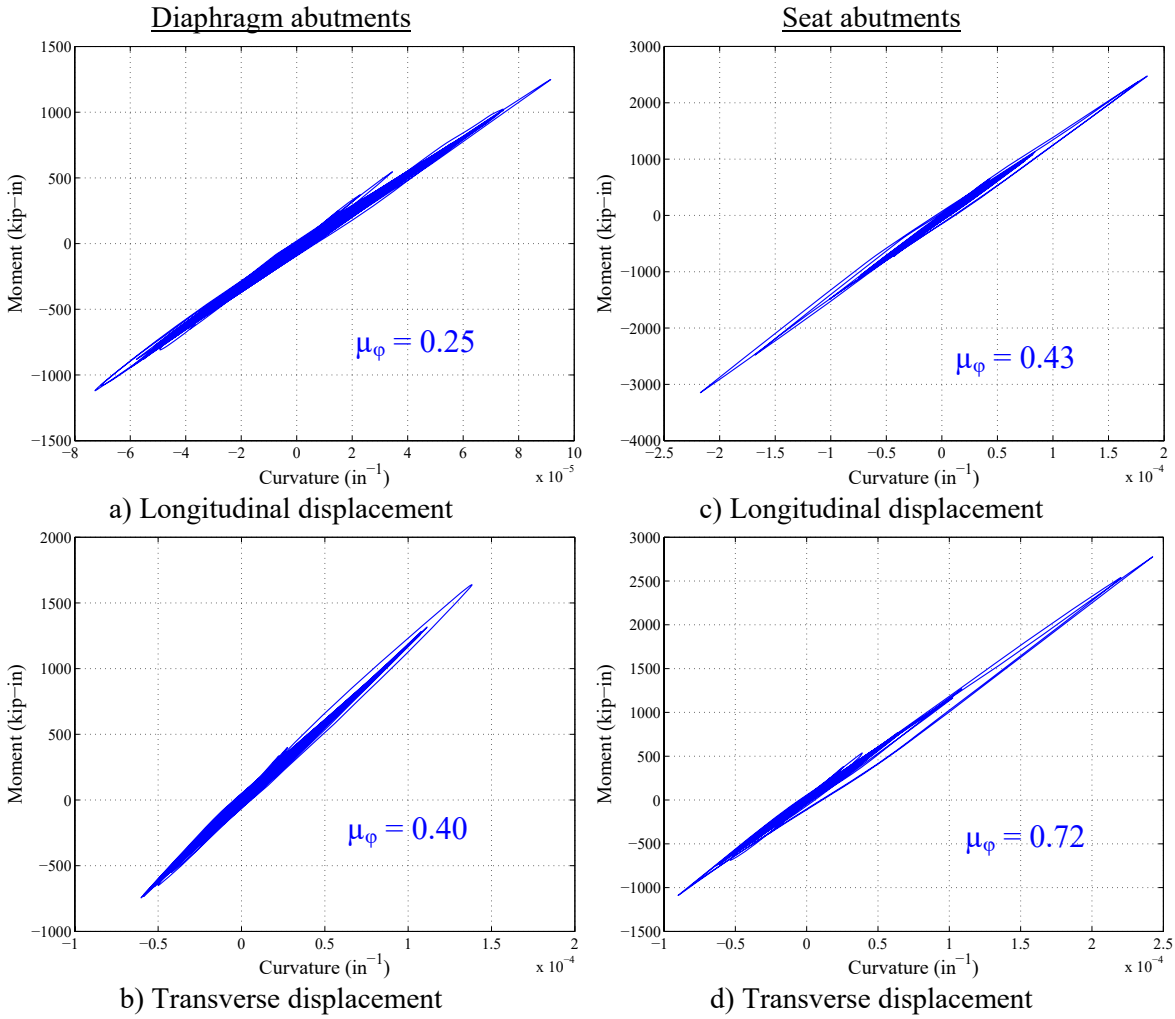

Figure 4.26: Response of MSCC-SL bridge columns in longitudinal and transverse direction

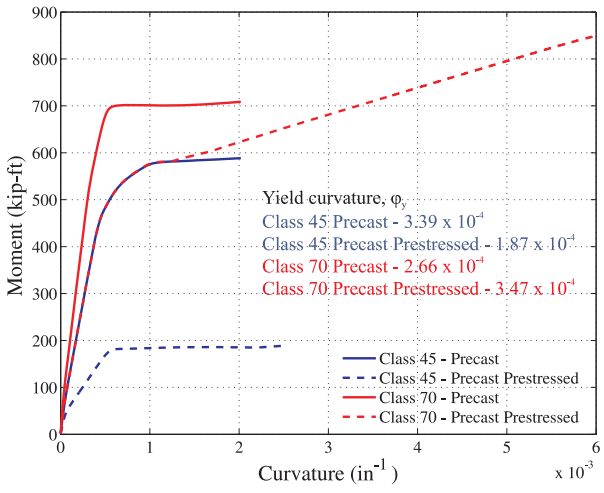

Figure 4.27: Moment curvature responses for different pile classes and pile types

From Figure 27, it is seen that PC piles have a higher moment and lower ductility capacity when compared to PPC piles. This may be attributed to the presence of larger amounts of primary longitudinal reinforcing bar in PC piles when compared to PPC piles. However, the enhanced ductility in the case of PPC piles is due to the presence of prestressing strands and improved confinement.

The curvature ductility of columns in bridges with seat abutments is higher than their diaphragm counterparts. This is because in the case of diaphragm abutments, the abutment system is completely engaged with the superstructure thereby reducing the demand on the columns. While in the case of seat abutments, majority of the superstructure forces go into the columns until the gap between the deck and the abutment backwall is closed, at which point abutments begin to engage and share forces and moments. The variation of curvature over the height of the column for a MSCC-SL bridge with Class 45 PC piles and seat abutments is shown in Figure 4.28. Only the portion of the column close to the superstructure yields in the transverse direction while the other sections remain elastic. Further, the curvature profile indicates the potential for the integral pile columns to undergo a double curvature bending.

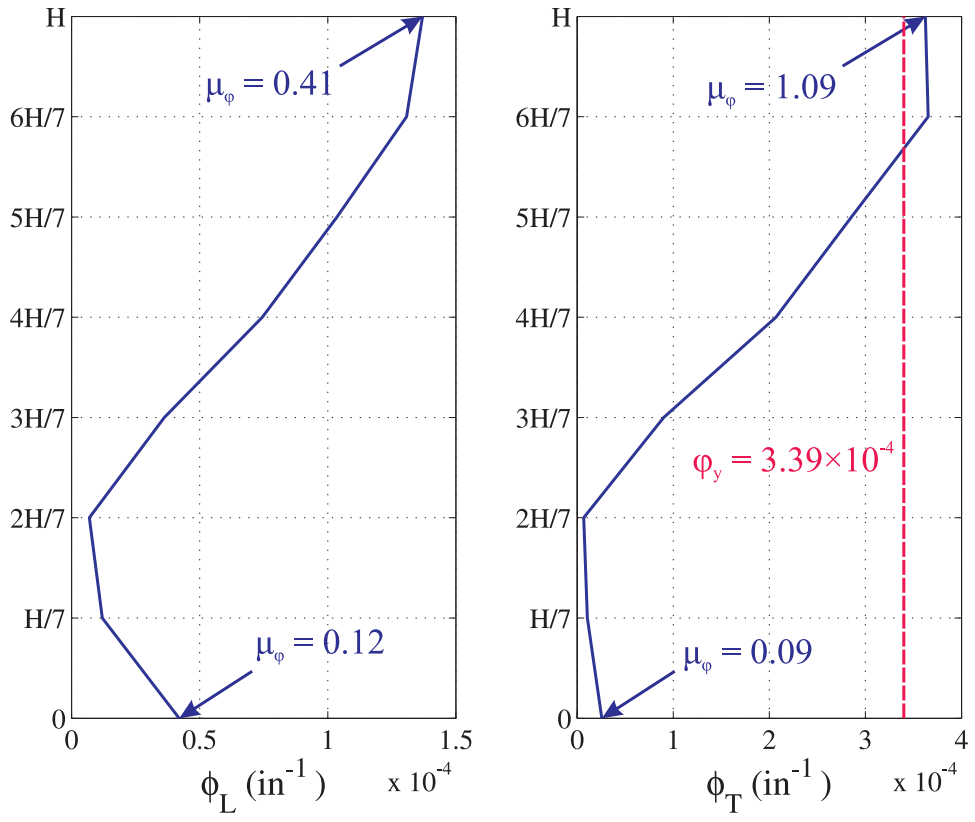

Figure 4.28: Variation of curvature over the height of the column for an MSCC-SL bridge with seat abutments

The response of the abutment backfill soil and piles in the longitudinal and transverse directions is shown in Figure 4.29. Class 45 PC piles are used in the simulations. The backfill soil responds only in passive action and it is seen that the passive displacement of the soil in seat abutments is greater than that of diaphragm abutments. On the other hand, the active displacement of piles in seat abutments is higher than the passive displacement and the trend is reverse in the case of diaphragm abutments. Further, it is seen that the transverse displacement of piles in diaphragm abutments is higher than that in the case of seat abutments. This is expected since the entire bridge structure frames into diaphragm abutments and behaves like a vertical cantilever in the transverse direction leading to greater displacements. It must be noted that piles alone contribute to the transverse resistance of the abutments.

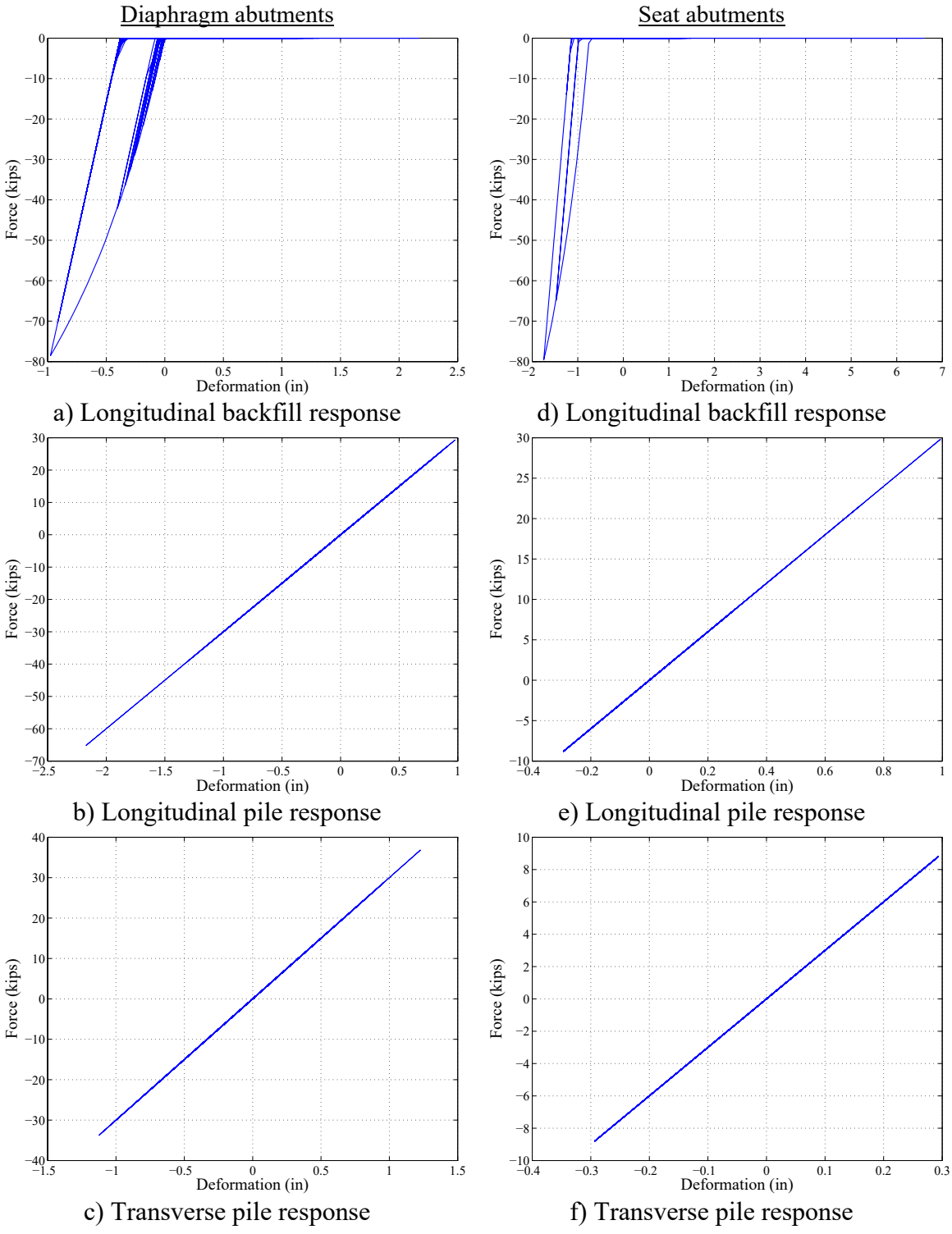

Figure 4.29: Response of abutment soil-pile system in MSCC-SL bridge with diaphragm and seat abutments

Unlike the case of the MSCC-BG bridges where the elastomeric bearing pads did not undergo significant deformations and nonlinearity, the elastomeric bearing pads in the case of MSCC-SL and seat abutments undergo significant deformations. This is due to the absence of restrainer cables and shear keys in this bridge class to share a proportion of the forces. Figure 4.30 shows the response of elastomeric bearing pads in slab bridges in longitudinal and transverse directions.

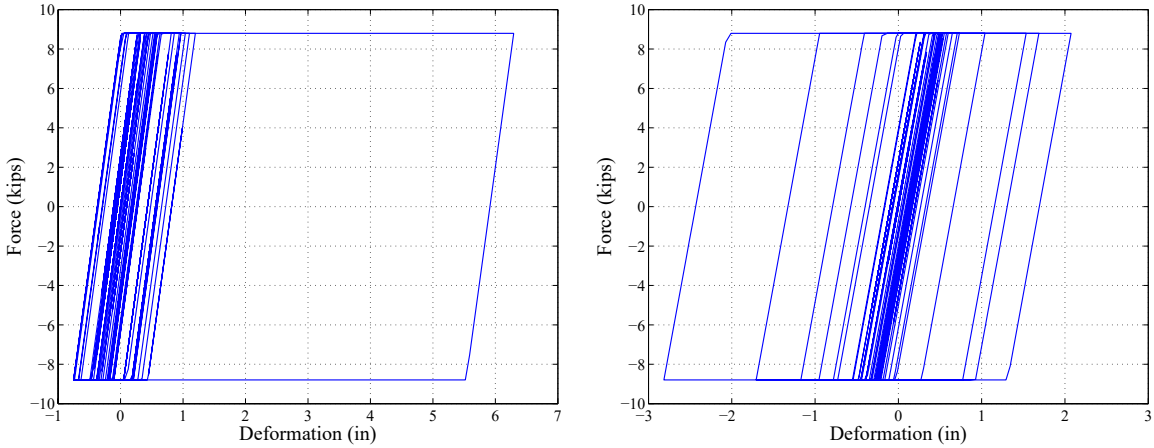

a) b)

Figure 4.30: Response of elastomeric bearing pads in MSCC-SL bridge with seat abutments in the a) longitudinal, and b) transverse direction

4.3.3 Multispan Continuous Concrete Tee Girder Bridges

4.3.3.1. General Layout

Multispan Tee girder bridges are normally adopted over span range of 30 ft to 80 ft and have typical depth to span ratios of 0.05. Their behavior is similar to MSCC-SL bridges described in the previous section. Tee girder bridges are integral at the bent and the superstructure consists of girders cast monolithically with the deck slab. As in the case of MSCC-SL bridges, MSCC-TG bridges have multi column bents (MCB) alone consisting of either integral pile columns (MSCC-TG-P) or circular columns founded on pile footings (MSCC-TG-M). Unlike, integral pile columns which did not undergo any

change across the design eras, circular columns underwent a major shift in response characteristics being described as brittle in the pre 1971 design era to ductile in the modern day bridges.

Deterministic responses from Tee girder bridges designed in the post 1990 design era are presented in this section. Three spans bridges are the most likely configurations for this bridge class. Three span analytical models are developed with the center span measuring 60 ft and the two adjacent spans measuring 50 ft for the sake of deterministic analysis and a typical layout is shown in Figure 4.31. The bridge is 50 ft wide and the superstructure deck is supported over 5 girders and consists of MCBs with 22 ft tall columns. The models employ both integral pile columns and MCB with circular columns for comparison purposes. As in the case of MSCC-SL bridges, Class 45 and 70, PC and PPC piles are employed for MCB with integral pile columns. The bridge bent has 10 columns per bent if Class 45 integral pile columns are adopted while they have 9 columns in the bent if Class 70 integral pile columns are adopted. In the case of MCB with circular columns, 3 ft diameter columns with 24 #11 longitudinal reinforcing bars and #4 stirrups at 3 in on center are employed. The bent has two columns if circular columns are adopted. Further details correlating the width of the bridge, number of column per bent and column center-to-center spacing is provided in Appendix A. The integral pile columns have translational and rotational springs at the base of the column to replicate the behavior of the portion of the pile extending beneath the surface of the ground. The stiffness of the translational and rotational springs is 30 kip/in and 80,000 kip-in/rad, respectively. On the other hand, MCB with circular columns are pinned at the base, and therefore only a translational spring of stiffness 800 kip/in is provided.

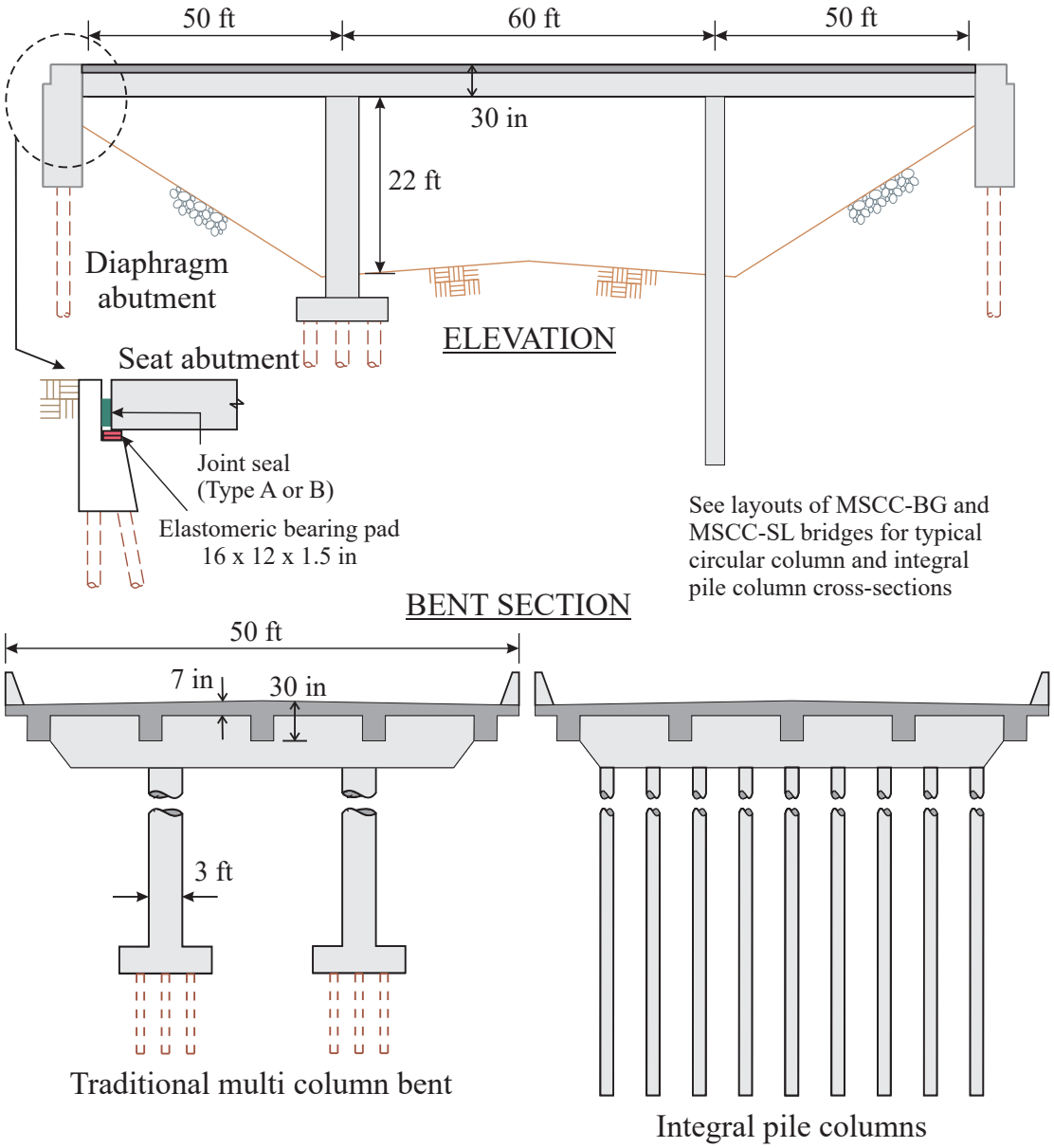

Figure 4.31: Typical layout of MSCC-TG bridges

The superstructure deck slab is 7 in thick and is supported on a series of Tee girder cast monolithic with the deck slab as shown in Figure 4.31. The girders are 12 in wide and the depth is proportioned based on the overall depth (girder depth plus slab thickness) to span ratio of 0.05. In this case, the Tee girders have a depth of 30 in. As in all the cases, the superstructure frames into the diaphragm abutments as a monolithic

connection. In the case of seat abutments, the deck slab-girder group rests on elastomeric bearing pads, (16 in × 12 in × 1.5 in) in dimension on the abutment seat. The gap between the superstructure and abutment backwall is 0.75 in. The abutment backfill soil and piles engage with the superstructure when this gap closes. As in the case of MSCC-SL bridges, review of bridge plans for MSCC-TG bridges did not reveal the presence of restrainer cables and shear keys and hence these are not considered in the bridge analytical models.

4.3.3.2. Eigen Value and Time History Analysis

Table 4.4 lists the first two modal periods for MSCC-TB bridges with diaphragm and seat abutments and MCB with circular columns. The modal periods for MSCC-TG bridges with integral pile columns is shown in Table 4.5. It is seen that bridges with integral pile columns are flexible when compared to bridges with circular columns. Further the modal periods for either pile class and pile type are very similar. Also it is seen that the fundamental periods for bridges with integral pile columns are similar for diaphragm and seat abutments, although, the second mode period differs depending on the abutment type. Further, the MSCC-SL bridges are stiffer when compared to MSCC-TG bridges (see Tables 4.3, 4.4, and 4.5).

Figure 4.32 shows the first two mode shapes for MSCC-TG with integral pile columns and MCB with circular columns having diaphragm and seat abutments. In all cases the first mode is a combination of transverse and torsional response and so is the second mode. The third mode is a longitudinal mode and the higher order modes invoke vertical and torsional response.

Table 1.4: Modal periods for MSCC-TG bridges with circular columns

Abutment type	First mode (sec)	Second mode (sec)
Diaphragm	0.55	0.31
Seat	0.61	0.58

Table 4.5: Modal periods for MSCC-TG bridges with integral pile columns

Abutment type	Pile class	Pile type	First mode (sec)	Second mode (sec)
Diaphragm	Class 45	Precast concrete	0.76	0.35
	Class 45	Precast prestressed concrete	0.75	0.35
	Class 70	Precast concrete	0.72	0.36
	Class 70	Precast prestressed concrete	0.71	0.35
Seat	Class 45	Precast concrete	0.79	0.62
	Class 45	Precast prestressed concrete	0.73	0.58
	Class 70	Precast concrete	0.78	0.63
	Class 70	Precast prestressed concrete	0.78	0.63

The typical response of circular columns and integral pile columns is similar to those shown in the previous sections. Although not shown here, it was seen that the curvature ductility of the integral pile columns was higher than that of MCB with circular columns. It should be noted that this can cause significant damage to the bridges with integral pile columns since they are brittle in nature. Further, as stated before, there has been no improvement in the pile details across the years which could render bridges with these column types more vulnerable than ductile circular columns belonging to this design era. Figure 4.33 shows a comparison between the response of typical bridge components in MSCC-TG bridges with integral pile columns and MCB with circular columns for both the abutment types.

Integral pile columns - Diaphragm abutments

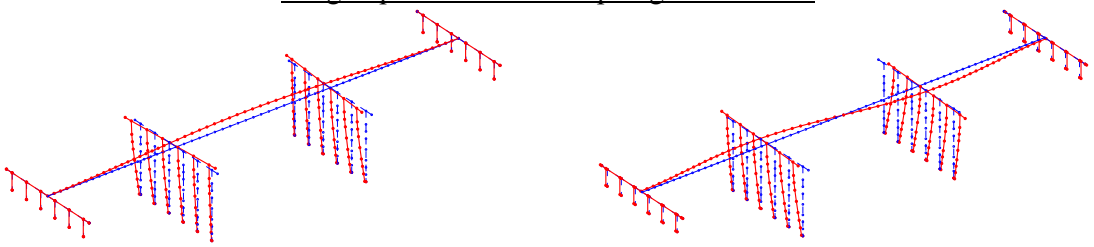

a) First mode b) Second mode

MCB with circular columns – Diaphragm abutments

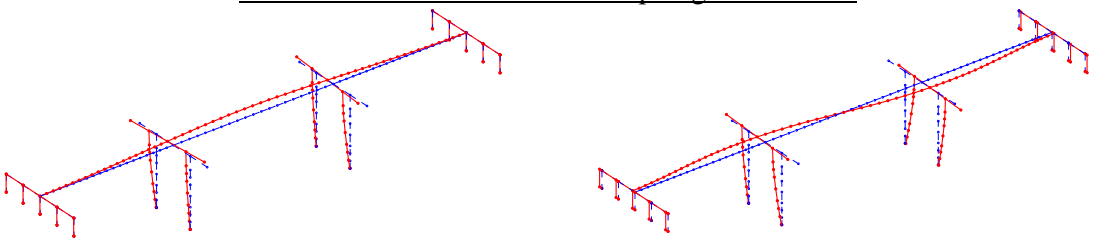

c) First mode d) Second mode

Integral pile columns - Seat abutments

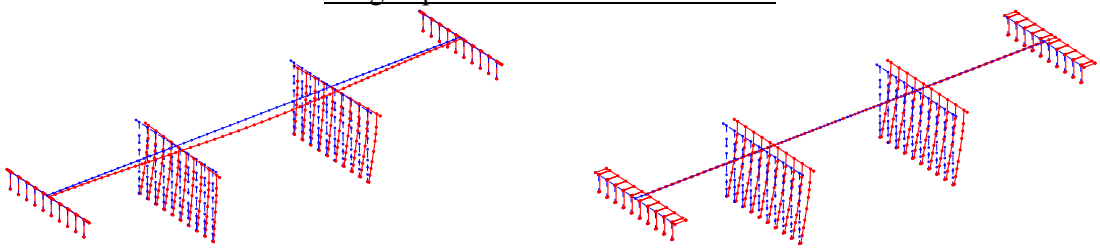

e) First mode f) Second mode

MCB with circular columns – Seat abutments

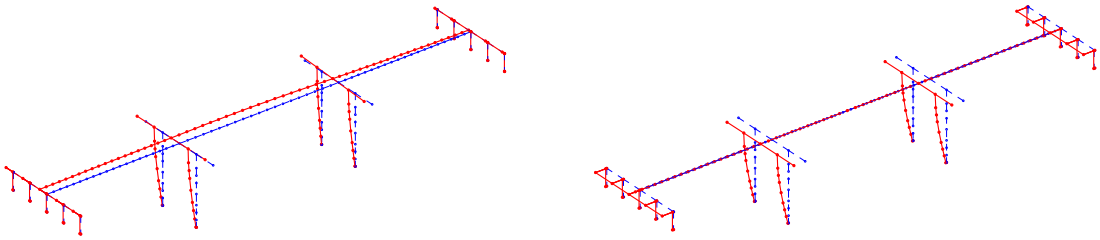

g) First mode h) Second mode

Figure 4.32: First and second mode shapes for MSCC-TG bridges

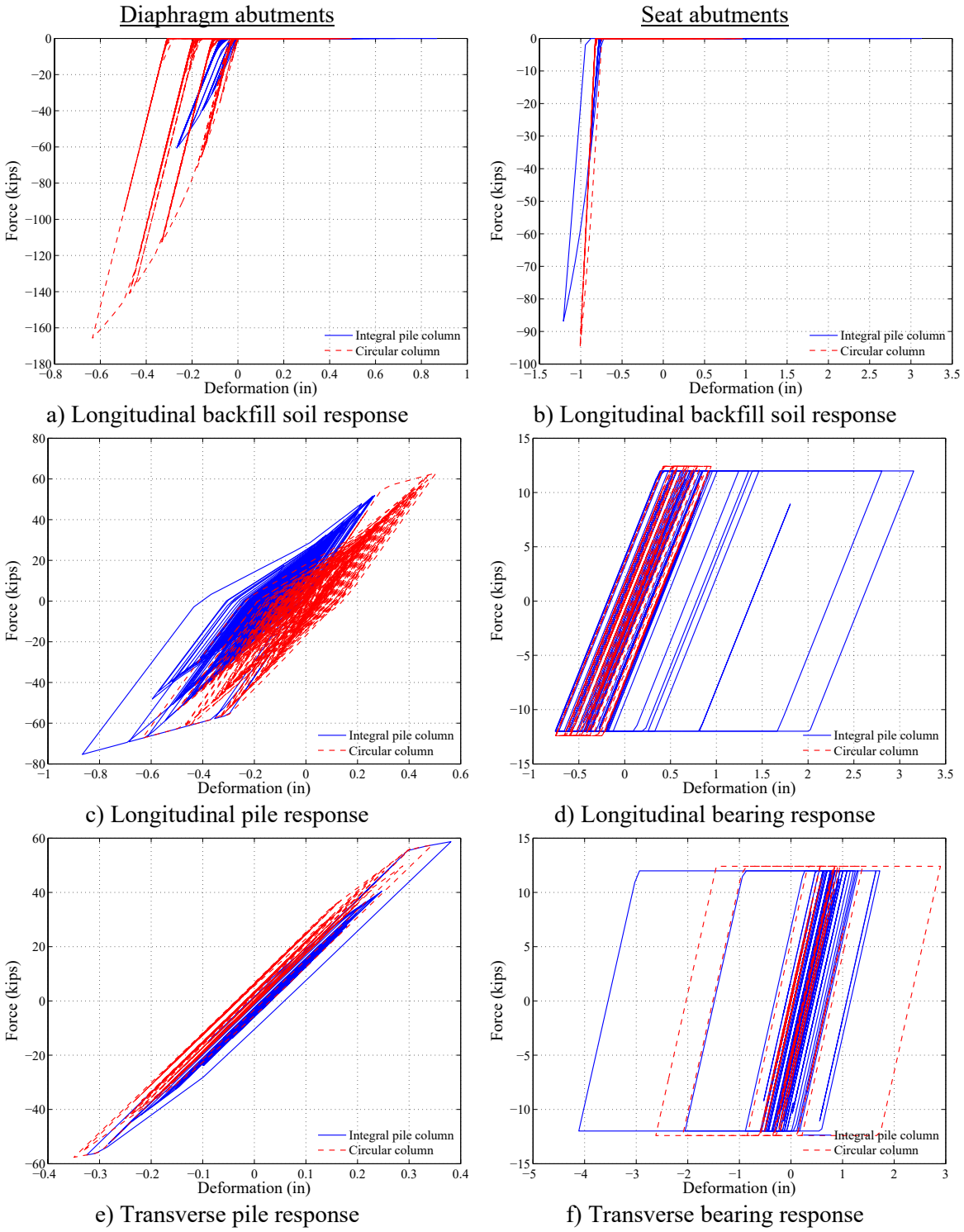

Figure 4.33: Response of components in MSCC-TG bridges with integral pile columns and circular multi column bents

The passive force and deformation response of the backfill soil in diaphragm abutments is higher for MCB with circular columns when compared to integral pile columns (Figure 4.33(a)). On the other hand, the backfill soil response is comparable for both column types in case of seat abutments as shown in Figure 4.33(b). Also, backfill soils experience greater nonlinearity and hence cause more energy dissipation in case of diaphragm abutments when compared to seat abutments. This may be attributed to the greater engagement of the superstructure and backwall in the case of diaphragm abutments when compared to seat abutments. With respect to the response of piles in the longitudinal direction in diaphragm abutments, it is seen that the active response of piles in bridges with MCB and circular columns dominates over the active response of piles in bridges with integral pile columns. However, the passive response of piles in diaphragm abutment bridges with integral pile columns is greater than that of MCB and circular columns. This is because the passive response of piles in bridges with integral pile columns takes a major share of the compressive force (Figure 4.33(c)) in contrast to the backfill soil in the case of bridges with circular MCB (Figure 4.33(a)). The behavior of piles in longitudinal direction is the opposite in the case of seat abutments. The response of piles in transverse direction is similar for both column types irrespective of the abutment type. Although the piles undergo inelasticity in the case of diaphragm abutments, they behave linearly in the case of seat abutments. The latter is expected since significant yielding of the elastomeric bearing pads is noticed in bridges with seat abutments, as shown in Figure 4.33(d) and 4.33(f).

With respect to bearings, it is seen that larger demands are imposed on the bearings in integral pile columns. This is consistent with the greater curvature ductility exhibited by the columns in these bridges which directly translates to an increased bearing displacement in the longitudinal direction (Figure 4.33(e)). In the transverse direction (Figure 4.33(f)), the bearing response is symmetric about the bridge centerline in the case of circular MCB while the bearings undergo increased nonlinearity in one

direction in bridges with integral pile columns. In other words, there is an apparent shift in the equilibrium position. This reflects the fact that significant residual displacements exist in these bridges due to the imposed ground motion.

4.3.4 Multispan Continuous Concrete I-Girder Bridges

4.3.4.1. General Layout

MSCC-IG bridges differ in response and performance when compared to MSCC-TG bridges although both bridge classes have the superstructure deck resting on girders. The fundamental differences in configuration and flow of forces were detailed in the previous sections. MSCC-IG are typically used for spans ranging between 30 ft and 150 ft and employ standard "I" and "Bulb-Tee" girders in the superstructure (see Appendix A for details). As in the case of slab and Tee girder bridges, three spans are the most likely number of spans in this case and hence three spans are considered for analytical modeling.

Figure 4.34 shows the general layout of MSCC-IG bridges. For the sake of deterministic analysis, a bridge with median value of the parameters designed in the 1971-1990 design era is considered. The center span measuring 60 ft is considered the longest and the two approach spans on either side measure 44 ft, such that the ratio of the maximum span to the approach span was found to be 1.4 based on the review of bridge plans. In general the choice and dimensions of the girder is dictated based on permissible depth-to-span ratio which is 0.05 for standard I-girders and 0.045 for Bulb-Tee girders. The deck slab is 7.5 in thick and details about Standard I- or Bulb-Tee girders can be found in Appendix A. The Standard I-girder has a flange with of 19 in and overall depth of 36 in with weight per unit run of 450 lb/ft. If Bulb-Tee girders were selected, the girder adopted would have a flange width of 48 in and overall depth of 55 in with weight per unit run of 964 lb/ft. The deterministic responses presented in this section employ

Standard I-girders in the superstructure. It must be noted that the choice of the girder type influences the mass and sectional properties (area and moment of inertia of the cross-section) of the superstructure elastic beam column elements. However, these do not affect the response of bridge components significantly since their variation is limited. The girders rest on (16 in × 12 in × 1.5 in) elastomeric bearing pads at the bent and at the seat abutments. As in all the other cases, both diaphragm and seat abutments are considered for deterministic and fragility analyses (in subsequent chapters). Both the abutment types have 6.0 ft high backwalls supported on Class 45 or 70, PC or PPC piles spaced 7 ft on center. A gap of 0.75 in is considered between the superstructure and the backwall in seat type abutments. Survey of bridge plans revealed the presence of longitudinal restrainer cables and transverse shear keys at the bent and seat abutments and these are considered in the analytical models. 14 ft long ¾ in diameter restrainer cables are considered at the seat type abutments and the bents with 0.625 in slack.

As in the case of MSCC-BG bridges, MSCC-IG bridges have SCBs and MCBs with two, three or four columns per bent. SCBs have the bridge deck slab supported on five girders and 6 ft diameter circular columns with potential plastic hinge zones at the base where the column frames into the pile cap and at the top where it frames into the bent beam. The bridge is 28 ft wide and consists of a single 22 ft tall column and the center-to-center spacing of the I-girders is 5.4 ft. The column cross-section has 72 -#11 longitudinal reinforcing bars and consists of #4 stirrups at 3 in on center. Translational and rotational springs are provided at the base of the column in the longitudinal and transverse directions to replicate the behavior of the underlying pile foundation. The stiffness of the translational and rotational springs is 1400 kip/in and 6.5×10^7 kip-in/rad, respectively.

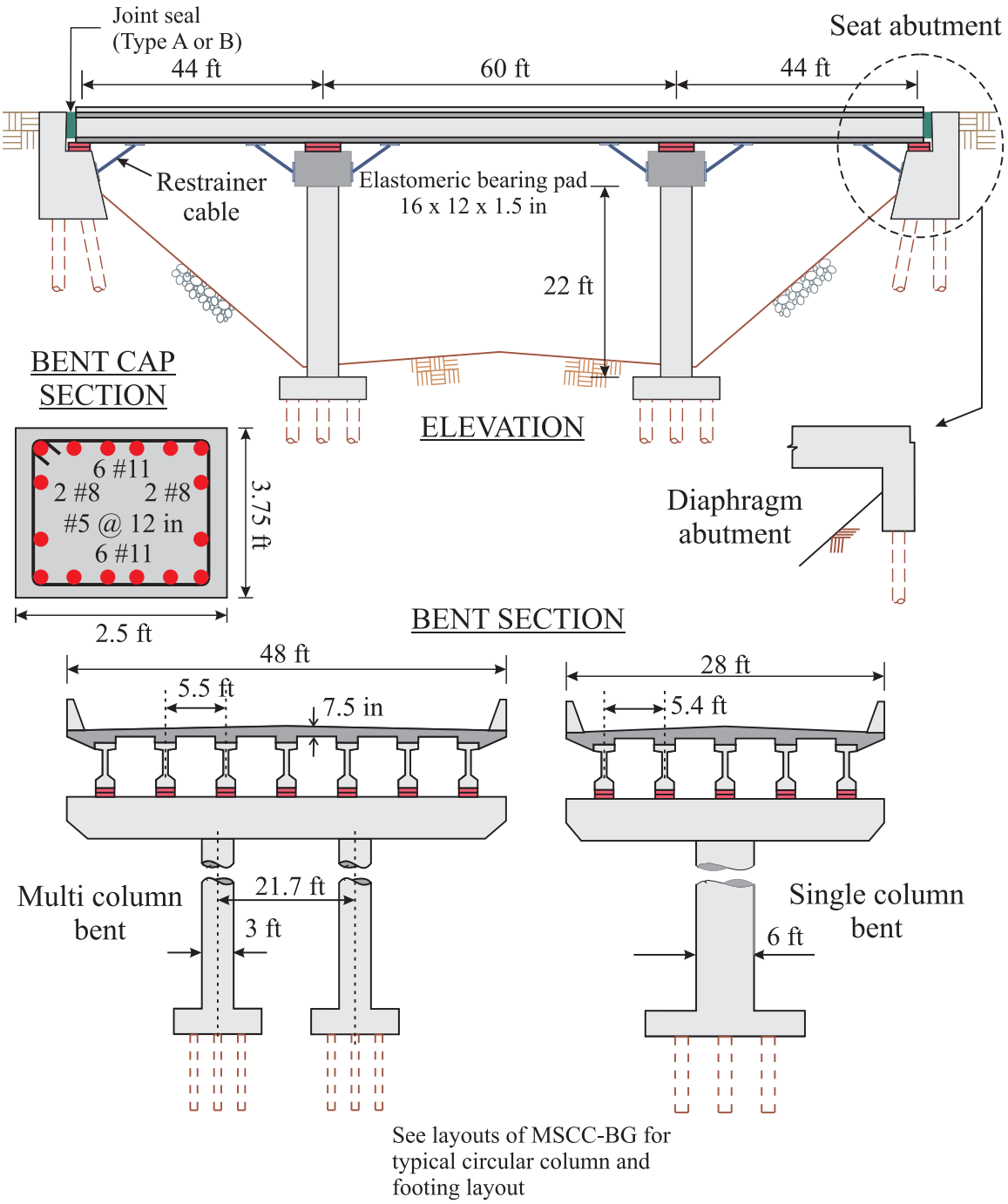

Figure 4.34: Typical layout of MSCC-IG bridges

On the other hand, the bridges with MCBs have bridge deck supported on seven girders and 3 ft diameter circular columns with 36 -#8 longitudinal reinforcing bars and

#4 stirrups at 3.5 in on center. As in the other cases, MCBs in MSCC-IG are not pinned to the base and have two translational and rotational springs of stiffness 800 kip/in and 3 × 10^7 kip-in/rad, respectively, in the longitudinal and transverse directions. In this section, the bridge has two columns in the bent with a center-to-center spacing of 21.7 ft and the bridge measures 48 ft in width, supported on seven Standard I-girders with 5.5 ft center-to-center spacing.

Unlike the previous cases where the bent is integral with the superstructure, MSCC-IG bridges have bearing supported superstructures and in this case, the columns frame into the bent beam. The bridge has a 2.5 ft × 3.75 ft rectangular bent beam reinforced with two rows of 6 -#11 bars at the top and bottom and 4 -#8 bars in the middle, as shown in Figure 4.35. The shear reinforcement consists of #5 stirrups at 12 in on center.

4.3.4.2. Eigen Value and Time History Analysis

The fundamental and second mode time periods for MSCC-IG bridges with SCBs and MCBs, diaphragm and seat abutments are indicated in Table 4.6. The results show that MCB are more flexible when compared to SCB and seat abutments are more flexible when compared to diaphragm abutments. The first two mode shapes for the cases mentioned in the Table 4.6 are shown in Figure 4.35. The fundamental mode is in the longitudinal direction for MCB irrespective of the abutment type and the second mode is in the transverse direction. However, SCBs do not have the same mode shapes for either abutment types. For diaphragm abutments, it is seen that the fundamental mode is in the transverse direction while the second mode is in the longitudinal direction. The mode shapes are reversed for SCB in bridges with seat abutments, where the fundamental mode is in the longitudinal direction and the second mode is in the transverse direction. Irrespective of the bent type, bridges with seat abutments are characterized by a longitudinal first mode and transverse second mode, as shown in Figure 4.35.

Table 4.6: Model time periods for MSCC-IG bridges with seat and diaphragm abutments

Abutment type	Number of columns	First mode (sec)	Second mode (sec)
Diaphragm	SCB	0.48	0.37
	MCB	0.57	0.42
Seat	SCB	0.68	0.57
	MCB	1.04	0.72

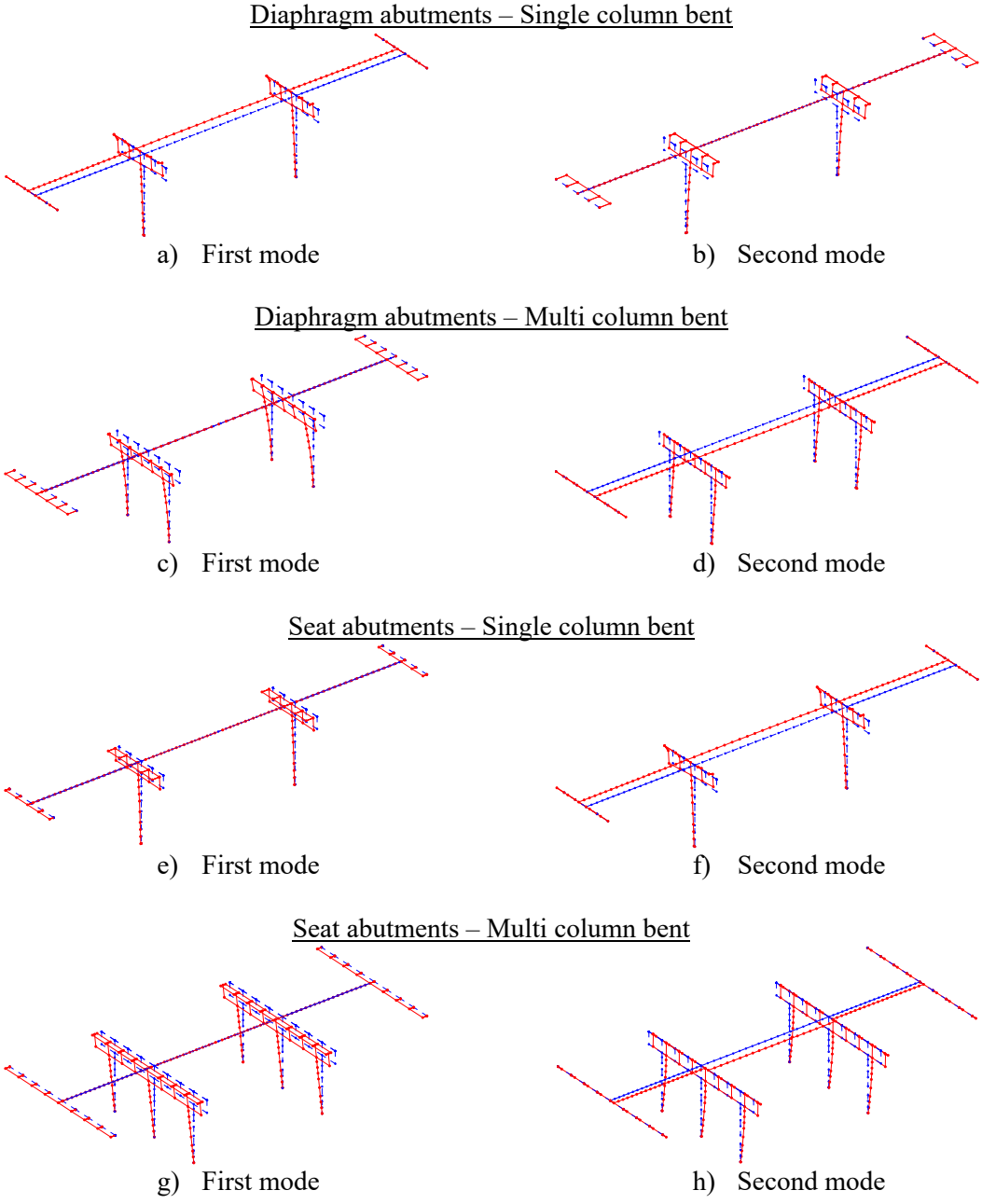

Figure 4.35: First and second mode shapes for MSCC-IG bridges with diaphragm and seat abutments

Figure 4.36 shows the variation of curvature over the height of the column for SCBs and MCBs in MSCC-IG bridges and diaphragm abutments. Clearly, the columns remain elastic under the imposed seismic load. Although not shown here, the same is observed in the case of seat abutments. Based on Figure 4.36, it can be seen that SCB are likely to develop plastic hinges at the base of the column while it is seen that the potential hinge location is at the top of the column close to the bent beam in the case of MCB.

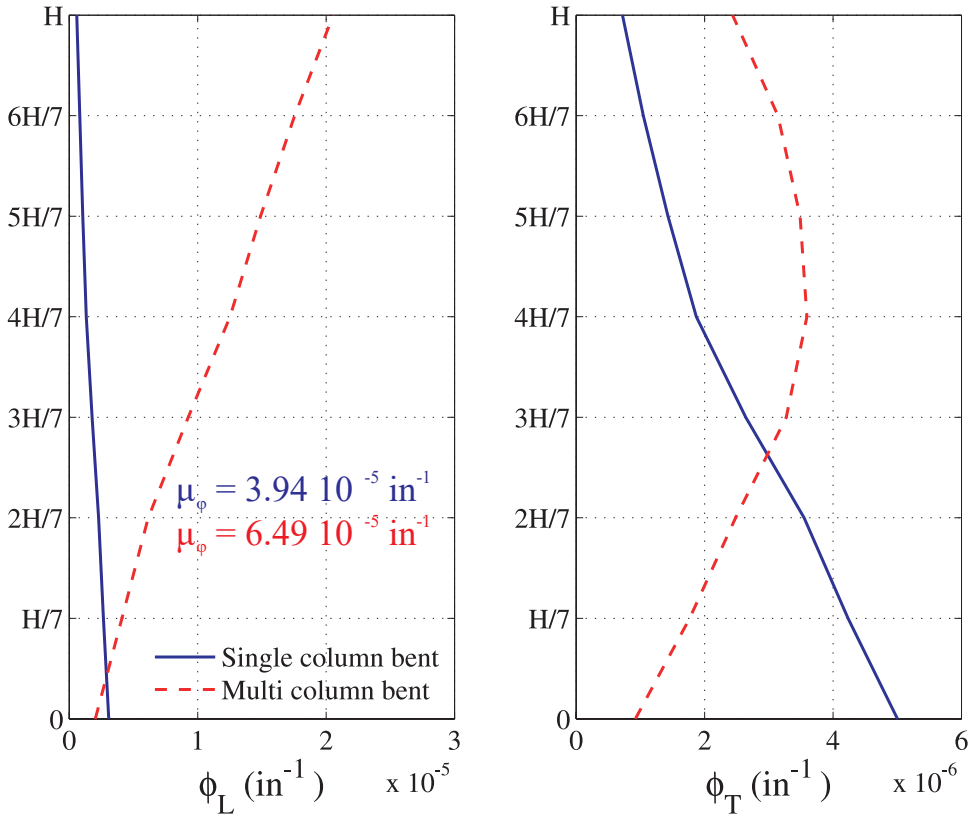

Figure 4.36: Variation of curvature over the height of the columns in MSCC-IG bridges with diaphragm abutments

The response of the abutment backfill soil and piles in the longitudinal and transverse directions for MSCC-IG bridges with diaphragm abutments, SCB and MCB bents is shown in Figure 4.37. Although a direct comparison between the responses of SCB and MCB is not possible due to differences in the bridge attributes (deck width,

number of girders etc.), qualitative comparisons are feasible. It is seen that the backfill soil in MCB undergo larger passive deformation when compared to that in the case of SCB. Both the active and passive displacement of piles is greater in the case of MCB in comparison to SCB. In the case of SCB, the piles undergo similar passive and active displacements while in the case of MCB, the passive deformation of piles is almost twice their active deformation. Further, it is seen that in the case of MCB, the piles reach their ultimate capacity in passive action and this might lead to significant damage to them and might require replacement. The transverse displacement of piles is similar in the case of both MCB and SCB and is less than the corresponding active and passive displacements. These responses are very similar in the case of seat abutments.

Single column bent

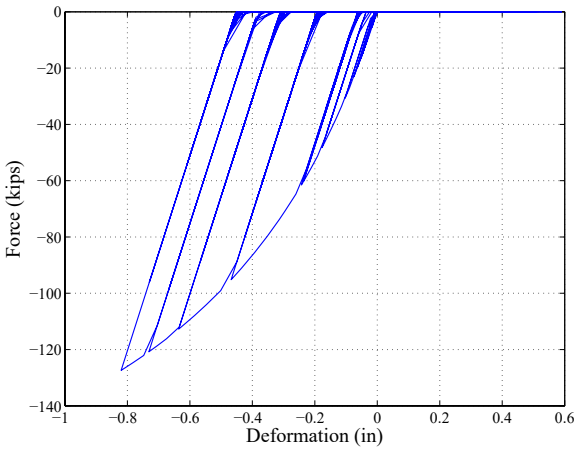

a) Abutment soil – longitudinal response

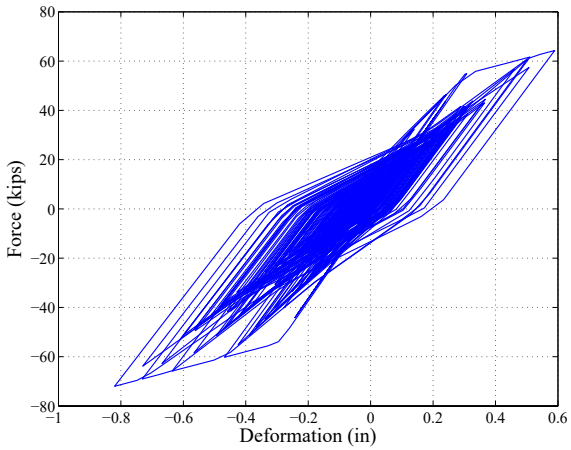

b) Longitudinal pile response

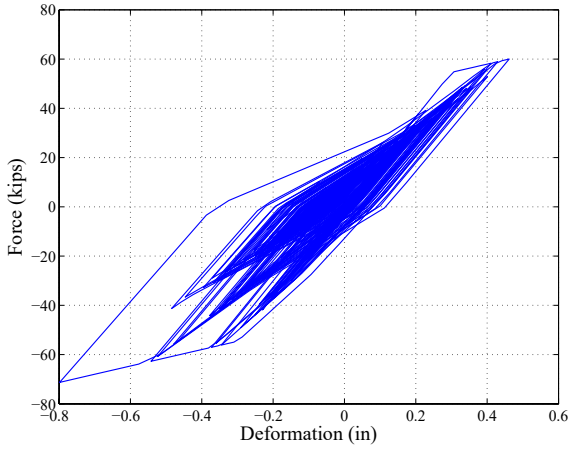

c) Transverse pile response

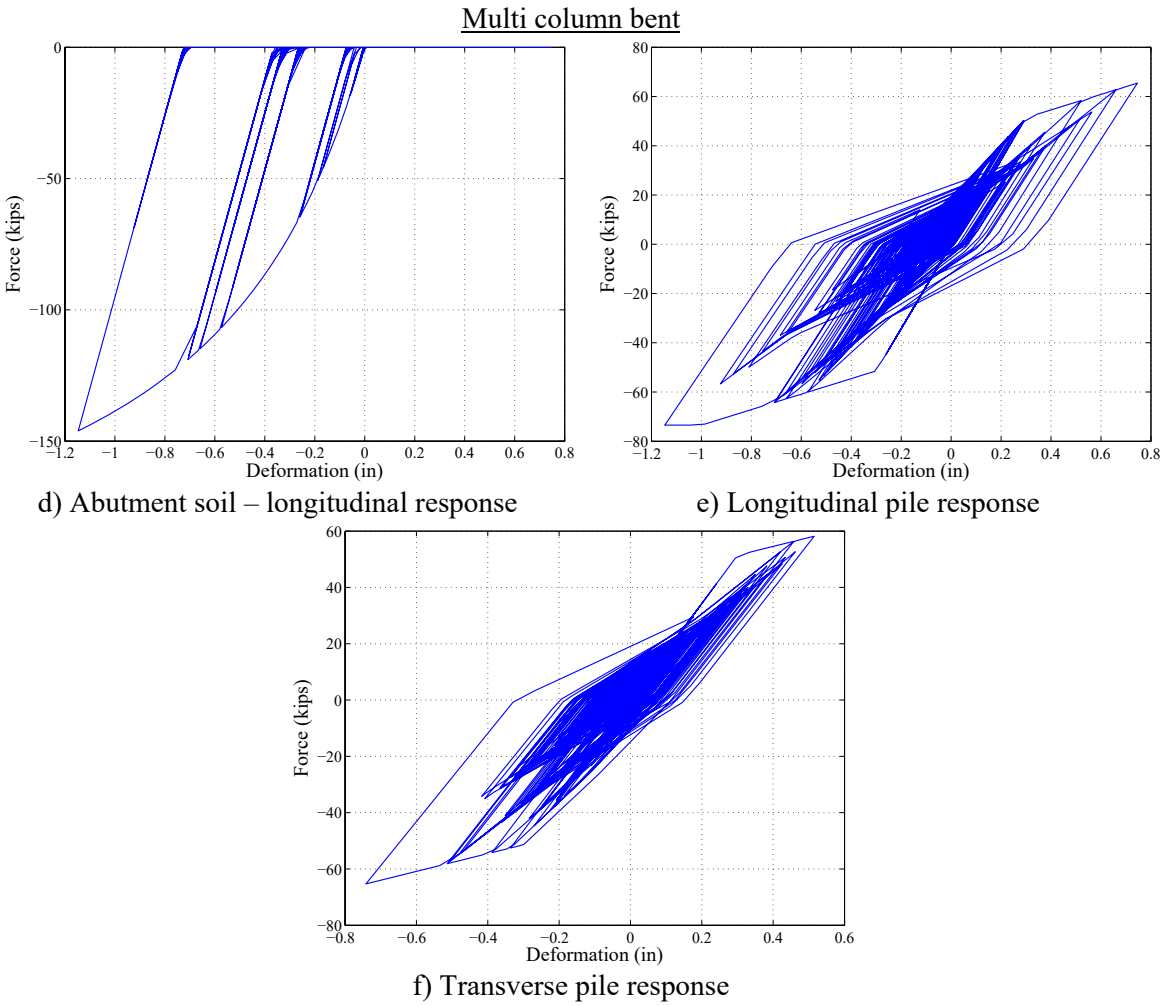

Figure 4.37: Abutment backfill soil-pile responses in longitudinal and transverse directions for MSCC-IG bridges with diaphragm abutments

The response of elastomeric bearing pads in the longitudinal direction and shear keys in the transverse directions for MSCC-IG bridges with SCB and MCB and seat abutments is shown in Figure 4.38. As in the case of abutment backfill soil and piles, elastomeric bearing pads undergo a larger displacement in the case of MCB when compared to SCB in both longitudinal and transverse directions. In the case of both SCB and MCB (Figure 4.38(a), (c)) it is seen that the bearing undergo significant yielding and might need replacement under one such scenario earthquake. Further, the ground motion used in deterministic analysis is seen to cause significant force and deformation demands

on the shear keys in the case of both SCB and MCB. The shear key is seen to be completely damaged in the case of MCB (Figure 4.38(d)). This is also reflected in the transverse response of the elastomeric bearing pad, shown in Figure 4.38(e). Initially the bearing pads are constrained by the presence of the shear keys thereby restricting their displacement to 0.75 in which is the gap present between the girder and the shear key in the transverse direction. The closure of the gap engages the shear keys leading to their eventual collapse. At this point, the bearings undergo significant deformation and the superstructure shifts transversely to a new equilibrium position, as replicated in the response of the bearings (see Figure 4.38(e)). The restrainers remain elastic at the bents and abutments in all cases.

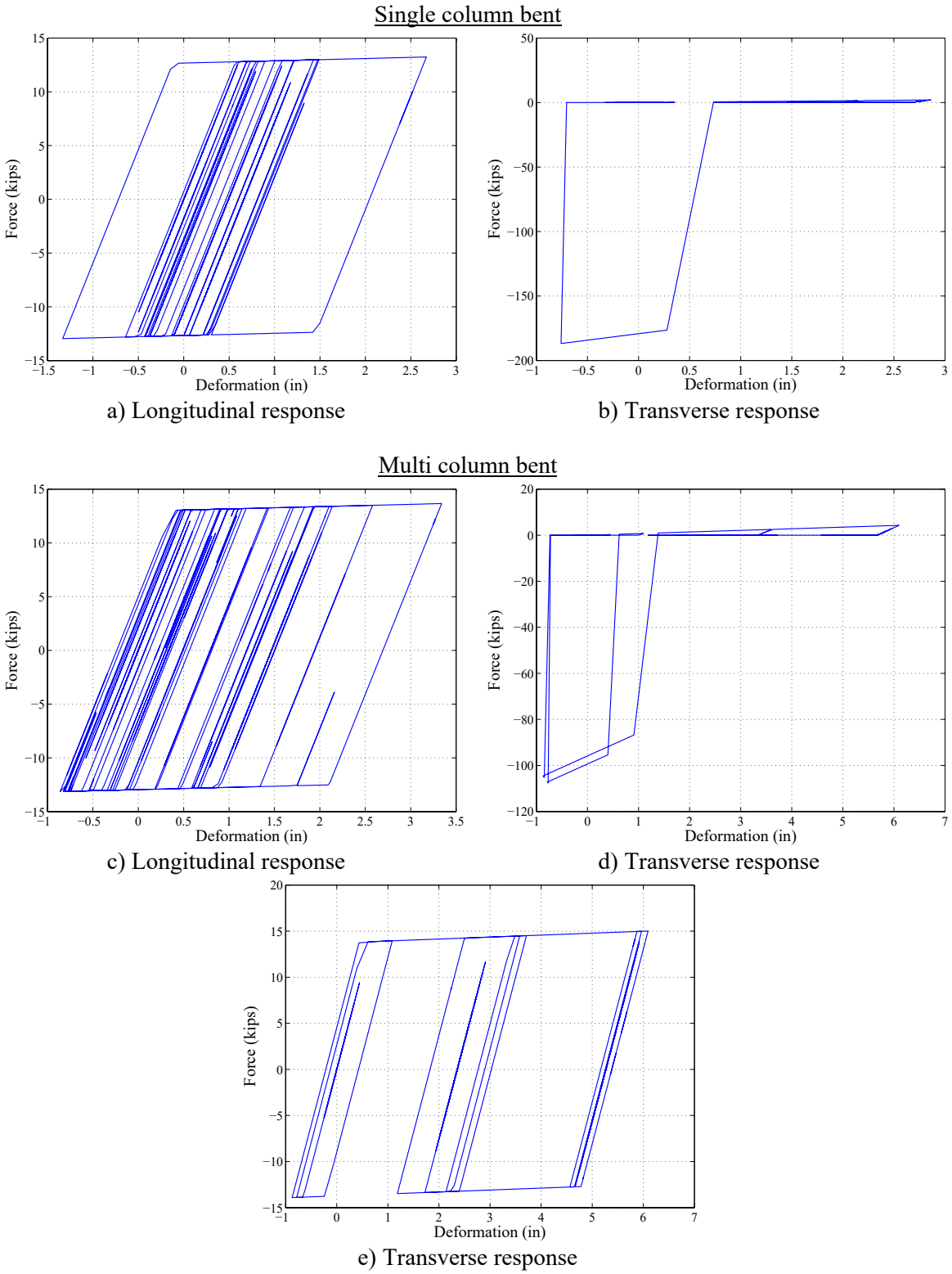

Figure 4.38: Longitudinal response of elastomeric bearing pads and transverse response of shear keys in MSCC-IG with seat abutments

4.4 Closure

In this chapter, extensive details are provided about the modeling strategies for bridge components: superstructure, single and multi column bents including columns and bent beam (wherever applicable), foundation systems, abutments including backfill soil and piles, restrainers and shear keys. These models are developed based on experimental data for the components and experience from their performance during past earthquakes. Detailed nonlinear three dimensional (3-D) analytical bridge models are created in OpenSEES by assembling the individual bridge component models.

Deterministic 3-D analytical models are developed and presented for four multispan concrete bridge classes with box-girders, slab, Tee and I-girders in the superstructure. Details are provided about the typical layout of each of these bridges across the three significant design eras considered in this study: pre 1971, 1971-1990 and post 1990 eras. Using a pair of orthogonal time histories from the PEER Transportation Systems Research Program having a moment magnitude of 7.62, hypocentral distance of 16.27 km, and peak ground accelerations of 0.96g and 0.63g, respectively, the deterministic bridge models are loaded along the two perpendicular bridge axes. The intention with presenting bridge component responses is not to facilitate drawing of conclusions, but rather pave the way for comparing the relative response of various bridge types and their components and to use it as a sanity check. A significant conclusion that can be drawn is that columns are not always the critical components as suggested in previous research in this area. It is seen that in a few bridge classes such as multispan continuous concrete I-girder bridges, columns remain elastic for the imposed seismic loading, while there is significant damage to the elastomeric bearings and shear keys. This suggests the need to consider and include multiple components in determining the vulnerability of the bridge system. The following is a brief summary of insights gained from the deterministic bridge component responses:

- **MSCC-BG bridges:** Evolution of column design philosophy is reflected in the response of bridge columns with post 1990 columns behaving in a ductile fashion when compared to their pre 1971 counterparts. Across all design eras, SCBs experience larger curvature ductility when compared to MCBs. Backfill soils and piles in diaphragm abutments experience greater nonlinearity when compared to seat type abutments. Abutments with sandy backfills exhibit larger forces and lower displacements when compared to abutments with clayey backfills. Columns in bridges with sandy backfills experience larger moments and curvatures when compared to columns in bridges with clayey backfills, thereby depicting the importance of backfill soil type on bridge component dynamic response characteristics.
- **MSCC-SL bridges:** The curvature ductility of columns in bridges with seat abutments is higher than their diaphragm counterparts. The columns in this bridge class show a tendency to undergo double curvature bending. Passive displacement of backfill soil in seat abutments is higher while the active and transverse displacement of piles is higher in the case of diaphragm abutments. The elastomeric bearing pads in seat abutments undergo significant nonlinearity in both longitudinal and transverse directions.
- **MSCC-TG bridges:** Curvature ductility of integral pile columns is higher than traditional MCBs. Passive force-deformation response of backfill soil in bridges with integral pile columns and diaphragm abutments is greater than traditional MCBs and diaphragm abutments. The backfill soil response is comparable for either bent types and seat type abutments. The elastomeric bearing pads in bridges with integral pile columns are subject to a greater demand when compared to traditional MCBs.
- **MSCC-IG bridges:** Plastic hinge tends to form at the base of the column in SCBs while they are likely to form close to the column top in the case of MCBs. The

passive deformation of the backfill soil and response of piles in all directions is higher in the case of MCBs when compared to SCBs. The same is the case with elastomeric bearing pads.

The component and system level responses presented in this chapter are for sample bridges in the bridge classes considered with typical values of the parameters. It is realized that the component responses might change as the values of the bridge modeling parameters change. A complete probabilistic evaluation will allow for the characterization and depiction of uncertainty in geometric and material parameters and will allow for drawing significant conclusions about the relative contribution of the bridge components to the overall system level performance.

CHAPTER 5

FRAGILITY FRAMEWORK

This chapter outlines the framework that will be adopted in the development of analytical fragility curves for the bridge classes considered in this study. Fragility curves provide an effective approach to compare design alternatives, particularly, the impact of evolution in design and detailing aspects by considering the vulnerability of multiple components and uncertainty in performance. The multiphase framework adopted here consists of independent assessment modules linked by pinch point variables such as intensity measures (IM) and engineering demand parameters (EDP) and is consistent with that proposed by Nielson (2005, 2007). Figure 5.1 shows a schematic of the framework and its essential components, which are listed below:

- Ground motion suite
- Stochastic finite element models
- Probabilistic seismic demand models (PSDM)
- Capacity estimates
- Fragility formulation (component and system level)

The first step is to assemble a suite of ground motions that is representative of the seismic hazard in the area of interest. The next step is to develop statistically significant and nominally identical bridge models by sampling on the structural parameters viz., material and geometric, to fully represent a wide range of bridges encompassing the bridge class considered. The stochastic finite element models and ground motions (components in two orthogonal directions) are randomly paired, and nonlinear time history analyses are performed to record the response of components that are deemed to contribute to the vulnerability of the bridge system.

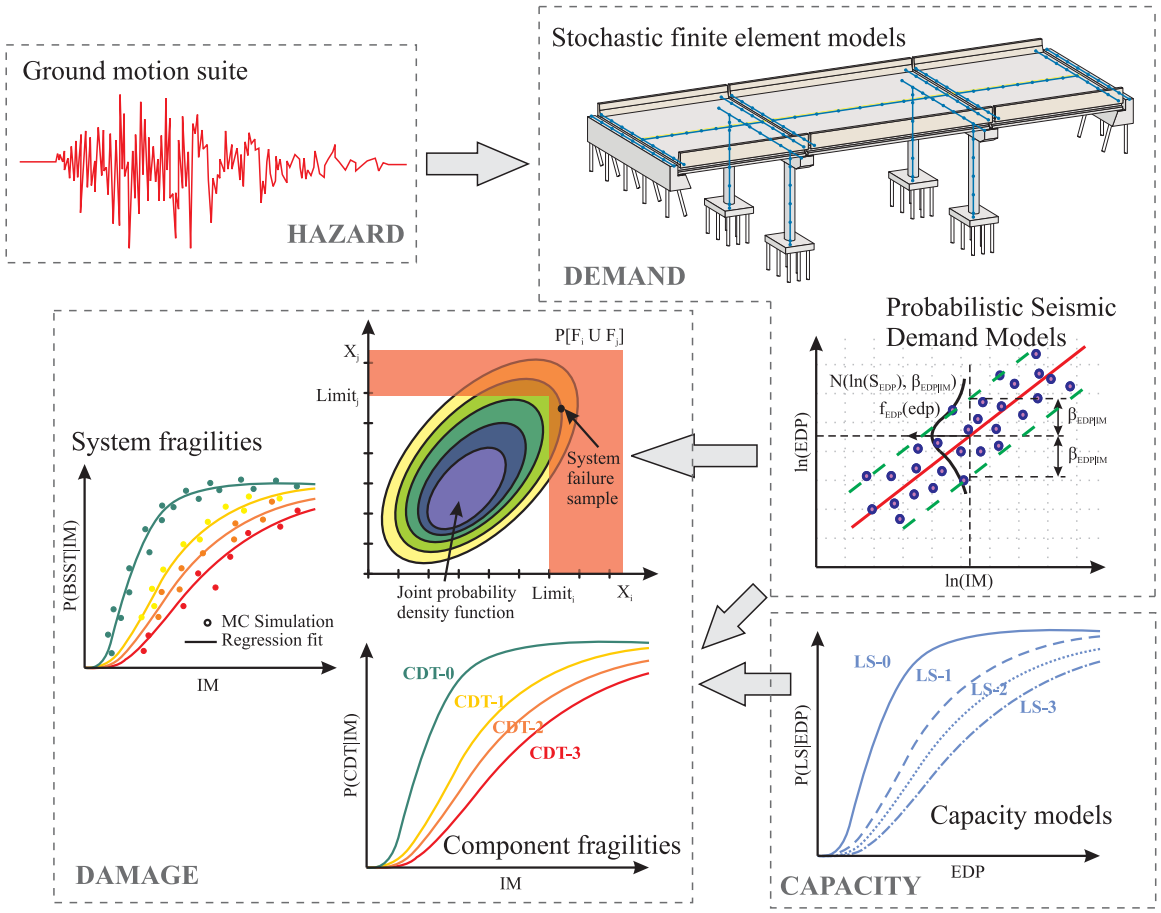

Figure 5.1: Schematic of the fragility framework

Probabilistic seismic demand models (PSDM) are developed for the component responses and this helps in establishing the "*demand*" side of the problem. The component capacities are determined based on a combination of experimental results and expert opinion involving coordination and one-on-one interaction with Caltrans maintenance and design staff, establishing the "*resistance*" side of the problem. However, probabilistic risk assessment procedures and performance based engineering, in general, are aimed at determining performance at different levels of structural capacity, each of them typically having an operational consequence or repair requirements. These are typically referred to as limit states or performance states and are quantified by values of engineering demand parameters based on experimental results or expert opinion based on

experience and observed damage during past earthquakes. Both the demand and capacity (or resistance) are assumed to be lognormal (Mackie and Stojadinovic, 2001; Cornell et al., 2002; Bazzurro and Cornell, 2002; Ellingwood and Wen, 2005; Nielson and DesRoches, 2007; Padgett et al., 2008; Celik and Ellingwood, 2010) and the component fragility can be derived using a closed form solution described in equation (5.1), where, D and C denote demand and capacity, S_D and S_C denote the median values of demand and capacity and $\beta_{D|IM}$ and β_C denote the dispersions (logarithmic standard deviation) of the demand and capacity, respectively. It must be noted that S_C and β_C are defined based on the limit state under consideration.

$$P[D > C \mid IM] = \Phi\left(\frac{\ln\left(S_D / S_C\right)}{\sqrt{\beta_{D|IM}^{\,2} + \beta_C^{\,2}}}\right) \tag{5.1}$$

In order to develop system fragility definitions, a joint probabilistic seismic demand model (JPSDM) is developed by combining the individual marginal PSDMs. It must be noted that the individual marginal demand distributions are not independent and a correlation structure is derived based on the analysis data. Realizations of the JPSDM are compared with those from the joint capacity distribution (based on the assumption of statistical independence) using Monte Carlo (MC) simulation to derive system fragility relationships. However, it should be noted that the components are combined in such a way that they have similar consequences in terms of traffic, repair, and closure implications. The subsequent sections in this chapter provide details about each part of the fragility framework. However, further details about the component and system level fragility formulation along with the results are presented in the next chapter.

5.1 Ground Motion Suite

Assembling a suite of ground motions that accurately characterizes the seismic hazard is crucial to developing fragility curves applicable to bridge classes spread over a wide geographic area. The general idea is to have a suite of ground motion time histories that cover a wide range of IMs expected in the area of interest based on seismic hazard analysis and for which the demand models and fragility curves are constructed. Another important aspect is to propagate uncertainty in the realization of other hazard characteristics such as magnitude and epicentral distance. A suite of 160 motions assembled by Baker et al. (2011) for the PEER Transportation Research Program is adopted for the fragility analysis. All of the ground motions in the suite were obtained from the PEER Next Generation Attenuation (NGA) Project ground motion library (Chiou et al., 2008) and these pertain to shallow crustal earthquakes with magnitudes ranging from 4.3 to 7.9. The Baker set consists of two sets of 120 broad-band ground motions having distribution of response spectra associated with moderately large earthquakes at small distances. Further it includes a set of 40 ground motions with strong velocity pulses characteristic of sites experiencing near-fault directivity effects. The details of the suite are as given below:

- Set 1a - Broad-band ground motions for a soil site: This set consists of 40 unscaled ground motions each selected in such a way that their response spectra match the median and logarithmic standard deviations predicted for a magnitude 7 strike slip earthquake at a distance of 10 km.
- Set 1b - Broad-band ground motions for a soil site: This set consists of 40 unscaled ground motions each selected in such a way that their response spectra match the median and logarithmic standard deviations predicted for a magnitude 6 strike slip earthquake at a distance of 25 km.
- Set 2 - Broad-band ground motions for a rock site: This set consists of 40 unscaled ground motions each selected in such a way that their response spectra

match the median and logarithmic standard deviations predicted for a magnitude 7 strike slip earthquake at a distance of 10 km.

- Set 3 – Pulse-like ground motions: This set consists of 40 unscaled ground motions containing strong strike-normal component velocity pulses of varying periods. This set helps in capturing the situations of near fault ruptures.

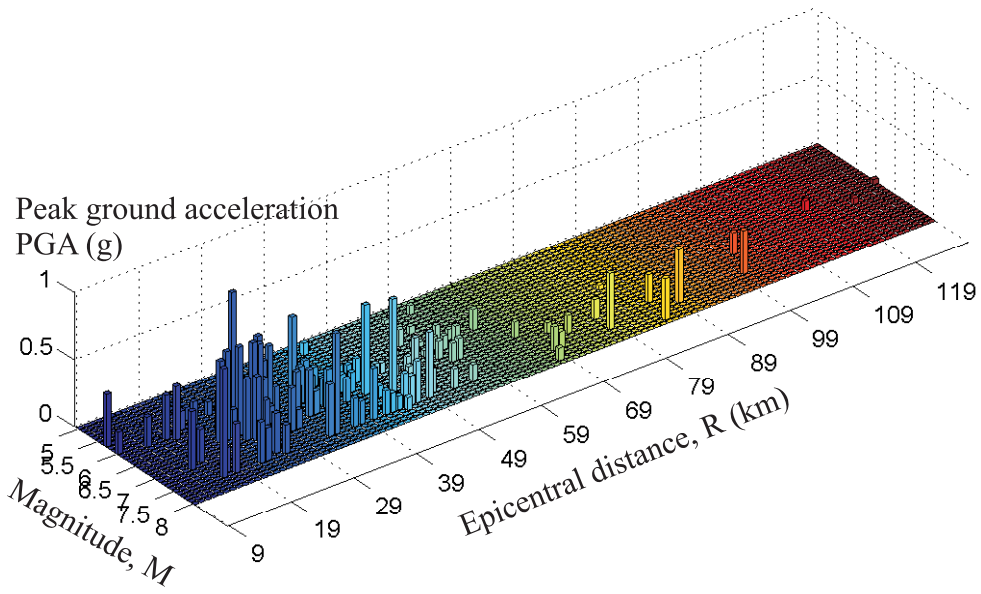

Figure 5.2: Distribution of magnitude, distance and PGA in the Baker suite of 160 ground motions (Baker et al., 2011)

Figure 5.2 shows the distribution of magnitude, distance and peak ground acceleration (PGA) for each of the 160 ground motion records in the suite. It is seen that the selected records cover a broad range of the aforementioned parameters. Based on interaction with the Caltrans design engineers (Caltrans, 2010-2012), it is noted that the highest probabilistic design hazard level in California is that corresponding to a hazard level of 10% probability of exceedance in 100 years and this is greatest for Palmdale. Figure 5.3 shows the response spectra in logarithmic scale for the unscaled records in the Baker set. Also shown is the Palmdale spectrum. The goal in selecting records for time history analyses is that the suite covers a reasonably broad range of intensity measure under consideration along with a range of spectral shapes, durations and pulse properties

that may occur in the area. However, as seen in Figure 5.2, the suite does not have a significant number of time histories in the higher range of IM of interest. Further, in order to have a sufficient number of time histories with IMs higher than the Palmdale spectrum, the entire suite of 160 motions are scaled by a factor of two and an expanded suite of 320 ground motions is used for the fragility analyses in the present study. The response spectra for the scaled ground motions are also shown in Figure 5.3. Summary data for the ground motions in the Baker suite along with significant amount of additional information, including the acceleration time history files are available on the project website: http://peer.berkeley.edu/transportation/projects/ground-motion-studies-for-transportation-systems.

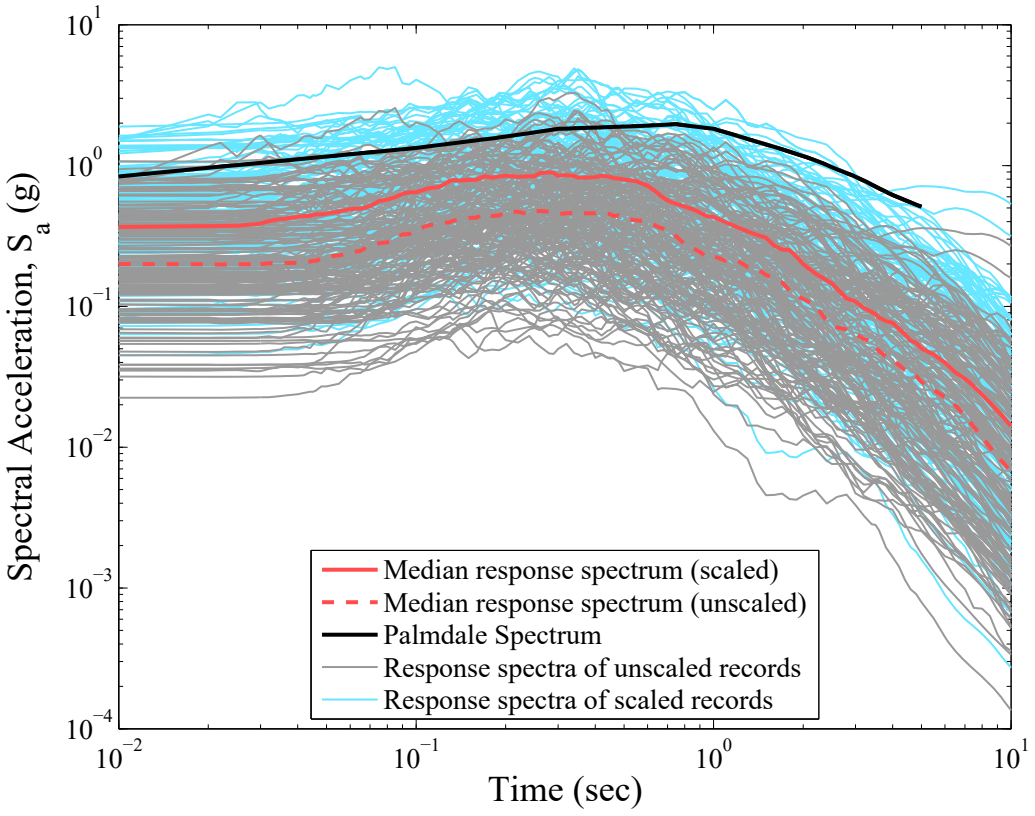

Figure 5.3: Response spectra for the scaled and unscaled ground motions in the Baker suite

5.2 Parameterized Stochastic Finite Element Models and Propagation of Uncertainty

Treatment of uncertainty in seismic reliability and performance assessment has been a subject of research for many years (Melchers, 1999; Ellingwood and Wen, 2005). Uncertainties can be classified under two main types: aleatoric and epistemic. There is inherent randomness in the occurrence of seismic events typically classified as aleatoric uncertainty. The historic data is limited and this leads to statistical error in the estimates of the aleatoric uncertainty. Further, there is uncertainty in the earthquake prediction model itself (due to limited data) and this is typically classified as epistemic uncertainty. These uncertainties do not arise as a result of the applied methodology or techniques; they reside in the historical and physical understanding of the natural processes involved. Epistemic uncertainties are fundamentally associated with the lack of knowledge and assumptions in modeling techniques and can generally be reduced with the acquisition of additional information and understanding (Ellingwood and Wen, 2005). They are present in both deterministic and probabilistic scenarios, although in the case of the former they are typically masked by factors of safety. In the case of probabilistic techniques for design and assessment, a good practice to integrate these two types of uncertainties is to present the final aleatoric frequencies with confidence bounds of epistemic uncertainties (typical of the relative frequency approach) or to integrate both of them in a single probability distribution using Bayesian techniques (Singhal and Kiremidjian, 1998; Ramanathan et al., 2012).

The uncertainty associated with the recorded ground motions in the suite is traditionally considered aleatoric in nature due to the inherent randomness in the seismological mechanisms. Uncertainty in structural geometric and material parameters is considered in this study in addition to the uncertainty from the ground motions and these are elaborated in the next section.

5.2.1 Uncertainty in Material Parameters

5.2.1.1 Concrete Compressive Strength and Reinforcing Steel Yield Strength

The bridge classes considered in this study use concrete as the construction material and the cast-in-place concrete used in bridge construction in California typically has design strength of 5000 psi at 28 days. Following the recommendations of Choi (2002), the compressive strength of concrete is modeled using a normal distribution with mean value, μ_{fc}, of 5000 psi and standard deviation, σ_{fc}, of 627 psi. Ellingwood and Hwang (1985) indicated that the yield strength, f_y, of Gr. 60 (f_y = 60 ksi) follows a lognormal distribution with the following parameters: median, λ = 4.21 ksi, and coefficient of variation, ζ = 0.08. These parameters are adopted in the present study to model the distribution of yield strength of the reinforcing bars.

5.2.1.2 Elastomeric Bearing Pad Attributes

All of the bridge classes considered in this study use elastomeric bearing pads at the seat abutments which consist of rubber pads that transmit forces by friction. In the case of MSCC-IG bridge class, the girders sit on bearing pads at the bents in addition to their presence at seat abutments. Caltrans (MTD 7-1, 1994) recommends the usage of rubber pads with a shear modulus, G, of 169 psi in the design of elastomeric bearing pads. Previous research (Lindley, 1992; Mtenga, 2007) showed variability in the shear modulus of bearing pads and further indicated strong correlation with the hardness of the material. Mtenga (2007) presented a range of G values for the bearing pads as a function of hardness and this range is used in this study. Since sufficient information is not available on the probability distribution of the shear modulus, a uniform distribution is assumed with lower and upper limits set at 80 ksi and 250 ksi, respectively. The shear modulus is used to determine the stiffness of the bearing pads for a given dimension.

The coefficient of friction, μ, is another key parameter that defines the response of the elastomeric bearing pads. An empirical expression (see equation (4.4)) is used for determining μ as a function of the normal stress, and to account for uncertainty in μ, a multiplication factor (MF) is considered. A lognormal distribution is assumed for the MF based on the recommendations of Mander et al. (1996) and Dutta (1999) with a median value, λ, of zero and logarithmic standard deviation, ζ of 0.10.

5.2.2 Uncertainty in Geometric and Structural Parameters

The distributions for geometric and structural parameters are mostly derived from the NBI and are based on review of a significant number of plans pertinent to bridges across design eras for the bridge classes considered in this study.

5.2.2.1 NBI based Bridge Geometric Parameters

Empirical distributions for bridge geometric parameters such as maximum span length, deck width, and column height were presented in Section 3.3 of Chapter 3. Although NBI provides information on the number of spans and probability mass functions were derived and presented in Chapter 3, this study uses the mode statistic for the number of spans due to the complexity involved in parameterizing this variable. The median value modification factor prescribed in HAZUS-MH (2011) is recommended to be used to determine fragilities for bridges with spans not equal to the mode statistic adopted here.

5.2.2.2 Abutment Backwall Height

Most of the structural parameters are attributed to uniform distribution due to a lack of significant data or information that can be used to associate a distribution of any other type. Based on the review of bridge plans, the height of the backwall in the case of diaphragm and seat abutments is assumed to be uniformly distributed between 3.5 ft and 8.5 ft.

5.2.2.3 Column Reinforcement Ratios

The longitudinal and transverse reinforcement ratios in the bridge columns are sampled from uniform distributions with limits established based on the review of bridge plans. Table 5.1 details the parameters of the uniform distribution describing the longitudinal and transverse reinforcement ratios. In the pre 1971 design era, the transverse reinforcement consists of #4 stirrups at 12 in on center, which was a common standard irrespective of the column size or reinforcement. Hence this parameter was not varied in the simulations for the bridges in this design era. Further, MSCC slab bridges employ integral pile columns whose cross-section is standard and hence the reinforcement is not varied in this case.

Table 5.1: Distributions for longitudinal and transverse reinforcement ratios in bridge columns

Bridge class	Design era	Longitudinal reinforcement ratio		Transverse reinforcement ratio	
		u_1*	u_2*	u_1*	u_2*
MSCC-BG	Pre 1971	1.4	2.4	N.A.	N.A.
	1971-1990	1.0	3.7	0.30	0.90
	Post 1990	1.0	3.5	0.40	1.70
MSCC-IG	Pre 1971	1.08	3.61	N.A.	N.A.
	1971-1990	1.18	5.31	0.31	1.07
	Post 1990	1.49	5.35	0.31	1.61
MSCC-TG	Pre 1971	1.08	3.61	N.A.	N.A.
	1971-1990	1.18	5.31	0.31	1.07
	Post 1990	1.49	5.35	0.31	1.61

*u_1, u_2 are the parameters describing a uniform distribution representing lower and upper bounds.

5.2.2.4 Gaps

The gap between the superstructure and abutment backwall is assumed to be uniformly distributed. As mentioned in Section 3.5.6 of Chapter 3, the gap uniformly ranges between 0 and 1.5 in across all bridge classes and design eras. However, in the case of the MSCC-BG bridges, simulations are performed for two ranges of gap sizes: smaller gaps uniformly distributed between 0 and 1.5 in and larger gaps uniformly distributed between 1.5 in and 6.0 in. Further, the transverse gap between the

superstructure and shear keys is assumed to be uniformly distributed between 0 and 1.5 in for the case of MSCC-BG and MSCC-IG bridge classes.

5.2.2.5 Restrainer Attributes

The length and initial slack of the restrainer cables are assumed to be random variables sampled from uniform distributions. The length of the cables is bounded between 8 ft and 20 ft and samples are drawn at 2 ft increments. The initial slack is sampled from a uniform distribution bounded between 0.25 in and 1.0 in.

5.2.2.6 Pile Effective Stiffness

Piles form an integral part of the foundation system beneath the abutments. Translational springs characterizing by the pile stiffness are provided in the longitudinal and transverse directions at the abutments. As stated in previous chapters, piles could be of many different types such as driven steel H section piles, CIDH concrete piles, PC piles or PPC piles. Based on input from the Caltrans design engineers (Caltrans, 2010-2012), the stiffness of the piles is assumed to follow a lognormal distribution with a logarithmic standard deviation, ζ, of 0.3. The median value is taken as 65 kips/in for steel H sections and 80 kips/in for all of the aforementioned concrete piles. It should be noted that the stiffness adopted here is much higher than the 40 kip/in value used in previous studies (Choi, 2002; Nielson, 2005; Padgett, 2007).

5.2.2.7 Foundation Translational and Rotational Spring Stiffnesses

The soil profile changes vastly over a wide geographic area and the stiffness of the foundation translation and rotational springs depends on the soil profile at a particular location. In order to obtain realistic estimates of bridge performance within a class, it is imperative to capture a wide range of soil profiles. Other factors such as the type of foundation system (see section 3.5.5), end conditions of the columns (pinned vs. restrained) and column details (size and reinforcement) affect the stiffness of the

foundation springs. Appendix A documents the different soil profiles considered in this study along with details of the common foundation systems. The different foundation systems and the soil profiles are modeled and analyzed in LPILE (2012) using substantial input from Shantz (2011) and Table 5.2 summarizes the parameters for the truncated normal distribution describing the stiffness of the foundation translation and rotational springs.

5.2.2.8 Other Bridge Structural Attributes

Several other attributes are uniformly distributed between the simulations such as type of backfill soil: sand versus clay; pile class: Class 45 versus Class 70; pile type: PC versus PPC piles. The type of backfill soil affects the hyperbolic force deformation response of the abutment in terms of the initial stiffness, ultimate strength and the deformations. The class and type of pile dictates the pile geometry and reinforcement details (amount and layout) and therefore affects the strength and stiffness characteristics. The type of girder (Standard I- versus Bulb-Tee) is also assumed to be uniformly distributed among the simulations due to their existence in the California bridge inventory. The type of girder affects the deck geometric properties such as cross-sectional area, moment of inertia and the mass.

Table 5.2: Probability distributions for foundation translational and rotational spring stiffnesses

Foundation type	Bridge class	Distribution type	Translational spring stiffness (kip/in)			Rotational spring stiffness (kip-in/rad)		
			μ	σ	μ_L	μ	σ	μ_L
Pile extension 16 in dia integral pile column	MSCC-SL, MSCC-TG	Truncated normal*	30	20	2	8×10^4	3×10^4	2×10^4
Pile shafts								
6ft dia – 1% long. steel – Fixed top	MSCC-BG	Truncated normal	600	350	100	5×10^6	3×10^6	0
6ft dia – 1% long. steel – Free top	MSCC-IG	Truncated normal	250	125	50	7×10^6	2×10^6	3×10^6
6ft dia – 3% long. steel – Fixed top	MSCC-BG	Truncated normal	700	400	200	6×10^6	4×10^6	0
6ft dia – 3% long. steel – Free top	MSCC-IG	Truncated normal	300	150	80	1×10^7	3×10^6	5×10^6
8ft dia – 1% long. steel – Fixed top	MSCC-BG	Truncated normal	900	500	200	6×10^6	4×10^6	0
8ft dia – 1% long. steel – Free top	MSCC-IG	Truncated normal	400	200	80	1.4×10^7	4×10^6	7×10^6
8ft dia – 3% long. steel – Fixed top	MSCC-BG	Truncated normal	1300	600	250	7×10^6	5×10^6	0
8ft dia – 3% long. steel – Free top	MSCC-IG	Truncated normal	500	250	100	2.3×10^7	7×10^6	1×10^7
Pile group – pile cap and piles								
6ft dia column – 1% long. steel	MSCC-IG, MSCC-BG	Truncated normal	1700	800	400	4.1×10^7	1.2×10^7	2.2×10^7
6ft dia column – 3% long. steel	MSCC-IG, MSCC-BG	Truncated normal	1400	600	600	6.5×10^7	1×10^7	5×10^7
3ft dia column – 1.5% long. steel	MSCC-IG, MSCC-BG, MSCC-TG	Truncated normal	800	600	175	0	0	0

*μ and σ represent the mean and standard deviation for the normal distribution and μ_L denotes the truncation limit

5.2.3 Uncertainty in Other Parameters

5.2.3.1 Mass

Mass factor is a parameter used to capture the uncertainty in mass from incidental sources and is applied as a factor to modify the mass of the superstructure. It should be noted that the mass factor does not account for the variations due to changes in bridge geometric parameters such as span length, deck width, column height etc., which are explicitly accounted for in the analytical modeling procedure. Various incidental sources accounting for the mass factor include the presence of parapets and barrier rails, variable deck slab thickness, electric poles and other equipment, re-pavement procedures, variation in the material densities etc. The mass factor is assumed to be uniformly distributed with bounds of 1.1 and 1.4. The bounds are established by estimating the additional mass observed from the review of bridge plans.

5.2.3.2 Damping

The recommendations of Fang et al. (1999) for tall buildings are extended to bridges (Nielson, 2005; Padgett, 2007) and the uncertainty in damping is modeled using a normal distribution. Bavirisetty et al. (2003) estimated the 2^{nd} and 98^{th} percentile of damping ratio in bridges to be 0.02 and 0.07 respectively and using these recommendations, the damping ratio is sampled from a normal distribution with mean, μ, of 0.045 and standard deviation, σ, of 0.0125.

5.2.3.3 Direction Factor

Previous studies (Nielson, 2005; Padgett, 2007; Ramanathan et al., 2010) considered the angle of incidence of the seismic load as a uniform random variable. However, recent studies by Mackie et al. (2011) demonstrated the negligible effect of the angle of incidence on the mean ensemble response of bridge components. Hence, the

incidence angle is not considered as a major source of uncertainty in this study. However, the fault normal and fault parallel components of the ground motion are randomly applied along the longitudinal and transverse axes of the bridge i.e., 50% of the simulations have the fault normal component applied along the longitudinal bridge axis while 50% of the simulations have the fault parallel component applied along the longitudinal axis.

5.2.4 Parameterized Stochastic Bridge Models

The previous sections listed the parameters that are varied to capture uncertainty in the bridge class attributes along with the suite of ground motions across the three significant design eras. Statistically significant yet nominally identical 3-D bridge models are developed by sampling across the range of parameters listed previously using Latin Hypercube Sampling (LHS) (McKay et al., 1979). LHS provides an effective scheme to cover the probability space of the random variables when compared to pure random sampling using naïve Monte Carlo Simulation (Celik and Ellingwood, 2010). Figure 5.4 shows a schematic of the procedure adopted to capture the demands in bridge components due to the imposed seismic hazards. One hundred and sixty analytical bridge models are generated consistent with the number of unscaled ground motions in the Baker suite and these are then paired randomly to create a bridge model-ground motion pair. The same bridge models are used for the suite of ground motions scaled by a factor of two. In each case, NLTHA is performed and the peak component demands are recorded to derive the relationship between the peak demands and the ground motion intensity measure, which is described in the next section.

The study considers the vulnerability of multiple components. The components of interest are columns, abutment seat (seat type abutments), elastomeric bearings, joint seal, restrainer cables, deck displacement, foundations, abutments, and shear keys. The response of the aforementioned components are recorded and the engineering demand parameters (EDP) representing the component responses are indicated in Table 5.3.

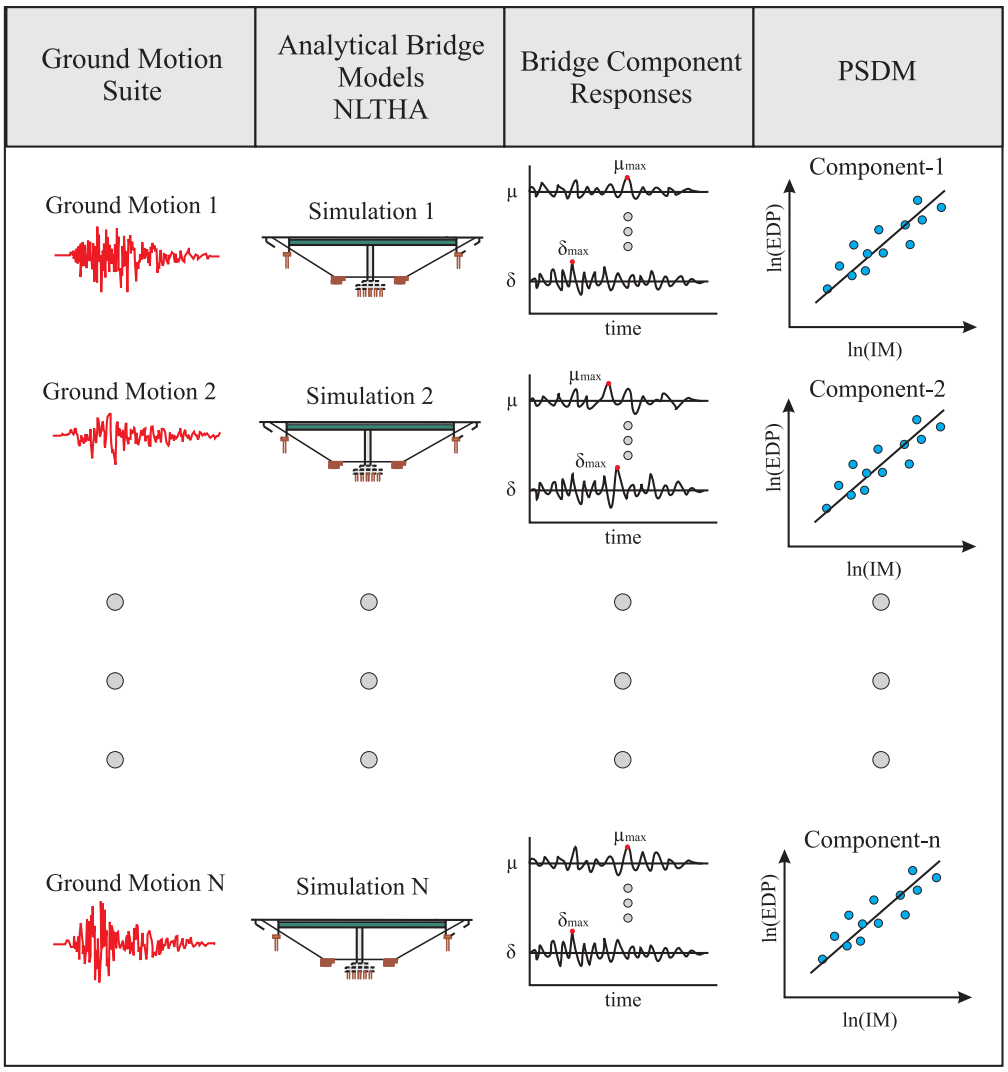

Figure 5.4: Schematic representation of the NLTHA procedure to derive peak component demands

Table 5.3: Engineering demand parameters for bridge components monitored in NLTHA

Component	Engineering demand parameter	Notation	Units
Columns	Curvature	φ	1/inch
Abutment seat	Displacement	δ_{seat}	Inches
Joint seal	Displacement	δ_{seal}	Inches
Elastomeric bearing pads	Displacement	δ_{brng}	Inches
Restrainer cables	Displacement	δ_{rest}	Inches
Deck	Displacement	δ_{deck}	Inches
Foundation translation	Displacement	δ_{fnd}	Inches
Foundation rotation	Rotation	θ_{pile}	Radians
Passive abutment displacement	Displacement	δ_p	Inches
Active abutment displacement	Displacement	δ_a	Inches
Transverse abutment displacement	Displacement	δ_t	Inches
Shear key	Displacement	δ_{key}	Inches

5.3 Probabilistic Seismic Demand Models

Probabilistic seismic analysis of structures involves the construction of seismic demand models, often stated as probabilistic models of structural response conditioned on a seismic intensity measure (IM). Demand models are probability distributions of structural demand conditioned on the IM, known as Probabilistic Seismic Demand Models (PSDMs). The seminal work by Cornell et al. (2002) formulated the conditional seismic demand-IM relationship, referred to as the PSDM, in terms of a two parameter lognormal distribution as in equation (5.2). This form and the one expressed in equation (5.3) have been readily adopted for bridge component probabilistic seismic demand analysis.

$$P[D \geq d \mid IM] = 1 - \Phi\left(\frac{\ln(d) - \ln(S_D)}{\beta_{D|IM}}\right) \tag{5.2}$$

In equation (5.2), $\Phi(\bullet)$ is the standard normal cumulative distribution function, S_D is the median value of the demand in terms of an IM, and $\beta_{D|IM}$ is the lognormal standard deviation, commonly referred to as the dispersion. The relationship between the median demand and IM was expressed in the power form given in Equation 5.3 as below,

$$S_D = a(IM)^b \tag{5.3}$$

Equation (5.3) can be expressed in the transformed space, shown in equation (5.4), where the model parameter $\ln(a)$ is the vertical intercept and the parameter b is the slope. They can be obtained by performing a linear regression analysis.

$$\ln(S_D) = \ln(a) + b \cdot \ln(IM) \tag{5.4}$$

The development of PSDMs in the case study presented herein involves subjecting a set of 3-D analytical bridge models to a suite of N ground motions and recording the peak demand measures, for instance, column curvature ductility, bearing

and abutment deformations. The median demand, as mentioned previously can be expressed as in equation (5.3) and the dispersion can be estimated based on equation (5.5).

$$\beta_{D|IM} \cong \sqrt{\frac{\sum\left(\ln\left(d_i\right)-\ln\left(aIM^{b}\right)\right)^2}{N-2}} \tag{5.5}$$

It must be noted that the characterization of median demand using a power-law formulation and constant dispersion are assumptions that are often made but are not necessarily the only possible models to express seismic demand as a function of an IM. However, these representations have been used widely and have been shown to perform very well (Mackie and Stojadinovic, 2001; Cornell et al., 2002; Bazzurro and Cornell, 2002; Ellingwood and Wen, 2005; Nielson and DesRoches, 2007; Padgett et al., 2008; Celik and Ellingwood, 2010; Ramanathan et al., 2012). Figure 5.5 shows a typical PSDM illustrating all the parameters involved in its description. The PSDMs for bridge components for various bridge classes across the design eras are presented in Appendix B.

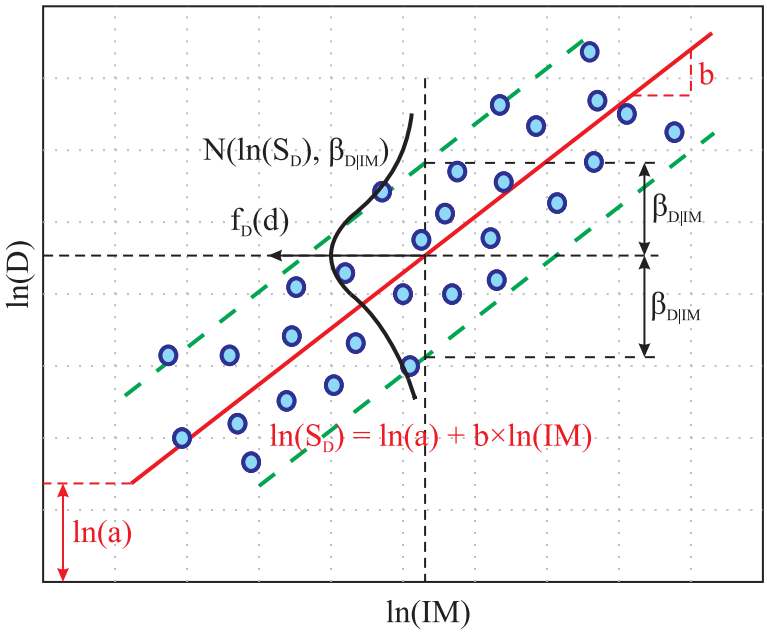

Figure 5.5: Illustration of a typical PSDM

Based on the formulations presented in equations (5.2) through (5.5) it is evident that the selection of an optimal IM can pay a predominant role on the accuracy of the model in estimating seismic demand. Their optimal selection is instrumental to obtain reasonable estimates of the vulnerability of various components as the uncertainty associated with the demand is dependent on the variable chosen as an IM to some extent, although this is not the only source of the uncertainty. Spectral acceleration at 1.0 sec, $S_a(1.0)$ is chosen as the IM in this study and the next section illustrates and substantiates the choice of $S_a(1.0)$ as the optimal IM.

5.4 Choice of an Optimal Intensity Measure

5.4.1 Introduction and Characteristics of an Optimal Intensity Measure

Probabilistic seismic demand models provide the first step in developing fragility curves, which are conditional probability statements of the likelihood that the structure will meet or exceed a specified level of damage for a IM. As stated previously, a PSDM is a conditional statement of the probability that a component experiences a demand for a given IM level, illustrating the importance of the IM as a conditional parameter in the probabilistic model. Their optimal selection is instrumental in obtaining reasonable estimates of the vulnerability of various components as the uncertainty associated with the demand model is dependent in part on the variable chosen as an IM.

Several researchers have explored the issue of selection of IMs. The Applied Technology Council report, ATC-13 (1985) uses the Modified Mercalli Scale as the IM while the more recent ATC documents such as ATC-63/FEMA P695 (2008), use S_a at the fundamental period of the structure as their preferred IM. The risk assessment software package, HAZUS-MH (2011) uses peak ground acceleration (PGA), peak ground displacement (PGD) and $S_a(1.0)$. Luco and Cornell (2007) proposed the use of structure specific IMs and showed that S_a at the fundamental period of the structure, T_1, $S_a(T_1)$,

performs very well. An IM that takes into account the second mode frequency content and inelasticity was also proposed and tested and was found to satisfy the essential characteristics of an IM (Luco and Cornell, 2007). Bazzurro and Cornell (2002) and Shome and Cornell (1999) proposed a vector IM comprised of $S_a(T_1)$ and the spectral acceleration ratio, $S_a(T_2)/S_a(T_1)$, where T_2 is the second mode period of the structure. They also considered a scalar IM that combines $S_a(T_2)$ and $S_a(T_1)$. Baker and Cornell (2005) also proposed a vector valued IM comprising of $S_a(T_1)$ and a second parameter which would either be the magnitude, distance or epsilon associated with the ground motion. It was also shown that epsilon has a significant ability to predict structural response. Mackie and Stojadinovic (2001) investigated the use of 24 IMs in their study of PSDMs for typical California bridges and suggested that $S_a(T_1)$ and spectral displacement (S_d) at the fundamental period, T_1, $S_d(T_1)$ are the ideal IMs as they were found to reduce uncertainty in the demand models. However, all the aforementioned studies are pertinent to deterministic scenarios and did not consider portfolio of structures with variable geometric properties. Padgett et al. (2008) and Shafieezadeh et al. (2011) explored IMs for portfolios of bridges with geometric variation and concluded that PGA is an optimal IM for probabilistic seismic demand analysis of classes of bridges based on metrics of sufficiency, practicality, proficiency, efficiency, and hazard computability.

The formulation of a PSDM was shown in equations (5.2) through (5.5). Based on the formulations presented in these equations, it is evident that the selection of an optimal IM can pay a predominant role on the accuracy of the model in estimating seismic demand. Their optimal selection is instrumental to obtain reasonable estimates of the vulnerability of various components as the uncertainty associated with the demand is dependent on the variable chosen as an IM to some extent, although this is not the only source of the uncertainty.

The natural question that arises following this development is “What properties make an IM optimal?” Giovenale et al. (2004) pointed out that *sufficiency*, *efficiency* and

hazard computability are the essential properties of a good IM. In addition, *practicality* (Lucoand Cornell, 2007) and *proficiency* (Padgett et al., 2008) are properties that need to be considered, the latter one being a composite measure of efficiency and practicality. The satisfaction of these fore mentioned properties further validates the strength and accuracy of the power law assumption of the PSDM for a given IM, among other conclusions. Shafieezadeh et al. (2011) provides a detailed discussion of each of these characteristics of optimal IMs, including how to quantify and interpret each property. Efficiency is commonly used to establish the superiority of an IM. An efficient IM reduces the amount of variation in the estimated demand for a given IM value and at the same time maintains it constant over the entire range of the chosen IM. A lower value of the logarithmic standard deviation of the seismic demand, commonly referred to as the dispersion, $\beta_{D|IM}$, indicates an efficient IM.

Another property to measure the validity of an IM is sufficiency. An IM needs to be sufficient in order to justify the usage of total probability theorem in PSDA. Sufficiency refers to the property where an IM is independent of ground motion characteristics like magnitude (M), epicentral distance (R), and epsilon (ε). This is quantified by the p-value which is a measure of the probability that the randomly distributed points from the analysis would result in a regression line as flat as possible (tending towards zero slope) than that observed actually. Statistically, it is the probability of getting a value of the test statistic as extreme as or more extreme than that observed by chance alone, if the null hypothesis is true. This is achieved by a linear regression of the residuals from the PSDM with respect to M, R and ε. Practicality is a measure of the dependence of the demand upon the IM level and the slope, b, is a good indicator of this dependence. When the slope, b, approaches zero, there is negligible dependence of the demand upon the IM, thereby indicating an impractical IM. A higher value of b indicates that the IM is more practical.

Proficiency is a composite measure of efficiency and practicality. This property is derived by rearranging the terms in the formulation presented in equation (5.2) after substitution by equation (5.4). The term in the denominator in the formulation given in equation (5.6) is defined as modified dispersion, ζ, expressed in equation (5.7) and is a measure of proficiency. A lower value of ζ indicates a more proficient IM thereby indicating a lower uncertainty in the demand model by the choice of the IM.

$$P[D \geq d \mid IM] = \Phi\left(\frac{\ln(IM) - \frac{\ln(d) - \ln(a)}{b}}{\frac{\beta_{D|IM}}{b}}\right) \tag{5.6}$$

$$\zeta = \frac{\beta_{D|IM}}{b} \tag{5.7}$$

These properties will be used to determine the most optimal IM for the bridge classes considered in this study. This study investigates the IMs listed in Table 5.4 to determine the optimality in developing fragility curves for portfolios of highway bridges. Only the results for the primary components are presented here since these directly map into the system level damage states and have more significance in comparison to the secondary components, each of which will be described in detail in the next section.

Table 5.4: Intensity measures investigated for optimality

Intensity measure	Definition
PGA	Peak ground acceleration
$S_a(0.2)$	Spectral acceleration at 0.2 sec
$S_a(0.3)$	Spectral acceleration at 0.3 sec
$S_a(1.0)$	Spectral acceleration at 1.0 sec

5.4.2 Practicality, Efficiency and Proficiency

The results from the tests for practicality, efficiency and proficiency are presented in this section. The dispersion, $\beta_{D|IM}$ is a measure of efficiency while the slope, b of the PSDM is a measure of practicality as previously stated. Proficiency is quantified by the modified dispersion value, ζ. An optimal IM would be characterized by smaller values of

$\beta_{D|IM}$ and ζ and larger values of b and R^2. Appendix C reports values of these measures for IMs mentioned in Table 5.4 and primary component demands for the bridge classes considered in this study. The controlling values of the aforementioned parameters: b, $\beta_{D|IM}$ and ζ are highlighted in the table and so is the most optimal IM for the particular sub-class under consideration. PGA is the most practical IM followed by $S_a(1.0)$ and $S_a(0.3)$. In terms of efficiency and proficiency, $S_a(1.0)$ is by far the optimal IM across the bridge classes. Figure 5.6 shows a sample PSDM for column curvature ductility and abutment seat displacement in a post 1990 designed MSCC-BG with multi column bents using $S_a(1.0)$ as the IM.

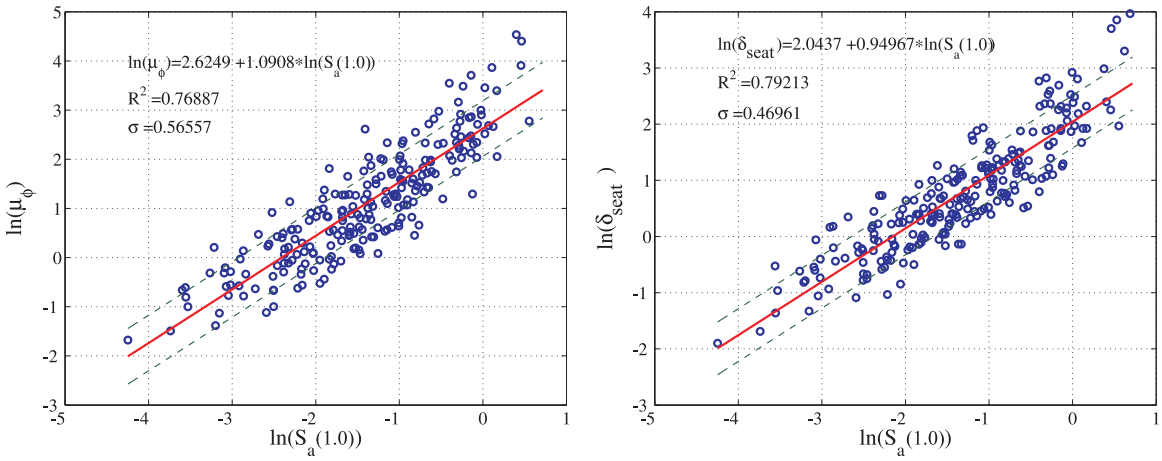

a) b)

Figure 5.6: PSDMs for a) column curvature ductility, and b) abutment seat displacement in post 1990 designed MSCC-BG-M bridges

5.4.3 Sufficiency

Sufficiency investigates the statistical independence of the IM with respect to ground motion characteristics. A sufficient IM ensures the accuracy of results obtained using the probabilistic structural assessment framework used commonly today (Mackie and Stojadinovic, 2001; Luco and Cornell, 2007):

$$\nu(LS) = \int_{DM}\int_{IM} G(LS \mid DM)\, dG(DM \mid IM)\, d\lambda(IM) \tag{5.8}$$

In equation (5.8), $G(LS|DM)$ denotes the probability of exceeding a limit state (LS) given the value of structural demand measure, $G(DM|IM)$ denotes the probability of exceeding a demand measure given the value of ground motion IM and $\lambda(IM)$ denotes the mean annual frequency of exceeding each value of the IM. Using the theorem of total probability yields the mean annual frequency of exceeding a limit state, $\nu(LS)$, as shown in Equation (5.8). Sufficiency of the IM ensures that the estimate of $G(DM|IM)$ is independent of ground motion parameters (or other hazard parameters), and enables this straightforward application of the theorem of total probability without introducing model bias or the need to consider joint probability density functions of multiple hazard parameters.

Sufficiency of an IM has been traditionally tested using ground motion characteristics like M and R and more recently, the epsilon, ε, parameter introduced by Baker and Cornell (2006). ε is a measure of the difference between spectral acceleration of a ground motion record and the mean of a corresponding attenuation relationship at a particular period and is evaluated by computing the difference between an individual records' $ln(S_a(T_1))$ and the mean predicted $ln(S_a(T_1))$ and then dividing the difference by the standard deviation of the ground motion prediction equation (Baker and Cornell, 2006). The ground motion prediction model developed by Abrahamson and Silva (2008) is used in the present study. As mentioned earlier the sufficiency property is quantified by the p-value which is estimated by performing a linear regression upon the residuals, $\varepsilon_d|IM$ from the PSDM with respect to characteristics such as M, R, and ε. By definition, p-value is the probability of rejecting the null hypothesis (Hines et al., 2003), which is this case is the independence of IM from ground motion characteristics like M, R, and ε. Higher p-value therefore give weaker evidence for rejecting the null hypothesis, meaning lower statistical significance and therefore a sufficient IM. Therefore, it is customary to reject the null hypothesis if the p-value is less than a particular significance level. Popular levels of significance are 0.1% (0.001), 1% (0.01) and 5% (0.05). This study uses a 5%

significance level to determine the sufficiency of the proposed IMs. Table D1 in Appendix C also reports the *p*-values with respect to M, R, and ε (denoted by p_M, p_R, p_ε, respectively) for the primary component demands for commonly used IMs. Based on the significance level, it is generally observed that all of the candidate IMs are sufficient in a majority of the cases. In general sufficiency typically serves as a prequalification test and the emphasis is placed on efficiency, proficiency, and practicality to choose the optimal IM. Figure 5.7 shows the linear regression on the residuals for column curvature ductility with respect to M, R and ε for a MSCC-IG-M in the 1971-1990 design era. Also shown are the *p*-values on the respective plots. The plots clearly demonstrate that the regression linear lines are almost horizontal (zero slope) thereby demonstrating the sufficiency property.

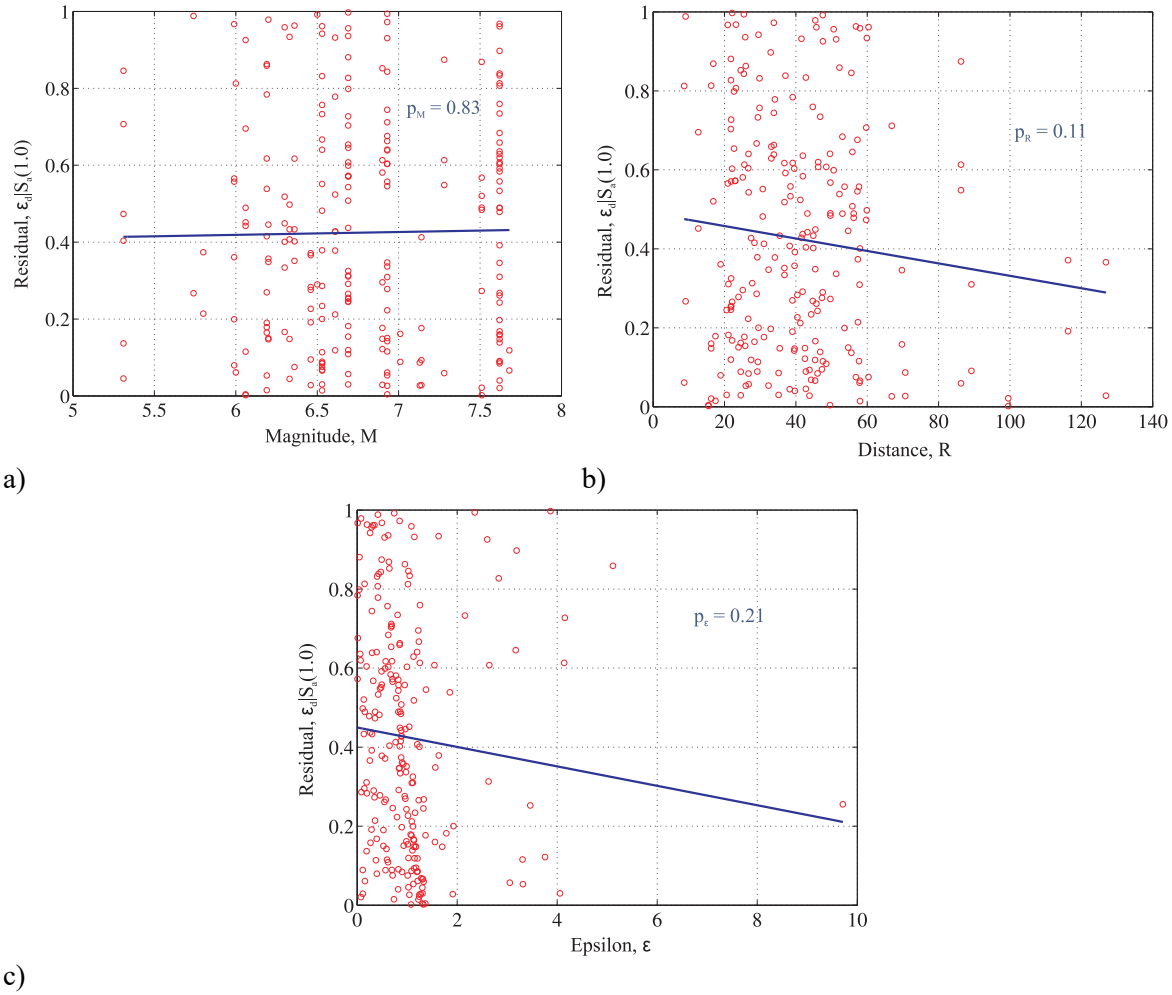

Figure 5.7: Plots showing the linear regression of the residuals for column curvature ductility in 1971-1990 designed MSCC-IG-M bridges with respect to a) magnitude, b) distance, and c) epsilon

5.4.4 Hazard Computability

Hazard computability is an important property for optimal IM selection as it dictates the ease with which probabilistic seismic hazard maps are available or can be developed to facilitate the convolution described in equation (5.8). The candidate IMs considered in this study satisfy this property since hazard curves are typically available in terms of PGA and S_a at specific periods such as 0.2 sec, and 1.0 sec. Many researchers (Luco and Cornell, 2007; Baker and Cornell, 2005; Bazzurro and Cornell, 2002; Shome and Cornell, 1999) demonstrated the superiority of $S_a(T_1)$ as an optimal IM for deterministic scenarios while Padgett et al. (2008) and Shafieezadeh et al. (2011)

highlighted the superiority of PGA as the optimal IM for portfolios of bridge structures. S_a at characteristic fundamental periods are effectively impossible to estimate across portfolios of bridge structures and further their values change across the class. Further, it is literally impossible to define hazard curves for these characteristic periods thereby making them prohibitive from a hazard computability stand point to be adopted as an optimal IM even if other properties determined them to a suitable candidate.

5.4.5 Optimal IMs across Bridge Classes and Seismic Performance Sub-bins

Table 5.5 details the optimal IM across the bridge classes (BC) and seismic performance sub-bins (SPS) considered in this study assessed based on the aforementioned properties. It is clearly seen that $S_a(1.0)$ dominates the selection and is therefore chosen as the preferred IM in this study. PGA is also seen to perform well in many cases and fragility curves will therefore also be presented using PGA as an IM.

Table 5.5: Optimal IM across the bridge classes and the respective SPS considered in this study

BC	SPS	E1-S0	E1-SX	E2-S0	E2-SX	E3-S0	E3-SX
MSCC-BG-S		PGA	$S_a(1.0)$	$S_a(1.0)$	$S_a(1.0)$	$S_a(1.0)$	$S_a(1.0)$
MSCC-BG-M		$S_a(1.0)$	$S_a(1.0)$	$S_a(1.0)$	$S_a(1.0)$	$S_a(1.0)$	$S_a(1.0)$
MSCC-SL-P		$S_a(1.0)$	$S_a(1.0)$	$S_a(1.0)$	$S_a(1.0)$	$S_a(1.0)$	$S_a(1.0)$
MSCC-TG-P		$S_a(1.0)$	$S_a(1.0)$	$S_a(1.0)$	$S_a(1.0)$	$S_a(1.0)$	$S_a(1.0)$
MSCC-TG-M		$S_a(1.0)$	$S_a(1.0)$	PGA	$S_a(1.0)$	$S_a(1.0)$	$S_a(1.0)$
MSCC-IG-S		PGA	$S_a(1.0)$	$S_a(1.0)$	$S_a(1.0)$	PGA	$S_a(1.0)$
MSCC-IG-M		$S_a(1.0)$	$S_a(1.0)$	$S_a(1.0)$	$S_a(1.0)$	$S_a(1.0)$	$S_a(1.0)$

5.5 Component Capacity or Limit State Models

Seismic fragility involves the convolution of the demand and capacity models. The formulation of the demand models was explained in the previous section. Definition of the component capacities or limit states is not a trivial task and is a crucial step in the fragility formulation. The individual limit states are characterized by representative values for the median, S_C, and dispersion, β_C, (see equation (5.1)) for the component

damage states distributions which are also assumed to be lognormal akin to the PSDMs. Discrete damage states are defined for each component corresponding to significant changes in its response and consequences to its own performance and performance of the bridge at the global or system level. Although the damage state definitions are discrete, the assumption is that a continuous range of damage exists between the discrete states to enable the closed-form computation of the component fragility curves. It is essential that the limit state definitions use the same metric as the EDP for the respective bridge components. Table 5.3 listed the bridge component EDPs that are used to monitor the response of specific components and assess their performance.

A significant contribution in the present study is that the damage state definitions for the components are derived in such a way that they align with the Caltrans design and operational experience. This will facilitate the evaluation of repair-related decision variables, repair cost and repair time, which are the end products in a typical risk assessment procedure. The major challenge lies in being able to group components that have similar consequences at the system level in terms of functionality and repair consequences. A common question that could arise is: "Do the complete collapse of columns have the same effect on bridge functionality as the complete damage to a shear key or tearing of an elastomeric bearing pad?" In order to be able to address the aforementioned concerns, two classes of components are proposed viz., primary and secondary. Primary components are defined as those that affect the vertical stability and load carrying capacity of the bridge. Extensive or complete damage to these components might lead to closure of the bridge. Columns and abutment seat belong to this category with regards to the bridge classes considered in this research. When looking at bridges with in-span hinges, which is out of the scope of the present study, the internal hinge is also considered as a primary components as excessive hinge opening (values exceeding the support seat length) could lead to unseating of the superstructure.

Secondary components may be defined as the ones that do not affect the vertical stability of the bridge. Failure of these components will not force closure of the bridge but might lead to restrictions on the travel speed and traffic conditions on the bridge. Table 5.6 lists the primary and secondary components in the bridge classes considered in this study for both diaphragm and seat abutments.

Table 5.6: List of primary and secondary components in the bridge classes considered in this study

Seat Abutments	Diaphragm Abutments
Primary components	
Columns	Columns
Abutment seat	
Secondary Components	
Joint seal	Maximum deck displacement
Elastomeric bearing pads	Bent foundation translation
Restrainers	Bent foundation rotation
Maximum deck displacement	Abutment passive displacement
Bent foundation translation	Abutment active displacement
Bent foundation rotation	Abutment transverse displacement
Abutment passive displacement	Joint seal*
Abutment active displacement	Elastomeric bearing pads*
Abutment transverse displacement	Restrainers*
Shear key displacement	Shear key displacement*

*These components are only present in the case of MSCC-IG bridges with diaphragm abutments

Tables 5.7 and 5.8 show the general description of the bridge system level damage states (BSST) and the component damage thresholds (CDT) for primary components, respectively. The bridge system level damage state descriptions, BSST-0 through BSST-3 are defined in Table 5.7 and are aimed at operational consequences in the aftermath of an earthquake. The CDT of primary components map directly to the BSSTs since the loss of a primary component affects the load carrying capacity and overall stability of the bridge system. In the case of secondary components, only two broad CDTs are defined, CDT-0 and CDT-1 and these map directly into BSST-0 and BSST-1, respectively. The damage state descriptions for CDT-0 and CDT-1 in the case of secondary components are shown in Table 5.9. The combinations of the Component

Damage Thresholds (CDT) of primary and secondary components, detailed in Table 5.7, are aimed at achieving similar consequences in terms of bridge operations (repair and traffic implications) in the aftermath of an earthquake. As described in Table 5.7, the primary components: columns and abutment seat (the latter only in the case of seat abutments) directly map into the BSSTs and equally contribute to the vulnerability across all damage states. On the other hand, the secondary components (detailed in Table 5.6) map into BSST-0 and BSST-1 since there complete failure will not have a similar consequence as that of the primary components. Both these tables are developed in close collaboration with Caltrans (Caltrans, 2010-2012) to ensure that the component mapping is in alignment with the inspection/maintenance closure decisions and the training guides for post-earthquake inspections (Sahs et al., 2008). The CDTs may be broadly defined as below:

- CDT–0 (Aesthetic damage) is a performance parameter threshold beyond which aesthetic damage of the component occurs. The associated repair is primarily aimed at restoring the aesthetics
- CDT–1 (Repairable minor functional damage) is a performance parameter threshold beyond which significant repairs are required to restore component functionality
- CDT–2 (Repairable major functional damage) is a performance parameter threshold beyond which extensive repairs are required to restore component functionality
- CDT–3 (Component replacement) is a performance parameter threshold beyond which component replacement is likely to be the most cost-effective means to restore component functionality

The CDT values can be described using a prescriptive (physics-based) approach, descriptive (judgmental-based) approach or by incorporating both (Padgett et al., 2007) using Bayesian updating principles. The prescriptive approach is based on the mechanics of the problem where a functional level is associated with component damage such as

spalling of cover concrete in a column, buckling or rupture of the longitudinal column reinforcement etc. The descriptive approach is based on the functionality level of the components post disaster and is usually in terms of repair cost and downtime. In this study a combination of both techniques are used to define the threshold value.

Having broadly defined the CDTs for various components, the threshold values are determined based on experimental studies from the literature and based on extensive input from the Caltrans design and bridge maintenance groups. The subsequent sections provide these median values, S_C, for the CDTs along with visible signs of associated damage and repair strategies. As mentioned before, the capacity distributions are assumed to be lognormal similar to the demand distributions. The uncertainty associated with the median values of the CDTs is prescribed in the form of a logarithmic standard deviation or dispersion, β_C. The assignment of dispersion is done in a subjective manner due to lack of enough information to quantify it and a dispersion value of 0.35 is adopted across the components and the respective damage states. This value is particularly a good estimate for columns and is consistent with the test results documented in the PEER column structural performance database (Berry and Eberhard, 2004).

Table 5.7: General description of bridge system level damage states along with component damage thresholds

Bridge system damage states	BSST-0 MINOR	BSST-1 MODERATE	BSST-2 EXTENSIVE	BSST-3 COMPLETE
ShakeCast Inspection Priority levels	Low	Medium	Medium-High	High
Likely Immediate Post-Event Traffic State	Open to normal public traffic – No Restrictions	Open to limited public traffic – speed/weight/lane restrictions	Emergency vehicles only – speed/weight/lane restrictions	Closed (until shored/braced) – potential for collapse
Traffic Operation Implications				
Is closure/detour needed?	Very unlikely	Unlikely	Likely	Very likely
Are traffic restrictions needed?	Unlikely	Likely	Very Likely	Very Likely - Detour
Emergency Repair Implications				
Is shoring/bracing needed?	Very unlikely	Unlikely	Likely	Very likely
Is roadway leveling needed?	Unlikely	Likely	Very Likely	Very Likely - Detour
Component Damage Threshold mapping				
Primary components	CDT-0 to 1	CDT-1 to 2	CDT-2 to 3	Above CDT-3
Secondary components	CDT-0	CDT-1	NA	NA

NA indicates that these CDTs are not defined for the secondary components

Table 5.8: Component level damage state descriptions – Component Damage Thresholds (CDT) for Primary Components

	CDT-0	CDT-1	CDT-2	CDT-3
Component damage states	No damage	Aesthetic damage	Repairable minor functional damage	Repairable major functional damage	Component replacement

Table 5.9: Component level damage state descriptions – Component Damage Thresholds (CDT) for Secondary Components

		CDT-0	**CDT-1**
Component damage states	No damage	Aesthetic damage/ Repairable minor functional damage	Repairable major functional damage/ Component replacement

5.5.1 Columns

Curvature ductility, μ_φ, is the chosen EDP for columns. The columns in the pre 1971 design era have very poor confinement of the longitudinal reinforcement due to the large spacing between the transverse reinforcement (#4 stirrups at 12 in on center is a commonly adopted standard). It is realized that curvature ductility has its limitations in terms of applicability to non-ductile columns which is characteristic of the pre 1971 design era; it is chosen to maintain consistency, with added conservatism to the threshold values. A lot of information is available on the performance of bridge columns and experimental results pertinent to columns are documented in Veletzos et al. (2006), Berry and Eberhard (2003, 2004), Mackie and Stojadinovic (2005). Four damage states, CDT-0 through 3 are chosen and the median μ_φ values characterizing these damage states along with observed damage and typically employed repair strategies are documented in Table 5.10. Pictorial representations of typical column force deformation relationships with expected damage is shown in Figures 5.8 through 5.10.

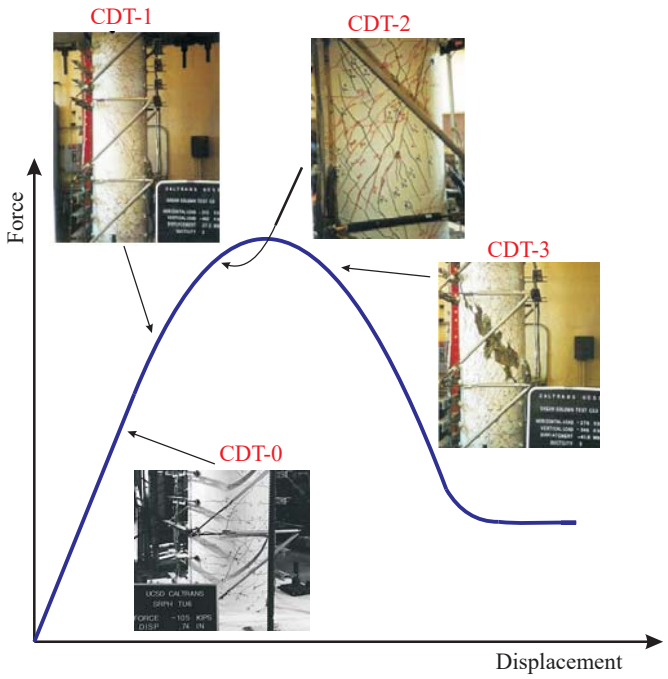

Figure 5.8: Depiction of CDTs for pre 1971 designed brittle columns (Sahs et al, 2008)

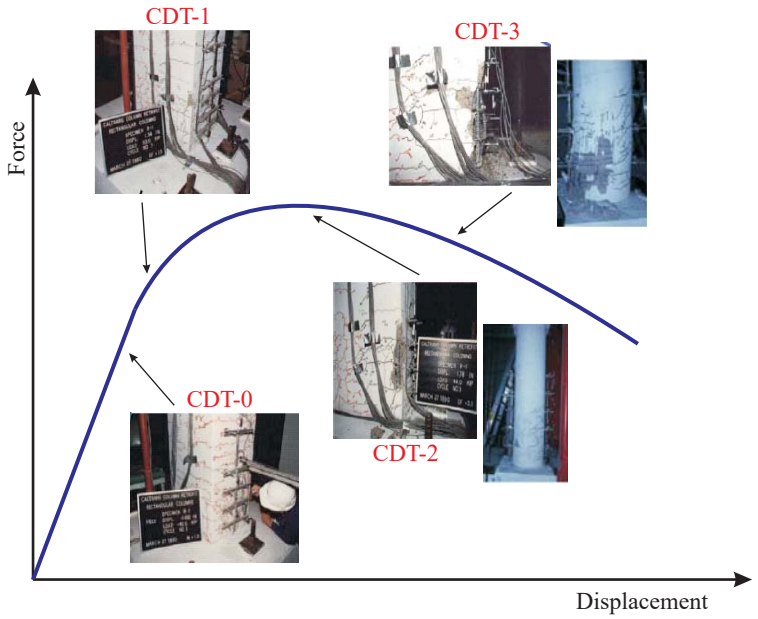

Figure 5.9: Depiction of CDTs for 1971-1990 era designed strength degrading column (Sahs et al, 2008)

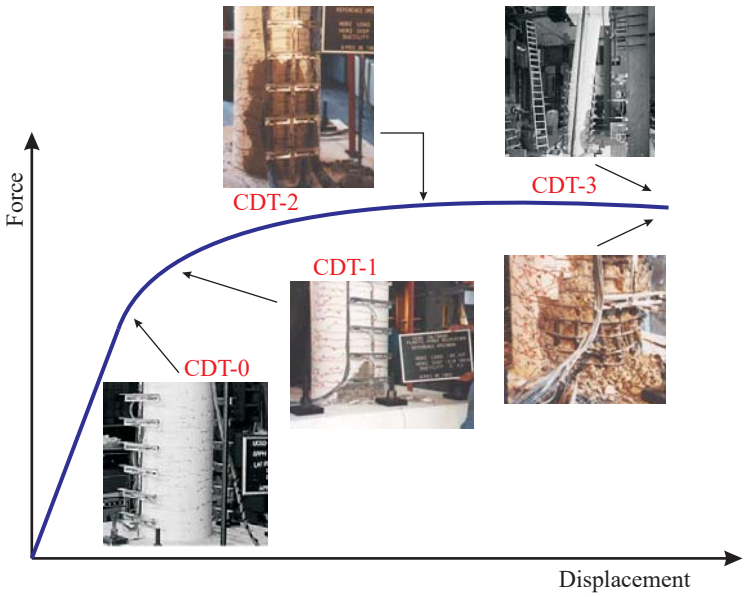

Figure 5.10: Depiction of CDTs for a post 1990 designed ductile column (Sahs et al, 2008)

Table 5.10: Median values of column CDTs along with damage description and likely emergency and permanent repair strategies

Design era	CDT level	μ_φ	Damage description	Typical emergency repair	Typical permanent repair
Pre 1971 Brittle column	CDT-0	0.80	Cracking	None	Seal and paint
	CDT-1	0.90	Minor cover spalling anywhere along the column height	None	Epoxy injection; minor concrete removal and patch; seal and paint
	CDT-2	1.00	Large shear cracks; major spalling; exposed core; confinement yield (no rupture)	Shoring very likely	Add Class-F jacket
	CDT-3	1.20	Loss of confinement; longitudinal bar buckling or rupture; core crushing	Closure/detour; shore deck if to re-open	Replace column or bridge
1971-1990 Strength degrading column	CDT-0	1.00	Cracking	None	Seal and paint
	CDT-1	2.00	Minor cover spalling anywhere along the column height	None	Epoxy injection; minor concrete removal and patch; seal and paint
	CDT-2	3.50	Major spalling; exposed core; confinement yield (no rupture)	Possibly shoring	Major concrete removal and patch; add Class-F jacket
	CDT-3	5.00	Loss of confinement; longitudinal bar buckling or rupture; core crushing; large residual drift	Closure/detour; shore deck if to re-open	Replace column or bridge
Post 1990 Ductile column	CDT-0	1.00	Cracking	None	Seal and paint
	CDT-1	4.00	Minor cover spalling concentrated at the top and bottom of the column	None	Epoxy injection; minor concrete removal and patch; seal and paint
	CDT-2	8.00	Major spalling; exposed core; confinement yield (no rupture)	Possibly shoring	Major concrete removal and patch; add Class-F jacket
	CDT-3	12.0	Loss of confinement; longitudinal bar buckling or rupture; core crushing; large residual drift	Closure/detour; shore deck if to re-open	Replace column or bridge

5.5.2 Abutment Seat and Joint Seal

A detailed description of the available seat width and joint seals assembled in the seats was provided in Section 3.5.6 of Chapter 3. Bridge classes with seat abutments have a potential for unseating at the abutments. Along with columns, the seat is considered a primary component. In addition to the evaluation of unseating potential, damage to the joint seal is also monitored considering the same EDP as the unseating potential. Similar to the unseating potential associated with the abutment seat, damage to joint sealant is commonly observed in bridges after earthquakes. The joints are typically sealed with some kind of a joint sealant and damage to the sealant is considered a secondary component. The different types of joint sealants were also mentioned in Chapter 3. Bridge seat widths chronologically increased from the 4 – 12 in (S1) range in the Pre 1971 design era to 12 – 18 in (S2) range in the 1971-1990 design era and 18 – 24 in (S3) and greater than 24 in (S4) range in the Post 1990 design era. The Phase I and II retrofit programs addressed this issue by retrofitting the pre 1971 and 1971-1990 to the post 1990 seat categories by the provision of restrainers and pipe seat extenders. Therefore, all the four categories of seat widths, S1 through S4 exist in the pre 1971 design era, while categories S2 through S4 exist in the 1971-1990 design era and only the S3 and S4 categories exist in the post 1990 design era bridges. Further, the joint gap is based on the movement rating (MR) of the bridge and a joint seal (Type A or B) is typically used for joints with MR less than 2 in, and a joint seal assembly (strip or modular) is used for joints with MR greater than 2 in. Joint seals are considered in the case of all the bridge classes considered in this study. In the case of MSCC-BG bridges, due to the presence of larger gaps with MR greater than 2 in for a few bridges, the effect of gap size is investigated on the fragility curves. The displacement of the joint and damage to the seal is highly correlated with damage to the abutment backwall in the case of seat type abutments. Table 5.11 gives the median CDT values for the joint seat and the CDT values

for the joint sealant are mentioned in Table 5.12. The joint opening is the EDP used in either case.

Table 5.11: Median values of CDT for abutment seat

Type	Gap size	Notation	Units	CDT-0	CDT-1	CDT-2	CDT-3
S1: 4-12 in seat	Small: MR < 2 in	AS1-S	Inches	0.5	1.0	2.0	3.0
S2: 12-18 in seat	Small: MR < 2 in	AS2-S	Inches	1.0	3.0	6.0	9.0
S3: 18-24 in seat	Small: MR < 2 in	AS3-S	Inches	1.0	3.0	10.0	15.0
S3: 18-24 in seat	Large: MR > 2 in	AS3-L	Inches	2.0	6.0	10.0	15.0
S4: >24 in seat	Small: MR < 2 in	AS4-S	Inches	1.0	3.0	14.0	21.0
S4: >24 in seat	Large: MR > 2 in	AS4-L	Inches	2.0	6.0	14.0	21.0

The CDT values for the abutment joint seat depend on two factors: seat width and the joint gap, which dictate the unseating potential and pounding damage potential, respectively. Seat width governs higher CDT values (CDT-2 and -3) where unseating is possible and joint gap is considered to govern the lower CDT levels (CDT-0 and -1). In all cases, except AS1-S, the CDT-3 threshold is set to a value 3 in less than the minimum seat width. CDT-0 is set to the approximate gap width, thereby corresponding to the initiation of joint pounding damage. The CDT-1 values are set to 300% of the gap width to correspond with significant levels of joint pounding (Caltrans, 2010-2012). In order to obtain an intermediate limit, CDT-2 is set to two-thirds of the CDT-3 threshold value to correspond to movement of more than one half of the minimum seat width, in consultation with Caltrans design engineers (Caltrans, 2010-2012). The CDT values used for the S1 or 4-12 in seat group are governed by the potential for unseating at 4 in.

Table 5.12: Median values of CDT for joint seal

Seat type	Units	CDT-0	CDT-1
Joint seal: Type A poured	Inches	0.75	--
Joint seal: Type B compression	Inches	0.75	--
Seal assembly: Strip	Inches	2.0	5.0
Seal assembly: Modular	Inches	4.0	10.0

The CDT values for joint seal are based on the MR of the bridges where the joints are installed. For Type A and Type B joint seals, only CDT-0 is defined due to lack of

unique higher-level damage model for sealed joints. This intuitively makes sense since once damaged or torn, the seals are expelled and replaced with new ones suggesting the necessity for just one CDT. The CDT-0 values are close to the MR of the system. In the case of Joint seal assemblies (strip and modular), the CDT-1 values are arbitrarily set to 250% of the CDT-0 values to correspond to anticipated damage of the mechanical elements of the assembly beyond damage to the seal component which is captured in CDT-0.

5.5.3 Superstructure Deck

The maximum displacement of the deck is considered to be a secondary component and the link between this EDP and damage to the deck is chosen based on the recommendations of Caltrans design engineers (Caltrans, 2010-2012). The maximum displacement provides an intuitive baseline for overall levels of seismic loading. The CDT values are chosen herein based on observed displacements during past earthquakes and with an intention to trigger an inspection priority accordingly more so with damage anticipated elsewhere in the bridge. The repair strategies typically involve injecting epoxy into the crack typically.

Table 5.13: CDT values for maximum deck displacement

Component	Units	CDT-0	CDT-1
Maximum deck displacement	Inches	4.00	12.00

5.5.4 Abutments - Passive, Active and Transverse Reponses

In general the abutment backwalls are designed to shear off. The design considerations ensure that no damage occurs to the stem wall other than the concrete that needs to be chipped out during repairs to the back wall. The CDT-0 value for the passive response is defined corresponding to 0.5% drift ratio measured at the top of the back wall. The CDT-1 value is fixed based on 2% of typical deck thickness (ATC/MCEER,

2002). The CDT values are listed in Table 5.14. The active and transverse response of the abutments is governed by the behavior of piles and the CDT values are specified corresponding to the first yield and ultimate deformation of the underlying piles. The typical repair strategies associated with the abutments involves repairs to the backwalls and in some cases, the replacement of the approach slab. In many cases, this might also involve the replacement of the shear keys (in the case of seat abutments) and this is considered as a separate secondary component in this study.

Table 5.14: CDT values for abutment passive, active and transverse response

Component	Units	CDT-0	CDT-1
Passive abutment response	Inches	3.00	10.0
Active abutment response	Inches	1.50	4.00
Transverse abutment response	Inches	1.00	4.00

5.5.5 Bent Foundation –Translation and Rotational Responses

Damage to the foundations is captured with the help of two EDPs: translation and rotation of the bent foundation. The translational CDT values are consistent with those provided for the abutments. The rotational CDT values are representative of the axial pile movement of ±0.5 in at the opposite edges of a 20 feet wide pile cap. The translation and rotation CDT values associated with the column foundations are tabulated in Table 5.15. The width of 20 feet was chosen as this was observed to be the largest possible width for pile caps based on the review of bridge plans. The typical repair strategy associated with bent foundations involves enlargement of the pile cap and provision of additional piles surrounding the existing ones. The enlarged pile cap is then tied to the existing pile cap by drilling into the existing cap and inserting dowel bars.

Table 5.15: CDT values for translation and rotational foundation response

Component	Units	CDT-0	CDT-1
Translation	Inches	1.00	4.00
Rotation	Radian	1.50	6.00

5.5.6 Elastomeric Bearing Pads, Restrainers and Shear Keys

The EDP associated with all these components is the displacement. Elastomeric bearing pads are manufactured to undergo large displacements without any significant strength degradation based on Caltrans specifications. The bearing pads remain elastic until about 100% shear strain and experience significant damage and tearing over 300 to 350% shear strain. The typical pads are close to 2 in thick and these dimensions are used to establish the CDT values documented in Table 5.16. The typical repair strategy is to replace the bearing pads when damage is notices upon inspection.

The restrainer CDT values are based on typical design values for restrained relative displacement between the two ends of the joint (abutment backwall and deck in this case) for various systems that includes both restrainer cable yield displacement and slack (BDA, 2009). The CDT-0 and CDT-1 values are set at 75% and 200% of the yield displacement. The CDT values are listed in Table 5.16.

The presence of external shear keys limits the service-level and excessive transverse displacement and are typically designed to break off or shear similar to the abutment backwall. The bridges considered in this study are assumed to have only exterior shear keys. Internal shear keys are typical in older bridges and most of these were removed and replaced with exterior shear keys during the Caltrans Phase-I and –II retrofit programs. The CDT values of the shear keys documented in Table 5.16 are based on the testing of these components in the University of California San Diego (Megally et al., 2002), as stated previously in Chapter 4. Repairs to shear key involves injecting epoxy into the minor cracks observed at displacements corresponding to CDT-0. However, shear keys are normally replaced when they are broken off at displacements close to CDT-1.

Table 5.16: CDT values for elastomeric bearing pads, restrainers and shear keys

Component	Units	CDT-0	CDT-1
Elastomeric bearing pads	Inches	1.00	4.00
Restrainers	Inches	1.50	4.00
Shear keys	Inches	1.50	5.00

5.5.7 Component Limit States Summary

Table 5.17: Summary of CDT values adopted in this study

Component	EDP	Units	Median values, S_C				β_C
			CDT-0	CDT-1	CDT-2	CDT-3	
Primary Components							
Columns							
Pre 1971	Curvature ductility	NA	0.8	0.9	1.0	1.2	0.35
1971-1990	Curvature ductility	NA	1.0	2.0	3.5	5.0	0.35
Post 1990	Curvature ductility	NA	1.0	4.0	8.0	12.0	0.35
Abutment seat							
AS1-S	Displacement	Inches	0.5	1.0	2.0	3.0	0.35
AS2-S	Displacement	Inches	1.0	3.0	6.0	9.0	0.35
AS3-S	Displacement	Inches	1.0	3.0	10.0	15.0	0.35
AS3-L	Displacement	Inches	2.0	6.0	10.0	15.0	0.35
AS4-S	Displacement	Inches	1.0	3.0	14.0	21.0	0.35
AS4-L	Displacement	Inches	2.0	6.0	14.0	21.0	0.35
Secondary Components							
Joint seal							
Type A	Displacement	Inches	0.5	NA	NA	NA	0.35
Type B	Displacement	Inches	1.0	NA	NA	NA	0.35
Strip	Displacement	Inches	2.0	5.0	NA	NA	0.35
Modular	Displacement	Inches	4.0	10.0	NA	NA	0.35
Bearings	Displacement	Inches	1.0	4.0	NA	NA	0.35
Restrainers	Displacement	Inches	1.5	4.0	NA	NA	0.35
Shear keys	Displacement	Inches	1.5	5.0	NA	NA	0.35
Deck	Displacement	Inches	4.0	12.0	NA	NA	0.35
Bent foundation							
Translation	Displacement	Inches	1.00	4.00	NA	NA	0.35
Rotation	Rotation	Radian	1.50	6.00	NA	NA	0.35
Abutments							
Passive	Displacement	Inches	3.00	10.0	NA	NA	0.35
Active	Displacement	Inches	1.50	4.00	NA	NA	0.35
Transverse	Displacement	Inches	1.00	4.00	NA	NA	0.35

The previous sections detailed the capacity models component wise along with details about the choice of the respective CDT values and typical repair strategies adopted. As stated previously, the capacity models are assumed to be lognormal characterized by a median value and dispersion. Table 5.17 provides a summary of the CDT values adopted for the bridge components.

5.6 Closure

The multi phase framework used in the development of fragility curves is presented in this chapter. Details are provided regarding the different components of the framework: ground motion suite, stochastic finite element models capturing a wide range of uncertainties, formulation of probabilistic seismic demand models and definition of capacity models. A suite of 160 ground motions developed by Baker et al. (2011) is considered for use in the development of fragility curves and details are presented regarding the composition of the suite. The treatment of uncertainty in the bridge models representing the respective bridge classes and seismic performance sub-bins is achieved through probability distributions of a wide range of material, geometric and other miscellaneous attributes in addition to the empirical geometric distributions generated using the NBI information. These include concrete compressive strength, reinforcing steel yield strength, bearing pad coefficient of friction, mass, damping etc. to mention a few. Having presented the formulation of the probabilistic seismic demand model (PSDM), extensive details are provided about the formulation of capacity models which will then be convolved with the PSDMs to aid in the development of component and system level fragility curves, which will be presented in the next chapter.

The study consider multiple component vulnerability, and classification of bridge components into two categories viz., primary and secondary is proposed based on the individual damage mapping to a system level consequence. Engineering demand parameters are identified to capture the response of components and drawing upon

literature and the expertise of Caltrans design and maintenance professionals, component damage thresholds and repair strategies are identified across the portfolio of bridge components deemed to contribute to the vulnerability of the bridge system.

Another important aspect addressed in this chapter is the selection criteria for an optimal intensity measure. Spectral acceleration at 1.0 sec is identified and proposed to be used as the intensity measure of choice for generating fragility curves based on test metrics such as efficiency, proficiency, practicality, sufficiency and hazard computability.

CHAPTER 6

SYSTEM AND COMPONENT FRAGILITY CURVES

The end goal of seismic risk assessment of highway bridge infrastructure systems is the quantification of the expected damage in terms of metrics such as cost or time in the event of an earthquake. Estimates of vulnerabilities at the system and component level plays a significant role in assessing probable bridge losses to facilitate critical decision making pertinent to post earthquake safety, preparedness, mitigation and management. Fragility curves, which are conditional probability statements that express the probability of meeting or exceeding specific user defined damage states, play a significant role in risk assessment. Component and system level fragility relationships further help in the assignment of inspection priorities and assessing the post-earthquake serviceability condition of bridges and their components.

The previous chapters in addressed the different aspects of the fragility framework arriving at the formulation of probabilistic seismic demand models (PSDMs) and capacity models. Each of these is characterized by median values and dispersions completely describing a lognormal distribution, representing the component responses in the case of PSDMs, and the capacity (or resistance) for defined damage states in the case of the capacity models. The component fragility can be derived using a closed form solution described in equation (6.1), where, D and C denote demand and capacity, S_D and S_C denote the median values of demand and capacity and $\beta_{D|IM}$ and β_C denote the dispersions (logarithmic standard deviation) of the demand and capacity, respectively.

$$P[D > C \mid IM] = \Phi\left(\frac{\ln\left(S_D / S_C\right)}{\sqrt{\beta_{D|IM}{}^2 + \beta_C{}^2}}\right) \tag{6.1}$$

It must be noted that S_C and β_C are defined based on the limit state under consideration. As stated in the previous chapter, the components contributing to the vulnerability of the bridge system are divided into primary and secondary components based on their influence on the stability and operational consequences in the aftermath of an earthquake (see Table 5.6 in Chapter 5). Spectral acceleration at 1.0 sec, $S_a(1.0)$, was established as the optimal intensity measure (IM) in Chapter 5 and fragility curves will be developed and presented using this IM. Substituting the formulation for the median demand, S_D described in the PSDM formulation, and subsequent simplification, as illustrated in equation (6.2), leads to the formulation in (6.3) which is representative of the lognormal distribution describing the component fragilities with median, λ_c and dispersion, ζ_c. Component fragility curves provide valuable information about the most vulnerable component in the bridge system thereby prioritizing inspection and retrofit.

$$P[LS \mid IM] = \Phi\left(\frac{\ln(a\,IM^{b}) - \ln(S_C)}{\sqrt{\beta_{D|IM}{}^2 + \beta_C{}^2}}\right) = \Phi\left(\frac{\ln(IM) - \left(\frac{\ln(S_C) - \ln(a)}{b}\right)}{\frac{\sqrt{\beta_{D|IM}{}^2 + \beta_C{}^2}}{b}}\right) \tag{6.2}$$

$$P[LS \mid IM] = \Phi\left(\frac{\ln(IM) - \ln(\lambda_c)}{\zeta_c}\right) \tag{6.3}$$

The logical step following the determination of component fragilities is to integrate these to enable the macroscopic view of the vulnerability of the bridge system. Contrary to some of the previous studies (Nielson, 2005; Padgett, 2007; Ramanathan et al., 2010, 2012), the components in this study are combined in a way such that they are have equal consequences in terms of repair and traffic implications in the aftermath of an earthquake. Although the aforementioned studies tried to address the issue of consequence based system level damage states by adjusting the component capacities, the adjusted capacities did not correlate well to description of damage at the component level. On the contrary, in the present study, the component level damage states were

defined in such a way that they were reflective of physical damage and the components were them combined based on the influence of their respective damages on the system level repair and traffic consequences. This was detailed in Table 5.7 of Chapter 5, where the primary components directly mapped to the bridge system level thresholds (BSSTs) while the secondary components at most contributed to BSST-1.

Several techniques to develop system level fragility curves were presented in Chapter 2. In this study, the estimate of system fragility curves is facilitated through the development of joint probabilistic seismic demand model (JPSDM), recognizing that the demands on various components have some level of correlation. If $\underline{X} = (X_1, X_2, \ldots.., X_n)$ represents the vector of demands, X_i, placed on the n components of the system, then the vector, $\underline{Y} = ln(\underline{X})$ represents the vector of component demands in the transformed lognormal space. Since the marginal component demands, X_i, are lognormally distributed, the transformed demands, Y_i, are normally distributed in the transformed space. The JPSDM is formulated in this space by assembling the vector of means, $\mu_{\underline{Y}}$ and the covariance matrix, $\sigma_{\underline{Y}}$. It must be noted that the covariance matrix, $\sigma_{\underline{Y}}$, considers the correlation coefficients between $ln(X_i)$ and not X_i. The correlation coefficients between the component demands are obtained by using the results of the NLTHA and the resulting covariance matrix is then assembled. A Monte Carlo simulation is then used to compare realizations of the demand (using the JPSDM defined by a conditional joint normal distribution in the transformed space) and component capacities to calculate the probability of system failure. It is important to note that correlation across the component capacities is not considered, although, a 100% correlation is assumed across damage states for a given component. Samples (10^6 in this case) are drawn from both the demand and capacity models and the probability of demand exceeding the capacity is evaluated for a particular IM value. The procedure is repeated for increasing values of the IM. Regression analysis is used to estimate the lognormal parameters, median and dispersion, which characterize the bridge system fragility. For a given system level damage state, the

series system assumption is used to generate fragility curves. However, the number of components comprising the series system varies based on the BSST under consideration and is dictated by the mapping of component level damage states defined previously. The mapping ensures the consistency of the series assumption in an attempt to achieve similar consequences in terms of repair and traffic implications at the system level.

The methodology presented in this section is used to develop system and component level fragility curves for the bridge classes and the respective seismic performance sub-bins (SPS) considered in this study. The nomenclature introduced in section 3.6 of Chapter 3 will be used to present the results. Finally, comparisons are also made with the fragilities in HAZUS-MH (2011) and insight is provided into the relative vulnerability of bridge classes and their seismic performance sub-bins, assess the effectiveness of seismic design philosophy currently adopted for the design of bridges, and guide future data collection that is presently absent in the NBI and the state databases.

6.1 Multispan Continuous Concrete Slab Bridges

Fragility curves are developed for MSCC-SL bridges with both seat and diaphragm abutments and the median values and dispersions are documented in Table 6.1. Since slab bridges employ integral pile columns which have seen no modifications in their geometry or reinforcing bar configuration over the decades, the fragilities reported in Table 6.1 are applicable across the design eras considered in this study. Table 6.1 also documents the average dispersion, ζ^*, which could be used as a single value of dispersion characterizing the fragility across all the four damage states. Appendix D documents the median and dispersion values for the component fragility curves for the bridge classes and SPS considered in this study.

Table 6.1: Multispan continuous slab bridge fragilities

Seismic performance sub-bin	BSST-0		BSST-1		BSST-2		BSST-3		
	λ	ζ	λ	ζ	λ	ζ	λ	ζ	ζ*
MSCC-SL-P-S0	0.175	0.700	0.737	0.628	1.024	0.653	1.277	0.654	0.66
MSCC-SL-P-S1-S	0.090	0.462	0.167	0.477	0.287	0.481	0.394	0.486	0.48
MSCC-SL-P-S2-S	0.120	0.459	0.351	0.495	0.499	0.597	0.627	0.649	0.55
MSCC-SL-P-S3-S	0.120	0.476	0.348	0.499	0.537	0.683	0.652	0.716	0.59
MSCC-SL-P-S4-S	0.121	0.476	0.345	0.499	0.543	0.683	0.654	0.716	0.60

The plot of median values across damage states is shown in Figure 6.1. In the figure, BC stands for the bridge class which is MSCC-SL in the present case and EX denotes the applicability across all the design eras. A simple technique to compare differences in the fragility curves is to evaluate the relative change in the median value of the fragility curves. This facilitates the determination of the effect of certain attributes on the overall vulnerability of the bridge system. A positive change indicates a less vulnerable structure while a negative change indicates a more vulnerable structure. Figure 6.2 illustrates this using fragility curves for MSCC-SL-P-EX-S1 and MSCC-SL-P-EX-S4 for the BSST-3 damage state. The following inferences can be drawn:

- Diaphragm abutments (BC-P-EX-S0) are less vulnerable when compared to seat type abutments (BC-P-EX-SX) across the range of seat widths considered (S1 through S4). The percentage change in median values between diaphragm and seat abutments with largest seat width (S4) is 200%, 143%, 92% and 96% for BSST-0, -1, -2, and -3, respectively.
- The vulnerability of bridges reduces with an increase in the seat width. However, the median and dispersion values for MSCC-SL-P-EX-S2 through -S4 is very similar as seen in Figure 6.1 and documented in Table 6.1. The consistency in fragility parameters is due to the fact that the columns dominate the overall vulnerability across the damage states and as such increased seat width beyond 18 in (S2 category) does not contribute to the reduction in vulnerability. This is

demonstrated in Figure 6.3 which shows a plot of system and component fragilities for MSCC-SL-P-EX-S1 and –S3 across all damage states. Clearly, in the case of MSCC-SL-P-EX-S1, the abutment seat is the most vulnerable component and the vulnerability of these is reduced when the seats are increased (S2 through S4) making columns the most vulnerable component in the latter cases. However, the present study shows relatively little impact on the system fragility if the seat width is increased beyond the 12 – 18 inch range but other components are not improved such as the columns, as suggested by similar values of median and dispersion for the SPS with seats S2 through S4.

- Alternatively, it can be concluded that the most effective technique would be to focus on retrofitting the columns once the seat has been increased to at least the 12 – 18 inch (S2) range. The results suggest that the columns govern the overall vulnerability with seats increased to categories S2 through S4. It is not to be misconstrued that shorter seat widths are just as effective or that seats do not contribute to the vulnerability. Improvement in the performance of columns by retrofitting or replacement of the non-ductile columns with ductile ones, will demonstrate the impact of increasing the seat width potentially.
- This further reinforces the relatively fragile performance of the pile sections which are adopted as columns in the case of slab bridges and recommends for the improvement of the standard pile details to lead to betterment in their performance.
- The difference in vulnerabilities of slab bridges with diaphragm and seat abutments underscores the necessity to capture the type of abutment in a bridge which is not captured in the NBI. However, information about actual seat width is only of secondary interest. Coarse information on seats, such as short versus longer seats is sufficient to inform the system level vulnerability sufficiently accurate.

Table 6.2 provides details about the most vulnerable component across damage states in the SPS considered for this bridge class.

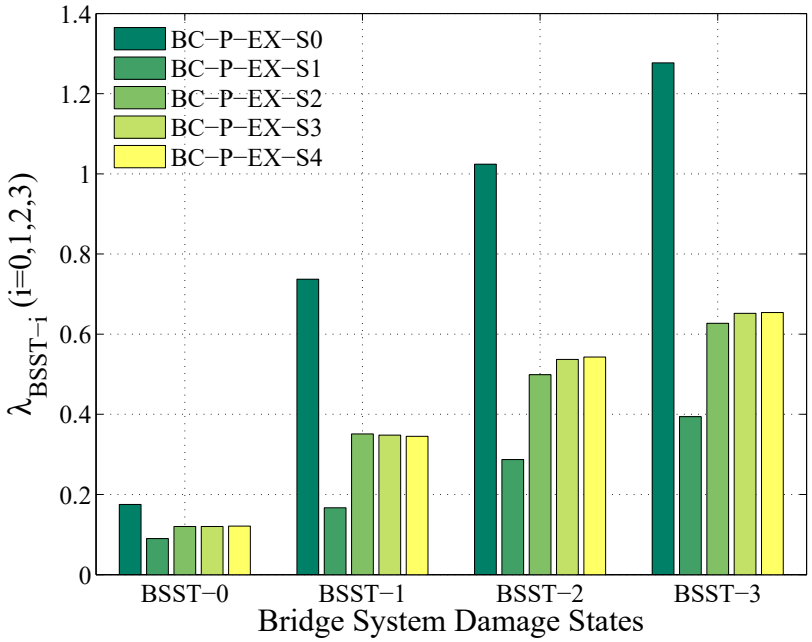

Figure 6.1: Plot of median values for MSCC-SL bridges across all damage states

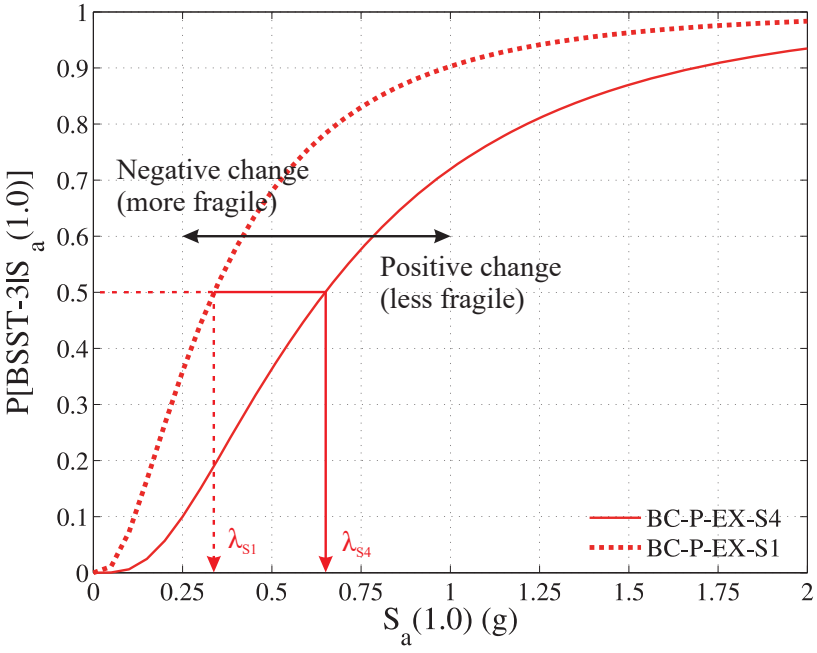

Figure 6.2: Illustration of change in median values and relative vulnerability

MSCC-SL-P-EX-S1

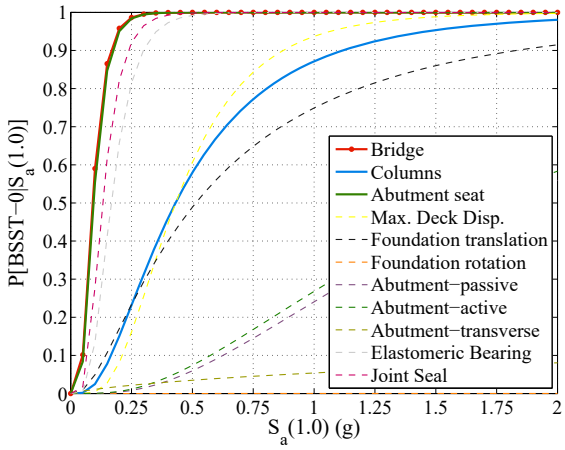

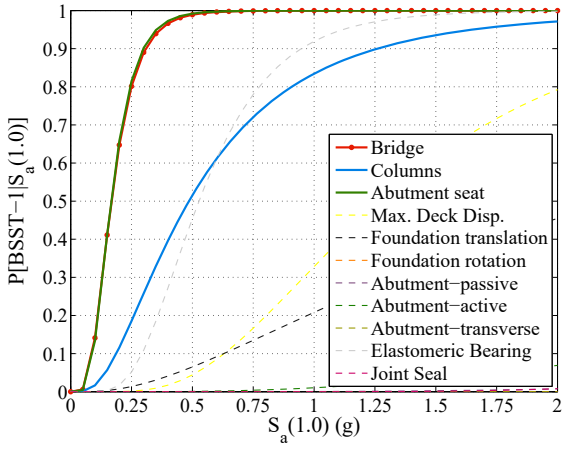

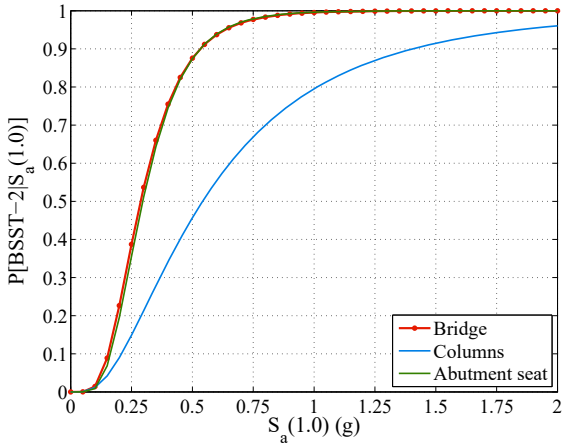

MSCC-SL-P-EX-S3

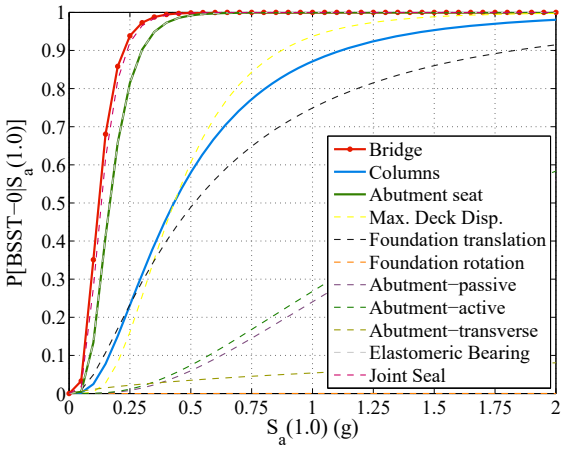

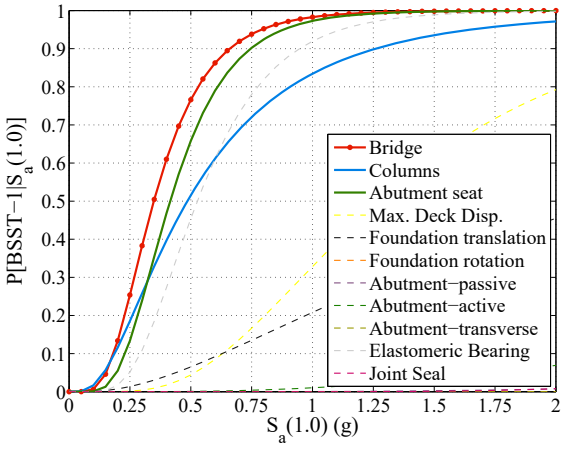

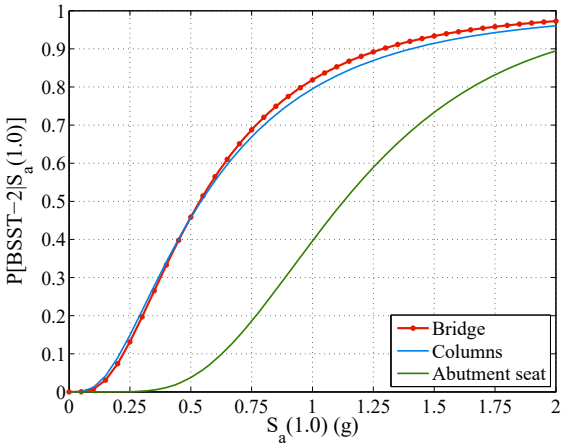

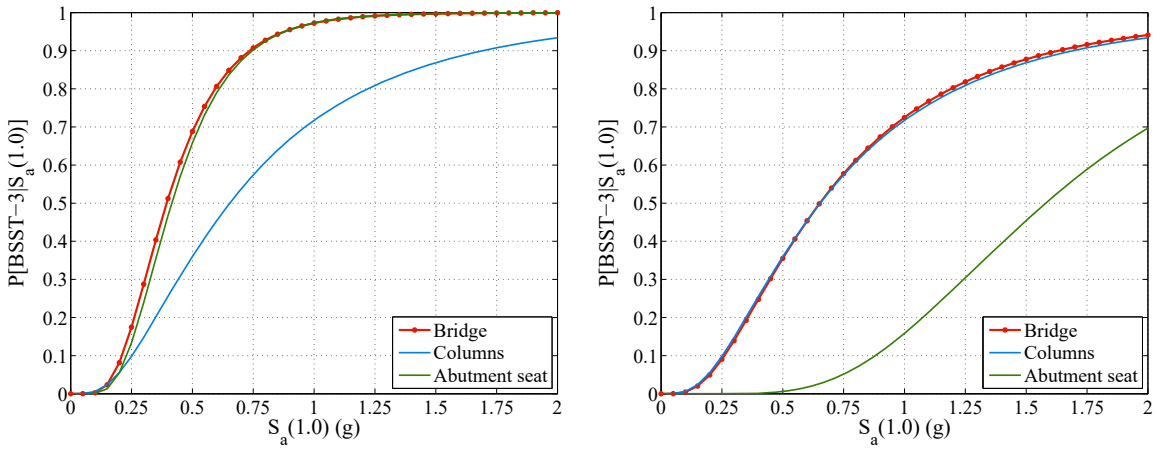

Figure 6.3: System and component level fragility curves for MSCC-SL bridges with seat type abutments and seat width class S1 and S3

Table 6.2: Details of the most vulnerable component across the SPS for MSCC-SL bridge class

Seismic performance sub-bin	BSST-0	BSST-1	BSST-2	BSST-3
MSCC-SL-P-EX-S0	Abut transverse	Columns	Columns	Columns
MSCC-SL-P-EX-S1	Abut seat	Abut seat	Abut seat	Abut seat
MSCC-SL-P-EX-S2	Joint seal	Abut seat	Columns	Columns
MSCC-SL-P-EX-S3	Joint seal	Abut seat	Columns	Columns
MSCC-SL-P-EX-S4	Joint seal	Abut seat	Columns	Columns

6.2 Multispan Continuous Concrete Single Frame Box-girder Bridges

Component and system level fragility curves are developed for MSCC-BG bridges with diaphragm and seat abutments, single and multi column bents across the three significant design eras considered in this study. Table 6.3 lists the median, λ, and dispersion, ζ, values for the SPS considered along with an average dispersion, ζ^*. Figure 6.4 shows a comparison of fragility curves for single (SCB) and multi column bents (MCB) in bridges with diaphragm abutments. A comparison of median fragilities for SCBs and MCBs with seat type abutments is shown in Figure 6.5. Based on these two figures and Table 6.3, inferences can be drawn based on the influence of the type of bent and abutment on the bridge fragility.

Table 6.3: Multispan continuous concrete box-girder bridge fragilities

Seismic performance sub-bin	BSST-0		BSST-1		BSST-2		BSST-3		
	λ	ζ	λ	ζ	λ	ζ	λ	ζ	ζ^*
Pre 1971 design era									
MSCC-BG-S-E1-S0	0.13	0.53	0.17	0.60	0.19	0.61	0.22	0.59	0.58
MSCC-BG-M-E1-S0	0.08	0.51	0.10	0.51	0.11	0.52	0.12	0.52	0.51
MSCC-BG-S-E1-S1	0.02	0.77	0.08	0.62	0.14	0.53	0.17	0.54	0.61
MSCC-BG-S-E1-S2	0.02	0.82	0.09	0.67	0.15	0.54	0.17	0.54	0.64
MSCC-BG-S-E1-S3	0.02	0.79	0.09	0.67	0.14	0.55	0.17	0.54	0.64
MSCC-BG-S-E1-S4	0.02	0.80	0.09	0.66	0.15	0.55	0.17	0.54	0.64
MSCC-BG-M-E1-S1	0.01	0.73	0.06	0.61	0.08	0.59	0.09	0.60	0.63
MSCC-BG-M-E1-S2	0.01	0.80	0.06	0.66	0.08	0.62	0.09	0.62	0.68
MSCC-BG-M-E1-S3	0.01	0.80	0.06	0.64	0.08	0.60	0.09	0.61	0.66
MSCC-BG-M-E1-S4	0.01	0.77	0.06	0.67	0.08	0.61	0.09	0.60	0.66
1971-1990 design era									
MSCC-BG-S-E2-S0	0.15	0.56	0.38	0.61	0.70	0.70	1.00	0.70	0.64
MSCC-BG-M-E2-S0	0.12	0.55	0.24	0.56	0.38	0.57	0.50	0.57	0.56
MSCC-BG-S-E2-S2	0.08	0.61	0.31	0.53	0.47	0.51	0.62	0.52	0.54
MSCC-BG-S-E2-S3	0.08	0.61	0.31	0.53	0.47	0.51	0.62	0.51	0.54
MSCC-BG-S-E2-S4	0.09	0.61	0.31	0.54	0.48	0.51	0.62	0.51	0.54
MSCC-BG-M-E2-S2	0.07	0.52	0.18	0.58	0.27	0.62	0.36	0.63	0.59
MSCC-BG-M-E2-S3	0.07	0.52	0.18	0.59	0.28	0.64	0.36	0.64	0.59
MSCC-BG-M-E2-S4	0.07	0.55	0.18	0.58	0.27	0.64	0.35	0.64	0.60
Post 1990 design era									
MSCC-BG-S-E3-S0	0.16	0.42	0.52	0.39	0.95	0.40	1.26	0.40	0.40
MSCC-BG-M-E3-S0	0.11	0.54	0.32	0.53	0.61	0.56	0.84	0.57	0.55
MSCC-BG-S-E3-S3	0.09	0.55	0.57	0.53	1.44	0.48	2.06	0.49	0.51
MSCC-BG-S-E3-S4	0.09	0.56	0.57	0.53	1.44	0.48	2.06	0.49	0.51
MSCC-BG-M-E3-S3	0.06	0.57	0.26	0.55	0.59	0.59	0.87	0.60	0.58
MSCC-BG-M-E3-S4	0.06	0.58	0.26	0.55	0.61	0.60	0.88	0.61	0.59

6.2.1 Trends based on Diaphragm Abutments

The following inferences can be drawn for SCBs and MCBs in bridges with diaphragm abutments across the three significant design eras considered in this study.

- The vulnerability of both SCBs and MCBs reduces with the evolution of the column design philosophy. Post 1990 era designed bridges with diaphragm

abutments are much less vulnerable when compared to their pre 1971 counterparts irrespective of the type of bent.

- In general, it is seen that SCBs are less vulnerable when compared to the MCBs. MCBs with diaphragm abutments are 46%, 50% and 34% more vulnerable in comparison to their SCB counterparts in the pre 1971, 1971-1990 and post 1990 design eras, respectively. Similar observations are seen in the case of seat abutments with MCBs, which are 47%, 42% and 57% more vulnerable than SCBs in the pre 1971, 1971-1990 and post 1990 design eras, respectively.
- The relative change in median values of post 1990 and 1971-1990 era SCBs with respect to their pre 1971 counterparts is 473% and 355% respectively, while the equivalent quantities in the case of MCBs is 592% and 317%, respectively – at the BSST-3 damage state. This indicates that the evolution of column design has a major impact in the reduction of vulnerability in MCBs when compared to SCBs although the former are more vulnerable when compared to the latter. The reduced vulnerability of SCBs when compared to MCBs may be attributed to a wide variety of reasons including the bridge geometry and dimensions, end conditions of the columns (pinned condition in the case of MCBs versus rotational restraint in the case of SCBs), to mention a few.
- Further the difference in vulnerabilities of SCBs and MCBs underscore the necessity to capture the type of bent in a bridge which is not available through the NBI.

Table 6.4 lists the most vulnerable component in MSCC-BG bridges with diaphragm abutments across the system damage states.

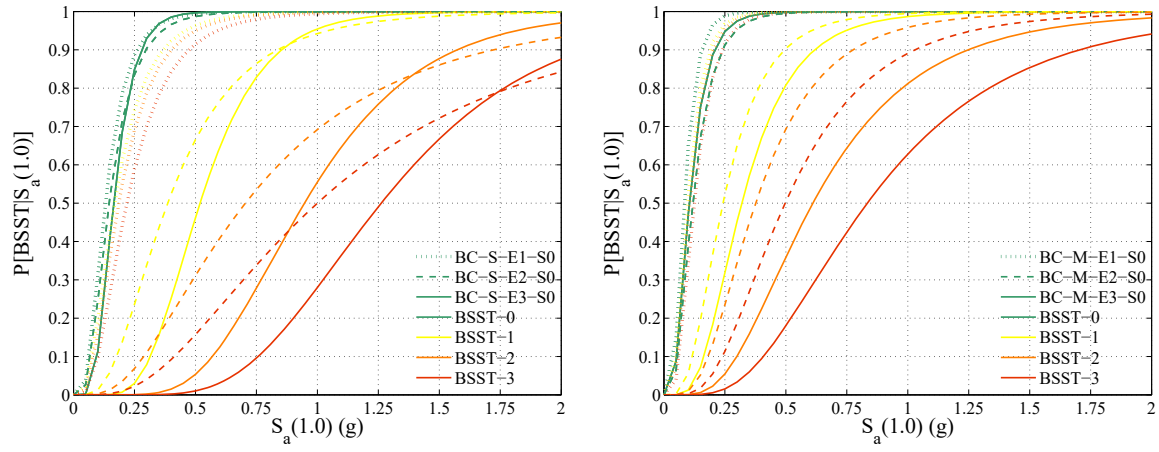

a) b)

Figure 6.4: Fragility curves for MSCC-BG bridges with diaphragm abutments across design eras having a) single column bents, and b) multi column bents

Table 6.4: Details of the most vulnerable component for MSCC-BG bridge class and diaphragm abutments

Seismic performance sub-bin	BSST-0	BSST-1	BSST-2	BSST-3
MSCC-BG-S-E1-S0	Columns	Columns	Columns	Columns
MSCC-BG-S-E2-S0	Abut transverse	Columns	Columns	Columns
MSCC-BG-S-E3-S0	Abut transverse	Columns	Columns	Columns
MSCC-BG-M-E1-S0	Columns	Columns	Columns	Columns
MSCC-BG-M-E2-S0	Abut transverse	Columns	Columns	Columns
MSCC-BG-M-E3-S0	Abut transverse	Columns	Columns	Columns

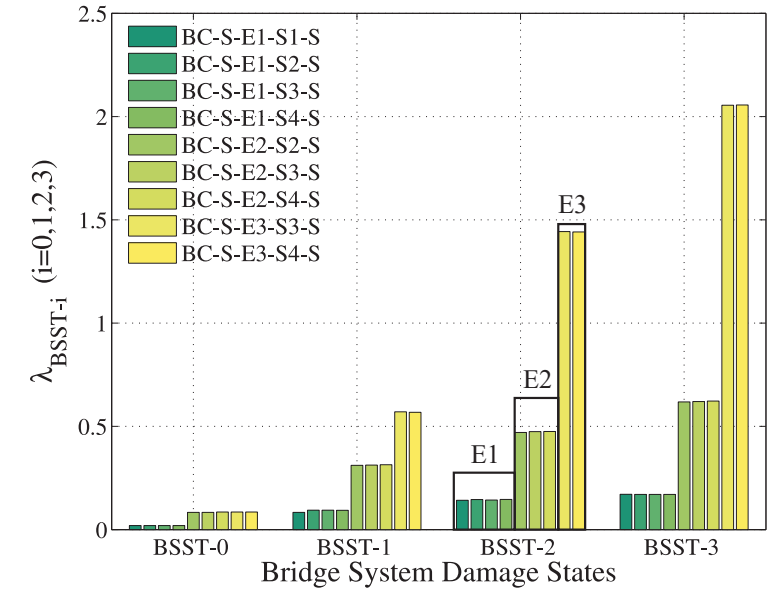

a)

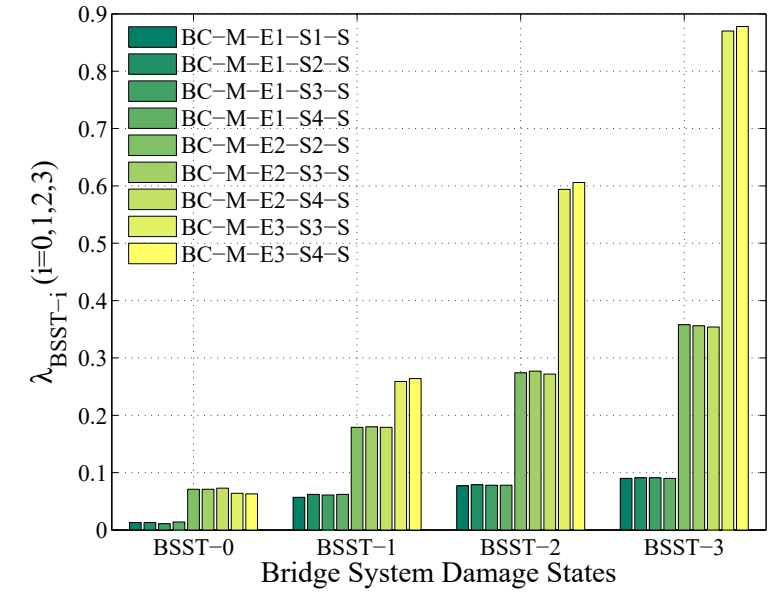

b)

Figure 6.5: Plot of median values for MSCC-BG bridges with seat abutments across design eras for a) single column bents, b) multi column bents

6.2.2 Trends based on Seat Abutments

The following inferences can be drawn for SCBs and MCBs in bridges with seat type abutments across the three significant design eras considered in this study. It must be noted that bridges in the E1 era have all possible ranges of seat widths (S1 through S4),

while those designed in the 1971-1990 design era have only three possible ranges (S2 through S4). Bridges designed post 1990 fall under the S3 and S4 categories and this is depicted in Figure 6.5(a). Additionally, the same trend exists with respect to seat width availability per era in the case of MSCC-TG and MSCC-IG bridge classes which are discussed subsequently in this chapter.

- As in the case of diaphragm abutments, it is seen that the vulnerability of both SCBs (Figure 6.5(a)) and MCBs (Figure 6.5(b)) decreases with an evolution of column design philosophy.
- For a given design era, it is seen that the median fragilities remain consistently similar across the range of seat widths. This is due to the fact that columns govern the vulnerability in most cases and the details of the most vulnerable component are documented in Table 6.5. This serves as an indicator to prioritize the efforts leading to betterment in the performance of columns which will then help realize the true impact of increasing the seat widths.
- In any case, it is seen that there is a tremendous reduction in the vulnerability of post 1990 and 1971-1990 designed bridges with both SCBs and MCBs when compared to their respective pre 1971 counterparts.
- SCBs with seat type abutments are much less vulnerable when compared to MCBs with seat abutments. The median fragilities for post 1990 designed bridges with SCBs is found to be 2.06g in contrast to 0.88g for MCBs therefore making the MCBs 57% more vulnerable when compared to the SCBs. This once again underscores the necessity to capture the type of bent which is not captured by NBI to date.

Table 6.5: Details of the most vulnerable component for MSCC-BG bridge class and seat abutments

Seismic performance sub-bin	BSST-0	BSST-1	BSST-2	BSST-3
MSCC-BG-S-E1-S1	Abut seat	Abut seat	Abut seat	Abut seat
MSCC-BG-S-E1-S2	Joint seal	Abut seat	Columns	Columns
MSCC-BG-S-E1-S3	Joint seal	Abut seat	Columns	Columns
MSCC-BG-S-E1-S4	Joint seal	Abut seat	Columns	Columns
MSCC-BG-M-E1-S1	Joint seal	Abut seat	Abut seat	Abut seat
MSCC-BG-M-E1-S2	Joint seal	Abut seat	Columns	Columns
MSCC-BG-M-E1-S3	Joint seal	Abut seat	Columns	Columns
MSCC-BG-M-E1-S4	Joint seal	Abut seat	Columns	Columns
MSCC-BG-S-E2-S2	Joint seal	Columns	Columns	Columns
MSCC-BG-S-E2-S3	Joint seal	Columns	Columns	Columns
MSCC-BG-S-E2-S4	Joint seal	Columns	Columns	Columns
MSCC-BG-M-E2-S2	Joint seal	Columns	Columns	Columns
MSCC-BG-M-E2-S3	Joint seal	Columns	Columns	Columns
MSCC-BG-M-E2-S4	Joint seal	Columns	Columns	Columns
MSCC-BG-S-E3-S3	Joint seal	Abut seat	Columns	Columns
MSCC-BG-S-E3-S4	Joint seal	Abut seat	Columns	Columns
MSCC-BG-M-E3-S3	Joint seal	Columns	Columns	Columns
MSCC-BG-M-E3-S4	Joint seal	Columns	Columns	Columns

6.2.3 Trends based on the Design Era

Figure 6.6 shows a plot of median values based on design era. The following are some of the inferences that can be drawn:

- In general, irrespective of the type of bent or abutment, pre 1971 era bridges are highly vulnerable when compared to 1971-1990 and post 1990 era bridges.
- Across all the design eras, for a particular abutment type, it is seen that SCBs are much less vulnerable when compared to MCBs. The reduction in vulnerability of SCBs in comparison to MCBs is consistent for both seat and diaphragm abutments. As mentioned previously, this underscores the necessity to capture the type of bent in order to obtain reasonably good estimates of the overall vulnerability of the bridge system.

- Across the first two design eras, diaphragm abutments are much less vulnerable when compared to seat type abutments. The reduction in vulnerability of diaphragm type in comparison to seat type is consistent for both SCBs and MCBs. The lower vulnerability of diaphragm abutments may be attributed to the complete engagement of the superstructure with the abutment and load transfer mechanisms. Further, in the case of seat abutments, the overall system fragility has an added contribution from the abutment seats in addition to the columns which is absent in the case of diaphragm abutments.
- However, in the post 1990 design era, the trend is reversed and seat abutments are seen to be less vulnerable when compared to diaphragm abutments. This may be attributed to the increased demands on the columns of the latter which is found to be the most vulnerable component.
- The differences in fragilities of diaphragm and seat abutments emphasize the necessity to capture the type of abutment in order to get a reasonable estimate of the overall bridge system fragility.

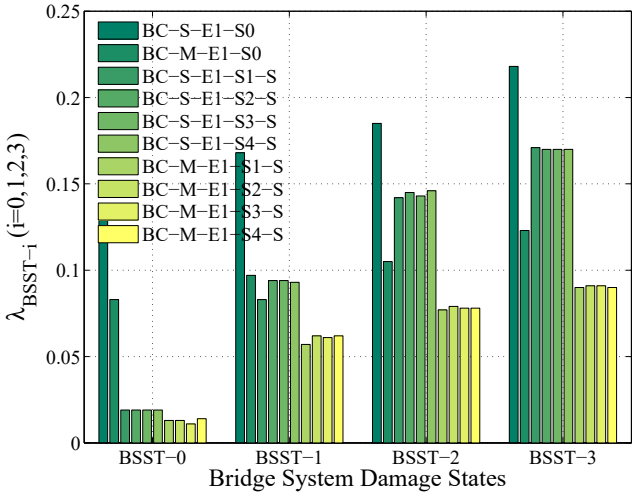

a)

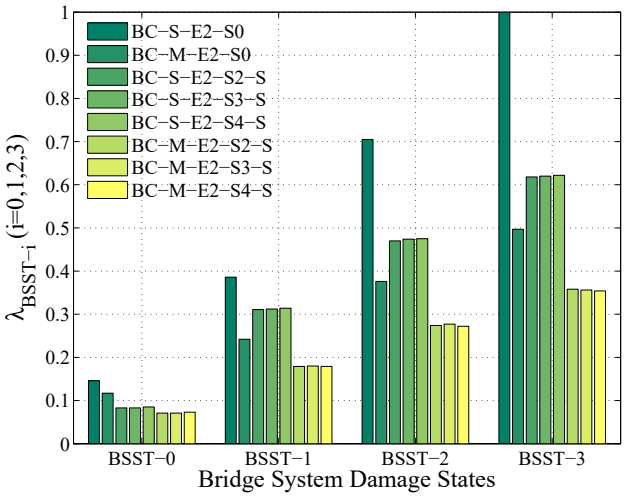

b)

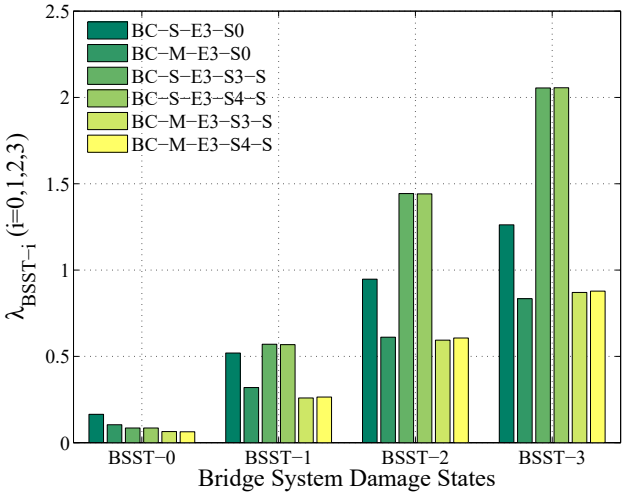

c)

Figure 6.6: Plot of median values of system fragility for a) pre 1971, b) 1971-1990, and c) post 1990 design era

6.2.4 Effect of Gap Size on the Fragility of Post 1990 MSCC-BG bridges

In order to determine the effect of the gap between the deck and abutment backwall on the vulnerability of the bridge system, fragility curves are developed for post 1990 MSCC-BG bridges with seat abutments using two ranges of gap sizes. NLTHA was conducted on two sets of 320 bridge models, the first set comprising of a small gap, denoted by S, between the deck and the abutment backwall which is considered as a uniform random variable between 0 and 1.5 in and a second set consisting of a larger gap, denoted by L, between the deck and the abutment backwall, also modeled as a uniform random number between 1.5 and 6.0 in. It must be noted that the gap size depends on the movement rating (MR) of the joint and further dictates the type of joint seal mechanism in place. Smaller gaps have Type A and B joint sealants while the larger ones have a joint seal assembly in place (either strip or modular type). Extensive details about the MR, gaps and joint seal types were provided in section 3.5.6 of Chapter 3. The comparison of gap sizes, therefore, takes into account the change in dynamic characteristics of the bridge as well as the contribution of joint seal components with different capacity definitions.

Figure 6.7 shows the comparison of median fragilities for post 1990 MSCC-BG bridges with small gap and larger gap, consisting of strip and modular joint seal assemblies. The median and dispersion values are reported in Table 6.6. The following inferences can be drawn by looking at Figure 6.7 and Table 6.6:

- The median values and dispersion for both strip and modular joint assemblies are similar across damage states for both SCBs and MCBs. This is due to the fact the joint seal does not dominate the vulnerability at the BSST-0 and -1 damage states for either case. This indicates that joints may be broadly classified based on the gap as small and large and significant additional effort is not required to further classify the gaps based on the seal mechanism.

- Bridges with large gaps and SCBs are less vulnerable when compared to small gaps. The reduced vulnerability of the abutment seat in the case of larger gaps may be attributed to the abutments not being engaged in this case. However, the trend is reversed in the case of MCBs where bridges with small gaps are less vulnerable when compared to those with large gaps. In this case, the higher vulnerability of the larger gaps may be attributed to the contribution of piles, which attract a major proportion of the force in comparison to the backfill soil. This can further be understood by a quick inspection of the component fragility curves shown in Figure 6.8, which shows the system and component level fragility curves for MSCC-BG-S-E3-S4-L and MSCC-BG-M-E3-S4-L with modular joint assembly. It is evident that in the case of MCBs, the relative contribution of abutment seat to the overall system vulnerability is much higher when compared to that in the case of SCBs, and also MCBs with smaller gaps.
- The investigation of the effect of joint gap size or MR of the joint reinforces the need to capture this attribute in order to obtain reasonable estimates of the system vulnerability. Attributing similar fragilities to either joint gap size may lead to underestimation or overestimation of the vulnerability depending on the bent type in the bridge.

Strip joint seal assembly

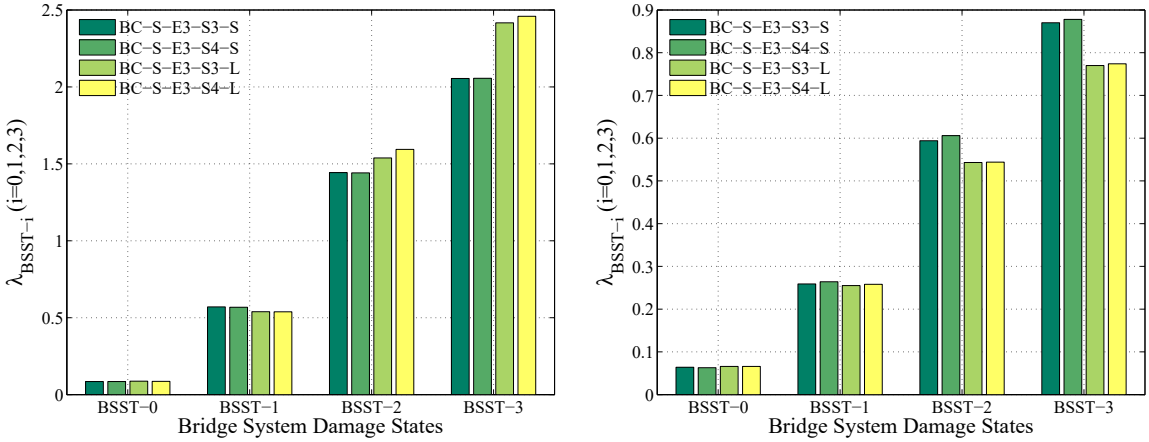

a) Single column bent b) Multi column bent

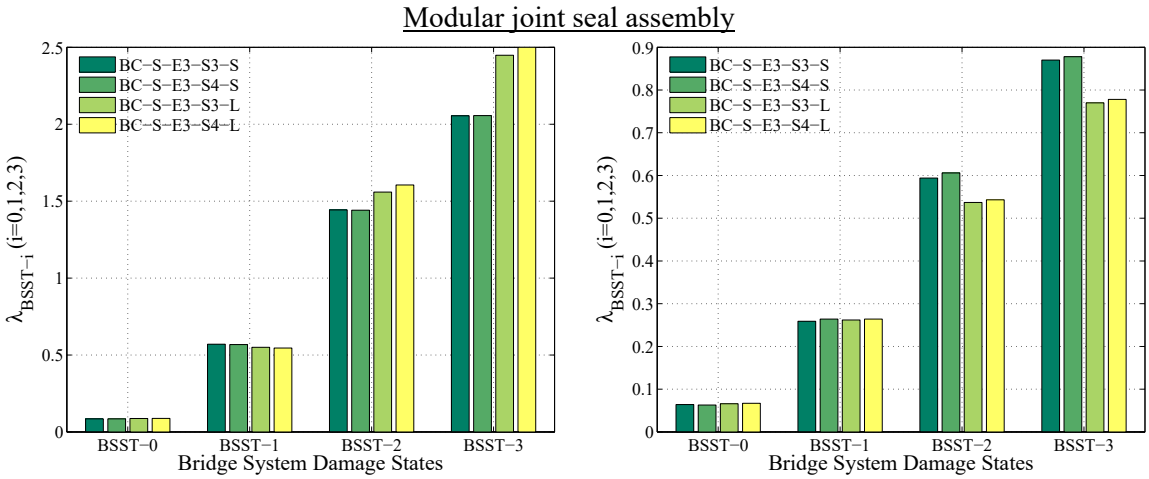

Figure 6.7: Comparison of median values for bridge fragility curves for post 1990 MSCC-BG bridges with small and large gaps installed with different joint seal units

Table 6.6: System fragilities for post 1990 designed MSCC-BG bridges with strip and modular joint seat assemblies

Seismic performance sub-bin	BSST-0		BSST-1		BSST-2		BSST-3		
	λ	ζ	λ	ζ	λ	ζ	λ	ζ	ζ*
Strip assembly									
MSCC-BG-S-E3-S3-L	0.09	0.61	0.54	0.58	1.54	0.74	2.42	0.74	0.67
MSCC-BG-S-E3-S4-L	0.09	0.60	0.54	0.58	1.59	0.76	2.46	0.74	0.67
MSCC-BG-M-E3-S3-L	0.07	0.55	0.26	0.53	0.54	0.59	0.77	0.58	0.56
MSCC-BG-M-E3-S4-L	0.07	0.55	0.26	0.54	0.54	0.59	0.77	0.59	0.56
Modular assembly									
MSCC-BG-S-E3-S3-L	0.09	0.62	0.55	0.60	1.56	0.73	2.45	0.75	0.67
MSCC-BG-S-E3-S4-L	0.09	0.64	0.55	0.59	1.61	0.76	2.50	0.77	0.69
MSCC-BG-M-E3-S3-L	0.07	0.54	0.26	0.54	0.54	0.58	0.77	0.58	0.56
MSCC-BG-M-E3-S4-L	0.07	0.56	0.26	0.55	0.54	0.59	0.78	0.59	0.57

MSCC-BG-S-E3-S4-L

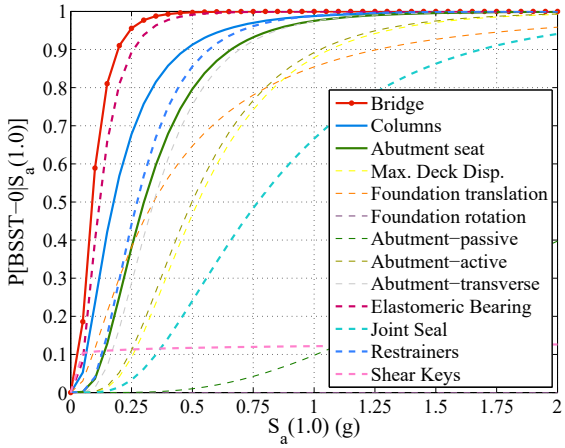

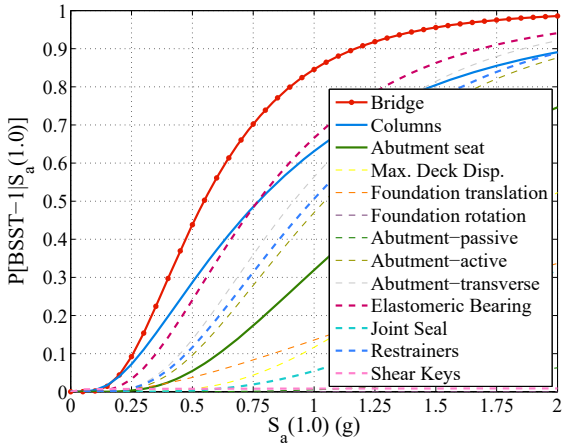

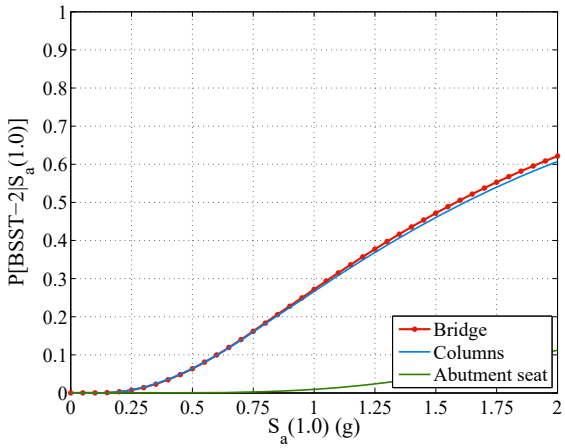

MSCC-BG-M-E3-S4-L

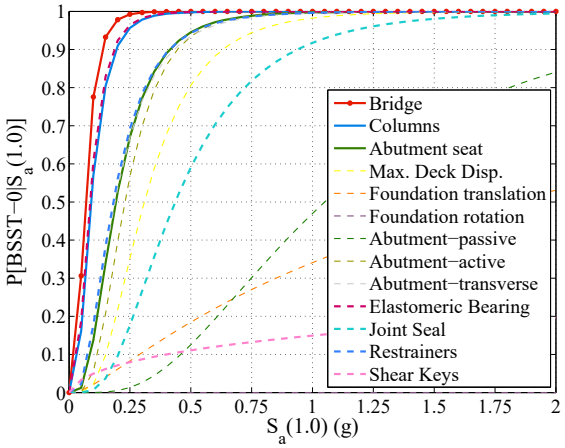

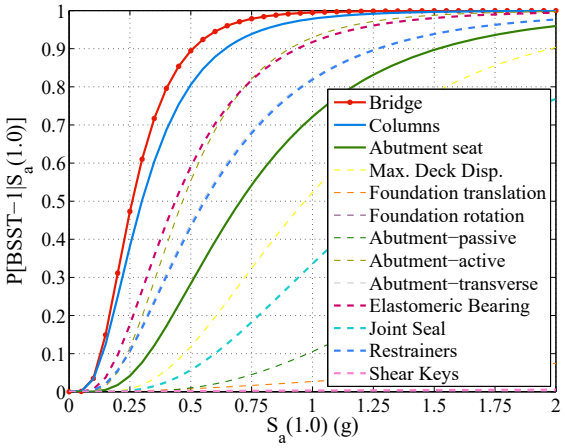

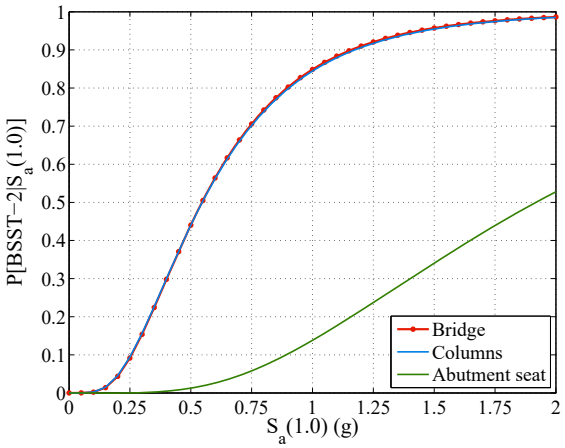

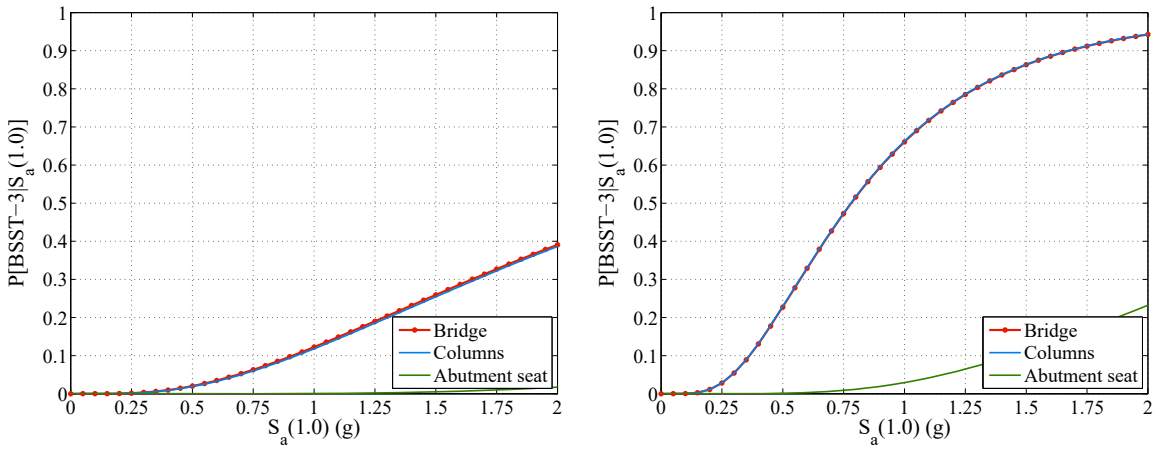

Figure 6.8: System and component level fragility curves for post 1990 MSCC-BG bridges with SCB and MCB equipped with modular joint seal assembly systems

6.3 Multispan Continuous Concrete Tee-girder Bridges

This section presents the results of fragility analysis of MSCC-TG bridges with MCB alone consisting of both integral pile columns (P) and traditional circular columns (M) with seat and diaphragm abutments. Table 6.7 lists the median, λ, and dispersion, ζ, values for the SPS considered along with an average dispersion, ζ^*. A comparison of median fragilities for integral pile columns and MCB in bridges with diaphragm and seat abutments is shown in Figure 6.9. Table 6.8 lists the most vulnerable component for the SPS considered in this bridge class.

Table 6.7**:** Multispan continuous concrete Tee-girder bridge fragilities

Seismic performance sub-bin	BSST-0		BSST-1		BSST-2		BSST-3		
	λ	ζ	λ	ζ	λ	ζ	λ	ζ	ζ*
Pre 1971 design era									
MSCC-TG-P-E1-S0	0.44	0.55	0.77	0.65	0.88	0.68	1.07	0.68	0.64
MSCC-TG-M-E1-S0	0.27	0.56	0.31	0.57	0.35	0.57	0.44	0.57	0.57
MSCC-TG-P-E1-S1	0.06	0.37	0.12	0.40	0.20	0.42	0.28	0.44	0.41
MSCC-TG-P-E1-S2	0.08	0.36	0.23	0.42	0.31	0.51	0.37	0.53	0.45
MSCC-TG-P-E1-S3	0.08	0.37	0.23	0.43	0.32	0.55	0.38	0.56	0.48
MSCC-TG-P-E1-S4	0.08	0.35	0.23	0.43	0.32	0.57	0.38	0.58	0.48
MSCC-TG-M-E1-S1	0.07	0.51	0.14	0.55	0.23	0.56	0.30	0.55	0.54
MSCC-TG-M-E1-S2	0.10	0.50	0.24	0.58	0.27	0.62	0.34	0.64	0.59
MSCC-TG-M-E1-S3	0.10	0.50	0.24	0.57	0.28	0.64	0.34	0.65	0.59
MSCC-TG-M-E1-S4	0.10	0.49	0.24	0.58	0.28	0.64	0.34	0.64	0.59
1971-1990 design era									
MSCC-TG-P-E2-S0	0.43	0.48	0.76	0.56	0.87	0.60	1.04	0.60	0.56
MSCC-TG-M-E2-S0	0.47	0.51	1.08	0.56	1.99	0.59	2.82	0.51	0.54
MSCC-TG-P-E2-S2	0.09	0.57	0.28	0.60	0.38	0.68	0.47	0.71	0.64
MSCC-TG-P-E2-S3	0.09	0.57	0.28	0.60	0.39	0.72	0.47	0.73	0.65
MSCC-TG-P-E2-S4	0.09	0.57	0.28	0.60	0.39	0.73	0.46	0.73	0.66
MSCC-TG-M-E2-S2	0.12	0.46	0.41	0.47	0.79	0.49	1.12	0.49	0.48
MSCC-TG-M-E2-S3	0.12	0.46	0.41	0.47	1.06	0.52	1.52	0.52	0.49
MSCC-TG-M-E2-S4	0.12	0.46	0.40	0.46	1.20	0.55	1.71	0.55	0.51
Post 1990 design era									
MSCC-TG-P-E3-S0	0.40	0.48	0.74	0.57	0.86	0.63	1.04	0.63	0.57
MSCC-TG-M-E3-S0	0.48	0.47	1.23	0.49	2.47	0.64	3.57	0.40	0.50
MSCC-TG-P-E3-S3	0.07	0.39	0.26	0.43	0.43	0.54	0.54	0.57	0.49
MSCC-TG-P-E3-S4	0.07	0.39	0.25	0.42	0.44	0.58	0.54	0.60	0.50
MSCC-TG-M-E3-S3	0.11	0.44	0.39	0.46	1.20	0.48	1.72	0.48	0.46
MSCC-TG-M-E3-S4	0.11	0.44	0.39	0.45	1.55	0.47	2.23	0.49	0.46

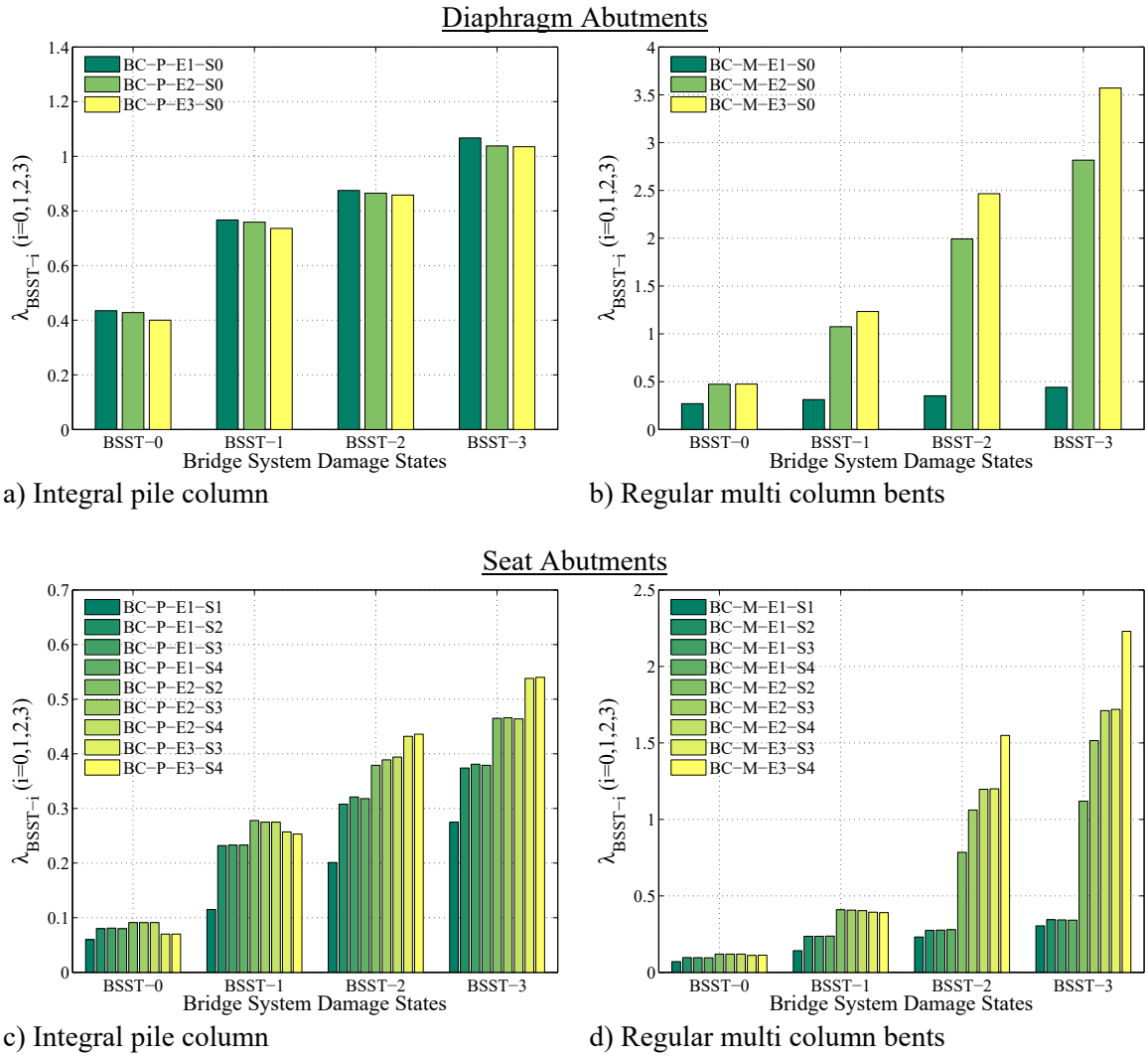

a) Integral pile column

b) Regular multi column bents

c) Integral pile column

d) Regular multi column bents

Figure 6.9: Comparison of median values of system fragility for MSCC-TG bridge class

Table 6.8: List of the most vulnerable component across damage states for the SPS in MSCC-TG bridge class

Seismic performance sub-bin	BSST-0	BSST-1	BSST-2	BSST-3
Diaphragm Abutments				
MSCC-TG-P-E1-S0	Deck disp.	Columns	Columns	Columns
MSCC-TG-P-E2-S0	Deck disp.	Columns	Columns	Columns
MSCC-TG-P-E3-S0	Deck disp.	Columns	Columns	Columns
MSCC-TG-M-E1-S0	Columns	Columns	Columns	Columns
MSCC-TG-M-E2-S0	Columns	Columns	Columns	Columns
MSCC-TG-M-E3-S0	Columns	Columns	Columns	Columns
Seat Abutments				
MSCC-TG-P-E1-S1	Abut seat	Abut seat	Abut seat	Abut seat
MSCC-TG-P-E1-S2	Joint seal	Columns	Columns	Columns
MSCC-TG-P-E1-S3	Joint seal	Columns	Columns	Columns
MSCC-TG-P-E1-S4	Joint seal	Columns	Columns	Columns
MSCC-TG-M-E1-S1	Abut seat	Abut seat	Columns	Columns
MSCC-TG-M-E1-S2	Joint seal	Columns	Columns	Columns
MSCC-TG-M-E1-S3	Joint seal	Columns	Columns	Columns
MSCC-TG-M-E1-S4	Joint seal	Columns	Columns	Columns
MSCC-TG-P-E2-S2	Joint seal	Abut seat	Columns	Columns
MSCC-TG-P-E2-S3	Joint seal	Abut seat	Columns	Columns
MSCC-TG-P-E2-S4	Joint seal	Abut seat	Columns	Columns
MSCC-TG-M-E2-S2	Joint seal	Abut seat	Abut seat	Abut seat
MSCC-TG-M-E2-S3	Joint seal	Abut seat	Columns	Columns
MSCC-TG-M-E2-S4	Joint seal	Abut seat	Columns	Columns
MSCC-TG-P-E3-S3	Joint seal	Abut seat	Columns	Columns
MSCC-TG-P-E3-S4	Joint seal	Abut seat	Columns	Columns
MSCC-TG-M-E3-S3	Joint seal	Abut seat	Abut seat	Abut seat
MSCC-TG-M-E3-S4	Joint seal	Abut seat	Abut seat	Abut seat

6.3.1 Trends based on Diaphragm Abutments

The following are some of the conclusions and inferences that can be drawn for MSCC-TG bridges with diaphragm abutments:

- The median fragilities for integral pile columns are very similar across the design eras (Figure 6.9(a)). This is due to the fact that there has been no evolution in the standard pile details through the design eras unlike traditional MCBs with circular columns which saw a radical shift in the design philosophy from brittle to ductile

behavior. This suggests that a single set of fragilities may be employed for MSCC-TG with integral pile columns and diaphragm abutments irrespective of the time of construction of the bridge.

- Contrasting the case of integral pile columns, the vulnerability of traditional MCBs reduces with the progression of design eras, as expected (Figure 6.9(b)).
- Pre 1971 design era bridges with integral pile columns are less vulnerable when compared to bridges with traditional MCBs. This may be attributed to the slightly better confinement in the former (reinforced and prestressed piles) when compared to traditional circular columns with very little confinement and hence minimal ductility capacity, which is characteristic of this design era columns.
- On the other hand, traditional MCBs in the 1971-1990 and post 1990 era bridges are less vulnerable when compared to integral pile columns. This underscores the effectiveness of the shift in design philosophy towards energy dissipation in the latter design eras.
- The difference in vulnerability of integral pile columns versus traditional MCBs underscores the necessity to capture this attribute which is not done to date in the NBI.

6.3.2 Trends based on Seat Abutments

- Traditional MCBs with seat type abutments have a tremendous reduction in their vulnerability with the evolution of seat ranges and column design philosophy (Figure 6.9(d)). The enhanced ductility capacity of the modern day columns coupled with generous seat width makes these much less vulnerable when compared to the pre 1971 bridges.
- Bridges with integral pile columns do not see a major reduction in system vulnerability with the evolution of seat widths (Figure 6.9(c)). Although abutment seats are primary components along with columns, the benefit of a larger seat

width is masked by the dominance of the brittle integral pile columns to the system vulnerability. Neglecting the subtle differences in the median fragilities, a single set of fragility curves can be used for MSCC-TG-P across the design eras for all ranges of seat widths, thereby reducing the effort to capture these attributes.

- Integral pile columns and traditional MCBs have similar fragilities in the pre 1971 design era, although integral pile columns are slightly less vulnerable. This is due to similar response characteristics and limited ductility capacity of either of them.
- However, in the latter two design eras, traditional MCBs are far less vulnerable when compared to integral pile columns. As stated previously, this once again stresses the need to capture the type of column in the bridge to obtain reasonable estimates of the vulnerability.

6.3.3 Trends based on Design Era

The plot of median fragilities based on design era is shown in Figure 6.10. The observations can be summarized as below:

- Across design eras, it is observed that irrespective of the column type, diaphragm abutments are less vulnerable when compared to seat abutments.
- In the pre-1971 design era, integral pile columns are less vulnerable when compared to traditional MCBs due to slightly better confinement in the former when compared to the latter. In the case of seat abutments, it is seen that there is insignificant reduction in the vulnerability of the bridge system beyond the 12-18 inch seat range (S2) for both integral pile columns and traditional MCBs. This is indicated by the similar values of median fragilities for seat ranges S2 through S4 across all damage states. It can therefore be concluded that the most effective technique would be to focus on retrofitting the columns once the seat has been increased to at least the 12 – 18 inch (S2) range. The results suggest that the

columns govern the overall vulnerability with seats increased to categories S2 through S4. This does not imply that shorter seat widths are just as effective or that seats do not contribute to the vulnerability. Improvement in the performance of columns by retrofitting or replacement of the non-ductile columns with ductile ones, will demonstrate the impact of increasing the seat width potentially.

- In the 1971-1990 and post 1990 design eras, traditional MCBs are less vulnerable when compared to integral pile columns due to enhanced energy dissipation and ductile characteristics. Unlike the situation in the pre 1971 era bridges, the vulnerability of traditional MCBs is reduced with an increase in the seat width. This is due to the relatively larger contribution of the abutment seat to the overall vulnerability in the latter design eras when compared to the pre 1971 design era where columns dominate the vulnerability almost entirely. This is illustrated in Figure 6.11. Unlike the case of MSCC-BG and MSCC-SL bridges, where columns dominate the vulnerability with the provision of increased seat widths beyond a certain range, the situation is not the same in the case of MSCC-TG bridges, where the provision of increased seat widths (S1 through S4) leads to a reduction in vulnerability successively. This necessitates the need to capture not only the presence of seat abutments in this bridge class, but also specific information regarding the actual seat width range, in order to obtain reliable estimates of the vulnerability.
- The median fragilities across seat ranges (S2 through S4) is similar for bridges with integral pile columns in the 1971-1990 and post 1990 design eras. This once again serves as an indicator to target the retrofit prioritization efforts towards columns to see the potential benefit of increased seat widths and reduced bridge system vulnerability.
- The percentage reduction in vulnerability between diaphragm and seat abutments for integral pile columns and traditional MCBs not consistent across the design

eras. Table 6.9 reports the percentage reduction in the vulnerability of diaphragm abutments in comparison to seat abutments for the two column types across the three design eras. Clearly it is seen that the trends are different for integral pile columns and traditional MCBs. This may be attributed to several factors such as change in the dynamic characteristics of the bridges, bridge geometry, end conditions of the column, relative vulnerability between bridge components, to mention a few.

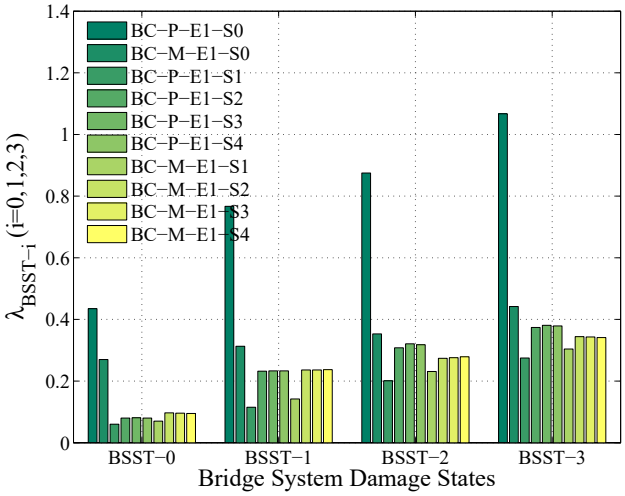

a)

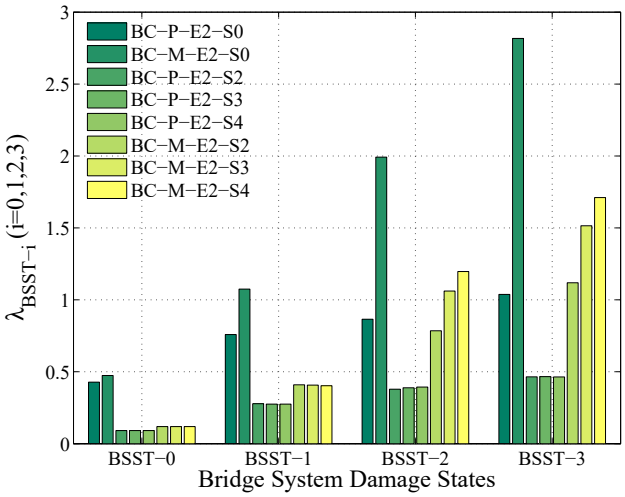

b)

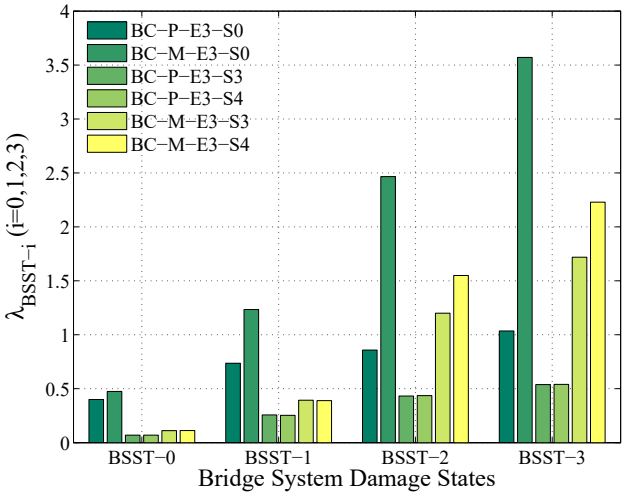

c)

Figure 6.10: Plot of median values of system fragility across damage states for MSCC-TG bridges designed a) pre 1971, b) 1971-1990, and c) post 1990

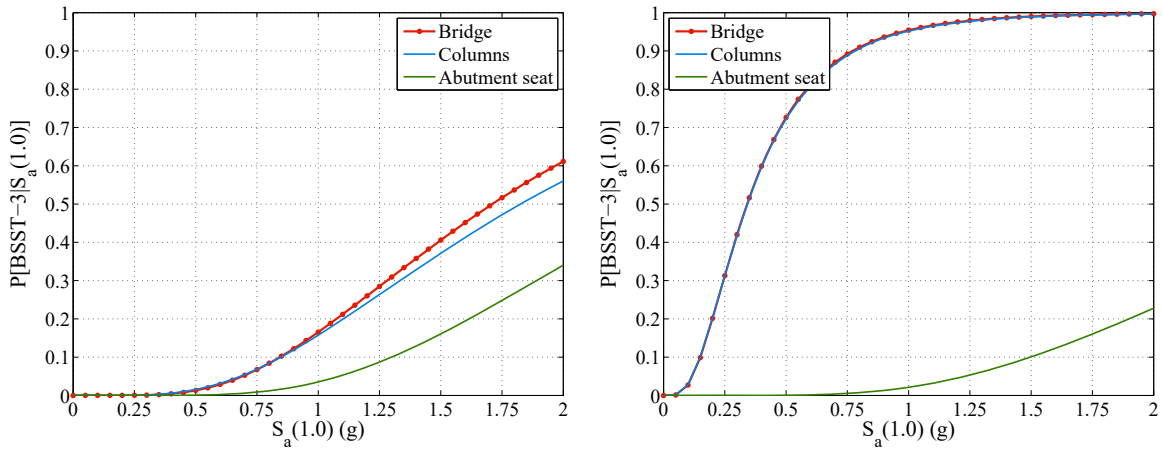

Figure 6.11: System and component fragility curves for a) MSCC-TG-M-E2-S4, and b) MSCC-TG-M-E1-S4

Table 6.9: Percentage reduction in vulnerability of diaphragm abutments with respect to seat abutments in MSCC-TG bridges

Design era	Bent (column) type	
	Integral pile columns	Traditional MCBs
Pre 1971	182%	29%
1971-1990	121%	65%
Post 1990	93%	60%

6.4 Multispan Continuous Concrete I-girder Bridges

Component and system level fragility curves are developed for MSCC-IG bridges with diaphragm and seat abutments, single and multi-column bents across the three significant design eras considered in this study. Table 6.10 lists the median, λ, and dispersion, ζ, values for the SPS considered along with an average dispersion, ζ^*. The following sub-sections provide discussion about the observed trends based on a number of criteria.

Table 6.10: Multispan continuous concrete I-girder bridge fragilities

Seismic performance sub-bin	BSST-0		BSST-1		BSST-2		BSST-3		
	λ	ζ	λ	ζ	λ	ζ	λ	ζ	ζ^*
Pre 1971 design era									
MSCC-IG-S-E1-S0	0.12	0.56	0.33	0.58	0.47	0.76	0.54	0.75	0.66
MSCC-IG-M-E1-S0	0.09	0.58	0.22	0.63	0.27	0.71	0.33	0.71	0.66
MSCC-IG-S-E1-S1	0.05	0.54	0.16	0.56	0.37	0.55	0.52	0.54	0.55
MSCC-IG-S-E1-S2	0.07	0.49	0.29	0.48	0.49	0.56	0.57	0.56	0.52
MSCC-IG-S-E1-S3	0.07	0.50	0.29	0.48	0.49	0.57	0.57	0.57	0.53
MSCC-IG-S-E1-S4	0.07	0.50	0.29	0.49	0.49	0.57	0.57	0.57	0.53
MSCC-IG-M-E1-S1	0.06	0.44	0.13	0.47	0.19	0.49	0.23	0.50	0.47
MSCC-IG-M-E1-S2	0.07	0.45	0.18	0.49	0.21	0.55	0.25	0.55	0.51
MSCC-IG-M-E1-S3	0.07	0.45	0.18	0.50	0.21	0.56	0.25	0.56	0.52
MSCC-IG-M-E1-S4	0.07	0.45	0.18	0.50	0.21	0.56	0.25	0.56	0.52
1971-1990 design era									
MSCC-IG-S-E2-S0	0.09	0.59	0.24	0.61	0.68	0.91	0.88	0.91	0.75
MSCC-IG-M-E2-S0	0.11	0.52	0.35	0.50	0.76	0.58	1.02	0.59	0.55
MSCC-IG-S-E2-S2	0.04	0.53	0.15	0.54	0.31	0.55	0.46	0.55	0.54
MSCC-IG-S-E2-S3	0.04	0.52	0.15	0.55	0.51	0.55	0.73	0.55	0.54
MSCC-IG-S-E2-S4	0.04	0.52	0.16	0.55	0.67	0.56	0.97	0.56	0.55
MSCC-IG-M-E2-S2	0.06	0.43	0.21	0.45	0.42	0.46	0.62	0.45	0.45
MSCC-IG-M-E2-S3	0.06	0.43	0.21	0.44	0.58	0.46	0.84	0.48	0.45
MSCC-IG-M-E2-S4	0.06	0.42	0.21	0.43	0.66	0.49	0.93	0.50	0.46
Post 1990 design era									
MSCC-IG-S-E3-S0	0.05	0.81	0.19	0.78	2.15	0.99	3.28	0.94	0.88
MSCC-IG-M-E3-S0	0.10	0.56	0.37	0.54	1.59	0.64	2.24	0.64	0.59
MSCC-IG-S-E3-S3	0.03	0.65	0.18	0.66	0.56	0.74	0.93	0.74	0.72
MSCC-IG-S-E3-S4	0.03	0.67	0.18	0.67	0.84	0.74	1.40	0.74	0.73
MSCC-IG-M-E3-S3	0.08	0.39	0.28	0.41	0.72	0.45	1.04	0.46	0.44
MSCC-IG-M-E3-S4	0.08	0.39	0.28	0.41	0.96	0.45	1.38	0.45	0.44

6.4.1 Trends based on Diaphragm Abutments

The plot of median values of system fragility for MSCC-IG bridges with diaphragm abutments across the three design eras is shown in Figure 6.12. The trends observed in this case are very similar to those observed in the case of MSCC-BG bridge class and can be summarized as below.

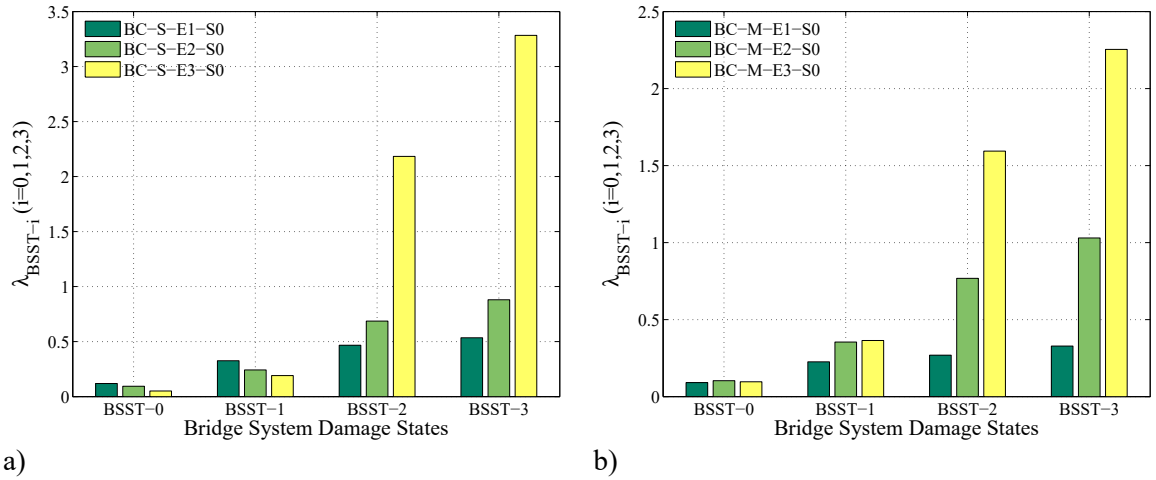

Figure 6.12: Plot of median fragilities for MSCC-IG with diaphragm abutments consisting of a) single column bents, b) multi column bents, across design eras

- The vulnerability of bridges decreases with the progression of the design era, which reinforces the effectiveness of the ductile design philosophy.
- SCBs are less vulnerable when compared to MCBs with diaphragm abutments. MSCC-IG bridges with diaphragm abutments and MCBs are 39%, 13% and 27% more vulnerable when compared to their SCB counterparts in the pre 1971, 1971-1990 and post 1990 design eras, respectively.
- This study recommends the need to capture the type of bent in the bridge owing to the differences in the median values and dispersions characterizing the system fragility due to this attribute.

6.4.2 Trends based on Seat Abutments

Figure 6.13 shows the comparison of median fragilities for I-girder bridge class with seat type abutments across the design eras considered in this study.

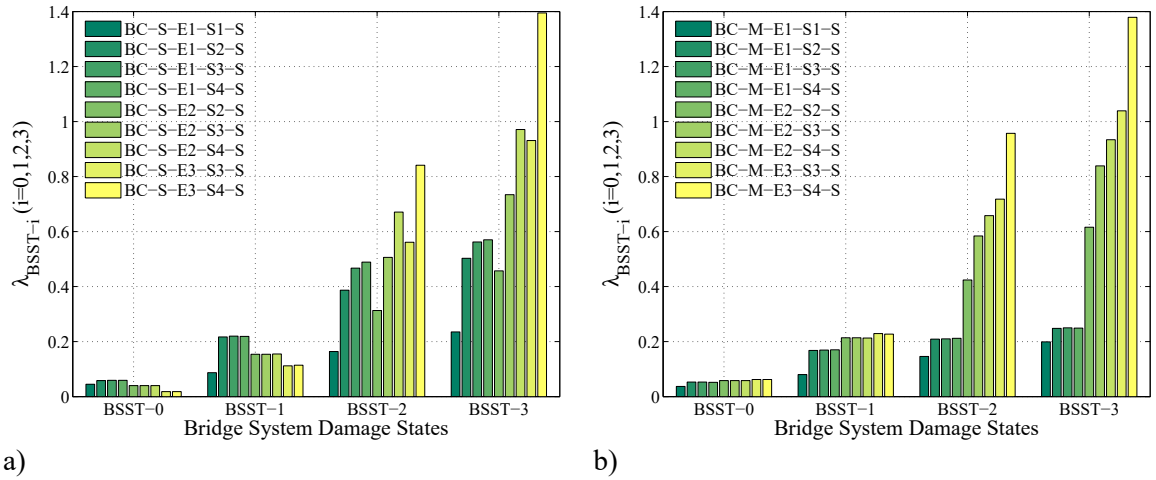

Figure 6.13: Plot of median fragilities for MSCC-IG with seat type abutments consisting of a) single column bents, b) multi column bents, across design eras

The important observations are summarized below.

- Akin to the case of diaphragm abutments, the vulnerability of bridges (both SCB and MCB) reduces across the design eras. However, in the case of seat abutments, it is seen that MCBs are less vulnerable when compared to the SCBs.
- In the pre 1971 design era it is seen that the median fragilities are similar for seat ranges S2 thru S4 and these are less vulnerable when compared to S1 as expected. This establishes the potential impact of increasing the seat widths beyond the S2 (12 – 18 in) range and focusing on modifying the response of columns in an attempt to reduce the overall vulnerability of the bridge system.
- However in the 1971-1990 and post 1990 design eras, there is a reduction in the vulnerability with the progression of seat ranges S2 through S4. This is due to the fact that the relative contribution of the abutment seat to the overall vulnerability is higher in these cases when compared to the situation in the pre 1971 designed bridges, where columns dominate the overall vulnerability.

- The results presented in this section underscore the importance of capturing attributes such as the bent type and type of abutment in order to obtain reliable estimates of the overall vulnerability of the bridge system.

Table 6.11 lists the most vulnerable component for the MSCC-IG bridge class and the different SPS associated with it.

Table 6.11: Details of the most vulnerable component for MSCC-IG bridge class

Seismic performance sub-bin	BSST-0	BSST-1	BSST-2	BSST-3
MSCC-IG-S-E1-S0	Bearings	Bearings	Columns	Columns
MSCC-IG-M-E1-S0	Bearings	Columns	Columns	Columns
MSCC-IG-S-E1-S1	Abut seat	Abut seat	Columns	Columns
MSCC-IG-S-E1-S2	Joint seal	Abut seat	Abut seat	Columns
MSCC-IG-S-E1-S3	Joint seal	Abut seat	Columns	Columns
MSCC-IG-S-E1-S4	Joint seal	Abut seat	Columns	Columns
MSCC-IG-M-E1-S1	Abut seat	Abut seat	Abut seat	Abut seat
MSCC-IG-M-E1-S2	Joint seal	Columns	Columns	Columns
MSCC-IG-M-E1-S3	Joint seal	Columns	Columns	Columns
MSCC-IG-M-E1-S4	Joint seal	Columns	Columns	Columns
MSCC-IG-S-E2-S0	Bearings	Bearings	Columns	Columns
MSCC-IG-M-E2-S0	Bearings	Bearings	Columns	Columns
MSCC-IG-S-E2-S2	Joint seal	Abut seat	Abut seat	Abut seat
MSCC-IG-S-E2-S3	Joint seal	Abut seat	Abut seat	Abut seat
MSCC-IG-S-E2-S4	Joint seal	Abut seat	Abut seat	Abut seat
MSCC-IG-M-E2-S2	Joint seal	Abut seat	Abut seat	Abut seat
MSCC-IG-M-E2-S3	Joint seal	Abut seat	Columns	Columns
MSCC-IG-M-E2-S4	Joint seal	Abut seat	Columns	Columns
MSCC-IG-S-E3-S0	Bearings	Bearings	Columns	Columns
MSCC-IG-M-E3-S0	Bearings	Bearings	Columns	Columns
MSCC-IG-S-E3-S3	Joint seal	Abut seat	Abut seat	Abut seat
MSCC-IG-S-E3-S4	Joint seal	Abut seat	Abut seat	Abut seat
MSCC-IG-M-E3-S3	Joint seal	Abut seat	Abut seat	Abut seat
MSCC-IG-M-E3-S4	Joint seal	Abut seat	Abut seat	Abut seat

6.4.3 Trends based on Design Era

The median values of system fragility curves for MSCC-IG bridges with SCBs and MCBs, seat and diaphragm abutments based on the design era are shown in Figure 6.14.

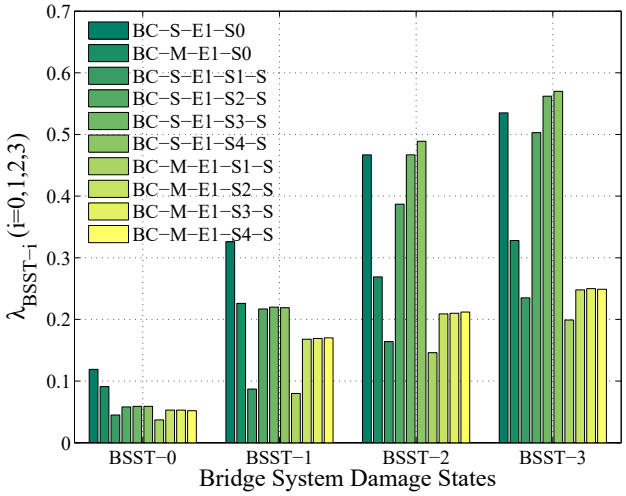

a)

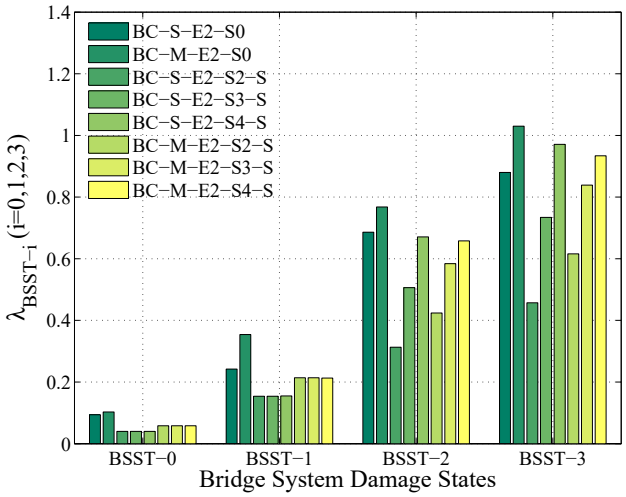

b)

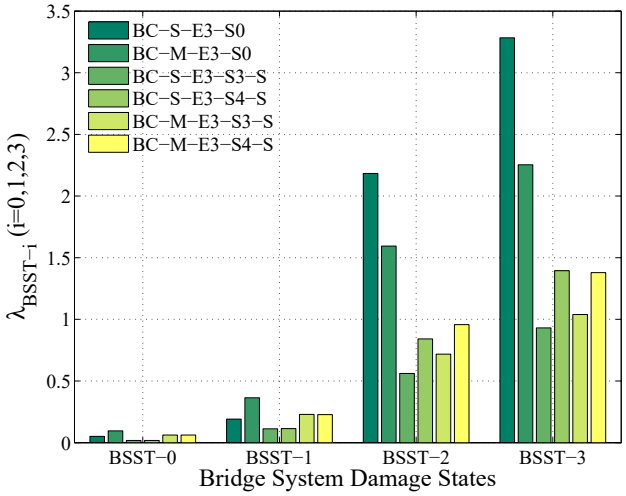

c)

Figure 6.14: Plot of median fragilities for MSCC-IG bridges designed in the a) pre 1971, b) 1971-1990, and c) post 1990 era

- Clearly, the vulnerability of the I-girder bridges reduces with the evolution of column design philosophy and seat widths moving from pre 1971 through 1971-1990 and post 1990 eras.
- MCBs and diaphragm abutments are less vulnerable when compared to MCBs and seat type abutments. However, the trend is quite complex in the case of SCBs where the seat abutments are less vulnerable when compared to diaphragm abutments in the pre 1971 and 1971-1990 design eras. However, SCBs and diaphragm abutments are less vulnerable when compared to SCBs and seat abutments in the post 1990 design era.

6.5 HAZUS Comparison

A detailed discussion about the assumptions, methodology and limitations of the HAZUS fragilities (HAZUS-MH, 2011) were discussed in Chapter 2. HAZUS fragilities were developed by synthesizing the information from the NBI alone unlike the present study where extensive data from bridge plans and in-house databases and the evolution of seismic design philosophy at the component level was used to supplement the information from NBI to obtain seismic performance sub-bins with similar characteristics. As was demonstrated in Chapter 5 and proceeding sections in this chapter, this led to significant variability in the median fragilities across design eras. Further, significant variation was seen with the SPS for the same design era. Despite the differences between the present study and HAZUS methodology, discussed previously, there are a couple of similarities. $S_a(1.0)$ is used as the intensity measure in both cases and so is the number of damage states characterizing the bridge system vulnerability. Although the vulnerability of bridges is governed by that of the columns alone in the case of HAZUS, the column damage state threshold values are chosen and the damage state descriptions are defined keeping in view the anticipated damage to the other bridge components and the HAZUS damage indicators are defined in Table 6.12.

Table 6.12: HAZUS damage state definitions (HAZUS-MH, 2011)

Damage state	Notation	Description
None	ds_1	None
Slight	ds_2	Minor spalling to the column requiring no more than cosmetic repair; minor cracking to the deck; minor cracking and spalling to the abutment; cracks in shear keys at the abutment
Moderate	ds_3	Moderate cracking (shear cracks) and spalling to the columns but is still structurally sound; moderate (< 2 in) movement of the abutment; extensive cracking and spalling of the shear keys; moderate settlement of the approach slab
Extensive	ds_4	Shear failure of the column causing strength degradation without collapse and columns is structurally unsafe; significant residual movement of superstructure-bent cap connection; vertical offset of the abutment; major settlement of the approach slab; shear key failure at the abutments
Complete	ds_5	Collapse of the column; loss of bearing support in the connection leading to unseating and imminent deck collapse; foundation failure leading to titling of the superstructure

The HAZUS median fragilities (λ_s, λ_m, λ_e, λ_c, corresponding to slight, moderate, extensive, and complete damage states, respectively) and dispersion (β_{ds}) are documented in Table 6.13. A single value of dispersion equal to 0.6 is prescribed across all the bridge classes. The equivalent bridge class notations between HAZUS and the present study are also noted to facilitate comparison. Figure 6.15 shows a plot of median values for MSCC-BG bridge class with single columns bents in the post 1990 design era and the HAZUS fragilities for illustrative purposes.

Table 6.13: Median values and dispersion for the HAZUS fragilities

Bridge class notation		Median fragilities				
Present study	HAZUS	λ_s	λ_m	λ_e	λ_c	β_{ds}
MSCC-BG-S-E1-SX	HWB8/HWB20	0.35	0.45	0.55	0.80	0.60
MSCC-BG-S-E2/3-SX	HWB9/HWB21	0.60	0.90	1.30	1.60	0.60
MSCC-TG-P/M-E1-SX MSCC-IG-S/M-E1-SX MSCC-BG-M-E1-SX MSCC-SL-P-EX-SX	HWB10/HWB22	0.60	0.90	1.10	1.50	0.60
MSCC-TG-P/M-E2/3-SX MSCC-IG-S/M-E2/3-SX MSCC-BG-M-E2/3-SX	HWB11/HWB23	0.90	0.90	1.10	1.50	0.60

Note: X stands for all possible combinations pertinent to the attribute under consideration

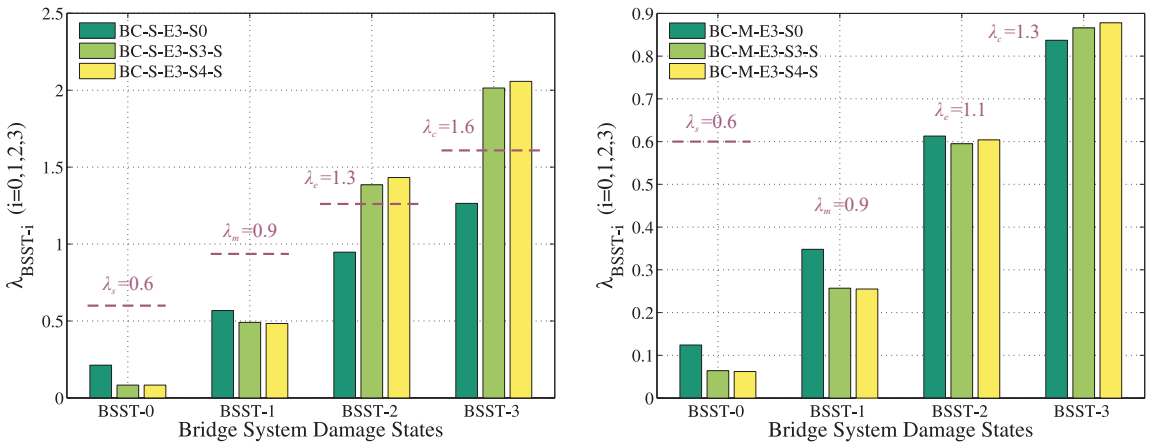

a) Single column bent b) Multi column bent

Figure 6.15: Comparison of median values of system fragility for MSCC-BG-S-E3 based on the present study and HAZUS

The following are some of the trends based on comparison:

- Bridges with diaphragm abutments are found to be more vulnerable than predicted by HAZUS, which does not distinguish this feature. The degree of vulnerability is higher for MCBs when compared to SCBs.
- Bridges with seat abutments and SCBs are more vulnerable relative to HAZUS at the BSST-0 and BSST-1 damage states while the trend reverses for the BSST-2

and -3 damage states where HAZUS predicts the bridge class to be more vulnerable.

- Bridges with seat abutments and MCBs are found to be more vulnerable than predicted by HAZUS.

The procedure of comparing the median values of the fragility at the system level is repeated for all of the bridge classes and the respective SPS across the design eras and the trends are summarized below. The percentage change in median values with respect to HAZUS is calculated in each case where a positive change in the median value indicates a less vulnerable bridge while a negative value indicates a more vulnerable bridge. These values are reported in Appendix E. In all cases, the bridges in this study are found to be more vulnerable than that predicted by HAZUS for the lower bridge system damage states, BSST-0 and BSST-1. This is mainly due to the contribution of the secondary components which account for the vulnerability at these lower damage states, which are perceived to necessitate repair.

- MSCC-BG bridges with SCBs and MCBs having both seat and diaphragm abutments in the pre 1971 and 1971-1990 design eras are more vulnerable than that predicted by HAZUS. The change in median values is very high for BSST-0 and -1 damage states when compared to the higher damage states in the bridge. In the post 1990 design era, MSCC-BG bridges with diaphragm abutments are more vulnerable than that predicted by HAZUS. The same is the case with MCBs and seat abutments. However, based on the results of this study, SCBs and seat abutments are less vulnerable than that predicted by HAZUS for the higher damage states BSST-2, and BSST-3. The dispersions obtained from the present study are close to the HAZUS values but are systematically lower for all the bridge classes considered in this study.
- The fragilities for MSCC-SL bridge class indicate that they are more vulnerable than those presented by HAZUS. The percentage change in the median values is

as high as 50% for the higher bridge damage states. The average dispersion is about 0.7 which is roughly 17% higher than the HAZUS prescribed value.

- MSCC-TG bridges with integral pile columns and traditional MCBs in the pre 1971 design era are more vulnerable than that predicted by HAZUS. In the 1971-1990 and post 1990 design eras, traditional MCBs are less vulnerable than that predicted by HAZUS. However, the integral pile columns in the 1971-1990 and post 1990 design eras are much more vulnerable (about 60% lower median value of the fragilities) than that predicted by HAZUS. The dispersions for this bridge class are generally found to be lower than that predicted by HAZUS, particularly for the integral pile columns.
- The results from this study indicate that MSCC-IG bridges in the pre 1971 design era are more vulnerable than that predicted by HAZUS. However, the SCBs in the 1971-1990 and post 1990 are less vulnerable and the percentage change in median values is as high as 160% in the case of MSCC-IG-S-E3-S4. The MCBs in the 1971-1990 design era are more vulnerable than that predicted by HAZUS, however, the trend is reversed in the case of post 1990 design era MCBs. In short, the post 1990 bridge fragilities from this study reveal much lower vulnerability than that predicted by HAZUS. The dispersions calculated in this study are lower than that proposed in HAZUS in a majority of the SPS for this bridge class.

6.6 Closure

Bridge component and system level seismic fragility curves are generated and presented for four multispan continuous concrete bridge classes with several seismic performance sub-bins across three significant design eras considered in this study. The curves are generated using Monte Carlo simulation by comparing realizations of the joint probabilistic seismic demand models with realizations of the capacity models, discussed in the previous chapter.

The following are some of the significant findings of this chapter:

- The vulnerability of all the bridge classes reduced with the evolution of column and ductile design philosophy and seat widths across the design eras considered.
- MSCC-BG bridges are the most fragile in the pre 1971 design era in comparison to the other bridge classes considered in this study. The multi column bents (MCB) are more vulnerable when compared to the single column bents (SCB).
- In the 1971-1990 design era, MSCC-BG bridges with MCBs and diaphragm abutments are the most vulnerable bridges followed by their seat abutment counterparts. MSCC-IG bridges with diaphragm abutments are the most vulnerable considering SCBs.
- MSCC-TG bridges with integral pile columns and seat abutments are the most fragile among the modern day bridges followed by MSCC-BG bridges with MCBs and diaphragm abutments.
- Across bridge classes and design eras, in general it was seen that SCBs and diaphragm abutments are relatively less vulnerable when compared to MCBs and seat abutments, barring a few exceptions.
- Comparison with HAZUS fragilities revealed the wide disparity between the results of the present study and the values prescribed in HAZUS. The results from this study indicate that a majority of the SPS in the pre 1971 and 1971-1990 design eras are more vulnerable than that predicted by HAZUS. However, the SPS in modern day bridges are less vulnerable that predicted by HAZUS in a majority of cases. Discrepancies with HAZUS are likely due to the mechanical analyses technique used to define component response distributions, system reliability definition, capacity models or damage state definitions, to mention a few.

CHAPTER 7

CONCLUSIONS AND FUTURE WORK

7.1 Summary and Conclusions

Quantification of the seismic performance of engineered structures using metrics that are readily understood and deployed by engineers, stake holders and policy makers in the decision-making framework is the fundamental aim of performance-based earthquake engineering. Bridges form the critical link in the highway infrastructure system and play a significant role in post earthquake response and recovery. Vulnerability estimation as well as quantitative and qualitative assessment of the seismic risk to highway bridges is therefore crucial in obtaining reliable estimates of the resilience of highway transportation systems. Fragility curves, which furnish the probabilities of exceeding user specified damage states or performance levels as a function of a ground motion intensity measure, have found widespread use in the area of seismic risk assessment. With the increased awareness of the high seismic hazard in California, potential vulnerabilities associated with the bridge classes and the high investments required for new construction, maintenance and retrofit, reliable estimation and quantification of the seismic risk is important which requires sufficiently accurate and reliable fragility relationships, which is the main objective of this study.

The 1971 San Fernando, 1989 Loma Prieta, and 1994 Northridge earthquakes in California motivated significant research on the seismic response, analysis, and design philosophy of bridges. These earthquakes resulted in collapse or major damage to many bridges that were at least nominally designed for seismic forces. Following the San Fernando earthquake, which exposed major deficiencies in bridges at that time, the elastic bridge design philosophy was significantly modified with a major focus on ductility and

inelasticity and special attention to detailing aspects. The Loma Prieta and Northridge earthquakes furthered this approach when significant damage was observed in bridges constructed prior to 1971. A majority of the bridges constructed after 1971 performed relatively well demonstrating the superiority of the improved design and retrofitting philosophy. In line with the temporal evolution of seismic design philosophy marked by the three design eras, pre 1971, 1971-1990, and post 1990, this study is devoted to developing fragility relationships for multispan concrete bridge classes in California capturing the unique design and detailing attributes pertinent to them.

A major task in the current research was to seek an understanding of the highway bridge inventory and capture the trends pertaining to the changes in design and detailing aspects of various bridge components across the three design eras. These include dimensions and reinforcement layout in columns, chronology of seat widths at the abutments and the bent, abutment types, foundation types, pile classes, restrainers and shear key attributes, to mention a few. Four multispan bridges classes, box-girders (MSCC-BG), slabs (MSCC-SL), Tee-girders (MSCC-TG) and I-girders (MSCC-IG) were identified and used for the development of fragility curves. In addition to the basic geometric information, such as span length, deck width, column height, and number of spans made available through the National Bridge Inventory (NBI), extensive details about the aforementioned bridge components and their respective evolutionary design features were obtained based on an extensive review of bridge plans and the California Department of Transportation (Caltrans) in-house databases. The characterization of this type of variability and its incorporation into the fragility formulation not only makes the resulting fragility models applicable to a wide geographic area, but also leads to the creation of improved bridge class sub-bins with consistent performance.

Three dimensional parameterized stochastic finite element models were developed using the finite element platform, OpenSEES. The models incorporate a high degree of detail with respect to the component modeling strategies and their ability to

capture damage due to the imposed seismic demand. Deterministic analyses of the bridge models were conducted to be used as a sanity check and study the relative response of bridge components to suggest criticalities and dynamic characteristics. An important conclusion was that columns are not always the critical components as perceived by some of the previous researchers. Significant damage can be expected to other components such as abutments, shear keys, and elastomeric bearing pads and neglect of these components in determining the vulnerability of the bridge system might not be appropriate. This is particularly important when using fragility curves for determining post earthquake repair and retrofit strategies, as in the present case, where exclusion of components other than columns might lead to damage in them being undetected.

A multiphase framework for the development of analytical fragility curves was described. Details about various parts of the framework including assembly of a ground motion suite, conducting nonlinear time history analysis (NLTHA), development of probabilistic seismic demand models (PSDM), definition of capacity models (or limit state models), formulation of component and bridge system level fragility curves was presented. A suite of 320 ground motions, 160 unscaled and 160 scaled (factor of two) ground motions assembled by Baker et al. (2011) were used in conducting NLTHA on bridge models capturing a wide range of geometric and material uncertainties, to aid in the development of PSDMs. In order to identify the optimal intensity measure (IM) to characterize component demands, an investigation was conducted on four commonly adopted and hazard computable IMs: peak ground acceleration, PGA, spectral acceleration (S_a) at 0.2 sec period, $S_a(0.2)$, $S_a(0.3)$ and $S_a(1.0)$. Metrics such as efficiency, practicality, sufficiency, and proficiency were tested and $S_a(1.0)$ was identified as the optimal IM for probabilistic seismic demand modeling and fragility analysis of typical classes of California bridges.

A significant contribution of the present study was providing damage state definitions for the components derived in such a way that they align with the Caltrans

design and operational experience. This will facilitate the application of the generated fragility curves in assessing repair and operational consequences in the aftermath of an earthquake, which is the intent of the present research. Components were grouped as primary and secondary in such a way that the component level damage has similar consequences at the bridge system level in terms of closure and repair implications. Threshold values of engineering demand parameters (EDPs) consistent with those used in the formulation of PSDMs, were identified by drawing upon the literature and expertise of Caltrans design and maintenance professionals to describe the capacity models. Typical repair strategies and visible damage patters consistent with the EDP threshold limit states values were also identified to facilitate correlation and observations in the field. Bridge component and system level fragility curves were obtained for the bridge classes and their respective seismic performance sub-bins based on the convolution of the demand and capacity models. Specifically system level fragility relationships were developed using Monte Carlo simulations and joint probabilistic seismic demand models (JPSDMs) with correlation between components considered.

Many of the key contributions of the study lie in the insights gleamed from the fragility analysis of the California bridge classes across the three design eras. The following are some of the notable findings from the fragility analysis:

- The vulnerability of all the bridge classes reduced with the evolution of column design philosophy and progressively increasing seat widths across the design eras considered.
- Multispan continuous concrete box-girder bridges with multi column bents (MCBs) and seat abutments were the most fragile in the pre 1971 design era, while MSCC-BG bridges with MCBs and diaphragm abutments are the most fragile in the 1971-1990 design era. MSCC-TG bridges with integral pile column bents and seat abutments are the most vulnerable among the modern day bridge classes.

- Across bridge classes and design eras, it was revealed that single column bents (SCBs) and diaphragm abutments are the least vulnerable.
- Comparison with HAZUS fragilities revealed the wide disparity between the results of the present study and the values prescribed in HAZUS. The results from this study indicate that a majority of the seismic performance sub-bins in the pre 1971 and 1971-1990 design eras are more vulnerable than that predicted by HAZUS. However, the seismic performance sub-bins in modern day bridge classes are less vulnerable that predicted by HAZUS in a majority of cases. Discrepancies with HAZUS are likely due to the structural modeling and analyses techniques used in the demand analysis, system reliability definition, capacity models or damage state definitions, to mention a few.

The results from this research across bridge classes underscored the necessity to capture various attributes that are not currently documented in the NBI or the state databases. Clearly, the evolution of seismic design philosophy had a profound impact on the reduction of vulnerability in the modern day bridges in comparison to their pre 1971 counterparts by as high as 60% in some cases. This stresses the need to capture unique design details and sub-bin bridge classes beyond their current classification in the NBI and HAZUS. Several other attributes such as the type of abutment (diaphragm versus seat), type of bent (single versus multi-column), foundation type (pile shafts versus pile group with a pile cap), and range of seat widths significantly affected the vulnerability. This stresses the need to capture these attributes in the NBI and state databases in order to be able to better classify the bridge classes akin to the classification in the present study and obtain reliable estimates of the vulnerability.

7.2 Research Impact

This study presented a rigorous probabilistic performance assessment framework to develop analytical seismic fragility curves for common concrete bridge classes in California. This resulted in a significant number of contributions which are as follows:

- An enhanced understanding of the evolution of seismic design philosophy along with a capture of trends in the design and detailing of several bridge components such as columns, seat widths, abutment and foundation types, and superstructure to substructure connectivity issues, over three significant design eras: pre 1971, 1971-1990, and post 1990 separated by the historic 1971 San Fernando and 1989 Loma Prieta California earthquakes.
- Modeling considerations and detailed formulations of three dimensional nonlinear finite element bridge models depicting the common Californian bridge classes. Extensive details regarding the variability in geometric and material properties across the bridge classes based on extensive review of bridge plans and Caltrans in-house databases.
- A detailed perspective on the component level damage states along with threshold values of engineering demand parameters, visible damage indicators, repair strategies and their implications on the bridge system level repair and traffic consequences consistent with Caltrans' perspective. This is particularly relevant in the field of post-earthquake inspection and management, where fragility curves are used in risk assessment and situational awareness packages such as ShakeCast or REDARS.
- Development of fragility curves considering the vulnerability of multiple components will facilitate stake holders and decision makers in the prioritization and selection of retrofit strategies based on performance metrics or cost-effectiveness strategies.

- The first systematic approach in sub-binning bridge classes based on the evolution of seismic design philosophy and developed fragility curves for each of these sub-bins considering variations in the bent type, abutment type, and range of seat widths. This leads to the development of improved sub-bins within a bridge class with consistent design and performance features in contrast to some of the previous studies that combine all the characteristics into a single bridge class.
- Fragility analysis reveal significant differences in vulnerability across the design era based sub-bins for the same bridge class. Further, differences are observed within the same sub-bin for attributes such as bent, abutment, and foundation types, to mention a few. This underscores the necessity to account for the creation of sub-bins based on design features as well as accounting for various attributes such as bent, abutment and foundation type.

7.3 Recommendations for Future Work

There are several potential arenas in which the present research can be extended. A few of these are described below:

- This study looked at the vulnerability assessment of straight and non-skewed bridges with a fixed number of spans (equal to the mode statistic obtained from the inventory analysis of the NBI data). HAZUS-MH provides median value modification factors to account for the effect of skew and number of spans and these were based on simplified static analyses. This warrants a thorough investigation, validation, and if necessary a revision to these equations by incorporating dynamic effects and three dimensional modeling strategies. Also the effect of curvature on the median fragilities should be studied, since a majority of highway interchanges have curved superstructure configurations.
- A majority of bridges with more than five spans have in-span hinges which lead to significant differences in the bridge dynamic behavior. Bridges with

intermediate hinges have evolved in their design philosophy which is unique in its consideration of balanced frame design approaches. This study should be extended to bridges with intermediate hinges and equations should be developed to modify the median fragilities akin to the modification factors for skew and number of spans.

- The sub-binning strategy should be extended to steel bridge classes capturing the evolution of seismic design philosophy in the design and detailing of steel connections, intermediate diaphragm and steel bearings, to mention a few in addition to the components captured in the present study.
- Bridge foundations and abutments may be founded on liquefiable soil and significant damage can be seen in regions with high seismic hazard. Methodologies incorporating the effect of liquefaction and ground deformation hazard through the use of macro-elements or p-y soil springs should be integrated in the fragility formulation presented in this study.
- Another area of bridge system investigations identified is a rational evaluation of costs and benefits of enhanced performance bridge structural elements and response modification devices such as base isolators, elastomeric isolation bearings, column retrofits, to mention a few. Rigorous application of the framework across the sub-bins with the potential retrofits against a complete bridge replacement using modern day design principles would enable a direct comparison of the total life cycle costs of new designs to their retrofit counterparts. Such comparisons will facilitate the understanding of effectiveness of new designs as well as the identification of new technologies and potential retrofits aimed at improved bridge performance and cost effectiveness.
- Another important aspect that deserves attention is the loss of capacity of bridge components resulting from degradation or cumulative damage due to repeated seismic events. This is of particular relevance in geographical areas where

bridges experience several mainshock-aftershock sequences, where no research is done considering the cumulative effect of multiple shocks on the load carrying capacity of bridges and this deserves a thorough investigation.

- In line with the preceding discussion, it is fairly important to consider deterioration in the component capacities due to factors such as aging and deterioration due to spalling of reinforced concrete, build of debris leading to corrosion of bridge components such as steel bearings, corrosion of the column longitudinal reinforcement etc. This is of particular significance now that more than one half of the nations' bridges are approaching the end of their design life and nearly a quarter need significant retrofit or replacement to eliminate the existing deficiencies according to published reports from the American Society of Civil Engineers (ASCE, 2009).

APPENDIX A

COMPONENT ATTRIBUTES AND MODELING ASSUMPTIONS

This Appendix is devoted to presenting details for the bridge classes to aid in the development of finite element models used for fragility analysis. The details are obtained based on an extensive review of bridge plans across the three significant design eras chosen in this study, and Caltrans in-house documents. Section A.1 presents details about attributes that are common to all bridge classes. For every bridge class, a table of modeling assumptions along with specific bridge component information is presented in the subsequent sections.

A.1 Attributes Common to all Bridge Classes

Details such the spacing of the abutment piles, soil profiles adopted in the determination of foundation translation and rotational springs are common to all the bridge classes and these are documented in this section.

A.1.1 Common Soil Profiles

The soil profile changes vastly over a wide geographic area and the stiffness of the foundation translation and rotational springs depends on the soil profile at a particular location. In order to obtain realistic estimates of bridge performance within a class, it is imperative to capture a wide range of soil profiles. Other factors such as the type of foundation system, end conditions of the columns (pinned vs. restrained) and column details (size and reinforcement) affect the stiffness of the foundation springs. The different foundation systems and the soil profiles are modeled and analyzed in LPILE and Table 5.2 in Chapter 5 summarized the parameters for the truncated normal distribution

describing the stiffness of the foundation translation and rotational springs. Typical soil profiles considered in the calculation of stiffnesses are presented in Table A.1.

Table A.1: Soil profiles considered in the stiffness calculations

Foundation type	Integral pile columns				
Soil profile	Soft		Depth of water table – 3 ft		
Description	Depth (ft)	Soil type	S_u (psf)*	ϕ*	γ (psf)*
	0 – 7	Clay	300	-	95
	7 – 17	Clay	600	-	100
	17 – 24	Sand	-	37	129
Soil profile	Stiff		Depth of water table – 30 ft		
Description	Depth (ft)	Soil type	S_u (psf)	ϕ	γ (psf)
	0 – 15	Sand	0	38	127
	15 – 43	Sand	0	40	130
Foundation type	Spread footing (pile cap) with piles				
Soil profile	Soft		Depth of water table – 3 ft		
Description	Depth (ft)	Soil type	S_u (psf)	ϕ	γ (psf)
	0 – 7	Clay	300	-	95
	7 – 17	Clay	600	-	100
	17 – 24	Sand	-	37	129
	24 – 48	Clay	1500	-	110
	48 – 58	Sand	-	36	130
	58 – 85	Sand	-	39	130
Soil profile	Stiff		Depth of water table – 30 ft		
Description	Depth (ft)	Soil type	S_u (psf)	ϕ	γ (psf)
	0 – 15	Sand	0	36	127
	15 – 41	Sand	0	38	130
	41 – 85	Sand	0	42	130

*S_u denotes the undrained shear strength, ϕ the angle of internal friction, and γ the unit weight

A.1.2 Typical Footing Configurations

Details of the typical footing configuration based on the soil profile and bridge column framing into it is described in Table A.2. It must be noted that MSCC-SL bridges employ integral pile columns. MSCC-TG bridges also employ integral pile columns in addition to traditional multi column bents (MCBs). Standard pile details were provided in section 4.3.2.1 (also see Figure 4.23) of Chapter 4. However, in the case of MSCC-BG and MSCC-IG bridges with MCBs, the foundation consists of a pile cap with a group of

piles underneath the columns. The same is the case with MSCC-IG with SCBs. MSCC-BG bridges with SCBs employ pile shafts as well as a system of pile cap and a group of piles. Details are presented in Table A.2.

Table A.2: Details of foundation systems

Bridge class	Column details	Soil profile	Foundation details
MSCC-BG MSCC-IG	6 ft dia. column – 1% long. steel	Soft	14 ft × 14 ft pile cap with 8 nos. of 24-in precast prestressed piles
		Stiff	15 ft × 15 ft pile cap with 16 nos. of 16-in precast prestressed piles
MSCC-BG MSCC-IG	6 ft dia. column – 3% long. steel	Soft	18 ft × 18 ft pile cap with 9 nos. of 24-in precast prestressed piles
		Stiff	16 ft × 14 ft pile cap with 20 nos. of 16-in precast prestressed piles
MSCC-BG MSCC-IG MSCC-TG	3 ft dia. column – 1.5% long. steel	Soft	9 ft × 9 ft pile cap with 6 nos. of 14×89 steel H section piles
		Stiff	10 ft × 10 ft pile cap with 6 nos. of 10-in cast-in-place concrete piles

A.1.3 Spacing of the Abutment Piles

Bridge Design Aids (BDA) 4-10 (2009) gives details about the pile spacing (shown in Figure A.1) depending on the pile class, typical bridge layout and support type (shown in Figure A.2), and span length.

ABUTMENT																	
	45T Pile Spacing"	I	9	8 3/4	8 1/2	8 1/4	8	8	7 3/4	7 1/2	7 1/4	7	6 3/4	6 1/2	6 1/4	6	5 3/4
	70T Pile Spacing"	I							12	11 1/2	11 1/4	11	10 1/2	10	9 3/4	9 1/4	9
	45T Pile Spacing"	IV	9 3/4	9 1/2	9 1/4	9	8 3/4	8 3/4	8 1/2	8 1/4	8	8	7 3/4	7 1/2	7 1/4	7	6 3/4
	70T Pile Spacing"	IV															
	45T Pile Spacing"	VII	8 1/2	8	7 3/4	7 1/2	7 1/4	7	6 3/4	6 1/2	6 1/4	6	5 3/4	5 1/2	5 1/4	5	4 3/4
	70T Pile Spacing"	VII				11 3/4	11 1/2	11	10 1/2	10	9 3/4	9 1/4	9	8 1/2	8	7 3/4	7 1/4
	Support Type		Length of Span "L"														
			16	18	20	22	24	26	28	30	32	34	36	38	40	42	44

Figure A.1: Typical abutment pile spacing (BDA 4-10, 2009)

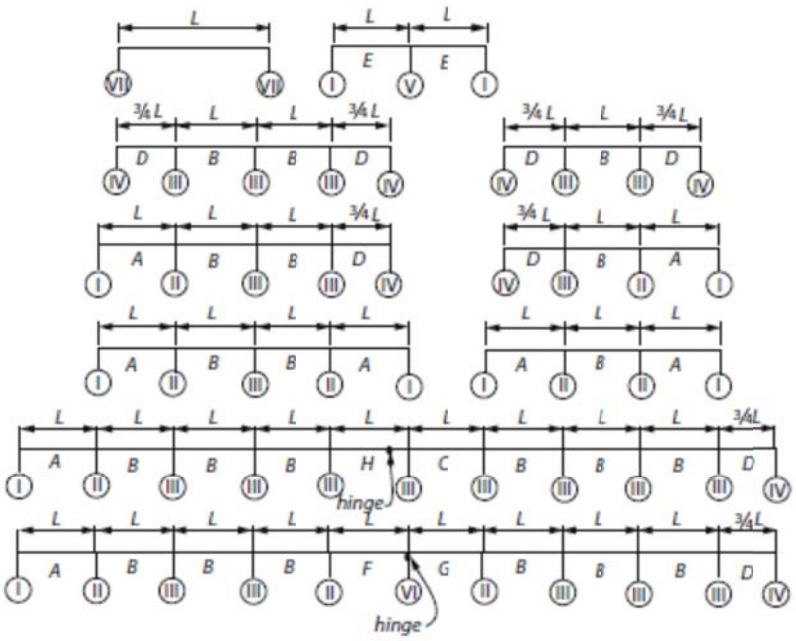

Figure A.2: Typical bridge layout to determine support type (BDA 4-10, 2009)

A.2 Multispan Continuous Concrete Box-girder Bridges

Table A.3: Bridge component details for MSCC-BG bridge class and its seismic performance sub-bins

Attribute	MSCC-BG bridge class		
	Pre 1971	1971-1990	Post 1990
Superstructure			
Number of spans	2	2	2
	This is the mode statistic based on inventory analysis		
Center span (ft)	90.0 – 180.0	90.0 – 180.0	90.0 – 180.0
Center/Edge span length	1.0	1.0	1.0
Deck width(ft)			
Minimum	25	30	30
Maximum	60	120	130
Box-girder details			
Top flange thickness (in)	See Table A.4		
	Note that this value can be decided only after determining the number of boxes and c/c spacing		
Bottom flange thickness	6.0	6.5	7.0
Wall thickness (in)	12.0	12.0	12.0
Overall girder depth	Proportioned based on typical depth-to-span ratios: Cast-in-place reinforced concrete: 0.055 Cast-in-place prestressed concrete: 0.04		
Min. number of boxes	3	3	3
Max. number of boxes	5	12	15
Number of boxes	See Table A.5		
	Having picked the number of boxes based on bridge width, the girder c/c distance is picked from Table A.1		
Elastomeric bearing pad			
Span ≤ 130 ft	14” × 14” × 2.5”	14” × 14” × 2.5”	14” × 14” × 2.5”
Span > 130 ft	20” × 14” × 2.5”	20” × 14” × 2.5”	20” × 14” × 2.5”
Columns			
Diameter (ft)			
Single column bent	6	6	7
Multi column bent	4	5	5 (2, 3, 4 col/bent) 4 (5 col/bent)
Long. reinf. ratio (%)	1.4 – 2.4	1.0 – 3.7	1.0 – 3.5
Tran. reinf. ratio (%)	#4 @ 12 in. o.c.	0.3 – 0.9	0.4 – 1.7
Number of columns per bent	See Table A.5		
Foundation			
Single column bent	Pile shaft + Pile cap with pile group	Pile shaft + Pile cap with pile group	Pile shaft + Pile cap with pile group
Multi column bent	Pile cap with pile group	Pile cap with pile group	Pile cap with pile group
	See Table 5.2 in Chapter 5 for foundation spring stiffnesses		

Abutments			
Backwall height (ft)	3.50 – 8.50	3.50 – 8.50	3.50 – 8.50
Pile spacing	See Figure A.2	See Figure A.2	See Figure A.2

Table A.4: Box-girder cell center-to-center spacing and deck slab thickness (MTD 10-20, 2008)

Reinforced concrete box-girders

REINFORCED CONCRETE BOX & STEEL GIRDERS w/ flange width >12" and < 24"						
"S"	"t"	Dimension	Transverse Bars		"D" Bars	"G" Bars
Girder CL to CL Spacing	Top Slab Thickness	"F"	Size	Spacing [1]	#5 Bars	#4 Bars
4'- 0"	7"	6"	#5	12"	3	2
4'- 3"	7"	6"	#5	12"	3	2
4'- 6"	7"	6"	#5	12"	3	2
4'- 9"	7"	7"	#5	12"	3	2
5'- 0"	7"	7"	#5	12"	4	2
5'- 3"	7"	7"	#5	12"	4	3
5'- 6"	7"	8"	#5	12"	4	3
5'- 9"	7"	8"	#5	11"	4	3
6'- 0"	7 1/8"	9"	#5	11"	5	3
6'- 3"	7 1/8"	9"	#5	11"	5	3
6'- 6"	7 1/4"	9"	#5	11"	5	3
6'- 9"	7 3/8"	10"	#5	11"	5	3
7'- 0"	7 1/2"	10"	#5	10"	6	3
7'- 3"	7 1/2"	11"	#5	10"	6	3
7'- 6"	7 5/8"	11"	#5	10"	6	3
7'- 9"	7 3/4"	11"	#5	10"	6	3
8'- 0"	7 3/4"	1'- 0"	#5	10"	7	3
8'- 3"	7 7/8"	1'- 0"	#5	10"	7	4
8'- 6"	8"	1'- 1"	#5	10"	7	4
8'- 9"	8 1/8"	1'- 1"	#5	10"	7	4
9'- 0"	8 1/8"	1'- 1"	#5	10"	7	4
9'- 3"	8 1/4"	1'- 2"	#5	10"	8	4
9'- 6"	8 3/8"	1'- 2"	#5	10"	8	4
9'- 9"	8 3/8"	1'- 2"	#5	10"	8	4
10'- 0"	8 1/2"	1'- 3"	#6	12"	10	4
10'- 3"	8 5/8"	1'- 3"	#6	11"	11	4
10'- 6"	8 5/8"	1'- 4"	#6	11"	11	4
10'- 9"	8 3/4"	1'- 4"	#6	11"	11	4
11'- 0"	8 7/8"	1'- 4"	#6	11"	11	4
11'- 3"	8 7/8"	1'- 5"	#6	11"	12	5
11'- 6"	9"	1'- 5"	#6	11"	12	5
11'- 9"	9 1/8"	1'- 6"	#6	11"	12	5
12'- 0"	9 1/8"	1'- 6"	#6	10"	13	5
12'- 3"	9 1/4"	1'- 6"	#6	10"	13	5
12'- 6"	9 3/8"	1'- 7"	#6	10"	13	5
12'- 9"	9 1/2"	1'- 7"	#6	10"	14	5
13'- 0"	9 1/2"	1'- 7"	#6	10"	14	5
13'- 3"	9 5/8"	1'- 8"	#6	10"	14	5
13'- 6"	9 3/4"	1'- 8"	#6	10"	14	5
13'- 9"	9 3/4"	1'- 9"	#6	10"	14	5
14'- 0"	9 7/8"	1'- 9"	#6	10"	14	5
14'- 3"	10"	1'- 9"	#6	10"	14	5
14'- 6"	10 1/8"	1'- 10"	#6	10"	15	5
14'- 9"	10 1/4"	1'- 10"	#6	10"	15	5
15'- 0"	10 3/8"	1'- 11"	#6	10"	15	5

Prestressed concrete box-girders

CIP PRESTRESSED BOX, PRECAST-I, & STEEL GIRDERS w/ flange width>=24"						
"S"	"t"	Dimension	Transverse Bars		"D" Bars	"G" Bars
Girder CL to CL Spacing	Top Slab Thickness	"F"	Size	Spacing [1]	#5 Bars	#4 Bars
4'- 0"	7"	5"	#5	12"	3	2
4'- 3"	7"	5"	#5	12"	3	2
4'- 6"	7"	6"	#5	12"	3	2
4'- 9"	7"	6"	#5	12"	3	2
5'- 0"	7"	6"	#5	12"	3	2
5'- 3"	7"	7"	#5	12"	3	2
5'- 6"	7"	7"	#5	12"	4	2
5'- 9"	7"	7"	#5	12"	4	3
6'- 0"	7"	8"	#5	12"	4	3
6'- 3"	7"	8"	#5	12"	4	3
6'- 6"	7 1/8"	9"	#5	12"	4	3
6'- 9"	7 1/8"	9"	#5	11"	5	3
7'- 0"	7 1/4"	9"	#5	11"	5	3
7'- 3"	7 3/8"	10"	#5	11"	5	3
7'- 6"	7 1/2"	10"	#5	11"	5	3
7'- 9"	7 1/2"	11"	#5	11"	5	3
8'- 0"	7 5/8"	11"	#5	11"	6	3
8'- 3"	7 3/4"	11"	#5	11"	6	3
8'- 6"	7 3/4"	1'- 0"	#5	11"	6	3
8'- 9"	7 7/8"	1'- 0"	#5	11"	6	4
9'- 0"	8"	1'- 1"	#5	11"	6	4
9'- 3"	8 1/8"	1'- 1"	#5	11"	7	4
9'- 6"	8 1/8"	1'- 1"	#5	11"	7	4
9'- 9"	8 1/4"	1'- 2"	#5	10"	8	4
10'- 0"	8 3/8"	1'- 2"	#5	10"	8	4
10'- 3"	8 3/8"	1'- 2"	#5	10"	8	4
10'- 6"	8 1/2"	1'- 3"	#5	10"	8	4
10'- 9"	8 5/8"	1'- 3"	#5	10"	8	4
11'- 0"	8 5/8"	1'- 4"	#6	11"	11	4
11'- 3"	8 3/4"	1'- 4"	#6	11"	11	4
11'- 6"	8 7/8"	1'- 4"	#6	11"	11	4
11'- 9"	8 7/8"	1'- 5"	#6	11"	12	5
12'- 0"	9"	1'- 5"	#6	11"	12	5
12'- 3"	9 1/8"	1'- 6"	#6	11"	12	5
12'- 6"	9 1/8"	1'- 6"	#6	11"	12	5
12'- 9"	9 1/4"	1'- 6"	#6	11"	12	5
13'- 0"	9 3/8"	1'- 7"	#6	10"	13	5
13'- 3"	9 1/2"	1'- 7"	#6	10"	14	5
13'- 6"	9 1/2"	1'- 7"	#6	10"	14	5
13'- 9"	9 5/8"	1'- 8"	#6	10"	14	5
14'- 0"	9 3/4"	1'- 8"	#6	10"	14	5
14'- 3"	9 3/4"	1'- 9"	#6	10"	14	5
14'- 6"	9 7/8"	1'- 9"	#6	10"	14	5
14'- 9"	10"	1'- 9"	#6	10"	14	5
15'- 0"	10 1/8"	1'- 10"	#6	10"	15	5

Table A.5: Number of cells in the box-girder and number of columns per bent as a function of deck width for MSCC-BG bridges

a) Pre 1971 design era

# boxes	# columns	Width range (ft)
3	1	Upto 40
5	2	> 40

b) 1971-1990 design era

# boxes	# columns	Width range (ft)
3	1	Upto 40
5	2	40 – 60
7	3	60 – 80
9	3	80 – 100
11	4	> 100

c) Post 1990 design era

# boxes	# columns	Width range (ft)
3	1	Upto 40
5	2	40 – 60
7	3	60 – 80
9	4	80 – 100
11	5	100 – 120
15	5	> 120

A.3 Multispan Continuous Concrete Slab Bridges

Table A.6: Bridge component details for MSCC-SL bridge class

Attribute	Values
Superstructure	
# of spans	3
Center span (ft)	16.0 – 50.0
Center/Edge span length	1.2
Deck width (ft)	≥ 35.0
Slab thickness	$Thickness = \max\left[\frac{S+10}{30}, 0.542\right]$ S is the maximum span length (ft) This is tabulated in Figure A.3
Elastomeric bearing pads	16” × 12” × 1.5”
Columns	Integral pile columns – See section 4.3.2.1 in Chapter 4 for details
Center-to-center spacing	See Figure A.1
Number of columns per bent	$Number\ of\ columns/bent = \frac{Width - 2y}{pile\ spacing} + 1$ y is the edge distance and is assumed to be 0.4 × pile spacing
Bent cap details	The presence of bent cap depends on the span length. Details about the bent cap dimensions and the reinforcement layout is shown in Figure A.4.
Foundation	Integral pile columns
Abutments	
Backwall height (ft)	3.5 – 8.5
Pile spacing	See Figure A.2

L=Length of Span			16′	18′	20′	22′	24′	26′	28′	30′	32′	34′	36′	38′	40′	42′	44′
REINFORCEMENT	Top of Slab	ⓐ bars	Size	#7	#7	#7	#7	#8	#8	#8	#9	#9	#9	#10	#10	#10	#10	#10
			Length[1]	34.0′	38.0′	42.0′	46.0′	50.0′	54.0′	58.0′	74.0′	78.0′	82.0′	90.0′	94.0′	98.0′	102′	106′
		ⓑ bars	Size	#7	#7	#7	#7	#7	#8	#8	#8	#9	#9	#9	#10	#10	#10	#10
			Length	12.0′	13.0′	15.0′	16.0′	17.0′	18.0′	19.0′	15.0′	16.0′	17.0′	18.0′	19.0′	20.0′	20.0′	21.0′
			Xb	6.0′	6.5′	7.5′	8.0′	8.5′	9.0′	9.5′	7.5′	8.0′	8.5′	9.0′	9.5′	10.0′	10.0′	10.5′
		ⓒ bars	Size	#7	#7	#7	#7	#7	#7	#8	#8	#8	#9	#9	#9	#9	#10	#10
			Length	6.0′	6.0′	6.0′	7.0′	7.0′	8.0′	8.0′	9.0′	11.0′	11.0′	11.0′	11.0′	12.0′	12.0′	14.0′
			Xc	3.0′	3.0′	3.0′	3.5′	3.5′	4.0′	4.0′	4.5′	5.5′	5.5′	5.5′	5.5′	6.0′	6.0′	7.0′
	Bottom of Slab	ⓓ bars	Size	#7	#7	#7	#8	#8	#8	#8	#8	#8	#9	#9	#9	#9	#9	#9
			Length[1]	36.0′	40.0′	44.0′	48.0′	52.0′	56.0′	60.0′	68.0′	72.0′	78.0′	82.0′	86.0′	90.0′	94.0′	98.0′
		ⓔ bars	Size	#7	#7	#7	#7	#7	#8	#8	#8	#8	#8	#8	#9	#9	#9	#9
			Length	16.5′	18.0′	20.0′	19.5′	21.0′	23.0′	24.5′	26.0′	27.5′	29.5′	31.0′	32.5′	34.5′	36.0′	37.5′
			Xe	0.5′	1.0′	1.0′	3.5′	4.0′	4.0′	4.5′	5.0′	5.5′	5.5′	6.0′	6.5′	6.5′	7.0′	7.5′
		ⓕ bars	Size	#7	#7	#7	#7	#7	#7	#7	#8	#8	#8	#8	#8	#8	#9	#9
			Length	12.0′	13.0′	14.5′	15.5′	17.0′	18.0′	19.0′	20.5′	22.0′	23.0′	24.5′	26.0′	27.5′	28.5′	30.0′
			Xf	3.5′	4.5′	5.0′	5.5′	6.0′	6.5′	7.0′	8.0′	8.5′	9.0′	9.5′	10.0′	10.5′	11.0′	11.5′
Distribution Steel			Size	#5	#5	#5	#5	#5	#5	#5	#5	#5	#5	#5	#5	#5	#5	#5
			Spacing	12"	12"	12"	12"	12"	12"	12"	12"	12"	12"	12"	12"	12"	12"	12"
Top of Slab Transverse Reinforcement			Size	#4	#4	#4	#4	#4	#4	#4	#4	#4	#5	#5	#5	#5	#5	#5
			Spacing	18"	18"	18"	15"	15"	15"	12"	12"	12"	18"	18"	15"	15"	15"	15"
T= Thickness of Slab[2]				10½"	11½"	12"	13"	14"	14½"	15½"	16"	17"	18"	18½"	19½"	20"	21"	22½"
Approximate quantities per foot of width		Concrete (ft³)		14.7	18.0	20.8	24.6	28.9	32.3	37.1	41.0	46.4	52.1	56.7	63.0	67.9	74.8	83.9
		Steel (lbs)		125	138	152	176	205	235	253	306	331	373	425	472	496	534	560
Camber at Mid-Span				.01′	.01′	.02′	.02′	.03′	.03′	.04′	.05′	.05′	.06′	.07′	.08′	.09′	.10′	.10′

Figure A.3: Deck slab thickness for MSCC-SL bridges as a function of span length (BDA 4-10, 2009)

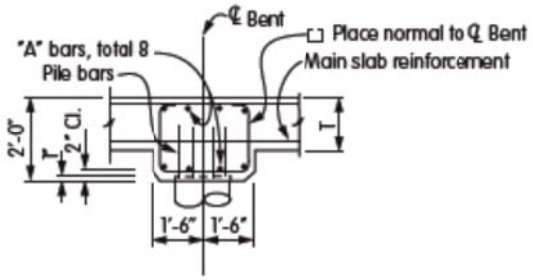

a) Bent cap – spans ≤ 28 ft

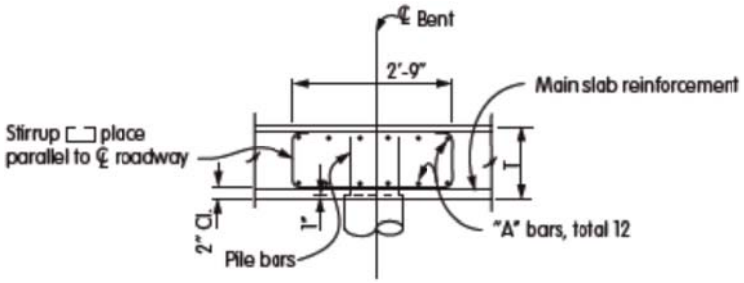

b) Bent cap – spans > 28 ft

		Support Type	Length of Span "L"														
			16	18	20	22	24	26	28	30	32	34	36	38	40	42	44
BENT CAP	45T Pile Spacing*	I	7 1/2	7 1/4	6 1/2	6	5 3/4	5 1/4	5	4 3/4	4 1/2	4 1/4	4				
	"A" bars (Skew 0-20)	I	#7	#7	#7	#7	#7	#7	#7	#6	#7	#6	#6				
	"A" bars (Skew 21-35)	I	#8	#8	#7	#7	#7	#7	#7	#6	#7	#7	#6				
	"A" bars (Skew 36-50)	I	#8	#8	#8	#8	#8	#8	#8	#7	#7	#7	#7				
	Stirrup Spacing	I	#5@12	#5@12	#5@12	#5@12	#5@12	#5@12	#5@12	#5@6	#5@7	#5@7	#5@9				
	70T Pile Spacing*	I	12	11 1/4	10 1/4	9 1/2	8 3/4	8 1/4	7 3/4	7 1/2	7	6 1/2	6	5 3/4	5 1/2	5	4 3/4
	"A" bars (Skew 0-20)	I	#8	#8	#8	#8	#8	#8	#8	#8	#7	#7	#7	#7	#7	#7	#7
	"A" bars (Skew 21-35)	I	#9	#9	#8	#8	#8	#8	#8	#8	#8	#8	#7	#7	#7	#7	#7
	"A" bars (Skew 36-50)	I	#10	#10	#10	#9	#9	#9	#9	#9	#9	#8	#8	#8	#7	#8	#8
	Stirrup Spacing	I	#5@8	#5@8	#5@8	#5@7	#5@7	#5@7	#5@7	#6@6	#5@4	#5@4	#5@5	#5@6	#5@7	#5@9	#5@10
	45T Pile Spacing*	III	8 1/4	7 3/4	7 1/2	7	6 1/2	6	5 3/4	5 1/2	5 1/4	5	4 3/4	4 1/2	4		
	"A" bars (Skew 0-20)	III	#7	#7	#7	#7	#7	#7	#7	#6	#7	#7	#6	#6	#6		
	"A" bars (Skew 21-35)	III	#8	#8	#8	#8	#8	#7	#7	#7	#7	#7	#7	#6	#6		
	"A" bars (Skew 36-50)	III	#8	#8	#8	#8	#8	#8	#8	#8	#7	#7	#7	#7	#7		
	Stirrup Spacing	III	#5@12	#5@12	#5@12	#5@12	#5@12	#5@12	#5@12	#5@6	#5@7	#5@8	#5@10	#5@11	#5@12		
	70T Pile Spacing*	III			11 3/4	10 3/4	10	9 1/2	9	8 1/2	8	7 3/4	7 1/4	6 3/4	6 1/4	6	5 1/2
	"A" bars (Skew 0-20)	III			#8	#8	#8	#8	#8	#8	#8	#7	#7	#7	#7	#7	#7
	"A" bars (Skew 21-35)	III			#9	#9	#8	#8	#8	#9	#8	#8	#8	#7	#7	#8	#7
	"A" bars (Skew 36-50)	III			#10	#10	#9	#9	#9	#10	#9	#9	#8	#8	#8	#8	#8
	Stirrup Spacing	III			#5@8	#5@8	#5@8	#5@7	#5@7	#6@6	#5@4	#5@4	#5@5	#5@5	#5@7	#5@8	#5@10
	45T Pile Spacing*	V	7 1/2	6 3/4	6 1/4	5 3/4	5 1/2	5	4 3/4	4 1/2	4 1/4						
	"A" bars (Skew 0-20)	V	#7	#7	#7	#7	#7	#7	#7	#6	#6						
	"A" bars (Skew 21-35)	V	#8	#7	#7	#7	#7	#7	#7	#6	#7						
	"A" bars (Skew 36-50)	V	#8	#8	#8	#8	#8	#8	#8	#7	#7						
	Stirrup Spacing	V	#5@12	#5@12	#5@12	#5@12	#5@12	#5@12	#5@12	#5@6	#5@7						
	70T Pile Spacing*	V	11 1/2	10 1/2	10	9	8 1/2	8	7 1/2	7	6 1/2	6	5 3/4	5 1/4	5	4 3/4	4 1/4
	"A" bars (Skew 0-20)	V	#8	#8	#8	#8	#8	#8	#8	#8	#7	#7	#7	#7	#7	#7	#6
	"A" bars (Skew 21-35)	V	#9	#8	#8	#8	#8	#8	#8	#8	#8	#7	#7	#7	#7	#7	#7
	"A" bars (Skew 36-50)	V	#10	#10	#9	#9	#9	#9	#9	#9	#9	#8	#8	#8	#7	#8	#8
	Stirrup Spacing	V	#5@8	#5@8	#5@8	#5@7	#5@7	#5@7	#5@7	#6@6	#5@4	#5@4	#5@5	#5@6	#5@8	#5@9	#5@10
	45T Pile Spacing*	VI	9 1/4	8 3/4	8 1/4	7 3/4	7 1/2	7	6 1/2	6 1/4	5 3/4	5 1/2	5 1/4	4 3/4	4 1/2	4 1/4	4
	"A" bars (Skew 0-20)	VI	#7	#7	#7	#7	#7	#7	#7	#6	#7	#7	#6	#6	#6	#5	#5
	"A" bars (Skew 21-35)	VI	#8	#8	#8	#8	#8	#7	#7	#7	#7	#7	#7	#6	#6	#6	#6
	"A" bars (Skew 36-50)	VI	#8	#8	#8	#8	#8	#8	#8	#8	#7	#7	#7	#7	#7	#7	#7
	Stirrup Spacing	VI	#5@12	#5@12	#5@12	#5@12	#5@12	#5@12	#5@12	#5@6	#5@9	#5@10	#5@12	#5@12	#5@12	#5@12	#5@12
	70T Pile Spacing*	VI					11 1/2	11	10 1/4	9 3/4	9	8 1/2	8 1/4	7 1/2	7 1/4	6 3/4	6 1/2
	"A" bars (Skew 0-20)	VI					#8	#8	#8	#8	#8	#7	#7	#7	#7	#7	#7
	"A" bars (Skew 21-35)	VI					#9	#9	#8	#9	#8	#8	#8	#7	#7	#8	#7
	"A" bars (Skew 36-50)	VI					#10	#10	#9	#10	#9	#9	#9	#8	#8	#8	#8
	Stirrup Spacing	VI					#5@8	#5@8	#5@8	#5@4	#5@4	#5@5	#5@5	#5@6	#5@7	#5@9	#5@10

c) Bent cap longitudinal and transverse reinforcement

Figure A.4: Bent cap details in MSCC-SL bridges as a function of span length (BDA 4-10, 2009)

A.4 Multispan Continuous Concrete Tee-girder Bridges

Table A.7: Bridge component details for MSCC-TG bridge class and the respective seismic performance sub-bins

Attribute	MSCC-TG bridge class		
	Pre 1971	1971-1990	Post 1990
Superstructure			
Number of spans	3	3	3
Center span (ft)	40.0 – 130.0	40.0 – 130.0	40.0 – 130.0
Center/Edge span length	1.4	1.4	1.33
Deck width (ft)	30.0 – 80.0	30.0 – 80.0	30.0 – 80.0
Deck slab thickness (in)	7.0	7.0	7.0
Number of Tee girders	See Table A.8	See Table A.8	See Table A.8
Tee girder details			
Width (in)	12.0	12.0	12.0
Depth (in)	Proportioned based on typical superstructure depth to span ratio of 0.065		
Elastomeric bearing pads			
Span ≤ 100 ft	16” × 12” × 1.5”	16” × 12” × 1.5”	16” × 12” × 1.5”
Span > 100 ft	20” × 14” × 2.0”	20” × 14” × 2.0”	20” × 14” × 2.0”
Columns			
Diameter (ft)			
Traditional multi column bent	3.0	3.0	3.0
Integral pile columns	Integral pile columns – See section 4.3.2.1 in Chapter 4 for all details		
Traditional multi column bents			
Long. reinf. ratio (%)	1.08 – 3.61	1.18 – 5.31	1.49 – 5.35
Trans. reinf. ratio (%)	#4 @ 12 in.	0.31 – 1.07	0.31 – 1.61
Number of columns per bent			
Integral pile columns	Same procedure as in MSCC-SL bridges (see Table A.6)		
Traditional multi column bent	See Table A.8	See Table A.8	See Table A.8
Foundation			
Integral pile column	Integral pile column	Integral pile column	Integral pile column
Traditional multi column bent	Pile cap with pile group	Pile cap with pile group	Pile cap with pile group
	See Table 5.2 in Chapter 5 for foundation spring stiffnesses		
Abutments			
Backwall height (ft)	3.50 – 8.50	3.50 – 8.50	3.50 – 8.50
Pile spacing	See Figure A.2	See Figure A.2	See Figure A.2

Table A.8: Number of superstructure girders and number of columns per bent as a function of deck width for MSCC-TG bridges

# columns	# girders	Width range (ft)
2	7	Upto 45
3	9	45 – 60
4	9	> 60

A.4 Multispan Continuous Concrete I-girder Bridges

Table A.9: Bridge component details for MSCC-IG bridge class and the respective seismic performance sub-bins

Attribute	MSCC-IG bridge class		
	Pre 1971	1971-1990	Post 1990
Superstructure			
Number of spans	3	3	3
	This is the mode statistic based on inventory analysis		
Center span (ft)	40.0 – 150.0	40.0 – 150.0	40.0 – 150.0
Center/Edge span length	1.4	1.4	1.33
Deck slab thickness (in)			
Standard I girder	7.5	7.5	7.5
Bulb Tee girder	7.0	7.0	7.0
Number of I-girders	See Table A.10	See Table A.10	See Table A.10
Girder type and dimensions	The choice of girder type and dimension is based on superstructure depth to span ratio – 0.05 for I-girders and 0.045 for Bulb-Tee girders See Figure A.5		
Girder spacing	1.5 times the superstructure depth		
Elastomeric bearing pad			
Span ≤ 50 ft	14” x 10” x 1”	14” x 10” x 1”	14” x 10” x 1”
50 ft < Span ≤ 100 ft	16” x 12” x 1.5”	16” x 12” x 1.5”	16” x 12” x 1.5”
Span > 100 ft	20” x 14” x 2”	20” x 14” x 2”	20” x 14” x 2”
Columns			
Diameter (ft)			
Single column bent	6	6	6
Multi column bent	3	3	3
Long. reinf. ratio (%)	1.08 – 3.61	1.18 – 5.31	1.49 – 5.35
Trans. reinf. ratio (%)	#4 @ 12 in. o.c.	0.31 – 1.07	0.31 – 1.61
Number of columns per bent	See Table A.10	See Table A.10	See Table A.10
Foundation			
Single column bent	Pile cap with pile group	Pile cap with pile group	Pile cap with pile group
Multi column bent	Pile cap with pile group	Pile cap with pile group	Pile cap with pile group
Abutments			
Backwall height (ft)	3.50 – 8.50	3.50 – 8.50	3.50 – 8.50
Pile spacing	See Figure A.2	See Figure A.2	See Figure A.2

Table A.10: Number of superstructure girders and number of columns per bent as a function of deck width for MSCC-IG bridges

# columns	# girders	Width range (ft)
1	5	Upto 45
2	7	45 – 60
3, 4	9	> 60

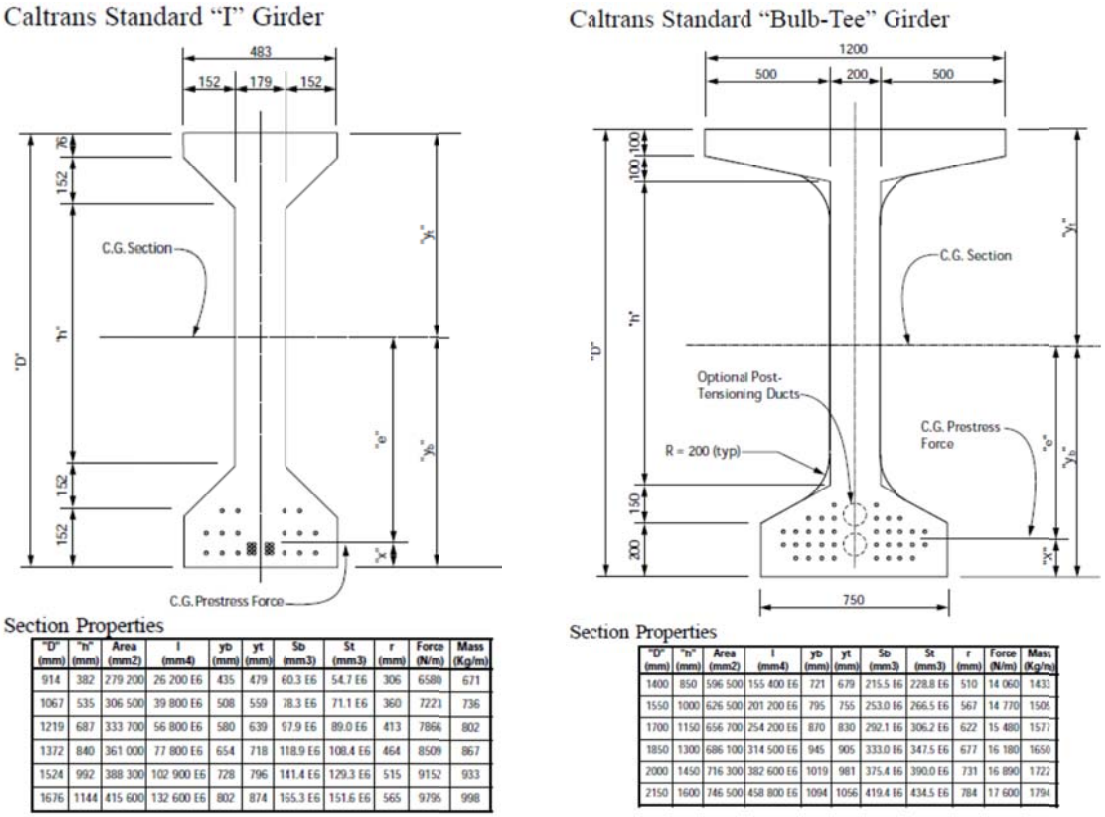

Section Properties

"D" (mm)	"h" (mm)	Area (mm2)	I (mm4)	yb (mm)	yt (mm)	Sb (mm3)	St (mm3)	r (mm)	Force (N/m)	Mass (Kg/m)
914	382	279 200	26 200 E6	435	479	60.3 E6	54.7 E6	306	6589	671
1067	535	306 500	39 800 E6	508	559	78.3 E6	71.1 E6	360	7221	736
1219	687	333 700	56 800 E6	580	639	97.9 E6	89.0 E6	413	7864	802
1372	840	361 000	77 800 E6	654	718	118.9 E6	108.4 E6	464	8509	867
1524	992	388 300	102 900 E6	728	796	141.4 E6	129.3 E6	515	9152	933
1676	1144	415 600	132 600 E6	802	874	165.3 E6	151.6 E6	565	9796	998

Section Properties

"D" (mm)	"h" (mm)	Area (mm2)	I (mm4)	yb (mm)	yt (mm)	Sb (mm3)	St (mm3)	r (mm)	Force (N/m)	Mass (Kg/m)
1400	850	596 500	155 400 E6	721	679	215.5 I6	228.8 E6	510	14 060	1433
1550	1000	626 500	201 200 E6	795	755	253.0 I6	266.5 E6	567	14 770	1505
1700	1150	656 700	254 200 E6	870	830	292.1 I6	306.2 E6	622	15 480	1577
1850	1300	686 100	314 500 E6	945	905	333.0 I6	347.5 E6	677	16 180	1650
2000	1450	716 300	382 600 E6	1019	981	375.4 I6	390.0 E6	731	16 890	1722
2150	1600	746 500	458 800 E6	1094	1056	419.4 I6	434.5 E6	784	17 600	1794

a) Caltrans Standard I-girder

b) Caltrans Standard Bulb-Tee girder

Figure A.5: Standard I-girders used in the California MSCC-IG bridges

APPENDIX B

PROBABILISTIC SEISMIC DEMAND MODELS AND CORRELATION MATRICES

The formulation of the probabilistic seismic demand model (PSDM) was described in section 5.3 of Chapter 5. The model parameters, a and b, describing the median demand and the coefficient of determination, R^2, of the linear fit are tabulated and presented in this Appendix. The dispersion, $\beta_{D|IM}$, characterizing the distribution of median demand is also tabulated across bridge classes and seismic performance sub-bins. Further, correlation coefficients are evaluated based on the simulation results in order to assemble the covariance matrix in the system fragility formulation. Specifically, correlation between the peak component demands are estimated from an analysis of the simulation results of the nonlinear time history analyses. These correlations have previously been found to be relatively consistent across all the ground motion intensities, and hence a single correlation matrix and covariance matrix is assembled for fragility analysis. The correlation coefficients of the natural logarithm of the component demands across bridge classes and the respective seismic performance sub-bins are also documented.

Table B.1: PSDMs for multispan continuous concrete box-girder bridge class and the respective seismic performance sub-bins

$ln(EDP)$	$ln(a)$	b	$\beta_{D\|IM}$	R^2	$ln(EDP)$	$ln(a)$	b	$\beta_{D\|IM}$	R^2
	MSCC-BG-S-E1-S0					MSCC-BG-M-E1-S0			
$ln(\mu_\varphi)$	1.85	1.09	0.54	0.81	$ln(\mu_\varphi)$	2.72	1.21	0.50	0.83
$ln(\delta_{deck})$	1.82	0.99	0.41	0.86	$ln(\delta_{deck})$	2.64	1.19	0.52	0.81
$ln(\delta_{fnd})$	0.21	0.68	0.49	0.67	$ln(\delta_{fnd})$	-1.11	0.49	0.96	0.18
$ln(\theta_{pile})$	-5.21	0.76	0.41	0.78	$ln(\theta_{pile})$	-2.92	1.22	0.52	0.82
$ln(\delta_p)$	1.29	0.92	0.48	0.79	$ln(\delta_p)$	2.05	1.15	0.51	0.82
$ln(\delta_a)$	1.29	0.90	0.48	0.78	$ln(\delta_a)$	2.06	1.14	0.50	0.82
$ln(\delta_t)$	1.79	1.02	0.42	0.86	$ln(\delta_t)$	2.62	1.23	0.53	0.82
	MSCC-BG-S-E1-SX					MSCC-BG-M-E1-SX			
$ln(\mu_\varphi)$	2.16	1.12	0.48	0.86	$ln(\mu_\varphi)$	3.26	1.28	0.67	0.76
$ln(\delta_{seat})$	1.41	0.74	0.33	0.86	$ln(\delta_{seat})$	2.12	0.91	0.42	0.76
$ln(\delta_{deck})$	1.96	0.87	0.39	0.84	$ln(\delta_{deck})$	3.10	1.25	0.60	0.79
$ln(\delta_{fnd})$	0.25	0.49	0.49	0.53	$ln(\delta_{fnd})$	-0.98	0.44	0.86	0.18
$ln(\theta_{pile})$	-5.04	0.67	0.39	0.76	$ln(\theta_{pile})$	-2.49	1.22	0.58	0.79
$ln(\delta_p)$	1.24	1.29	0.73	0.78	$ln(\delta_p)$	1.68	1.29	0.59	0.80
$ln(\delta_a)$	1.84	1.22	0.58	0.83	$ln(\delta_a)$	2.57	1.39	0.48	0.88
$ln(\delta_t)$	2.85	0.94	1.24	0.38	$ln(\delta_t)$	3.47	1.09	0.99	0.51
$ln(\delta_{brng})$	2.55	0.65	0.91	0.38	$ln(\delta_{brng})$	2.95	0.69	0.69	0.51
$ln(\delta_{seal})$	1.41	0.74	0.33	0.38	$ln(\delta_{seal})$	2.12	0.91	0.42	0.51
$ln(\delta_{rest})$	1.38	0.75	0.35	0.38	$ln(\delta_{rest})$	2.11	0.95	0.43	0.51
$ln(\delta_{key})$	-0.10	0.31	0.54	0.38	$ln(\delta_{key})$	-0.14	0.22	0.59	0.51
	MSCC-BG-S-E2-S0					MSCC-BG-M-E2-S0			
$ln(\mu_\varphi)$	1.61	1.02	0.62	0.68	$ln(\mu_\varphi)$	2.54	1.31	0.66	0.79
$ln(\delta_{deck})$	1.85	0.99	0.40	0.83	$ln(\delta_{deck})$	2.40	1.15	0.55	0.81
$ln(\delta_{fnd})$	0.25	0.70	0.47	0.63	$ln(\delta_{fnd})$	-0.41	0.68	0.73	0.47
$ln(\theta_{pile})$	-5.27	0.72	0.31	0.81	$ln(\theta_{pile})$	-3.19	1.19	0.55	0.82
$ln(\delta_p)$	1.44	1.04	0.47	0.80	$ln(\delta_p)$	1.93	1.15	0.47	0.86
$ln(\delta_a)$	1.45	1.03	0.47	0.80	$ln(\delta_a)$	1.94	1.14	0.47	0.86
$ln(\delta_t)$	1.77	0.99	0.41	0.83	$ln(\delta_t)$	2.30	1.14	0.58	0.79
	MSCC-BG-S-E2-S0					MSCC-BG-M-E2-S0			
$ln(\mu_\varphi)$	2.24	1.32	0.58	0.81	$ln(\mu_\varphi)$	3.02	1.37	0.81	0.74
$ln(\delta_{seat})$	1.41	0.76	0.37	0.81	$ln(\delta_{seat})$	1.97	0.93	0.37	0.74
$ln(\delta_{deck})$	2.11	1.00	0.36	0.86	$ln(\delta_{deck})$	2.83	1.21	0.64	0.78
$ln(\delta_{fnd})$	0.60	0.73	0.47	0.67	$ln(\delta_{fnd})$	-0.36	0.59	0.72	0.41
$ln(\theta_{pile})$	-5.00	0.75	0.29	0.84	$ln(\theta_{pile})$	-2.77	1.23	0.62	0.79
$ln(\delta_p)$	1.45	1.70	0.69	0.84	$ln(\delta_p)$	1.77	1.60	0.91	0.75
$ln(\delta_a)$	1.76	1.49	0.54	0.86	$ln(\delta_a)$	2.37	1.48	0.54	0.88
$ln(\delta_t)$	1.57	1.50	0.86	0.72	$ln(\delta_t)$	2.66	1.68	0.97	0.75
$ln(\delta_{brng})$	1.66	0.86	0.37	0.72	$ln(\delta_{brng})$	1.98	0.92	0.36	0.75
$ln(\delta_{seal})$	1.41	0.76	0.37	0.72	$ln(\delta_{seal})$	1.97	0.93	0.37	0.75
$ln(\delta_{rest})$	1.40	0.78	0.36	0.72	$ln(\delta_{rest})$	1.95	0.95	0.39	0.75
$ln(\delta_{key})$	-0.48	0.11	0.78	0.72	$ln(\delta_{key})$	-0.31	0.26	0.66	0.75

MSCC-BG-S-E3-S0					MSCC-BG-M-E3-S0				
$ln(\mu_{\varphi})$	2.15	1.41	0.44	0.91	$ln(\mu_{\varphi})$	2.72	1.30	0.64	0.79
$ln(\delta_{deck})$	1.80	1.03	0.31	0.91	$ln(\delta_{deck})$	2.54	1.17	0.56	0.80
$ln(\delta_{fnd})$	0.48	0.79	0.38	0.79	$ln(\delta_{fnd})$	-0.44	0.69	0.76	0.44
$ln(\theta_{pile})$	-4.99	0.94	0.32	0.89	$ln(\theta_{pile})$	-3.03	1.19	0.58	0.79
$ln(\delta_{p})$	1.32	1.01	0.39	0.86	$ln(\delta_{p})$	2.03	1.20	0.41	0.89
$ln(\delta_{a})$	1.33	0.99	0.39	0.85	$ln(\delta_{a})$	2.03	1.18	0.41	0.89
$ln(\delta_{t})$	1.75	1.03	0.35	0.89	$ln(\delta_{t})$	2.46	1.17	0.60	0.77
MSCC-BG-S-E3-SX-S					MSCC-BG-M-E3-SX-S				
$ln(\mu_{\varphi})$	1.66	1.14	0.41	0.87	$ln(\mu_{\varphi})$	2.62	1.09	0.57	0.77
$ln(\delta_{seat})$	1.16	0.67	0.26	0.87	$ln(\delta_{seat})$	2.04	0.95	0.47	0.77
$ln(\delta_{deck})$	1.81	0.83	0.28	0.89	$ln(\delta_{deck})$	2.42	0.96	0.42	0.82
$ln(\delta_{fnd})$	0.47	0.46	0.40	0.55	$ln(\delta_{fnd})$	-0.35	0.68	0.72	0.46
$ln(\theta_{pile})$	-5.13	0.72	0.26	0.87	$ln(\theta_{pile})$	-3.10	1.00	0.40	0.85
$ln(\delta_{p})$	1.04	1.05	0.68	0.68	$ln(\delta_{p})$	1.58	1.34	0.87	0.70
$ln(\delta_{a})$	1.21	0.96	0.51	0.75	$ln(\delta_{a})$	2.39	1.44	0.64	0.83
$ln(\delta_{t})$	1.32	1.04	0.67	0.68	$ln(\delta_{t})$	2.30	1.37	0.78	0.74
$ln(\delta_{brng})$	1.52	0.78	0.30	0.68	$ln(\delta_{brng})$	2.03	0.91	0.43	0.74
$ln(\delta_{seal})$	1.16	0.67	0.26	0.68	$ln(\delta_{seal})$	2.04	0.95	0.47	0.74
$ln(\delta_{rest})$	1.16	0.67	0.26	0.68	$ln(\delta_{rest})$	2.06	0.97	0.46	0.74
$ln(\delta_{key})$	-0.53	0.17	0.75	0.68	$ln(\delta_{key})$	-0.38	0.14	0.62	0.74
MSCC-BG-S-E3-SX-L					MSCC-BG-M-E3-SX-L				
$ln(\mu_{\varphi})$	1.63	0.94	0.63	0.66	$ln(\mu_{\varphi})$	2.77	1.15	0.59	0.79
$ln(\delta_{seat})$	1.44	0.70	0.27	0.66	$ln(\delta_{seat})$	2.09	0.86	0.39	0.79
$ln(\delta_{deck})$	1.93	0.84	0.31	0.86	$ln(\delta_{deck})$	2.52	0.96	0.41	0.84
$ln(\delta_{fnd})$	0.68	0.63	0.54	0.55	$ln(\delta_{fnd})$	-0.37	0.64	0.84	0.36
$ln(\theta_{pile})$	-4.97	0.64	0.33	0.75	$ln(\theta_{pile})$	-3.03	1.00	0.42	0.85
$ln(\delta_{p})$	-0.13	1.41	0.88	0.70	$ln(\delta_{p})$	1.02	1.58	0.96	0.73
$ln(\delta_{a})$	1.33	1.33	0.66	0.79	$ln(\delta_{a})$	2.44	1.39	0.63	0.83
$ln(\delta_{t})$	1.51	1.40	0.69	0.79	$ln(\delta_{t})$	2.16	1.30	0.76	0.73
$ln(\delta_{brng})$	1.58	0.74	0.28	0.79	$ln(\delta_{brng})$	2.09	0.85	0.37	0.73
$ln(\delta_{seal})$	1.44	0.70	0.27	0.79	$ln(\delta_{seal})$	2.09	0.86	0.39	0.73
$ln(\delta_{rest})$	1.39	0.76	0.26	0.79	$ln(\delta_{rest})$	1.90	0.87	0.44	0.73
$ln(\delta_{key})$	-0.74	0.03	0.91	0.79	$ln(\delta_{key})$	-0.34	0.19	0.62	0.73

Table B.2: PSDMs for multispan continuous concrete slab bridge class and the respective seismic performance sub-bins

$ln(EDP)$	$ln(a)$	b	$\beta_{D\|IM}$	R^2	$ln(EDP)$	$ln(a)$	b	$\beta_{D\|IM}$	R^2
MSCC-SL-P-EX-S0					MSCC-SL-P-EX-SX				
$ln(\mu_\varphi)$	-0.02	0.83	0.41	0.80	$ln(\mu_\varphi)$	0.60	0.97	0.63	0.68
$ln(\delta_{deck})$	1.48	0.77	0.47	0.73	$ln(\delta_{\text{seat}})$	1.89	0.78	0.63	0.68
$ln(\delta_{fnd})$	-0.26	0.62	0.72	0.45	$ln(\delta_{deck})$	2.24	1.01	0.43	0.83
$ln(\theta_{pile})$	-4.01	0.77	0.40	0.80	$ln(\delta_{fnd})$	0.63	0.94	0.87	0.52
$ln(\delta_p)$	1.16	0.75	0.46	0.73	$ln(\theta_{pile})$	-3.42	0.96	0.40	0.84
$ln(\delta_a)$	1.16	0.75	0.46	0.73	$ln(\delta_p)$	0.77	0.57	0.31	0.77
$ln(\delta_t)$	1.34	0.77	0.44	0.76	$ln(\delta_a)$	1.98	0.96	0.45	0.81
$ln(\mu_\varphi)$	-0.02	0.83	0.41	0.80	$ln(\delta_t)$	-1.02	0.19	0.53	0.10
					$ln(\delta_{brng})$	2.16	1.20	0.42	0.10
					$ln(\delta_{seal})$	1.89	0.78	0.63	0.10

Table B.3: PSDMs for multispan continuous concrete Tee-girder bridge class and the respective seismic performance sub-bins

$ln(EDP)$	$ln(a)$	b	$\beta_{D\|IM}$	R^2	$ln(EDP)$	$ln(a)$	b	$\beta_{D\|IM}$	R^2
	MSCC-TG-P-E1-S0					MSCC-TG-M-E1-S0			
$ln(\mu_\varphi)$	0.12	0.91	0.51	0.79	$ln(\mu_\varphi)$	0.86	0.83	0.33	0.84
$ln(\delta_{deck})$	1.96	0.88	0.28	0.92	$ln(\delta_{deck})$	1.63	0.85	0.36	0.82
$ln(\delta_{fnd})$	-0.58	0.66	0.67	0.51	$ln(\delta_{fnd})$	-2.38	0.70	0.44	0.67
$ln(\theta_{pile})$	-4.07	0.81	0.29	0.90	$ln(\theta_{pile})$	-3.70	0.80	0.49	0.70
$ln(\delta_p)$	0.21	0.73	0.62	0.58	$ln(\delta_p)$	-0.30	0.56	0.44	0.54
$ln(\delta_a)$	0.21	0.73	0.62	0.58	$ln(\delta_a)$	-0.30	0.55	0.45	0.52
$ln(\delta_t)$	-0.59	0.69	0.57	0.61	$ln(\delta_t)$	-0.73	0.70	0.44	0.63
	MSCC-TG-P-E1-SX					MSCC-TG-M-E1-SX			
$ln(\mu_\varphi)$	1.21	1.06	0.52	0.77	$ln(\mu_\varphi)$	1.10	0.85	0.43	0.78
$ln(\delta_{seat})$	2.45	1.14	0.31	0.77	$ln(\delta_{seat})$	1.93	1.01	0.42	0.78
$ln(\delta_{deck})$	2.43	0.96	0.30	0.90	$ln(\delta_{deck})$	1.93	0.91	0.40	0.83
$ln(\delta_{fnd})$	0.06	0.82	0.58	0.63	$ln(\delta_{fnd})$	-2.18	0.69	0.65	0.49
$ln(\theta_{pile})$	-3.46	0.93	0.41	0.82	$ln(\theta_{pile})$	-3.66	0.86	0.37	0.82
$ln(\delta_p)$	0.35	0.36	0.35	0.47	$ln(\delta_p)$	1.12	0.70	0.31	0.82
$ln(\delta_a)$	2.17	1.04	0.35	0.89	$ln(\delta_a)$	1.13	0.70	0.31	0.81
$ln(\delta_t)$	-2.75	0.12	0.20	0.21	$ln(\delta_t)$	-2.71	0.16	0.20	0.34
$ln(\delta_{brng})$	2.45	1.14	0.31	0.21	$ln(\delta_{brng})$	1.93	1.01	0.42	0.34
$ln(\delta_{seal})$	2.45	1.14	0.31	0.21	$ln(\delta_{seal})$	1.93	1.01	0.42	0.34
	MSCC-TG-P-E2-S0					MSCC-TG-M-E2-S0			
$ln(\mu_\varphi)$	0.14	0.99	0.47	0.79	$ln(\mu_\varphi)$	0.61	0.93	0.42	0.84
$ln(\delta_{deck})$	2.02	0.92	0.27	0.91	$ln(\delta_{deck})$	1.71	1.00	0.37	0.89
$ln(\delta_{fnd})$	-0.32	1.02	0.56	0.76	$ln(\delta_{fnd})$	-1.82	0.90	0.74	0.62
$ln(\theta_{pile})$	-3.83	0.95	0.31	0.90	$ln(\theta_{pile})$	-3.64	0.95	0.69	0.68
$ln(\delta_p)$	0.45	0.89	0.60	0.65	$ln(\delta_p)$	-0.29	0.75	0.53	0.64
$ln(\delta_a)$	0.45	0.89	0.60	0.65	$ln(\delta_a)$	-0.28	0.76	0.53	0.65
$ln(\delta_t)$	0.00	1.09	0.61	0.72	$ln(\delta_t)$	-0.45	0.98	0.48	0.77
	MSCC-TG-P-E2-S0					MSCC-TG-M-E2-S0			
$ln(\mu_\varphi)$	0.96	1.03	0.67	0.70	$ln(\mu_\varphi)$	1.00	1.01	0.49	0.77
$ln(\delta_{seat})$	2.32	1.14	0.57	0.70	$ln(\delta_{seat})$	2.02	1.14	0.45	0.77
$ln(\delta_{deck})$	2.38	1.00	0.45	0.82	$ln(\delta_{deck})$	1.94	0.98	0.46	0.78
$ln(\delta_{fnd})$	-0.18	0.75	0.86	0.43	$ln(\delta_{fnd})$	-1.84	0.57	0.76	0.31
$ln(\theta_{pile})$	-3.56	0.92	0.52	0.76	$ln(\theta_{pile})$	-3.56	1.00	0.42	0.82
$ln(\delta_p)$	0.53	0.55	0.32	0.74	$ln(\delta_p)$	1.15	0.79	0.34	0.82
$ln(\delta_a)$	1.97	1.03	0.58	0.76	$ln(\delta_a)$	1.17	0.79	0.35	0.82
$ln(\delta_t)$	-2.71	0.18	0.23	0.38	$ln(\delta_t)$	-2.64	0.22	0.22	0.46
$ln(\delta_{brng})$	2.32	1.14	0.57	0.38	$ln(\delta_{brng})$	2.02	1.14	0.45	0.46
$ln(\delta_{seal})$	2.32	1.14	0.57	0.38	$ln(\delta_{seal})$	2.02	1.14	0.45	0.46
	MSCC-TG-P-E3-S0					MSCC-TG-M-E3-S0			
$ln(\mu_\varphi)$	0.15	0.97	0.49	0.76	$ln(\mu_\varphi)$	0.64	0.96	0.33	0.88
$ln(\delta_{deck})$	2.21	1.04	0.32	0.91	$ln(\delta_{deck})$	1.60	0.85	0.34	0.84
$ln(\delta_{fnd})$	-0.40	0.92	0.64	0.66	$ln(\delta_{fnd})$	-2.05	0.63	0.59	0.51

$ln(\theta_{pile})$	-3.90	0.94	0.36	0.87	$ln(\theta_{pile})$	-3.64	0.91	0.45	0.79
$ln(\delta_p)$	0.51	0.94	0.58	0.72	$ln(\delta_p)$	-0.38	0.61	0.48	0.57
$ln(\delta_a)$	0.51	0.94	0.58	0.72	$ln(\delta_a)$	-0.36	0.61	0.47	0.59
$ln(\delta_t)$	-0.19	0.93	0.67	0.64	$ln(\delta_t)$	-0.57	0.85	0.46	0.73
	MSCC-TG-P-E3-SX					MSCC-TG-M-E3-SX			
$ln(\mu_\varphi)$	0.72	0.87	0.39	0.80	$ln(\mu_\varphi)$	1.16	1.07	0.46	0.83
$ln(\delta_{seat})$	2.34	1.04	0.31	0.80	$ln(\delta_{seat})$	2.07	1.14	0.42	0.83
$ln(\delta_{deck})$	2.37	0.89	0.25	0.92	$ln(\delta_{deck})$	2.08	1.09	0.41	0.87
$ln(\delta_{fnd})$	-0.45	0.79	0.63	0.60	$ln(\delta_{fnd})$	-1.62	0.77	0.59	0.60
$ln(\theta_{pile})$	-3.66	0.84	0.29	0.89	$ln(\theta_{pile})$	-3.53	1.02	0.38	0.87
$ln(\delta_p)$	0.42	0.54	0.35	0.70	$ln(\delta_p)$	1.13	0.85	0.36	0.84
$ln(\delta_a)$	2.08	1.01	0.38	0.87	$ln(\delta_a)$	1.15	0.85	0.36	0.84
$ln(\delta_t)$	-2.66	0.13	0.19	0.23	$ln(\delta_t)$	-2.81	0.13	0.23	0.24
$ln(\delta_{brng})$	2.34	1.04	0.31	0.23	$ln(\delta_{brng})$	2.07	1.14	0.42	0.24
$ln(\delta_{seal})$	2.34	1.04	0.31	0.23	$ln(\delta_{seal})$	2.07	1.14	0.42	0.24

Table B.4: PSDMs for multispan continuous concrete I-girder bridge class and the respective seismic performance sub-bins

$ln(EDP)$	$ln(a)$	b	$\beta_{D\|IM}$	R^2	$ln(EDP)$	$ln(a)$	b	$\beta_{D\|IM}$	R^2
	MSCC-IG-S-E1-S0					MSCC-IG-M-E1-S0			
$ln(\mu_\varphi)$	1.02	1.35	0.96	0.67	$ln(\mu_\varphi)$	1.23	0.93	0.56	0.73
$ln(\delta_{deck})$	2.50	1.11	0.51	0.83	$ln(\delta_{deck})$	2.20	0.89	0.37	0.86
$ln(\delta_{fnd})$	0.08	1.20	0.85	0.67	$ln(\delta_{fnd})$	-1.35	0.51	0.71	0.33
$ln(\theta_{pile})$	-5.38	0.95	0.69	0.67	$ln(\theta_{pile})$	-3.71	0.87	0.43	0.80
$ln(\delta_p)$	-0.51	0.58	0.36	0.67	$ln(\delta_p)$	-0.05	0.91	0.43	0.79
$ln(\delta_a)$	-0.48	0.46	0.36	0.55	$ln(\delta_a)$	0.01	0.82	0.44	0.75
$ln(\delta_t)$	0.19	0.66	0.52	0.61	$ln(\delta_t)$	0.10	0.72	0.43	0.70
$ln(\delta_{brng})$	2.61	1.22	0.57	0.61	$ln(\delta_{brng})$	2.28	0.95	0.45	0.70
$ln(\delta_{rest})$	0.26	0.48	0.36	0.61	$ln(\delta_{rest})$	0.07	0.30	0.28	0.70
$ln(\delta_{key})$	-0.32	0.54	0.55	0.61	$ln(\delta_{key})$	-0.80	0.24	0.39	0.70
	MSCC-IG-S-E1-SX					MSCC-IG-M-E1-SX			
$ln(\mu_\varphi)$	0.84	1.17	0.56	0.84	$ln(\mu_\varphi)$	1.64	1.05	0.46	0.82
$ln(\delta_{seat})$	1.17	0.67	0.28	0.84	$ln(\delta_{seat})$	2.15	1.08	0.37	0.82
$ln(\delta_{deck})$	2.75	1.09	0.39	0.91	$ln(\delta_{deck})$	2.59	0.93	0.34	0.87
$ln(\delta_{fnd})$	-0.18	0.92	0.54	0.76	$ln(\delta_{fnd})$	-1.48	0.69	0.64	0.51
$ln(\theta_{pile})$	-5.41	0.85	0.39	0.84	$ln(\theta_{pile})$	-3.33	0.95	0.37	0.85
$ln(\delta_p)$	0.06	1.06	0.47	0.86	$ln(\delta_p)$	0.20	0.93	0.43	0.81
$ln(\delta_a)$	-0.04	1.06	0.42	0.88	$ln(\delta_a)$	-0.10	0.89	0.42	0.80
$ln(\delta_t)$	1.35	1.60	0.86	0.83	$ln(\delta_t)$	1.10	0.93	0.57	0.72
$ln(\delta_{brng})$	2.66	1.09	0.42	0.83	$ln(\delta_{brng})$	2.49	0.99	0.36	0.72
$ln(\delta_{seal})$	1.17	0.67	0.28	0.83	$ln(\delta_{seal})$	2.15	1.08	0.37	0.72
$ln(\delta_{rest})$	0.80	0.57	0.29	0.83	$ln(\delta_{rest})$	0.22	0.51	0.31	0.72
$ln(\delta_{key})$	-0.21	0.53	0.48	0.83	$ln(\delta_{key})$	-1.18	0.14	0.46	0.72
	MSCC-IG-S-E2-S0					MSCC-IG-M-E2-S0			
$ln(\mu_\varphi)$	1.79	1.40	1.22	0.54	$ln(\mu_\varphi)$	1.58	1.21	0.62	0.81
$ln(\delta_{deck})$	3.09	1.24	0.59	0.80	$ln(\delta_{deck})$	2.24	0.96	0.33	0.90
$ln(\delta_{fnd})$	1.17	1.52	0.95	0.68	$ln(\delta_{fnd})$	-1.14	0.70	0.73	0.48
$ln(\theta_{pile})$	-4.66	1.16	0.85	0.62	$ln(\theta_{pile})$	-3.45	1.01	0.45	0.85
$ln(\delta_p)$	-0.09	0.82	0.40	0.79	$ln(\delta_p)$	-0.16	0.83	0.48	0.74
$ln(\delta_a)$	-0.38	0.64	0.36	0.73	$ln(\delta_a)$	-0.12	0.73	0.47	0.70
$ln(\delta_t)$	1.21	1.18	0.55	0.79	$ln(\delta_t)$	0.25	0.76	0.45	0.72
$ln(\delta_{brng})$	3.36	1.42	0.77	0.79	$ln(\delta_{brng})$	2.33	1.03	0.42	0.72
$ln(\delta_{rest})$	0.44	0.55	0.27	0.79	$ln(\delta_{rest})$	0.05	0.33	0.28	0.72
$ln(\delta_{key})$	-0.54	0.51	0.48	0.79	$ln(\delta_{key})$	-0.67	0.32	0.39	0.72
	MSCC-IG-S-E2-S0					MSCC-IG-M-E2-S0			
$ln(\mu_\varphi)$	1.02	1.09	0.67	0.73	$ln(\mu_\varphi)$	1.61	1.03	0.44	0.83
$ln(\delta_{seat})$	1.51	0.81	0.33	0.73	$ln(\delta_{seat})$	2.24	1.12	0.34	0.83
$ln(\delta_{deck})$	3.04	1.02	0.45	0.84	$ln(\delta_{deck})$	2.71	1.00	0.34	0.90
$ln(\delta_{fnd})$	0.09	0.72	0.72	0.49	$ln(\delta_{fnd})$	-1.71	0.36	0.62	0.26
$ln(\theta_{pile})$	-5.18	0.76	0.40	0.79	$ln(\theta_{pile})$	-3.19	1.02	0.32	0.91
$ln(\delta_p)$	0.46	1.16	0.58	0.80	$ln(\delta_p)$	0.18	0.92	0.35	0.87
$ln(\delta_a)$	0.09	1.04	0.59	0.74	$ln(\delta_a)$	-0.15	0.87	0.37	0.84

$ln(\delta_t)$	2.00	1.71	0.86	0.81	$ln(\delta_t)$	1.63	1.24	0.67	0.77
$ln(\delta_{brng})$	3.03	1.07	0.48	0.81	$ln(\delta_{brng})$	2.67	1.09	0.37	0.77
$ln(\delta_{seal})$	1.51	0.81	0.33	0.81	$ln(\delta_{seal})$	2.24	1.12	0.34	0.77
$ln(\delta_{rest})$	1.10	0.72	0.37	0.81	$ln(\delta_{rest})$	0.26	0.52	0.22	0.77
$ln(\delta_{key})$	-0.15	0.63	0.45	0.81	$ln(\delta_{key})$	-1.27	0.15	0.46	0.77
	MSCC-IG-S-E3-S0					MSCC-IG-M-E3-S0			
$ln(\mu_\varphi)$	1.18	1.07	1.08	0.50	$ln(\mu_\varphi)$	1.53	1.18	0.67	0.76
$ln(\delta_{deck})$	2.83	1.03	0.52	0.81	$ln(\delta_{deck})$	2.29	0.98	0.38	0.87
$ln(\delta_{fnd})$	0.65	0.89	0.92	0.50	$ln(\delta_{fnd})$	-0.90	0.65	0.72	0.43
$ln(\theta_{pile})$	-4.84	0.84	0.77	0.55	$ln(\theta_{pile})$	-3.41	0.98	0.49	0.79
$ln(\delta_p)$	-0.12	0.73	0.50	0.65	$ln(\delta_p)$	-0.17	0.77	0.43	0.72
$ln(\delta_a)$	-0.31	0.56	0.50	0.50	$ln(\delta_a)$	-0.01	0.76	0.43	0.72
$ln(\delta_t)$	1.06	0.89	0.66	0.64	$ln(\delta_t)$	0.19	0.74	0.50	0.65
$ln(\delta_{brng})$	3.11	1.05	0.80	0.64	$ln(\delta_{brng})$	2.40	1.03	0.47	0.65
$ln(\delta_{rest})$	0.38	0.43	0.27	0.64	$ln(\delta_{rest})$	0.18	0.37	0.28	0.65
$ln(\delta_{key})$	-0.33	0.42	0.48	0.64	$ln(\delta_{key})$	-0.85	0.26	0.44	0.65
	MSCC-IG-S-E3-SX					MSCC-IG-M-E3-SX			
$ln(\mu_\varphi)$	0.41	0.77	0.55	0.62	$ln(\mu_\varphi)$	1.50	1.08	0.39	0.87
$ln(\delta_{seat})$	1.43	0.82	0.29	0.62	$ln(\delta_{seat})$	2.26	1.12	0.34	0.87
$ln(\delta_{deck})$	2.90	0.92	0.45	0.76	$ln(\delta_{deck})$	2.66	0.98	0.35	0.88
$ln(\delta_{fnd})$	-0.06	0.23	0.44	0.17	$ln(\delta_{fnd})$	-1.44	0.57	0.67	0.38
$ln(\theta_{pile})$	-5.51	0.36	0.31	0.53	$ln(\theta_{pile})$	-3.19	1.03	0.36	0.89
$ln(\delta_p)$	0.07	1.10	0.50	0.81	$ln(\delta_p)$	0.20	0.93	0.38	0.85
$ln(\delta_a)$	-0.26	0.92	0.53	0.72	$ln(\delta_a)$	-0.17	0.84	0.36	0.83
$ln(\delta_t)$	1.75	1.26	0.86	0.70	$ln(\delta_t)$	1.69	1.30	0.74	0.77
$ln(\delta_{brng})$	2.77	0.80	0.48	0.70	$ln(\delta_{brng})$	2.66	1.11	0.38	0.77
$ln(\delta_{seal})$	1.43	0.82	0.29	0.70	$ln(\delta_{seal})$	2.26	1.12	0.34	0.77
$ln(\delta_{rest})$	1.00	0.74	0.26	0.70	$ln(\delta_{rest})$	0.26	0.53	0.24	0.77
$ln(\delta_{key})$	-0.57	0.29	0.44	0.70	$ln(\delta_{key})$	-1.16	0.21	0.49	0.77

Table B.5: Correlation Coefficients of the component demands of multispan continuous concrete box-girder bridge class and the respective seismic performance sub-bins

MSCC-BG-S-E1-S0

	$ln(\mu_\varphi)$	$ln(\delta_{deck})$	$ln(\delta_{fnd})$	$ln(\theta_{pile})$	$ln(\delta_p)$	$ln(\delta_a)$	$ln(\delta_t)$
$ln(\mu_\varphi)$	1.00	0.95	0.75	0.91	0.88	0.88	0.94
$ln(\delta_{deck})$	0.95	1.00	0.85	0.93	0.94	0.94	0.98
$ln(\delta_{fnd})$	0.75	0.85	1.00	0.84	0.79	0.79	0.84
$ln(\theta_{pile})$	0.91	0.93	0.84	1.00	0.87	0.87	0.92
$ln(\delta_p)$	0.88	0.94	0.79	0.87	1.00	1.00	0.90
$ln(\delta_a)$	0.88	0.94	0.79	0.87	1.00	1.00	0.90
$ln(\delta_t)$	0.94	0.98	0.84	0.92	0.90	0.90	1.00

MSCC-BG-M-E1-S0

	$ln(\mu_\varphi)$	$ln(\delta_{deck})$	$ln(\delta_{fnd})$	$ln(\theta_{pile})$	$ln(\delta_p)$	$ln(\delta_a)$	$ln(\delta_t)$
$ln(\mu_\varphi)$	1.00	0.98	0.70	0.98	0.82	0.83	0.98
$ln(\delta_{deck})$	0.98	1.00	0.75	1.00	0.81	0.81	1.00
$ln(\delta_{fnd})$	0.70	0.75	1.00	0.75	0.53	0.53	0.75
$ln(\theta_{pile})$	0.98	1.00	0.75	1.00	0.80	0.80	0.99
$ln(\delta_p)$	0.82	0.81	0.53	0.80	1.00	1.00	0.80
$ln(\delta_a)$	0.83	0.81	0.53	0.80	1.00	1.00	0.80
$ln(\delta_t)$	0.98	1.00	0.75	0.99	0.80	0.80	1.00

MSCC-BG-S-E1-SX

	$ln(\mu_\varphi)$	$ln(\delta_{seat})$	$ln(\delta_{deck})$	$ln(\delta_{fnd})$	$ln(\theta_{pile})$	$ln(\delta_p)$	$ln(\delta_a)$	$ln(\delta_t)$	$ln(\delta_{brng})$	$ln(\delta_{seal})$	$ln(\delta_{rest})$	$ln(\delta_{key})$
$ln(\mu_\varphi)$	1.00	0.87	0.95	0.68	0.88	0.84	0.86	0.59	0.57	0.87	0.84	0.31
$ln(\delta_{seat})$	0.87	1.00	0.91	0.72	0.86	0.89	0.94	0.56	0.56	1.00	0.99	0.25
$ln(\delta_{deck})$	0.95	0.91	1.00	0.80	0.93	0.89	0.91	0.68	0.68	0.91	0.89	0.27
$ln(\delta_{fnd})$	0.68	0.72	0.80	1.00	0.85	0.78	0.78	0.65	0.65	0.72	0.73	0.29
$ln(\theta_{pile})$	0.88	0.86	0.93	0.85	1.00	0.88	0.88	0.63	0.64	0.86	0.86	0.33
$ln(\delta_p)$	0.84	0.89	0.89	0.78	0.88	1.00	0.97	0.65	0.65	0.89	0.90	0.27
$ln(\delta_a)$	0.86	0.94	0.91	0.78	0.88	0.97	1.00	0.64	0.63	0.94	0.94	0.26
$ln(\delta_t)$	0.59	0.56	0.68	0.65	0.63	0.65	0.64	1.00	0.97	0.56	0.57	0.10
$ln(\delta_{brng})$	0.57	0.56	0.68	0.65	0.64	0.65	0.63	0.97	1.00	0.56	0.58	0.10
$ln(\delta_{seal})$	0.87	1.00	0.91	0.72	0.86	0.89	0.94	0.56	0.56	1.00	0.99	0.25
$ln(\delta_{rest})$	0.84	0.99	0.89	0.73	0.86	0.90	0.94	0.57	0.58	0.99	1.00	0.27
$ln(\delta_{key})$	0.31	0.25	0.27	0.29	0.33	0.27	0.26	0.10	0.10	0.25	0.27	1.00

MSCC-BG-M-E1-SX

	$ln(\mu_\varphi)$	$ln(\delta_{seat})$	$ln(\delta_{deck})$	$ln(\delta_{fnd})$	$ln(\theta_{pile})$	$ln(\delta_p)$	$ln(\delta_a)$	$ln(\delta_t)$	$ln(\delta_{brng})$	$ln(\delta_{seal})$	$ln(\delta_{rest})$	$ln(\delta_{key})$
$ln(\mu_\varphi)$	1.00	0.77	0.98	0.72	0.98	0.73	0.78	0.87	0.77	0.77	0.77	0.23
$ln(\delta_{seat})$	0.77	1.00	0.78	0.49	0.77	0.81	0.93	0.65	0.65	1.00	0.98	0.17
$ln(\delta_{deck})$	0.98	0.78	1.00	0.74	1.00	0.75	0.78	0.90	0.78	0.78	0.78	0.20
$ln(\delta_{fnd})$	0.72	0.49	0.74	1.00	0.74	0.47	0.49	0.71	0.68	0.49	0.50	0.04
$ln(\theta_{pile})$	0.98	0.77	1.00	0.74	1.00	0.73	0.77	0.90	0.77	0.77	0.77	0.20
$ln(\delta_p)$	0.73	0.81	0.75	0.47	0.73	1.00	0.93	0.66	0.61	0.81	0.82	0.22
$ln(\delta_a)$	0.78	0.93	0.78	0.49	0.77	0.93	1.00	0.67	0.64	0.93	0.92	0.21
$ln(\delta_t)$	0.87	0.65	0.90	0.71	0.90	0.66	0.67	1.00	0.90	0.65	0.65	0.15
$ln(\delta_{brng})$	0.77	0.65	0.78	0.68	0.77	0.61	0.64	0.90	1.00	0.65	0.65	0.09
$ln(\delta_{seal})$	0.77	1.00	0.78	0.49	0.77	0.81	0.93	0.65	0.65	1.00	0.98	0.17
$ln(\delta_{rest})$	0.77	0.98	0.78	0.50	0.77	0.82	0.92	0.65	0.65	0.98	1.00	0.17
$ln(\delta_{key})$	0.23	0.17	0.20	0.04	0.20	0.22	0.21	0.15	0.09	0.17	0.17	1.00

MSCC-BG-S-E2-S0

	$ln(\mu_\varphi)$	$ln(\delta_{deck})$	$ln(\delta_{fnd})$	$ln(\theta_{pile})$	$ln(\delta_p)$	$ln(\delta_a)$	$ln(\delta_t)$
$ln(\mu_\varphi)$	1.00	0.92	0.64	0.87	0.80	0.80	0.92
$ln(\delta_{deck})$	0.92	1.00	0.81	0.94	0.92	0.92	0.99
$ln(\delta_{fnd})$	0.64	0.81	1.00	0.85	0.73	0.73	0.81
$ln(\theta_{pile})$	0.87	0.94	0.85	1.00	0.84	0.84	0.93
$ln(\delta_p)$	0.80	0.92	0.73	0.84	1.00	1.00	0.87
$ln(\delta_a)$	0.80	0.92	0.73	0.84	1.00	1.00	0.87
$ln(\delta_t)$	0.92	0.99	0.81	0.93	0.87	0.87	1.00

MSCC-BG-M-E2-S0

	$ln(\mu_\varphi)$	$ln(\delta_{deck})$	$ln(\delta_{fnd})$	$ln(\theta_{pile})$	$ln(\delta_p)$	$ln(\delta_a)$	$ln(\delta_t)$
$ln(\mu_\varphi)$	1.00	0.98	0.77	0.98	0.81	0.81	0.97
$ln(\delta_{deck})$	0.98	1.00	0.82	1.00	0.81	0.81	1.00
$ln(\delta_{fnd})$	0.77	0.82	1.00	0.80	0.63	0.63	0.82
$ln(\theta_{pile})$	0.98	1.00	0.80	1.00	0.80	0.80	0.99
$ln(\delta_p)$	0.81	0.81	0.63	0.80	1.00	1.00	0.79
$ln(\delta_a)$	0.81	0.81	0.63	0.80	1.00	1.00	0.79
$ln(\delta_t)$	0.97	1.00	0.82	0.99	0.79	0.79	1.00

MSCC-BG-S-E2-SX

	$ln(\mu_\varphi)$	$ln(\delta_{seat})$	$ln(\delta_{deck})$	$ln(\delta_{fnd})$	$ln(\theta_{pile})$	$ln(\delta_p)$	$ln(\delta_a)$	$ln(\delta_t)$	$ln(\delta_{brng})$	$ln(\delta_{seal})$	$ln(\delta_{rest})$	$ln(\delta_{key})$
$ln(\mu_\varphi)$	1.00	0.83	0.94	0.73	0.92	0.82	0.86	0.82	0.89	0.83	0.84	0.09
$ln(\delta_{seat})$	0.83	1.00	0.90	0.77	0.84	0.88	0.96	0.75	0.96	1.00	1.00	0.03
$ln(\delta_{deck})$	0.94	0.90	1.00	0.89	0.96	0.90	0.94	0.90	0.93	0.90	0.91	0.10
$ln(\delta_{fnd})$	0.73	0.77	0.89	1.00	0.87	0.81	0.83	0.80	0.77	0.77	0.76	0.16
$ln(\theta_{pile})$	0.92	0.84	0.96	0.87	1.00	0.88	0.91	0.89	0.88	0.84	0.84	0.04
$ln(\delta_p)$	0.82	0.88	0.90	0.81	0.88	1.00	0.96	0.82	0.86	0.88	0.89	0.04
$ln(\delta_a)$	0.86	0.96	0.94	0.83	0.91	0.96	1.00	0.83	0.92	0.96	0.96	0.04
$ln(\delta_t)$	0.82	0.75	0.90	0.80	0.89	0.82	0.83	1.00	0.80	0.75	0.76	0.05
$ln(\delta_{brng})$	0.89	0.96	0.93	0.77	0.88	0.86	0.92	0.80	1.00	0.96	0.96	0.06
$ln(\delta_{seal})$	0.83	1.00	0.90	0.77	0.84	0.88	0.96	0.75	0.96	1.00	1.00	0.03
$ln(\delta_{rest})$	0.84	1.00	0.91	0.76	0.84	0.89	0.96	0.76	0.96	1.00	1.00	0.03
$ln(\delta_{key})$	0.09	0.03	0.10	0.16	0.04	0.04	0.04	0.05	0.06	0.03	0.03	1.00

MSCC-BG-M-E2-SX

	$ln(\mu_\varphi)$	$ln(\delta_{seat})$	$ln(\delta_{deck})$	$ln(\delta_{fnd})$	$ln(\theta_{pile})$	$ln(\delta_p)$	$ln(\delta_a)$	$ln(\delta_t)$	$ln(\delta_{brng})$	$ln(\delta_{seal})$	$ln(\delta_{rest})$	$ln(\delta_{key})$
$ln(\mu_\varphi)$	1.00	0.81	0.98	0.79	0.98	0.69	0.80	0.95	0.82	0.81	0.80	0.15
$ln(\delta_{seat})$	0.81	1.00	0.80	0.61	0.80	0.78	0.93	0.80	0.99	1.00	0.99	0.26
$ln(\delta_{deck})$	0.98	0.80	1.00	0.82	1.00	0.68	0.80	0.97	0.81	0.80	0.79	0.14
$ln(\delta_{fnd})$	0.79	0.61	0.82	1.00	0.81	0.54	0.63	0.80	0.61	0.61	0.59	0.18
$ln(\theta_{pile})$	0.98	0.80	1.00	0.81	1.00	0.68	0.80	0.96	0.81	0.80	0.79	0.14
$ln(\delta_p)$	0.69	0.78	0.68	0.54	0.68	1.00	0.91	0.71	0.78	0.78	0.79	0.18
$ln(\delta_a)$	0.80	0.93	0.80	0.63	0.80	0.91	1.00	0.81	0.93	0.93	0.93	0.21
$ln(\delta_t)$	0.95	0.80	0.97	0.80	0.96	0.71	0.81	1.00	0.80	0.80	0.78	0.11
$ln(\delta_{brng})$	0.82	0.99	0.81	0.61	0.81	0.78	0.93	0.80	1.00	0.99	0.99	0.26
$ln(\delta_{seal})$	0.81	1.00	0.80	0.61	0.80	0.78	0.93	0.80	0.99	1.00	0.99	0.26
$ln(\delta_{rest})$	0.80	0.99	0.79	0.59	0.79	0.79	0.93	0.78	0.99	0.99	1.00	0.26
$ln(\delta_{key})$	0.15	0.26	0.14	0.18	0.14	0.18	0.21	0.11	0.26	0.26	0.26	1.00

MSCC-BG-S-E3-S0

	$ln(\mu_\varphi)$	$ln(\delta_{deck})$	$ln(\delta_{fnd})$	$ln(\theta_{pile})$	$ln(\delta_p)$	$ln(\delta_a)$	$ln(\delta_t)$
$ln(\mu_\varphi)$	1.00	0.90	0.66	0.88	0.86	0.86	0.91
$ln(\delta_{deck})$	0.90	1.00	0.86	0.96	0.91	0.91	0.99
$ln(\delta_{fnd})$	0.66	0.86	1.00	0.86	0.72	0.72	0.87
$ln(\theta_{pile})$	0.88	0.96	0.86	1.00	0.87	0.86	0.95
$ln(\delta_p)$	0.86	0.91	0.72	0.87	1.00	1.00	0.88
$ln(\delta_a)$	0.86	0.91	0.72	0.86	1.00	1.00	0.88
$ln(\delta_t)$	0.91	0.99	0.87	0.95	0.88	0.88	1.00

MSCC-BG-M-E3-S0

	$ln(\mu_\varphi)$	$ln(\delta_{deck})$	$ln(\delta_{fnd})$	$ln(\theta_{pile})$	$ln(\delta_p)$	$ln(\delta_a)$	$ln(\delta_t)$
$ln(\mu_\varphi)$	1.00	0.98	0.83	0.98	0.84	0.84	0.98
$ln(\delta_{deck})$	0.98	1.00	0.85	1.00	0.82	0.82	1.00
$ln(\delta_{fnd})$	0.83	0.85	1.00	0.84	0.70	0.70	0.85
$ln(\theta_{pile})$	0.98	1.00	0.84	1.00	0.82	0.82	0.99
$ln(\delta_p)$	0.84	0.82	0.70	0.82	1.00	1.00	0.80
$ln(\delta_a)$	0.84	0.82	0.70	0.82	1.00	1.00	0.80
$ln(\delta_t)$	0.98	1.00	0.85	0.99	0.80	0.80	1.00

MSCC-BG-S-E3-SX-S

	$ln(\mu_\varphi)$	$ln(\delta_{seat})$	$ln(\delta_{deck})$	$ln(\delta_{fnd})$	$ln(\theta_{pile})$	$ln(\delta_p)$	$ln(\delta_a)$	$ln(\delta_t)$	$ln(\delta_{brng})$	$ln(\delta_{seal})$	$ln(\delta_{rest})$	$ln(\delta_{key})$
$ln(\mu_\varphi)$	1.00	0.86	0.91	0.53	0.89	0.75	0.82	0.80	0.87	0.86	0.86	0.11
$ln(\delta_{seat})$	0.86	1.00	0.92	0.68	0.88	0.75	0.86	0.81	0.92	1.00	1.00	0.27
$ln(\delta_{deck})$	0.91	0.92	1.00	0.77	0.93	0.84	0.92	0.87	0.98	0.92	0.92	0.28
$ln(\delta_{fnd})$	0.53	0.68	0.77	1.00	0.76	0.62	0.68	0.71	0.77	0.68	0.68	0.41
$ln(\theta_{pile})$	0.89	0.88	0.93	0.76	1.00	0.76	0.84	0.85	0.89	0.88	0.88	0.21
$ln(\delta_p)$	0.75	0.75	0.84	0.62	0.76	1.00	0.96	0.79	0.78	0.75	0.75	0.16
$ln(\delta_a)$	0.82	0.86	0.92	0.68	0.84	0.96	1.00	0.81	0.86	0.86	0.86	0.24
$ln(\delta_t)$	0.80	0.81	0.87	0.71	0.85	0.79	0.81	1.00	0.86	0.81	0.81	0.04
$ln(\delta_{brng})$	0.87	0.92	0.98	0.77	0.89	0.78	0.86	0.86	1.00	0.92	0.92	0.33
$ln(\delta_{seal})$	0.86	1.00	0.92	0.68	0.88	0.75	0.86	0.81	0.92	1.00	1.00	0.27
$ln(\delta_{rest})$	0.86	1.00	0.92	0.68	0.88	0.75	0.86	0.81	0.92	1.00	1.00	0.27
$ln(\delta_{key})$	0.11	0.27	0.28	0.41	0.21	0.16	0.24	0.04	0.33	0.27	0.27	1.00

MSCC-BG-M-E3-SX-S

	$ln(\mu_\varphi)$	$ln(\delta_{seat})$	$ln(\delta_{deck})$	$ln(\delta_{fnd})$	$ln(\theta_{pile})$	$ln(\delta_p)$	$ln(\delta_a)$	$ln(\delta_t)$	$ln(\delta_{brng})$	$ln(\delta_{seal})$	$ln(\delta_{rest})$	$ln(\delta_{key})$
$ln(\mu_\varphi)$	1.00	0.84	0.97	0.77	0.98	0.64	0.81	0.95	0.85	0.84	0.84	0.09
$ln(\delta_{seat})$	0.84	1.00	0.84	0.65	0.83	0.80	0.96	0.82	0.99	1.00	1.00	0.10
$ln(\delta_{deck})$	0.97	0.84	1.00	0.80	1.00	0.64	0.80	0.97	0.85	0.84	0.84	0.11
$ln(\delta_{fnd})$	0.77	0.65	0.80	1.00	0.78	0.52	0.63	0.79	0.65	0.65	0.65	0.19
$ln(\theta_{pile})$	0.98	0.83	1.00	0.78	1.00	0.63	0.79	0.97	0.84	0.83	0.83	0.10
$ln(\delta_p)$	0.64	0.80	0.64	0.52	0.63	1.00	0.91	0.68	0.79	0.80	0.81	0.09
$ln(\delta_a)$	0.81	0.96	0.80	0.63	0.79	0.91	1.00	0.81	0.95	0.96	0.97	0.10
$ln(\delta_t)$	0.95	0.82	0.97	0.79	0.97	0.68	0.81	1.00	0.83	0.82	0.82	0.08
$ln(\delta_{brng})$	0.85	0.99	0.85	0.65	0.84	0.79	0.95	0.83	1.00	0.99	0.99	0.10
$ln(\delta_{seal})$	0.84	1.00	0.84	0.65	0.83	0.80	0.96	0.82	0.99	1.00	1.00	0.10
$ln(\delta_{rest})$	0.84	1.00	0.84	0.65	0.83	0.81	0.97	0.82	0.99	1.00	1.00	0.10
$ln(\delta_{key})$	0.09	0.10	0.11	0.19	0.10	0.09	0.10	0.08	0.10	0.10	0.10	1.00

MSCC-BG-S-E3-SX-L

	$ln(\mu_\varphi)$	$ln(\delta_{seat})$	$ln(\delta_{deck})$	$ln(\delta_{fnd})$	$ln(\theta_{pile})$	$ln(\delta_p)$	$ln(\delta_a)$	$ln(\delta_t)$	$ln(\delta_{brng})$	$ln(\delta_{seal})$	$ln(\delta_{rest})$	$ln(\delta_{key})$
$ln(\mu_\varphi)$	1.00	0.74	0.86	0.57	0.87	0.70	0.76	0.80	0.81	0.74	0.76	0.08
$ln(\delta_{seat})$	0.74	1.00	0.95	0.85	0.90	0.89	0.96	0.81	0.98	1.00	0.97	0.01
$ln(\delta_{deck})$	0.86	0.95	1.00	0.84	0.95	0.91	0.95	0.90	0.97	0.95	0.93	0.06
$ln(\delta_{fnd})$	0.57	0.85	0.84	1.00	0.82	0.74	0.81	0.79	0.86	0.85	0.82	0.02
$ln(\theta_{pile})$	0.87	0.90	0.95	0.82	1.00	0.81	0.89	0.87	0.92	0.90	0.88	0.02
$ln(\delta_p)$	0.70	0.89	0.91	0.74	0.81	1.00	0.95	0.80	0.87	0.89	0.84	0.13
$ln(\delta_a)$	0.76	0.96	0.95	0.81	0.89	0.95	1.00	0.81	0.94	0.96	0.94	0.03
$ln(\delta_t)$	0.80	0.81	0.90	0.79	0.87	0.80	0.81	1.00	0.84	0.81	0.80	0.24
$ln(\delta_{brng})$	0.81	0.98	0.97	0.86	0.92	0.87	0.94	0.84	1.00	0.98	0.95	0.04
$ln(\delta_{seal})$	0.74	1.00	0.95	0.85	0.90	0.89	0.96	0.81	0.98	1.00	0.97	0.01
$ln(\delta_{rest})$	0.76	0.97	0.93	0.82	0.88	0.84	0.94	0.80	0.95	0.97	1.00	0.03
$ln(\delta_{key})$	0.08	0.01	0.06	0.02	0.02	0.13	0.03	0.24	0.04	0.01	0.03	1.00

MSCC-BG-M-E3-SX-L

	$ln(\mu_\varphi)$	$ln(\delta_{seat})$	$ln(\delta_{deck})$	$ln(\delta_{fnd})$	$ln(\theta_{pile})$	$ln(\delta_p)$	$ln(\delta_a)$	$ln(\delta_t)$	$ln(\delta_{brng})$	$ln(\delta_{seal})$	$ln(\delta_{rest})$	$ln(\delta_{key})$
$ln(\mu_\varphi)$	1.00	0.76	0.98	0.73	0.98	0.74	0.78	0.96	0.77	0.76	0.75	0.17
$ln(\delta_{seat})$	0.76	1.00	0.76	0.53	0.75	0.83	0.95	0.76	1.00	1.00	0.97	0.20
$ln(\delta_{deck})$	0.98	0.76	1.00	0.76	1.00	0.73	0.77	0.97	0.76	0.76	0.75	0.14
$ln(\delta_{fnd})$	0.73	0.53	0.76	1.00	0.75	0.49	0.55	0.74	0.54	0.53	0.51	0.16
$ln(\theta_{pile})$	0.98	0.75	1.00	0.75	1.00	0.73	0.76	0.97	0.75	0.75	0.74	0.14
$ln(\delta_p)$	0.74	0.83	0.73	0.49	0.73	1.00	0.91	0.74	0.83	0.83	0.82	0.18
$ln(\delta_a)$	0.78	0.95	0.77	0.55	0.76	0.91	1.00	0.78	0.95	0.95	0.93	0.18
$ln(\delta_t)$	0.96	0.76	0.97	0.74	0.97	0.74	0.78	1.00	0.76	0.76	0.74	0.08
$ln(\delta_{brng})$	0.77	1.00	0.76	0.54	0.75	0.83	0.95	0.76	1.00	1.00	0.96	0.19
$ln(\delta_{seal})$	0.76	1.00	0.76	0.53	0.75	0.83	0.95	0.76	1.00	1.00	0.97	0.20
$ln(\delta_{rest})$	0.75	0.97	0.75	0.51	0.74	0.82	0.93	0.74	0.96	0.97	1.00	0.18
$ln(\delta_{key})$	0.17	0.20	0.14	0.16	0.14	0.18	0.18	0.08	0.19	0.20	0.18	1.00

Table B.6: Correlation Coefficients of the component demands of multispan continuous concrete slab bridge class and the respective seismic performance sub-bins

MSCC-SL-P-EX-S0

	$ln(\mu_\varphi)$	$ln(\delta_{deck})$	$ln(\delta_{fnd})$	$ln(\theta_{pile})$	$ln(\delta_p)$	$ln(\delta_a)$	$ln(\delta_t)$
$ln(\mu_\varphi)$	1.00	0.87	0.63	0.88	0.80	0.80	0.85
$ln(\delta_{deck})$	0.87	1.00	0.92	0.96	0.95	0.95	0.97
$ln(\delta_{fnd})$	0.63	0.92	1.00	0.84	0.89	0.89	0.89
$ln(\theta_{pile})$	0.88	0.96	0.84	1.00	0.91	0.91	0.94
$ln(\delta_p)$	0.80	0.95	0.89	0.91	1.00	1.00	0.90
$ln(\delta_a)$	0.80	0.95	0.89	0.91	1.00	1.00	0.90
$ln(\delta_t)$	0.85	0.97	0.89	0.94	0.90	0.90	1.00

MSCC-SL-P-EX-SX

	$ln(\mu_\varphi)$	$ln(\delta_{seat})$	$ln(\delta_{deck})$	$ln(\delta_{fnd})$	$ln(\theta_{pile})$	$ln(\delta_p)$	$ln(\delta_a)$	$ln(\delta_t)$	$ln(\delta_{brng})$	$ln(\delta_{seal})$
$ln(\mu_\varphi)$	1.00	0.81	0.91	0.76	0.92	0.39	0.88	0.09	0.91	0.81
$ln(\delta_{seat})$	0.81	1.00	0.84	0.75	0.83	0.44	0.85	0.17	0.82	1.00
$ln(\delta_{deck})$	0.91	0.84	1.00	0.92	0.96	0.62	0.98	0.36	0.96	0.84
$ln(\delta_{fnd})$	0.76	0.75	0.92	1.00	0.90	0.60	0.91	0.56	0.82	0.75
$ln(\theta_{pile})$	0.92	0.83	0.96	0.90	1.00	0.47	0.93	0.20	0.94	0.83
$ln(\delta_p)$	0.39	0.44	0.62	0.60	0.47	1.00	0.64	0.62	0.56	0.44
$ln(\delta_a)$	0.88	0.85	0.98	0.91	0.93	0.64	1.00	0.38	0.94	0.85
$ln(\delta_t)$	0.09	0.17	0.36	0.56	0.20	0.62	0.38	1.00	0.21	0.17
$ln(\delta_{brng})$	0.91	0.82	0.96	0.82	0.94	0.56	0.94	0.21	1.00	0.82
$ln(\delta_{seal})$	0.81	1.00	0.84	0.75	0.83	0.44	0.85	0.17	0.82	1.00

Table B.7: Correlation Coefficients of the component demands of multispan continuous concrete Tee-girder bridge class and the respective seismic performance sub-bins

MSCC-TG-P-E1-S0

	$ln(\mu_\varphi)$	$ln(\delta_{deck})$	$ln(\delta_{fnd})$	$ln(\theta_{pile})$	$ln(\delta_p)$	$ln(\delta_a)$	$ln(\delta_t)$
$ln(\mu_\varphi)$	1.00	0.89	0.37	0.86	0.70	0.70	0.72
$ln(\delta_{deck})$	0.89	1.00	0.60	0.96	0.75	0.75	0.77
$ln(\delta_{fnd})$	0.37	0.60	1.00	0.65	0.58	0.58	0.57
$ln(\theta_{pile})$	0.86	0.96	0.65	1.00	0.80	0.80	0.82
$ln(\delta_p)$	0.70	0.75	0.58	0.80	1.00	1.00	0.89
$ln(\delta_a)$	0.70	0.75	0.58	0.80	1.00	1.00	0.89
$ln(\delta_t)$	0.72	0.77	0.57	0.82	0.89	0.89	1.00

MSCC-TG-M-E1-S0

	$ln(\mu_\varphi)$	$ln(\delta_{deck})$	$ln(\delta_{fnd})$	$ln(\theta_{pile})$	$ln(\delta_p)$	$ln(\delta_a)$	$ln(\delta_t)$
$ln(\mu_\varphi)$	1.00	0.95	0.72	0.81	0.71	0.71	0.76
$ln(\delta_{deck})$	0.95	1.00	0.64	0.81	0.77	0.77	0.76
$ln(\delta_{fnd})$	0.72	0.64	1.00	0.59	0.52	0.52	0.66
$ln(\theta_{pile})$	0.81	0.81	0.59	1.00	0.67	0.67	0.64
$ln(\delta_p)$	0.71	0.77	0.52	0.67	1.00	1.00	0.84
$ln(\delta_a)$	0.71	0.77	0.52	0.67	1.00	1.00	0.84
$ln(\delta_t)$	0.76	0.76	0.66	0.64	0.84	0.84	1.00

MSCC-TG-P-E1-SX

	$ln(\mu_\varphi)$	$ln(\delta_{seat})$	$ln(\delta_{deck})$	$ln(\delta_{fnd})$	$ln(\theta_{pile})$	$ln(\delta_p)$	$ln(\delta_a)$	$ln(\delta_t)$	$ln(\delta_{brng})$	$ln(\delta_{seal})$
$ln(\mu_\varphi)$	1.00	0.80	0.86	0.69	0.95	0.41	0.74	0.26	0.80	0.80
$ln(\delta_{seat})$	0.80	1.00	0.96	0.59	0.82	0.61	0.96	0.40	1.00	1.00
$ln(\delta_{deck})$	0.86	0.96	1.00	0.70	0.90	0.58	0.90	0.44	0.96	0.96
$ln(\delta_{fnd})$	0.69	0.59	0.70	1.00	0.81	0.36	0.51	0.25	0.59	0.59
$ln(\theta_{pile})$	0.95	0.82	0.90	0.81	1.00	0.49	0.75	0.31	0.82	0.82
$ln(\delta_p)$	0.41	0.61	0.58	0.36	0.49	1.00	0.62	0.22	0.61	0.61
$ln(\delta_a)$	0.74	0.96	0.90	0.51	0.75	0.62	1.00	0.41	0.96	0.96
$ln(\delta_t)$	0.26	0.40	0.44	0.25	0.31	0.22	0.41	1.00	0.40	0.40
$ln(\delta_{brng})$	0.80	1.00	0.96	0.59	0.82	0.61	0.96	0.40	1.00	1.00
$ln(\delta_{seal})$	0.80	1.00	0.96	0.59	0.82	0.61	0.96	0.40	1.00	1.00

MSCC-TG-M-E1-SX

	$ln(\mu_\varphi)$	$ln(\delta_{seat})$	$ln(\delta_{deck})$	$ln(\delta_{fnd})$	$ln(\theta_{pile})$	$ln(\delta_p)$	$ln(\delta_a)$	$ln(\delta_t)$	$ln(\delta_{brng})$	$ln(\delta_{seal})$
$ln(\mu_\varphi)$	1.00	0.97	0.97	0.73	0.98	0.78	0.78	0.49	0.97	0.97
$ln(\delta_{seat})$	0.97	1.00	1.00	0.73	0.99	0.80	0.80	0.44	1.00	1.00
$ln(\delta_{deck})$	0.97	1.00	1.00	0.73	0.99	0.79	0.79	0.47	1.00	1.00
$ln(\delta_{fnd})$	0.73	0.73	0.73	1.00	0.74	0.53	0.53	0.32	0.73	0.73
$ln(\theta_{pile})$	0.98	0.99	0.99	0.74	1.00	0.79	0.79	0.46	0.99	0.99
$ln(\delta_p)$	0.78	0.80	0.79	0.53	0.79	1.00	1.00	0.54	0.80	0.80
$ln(\delta_a)$	0.78	0.80	0.79	0.53	0.79	1.00	1.00	0.54	0.80	0.80
$ln(\delta_t)$	0.49	0.44	0.47	0.32	0.46	0.54	0.54	1.00	0.44	0.44
$ln(\delta_{brng})$	0.97	1.00	1.00	0.73	0.99	0.80	0.80	0.44	1.00	1.00
$ln(\delta_{seal})$	0.97	1.00	1.00	0.73	0.99	0.80	0.80	0.44	1.00	1.00

MSCC-TG-P-E2-S0

	$ln(\mu_\varphi)$	$ln(\delta_{deck})$	$ln(\delta_{fnd})$	$ln(\theta_{pile})$	$ln(\delta_p)$	$ln(\delta_a)$	$ln(\delta_t)$
$ln(\mu_\varphi)$	1.00	0.83	0.56	0.84	0.72	0.72	0.75
$ln(\delta_{deck})$	0.83	1.00	0.80	0.95	0.74	0.74	0.80
$ln(\delta_{fnd})$	0.56	0.80	1.00	0.84	0.61	0.61	0.63
$ln(\theta_{pile})$	0.84	0.95	0.84	1.00	0.78	0.78	0.81
$ln(\delta_p)$	0.72	0.74	0.61	0.78	1.00	1.00	0.85
$ln(\delta_a)$	0.72	0.74	0.61	0.78	1.00	1.00	0.85
$ln(\delta_t)$	0.75	0.80	0.63	0.81	0.85	0.85	1.00

MSCC-TG-M-E2-S0

	$ln(\mu_\varphi)$	$ln(\delta_{deck})$	$ln(\delta_{fnd})$	$ln(\theta_{pile})$	$ln(\delta_p)$	$ln(\delta_a)$	$ln(\delta_t)$
$ln(\mu_\varphi)$	1.00	0.93	0.67	0.78	0.64	0.65	0.78
$ln(\delta_{deck})$	0.93	1.00	0.65	0.75	0.74	0.74	0.87
$ln(\delta_{fnd})$	0.67	0.65	1.00	0.79	0.23	0.23	0.40
$ln(\theta_{pile})$	0.78	0.75	0.79	1.00	0.35	0.35	0.50
$ln(\delta_p)$	0.64	0.74	0.23	0.35	1.00	1.00	0.84
$ln(\delta_a)$	0.65	0.74	0.23	0.35	1.00	1.00	0.84
$ln(\delta_t)$	0.78	0.87	0.40	0.50	0.84	0.84	1.00

MSCC-TG-P-E2-SX

	$ln(\mu_\varphi)$	$ln(\delta_{seat})$	$ln(\delta_{deck})$	$ln(\delta_{fnd})$	$ln(\theta_{pile})$	$ln(\delta_p)$	$ln(\delta_a)$	$ln(\delta_t)$	$ln(\delta_{brng})$	$ln(\delta_{seal})$
$ln(\mu_\varphi)$	1.00	0.96	0.97	0.83	0.97	0.44	0.95	0.42	0.96	0.96
$ln(\delta_{seat})$	0.96	1.00	0.99	0.85	0.96	0.59	0.98	0.48	1.00	1.00
$ln(\delta_{deck})$	0.97	0.99	1.00	0.86	0.97	0.55	0.97	0.51	0.99	0.99
$ln(\delta_{fnd})$	0.83	0.85	0.86	1.00	0.90	0.47	0.83	0.41	0.85	0.85
$ln(\theta_{pile})$	0.97	0.96	0.97	0.90	1.00	0.48	0.95	0.44	0.96	0.96
$ln(\delta_p)$	0.44	0.59	0.55	0.47	0.48	1.00	0.55	0.60	0.59	0.59
$ln(\delta_a)$	0.95	0.98	0.97	0.83	0.95	0.55	1.00	0.44	0.98	0.98
$ln(\delta_t)$	0.42	0.48	0.51	0.41	0.44	0.60	0.44	1.00	0.48	0.48
$ln(\delta_{brng})$	0.96	1.00	0.99	0.85	0.96	0.59	0.98	0.48	1.00	1.00
$ln(\delta_{seal})$	0.96	1.00	0.99	0.85	0.96	0.59	0.98	0.48	1.00	1.00

MSCC-TG-M-E2-SX

	$ln(\mu_\varphi)$	$ln(\delta_{seat})$	$ln(\delta_{deck})$	$ln(\delta_{fnd})$	$ln(\theta_{pile})$	$ln(\delta_p)$	$ln(\delta_a)$	$ln(\delta_t)$	$ln(\delta_{brng})$	$ln(\delta_{seal})$
$ln(\mu_\varphi)$	1.00	0.96	0.96	0.65	0.97	0.76	0.77	0.57	0.96	0.96
$ln(\delta_{seat})$	0.96	1.00	0.99	0.63	0.99	0.80	0.80	0.54	1.00	1.00
$ln(\delta_{deck})$	0.96	0.99	1.00	0.63	0.99	0.77	0.77	0.54	0.99	0.99
$ln(\delta_{fnd})$	0.65	0.63	0.63	1.00	0.63	0.49	0.49	0.42	0.63	0.63
$ln(\theta_{pile})$	0.97	0.99	0.99	0.63	1.00	0.78	0.78	0.53	0.99	0.99
$ln(\delta_p)$	0.76	0.80	0.77	0.49	0.78	1.00	1.00	0.62	0.80	0.80
$ln(\delta_a)$	0.77	0.80	0.77	0.49	0.78	1.00	1.00	0.63	0.80	0.80
$ln(\delta_t)$	0.57	0.54	0.54	0.42	0.53	0.62	0.63	1.00	0.54	0.54
$ln(\delta_{brng})$	0.96	1.00	0.99	0.63	0.99	0.80	0.80	0.54	1.00	1.00
$ln(\delta_{seal})$	0.96	1.00	0.99	0.63	0.99	0.80	0.80	0.54	1.00	1.00

MSCC-TG-P-E3-S0

	$ln(\mu_\varphi)$	$ln(\delta_{deck})$	$ln(\delta_{fnd})$	$ln(\theta_{pile})$	$ln(\delta_p)$	$ln(\delta_a)$	$ln(\delta_t)$
$ln(\mu_\varphi)$	1.00	0.87	0.50	0.85	0.74	0.74	0.71
$ln(\delta_{deck})$	0.87	1.00	0.74	0.97	0.83	0.83	0.85
$ln(\delta_{fnd})$	0.50	0.74	1.00	0.77	0.68	0.68	0.65
$ln(\theta_{pile})$	0.85	0.97	0.77	1.00	0.85	0.85	0.85
$ln(\delta_p)$	0.74	0.83	0.68	0.85	1.00	1.00	0.87
$ln(\delta_a)$	0.74	0.83	0.68	0.85	1.00	1.00	0.87
$ln(\delta_t)$	0.71	0.85	0.65	0.85	0.87	0.87	1.00

MSCC-TG-M-E3-S0

	$ln(\mu_\varphi)$	$ln(\delta_{deck})$	$ln(\delta_{fnd})$	$ln(\theta_{pile})$	$ln(\delta_p)$	$ln(\delta_a)$	$ln(\delta_t)$
$ln(\mu_\varphi)$	1.00	0.93	0.66	0.83	0.72	0.72	0.84
$ln(\delta_{deck})$	0.93	1.00	0.73	0.88	0.75	0.75	0.83
$ln(\delta_{fnd})$	0.66	0.73	1.00	0.65	0.61	0.61	0.59
$ln(\theta_{pile})$	0.83	0.88	0.65	1.00	0.72	0.71	0.75
$ln(\delta_p)$	0.72	0.75	0.61	0.72	1.00	1.00	0.82
$ln(\delta_a)$	0.72	0.75	0.61	0.71	1.00	1.00	0.82
$ln(\delta_t)$	0.84	0.83	0.59	0.75	0.82	0.82	1.00

MSCC-TG-P-E3-SX

	$ln(\mu_\varphi)$	$ln(\delta_{seat})$	$ln(\delta_{deck})$	$ln(\delta_{fnd})$	$ln(\theta_{pile})$	$ln(\delta_p)$	$ln(\delta_a)$	$ln(\delta_t)$	$ln(\delta_{brng})$	$ln(\delta_{seal})$
$ln(\mu_\varphi)$	1.00	0.88	0.89	0.37	0.88	0.65	0.86	0.37	0.88	0.88
$ln(\delta_{seat})$	0.88	1.00	0.98	0.62	0.95	0.67	0.95	0.45	1.00	1.00
$ln(\delta_{deck})$	0.89	0.98	1.00	0.63	0.96	0.68	0.92	0.46	0.98	0.98
$ln(\delta_{fnd})$	0.37	0.62	0.63	1.00	0.64	0.49	0.56	0.44	0.62	0.62
$ln(\theta_{pile})$	0.88	0.95	0.96	0.64	1.00	0.70	0.89	0.40	0.95	0.95
$ln(\delta_p)$	0.65	0.67	0.68	0.49	0.70	1.00	0.67	0.41	0.67	0.67
$ln(\delta_a)$	0.86	0.95	0.92	0.56	0.89	0.67	1.00	0.46	0.95	0.95
$ln(\delta_t)$	0.37	0.45	0.46	0.44	0.40	0.41	0.46	1.00	0.45	0.45
$ln(\delta_{brng})$	0.88	1.00	0.98	0.62	0.95	0.67	0.95	0.45	1.00	1.00
$ln(\delta_{seal})$	0.88	1.00	0.98	0.62	0.95	0.67	0.95	0.45	1.00	1.00

MSCC-TG-M-E3-SX

	$ln(\mu_\varphi)$	$ln(\delta_{seat})$	$ln(\delta_{deck})$	$ln(\delta_{fnd})$	$ln(\theta_{pile})$	$ln(\delta_p)$	$ln(\delta_a)$	$ln(\delta_t)$	$ln(\delta_{brng})$	$ln(\delta_{seal})$
$ln(\mu_\varphi)$	1.00	0.96	0.95	0.69	0.98	0.78	0.78	0.45	0.96	0.96
$ln(\delta_{seat})$	0.96	1.00	1.00	0.70	0.99	0.82	0.82	0.49	1.00	1.00
$ln(\delta_{deck})$	0.95	1.00	1.00	0.69	0.99	0.81	0.81	0.50	1.00	1.00
$ln(\delta_{fnd})$	0.69	0.70	0.69	1.00	0.69	0.62	0.62	0.47	0.70	0.70
$ln(\theta_{pile})$	0.98	0.99	0.99	0.69	1.00	0.81	0.81	0.49	0.99	0.99
$ln(\delta_p)$	0.78	0.82	0.81	0.62	0.81	1.00	1.00	0.53	0.82	0.82
$ln(\delta_a)$	0.78	0.82	0.81	0.62	0.81	1.00	1.00	0.53	0.82	0.82
$ln(\delta_t)$	0.45	0.49	0.50	0.47	0.49	0.53	0.53	1.00	0.49	0.49
$ln(\delta_{brng})$	0.96	1.00	1.00	0.70	0.99	0.82	0.82	0.49	1.00	1.00
$ln(\delta_{seal})$	0.96	1.00	1.00	0.70	0.99	0.82	0.82	0.49	1.00	1.00

Table B.8: Correlation Coefficients of the component demands of multispan continuous concrete I-girder bridge class and the respective seismic performance sub-bins

MSCC-IG-S-E1-S0

	$ln(\mu_\varphi)$	$ln(\delta_{deck})$	$ln(\delta_{fnd})$	$ln(\theta_{pile})$	$ln(\delta_p)$	$ln(\delta_a)$	$ln(\delta_t)$	$ln(\delta_{brng})$	$ln(\delta_{rest})$	$ln(\delta_{key})$
$ln(\mu_\varphi)$	1.00	0.90	0.91	0.98	0.70	0.64	0.83	0.94	0.73	0.37
$ln(\delta_{deck})$	0.90	1.00	0.89	0.90	0.78	0.75	0.89	0.98	0.79	0.35
$ln(\delta_{fnd})$	0.91	0.89	1.00	0.96	0.71	0.66	0.83	0.91	0.71	0.27
$ln(\theta_{pile})$	0.98	0.90	0.96	1.00	0.72	0.66	0.83	0.94	0.71	0.32
$ln(\delta_p)$	0.70	0.78	0.71	0.72	1.00	0.93	0.75	0.76	0.68	0.29
$ln(\delta_a)$	0.64	0.75	0.66	0.66	0.93	1.00	0.75	0.72	0.70	0.30
$ln(\delta_t)$	0.83	0.89	0.83	0.83	0.75	0.75	1.00	0.90	0.69	0.30
$ln(\delta_{brng})$	0.94	0.98	0.91	0.94	0.76	0.72	0.90	1.00	0.77	0.37
$ln(\delta_{rest})$	0.73	0.79	0.71	0.71	0.68	0.70	0.69	0.77	1.00	0.29
$ln(\delta_{key})$	0.37	0.35	0.27	0.32	0.29	0.30	0.30	0.37	0.29	1.00

MSCC-IG-M-E1-S0

	$ln(\mu_\varphi)$	$ln(\delta_{deck})$	$ln(\delta_{fnd})$	$ln(\theta_{pile})$	$ln(\delta_p)$	$ln(\delta_a)$	$ln(\delta_t)$	$ln(\delta_{brng})$	$ln(\delta_{rest})$	$ln(\delta_{key})$
$ln(\mu_\varphi)$	1.00	0.83	0.66	0.95	0.66	0.68	0.80	0.87	0.64	0.26
$ln(\delta_{deck})$	0.83	1.00	0.56	0.87	0.78	0.78	0.87	0.95	0.67	0.37
$ln(\delta_{fnd})$	0.66	0.56	1.00	0.67	0.35	0.38	0.48	0.64	0.48	0.14
$ln(\theta_{pile})$	0.95	0.87	0.67	1.00	0.70	0.72	0.82	0.92	0.70	0.26
$ln(\delta_p)$	0.66	0.78	0.35	0.70	1.00	0.97	0.80	0.69	0.60	0.42
$ln(\delta_a)$	0.68	0.78	0.38	0.72	0.97	1.00	0.83	0.69	0.60	0.41
$ln(\delta_t)$	0.80	0.87	0.48	0.82	0.80	0.83	1.00	0.83	0.55	0.38
$ln(\delta_{brng})$	0.87	0.95	0.64	0.92	0.69	0.69	0.83	1.00	0.70	0.28
$ln(\delta_{rest})$	0.64	0.67	0.48	0.70	0.60	0.60	0.55	0.70	1.00	0.27
$ln(\delta_{key})$	0.26	0.37	0.14	0.26	0.42	0.41	0.38	0.28	0.27	1.00

MSCC-IG-S-E1-SX

	$ln(\mu_\varphi)$	$ln(\delta_{seat})$	$ln(\delta_{deck})$	$ln(\delta_{fnd})$	$ln(\theta_{pile})$	$ln(\delta_p)$	$ln(\delta_a)$	$ln(\delta_t)$	$ln(\delta_{brng})$	$ln(\delta_{seal})$	$ln(\delta_{rest})$	$ln(\delta_{key})$
$ln(\mu_\varphi)$	1.00	0.70	0.94	0.84	0.97	0.77	0.77	0.85	0.94	0.70	0.62	0.54
$ln(\delta_{seat})$	0.70	1.00	0.74	0.53	0.68	0.91	0.92	0.68	0.74	1.00	0.97	0.62
$ln(\delta_{deck})$	0.94	0.74	1.00	0.84	0.93	0.80	0.80	0.87	0.99	0.74	0.69	0.58
$ln(\delta_{fnd})$	0.84	0.53	0.84	1.00	0.89	0.67	0.65	0.73	0.86	0.53	0.48	0.44
$ln(\theta_{pile})$	0.97	0.68	0.93	0.89	1.00	0.76	0.76	0.84	0.94	0.68	0.62	0.55
$ln(\delta_p)$	0.77	0.91	0.80	0.67	0.76	1.00	0.98	0.70	0.80	0.91	0.85	0.61
$ln(\delta_a)$	0.77	0.92	0.80	0.65	0.76	0.98	1.00	0.72	0.81	0.92	0.87	0.63
$ln(\delta_t)$	0.85	0.68	0.87	0.73	0.84	0.70	0.72	1.00	0.88	0.68	0.66	0.52
$ln(\delta_{brng})$	0.94	0.74	0.99	0.86	0.94	0.80	0.81	0.88	1.00	0.74	0.69	0.57
$ln(\delta_{seal})$	0.70	1.00	0.74	0.53	0.68	0.91	0.92	0.68	0.74	1.00	0.97	0.62
$ln(\delta_{rest})$	0.62	0.97	0.69	0.48	0.62	0.85	0.87	0.66	0.69	0.97	1.00	0.55
$ln(\delta_{key})$	0.54	0.62	0.58	0.44	0.55	0.61	0.63	0.52	0.57	0.62	0.55	1.00

MSCC-IG-M-E1-SX

	$ln(\mu_\varphi)$	$ln(\delta_{seat})$	$ln(\delta_{deck})$	$ln(\delta_{fnd})$	$ln(\theta_{pile})$	$ln(\delta_p)$	$ln(\delta_a)$	$ln(\delta_t)$	$ln(\delta_{brng})$	$ln(\delta_{seal})$	$ln(\delta_{rest})$	$ln(\delta_{key})$
$ln(\mu_\varphi)$	1.00	0.84	0.91	0.62	0.93	0.77	0.76	0.72	0.89	0.84	0.79	0.20
$ln(\delta_{seat})$	0.84	1.00	0.93	0.58	0.93	0.87	0.86	0.65	0.92	1.00	0.80	0.27
$ln(\delta_{deck})$	0.91	0.93	1.00	0.66	0.97	0.83	0.81	0.74	0.98	0.93	0.82	0.24
$ln(\delta_{fnd})$	0.62	0.58	0.66	1.00	0.68	0.56	0.56	0.55	0.67	0.58	0.59	0.26
$ln(\theta_{pile})$	0.93	0.93	0.97	0.68	1.00	0.84	0.83	0.71	0.96	0.93	0.83	0.24

$ln(\delta_p)$	0.77	0.87	0.83	0.56	0.84	1.00	0.95	0.62	0.81	0.87	0.82	0.27
$ln(\delta_a)$	0.76	0.86	0.81	0.56	0.83	0.95	1.00	0.59	0.79	0.86	0.81	0.24
$ln(\delta_t)$	0.72	0.65	0.74	0.55	0.71	0.62	0.59	1.00	0.77	0.65	0.52	0.09
$ln(\delta_{brng})$	0.89	0.92	0.98	0.67	0.96	0.81	0.79	0.77	1.00	0.92	0.79	0.21
$ln(\delta_{seal})$	0.84	1.00	0.93	0.58	0.93	0.87	0.86	0.65	0.92	1.00	0.80	0.27
$ln(\delta_{rest})$	0.79	0.80	0.82	0.59	0.83	0.82	0.81	0.52	0.79	0.80	1.00	0.23
$ln(\delta_{key})$	0.20	0.27	0.24	0.26	0.24	0.27	0.24	0.09	0.21	0.27	0.23	1.00

MSCC-IG-S-E2-S0

	$ln(\mu_\varphi)$	$ln(\delta_{deck})$	$ln(\delta_{fnd})$	$ln(\theta_{pile})$	$ln(\delta_p)$	$ln(\delta_a)$	$ln(\delta_t)$	$ln(\delta_{brng})$	$ln(\delta_{rest})$	$ln(\delta_{key})$
$ln(\mu_\varphi)$	1.00	0.66	0.91	0.91	0.97	0.71	0.63	0.89	0.95	0.66
$ln(\delta_{deck})$	0.66	1.00	0.82	0.76	0.73	0.85	0.80	0.77	0.78	1.00
$ln(\delta_{fnd})$	0.91	0.82	1.00	0.94	0.95	0.86	0.79	0.92	0.98	0.82
$ln(\theta_{pile})$	0.91	0.76	0.94	1.00	0.97	0.78	0.69	0.89	0.95	0.76
$ln(\delta_p)$	0.97	0.73	0.95	0.97	1.00	0.76	0.66	0.91	0.97	0.73
$ln(\delta_a)$	0.71	0.85	0.86	0.78	0.76	1.00	0.93	0.84	0.82	0.85
$ln(\delta_t)$	0.63	0.80	0.79	0.69	0.66	0.93	1.00	0.73	0.73	0.80
$ln(\delta_{brng})$	0.89	0.77	0.92	0.89	0.91	0.84	0.73	1.00	0.94	0.77
$ln(\delta_{rest})$	0.95	0.78	0.98	0.95	0.97	0.82	0.73	0.94	1.00	0.78
$ln(\delta_{key})$	0.66	1.00	0.82	0.76	0.73	0.85	0.80	0.77	0.78	1.00

MSCC-IG-M-E2-S0

	$ln(\mu_\varphi)$	$ln(\delta_{deck})$	$ln(\delta_{fnd})$	$ln(\theta_{pile})$	$ln(\delta_p)$	$ln(\delta_a)$	$ln(\delta_t)$	$ln(\delta_{brng})$	$ln(\delta_{rest})$	$ln(\delta_{key})$
$ln(\mu_\varphi)$	1.00	0.64	0.87	0.69	0.96	0.67	0.67	0.77	0.92	0.64
$ln(\delta_{deck})$	0.64	1.00	0.68	0.49	0.68	0.68	0.70	0.58	0.69	1.00
$ln(\delta_{fnd})$	0.87	0.68	1.00	0.64	0.90	0.75	0.75	0.86	0.96	0.68
$ln(\theta_{pile})$	0.69	0.49	0.64	1.00	0.73	0.38	0.39	0.51	0.73	0.49
$ln(\delta_p)$	0.96	0.68	0.90	0.73	1.00	0.68	0.67	0.78	0.95	0.68
$ln(\delta_a)$	0.67	0.68	0.75	0.38	0.68	1.00	0.96	0.82	0.70	0.68
$ln(\delta_t)$	0.67	0.70	0.75	0.39	0.67	0.96	1.00	0.84	0.70	0.70
$ln(\delta_{brng})$	0.77	0.58	0.86	0.51	0.78	0.82	0.84	1.00	0.82	0.58
$ln(\delta_{rest})$	0.92	0.69	0.96	0.73	0.95	0.70	0.70	0.82	1.00	0.69
$ln(\delta_{key})$	0.64	1.00	0.68	0.49	0.68	0.68	0.70	0.58	0.69	1.00

MSCC-IG-S-E2-SX

	$ln(\mu_\varphi)$	$ln(\delta_{seat})$	$ln(\delta_{deck})$	$ln(\delta_{fnd})$	$ln(\theta_{pile})$	$ln(\delta_p)$	$ln(\delta_a)$	$ln(\delta_t)$	$ln(\delta_{brng})$	$ln(\delta_{seal})$	$ln(\delta_{rest})$	$ln(\delta_{key})$
$ln(\mu_\varphi)$	1.00	0.71	0.91	0.81	0.96	0.69	0.66	0.81	0.91	0.71	0.72	0.43
$ln(\delta_{seat})$	0.71	1.00	0.77	0.61	0.74	0.90	0.88	0.74	0.77	1.00	0.94	0.63
$ln(\delta_{deck})$	0.91	0.77	1.00	0.86	0.93	0.75	0.74	0.85	0.99	0.77	0.79	0.52
$ln(\delta_{fnd})$	0.81	0.61	0.86	1.00	0.88	0.54	0.51	0.74	0.87	0.61	0.66	0.49
$ln(\theta_{pile})$	0.96	0.74	0.93	0.88	1.00	0.69	0.65	0.78	0.93	0.74	0.74	0.41
$ln(\delta_p)$	0.69	0.90	0.75	0.54	0.69	1.00	0.96	0.73	0.74	0.90	0.85	0.57
$ln(\delta_a)$	0.66	0.88	0.74	0.51	0.65	0.96	1.00	0.71	0.72	0.88	0.85	0.57
$ln(\delta_t)$	0.81	0.74	0.85	0.74	0.78	0.73	0.71	1.00	0.85	0.74	0.73	0.55
$ln(\delta_{brng})$	0.91	0.77	0.99	0.87	0.93	0.74	0.72	0.85	1.00	0.77	0.79	0.55
$ln(\delta_{seal})$	0.71	1.00	0.77	0.61	0.74	0.90	0.88	0.74	0.77	1.00	0.94	0.63
$ln(\delta_{rest})$	0.72	0.94	0.79	0.66	0.74	0.85	0.85	0.73	0.79	0.94	1.00	0.59
$ln(\delta_{key})$	0.43	0.63	0.52	0.49	0.41	0.57	0.57	0.55	0.55	0.63	0.59	1.00

MSCC-IG-M-E2-SX

	$ln(\mu_\varphi)$	$ln(\delta_{seat})$	$ln(\delta_{deck})$	$ln(\delta_{fnd})$	$ln(\theta_{pile})$	$ln(\delta_p)$	$ln(\delta_a)$	$ln(\delta_t)$	$ln(\delta_{brng})$	$ln(\delta_{seal})$	$ln(\delta_{rest})$	$ln(\delta_{key})$
$ln(\mu_\varphi)$	1.00	0.75	0.84	0.55	0.89	0.76	0.75	0.77	0.85	0.75	0.69	0.18
$ln(\delta_{seat})$	0.75	1.00	0.90	0.36	0.89	0.87	0.86	0.66	0.89	1.00	0.85	0.25
$ln(\delta_{deck})$	0.84	0.90	1.00	0.52	0.96	0.83	0.81	0.80	0.98	0.90	0.81	0.17
$ln(\delta_{fnd})$	0.55	0.36	0.52	1.00	0.54	0.41	0.36	0.58	0.54	0.36	0.33	0.13
$ln(\theta_{pile})$	0.89	0.89	0.96	0.54	1.00	0.82	0.81	0.79	0.97	0.89	0.81	0.21
$ln(\delta_p)$	0.76	0.87	0.83	0.41	0.82	1.00	0.95	0.68	0.81	0.87	0.81	0.25
$ln(\delta_a)$	0.75	0.86	0.81	0.36	0.81	0.95	1.00	0.67	0.80	0.86	0.79	0.25
$ln(\delta_t)$	0.77	0.66	0.80	0.58	0.79	0.68	0.67	1.00	0.81	0.66	0.61	0.03
$ln(\delta_{brng})$	0.85	0.89	0.98	0.54	0.97	0.81	0.80	0.81	1.00	0.89	0.80	0.19
$ln(\delta_{seal})$	0.75	1.00	0.90	0.36	0.89	0.87	0.86	0.66	0.89	1.00	0.85	0.25
$ln(\delta_{rest})$	0.69	0.85	0.81	0.33	0.81	0.81	0.79	0.61	0.80	0.85	1.00	0.24
$ln(\delta_{key})$	0.18	0.25	0.17	0.13	0.21	0.25	0.25	0.03	0.19	0.25	0.24	1.00

MSCC-IG-S-E3-S0

	$ln(\mu_\varphi)$	$ln(\delta_{deck})$	$ln(\delta_{fnd})$	$ln(\theta_{pile})$	$ln(\delta_p)$	$ln(\delta_a)$	$ln(\delta_t)$	$ln(\delta_{brng})$	$ln(\delta_{rest})$	$ln(\delta_{key})$
$ln(\mu_\varphi)$	1.00	0.64	0.89	0.89	0.98	0.53	0.47	0.86	0.95	0.64
$ln(\delta_{deck})$	0.64	1.00	0.78	0.66	0.69	0.78	0.80	0.79	0.74	1.00
$ln(\delta_{fnd})$	0.89	0.78	1.00	0.89	0.92	0.72	0.65	0.92	0.98	0.78
$ln(\theta_{pile})$	0.89	0.66	0.89	1.00	0.94	0.60	0.51	0.84	0.92	0.66
$ln(\delta_p)$	0.98	0.69	0.92	0.94	1.00	0.58	0.52	0.88	0.97	0.69
$ln(\delta_a)$	0.53	0.78	0.72	0.60	0.58	1.00	0.94	0.72	0.64	0.78
$ln(\delta_t)$	0.47	0.80	0.65	0.51	0.52	0.94	1.00	0.69	0.57	0.80
$ln(\delta_{brng})$	0.86	0.79	0.92	0.84	0.88	0.72	0.69	1.00	0.92	0.79
$ln(\delta_{rest})$	0.95	0.74	0.98	0.92	0.97	0.64	0.57	0.92	1.00	0.74
$ln(\delta_{key})$	0.64	1.00	0.78	0.66	0.69	0.78	0.80	0.79	0.74	1.00

MSCC-IG-M-E3-S0

	$ln(\mu_\varphi)$	$ln(\delta_{deck})$	$ln(\delta_{fnd})$	$ln(\theta_{pile})$	$ln(\delta_p)$	$ln(\delta_a)$	$ln(\delta_t)$	$ln(\delta_{brng})$	$ln(\delta_{rest})$	$ln(\delta_{key})$
$ln(\mu_\varphi)$	1.00	0.66	0.90	0.75	0.96	0.72	0.72	0.80	0.93	0.66
$ln(\delta_{deck})$	0.66	1.00	0.74	0.53	0.72	0.65	0.68	0.62	0.74	1.00
$ln(\delta_{fnd})$	0.90	0.74	1.00	0.67	0.91	0.79	0.80	0.85	0.96	0.74
$ln(\theta_{pile})$	0.75	0.53	0.67	1.00	0.75	0.54	0.53	0.58	0.73	0.53
$ln(\delta_p)$	0.96	0.72	0.91	0.75	1.00	0.72	0.72	0.79	0.96	0.72
$ln(\delta_a)$	0.72	0.65	0.79	0.54	0.72	1.00	0.95	0.81	0.75	0.65
$ln(\delta_t)$	0.72	0.68	0.80	0.53	0.72	0.95	1.00	0.85	0.75	0.68
$ln(\delta_{brng})$	0.80	0.62	0.85	0.58	0.79	0.81	0.85	1.00	0.82	0.62
$ln(\delta_{rest})$	0.93	0.74	0.96	0.73	0.96	0.75	0.75	0.82	1.00	0.74
$ln(\delta_{key})$	0.66	1.00	0.74	0.53	0.72	0.65	0.68	0.62	0.74	1.00

MSCC-IG-S-E3-SX

	$ln(\mu_\varphi)$	$ln(\delta_{seat})$	$ln(\delta_{deck})$	$ln(\delta_{fnd})$	$ln(\theta_{pile})$	$ln(\delta_p)$	$ln(\delta_a)$	$ln(\delta_t)$	$ln(\delta_{brng})$	$ln(\delta_{seal})$	$ln(\delta_{rest})$	$ln(\delta_{key})$
$ln(\mu_\varphi)$	1.00	0.63	0.83	0.60	0.88	0.56	0.58	0.67	0.84	0.63	0.67	0.39
$ln(\delta_{seat})$	0.63	1.00	0.70	0.38	0.59	0.86	0.80	0.61	0.68	1.00	0.94	0.48
$ln(\delta_{deck})$	0.83	0.70	1.00	0.69	0.87	0.58	0.58	0.65	0.99	0.70	0.72	0.37
$ln(\delta_{fnd})$	0.60	0.38	0.69	1.00	0.82	0.29	0.30	0.49	0.73	0.38	0.40	0.20
$ln(\theta_{pile})$	0.88	0.59	0.87	0.82	1.00	0.51	0.52	0.63	0.89	0.59	0.62	0.40
$ln(\delta_p)$	0.56	0.86	0.58	0.29	0.51	1.00	0.94	0.62	0.56	0.86	0.80	0.40
$ln(\delta_a)$	0.58	0.80	0.58	0.30	0.52	0.94	1.00	0.63	0.56	0.80	0.77	0.37
$ln(\delta_t)$	0.67	0.61	0.65	0.49	0.63	0.62	0.63	1.00	0.66	0.61	0.65	0.30

$ln(\delta_{brng})$	0.84	0.68	0.99	0.73	0.89	0.56	0.56	0.66	1.00	0.68	0.70	0.35
$ln(\delta_{seal})$	0.63	1.00	0.70	0.38	0.59	0.86	0.80	0.61	0.68	1.00	0.94	0.48
$ln(\delta_{rest})$	0.67	0.94	0.72	0.40	0.62	0.80	0.77	0.65	0.70	0.94	1.00	0.50
$ln(\delta_{key})$	0.39	0.48	0.37	0.20	0.40	0.40	0.37	0.30	0.35	0.48	0.50	1.00

MSCC-IG-M-E3-SX

	$ln(\mu_{\varphi})$	$ln(\delta_{seat})$	$ln(\delta_{deck})$	$ln(\delta_{fnd})$	$ln(\theta_{pile})$	$ln(\delta_{p})$	$ln(\delta_{a})$	$ln(\delta_{t})$	$ln(\delta_{brng})$	$ln(\delta_{seal})$	$ln(\delta_{rest})$	$ln(\delta_{key})$
$ln(\mu_{\varphi})$	1.00	0.78	0.85	0.54	0.88	0.72	0.73	0.77	0.85	0.78	0.70	0.24
$ln(\delta_{seat})$	0.78	1.00	0.90	0.45	0.91	0.87	0.87	0.73	0.89	1.00	0.82	0.22
$ln(\delta_{deck})$	0.85	0.90	1.00	0.59	0.96	0.79	0.79	0.82	0.98	0.90	0.81	0.20
$ln(\delta_{fnd})$	0.54	0.45	0.59	1.00	0.57	0.43	0.40	0.57	0.61	0.45	0.56	0.16
$ln(\theta_{pile})$	0.88	0.91	0.96	0.57	1.00	0.80	0.81	0.81	0.96	0.91	0.81	0.22
$ln(\delta_{p})$	0.72	0.87	0.79	0.43	0.80	1.00	0.96	0.66	0.78	0.87	0.78	0.21
$ln(\delta_{a})$	0.73	0.87	0.79	0.40	0.81	0.96	1.00	0.67	0.77	0.87	0.76	0.19
$ln(\delta_{t})$	0.77	0.73	0.82	0.57	0.81	0.66	0.67	1.00	0.86	0.73	0.68	0.14
$ln(\delta_{brng})$	0.85	0.89	0.98	0.61	0.96	0.78	0.77	0.86	1.00	0.89	0.80	0.19
$ln(\delta_{seal})$	0.78	1.00	0.90	0.45	0.91	0.87	0.87	0.73	0.89	1.00	0.82	0.22
$ln(\delta_{rest})$	0.70	0.82	0.81	0.56	0.81	0.78	0.76	0.68	0.80	0.82	1.00	0.31
$ln(\delta_{key})$	0.24	0.22	0.20	0.16	0.22	0.21	0.19	0.14	0.19	0.22	0.31	1.00

APPENDIX C

OPTIMAL INTENSITY MEASURE INVESTIGATION

This appendix presents the results from the investigation of optimal intensity measures across the bridge classes and seismic performance sub-bins considered in this study. This was detailed in section 5.4 of Chapter 5. Efficiency, practicality, proficiency, and sufficiency are some of the essential properties of an optimal IM and the results are presented in Table C.1.

Table C.1: Investigation of efficiency, proficiency, practicality and sufficiency properties to investigate optimality of intensity measures

			Column curvature ductility, μ_φ								Abutment seat displacement, δ_{seat}							
Bridge class	SPS	IM	$log(a)$	b	R^2	$\beta_{D\|IM}$	ζ	p_M	p_R	p_ε	$log(a)$	b	R^2	$\beta_{D\|IM}$	ζ	p_M	p_R	p_ε
MSCC-BG-S	E1-S0	PGA	2.28	1.28	0.82	0.53	0.41	0.84	0.12	0.91								
		$S_{a\text{-}0.3}$	1.20	1.24	0.79	0.56	0.45	0.53	0.56	0.77								
		$S_{a\text{-}0.2}$	1.28	1.29	0.72	0.67	0.52	0.66	0.83	0.39								
		$S_{a\text{-}1.0}$	1.85	1.09	0.81	0.54	0.49	0.66	0.54	0.73								
	E1-SX	PGA	2.27	1.09	0.74	0.60	0.55	0.31	0.93	0.95	1.52	0.75	0.70	0.45	0.60	0.69	0.31	0.01
		$S_{a\text{-}0.3}$	1.42	1.11	0.70	0.66	0.59	1.00	0.52	0.01	0.95	0.75	0.69	0.45	0.60	0.16	1.00	0.76
		$S_{a\text{-}0.2}$	1.37	1.03	0.64	0.70	0.68	0.54	0.32	0.59	0.88	0.69	0.60	0.51	0.74	0.22	0.76	0.60
		$S_{a\text{-}1.0}$	2.16	1.12	0.86	0.48	0.43	0.44	0.36	0.23	1.41	0.74	0.85	0.33	0.45	0.87	0.79	0.66
	E2-S0	PGA	1.87	1.09	0.61	0.66	0.61	0.29	0.67	0.42								
		$S_{a\text{-}0.3}$	0.93	1.22	0.57	0.74	0.60	0.55	0.22	0.67								
		$S_{a\text{-}0.2}$	0.98	0.98	0.46	0.77	0.79	0.31	0.24	0.24								
		$S_{a\text{-}1.0}$	1.61	1.02	0.68	0.62	0.61	0.21	0.96	0.08								
	E2-SX	PGA	2.41	1.14	0.72	0.64	0.56	0.36	0.28	0.56	1.53	0.72	0.63	0.47	0.65	0.70	0.61	0.65
		$S_{a\text{-}0.3}$	1.34	1.21	0.76	0.62	0.52	0.66	0.62	0.25	0.95	0.79	0.63	0.52	0.66	0.72	0.29	0.18
		$S_{a\text{-}0.2}$	1.46	1.16	0.62	0.79	0.68	0.54	0.64	0.07	0.93	0.74	0.59	0.52	0.70	0.09	0.09	0.11
		$S_{a\text{-}1.0}$	2.24	1.32	0.81	0.58	0.44	0.27	0.08	0.22	1.41	0.76	0.77	0.37	0.49	0.54	0.06	0.96
	E3-S0	PGA	2.21	1.33	0.84	0.52	0.39	0.50	0.68	0.25								
		$S_{a\text{-}0.3}$	0.96	1.22	0.79	0.58	0.48	0.76	0.89	0.74								
		$S_{a\text{-}0.2}$	1.09	1.30	0.73	0.68	0.52	0.24	0.48	0.98								
		$S_{a\text{-}1.0}$	2.15	1.41	0.91	0.44	0.31	0.96	0.93	0.89								
	E3-SX	PGA	2.14	1.32	0.86	0.41	0.31	0.63	0.85	0.03	1.38	0.77	0.69	0.39	0.51	0.25	0.43	0.44
		$S_{a\text{-}0.3}$	1.05	1.29	0.75	0.57	0.45	0.08	0.02	0.09	0.76	0.72	0.71	0.36	0.50	0.29	0.04	0.15
		$S_{a\text{-}0.2}$	1.00	1.28	0.70	0.62	0.48	0.28	0.12	0.79	0.75	0.71	0.57	0.46	0.64	0.50	0.45	0.51
		$S_{a\text{-}1.0}$	1.66	1.14	0.87	0.41	0.37	0.33	0.01	0.53	1.16	0.67	0.85	0.26	0.38	0.81	0.13	0.00

MSCC-BG-M	E1-S0	PGA	2.63	1.11	0.57	0.81	0.73	0.75	0.36	0.21								
		$S_{a\text{-}0.3}$	1.67	1.09	0.55	0.82	0.75	0.31	0.53	0.70								
		$S_{a\text{-}0.2}$	1.56	0.90	0.41	0.91	1.00	0.02	0.72	0.90								
		$S_{a\text{-}1.0}$	2.72	1.21	0.83	0.50	0.41	0.64	0.90	0.33								
	E1-SX	PGA	3.30	1.20	0.53	0.90	0.75	0.70	0.82	0.64	2.23	0.91	0.57	0.61	0.67	0.76	0.64	0.11
		$S_{a\text{-}0.3}$	2.21	1.14	0.50	0.93	0.81	0.64	0.82	0.62	1.44	0.88	0.56	0.61	0.70	0.60	0.25	0.58
		$S_{a\text{-}0.2}$	2.24	1.08	0.38	1.03	0.95	0.37	0.78	0.31	1.46	0.85	0.43	0.71	0.84	0.44	0.01	0.12
		$S_{a\text{-}1.0}$	3.26	1.28	0.76	0.67	0.53	0.02	0.38	0.55	2.12	0.91	0.80	0.42	0.46	0.12	1.00	0.87
	E2-S0	PGA	2.74	1.37	0.66	0.85	0.62	0.09	0.34	0.12								
		$S_{a\text{-}0.3}$	1.61	1.35	0.62	0.93	0.69	0.75	0.38	0.49								
		$S_{a\text{-}0.2}$	1.53	1.24	0.52	1.01	0.81	0.78	0.58	0.18								
		$S_{a\text{-}1.0}$	2.54	1.31	0.79	0.66	0.50	0.80	0.49	0.08								
	E2-SX	PGA	3.06	1.35	0.55	1.02	0.75	0.72	0.99	0.17	2.07	0.96	0.68	0.54	0.56	0.70	0.44	0.12
		$S_{a\text{-}0.3}$	1.97	1.33	0.54	1.03	0.77	0.49	0.83	0.02	1.25	0.89	0.64	0.56	0.62	0.93	0.24	0.45
		$S_{a\text{-}0.2}$	1.87	1.20	0.42	1.16	0.97	0.43	0.93	0.48	1.23	0.85	0.53	0.65	0.77	0.44	0.24	0.67
		$S_{a\text{-}1.0}$	3.02	1.37	0.74	0.81	0.59	0.56	0.77	0.16	1.97	0.93	0.86	0.37	0.40	0.80	0.26	0.10
	E3-S0	PGA	3.15	1.52	0.67	0.83	0.55	0.62	0.36	0.18								
		$S_{a\text{-}0.3}$	1.86	1.42	0.63	0.87	0.62	0.99	0.44	0.14								
		$S_{a\text{-}0.2}$	1.78	1.27	0.56	0.89	0.70	0.04	0.32	0.30								
		$S_{a\text{-}1.0}$	2.72	1.30	0.79	0.64	0.49	0.65	0.43	0.76								
	E3-SX	PGA	2.61	1.04	0.51	0.82	0.79	0.91	0.86	0.07	2.14	0.97	0.62	0.65	0.67	0.62	0.12	0.89
		$S_{a\text{-}0.3}$	1.78	1.02	0.48	0.89	0.87	0.11	0.41	0.69	1.34	0.95	0.65	0.62	0.65	0.92	0.52	0.56
		$S_{a\text{-}0.2}$	1.72	0.95	0.39	0.96	1.01	0.22	0.65	0.77	1.28	0.88	0.51	0.73	0.84	0.97	0.52	0.02
		$S_{a\text{-}1.0}$	2.62	1.09	0.77	0.57	0.52	0.67	0.82	0.81	2.04	0.95	0.79	0.47	0.49	0.02	0.83	0.69
MSCC-SL-P	EX-S0	PGA	0.19	0.95	0.75	0.46	0.49	0.78	0.00	0.00								
		$S_{a\text{-}0.3}$	-0.53	1.01	0.78	0.45	0.45	1.00	0.02	0.00								

		$S_{a\text{-}0.2}$	-0.60	0.89	0.65	0.53	0.59	0.82	0.01	0.00								
		$S_{a\text{-}1.0}$	-0.02	0.83	0.80	0.41	0.50	0.58	0.09	0.00								
	EX-SX	PGA	0.69	0.98	0.54	0.75	0.77	0.39	0.04	0.06	2.06	0.80	0.48	0.68	0.85	0.28	0.06	0.95
		$S_{a\text{-}0.3}$	-0.12	0.97	0.54	0.74	0.76	0.81	0.05	0.00	1.39	0.78	0.48	0.67	0.87	0.68	0.58	0.83
		$S_{a\text{-}0.2}$	-0.17	0.88	0.42	0.84	0.95	0.48	0.17	0.31	1.42	0.76	0.43	0.70	0.92	0.62	0.11	0.25
		$S_{a\text{-}1.0}$	0.60	0.97	0.68	0.63	0.65	0.56	0.03	0.00	1.89	0.78	0.58	0.63	0.81	0.40	0.92	0.87
MSCC-TG-P	E1-S0	PGA	0.51	1.11	0.78	0.54	0.49	0.76	0.02	0.19								
		$S_{a\text{-}0.3}$	-0.46	1.00	0.74	0.52	0.53	0.41	0.20	0.01								
		$S_{a\text{-}0.2}$	-0.43	1.05	0.72	0.59	0.56	0.62	0.07	0.03								
		$S_{a\text{-}1.0}$	0.12	0.91	0.79	0.51	0.55	0.04	0.16	0.00								
	E1-SX	PGA	1.41	1.09	0.66	0.61	0.56	1.00	0.71	0.91	2.78	1.23	0.78	0.52	0.42	0.41	0.27	0.84
		$S_{a\text{-}0.3}$	0.44	1.06	0.66	0.62	0.59	0.26	0.80	0.66	1.64	1.15	0.79	0.50	0.44	0.13	0.40	0.04
		$S_{a\text{-}0.2}$	0.44	0.96	0.56	0.66	0.68	0.05	0.69	0.19	1.61	1.06	0.68	0.61	0.58	0.83	0.34	0.87
		$S_{a\text{-}1.0}$	1.21	1.06	0.77	0.52	0.49	0.03	0.65	0.23	2.45	1.14	0.92	0.31	0.27	0.61	0.84	0.69
	E2-S0	PGA	0.17	0.89	0.65	0.54	0.61	0.28	0.90	0.36								
		$S_{a\text{-}0.3}$	-0.52	0.95	0.70	0.54	0.57	0.75	0.60	0.40								
		$S_{a\text{-}0.2}$	-0.55	0.88	0.63	0.55	0.63	0.40	0.62	0.70								
		$S_{a\text{-}1.0}$	0.14	0.99	0.79	0.47	0.48	0.84	0.36	0.00								
	E2-SX	PGA	1.17	1.09	0.61	0.75	0.69	0.66	0.53	0.74	2.59	1.19	0.70	0.68	0.57	0.92	0.73	0.25
		$S_{a\text{-}0.3}$	0.28	1.09	0.60	0.76	0.70	0.74	0.92	0.07	1.60	1.19	0.70	0.68	0.57	0.56	0.45	0.86
		$S_{a\text{-}0.2}$	0.24	0.98	0.52	0.80	0.81	0.75	0.60	0.15	1.56	1.08	0.58	0.79	0.73	0.29	0.63	0.29
		$S_{a\text{-}1.0}$	0.96	1.03	0.70	0.67	0.65	0.93	0.30	0.11	2.32	1.14	0.80	0.57	0.50	0.24	0.25	0.11
	E3-S0	PGA	0.33	0.99	0.71	0.56	0.56	0.94	0.01	0.02								
		$S_{a\text{-}0.3}$	-0.52	0.98	0.70	0.55	0.56	0.94	0.01	0.31								
		$S_{a\text{-}0.2}$	-0.48	0.97	0.70	0.53	0.55	0.93	0.00	0.00								
		$S_{a\text{-}1.0}$	0.15	0.97	0.76	0.49	0.51	0.92	0.03	0.00								
	E3-SX	PGA	0.84	0.88	0.64	0.52	0.59	0.91	0.10	0.00	2.64	1.14	0.79	0.46	0.41	0.34	0.50	0.32

		$S_{a\text{-}0.3}$	0.14	0.89	0.69	0.48	0.54	0.56	0.45	0.57	1.70	1.21	0.82	0.46	0.38	0.28	0.70	0.93
		$S_{a\text{-}0.2}$	0.10	0.80	0.55	0.57	0.71	0.56	0.35	0.15	1.71	1.16	0.73	0.56	0.48	0.57	0.99	0.43
		$S_{a\text{-}1.0}$	0.72	0.87	0.80	0.39	0.45	0.04	0.86	0.05	2.34	1.04	0.92	0.31	0.30	0.45	0.36	0.65
MSCC-TG-M	E1-S0	PGA	0.99	0.91	0.78	0.39	0.43	0.54	0.04	0.33								
		$S_{a\text{-}0.3}$	0.28	0.93	0.78	0.40	0.43	0.97	0.17	0.63								
		$S_{a\text{-}0.2}$	0.22	0.92	0.70	0.44	0.48	0.83	0.01	0.01								
		$S_{a\text{-}1.0}$	0.86	0.83	0.84	0.33	0.40	0.50	0.03	0.00								
	E1-SX	PGA	1.33	0.96	0.73	0.46	0.48	0.84	0.01	0.17	2.17	1.11	0.79	0.46	0.41	0.94	0.63	0.00
		$S_{a\text{-}0.3}$	0.50	0.95	0.66	0.53	0.56	0.90	0.20	0.96	1.22	1.06	0.69	0.57	0.54	0.42	0.31	0.23
		$S_{a\text{-}0.2}$	0.51	0.89	0.61	0.56	0.63	0.06	0.14	0.98	1.28	1.06	0.68	0.57	0.54	0.24	0.61	0.52
		$S_{a\text{-}1.0}$	1.10	0.85	0.78	0.43	0.50	0.99	0.63	0.64	1.93	1.01	0.82	0.42	0.42	0.84	0.14	0.16
	E2-S0	PGA	0.92	1.16	0.86	0.39	0.33	0.34	0.61	0.90								
		$S_{a\text{-}0.3}$	0.07	1.20	0.86	0.40	0.33	0.03	0.66	0.20								
		$S_{a\text{-}0.2}$	0.05	1.12	0.76	0.50	0.45	0.03	0.64	0.09								
		$S_{a\text{-}1.0}$	0.61	0.93	0.84	0.42	0.45	0.82	0.48	0.33								
	E2-SX	PGA	1.09	1.03	0.63	0.59	0.58	0.78	0.85	0.92	2.09	1.18	0.70	0.59	0.51	0.41	0.02	0.09
		$S_{a\text{-}0.3}$	0.19	1.01	0.62	0.62	0.61	0.85	0.36	0.54	1.08	1.14	0.70	0.59	0.52	0.92	0.94	0.49
		$S_{a\text{-}0.2}$	0.19	0.96	0.52	0.69	0.72	0.59	0.70	0.38	1.06	1.10	0.64	0.63	0.57	0.99	0.25	0.51
		$S_{a\text{-}1.0}$	1.00	1.01	0.77	0.49	0.49	0.88	0.17	0.02	2.02	1.14	0.83	0.45	0.39	0.13	0.81	0.14
	E3-S0	PGA	0.87	1.02	0.84	0.35	0.35	0.95	0.84	0.01								
		$S_{a\text{-}0.3}$	0.03	1.03	0.86	0.35	0.34	0.31	0.22	0.00								
		$S_{a\text{-}0.2}$	-0.05	0.94	0.74	0.44	0.47	0.54	0.47	0.09								
		$S_{a\text{-}1.0}$	0.64	0.96	0.88	0.33	0.34	0.95	0.19	0.00								
	E3-SX	PGA	1.20	1.02	0.76	0.48	0.47	0.23	0.59	0.82	2.21	1.15	0.80	0.50	0.44	0.77	0.97	0.79
		$S_{a\text{-}0.3}$	0.32	0.98	0.72	0.56	0.58	0.68	0.94	0.51	1.18	1.10	0.77	0.56	0.51	0.72	0.21	0.15
		$S_{a\text{-}0.2}$	0.29	0.88	0.63	0.59	0.67	0.01	0.21	0.03	1.17	1.03	0.70	0.61	0.60	0.08	0.42	0.52
		$S_{a\text{-}1.0}$	1.16	1.07	0.83	0.46	0.43	0.11	0.92	0.34	2.07	1.14	0.88	0.42	0.37	0.74	0.58	0.07

MSCC-IG-S	E1-S0	PGA	1.22	1.72	0.67	0.99	0.58	0.94	0.36	0.95								
		$S_{a\text{-}0.3}$	-0.07	1.70	0.64	1.02	0.60	0.19	0.64	0.40								
		$S_{a\text{-}0.2}$	-0.21	1.78	0.65	1.00	0.56	0.30	0.41	0.48								
		$S_{a\text{-}1.0}$	1.02	1.35	0.67	0.96	0.71	0.59	0.69	0.62								
	E1-SX	PGA	0.91	1.09	0.72	0.66	0.61	0.04	0.22	0.79	1.43	0.81	0.87	0.29	0.36	0.01	0.53	0.06
		$S_{a\text{-}0.3}$	-0.07	1.13	0.77	0.59	0.52	0.16	0.79	0.44	0.76	0.78	0.83	0.33	0.42	0.00	0.18	0.13
		$S_{a\text{-}0.2}$	0.02	1.11	0.74	0.63	0.57	0.08	0.63	0.40	0.75	0.72	0.77	0.37	0.52	0.19	0.13	0.10
		$S_{a\text{-}1.0}$	0.84	1.17	0.84	0.56	0.48	0.63	0.66	0.26	1.17	0.67	0.88	0.28	0.42	0.01	0.23	0.37
	E2-S0	PGA	2.02	1.77	0.65	1.22	0.69	0.18	0.77	0.10								
		$S_{a\text{-}0.3}$	0.66	1.85	0.66	1.20	0.65	0.00	0.74	0.16								
		$S_{a\text{-}0.2}$	0.57	1.83	0.69	1.15	0.63	0.03	0.86	0.80								
		$S_{a\text{-}1.0}$	1.79	1.40	0.54	1.22	0.87	0.32	0.73	0.03								
	E2-SX	PGA	1.16	1.26	0.63	0.78	0.62	0.18	0.51	0.17	1.56	0.86	0.76	0.40	0.47	0.64	0.83	0.47
		$S_{a\text{-}0.3}$	0.18	1.08	0.55	0.84	0.78	0.60	0.16	0.23	0.84	0.81	0.75	0.40	0.50	0.91	0.10	0.04
		$S_{a\text{-}0.2}$	0.36	1.11	0.61	0.73	0.66	0.53	0.25	0.82	0.83	0.85	0.74	0.42	0.50	0.97	0.82	0.23
		$S_{a\text{-}1.0}$	1.02	1.09	0.73	0.67	0.61	0.08	0.81	0.38	1.51	0.81	0.85	0.33	0.41	0.55	0.06	0.83
	E3-S0	PGA	1.27	1.12	0.39	1.13	1.01	0.30	0.94	0.51								
		$S_{a\text{-}0.3}$	0.39	1.20	0.47	1.03	0.86	0.35	0.77	0.04								
		$S_{a\text{-}0.2}$	0.46	0.96	0.33	1.02	1.07	0.16	0.00	0.47								
		$S_{a\text{-}1.0}$	1.18	1.07	0.50	1.08	1.02	0.22	0.76	0.95								
	E3-SX	PGA	0.51	0.81	0.57	0.59	0.72	0.53	0.58	0.08	1.56	0.84	0.83	0.32	0.38	0.13	0.83	0.27
		$S_{a\text{-}0.3}$	-0.12	0.74	0.53	0.56	0.75	0.68	0.96	0.06	0.89	0.81	0.81	0.33	0.41	0.49	0.59	0.25
		$S_{a\text{-}0.2}$	-0.10	0.75	0.51	0.57	0.76	0.77	0.64	0.62	0.89	0.84	0.80	0.34	0.41	0.02	0.91	0.36
		$S_{a\text{-}1.0}$	0.41	0.77	0.62	0.55	0.71	0.56	0.69	0.60	1.43	0.82	0.89	0.29	0.35	0.64	0.55	0.49
MSCC-IG-M	E1-S0	PGA	1.44	1.04	0.66	0.62	0.60	0.28	0.05	0.09								
		$S_{a\text{-}0.3}$	0.58	0.98	0.68	0.59	0.61	0.05	0.22	0.79								

	$S_{a\text{-}0.2}$	0.68	1.05	0.65	0.64	0.61	0.44	0.34	0.90								
	$S_{a\text{-}1.0}$	1.23	0.93	0.73	0.56	0.61	0.82	0.28	0.88								
E1-SX	PGA	1.74	0.92	0.65	0.55	0.59	0.54	0.11	0.12	2.37	1.10	0.73	0.56	0.50	0.27	0.32	0.37
	$S_{a\text{-}0.3}$	0.91	0.91	0.66	0.55	0.61	0.90	0.72	0.08	1.32	1.03	0.73	0.53	0.52	0.10	0.33	0.70
	$S_{a\text{-}0.2}$	0.91	0.78	0.49	0.64	0.81	0.55	0.44	0.71	1.34	0.98	0.63	0.62	0.63	0.18	0.41	0.59
	$S_{a\text{-}1.0}$	1.64	1.05	0.82	0.46	0.44	0.50	0.00	0.85	2.15	1.08	0.89	0.37	0.34	0.25	0.07	0.07
E2-S0	PGA	1.95	1.40	0.74	0.69	0.49	0.79	0.15	0.91								
	$S_{a\text{-}0.3}$	0.73	1.31	0.72	0.71	0.54	0.55	0.12	0.01								
	$S_{a\text{-}0.2}$	0.76	1.25	0.66	0.75	0.60	0.72	0.07	0.24								
	$S_{a\text{-}1.0}$	1.58	1.21	0.81	0.62	0.51	0.83	0.10	0.20								
E2-SX	PGA	1.64	0.99	0.75	0.47	0.47	0.59	0.53	0.41	2.57	1.23	0.85	0.42	0.34	0.47	0.67	0.96
	$S_{a\text{-}0.3}$	0.90	1.09	0.74	0.52	0.48	0.14	0.47	0.31	1.47	1.17	0.86	0.40	0.34	0.76	0.44	0.01
	$S_{a\text{-}0.2}$	0.85	0.94	0.65	0.58	0.61	0.92	0.33	0.81	1.49	1.13	0.77	0.52	0.46	0.02	0.94	0.21
	$S_{a\text{-}1.0}$	1.61	1.03	0.83	0.44	0.43	0.84	0.72	0.29	2.24	1.12	0.92	0.34	0.30	0.75	0.42	0.43
E3-S0	PGA	1.76	1.32	0.74	0.70	0.53	0.07	0.27	0.00								
	$S_{a\text{-}0.3}$	0.74	1.41	0.76	0.69	0.49	0.48	0.52	0.44								
	$S_{a\text{-}0.2}$	0.75	1.42	0.72	0.70	0.49	0.57	0.59	0.57								
	$S_{a\text{-}1.0}$	1.53	1.18	0.76	0.67	0.56	0.05	0.69	0.77								
E3-SX	PGA	1.62	1.07	0.76	0.49	0.46	0.95	0.73	0.54	2.50	1.19	0.83	0.44	0.37	0.73	0.44	0.01
	$S_{a\text{-}0.3}$	0.73	1.16	0.78	0.51	0.44	0.68	0.08	0.53	1.41	1.16	0.81	0.46	0.39	0.09	0.96	0.94
	$S_{a\text{-}0.2}$	0.71	1.04	0.68	0.58	0.55	0.49	0.77	0.22	1.38	1.09	0.74	0.52	0.48	0.73	0.50	0.30
	$S_{a\text{-}1.0}$	1.50	1.08	0.87	0.39	0.37	0.92	0.02	0.53	2.26	1.12	0.91	0.34	0.30	0.85	0.16	0.11

The shaded quantities represent the most efficient (lower $\beta_{D|IM}$), practical (higher b), proficient (lower ζ), and sufficient (higher p_M, p_R, p_ε)

APPENDIX D

COMPONENT FRAGILITY CURVES FOR BRIDGE CLASSES AND SEISMIC PERFORMANCE SUB-BINS

Chapter 6 presented the approach for developing fragility curves for the components that contribute to the vulnerability of bridge classes and their respective seismic performance sub-bins. The median and dispersion (logarithmic standard deviation) for the components across the four damage states is documented in the subsequent tables. The median value is in units of acceleration due to gravity, g. When the component median fragility value is greater than 5.0, the corresponding median and dispersion values are reported as 99.0 and 0.00, respectively, to indicate that the contribution of the component to the system vulnerability is negligible.

Table D.1: Component level fragility relationships for multispan continuous concrete box-girder bridge class and the respective seismic performance sub-bins

Bridge class (CBC + SPS)	CDT-0		CDT-1		CDT-2		CDT-3	
	λ	ζ	λ	ζ	λ	ζ	λ	ζ
Pre 1971 design era								
MSCC-BG-S-E1-S0								
Column	0.15	0.59	0.17	0.59	0.18	0.59	0.22	0.59
Deck-max	0.64	0.54	1.95	0.54				
Fnd-tran	0.74	0.88	5.66	0.88				
Fnd-rot	99.0	0.00	99.0	0.00				
Abt-Pass	0.81	0.65	3.01	0.65				
Abt-Act	0.38	0.66	1.11	0.66				
Abt-tran	0.17	0.54	0.67	0.54				
MSCC-BG-M-E1-S0								
Column	0.09	0.51	0.10	0.51	0.11	0.51	0.12	0.51
Deck-max	0.35	0.52	0.88	0.52				
Fnd-tran	99.0	0.00	99.0	0.00				
Fnd-rot	99.0	0.00	99.0	0.00				
Abt-Pass	0.44	0.54	1.24	0.54				
Abt-Act	0.24	0.54	0.56	0.54				
Abt-tran	0.12	0.51	0.37	0.51				
MSCC-BG-S-E1-S1								
Column	0.12	0.53	0.13	0.53	0.14	0.53	0.17	0.53
Abt-seat	0.01	1.49	0.02	1.49	0.06	1.49	0.11	1.49
Deck-max	0.51	0.60	1.82	0.60				
Fnd-tran	0.60	1.24	99.0	0.00				
Fnd-rot	99.0	0.00	99.0	0.00				
Abt-Pass	0.90	0.63	2.28	0.63				
Abt-Act	0.31	0.56	0.69	0.56				
Abt-tran	0.05	1.38	0.21	1.38				
Bearing	0.02	1.49	0.17	1.49				
Joint Seal	0.01	1.49	99.0	0.00				
Restrainer	0.27	0.66	1.01	0.66				
Shear key	99.0	0.00	99.0	0.00				
MSCC-BG-S-E1-S2								
MSCC-BG-S-E1-S3								
MSCC-BG-S-E1-S4								
Column	0.12	0.53	0.13	0.53	0.14	0.53	0.17	0.53
Abt-seat	0.02	1.49	0.11	1.49	0.31	1.49	0.58	1.49
Deck-max	0.51	0.60	1.82	0.60				
Fnd-tran	0.60	1.24	99.0	0.00				
Fnd-rot	99.0	0.00	99.0	0.00				
Abt-Pass	0.90	0.63	2.28	0.63				
Abt-Act	0.31	0.56	0.69	0.56				
Abt-tran	0.05	1.38	0.21	1.38				
Bearing	0.02	1.49	0.17	1.49				
Joint Seal	0.01	1.49	99.0	0.00				

Restrainer	0.27	0.66	99.0	0.00				
Shear key	99.0	0.00	99.0	0.00				
MSCC-BG-M-E1-S1								
Column	0.07	0.59	0.07	0.59	0.08	0.59	0.09	0.59
Abt-seat	0.01	1.11	0.01	1.11	0.04	1.11	0.07	1.11
Deck-max	0.26	0.56	0.61	0.56				
Fnd-tran	99.0	0.00	99.0	0.00				
Fnd-rot	99.0	0.00	99.0	0.00				
Abt-Pass	0.64	0.53	1.62	0.53				
Abt-Act	0.21	0.43	0.43	0.43				
Abt-tran	0.04	0.96	0.15	0.96				
Bearing	0.01	1.11	0.11	1.11				
Joint Seal	0.01	1.11	99.0	0.00				
Restrainer	0.17	0.58	0.47	0.58				
Shear key	99.0	0.00	99.0	0.00				
MSCC-BG-M-E1-S2								
MSCC-BG-M-E1-S3								
MSCC-BG-M-E1-S4								
Column	0.07	0.59	0.07	0.59	0.08	0.59	0.09	0.59
Abt-seat	0.01	1.11	0.07	1.11	0.40	1.11	0.71	1.11
Deck-max	0.26	0.56	0.61	0.56				
Fnd-tran	99.0	0.00	99.0	0.00				
Fnd-rot	99.0	0.00	99.0	0.00				
Abt-Pass	0.64	0.53	1.62	0.53				
Abt-Act	0.21	0.43	0.43	0.43				
Abt-tran	0.04	0.96	0.15	0.96				
Bearing	0.01	1.11	0.11	1.11				
Joint Seal	0.01	1.11	99.0	0.00				
Restrainer	0.17	0.58	0.47	0.58				
Shear key	99.0	0.00	99.0	0.00				
<u>1971-1990 design era</u>								
MSCC-BG-S-E2-S0								
Column	0.21	0.70	0.41	0.70	0.70	0.70	1.00	0.70
Deck-max	0.63	0.54	1.91	0.54				
Fnd-tran	0.70	0.84	5.01	0.84				
Fnd-rot	99.0	0.00	99.0	0.00				
Abt-Pass	0.72	0.57	2.29	0.57				
Abt-Act	0.36	0.57	0.94	0.57				
Abt-tran	0.17	0.54	0.68	0.54				
MSCC-BG-M-E2-S0								
Column	0.14	0.57	0.25	0.57	0.38	0.57	0.49	0.57
Deck-max	0.41	0.56	1.08	0.56				
Fnd-tran	1.82	1.19	99.0	0.00				
Fnd-rot	99.0	0.00	99.0	0.00				
Abt-Pass	0.48	0.51	1.38	0.51				
Abt-Act	0.26	0.51	0.61	0.51				

Abt-tran	0.13	0.60	0.45	0.60				
MSCC-BG-S-E2-S2								
MSCC-BG-S-E2-S3								
MSCC-BG-S-E2-S4								
Column	0.18	0.51	0.31	0.51	0.47	0.51	0.62	0.51
Abt-seat	0.14	0.60	0.52	0.60	2.12	0.60	3.40	0.60
Deck-max	0.48	0.50	1.45	0.50				
Fnd-tran	0.44	0.80	2.95	0.80				
Fnd-rot	99.0	0.00	99.0	0.00				
Abt-Pass	0.81	0.45	1.65	0.45				
Abt-Act	0.40	0.43	0.78	0.43				
Abt-tran	0.35	0.62	0.88	0.62				
Bearing	0.14	0.60	0.73	0.60				
Joint Seal	0.10	0.60	99.0	0.00				
Restrainer	0.28	0.65	0.98	0.65				
Shear key	99.0	0.00	99.0	0.00				
MSCC-BG-M-E2-S2								
MSCC-BG-M-E2-S3								
MSCC-BG-M-E2-S4								
Column	0.11	0.64	0.18	0.64	0.28	0.64	0.36	0.64
Abt-seat	0.12	0.55	0.38	0.55	2.05	0.55	3.19	0.55
Deck-max	0.30	0.60	0.75	0.60				
Fnd-tran	1.82	1.35	99.0	0.00				
Fnd-rot	99.0	0.00	99.0	0.00				
Abt-Pass	0.66	0.61	1.40	0.61				
Abt-Act	0.26	0.44	0.51	0.44				
Abt-tran	0.21	0.61	0.47	0.61				
Bearing	0.12	0.55	0.53	0.55				
Joint Seal	0.09	0.55	99.0	0.00				
Restrainer	0.20	0.55	0.55	0.55				
Shear key	99.0	0.00	99.0	0.00				
<u>Post 1990 design era</u>								
MSCC-BG-S-E3-S0								
Column	0.22	0.40	0.58	0.40	0.95	0.40	1.26	0.40
Deck-max	0.67	0.45	1.95	0.45				
Fnd-tran	0.55	0.65	3.16	0.65				
Fnd-rot	99.0	0.00	99.0	0.00				
Abt-Pass	0.80	0.52	2.64	0.52				
Abt-Act	0.39	0.53	1.06	0.53				
Abt-tran	0.18	0.48	0.70	0.48				
MSCC-BG-M-E3-S0								
Column	0.12	0.56	0.36	0.56	0.61	0.56	0.84	0.56
Deck-max	0.37	0.56	0.95	0.56				
Fnd-tran	1.89	1.21	99.0	0.00				
Fnd-rot	99.0	0.00	99.0	0.00				
Abt-Pass	0.46	0.45	1.26	0.45				

Abt-Act	0.25	0.45	0.58	0.45				
Abt-tran	0.12	0.59	0.40	0.59				
MSCC-BG-S-E3-S3								
MSCC-BG-S-E3-S4								
Column	0.23	0.48	0.78	0.48	1.44	0.48	2.06	0.48
Abt-seat	0.14	0.60	0.58	0.60	4.21	0.60	7.07	0.60
Deck-max	0.60	0.54	2.26	0.54				
Fnd-tran	0.36	1.15	99.0	0.00				
Fnd-rot	99.0	0.00	99.0	0.00				
Abt-Pass	1.06	0.73	3.35	0.73				
Abt-Act	0.43	0.65	1.21	0.65				
Abt-tran	0.28	0.73	1.07	0.73				
Bearing	0.14	0.60	0.85	0.60				
Joint Seal	0.10	0.60	99.0	0.00				
Restrainer	0.33	0.65	1.41	0.65				
Shear key	99.0	0.00	99.0	0.00				
MSCC-BG-M-E3-S3								
MSCC-BG-M-E3-S4								
Column	0.09	0.61	0.32	0.61	0.61	0.61	0.88	0.61
Abt-seat	0.11	0.61	0.36	0.61	1.95	0.61	3.04	0.61
Deck-max	0.34	0.57	1.07	0.57				
Fnd-tran	1.68	1.18	99.0	0.00				
Fnd-rot	99.0	0.00	99.0	0.00				
Abt-Pass	0.70	0.70	1.71	0.70				
Abt-Act	0.25	0.51	0.50	0.51				
Abt-tran	0.19	0.63	0.51	0.63				
Bearing	0.11	0.61	0.49	0.61				
Joint Seal	0.08	0.61	99.0	0.00				
Restrainer	0.18	0.60	0.50	0.60				
Shear key	99.0	0.00	99.0	0.00				

Table D.2: Component level fragility relationships for multispan continuous concrete slab bridge class and the respective seismic performance sub-bins

Bridge class (CBC + SPS)	CDT-0		CDT-1		CDT-2		CDT-3	
	λ	ζ	λ	ζ	λ	ζ	λ	ζ
MSCC-SL-P-EX-S0								
Column	0.79	0.65	0.91	0.65	1.03	0.65	1.28	0.65
Deck-max	0.88	0.76	3.65	0.76				
Fnd-tran	1.52	1.29	99.0	0.00				
Fnd-rot	99.0	0.00	99.0	0.00				
Abt-Pass	0.92	0.78	4.60	0.78				
Abt-Act	0.77	0.64	2.23	0.64				
Abt-tran	0.18	0.73	1.06	0.73				
MSCC-SL-P-EX-S1								
Column	0.43	0.74	0.49	0.74	0.54	0.74	0.65	0.74
Abt-seat	0.09	0.46	0.17	0.46	0.30	0.46	0.42	0.46
Deck-max	0.43	0.55	1.28	0.55				
Fnd-tran	0.51	0.99	2.24	0.99				
Fnd-rot	99.0	0.00	99.0	0.00				
Abt-Pass	1.77	0.81	99.0	0.00				
Abt-Act	1.68	0.84	99.0	0.00				
Abt-tran	99.0	0.00	99.0	0.00				
Bearing	0.17	0.46	0.53	0.46				
Joint Seal	0.13	0.46	99.0	0.00				
MSCC-SL-P-EX-S2								
MSCC-SL-P-EX-S3								
MSCC-SL-P-EX-S4								
Column	0.43	0.74	0.49	0.74	0.54	0.74	0.65	0.74
Abt-seat	0.17	0.46	0.42	0.46	1.49	0.46	2.09	0.46
Deck-max	0.43	0.55	1.28	0.55				
Fnd-tran	0.51	0.99	2.24	0.99				
Fnd-rot	99.0	0.00	99.0	0.00				
Abt-Pass	1.77	0.81	99.0	0.00				
Abt-Act	1.68	0.84	99.0	0.00				
Abt-tran	99.0	0.00	99.0	0.00				
Bearing	0.17	0.46	0.53	0.46				
Joint Seal	0.13	0.46	99.0	0.00				

Table D.3: Component level fragility relationships for multispan continuous concrete Tee-girder bridge class and the respective seismic performance sub-bins

Bridge class (CBC + SPS)	CDT-0		CDT-1		CDT-2		CDT-3	
	λ	ζ	λ	ζ	λ	ζ	λ	ζ
Pre 1971 design era								
MSCC-TG-P-E1-S0								
MSCC-TG-P-E2-S0								
MSCC-TG-P-E3-S0								
Column	0.69	0.67	0.78	0.67	0.88	0.67	1.07	0.67
Deck-max	0.52	0.51	1.82	0.51				
Fnd-tran	2.41	1.14	99.0	0.00				
Fnd-rot	99.0	0.00	99.0	0.00				
Abt-Pass	3.42	0.98	99.0	0.00				
Abt-Act	99.0	0.00	99.0	0.00				
Abt-tran	2.34	0.97	99.0	0.00				
MSCC-TG-M-E1-S0								
Column	0.27	0.58	0.32	0.58	0.36	0.58	0.45	0.58
Deck-max	0.75	0.59	2.74	0.59				
Fnd-tran	99.0	0.00	99.0	0.00				
Fnd-rot	99.0	0.00	99.0	0.00				
Abt-Pass	99.0	0.00	99.0	0.00				
Abt-Act	3.82	1.01	99.0	0.00				
Abt-tran	2.84	0.81	99.0	0.00				
MSCC-TG-P-E1-S1								
Column	0.26	0.59	0.29	0.59	0.32	0.59	0.38	0.59
Abt-seat	0.06	0.41	0.12	0.41	0.21	0.41	0.31	0.41
Deck-max	0.34	0.48	1.06	0.48				
Fnd-tran	0.93	0.82	4.98	0.82				
Fnd-rot	99.0	0.00	99.0	0.00				
Abt-Pass	99.0	0.00	99.0	0.00				
Abt-Act	2.90	0.65	99.0	0.00				
Abt-tran	99.0	0.00	99.0	0.00				
Bearing	0.12	0.41	0.39	0.41				
Joint Seal	0.09	0.41	99.0	0.00				
MSCC-TG-P-E1-S2								
MSCC-TG-P-E1-S3								
MSCC-TG-P-E1-S4								
Column	0.26	0.59	0.29	0.59	0.32	0.59	0.38	0.59
Abt-seat	0.12	0.41	0.31	0.41	0.88	0.41	1.25	0.41
Deck-max	0.34	0.48	1.06	0.48				
Fnd-tran	0.93	0.82	4.98	0.82				
Fnd-rot	99.0	0.00	99.0	0.00				
Abt-Pass	99.0	0.00	99.0	0.00				
Abt-Act	2.90	0.65	99.0	0.00				
Abt-tran	99.0	0.00	99.0	0.00				
Bearing	0.12	0.41	0.39	0.41				
Joint Seal	0.09	0.41	99.0	0.00				

MSCC-TG-M-E1-S1								
Column	0.21	0.65	0.24	0.65	0.28	0.65	0.34	0.65
Abt-seat	0.08	0.54	0.15	0.54	0.30	0.54	0.44	0.54
Deck-max	0.55	0.58	1.84	0.58				
Fnd-tran	99.0	0.00	99.0	0.00				
Fnd-rot	99.0	0.00	99.0	0.00				
Abt-Pass	0.97	0.67	99.0	0.00				
Abt-Act	1.15	0.53	99.0	0.00				
Abt-tran	99.0	0.00	99.0	0.00				
Bearing	0.15	0.54	0.58	0.54				
Joint Seal	0.11	0.54	99.0	0.00				
MSCC-TG-M-E1-S2								
MSCC-TG-M-E1-S3								
MSCC-TG-M-E1-S4								
Column	0.21	0.65	0.24	0.65	0.28	0.65	0.34	0.65
Abt-seat	0.15	0.54	0.44	0.54	2.01	0.54	2.99	0.54
Deck-max	0.55	0.58	1.84	0.58				
Fnd-tran	99.0	0.00	99.0	0.00				
Fnd-rot	99.0	0.00	99.0	0.00				
Abt-Pass	0.97	0.67	99.0	0.00				
Abt-Act	1.15	0.53	99.0	0.00				
Abt-tran	99.0	0.00	99.0	0.00				
Bearing	0.15	0.54	0.58	0.54				
Joint Seal	0.11	0.54	99.0	0.00				
1971-1990 design era								
MSCC-TG-M-E2-S0								
Column	0.52	0.59	1.09	0.59	2.00	0.59	2.93	0.59
Deck-max	0.72	0.51	2.17	0.51				
Fnd-tran	99.0	0.00	99.0	0.00				
Fnd-rot	99.0	0.00	99.0	0.00				
Abt-Pass	99.0	0.00	99.0	0.00				
Abt-Act	3.47	0.93	99.0	0.00				
Abt-tran	1.59	0.61	99.0	0.00				
MSCC-TG-P-E2-S2								
MSCC-TG-P-E2-S3								
MSCC-TG-P-E2-S4								
Column	0.31	0.74	0.35	0.74	0.39	0.74	0.47	0.74
Abt-seat	0.13	0.59	0.34	0.59	0.99	0.59	1.41	0.59
Deck-max	0.37	0.57	1.11	0.57				
Fnd-tran	1.28	1.24	99.0	0.00				
Fnd-rot	99.0	0.00	99.0	0.00				
Abt-Pass	2.78	0.86	99.0	0.00				
Abt-Act	2.42	0.57	6.46	0.57				
Abt-tran	99.0	0.00	99.0	0.00				
Bearing	0.13	0.59	0.44	0.59				
Joint Seal	0.10	0.59	99.0	0.00				

MSCC-TG-M-E2-S2								
Column	0.37	0.60	0.74	0.60	1.28	0.60	1.83	0.60
Abt-seat	0.17	0.50	0.45	0.50	0.82	0.50	1.17	0.50
Deck-max	0.57	0.59	1.75	0.59				
Fnd-tran	99.0	0.00	99.0	0.00				
Fnd-rot	99.0	0.00	99.0	0.00				
Abt-Pass	0.94	0.62	4.33	0.62				
Abt-Act	0.90	0.44	1.73	0.44				
Abt-tran	99.0	0.00	99.0	0.00				
Bearing	0.17	0.50	0.58	0.50				
Joint Seal	0.13	0.50	99.0	0.00				
MSCC-TG-M-E2-S3								
Column	0.37	0.60	0.74	0.60	1.28	0.60	1.83	0.60
Abt-seat	0.17	0.50	0.45	0.50	1.28	0.50	1.83	0.50
Deck-max	0.57	0.59	1.75	0.59				
Fnd-tran	99.0	0.00	99.0	0.00				
Fnd-rot	99.0	0.00	99.0	0.00				
Abt-Pass	0.94	0.62	4.33	0.62				
Abt-Act	0.90	0.44	1.73	0.44				
Abt-tran	99.0	0.00	99.0	0.00				
Bearing	0.17	0.50	0.58	0.50				
Joint Seal	0.13	0.50	99.0	0.00				
MSCC-TG-M-E2-S4								
Column	0.37	0.60	0.74	0.60	1.28	0.60	1.83	0.60
Abt-seat	0.17	0.50	0.45	0.50	1.72	0.50	2.45	0.50
Deck-max	0.57	0.59	1.75	0.59				
Fnd-tran	99.0	0.00	99.0	0.00				
Fnd-rot	99.0	0.00	99.0	0.00				
Abt-Pass	0.94	0.62	4.33	0.62				
Abt-Act	0.90	0.44	1.73	0.44				
Abt-tran	99.0	0.00	99.0	0.00				
Bearing	0.17	0.50	0.58	0.50				
Joint Seal	0.13	0.50	99.0	0.00				
Post 1990 design era								
MSCC-TG-M-E3-S0								
Column	0.51	0.50	2.18	0.50	4.48	0.50	6.84	0.50
Deck-max	0.78	0.57	2.84	0.57				
Fnd-tran	99.0	0.00	99.0	0.00				
Fnd-rot	99.0	0.00	99.0	0.00				
Abt-Pass	99.0	0.00	99.0	0.00				
Abt-Act	4.02	0.90	99.0	0.00				
Abt-tran	1.94	0.68	99.0	0.00				
MSCC-TG-P-E3-S3								
MSCC-TG-P-E3-S4								
Column	0.34	0.60	0.39	0.60	0.44	0.60	0.54	0.60

Abt-seat	0.11	0.45	0.30	0.45	1.34	0.45	1.97	0.45
Deck-max	0.33	0.48	1.14	0.48				
Fnd-tran	1.77	0.92	99.0	0.00				
Fnd-rot	99.0	0.00	99.0	0.00				
Abt-Pass	3.52	0.92	99.0	0.00				
Abt-Act	2.88	0.66	99.0	0.00				
Abt-tran	99.0	0.00	99.0	0.00				
Bearing	0.11	0.45	0.40	0.45				
Joint Seal	0.08	0.45	99.0	0.00				
MSCC-TG-M-E3-S3								
Column	0.34	0.54	1.24	0.54	2.36	0.54	3.44	0.54
Abt-seat	0.16	0.48	0.42	0.48	1.22	0.48	1.75	0.48
Deck-max	0.53	0.49	1.46	0.49				
Fnd-tran	99.0	0.00	99.0	0.00				
Fnd-rot	99.0	0.00	99.0	0.00				
Abt-Pass	0.96	0.59	3.98	0.59				
Abt-Act	1.24	0.52	2.57	0.52				
Abt-tran	99.0	0.00	99.0	0.00				
Bearing	0.16	0.48	0.55	0.48				
Joint Seal	0.13	0.48	99.0	0.00				
MSCC-TG-M-E3-S4								
Column	0.34	0.54	1.24	0.54	2.36	0.54	3.44	0.54
Abt-seat	0.16	0.48	0.42	0.48	1.64	0.48	2.35	0.48
Deck-max	0.53	0.49	1.46	0.49				
Fnd-tran	99.0	0.00	99.0	0.00				
Fnd-rot	99.0	0.00	99.0	0.00				
Abt-Pass	0.96	0.59	3.98	0.59				
Abt-Act	1.24	0.52	2.57	0.52				
Abt-tran	99.0	0.00	99.0	0.00				
Bearing	0.16	0.48	0.55	0.48				
Joint Seal	0.13	0.48	99.0	0.00				

Table D.4: Component level fragility relationships for multispan continuous concrete I-girder bridge class and the respective seismic performance sub-bins

Bridge class (CBC + SPS)	CDT-0		CDT-1		CDT-2		CDT-3	
	λ	ζ	λ	ζ	λ	ζ	λ	ζ
Pre 1971 design era								
MSCC-IG-S-E1-S0								
Column	0.40	0.76	0.44	0.76	0.47	0.76	0.54	0.76
Deck-max	0.37	0.56	0.98	0.56				
Fnd-tran	0.94	0.77	2.99	0.77				
Fnd-rot	99.0	0.00	99.0	0.00				
Abt-Pass	99.0	0.00	99.0	0.00				
Abt-Act	99.0	0.00	99.0	0.00				
Abt-tran	0.75	0.95	6.13	0.95				
Bearing	0.12	0.55	0.37	0.55				
Restrainer	1.35	1.06	99.0	0.00				
Shear key	3.89	1.22	99.0	0.00				
MSCC-IG-M-E1-S0								
Column	0.21	0.71	0.24	0.71	0.27	0.71	0.32	0.71
Deck-max	0.40	0.57	1.38	0.57				
Fnd-tran	99.0	0.00	99.0	0.00				
Fnd-rot	99.0	0.00	99.0	0.00				
Abt-Pass	3.54	0.62	99.0	0.00				
Abt-Act	1.62	0.68	99.0	0.00				
Abt-tran	0.87	0.77	99.0	0.00				
Bearing	0.09	0.59	0.39	0.59				
Restrainer	3.05	1.49	99.0	0.00				
Shear key	99.0	0.00	99.0	0.00				
MSCC-IG-S-E1-S1								
Column	0.40	0.57	0.45	0.57	0.49	0.57	0.57	0.57
Abt-seat	0.05	0.50	0.09	0.50	0.16	0.50	0.24	0.50
Deck-max	0.29	0.48	0.79	0.48				
Fnd-tran	1.21	0.70	99.0	0.00				
Fnd-rot	99.0	0.00	99.0	0.00				
Abt-Pass	2.66	0.55	99.0	0.00				
Abt-Act	1.52	0.52	3.84	0.52				
Abt-tran	0.43	0.58	1.02	0.58				
Bearing	0.09	0.50	0.31	0.50				
Joint Seal	0.07	0.50	4.62	0.50				
Restrainer	0.50	0.80	2.83	0.80				
Shear key	3.22	1.13	99.0	0.00				
MSCC-IG-S-E1-S2								
MSCC-IG-S-E1-S3								
MSCC-IG-S-E1-S4								
Column	0.40	0.57	0.45	0.57	0.49	0.57	0.57	0.57
Abt-seat	0.09	0.50	0.24	0.50	0.98	0.50	1.43	0.50
Deck-max	0.29	0.48	0.79	0.48				
Fnd-tran	1.21	0.70	99.0	0.00				

Fnd-rot	99.0	0.00	99.0	0.00				
Abt-Pass	2.66	0.55	99.0	0.00				
Abt-Act	1.52	0.52	3.84	0.52				
Abt-tran	0.43	0.58	1.02	0.58				
Bearing	0.09	0.50	0.31	0.50				
Joint Seal	0.07	0.50	4.62	0.50				
Restrainer	0.50	0.80	2.83	0.80				
Shear key	3.22	1.13	99.0	0.00				
MSCC-IG-M-E1-S1								
Column	0.17	0.55	0.19	0.55	0.21	0.55	0.25	0.55
Abt-seat	0.04	0.51	0.08	0.51	0.16	0.51	0.24	0.51
Deck-max	0.27	0.52	0.89	0.52				
Fnd-tran	99.0	0.00	99.0	0.00				
Fnd-rot	99.0	0.00	99.0	0.00				
Abt-Pass	2.61	0.60	99.0	0.00				
Abt-Act	1.76	0.61	99.0	0.00				
Abt-tran	0.31	0.73	1.36	0.73				
Bearing	0.08	0.51	0.33	0.51				
Joint Seal	0.06	0.51	6.36	0.51				
Restrainer	1.45	0.92	99.0	0.00				
Shear key	99.0	0.00	99.0	0.00				
MSCC-IG-M-E1-S2								
MSCC-IG-M-E1-S3								
MSCC-IG-M-E1-S4								
Column	0.17	0.55	0.19	0.55	0.21	0.55	0.25	0.55
Abt-seat	0.08	0.51	0.24	0.51	0.83	0.51	1.25	0.51
Deck-max	0.27	0.52	0.89	0.52				
Fnd-tran	99.0	0.00	99.0	0.00				
Fnd-rot	99.0	0.00	99.0	0.00				
Abt-Pass	2.61	0.60	99.0	0.00				
Abt-Act	1.76	0.61	99.0	0.00				
Abt-tran	0.31	0.73	1.36	0.73				
Bearing	0.08	0.51	0.33	0.51				
Joint Seal	0.06	0.51	99.0	0.00				
Restrainer	1.45	0.92	99.0	0.00				
Shear key	99.0	0.00	99.0	0.00				
<u>1971-1990 design era</u>								
MSCC-IG-S-E2-S0								
Column	0.28	0.91	0.46	0.91	0.68	0.91	0.88	0.91
Deck-max	0.25	0.55	0.61	0.55				
Fnd-tran	0.46	0.67	1.15	0.67				
Fnd-rot	99.0	0.00	99.0	0.00				
Abt-Pass	4.24	0.64	99.0	0.00				
Abt-Act	3.41	0.78	99.0	0.00				
Abt-tran	0.36	0.55	1.16	0.55				
Bearing	0.10	0.60	0.25	0.60				
Restrainer	0.95	0.79	99.0	0.00				

Shear key	99.0	0.00	99.0	0.00				
MSCC-IG-M-E2-S0								
Column	0.27	0.59	0.48	0.59	0.76	0.59	1.03	0.59
Deck-max	0.41	0.50	1.30	0.50				
Fnd-tran	99.0	0.00	99.0	0.00				
Fnd-rot	99.0	0.00	99.0	0.00				
Abt-Pass	4.54	0.71	99.0	0.00				
Abt-Act	2.04	0.80	99.0	0.00				
Abt-tran	0.72	0.75	4.44	0.75				
Bearing	0.11	0.53	0.40	0.53				
Restrainer	2.88	1.34	99.0	0.00				
Shear key	99.0	0.00	99.0	0.00				
MSCC-IG-S-E2-S2								
Column	0.39	0.69	0.74	0.69	1.24	0.69	1.72	0.69
Abt-seat	0.06	0.56	0.17	0.56	0.32	0.56	0.46	0.56
Deck-max	0.20	0.56	0.58	0.56				
Fnd-tran	0.89	1.11	99.0	0.00				
Fnd-rot	99.0	0.00	99.0	0.00				
Abt-Pass	1.74	0.59	4.91	0.59				
Abt-Act	1.35	0.66	3.46	0.66				
Abt-tran	0.31	0.54	0.70	0.54				
Bearing	0.06	0.56	0.22	0.56				
Joint Seal	0.05	0.56	3.34	0.56				
Restrainer	0.38	0.70	1.49	0.70				
Shear key	2.39	0.90	99.0	0.00				
MSCC-IG-S-E2-S3								
Column	0.39	0.69	0.74	0.69	1.24	0.69	1.72	0.69
Abt-seat	0.06	0.56	0.17	0.56	0.51	0.56	0.74	0.56
Deck-max	0.20	0.56	0.58	0.56				
Fnd-tran	0.89	1.11	99.0	0.00				
Fnd-rot	99.0	0.00	99.0	0.00				
Abt-Pass	1.74	0.59	4.91	0.59				
Abt-Act	1.35	0.66	3.46	0.66				
Abt-tran	0.31	0.54	0.70	0.54				
Bearing	0.06	0.56	0.22	0.56				
Joint Seal	0.05	0.56	3.34	0.56				
Restrainer	0.38	0.70	1.49	0.70				
Shear key	2.39	0.90	99.0	0.00				
MSCC-IG-S-E2-S4								
Column	0.39	0.69	0.74	0.69	1.24	0.69	1.72	0.69
Abt-seat	0.06	0.56	0.17	0.56	0.70	0.56	1.02	0.56
Deck-max	0.20	0.56	0.58	0.56				
Fnd-tran	0.89	1.11	99.0	0.00				
Fnd-rot	99.0	0.00	99.0	0.00				
Abt-Pass	1.74	0.59	4.91	0.59				
Abt-Act	1.35	0.66	3.46	0.66				

Abt-tran	0.31	0.54	0.70	0.54				
Bearing	0.06	0.56	0.22	0.56				
Joint Seal	0.05	0.56	3.34	0.56				
Restrainer	0.38	0.70	1.49	0.70				
Shear key	2.39	0.90	99.0	0.00				
MSCC-IG-M-E2-S2								
Column	0.21	0.55	0.41	0.55	0.71	0.55	1.00	0.55
Abt-seat	0.09	0.47	0.24	0.47	0.45	0.47	0.65	0.47
Deck-max	0.26	0.49	0.80	0.49				
Fnd-tran	99.0	0.00	99.0	0.00				
Fnd-rot	99.0	0.00	99.0	0.00				
Abt-Pass	2.72	0.54	99.0	0.00				
Abt-Act	1.89	0.59	99.0	0.00				
Abt-tran	0.27	0.61	0.82	0.61				
Bearing	0.09	0.47	0.31	0.47				
Joint Seal	0.07	0.47	4.57	0.47				
Restrainer	1.33	0.79	99.0	0.00				
Shear key	99.0	0.00	99.0	0.00				
MSCC-IG-M-E2-S3								
Column	0.21	0.55	0.41	0.55	0.71	0.55	1.00	0.55
Abt-seat	0.09	0.47	0.24	0.47	0.71	0.47	1.04	0.47
Deck-max	0.26	0.49	0.80	0.49				
Fnd-tran	99.0	0.00	99.0	0.00				
Fnd-rot	99.0	0.00	99.0	0.00				
Abt-Pass	2.72	0.54	99.0	0.00				
Abt-Act	1.89	0.59	99.0	0.00				
Abt-tran	0.27	0.61	0.82	0.61				
Bearing	0.09	0.47	0.31	0.47				
Joint Seal	0.07	0.47	4.57	0.47				
Restrainer	1.33	0.79	99.0	0.00				
Shear key	99.0	0.00	99.0	0.00				
MSCC-IG-M-E2-S4								
Column	0.21	0.55	0.41	0.55	0.71	0.55	1.00	0.55
Abt-seat	0.09	0.47	0.24	0.47	0.97	0.47	1.41	0.47
Deck-max	0.26	0.49	0.80	0.49				
Fnd-tran	99.0	0.00	99.0	0.00				
Fnd-rot	99.0	0.00	99.0	0.00				
Abt-Pass	2.72	0.54	99.0	0.00				
Abt-Act	1.89	0.59	99.0	0.00				
Abt-tran	0.27	0.61	0.82	0.61				
Bearing	0.09	0.47	0.31	0.47				
Joint Seal	0.07	0.47	4.57	0.47				
Restrainer	1.33	0.79	99.0	0.00				
Shear key	99.0	0.00	99.0	0.00				
<u>Post 1990 design era</u>								
MSCC-IG-S-E3-S0								

Column	0.33	1.07	1.21	1.07	2.32	1.07	3.39	1.07
Deck-max	0.24	0.62	0.71	0.62				
Fnd-tran	0.48	1.10	2.29	1.10				
Fnd-rot	99.0	0.00	99.0	0.00				
Abt-Pass	99.0	0.00	99.0	0.00				
Abt-Act	3.56	1.09	99.0	0.00				
Abt-tran	0.31	0.84	1.45	0.84				
Bearing	0.05	0.83	0.19	0.83				
Restrainer	1.06	1.03	99.0	0.00				
Shear key	99.0	0.00	99.0	0.00				
MSCC-IG-M-E3-S0								
Column	0.27	0.64	0.89	0.64	1.59	0.64	2.25	0.64
Deck-max	0.40	0.53	1.22	0.53				
Fnd-tran	4.00	1.23	99.0	0.00				
Fnd-rot	99.0	0.00	99.0	0.00				
Abt-Pass	99.0	0.00	99.0	0.00				
Abt-Act	1.73	0.73	99.0	0.00				
Abt-tran	0.78	0.83	99.0	0.00				
Bearing	0.10	0.57	0.37	0.57				
Restrainer	1.84	1.20	99.0	0.00				
Shear key	99.0	0.00	99.0	0.00				
MSCC-IG-S-E3-S3								
Column	0.59	0.84	3.55	0.84	99.0	0.00	99.0	0.00
Abt-seat	0.03	0.74	0.12	0.74	0.56	0.74	0.93	0.74
Deck-max	0.20	0.62	0.64	0.62				
Fnd-tran	1.31	2.43	99.0	0.00				
Fnd-rot	99.0	0.00	99.0	0.00				
Abt-Pass	2.56	0.56	99.0	0.00				
Abt-Act	2.07	0.69	99.0	0.00				
Abt-tran	0.25	0.74	0.75	0.74				
Bearing	0.03	0.74	0.18	0.74				
Joint Seal	0.02	0.74	99.0	0.00				
Restrainer	0.45	0.60	1.69	0.60				
Shear key	99.0	0.00	99.0	0.00				
MSCC-IG-S-E3-S4								
Column	0.59	0.84	3.55	0.84	99.0	0.00	99.0	0.00
Abt-seat	0.03	0.74	0.12	0.74	0.85	0.74	1.41	0.74
Deck-max	0.20	0.62	0.64	0.62				
Fnd-tran	1.31	2.43	99.0	0.00				
Fnd-rot	99.0	0.00	99.0	0.00				
Abt-Pass	2.56	0.56	99.0	0.00				
Abt-Act	2.07	0.69	99.0	0.00				
Abt-tran	0.25	0.74	0.75	0.74				
Bearing	0.03	0.74	0.18	0.74				
Joint Seal	0.02	0.74	99.0	0.00				
Restrainer	0.45	0.60	1.69	0.60				
Shear key	99.0	0.00	99.0	0.00				

MSCC-IG-M-E3-S3								
Column	0.25	0.49	0.90	0.49	1.72	0.49	2.51	0.49
Abt-seat	0.09	0.46	0.25	0.46	0.73	0.46	1.04	0.46
Deck-max	0.27	0.51	0.83	0.51				
Fnd-tran	99.0	0.00	99.0	0.00				
Fnd-rot	99.0	0.00	99.0	0.00				
Abt-Pass	2.64	0.56	99.0	0.00				
Abt-Act	2.00	0.60	99.0	0.00				
Abt-tran	0.27	0.63	0.79	0.63				
Bearing	0.09	0.46	0.32	0.46				
Joint Seal	0.07	0.46	4.44	0.46				
Restrainer	1.33	0.80	99.0	0.00				
Shear key	99.0	0.00	99.0	0.00				
MSCC-IG-M-E3-S4								
Column	0.25	0.49	0.90	0.49	1.72	0.49	2.51	0.49
Abt-seat	0.09	0.46	0.25	0.46	0.98	0.46	1.41	0.46
Deck-max	0.27	0.51	0.83	0.51				
Fnd-tran	99.0	0.00	99.0	0.00				
Fnd-rot	99.0	0.00	99.0	0.00				
Abt-Pass	2.64	0.56	99.0	0.00				
Abt-Act	2.00	0.60	99.0	0.00				
Abt-tran	0.27	0.63	0.79	0.63				
Bearing	0.09	0.46	0.32	0.46				
Joint Seal	0.07	0.46	4.44	0.46				
Restrainer	1.33	0.80	99.0	0.00				
Shear key	99.0	0.00	99.0	0.00				

APPENDIX E

COMPARISON OF THE BRIDGE CLASS SYSTEM FRAGILITIES WITH HAZUS

Table E.1: Percentage change in the median values and dispersions of the bridge class fragilities with respect to HAZUS fragilities

Bridge class (CBC + SPS)	BSST median values, λ					% change in λ and ζ				
	0	1	2	3	ζ*	0	1	2	3	ζ*
HAZUS fragilities										
MSCC-BG-S-E1	0.35	0.45	0.55	0.80	0.60					
MSCC-BG-S-E2/E3	0.60	0.90	1.30	1.60	0.60					
MSCC-BG-M-E1	0.60	0.90	1.10	1.50	0.60					
MSCC-BG-M-E2/E3	0.90	0.90	1.10	1.50	0.60					
Current study										
MSCC-BG-S-E1-S0	0.13	0.17	0.19	0.22	0.59	-63	-63	-66	-73	-2
MSCC-BG-M-E1-S0	0.08	0.10	0.11	0.12	0.51	-86	-89	-90	-92	-16
MSCC-BG-S-E1-S1	0.02	0.08	0.14	0.17	0.61	-95	-82	-74	-79	2
MSCC-BG-S-E1-S2	0.02	0.09	0.15	0.17	0.64	-95	-79	-74	-79	7
MSCC-BG-S-E1-S3	0.02	0.09	0.14	0.17	0.64	-95	-79	-74	-79	6
MSCC-BG-S-E1-S4	0.02	0.09	0.15	0.17	0.64	-95	-79	-73	-79	6
MSCC-BG-M-E1-S1	0.01	0.06	0.08	0.09	0.63	-98	-94	-93	-94	5
MSCC-BG-M-E1-S2	0.01	0.06	0.08	0.09	0.68	-98	-93	-93	-94	13
MSCC-BG-M-E1-S3	0.01	0.06	0.08	0.09	0.66	-98	-93	-93	-94	11
MSCC-BG-M-E1-S4	0.01	0.06	0.08	0.09	0.66	-98	-93	-93	-94	11
MSCC-BG-S-E2-S0	0.15	0.39	0.71	1.00	0.64	-76	-57	-46	-38	6
MSCC-BG-M-E2-S0	0.12	0.24	0.38	0.50	0.56	-87	-73	-66	-67	-6
MSCC-BG-S-E2-S2	0.08	0.31	0.47	0.62	0.54	-86	-65	-64	-61	-10
MSCC-BG-S-E2-S3	0.08	0.31	0.47	0.62	0.54	-86	-65	-64	-61	-10
MSCC-BG-S-E2-S4	0.09	0.31	0.48	0.62	0.54	-86	-65	-63	-61	-9
MSCC-BG-M-E2-S2	0.07	0.18	0.27	0.36	0.59	-92	-80	-75	-76	-2
MSCC-BG-M-E2-S3	0.07	0.18	0.28	0.36	0.59	-92	-80	-75	-76	-1
MSCC-BG-M-E2-S4	0.07	0.18	0.27	0.35	0.60	-92	-80	-75	-76	0
MSCC-BG-S-E3-S0	0.16	0.52	0.95	1.26	0.40	-73	-42	-27	-21	-34
MSCC-BG-M-E3-S0	0.10	0.32	0.61	0.83	0.54	-88	-65	-44	-44	-10
MSCC-BG-S-E3-S3	0.09	0.57	1.44	2.06	0.51	-86	-37	11	28	-15

MSCC-BG-S-E3-S4	0.09	0.57	1.44	2.06	0.51	-86	-37	11	29	-14
MSCC-BG-M-E3-S3	0.06	0.26	0.59	0.87	0.58	-93	-71	-46	-42	-4
MSCC-BG-M-E3-S4	0.06	0.26	0.61	0.88	0.59	-93	-71	-45	-41	-3
HAZUS fragilities										
MSCC-SL	0.60	0.90	1.10	1.50	0.60					
Current study										
MSCC-SL-P-S0	0.17	0.70	1.03	1.28	0.66	-72	-22	-6	-15	9
MSCC-SL-P-S1-S	0.03	0.09	0.21	0.34	0.82	-94	-90	-81	-77	37
MSCC-SL-P-S2-S	0.06	0.28	0.48	0.62	0.70	-91	-69	-56	-58	17
MSCC-SL-P-S3-S	0.06	0.29	0.53	0.65	0.70	-91	-68	-52	-57	17
MSCC-SL-P-S4-S	0.06	0.29	0.53	0.65	0.70	-91	-68	-51	-57	16
HAZUS fragilities										
MSCC-TG-S/M-E1	0.60	0.90	1.10	1.50	0.60					
MSCC-TG-S/M-E2/E3	0.90	0.90	1.10	1.50	0.60					
Current study										
MSCC-TG-P-E1-S0	0.44	0.77	0.88	1.07	0.64	-28	-15	-20	-29	6
MSCC-TG-M-E1-S0	0.27	0.31	0.35	0.44	0.57	-55	-65	-68	-71	-5
MSCC-TG-P-E1-S1	0.06	0.12	0.20	0.28	0.41	-90	-87	-82	-82	-32
MSCC-TG-P-E1-S2	0.08	0.23	0.31	0.37	0.45	-87	-74	-72	-75	-24
MSCC-TG-P-E1-S3	0.08	0.23	0.32	0.38	0.48	-87	-74	-71	-75	-21
MSCC-TG-P-E1-S4	0.08	0.23	0.32	0.38	0.48	-87	-74	-71	-75	-20
MSCC-TG-M-E1-S1	0.07	0.14	0.23	0.30	0.54	-88	-84	-79	-80	-10
MSCC-TG-M-E1-S2	0.10	0.24	0.27	0.34	0.59	-84	-74	-75	-77	-2
MSCC-TG-M-E1-S3	0.10	0.24	0.28	0.34	0.59	-84	-74	-75	-77	-2
MSCC-TG-M-E1-S4	0.10	0.24	0.28	0.34	0.59	-84	-74	-75	-77	-2
MSCC-TG-P-E2-S0	0.43	0.76	0.87	1.04	0.56	-52	-16	-21	-31	-7
MSCC-TG-M-E2-S0	0.47	1.08	1.99	2.82	0.54	-47	19	81	88	-9
MSCC-TG-P-E2-S2	0.09	0.28	0.38	0.47	0.64	-90	-69	-66	-69	7
MSCC-TG-P-E2-S3	0.09	0.28	0.39	0.47	0.65	-90	-69	-65	-69	9
MSCC-TG-P-E2-S4	0.09	0.28	0.39	0.46	0.66	-90	-69	-64	-69	10
MSCC-TG-M-E2-S2	0.12	0.41	0.79	1.12	0.48	-87	-55	-29	-25	-20
MSCC-TG-M-E2-S3	0.12	0.41	1.06	1.52	0.49	-87	-55	-4	1	-18
MSCC-TG-M-E2-S4	0.12	0.40	1.20	1.71	0.51	-87	-55	9	14	-15
MSCC-TG-P-E3-S0	0.40	0.74	0.86	1.04	0.57	-56	-18	-22	-31	-4
MSCC-TG-M-E3-S0	0.48	1.23	2.47	3.57	0.50	-47	37	124	138	-17
MSCC-TG-P-E3-S3	0.07	0.26	0.43	0.54	0.49	-92	-71	-61	-64	-19
MSCC-TG-P-E3-S4	0.07	0.25	0.44	0.54	0.50	-92	-72	-60	-64	-17

MSCC-TG-M-E3-S3	0.11	0.39	1.20	1.72	0.46	-88	-56	9	15	-23
MSCC-TG-M-E3-S4	0.11	0.39	1.55	2.23	0.46	-88	-57	41	49	-23
HAZUS fragilities										
MSCC-IG-S/M-E1	0.60	0.90	1.10	1.50	0.60					
MSCC-IG-S/M-E2/E3	0.90	0.90	1.10	1.50	0.60					
Current study										
MSCC-BG-S-E1-S0	0.12	0.33	0.47	0.54	0.66	-81	-64	-57	-64	11
MSCC-BG-M-E1-S0	0.09	0.22	0.27	0.33	0.66	-85	-75	-76	-78	9
MSCC-BG-S-E1-S1	0.05	0.16	0.37	0.52	0.55	-91	-82	-66	-66	-9
MSCC-BG-S-E1-S2	0.07	0.29	0.49	0.57	0.52	-88	-68	-56	-62	-13
MSCC-BG-S-E1-S3	0.07	0.29	0.49	0.57	0.53	-88	-68	-56	-62	-12
MSCC-BG-S-E1-S4	0.07	0.29	0.49	0.57	0.53	-88	-68	-56	-62	-12
MSCC-BG-M-E1-S1	0.06	0.13	0.19	0.23	0.47	-90	-86	-83	-84	-21
MSCC-BG-M-E1-S2	0.07	0.18	0.21	0.25	0.51	-88	-80	-81	-83	-15
MSCC-BG-M-E1-S3	0.07	0.18	0.21	0.25	0.52	-88	-80	-81	-83	-14
MSCC-BG-M-E1-S4	0.07	0.18	0.21	0.25	0.52	-88	-80	-81	-84	-14
MSCC-BG-S-E2-S0	0.09	0.24	0.68	0.88	0.75	-90	-73	-38	-41	25
MSCC-BG-M-E2-S0	0.11	0.35	0.76	1.02	0.55	-88	-61	-31	-32	-9
MSCC-BG-S-E2-S2	0.06	0.21	1.00	1.49	0.57	-94	-76	-9	-1	-6
MSCC-BG-S-E2-S3	0.06	0.21	1.20	1.68	0.60	-94	-76	9	12	-1
MSCC-BG-S-E2-S4	0.06	0.22	1.24	1.72	0.60	-94	-76	13	14	1
MSCC-BG-M-E2-S2	0.08	0.26	0.56	0.80	0.43	-92	-71	-49	-47	-28
MSCC-BG-M-E2-S3	0.08	0.26	0.67	0.95	0.44	-92	-71	-39	-37	-26
MSCC-BG-M-E2-S4	0.08	0.26	0.69	0.98	0.47	-92	-71	-37	-34	-22
MSCC-BG-S-E3-S0	0.05	0.19	2.15	3.05	0.88	-94	-79	95	103	47
MSCC-BG-M-E3-S0	0.10	0.37	1.59	2.24	0.59	-89	-59	44	49	-1
MSCC-BG-S-E3-S3	0.03	0.18	2.76	3.41	0.66	-97	-80	151	127	10
MSCC-BG-S-E3-S4	0.03	0.18	3.59	3.87	0.75	-97	-80	227	158	25
MSCC-BG-M-E3-S3	0.08	0.28	1.00	1.44	0.41	-91	-69	-9	-4	-32
MSCC-BG-M-E3-S4	0.08	0.28	1.25	1.80	0.41	-91	-69	14	20	-32

The entities shaded in red indicate more vulnerability with respect to HAZUS (negative change in median fragilities) while those shaded in green indicate less vulnerability with respect to HAZUS (positive change in median fragilities).

REFERENCES

Abrahamson, N., Silva, W. (2008). *Summary of the Abrahamson & Silva NGA Ground-Motion Relations,* Earthquake Spectra, 24(1), pp: 67-97.

Ang, A. H.-S., Tang, W. H. (1975). *Probability Concepts in Engineering Planning and Design*, Vol. 1, John Wiley and Sons, New York.

ACI (2008). *Building Code Requirements for Structural Concrete (ACI 318-08) and Commentary*, American Concrete Institute, Farmington Hills, MI.

ASCE (2009). *ASCE: Infrastructure fact sheet*, <http://www.infrastructurereportcard.org/sites/default/files/RC2009_bridges.pdf>.

ATC (1981). *Seismic Design Guidelines for Highway Bridges*, Report No. ATC-6, Applied Technology Council, Redwood City, CA.

ATC (1985). *Earthquake damage evaluation data for California*, Report No. ATC-13, Applied Technology Council, Redwood City, CA.

ATC (1991). *Seismic Vulnerability and Impact of Disruption of Lifelines in the Coterminous United States*, Report No. ATC-25, Applied Technology Council, Redwood City, CA.

ATC (1996). *Improved Seismic Design Criteria for California Bridges: Provisional Recommendations*, Report No. ATC-32, Applied Technology Council, Redwood City, CA.

ATC (1996). *Seismic Evaluation and Retrofit of Concrete Buildings*, Report No. ATC-40, Applied Technology Council, Redwood City, CA.

ATC-63 (2008). *Quantification of Building Seismic Performance Factors*. ATC-63/FEMA P695, Applied Technology Council, Redwood City, CA.

ATC/MCEER (2002). *Comprehensive Specification for the Seismic Design of Bridges*, Report No. NCHRP 471, National Cooperative Highway Research program, Transportation Research Board, Washington, DC.

Baker, J. W., Cornell, A. C. (2006). *Vector-Valued Ground Motion Intensity Measures for Probabilistic Seismic Demand Analysis*, Report No. PEER 2006/08, Pacific Earthquake Engineering Research Center, University of California, Berkeley, CA.

Baker, J. W., Ling, T., Shahi, S. K., Jayaram, N. (2011). *New Ground Motion Selection Procedures and Selected Motions for the PEER Transportation Research Program*, Draft Report, Pacific Earthquake Engineering Research Center, University of California, Berkeley, CA.

Banerjee, S., Shinozuka, M. (2007). *Nonlinear Static Procedure for Seismic Vulnerability Assessment of Bridges*, Computer-Aided Civil and Infrastructure Engineering, 22, pp: 293-305.

Basoz, N., Kiremidjian, A. S. (1997). *Evaluation of Bridge Damage Data from the Loma Prieta and Northridge CA Earthquakes*, Report No. MCEER-98-0004, MCEER, University at Buffalo, The State University of New York, Buffalo, NY.

Basoz, N., Mander, J. B. (1999). *Enhancement of the Lifeline Transportation Module in HAZUS*, Report No. Draft #7, National Institute of Building Sciences, Washington, DC.

Bavirisetty, R., Vinayagamoorthy, M., Duan, L. (2003). *Dynamic Analysis*, Bridge Engineering – Seismic Design, Edited by Wai-Fah Chen and Lian Duan, CRC Press LLC, Boca Raton, FL, ISBN: 0-8493-1683-9/02.

Bazurro, P., Cornell, A. C. (1994). *Seismic hazard analysis for non-linear structures. I: Methodology*, Journal of Structural Engineering, 120(11), pp: 3320-3344.

Bazurro, P., Cornell, A. C. (1994). *Seismic hazard analysis for non-linear structures. II: Applications*, Journal of Structural Engineering, 120(11), pp: 3345-3365.

Bazzurro, P., Cornell, A. C. (2002). *Vector-values probabilistic seismic hazard analysis (VP-SHA),* Proceedings of the 7th U.S. National Conference on Earthquake Engineering, Boston, MA.

BDA (1988). *Bridge Design Aids,* California Department of Transportation, Sacramento, CA.

BDA (1989). *Bridge Design Aids,* California Department of Transportation, Sacramento, CA.

BDA (1995). *Bridge Design Aids,* California Department of Transportation, Sacramento, CA.

BDA (2004). *Bridge Design Aids,* California Department of Transportation, Sacramento, CA.

BDA (2009). *Bridge Design Aids,* California Department of Transportation, Sacramento, CA.

BDS (1990). *Bridge Design Specifications*, California Department of Transportation, Sacramento, CA.

Berry, M. P., Eberhard, M. O. (2003). *Performance models for flexural damage in reinforced concrete columns*, Report No. 2003/18, Pacific Earthquake Engineering Research Center, University of California, Berkeley, CA.

Berry, M. P., Eberhard, M. O. (2004). *PEER Structural Performance Database User's Manual*, Pacific Earthquake Engineering Research Center, University of California, Berkeley, CA.

Bruneau, M., Chang, S. E., Eguchi, R. T., Lee, G. C., O'Rourke, T. D., Reinhorn, A. M., Shinozuka, M., Tierney, K., Wallace, W. A., and Winterfeldt, D. (2003). *A Framework to Quantitatively Assess and Enhance the Seismic Resilience of Communities*, Earthquake Spectra, 19, pp: 733-752.

BSSC (1997). *NEHRP Guidelines for the seismic rehabilitation of buildings,* Report No. FEMA-273, Building Seismic Safety Council, Washington, DC.

Bucher, C. G., Bourgund, U. (1990). *A fast and efficient response surface approach for structural reliability problems*, Structural Safety, 7(1), pp: 57-66.

Caltrans (2007). *Reinforced Concrete Bridge Capacity Assessment Training Manual*, Report submitted to Structure Maintenance and Investigations, California Department of Transportation, Sacramento, CA.

Caltrans (2008). *Foundation Manual*, Office of Structure Construction, California Department of Transportation, Sacramento, CA.

Caltrans (2010-2012). *Personal communication with the P266 Fragility Project Advisory Panel members including* Roblee, C., Yashinsky, M., Mahan, M., Shantz, T., Setberg, H., Turner, L., Sahs, S., Adams, D. T., Keever, M. (2011), California Department of Transportation, Sacramento, CA.

Celik, O. C., Ellingwood, B. R. (2010). *Seismic fragilities for non-ductile reinforced concrete frames – Role of aleatoric and epistemic uncertainties*, Structural Safety, 32, pp: 1-12.

Chang, G. A., Mander, J. B. (1994). *Seismic Energy Based Fatigue Damage Analysis of Bridge Columns*: *Part 1 – Evaluation of Seismic Capacity*, Technical Report NCEER-94-0006, State University of New York, Buffalo, NY.

Chiou, B., Darragh, R., Gregor, N., Silva, W. (2008). *NGA Project Strong-Motion Database*, Earthquake Spectra, 24(1), pp: 23-44.

Choi, E. (2002). *Seismic analysis and retrofit of Mid-America bridges*, Ph.D. thesis, School of Civil and Environmental Engineering, Georgia Institute of Technology, Georgia.

Choi, E., DesRoches, R., Nielson, B. G. (2004). *Seismic Fragility of Typical Bridges in Moderate Seismic Zones*, Engineering Structures, 26(2), pp: 187-199.

Chopra, A. K. (2007). Dynamics *of Structures: Theory and Applications to Earthquake Engineering*, Third Edition, Prentice Hall, NY.

Cornell, A. C., Krawinkler, H. (2000). *Progress and challenges in seismic performance assessment*, PEER Center News <http://peer.berkeley.edu/news/2000spring/index.html>.

Cornell, A. C., Jayaler, F., Hamburger, R. O., Foutch, A. D. (2002). *Probabilistic Basis for 2000 SAC Federal Emergency Management Agency Steel Moment Frame Guidelines*, Journal of Structural Engineering, 128(4), pp: 526-533.

Der Kiureghian, A. (1981). *A Response Spectrum Method for Random Vibration Analysis of MDF Systems*, Earthquake Engineering and Structural Dynamics, 9, pp: 419-435.

Der Kiureghian, A. (2002). *Bayesian Methods for Seismic Fragility Assessment of Lifeline Components*, Acceptable Risk Processes: Lifelines and Natural Hazards, Monograph No. 21, A. D. Kiureghian ed., Technical Council for Lifeline Earthquake Engineering, ASCE, Reston, VA.

Duan, L., Li, F. (2003). *Seismic Design Philosophies and Performance-Based Design Criteria*, Bridge Engineering – Seismic Design, Edited by Wai-Fah Chen and Lian Duan, CRC Press LLC, Boca Raton, FL, ISBN: 0-8493-1683-9/02.

Duenas-Osorio, L., Padgett, J. E. (2011). *Seismic Reliability Assessment of Bridges with User-Defined System Failure Events*, Journal of Engineering Mechanics, 137(10), pp: 680-690.

Dutta, A. (1999). *On Energy Based Seismic Analysis and Design of Highway Bridges*, Ph.D. Thesis, University at Buffalo, The State University of New York, Buffalo, NY.

Ellingwood, B. R., Hwang, H. (1985). *Probabilistic Descriptions of Resistance of Safety-Related Structures in Nuclear Plants*, Nuclear Engineering and Design, 88(2), 169-178.

Ellingwood, B. R., Wen, Y.-K. (2005). *Risk-Benefit-Based Design Decisions for Low-Probability/High Consequence Earthquake Events in Mid-America*, Progress on Structural Engineering and Materials, 7(2), pp: 56-70.

Elnashai, A., Borzi, B., Vlachos, S. (2004). *Deformation-Based Vulnerability Functions for RC Bridges*, Structural Engineering and Mechanics, 17(2), pp: 215-244.

Fajfar, P. (2000). *A nonlinear analysis method for performance-based seismic design*, Earthquake Spectra, 16(3), pp: 573-592.

Fang, J., Li, Q., Jeary, A., Liu, D. (1999). *Damping of Tall Buildings: Its Evaluation and Probabilistic Characteristics*, Structural Design of Tall Buildings, 8(2), pp: 145-153.

FEMA-273 (1997). *NEHRP Guidelines for the Seismic Rehabilitation of Buildings*, Report No. FEMA-273, Building Seismic Safety Council Seismic Rehabilitation Project, Federal Emergency Management Agency, Washington, DC,

FEMA-350 (2000). *Recommended seismic design criteria for new steel moment-frame buildings*, Report No. FEMA-350, SAC Joint Venture, Federal Emergency Management Agency, Washington, DC.

FEMA-351 (2000). *Recommended seismic evaluation and upgrade criteria for existing welded steel moment-frame buildings*, Report No. FEMA-351, SAC Joint Venture, Federal Emergency Management Agency, Washington, DC.

FEMA (2006). *FEMA 454: Designing for Earthquakes: A Manual for Architects, Federal Emergency Management Agency*, U.S. Department of Homeland Security, Washington, DC.

FHWA (2010). *Conditions and Performance Report*, U.S. Department of Transportation, Federal Highway Administration, Washington, DC.

Filippou, F. C., Popov, E. P. Bertero, V. V. (1983). *Effects of Bond Deterioration on Hysteretic Behavior of Reinforced Concrete Joints*, Report No. EERC 83-19, Earthquake Engineering Research Center, University of California, Berkeley, CA.

Gardoni, P., Der Kiureghian, A., Mosalam, K. M. (2002). *Probabilistic capacity models and fragility estimates for reinforced concrete columns based on experimental observations*, Journal of Engineering Mechanics, 128(10), pp: 1024-1038.

Gardoni, P., Mosalam, K. M., Der Kiureghian, A. (2003). *Probabilistic seismic demand models and fragility estimates for RC bridges*, Journal of Earthquake Engineering, 7(1), pp: 79-106.

Ghosh, J., Padgett, J. E., Duenas-Osorio, L. (2012). *Comparative Assessment of Different Surrogate Modeling Strategies with Application to Aging Bridge Seismic Fragility Analysis*, Proceedings of the 2012 Joint Conference of the Engineering Mechanics Institute and the 11th ASCE Joint Specialty Conference on Probabilistic Mechanics and Structural Reliability, Notre Dame, IN.

Giovenale, P., Cornell, A. C., Esteva, L. (2004). *Comparing the adequacy of alternate ground motion intensity measures for the estimation of structural responses*, Earthquake Engineering and Structural Dynamics, 33(8), pp: 951-979.

Goel R. K., Chopra, A. K. (1997). *Evaluation of Bridge Abutment Capacity and Stiffness during Earthquake*, Earthquake Spectra, 13(1), pp. 1-21.

Guan, X. L., Melchers, R. E. (2001). *Effect of response surface parameter variation on structural reliability estimates*, Structural Safety, 23(4), pp: 429-444.

HAZUS (1997). *Technical Manual,* Federal Emergency Management Agency, Washington DC.

HAZUS-MH (2011). *Multi-Hazard Loss Estimation Methodology: Earthquake Model HAZUS-MH MR5 Technical Manual,* Federal Emergency Management Agency, Washington DC.

Hines, W., Montgomery, D., Goldsman, D., Borror, C. (2003). *Probability and Statistics in Engineering*, Wiley, New York.

Huang, Q., Gardoni, P., Hurlebaus, S. (2010). *Probabilistic Seismic Demand Models and Fragility Estimates for Reinforced Concrete Highway Bridges with One Single-Column Bent*, Journal of Engineering Mechanics, 136(11), pp: 1340-1353.

Hwang, H., Huo, J. R. (1998). *Probabilistic Seismic Damage Assessment of Highway Bridges*, Proceedings of the 6th U.S. National Conference on Earthquake Engineering, Seattle, WA.

Hwang, H., Jernigan, J. B., Lin, Y. W. (2000). *Evaluation of seismic damage to Memphis bridges and highway systems*, Journal of Bridge Engineering, 5(4), pp: 322-330.

Hwang, H., Liu, J., Chiu, Y. (2000a). *Seismic Fragility Analysis of Highway Bridges*, Center for Earthquake Research and Information, The University of Memphis, Memphis, TN.

Jeong, S. H., Elnashai, A. S. (2007). *Probabilistic Fragility Analysis Parameterized by Fundamental Response Quantities*, Engineering Structures, 29, pp: 1238-1251.

Kaplan, S., Garrick, B. J. (1981). *On the quantitative definition of risk*, Risk analysis, 1(1), pp: 11-27.

Keady, K. L., Alameddine F., Sardo, T. E. (2003). *Seismic Retrofit Technology*, Bridge Engineering – Seismic Design, Edited by Wai-Fah Chen and Lian Duan, CRC Press LLC, Boca Raton, FL, ISBN: 0-8493-1683-9/02.

Kim, S. H., Shinozuka, M. (2004). *Development of fragility curves of bridges retrofitted by column jacketing*, Probabilistic Engineering Mechanics, 19, pp: 105-112.

Kim, S. H., Mha, H. S., Lee, S. W. (2006). *Effects of bearing damage upon seismic behavior of a multi-span girder bridge*, Engineering Structures, 28(7), pp: 1071-1080.

Koutsourelakis, P. S. (2010). *Assessing structural vulnerability against earthquakes using multi-dimensional fragility surfaces: A Bayesian framework*, Probabilistic Engineering Mechanics, 25, pp: 49-60.

Liao, D., Yen, P. W. (2010). *A linkage tool for analyzing earthquake traffic impact in micro level based on seismic risk assessment and traffic simulation*, ACM International Conference Processing Series, 2010, COM. Geo 2010 – 1st International Conference and Exhibition on Computing for Geospatial Research and Application, Washington, DC.

Lin, K. W., Wald, D. J. (2008). *ShakeCast Manual Open-File Report 2008-1158*, United States Geological Survey, United States Department of Interior, Washington, D.C.

Lindley, P. B. (1992). *Engineering design with natural rubber*, Malaysia Natural Rubber Producers Research Association, Hertford, England, United Kingdom.

LPILE (2012). *LPILE v6.0 – A Program for the Analysis and Design of Piles and Drilled Shafts Under Lateral Loads*, Ensoft, Inc. Engineering Software, Austin, Texas.

Luco, N., Cornell, A. C. (2000). *Effects of connection fractures on SMRF seismic drift demands*, Journal of Structural Engineering, 126, pp: 127-136.

Luco, N., Cornell, A. C. (2007). Structure-specific scalar intensity measures for near-source and ordinary earthquake ground motions, Earthquake Spectra, 23(2), pp:357-392.

Luna, R., Hoffman, D., Lawrence, W. T. (2008). *Estimation of earthquake loss due to bridge damage in the St. Louis Metropolitan Area. I: Direct losses*, Natural Hazards Review, 9(1**)**, pp: 1-11.

Lupoi, G., Franchin, P., Lupoi, A., Pinto, P. (2006). *Seismic fragility analysis of structural systems*, Journal of Engineering Mechanics, 132(4), pp: 385-395.

Mackie, K., Stojadinovic, B. (2001). *Probabilistic seismic demand model for California bridges,* Journal of Bridge Engineering, 6, pp: 468-480.

Mackie, K., Stojadinovic, B. (2004). *Fragility curves for reinforced concrete highway over-pass bridges*, 13th World Conference on Earthquake Engineering, Vancouver, B.C., Canada.

Mackie, K., and Stojadinovic, B. (2005). *Fragility Basis for California Highway Overpass Bridge Seismic Decision Making*, PEER Report 2005/02, Pacific Earthquake Engineering Research Center, University of California, Berkeley, CA.

Mackie, K. R., Wong, J.-M., Stojadinovic, B. (2008). *Integrated Probabilistic Performance-Based Evaluation of Benchmark Reinforced Concrete Bridges*,

Report No. PEER 2007/09, Pacific Earthquake Engineering Research Center, University of California, Berkeley, CA.

Mackie, K. R., Cronin, K. J., Nielson, B. G. (2011). *Response Sensitivity of Highway Bridges to Randomly Oriented Multi-Component Earthquake Excitation*, Journal of Earthquake Engineering, 15(6), pp: 850-876.

Mander, J. B., Kim, D. K., Chen, S. S., and Premus, G. J. (1996). *Response of steel bridge bearings to reverse cyclic loading*, Technical Report NCEER-96-0014, NCEER, State University of New York – University at Buffalo, Buffalo, NY.

Mander, J. B., and Basoz, N. (1999). *Seismic fragility curve theory for highway bridges*, 5th US Conference on Lifeline Earthquake Engineering, Seattle, WA.

Mander, J. B., Dhakal, R. P., Mashiko, N., Solberg, K. M. (2007). *Incremental dynamic analysis applied to seismic financial risk assessment of bridges*, Engineering Structures, 29, pp: 2662-2672.

Maroney, B., Ramstad, K., Kutter, B. (1993). *Experimental Testing of Laterally Loaded Large Scale Bridge Abutments*, Structural Engineering in Natural Hazards Mitigation, Irvine, CA, American Society of Civil Engineers.

Maroney, B., Kutter, B., Romastad, K., Chai, Y. H., Vanderbilt, E. (1994*). Interpretation of Large Scale Bridge Abutment Test Results*, Proceedings of the 3rd Annual Seismic Research Workshop, California Department of Transportation, Sacramento, CA.

Martin, G. R., Yan, L. (1995). *Modeling Passive Earth Pressure for Bridge Abutments, Earthquake-Induced Movements and Seismic Remediation of Existing Foundations and Abutments*, ASCE 1995 Annual National Convention, Vol. Geotechnical Special Publication 55, San Diego, CA.

McKay, M. D., Conover, W. J., Beckman, R. J. (1979). *A comparison of three methods for selecting values of input variables in the analysis of output from a computer code*, Technometrics, 21, pp: 239-245.

McKenna, F., Scott, M., Fenves, G. L. (2010). *Nonlinear Finite-Element Analysis Software Architecture Using Object Composition*, Journal of Computing in Civil Engineering, Vol. 24, No. 1, pp. 95-107.

Megally, S. H., Silva, P. F., Seible, F. (2002). *Seismic Response of Sacrificial Shear Keys in Bridge Abutments*, Structural Systems Research Project SSRP-2001/24, University of California, San Diego, La Jolla, CA.

Melchers, R. E. (1999). *Structural Reliability Analysis and Prediction*, John Wiley and Sons, 2nd Edition, ISBN: 978-0471987710.

Menegotto, M., Pinto, P. E. (1973). *Method of Analysis for Cyclically Loaded Reinforced Concrete Plane Frames Including Changes in Geometry and Non-Elastic Behavior of Elements Under Combined Normal Force and Bending*, Proceedings of the IABSE Symposium on Resistance and Ultimate Deformability of Structures Acted on by Well-Defined Repeated Loads, Lisbon, Portugal, pp: 15-22.

Moehle, J., Fenves, G., Mayes, R., Priestley, N., Seible, F., Uang, C.-M., Werner, S., Aschheim, M. (1995). *Highway Bridges and Traffic Management*, Earthquake Spectra, 11, pp: 287-372.

Moehle, J. P., Eberhard, M. O. (2003). *Earthquake Damage to Bridges*, Bridge Engineering – Seismic Design, Edited by Wai-Fah Chen and Lian Duan, CRC Press LLC, Boca Raton, FL, ISBN: 0-8493-1683-9/02.

Moore, J. E., Kiremidjian, A., Chiu, S. (2000). *Seismic risk model for a designated highway system*: *Oakland/San Francisco Bay Area*, PEER Report No. 2002/02, U.S.-Japan Workshop on the Effects of Near-Field Earthquake Shaking, Pacific Earthquake Engineering Research Center, University of California, Berkeley, CA.

MTD 5-1 (1992). *Bridge Memo to Designers (5-1)*, California Department of Transportation, Sacramento, CA.

MTD 7-1 (1994). Bridge *Memo to Designers (7-1)*, California Department of Transportation, Sacramento. CA.

MTD 20-4 (1995). *Bridge Memo to Designers (20-4)*, California Department of Transportation, Sacramento, CA.

MTD 20-1 (1999). *Bridge Memo to Designers (20-1) – Seismic Design Methodology*, California Department of Transportation, Sacramento, CA.

Mtenga, P. V. (2007). *Elastomeric Bearing Pads under Combined Loading*, Report to the Florida Department of Transportation, Contract No: BC352-16, Tallahassee, FL.

Muthukumar, S. (2003). *A Contact Element Approach with Hysteresis Damping for the Analysis and Design of Pounding in Bridges*, Ph.D. Dissertation, Georgia Institute of Technology.

NBI Coding Guide (1995). *Recording and Coding Guide for the Structure Inventory and Appraisal of the Nation's Bridges*, Report No. FHWA-PD-96-001, U.S. Department of Transportation, Federal Highway Administration, Office of Engineering Bridge Division, Washington, DC.

NBI (2010). *National Bridge Inventory Data*, U.S. Department of Transportation, Federal Highway Administration, Washington, DC, available at: http://www.fhwa.dot.gov/bridge/nbi/ascii.cfm.

Nielson, B. G. (2005). *Analytical Fragility Curves for Highway Bridges in Moderate Seismic Zones*, Ph.D. Dissertation, Georgia Institute of Technology, Atlanta, GA.

Nielson, B. G., DesRoches, R. (2007). *Analytical Seismic Fragility Curves for Typical Bridges in the Central and Southeastern United States*, Earthquake Spectra, 23, pp: 615-633.

Padgett, J. E. (2007). *Seismic Vulnerability Assessment of Retrofitted Bridges using Probabilistic Methods*, Ph.D. Dissertation, Georgia Institute of Technology, Atlanta, GA.

Padgett, J. E., DesRoches, R. (2007). *Bridge Functionality Relationships for Improved Seismic Risk Assessment of Transportation Networks*, Earthquake Spectra, 23(1), pp: 115-130.

Padgett, J. E., DesRoches, R. (2008). *Methodology for Development of Analytical Fragility Curves for Retrofitted Bridges*, Earthquake Engineering and Structural Dynamics, 37(8), pp: 1157-1174.

Padgett, J. E., Nielson, B. G., DesRoches, R. (2008). Selection of optimal intensity measures in probabilistic seismic demand models of highway bridge portfolios, Earthquake Engineering and Structural Dynamics, 37(5), pp: 711-725.

Padgett, J. E., Dennemann, K., Ghosh, J. (2010). *Risk-based seismic life-cycle cost-benefit (LCC-B) analysis for bridge retrofit assessment*, Structural Safety, 32(3), pp: 165-173.

Pan, Y., Agrawal, A. K., Ghosn, M., Alampalli, S. (2010). *Seismic Fragility of Multispan Simply Supported Steel Highway Bridges in New York State. II: Fragility Analysis, Fragility Curves, and Fragility Surfaces*, Journal of Bridge Engineering, 15(5), pp: 462-472.

Priestley, M. J. N., Seible, F., Calvi, G. M. (1996). *Seismic Design and Retrofit of Bridges*, John Wiley & Sons, Inc., New York, NY, ISBN: 0-471-57998-X.

Rajashekhar, M. R., Ellingwood, B. R. (1993). *A new look at the response surface approach for reliability analysis*, Structural Safety, 12(3), pp: 205-220.

Ramanathan, K., DesRoches, R., Padgett, J. E. (2010). *Analytical Fragility Curves for Multispan Continuous Steel Girder Bridges in Moderate Seismic Zones*, Transportation Research Record: Journal of the Transportation Research Board, 2202, pp: 173-182.

Ramanathan, K., DesRoches, R., Padgett, J. E. (2012). *A Comparison of Pre- and Post-Seismic Design Considerations in Moderate Seismic Zones through the Fragility Assessment of Multispan Bridge Classes*, Engineering Structures (In Review).

Rosenblueth, E. (1951). *A Basis for Aseismic Design*, Ph.D. Thesis, University of Illinois, Urbana, IL.

Sahs, S., Veletzos, M., Panagiutou, M., Restrepo, J. (2008). *Visual Inspection and Capacity Assessment of Earthquake Damaged Reinforced Concrete Bridge Elements: Integrate Research and Deployment Final Report*, California Department of Transportation, Sacramento, CA.

Saiidi, M., Maragakis, E. A., Feng, S. (1996). *Parameters in Bridge Restrainer Design for Seismic Retrofit*, Journal of Structural Engineering, 122(1), pp. 61-68.

Saiidi, M., Randall, M., Maragakis, E., Isakovic, T. (2001). *Seismic Restrainer Design Methods for Simply Supported Bridges*, Journal of Bridge Engineering, 6(5), pp. 307-315.

Scharge, L. (1981). *Anchoring of Bearings by Friction, Joint Sealing and Bearing Systems for Concrete Structures*, World Congress on Joints and Bearings, Vol. 1, American Concrete Institute, Niagara Falls, NY.

SDC (1990). *Caltrans Structures Seismic Design Reference*, California Department of Transportation, Sacramento, CA.

SDC (1999). *Seismic Design Criteria*, Version 1, California Department of Transportation, Sacramento, CA.

SDC (2010). *Seismic Design Criteria*, Version 1.6, California Department of Transportation, Sacramento, CA.

Shafieezadeh, A., Ramanathan, K., DesRoches, R., Padgett, J. E. (2011). *Fractional order intensity measures for probabilistic seismic demand modeling applied to highway bridges*, Earthquake Engineering and Structural Dynamics, DOI: 10.1002/eqe.1135.

Shamsabadi, A., Yan, L. (2008). *Closed-Form Force-Displacement Backbone Curves for Bridge Abutment Backfill Systems*, Proceedings of the Geotechnical Earthquake Engineering and Soil Dynamics IV Congress, American Society of Civil Engineers.

Shantz, T. (2011). *Personal Communication Regarding Modeling the Stiffness for Foundation Translational and Rotational Springs*, California Department of Transportation, Sacramento, CA.

Shinozuka, M., Feng, M. Q., Kim, H.-K., Kim, S.-H. (2000). *Nonlinear Static Procedure for Fragility Curve Development*, Journal of Engineering Mechanics, 126(12), pp: 1287-1296.

Shinozuka, M., Feng, M. Q., Kim, H., Uzawa, T. Ueda, T. (2003). *Statistical Analysis of Fragility Curves*, Report No. MCEER-03-0002*,* MCEER, University at Buffalo, The State University of New York, Buffalo, NY.

Shome, N., Cornell, A. C. (1999). *Probabilistic Seismic Demand Analysis of Nonlinear Structures,* Reliability of Marine Structures Program Report No. RMS-35, Department of Civil and Environmental Engineering, Stanford University, CA.

Singhal, A., Kiremidjian, A. S. (1996). *Bayesian updating of fragilities with application to RC frames*, Journal of Structural Engineering, 124(8), pp: 922-929.

Song, J., Kang, W.-H. (2009). *System reliability and sensitivity under statistical dependence by matrix-based system reliability method*, Structural Safety, 31(2), pp: 148-156.

Vamvatsikos, D., Cornell, A. C. (2002). *Incremental Dynamic Analysis*, Earthquake Engineering and Structural Dynamics*,* 31, pp: 491-514.

Veletzos M. J., Panagiotou, M., Restrepo, J. I. (2006). *Post Seismic Inspection and Capacity Assessment of Reinforced Concrete Bridges*, Report No. SSRP-06/19, Report submitted to the California Department of Transportation, University of California, San Diego, CA.

Wight, J., MacGregor, J. (2011). *Reinforced Concrete: Mechanics and Design*, 6th Edition, Prentice Hall, ISBN-10: 0132176521, ISBN-13: 9780132176521.

Werner, S. D., Lavoie, J.-P., Eitzel, C., Cho, S., Huyck, C., Ghosh, S., Eguchi, R. T., Taylor, C. E., Moore II, J. E. (2003). *REDARS 1: Demonstration Software for Seismic Risk Analysis of Highway Systems*, <http://mceer.buffalo.edu/publications/resaccom/03-SP01/02werner.pdf>

Werner, S. D., Taylor, C. E., Sungbin, C., Lavoie, J.-P., Huyck, C. K., Eitzel, C., Eguchi, R. T., Moore, J. E. (2004). *New developments in the seismic risk analysis of highway systems*, Proceedings of the 13th World Conference on Earthquake Engineering, Vancouver, Canada.

Whitman, R. V., Biggs, J. M., Brennan III, J. E., Cornell, A. C., de Neufville, R. L., Vanmarcke, E. H. (1975). *Seismic Design Decision Analysis*, Journal of Structural Division, 101(ST5), pp: 1067-1084.

Yamazaki, F., Hamada, T., Motoyama, H., Yamauchi, H. (1999). *Earthquake Damage Assessment of Expressway Bridges in Japan*, Technical Council on Lifeline Earthquake Engineering Monograph, 16, pp: 361-370.

Yashinsky, M. (1995). *Northridge Earthquake: Lifeline Performance and Post-Earthquake Response*, Technical Council on Lifeline Earthquake Engineering Monograph No. 8, Washington, D.C.

Yashinsky, M., Karshenas, M. J. (2003) *Fundamentals of Seismic Protection for Bridges*, EERI Monograph #9, Oakland, CA.

Yu. O., Allen, D. L., and Drnevich, V. P. (1991). *Seismic Vulnerability Assessment of Bridges on Earthquake Priority Routes in Western Kentucky*, 3rd US National Conference on Lifeline Earthquake Engineering, Los Angeles, CA.

Zhang, J., Huo, Y. (2009). *Evaluating effectiveness and optimum design of isolation devices for highway bridges using the fragility function method*, Engineering Structures, 31, pp: 1648-1660.

Zhong, J., Gardoni, P., Rosowsky, D., Haukaas, T. (2008). *Probabilistic seismic demand models and fragility estimates for reinforced concrete bridges with two-column bents*, Journal of Engineering Mechanics, 134(6), pp: 495-504.

Zhou, Y., Banerjee, S., Shinozuka, M. (2010). *Socio-economic effect of seismic retrofit of bridges for highway transportation networks: A pilot study*, Structure and Infrastructure Engineering, 6(1-2), pp: 145-157.

Feasibility Studies for Improving Caltrans' Bridge Fragility Relationships

Final Report

Part II

BRIDGE-SPECIFIC FRAGILITY FRAMEWORK AND DESIGN SUPPORT TOOL FOR TWO-SPAN INTEGRAL BOX GIRDER BRIDGES IN CALIFORNIA

Technical Report by Jazalyn Dukes, Reginald DesRoches and Jamie E. Padgett

TABLE OF CONTENTS

CHAPTER 1

INTRODUCTION AND MOTIVATION OF THE DESIGN SUPPORT TOOL

The California Department of Transportation (Caltrans) seismic bridge design process for an Ordinary Bridge described in the Seismic Design Criteria (SDC) directs the design engineer to meet minimum requirements resulting in bridge design that should remain standing in the event of a Design Seismic Hazard or a Design Earthquake (Caltrans, 2010). A bridge can be designed to sustain significant damage, however it should avoid the collapse limit state, where the bridge is unable to resist loads due to self-weight (Caltrans, Seismic Design Methodology, 2010). Seismic hazards, in the form of a design spectrum or ground motion time histories, are used to determine the demands of the bridge components and bridge system. These demands are compared to the capacity of the components to make sure the bridge meets key performance criteria. The SDC also specifies design detailing of various components, including abutments, foundations, hinge seats and bent caps. The expectation of following the guidelines set forth by the SDC during the design process is the design of a bridge that will avoid collapse under anticipated seismic loads.

The procedure set forth in the SDC is a prescriptive approach which does not provide quantitative information on how a bridge will perform for a Design Earthquake. Although the SDC is designed to produce bridge designs that will not collapse during a Design Earthquake, the collapse capacity of the structure is uncertain in itself (Luco, Ellingwood, Hamburger, Hooper, Kimball, & Kircher, 2007) and is not addressed by the SDC. The current approach does not account for the performance of the bridge at hazard levels other than the Design Seismic Hazard. The current design process does not directly

provide information on the expected performance as a function of varying different design details. Finally, this approach does not provide insight into the performance of the bridge at performance levels other than the collapse limit state. Therefore, there is a need for a supplement to this design process that will provide statistical information on the performance of a bridge at a Design Seismic Hazard, as well as for other hazard levels. Quantification of the uncertainty of the collapse capacity of the bridge and the sources of uncertainty would also be beneficial to append to the design process. There is also a need for designers to have an understanding of the effects of certain design decisions on the probabilistic performance of a bridge, and the performance of the bridge at different performance levels.

The goal of this project is to introduce probabilistic fragility analysis into the Caltrans design process and address the aforementioned shortcomings of the current design process. The motivation for this project is to improve the designer's understanding of the probabilistic performance of their bridge design as a function of several design details. To accomplish these goals, a new bridge fragility method is presented as well as a design support tool that provides design engineers with instant access to fragility information during the design process. These products are presented for one specific bridge type that is common in California, the two-span concrete box girder bridge. The end product, the design support tool, is a bridge-specific fragility generator that provides probabilistic performance information on the bridge design. With this tool, a designer can check the bridge design after going through the SDC procedure to determine the performance of the bridge and its components at any hazard level. The designer would then be able to determine the effect of a change in the design on the performance and therefore make more informed design decisions.

CHAPTER 2

CALTRANS CURRENT SEISMIC DESIGN PROCESS

2.1 Early Seismic Code Provisions for Bridge Design in Caltrans

Seismic design in the US has evolved significantly over the past 100 years, with most of the innovation in design coming after large earthquake events. In the United States, seismic design codes began to be developed after the 1906 San Francisco earthquake (FEMA, 2006). Seismic design concepts graduated from those based on wind loads and static force concepts, to dynamic design concepts using acceleration spectra. In recent history, the nonlinear behavior of components has been able to be modeled with computer analysis programs and verified with extensive lab tests. California has always been in the forefront of evolving seismic design in the US due to the high seismic activity in the state, with many universities playing key roles in testing and developing these new design concepts and ideas (FEMA, 2006).

The first seismic design provision in California for bridges was developed in 1940. The design criteria stated that bridges should be designed for a seismic force placed horizontally at the center of mass in any direction. The force was a percentage of the dead load which was determined by the design engineer. In 1943, and design criteria was more specific. It stated that the seismic force applied to the center of gravity of the weight of the structure should be between 2% and 6% of the dead load of the structure, depending on the type of foundation. As was mentioned before, these criteria were soon adopted in the nationwide standards of AASHTO. In 1965, the criteria incorporated more characteristics of the bridge into the calculation of the seismic force. Eqn. 1 shows the formula for finding this force. The coefficient K represents the energy absorption of the structure, and is determined based on the bent system (wall, versus single and multi-

column piers). The coefficient C represents the structure's stiffness, and is based on the natural period of vibration. The minimum force was 2% of the dead load of the structure, and the engineer was instructed to give special consideration to structures founded on soft soils, and structures with massive piers (Moehle, et al., 1995)

$$EQ = K * C * D \tag{1}$$

The 1971 San Fernando earthquake prompted major changes in the seismic bridge design code. For bridges in construction, lateral design forces were increased by a factor of 2 or 2.5. Design for new bridges then had to account for many new factors, including fault proximity, site conditions, dynamic response and ductile design for reinforced concrete structures. These changes were included in the 1974 seismic code for Caltrans (Sahs, Veletzos, Panagiutou, & Restrepo, 2008). Practice in design continued to evolve to improve the reinforcement details of columns and to design for plastic shear in the column. From this era, the criteria for design provided more details for the proportions of the components that would lead to ductile response in the columns, and elastic response in other parts of the bridge (Moehle, et al., 1995). After the 1989 Loma Prieta earthquake, Caltrans decided to ask the Applied Technology Council (ATC) to review and revise their design criteria. However, the results were not completed nor implemented at the time of the 1994 Northridge earthquake. As a result, very little changes were made to the code until after the 1994 Northridge earthquake occurred (Sahs, Veletzos, Panagiutou, & Restrepo, 2008).

Once the ATC completes its ATC-32 report for Caltrans, Caltrans incorporated nearly all of the recommendations made therein into its design code in 1996. Figure 1 shows how the seismic design spectra have changed throughout the years based on the code provisions (Moehle, et al., 1995). The new recommendations included a capacity design approach to ensure flexural failure in the column, which would be made possible by carefully designing the joints, column geometry, footing connection, among other things (Sahs, Veletzos, Panagiutou, & Restrepo, 2008).

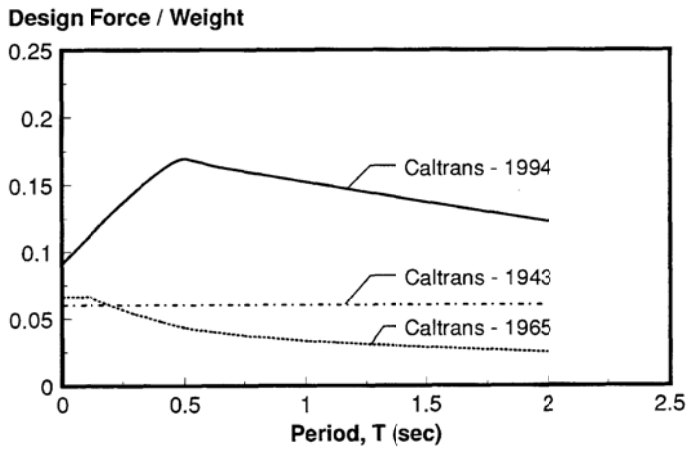

Figure 1: Caltrans design spectrum for a certain type of bridge(Moehle, et al., 1995).

Because the design concepts and codes were continually changing throughout the years, the design of structures and particularly bridges varied based on the period of design. Subsequently, each design period had its vulnerabilities to seismic forces (Sahs, Veletzos, Panagiutou, & Restrepo, 2008). In general, bridges built in California before 1971, had the following design details: column shear reinforcement of #4 at 12", short set width at expansion joints, inadequate lap splices and development of longitudinal reinforcement in the footing. The potential vulnerabilities in bridges designed during that period are column shear failure, column longitudinal reinforcement pull-out, and unseating of expansion hinges. The 1971 San Fernando earthquake resulted in a major change in the seismic codes, and thus the bridge designs. Bridges built between 1971 and 1994 had closer spacing and improved column shear detailing, column longitudinal splices prohibited at maximum moment locations, short seat widths at expansion joint hinges, poor flare detailing, and inadequate joint reinforcement. The possible vulnerabilities of bridges designed during this time that were not retrofitted are column shear failure of plastic hinge regions, shear failure of flared columns, and unseating of expansion joint hinges. Again, large earthquake events, the 1989 Loma Prieta and 1995 Northridge earthquakes in California, forced major changes in seismic design of bridges. For bridges designed after 1994, new design details included long seats widths at

expansion joints, improved flare column details, no lap splices in plastic hinge zones, shear reinforcement in footings, and joint reinforcement (Sahs, Veletzos, Panagiutou, & Restrepo, 2008).

2.2 Current Seismic Design Practice in CT SDC

The current seismic design code available for bridges is the Caltrans Seismic Design Criteria (SDC) version 1.6 released in 2010 (Caltrans, Seismic Design Criteria, 2010). The SDC specifies the minimum requirements for seismic design of bridges that go along with the performance goals for ordinary bridges. Within this document, it goes through the requirements for determining the demands and capacities of structural components, comparing the demand versus capacity, lists appropriate analysis methods of the structure, how to assess the seismicity of a site and the foundation performance, and details specifying design requirements to be met. Of particular interest to this project is the section dedicated to the design of the bridge. It has the requirements for frame design, superstructure, bent caps, joint design, bearings, columns and pier walls, foundations and abutments. The first requirements are that the frame is balanced in terms of stiffness, mass and geometry. The SDC gives recommendations to follow to ensure a balanced frame, which is intended to increase the chance of the structure responding in the fundamental mode of vibration. This type of response may reduce the chance of producing a nonlinear response that cannot be modeled accurately. Balancing the fundamental periods between frames is also meant to reduce the relative displacements due to out-of-phase movements (Caltrans, Seismic Design Criteria, 2010)

In the past, unseating of the deck from hinges or abutments was a source of major damage following large earthquake events. In the SDC, a minimum hinge seat width is specified as being greater than or equal to 24 inches to address that issue. The SDC lists equations used to determine the seat width of an internal hinge or abutment seat, which is based on thermal movement, prestressing effects, creep, and shrinkage in addition to

earthquake displacements. Hinge restrainers are installed as a backup component at hinges to prevent unseating, but there is no method for design of these components, only guidelines. Pipe seat extenders can replace hinge restrainers if they provide vertical support beyond the hinge seat width. They are designed to withstand the induced moments under single or double curvature.

The Caltrans SDC goes on to list additional specifications to ensure proper performance at all bridge components. For bent caps, a section describes requirements for integral and non-integral bent caps. A section for superstructure joint design gives equations to ensure proper performance and proportioning of joints, and different requirements for t-joints and knee joints, as well as proper detailing for bent caps and joints. For the design of columns, not many directives are given. A suggestion is given to control the ratio of the column dimension to the superstructure depth to between 0.7 and 1.0. The SDC also gives the analytical plastic hinge length for different column types. Details for column flares were, mainly stating care should be taken to avoid a flare design that would increase the seismic shear demand on the column. Other components addressed are bearings, foundation and pile performance, and abutment design.

As was demonstrated, current seismic design leaves little to be considered in terms of requirements for the capacity of many bridge components. Bridges designed today not only have to meet general bridge design requirements, but also have to make sure everything is designed to withstand an expected earthquake load. The flowcharts in Appendix A describe the steps that need to be taken to ensure a proper seismic design of a new bridge. The steps detailed in the flowchart are used by Caltrans design engineers to check the design of each bridge and ensure compliance with the SDC (Setberg, 2011). Each design check should be considered during the design process and after the design is complete. The design checks mostly deal with the relative stiffness of the structure, ductility of columns, and the structure displacement demand.

This section described the past and present bridge seismic design process along with important design checks to be employed during the design of the bridge. This process, however, does not provide the designer with critical information about specific performance of the bridge at a chosen design hazard level. It does not account for the uncertainty inherent in the capacity of the structure against collapse for a design event. Neither does the process produce the effects on that performance given a change in any design detail. Fragility analysis determines the probability of a structure or system experiencing a seismic demand exceeding the structural capacity defined by a limit state (Hwang, Liu, & Chiu, 2001). Fragility curves graphically show the performance of a bridge or bridge component at different ground shaking levels and at different damage levels. Thus, fragility analysis and fragility curves can be used to fill the gap of quantitative performance evaluation in the seismic design process. Later sections will describe how fragility can be used in the design process that will enable performance-based design decisions.

2.3 Use of Design Tool in Design Process

As described earlier, the current seismic design process in Caltrans is a prescriptive approach designed to ensure a no-collapse state after a Design Earthquake event. The procedure set forth in the SDC does not provide for any details on the anticipated performance or uncertainty attached to the performance of the bridge or its components at the Design Seismic Hazard or any other hazard level. The bridge specific design tool developed for this project does not aim to supersede the SDC, but to supplement it as a design check. After the bridge design is finalized using the SDC, this tool can be used to check that the design meets the criteria of no-collapse for a Design Earthquake set forth in the SDC. The design tool can also be used by a designer to quantify the effect of modifying aspects of the design on the response of the bridge. With

the design tool, a design engineer can input key design aspects of their bridge, and a fragility curve will be instantly created that is specific to that bridge.

Figure 2 shows a snapshot of this design tool developed in an Excel spreadsheet. As is shown, the design engineer inputs certain aspects of the design into appropriate cells, such as longitudinal steel ratio and other geometric properties of the bridge. The output of the tool includes fragility curves, specific fragility points at specified hazard levels, and an estimation of the fundamental period of the structure. System fragility curves as well as individual component fragility curves can be developed within the tool based on a fragility methodology described in a later section. Specific probabilities of failure can be displayed for any ground motion intensity level specified by the designer. The design tool can also receive upper and lower bound input for each design parameter to provide the user the option to produce fragility curves based on the original design parameters and on the upper and lower bounds of the design parameters in order to determine the effect of design decisions on the performance of the bridge.

This tool can be expanded to all types of bridge classes in California, and also to other structures where applicable. The results of this research are a primary step to determining the future of incorporating fragility analysis in the bridge seismic design process of Caltrans. This design support tool is an initial test of the concepts of bridge specific fragility as it relates to the design process used in Caltrans. The future of this concept will be based on the reception and feedback on the tool by Caltrans engineers. There are other possibilities with this methodology and tool, such as for retrofit designs, use in retrofit planning, and use in ShakeCast and other tools that require fragility analysis.

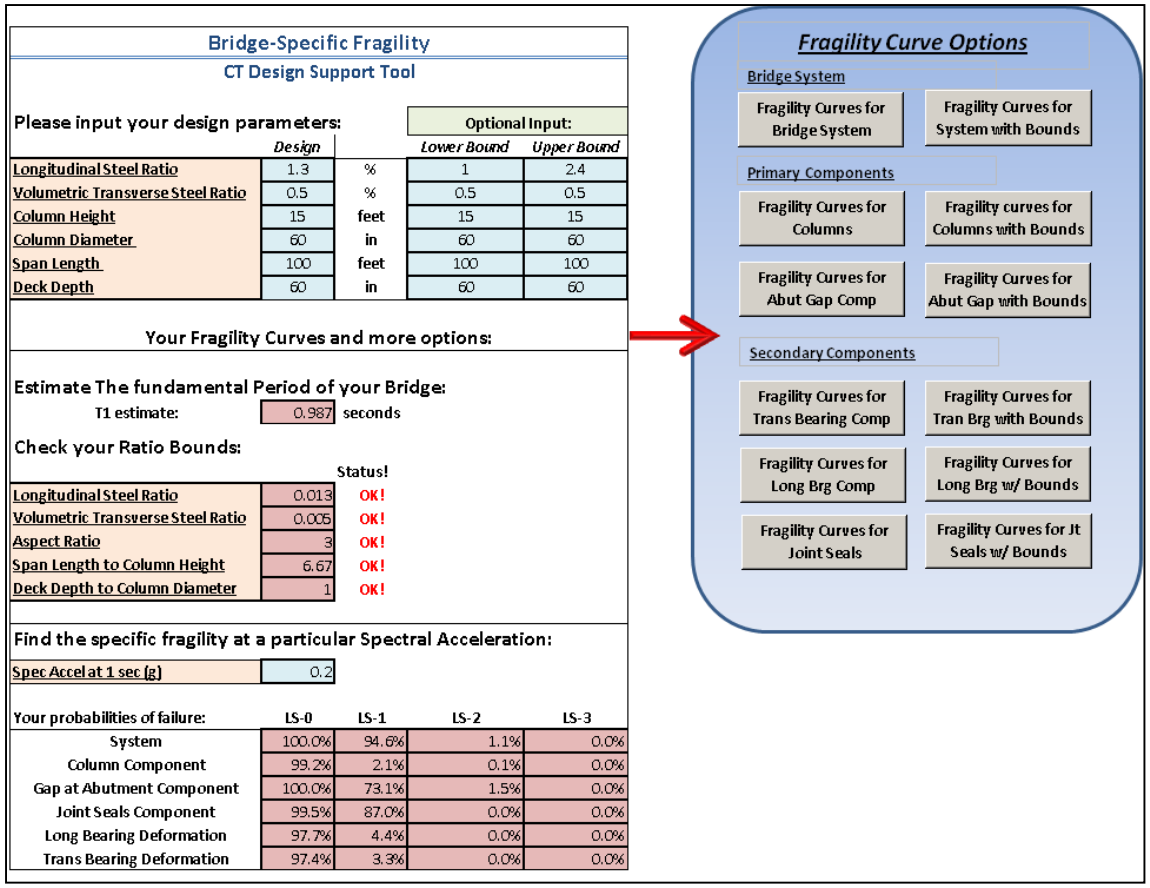

Figure 2: Illustration of design support tool format.

CHAPTER 3

TWO SPAN INTEGRAL CONCRETE BOX GIRDER BRIDGE

3.1 Inventory Analysis

The bridge type used to develop this first design tool is the multi-span continuous (MSC) concrete box girder bridge. According to an inventory analysis of the bridge classes in California, this bridge class is the most common in California, making up 21% of the state bridge inventory. A chart showing the bridge classes that comprise the California state bridge inventory is given in Figure 3. Further analysis of the inventory shows that most (~40%) of the MSC concrete box girder bridges have two spans, as shown in Figure 4. A bridge sample of modern (post year 2000) bridge plans revealed upwards of 70 bridges with these characteristics, which indicates that this bridge class is still being designed and constructed frequently in California. Based on this information, this bridge type was chosen to use as the bridge type on which to create this design tool and test the concept of bridge-specific fragility analysis in bridge design. In future versions of the design tool, additional bridge types could be included.

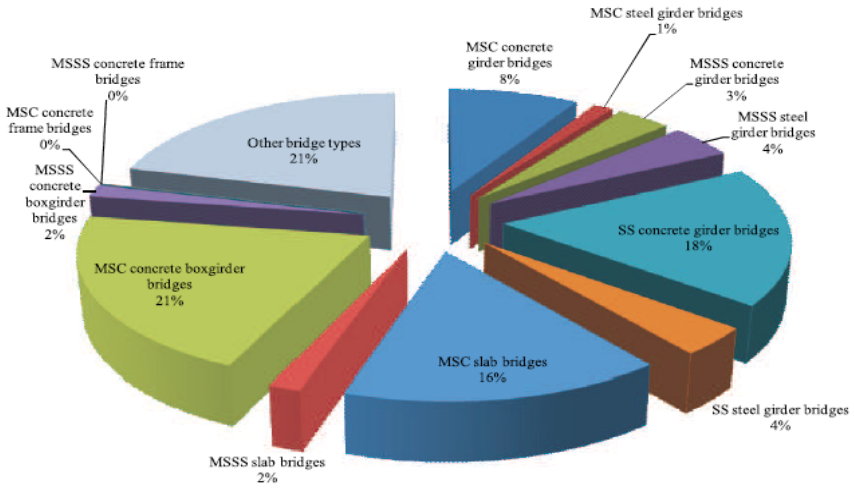

Figure 3: Pie Chart of California Bridge class inventory

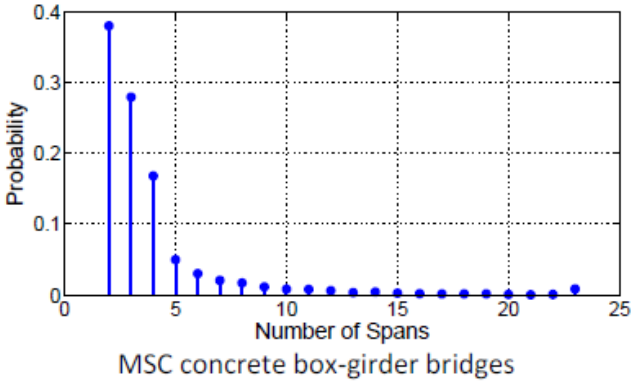

Figure 4: Statistics on the number of spans in box girder bridge class.

In addition to these characteristics, additional details about the bridge type were controlled for the purpose of developing this design tool. Figure 5 shows a typical configuration of the bridge type for which this version of the design tool was developed. A seat type abutment, which was present in the majority of sampled bridge plans, was assumed to be standard for this tool. A multi-column bent in the bridge is also a requirement to use this tool, meaning a bridge design with a single column or a pier wall would not be applicable for this version of the tool. The footings under the columns, as well as the abutments, were assumed to be supported on piles. The skew angle of the bridges was assumed to be zero, and the bridges are modeled as straight.

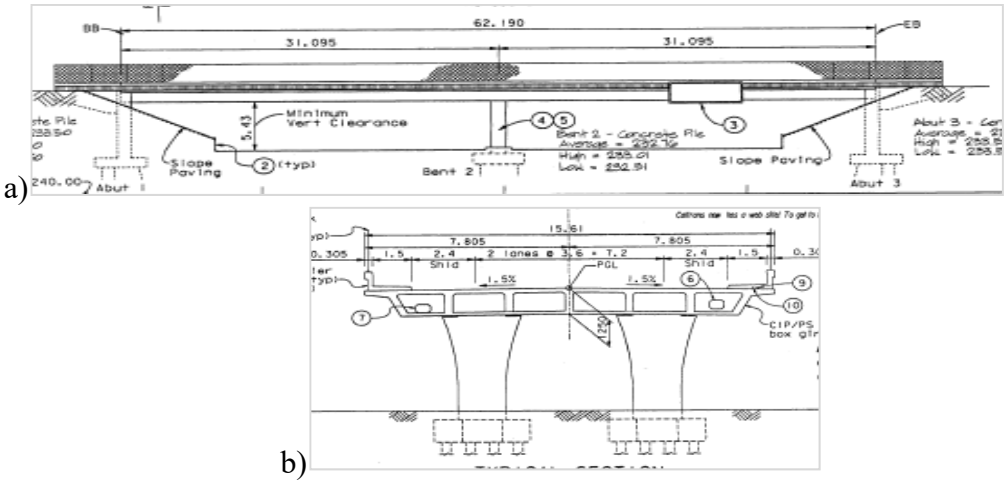

Figure 5: Typical configuration of two-span box girder bridge a) Elevation view, and b) Plan view.

3.2 Sample of Bridge Plans

Since this tool is developed for use with new bridge designs, information about recently built bridges in this class needed to be obtained. A sample of 40 bridge plans from the California state bridge inventory were compiled to gather important details and characteristics of the bridges to use in this project. All of the bridges sampled were constructed after the year 2000, since, for this project, this is considered to be the modern design era which would employ the current design practices in use in Caltrans. Other restrictions imposed when choosing bridge plans included a skew of less than 20 degrees, two spans, and multi-column bents.

These plans were analyzed and bridge data compiled for use in finite element bridge models developed for this project. Some of the properties of the bridges gathered from the bridge plans include span length, deck width, number of columns, column dimensions, reinforcement details, footing details, among others. For most of these properties, the minimum and maximum values from the sample were taken and used in the development of the finite element models in OpenSees. These properties and the ranges found from the analysis of the sample are listed later in the section. These properties were varied randomly in the development of the bridge models to create statistically similar yet distinct bridges within this bridge class. Creating bridges that in this manner addresses the differences found in the array of bridges in this bridge class as well as in the uncertainty in the capacity of the structures due to uncertain construction detailing, among other reasons (Luco, Ellingwood, Hamburger, Hooper, Kimball, & Kircher, 2007). Table 1 shows the properties that were varied randomly to create bridge models for this research. A few of the properties were determined to be key parameters in determining the response of a bridge under seismic loads. These design parameters will be discussed later.

3.3 OpenSees Model Details

Finite element bridge models needed to be constructed in order to analyze with a suite of ground motions to gather bridge response data to use for the bridge specific fragility design support tool. The Open System for Earthquake Engineering Simulation (OpenSees) is an open source software framework developed for use in earthquake engineering applications by the Pacific Earthquake Engineering Research Center (PEER). OpenSees is advanced in offering many different types of elements and nonlinear analysis to accommodate many structure and analysis types needed for research. This program was used to develop and analyze finite element bridge models used in this project.

Structure, component and material behavior of the bridges were carefully considered in the construction of the finite element bridge models in OpenSees. Figure 6 shows a typical layout of the nodes and elements that define the bridge model. Following are brief descriptions of the modeling materials and elements used in the creation of the bridge models.

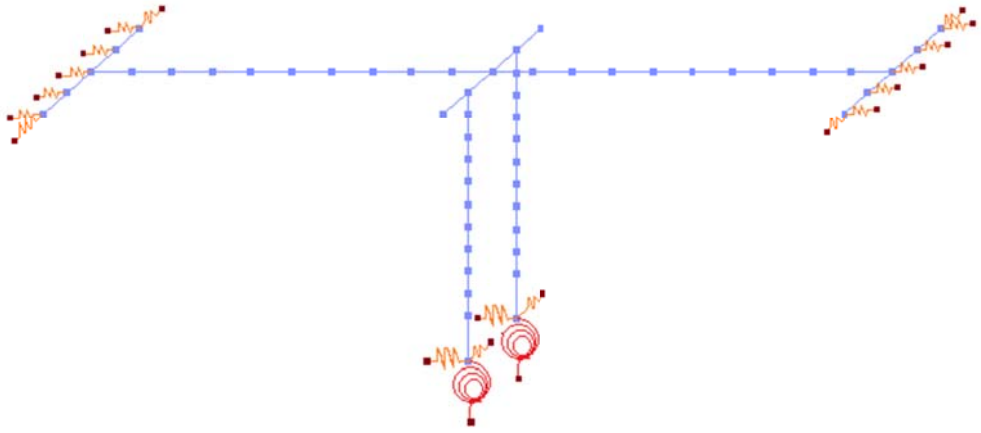

Figure 6: Typical layout of OpenSees models.

The columns of the bridge models were modeled using nonlinear beam column elements in OpenSees. The cross sections of the columns were defined with fiber material elements, as shown in Figure 7. The fiber elements allow the different properties of

unconfined and confined concrete to be specified, as well as the longitudinal steel properties. Properties of the unconfined and confined concrete strengths were derived from the theories of Mander et al. (1998), as shown in Figure 8.

The abutment behavior was characterized by the behavior of the supporting piles and the soil behind the backwall. The abutment piles were represented by nonlinear springs that behaved in a hysteretic manner in the longitudinal and transverse directions. The soil behind the abutment was represented by a hyperbolic gap material, developed by Shamsabadi et al. (Shamsabadi, Rollins, & Kapuskar, 2007). The behavior of the hyperbolic gap material is shown in Figure 9. The soil behavior is assumed only to engage in the passive longitudinal direction, while the piles act in the passive and active longitudinal direction as well as the transverse direction. The material is based off of the ultimate passive resistance and the stiffness of the soil (Mazzoni, McKenna, Scott, & Fenves, 2009). The average soil stiffness behind the abutment was randomly chosen as either 50 kip/in or 25 kip/in, which represents a granular soil or clay soil, respectively (Shamsabadi, Rollins, & Kapuskar, 2007).

The behavior of the pile cap and piles under the columns of the bridge are represented by linear elastic translational and rotational springs. The translational springs include the stiffness of the piles as well as the pile cap. The stiffness of the pile cap is fixed at 30 kip/in, and the median stiffness of the piles in the model were randomly chosen as either 65 kip/in or 80 kip/in, per the standard pile stiffnesses used in modern bridges (Roblee, Yashinsky, & Mahan, Bridge Specific Fragility Discussion, 2011). An illustration of these springs is shown in Figure 10. The rotational springs would be calculated based on the pile arrangement and size of the footing. However, since the bridges modeled here are all multi-column, the columns are assumed to behave as though pinned at the base. Therefore, for these models, the rotational springs were taken as negligible to simulate a pinned connection at the footings.

The deck was modeled as an elastic beam column element, as the deck is assumed to remain elastic during earthquake loading (Nielson & DesRoches, 2007). Impact elements were included to address the effect of the bridge deck pounding the abutment backwall. The element used to model this behavior is an elastic-plastic spring element. The elastomeric bearing pads that support the superstructure at the abutments will be modeled with translational bilinear spring elements in the transverse and longitudinal directions.

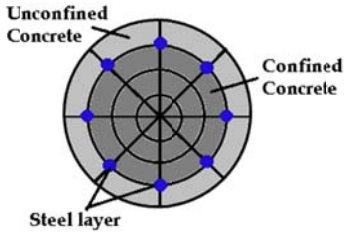

Figure 7: Fiber cross section of column element.

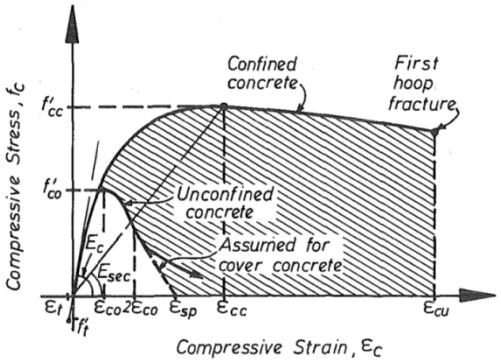

Figure 8: Stress-strain curve of confined and unconfined concrete (Mander, Priestley, & Park, 1988).

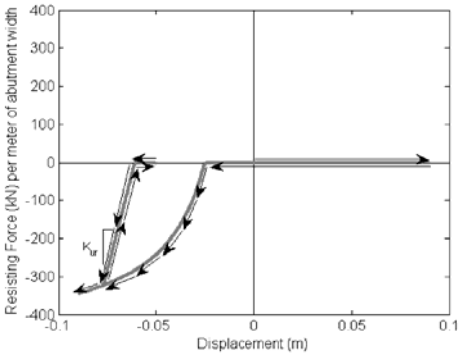

Figure 9: Hyperbolic gap material behavior (Mazzoni, McKenna, Scott, & Fenves, 2009).

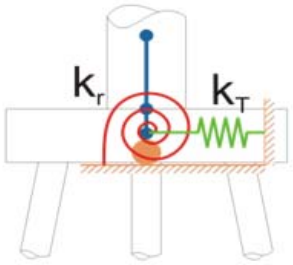

Figure 10: Illustration of foundation springs.

The bridge models that were developed for this project were parameterized to reflect the uncertainty in properties of the bridges. Distributions of geometric properties of the bridges, such as width of the deck and the number of foundation piles, were determined form an analysis of the sample of bridges described earlier. The distributions of some material properties, such as concrete and steel strength, are adopted from literature studies, while other parameters, such as the shear modulus of the bearing, were varied based on 50% and 150% bounds of the deterministic values of these parameters (Nielson & DesRoches, 2007). These uncertainty parameters are listed in Table 1. Bridge properties whose values were dependent on uncertainty parameters are listed in Table 2. These distributions were developed from the analysis of the bridge plan sample of modern bridges. Parameters that were fixed for all of the bridge models are listed in Table 3. Random samples of these parameters based on the assigned distributions combined to form analytical bridge models used in this study. Along with the design parameters that will be instrumental to the development of bridge specific fragility method (to be introduced later), a set of bridge models will be produced that will encompass the range of modern bridge designs that may be found in the inventory.

Table 1: Uncertainty parameters for parameterized bridge models

Uncertainty Parameters for Bridge Models			
	Distribution	**Parameter 1**	**Parameter 2**
Width of bridge (w)	Uniform	500 in	1600 in
Width of bent cap	Uniform	70 in	100 in
Concrete Strength	Normal	4.9 ksi	0.6 ksi
Steel Strength	Lognormal	4.27 ksi	0.072 ksi
Shear modulus of bearing	Uniform	0.1015 ksi	0.1668 ksi
Bearing pad coefficient of friction	Uniform	0.35	0.4
Pile Stiffness	Discrete Uniform	65 kip/in	80 kip/in
Number of foundation piles	Discrete Uniform	9, 12, 16	
Gap at abutment	Uniform	0 in	1.5 in
Soil Type	Discrete Uniform	1 (sand)	2(clay)
Abutment Backwall Height	Uniform	3.5 ft	8.5 ft
Angle of incidence of earthquake	Uniform	0	6.28

Table 2: Bridge properties that are dependent on Uncertainty Parameters

Property	**Values**
Number of girders	5, for w < 800 in 9, for 800 in < w < 1200 in 13, for w > 1200 in
Number of columns	2, for w < 800 in 3, for 800 in < w < 1200 in 4, for w > 1200 in
Number of abutment piles	Uniform between 12 and 24, for w < 800 in Uniform between 20 and 40, for 800 in < w < 1200 in Uniform between 30 and 80, for w > 1200 in
Soil Stiffness	50 kip/in for sand soil 25 kip/in for clay soil

w=width of the bridge

Table 3: Fixed parameters for parameterized bridge models

Fixed Properties of Bridge models	
Longitudinal Steel Bar size	#11
Transverse confinement Steel size	#6
Diameter of Column	60 in
Cover depth of concrete	2 in
Thickness of girders	12 in

CHAPTER 4

DESIGN PARAMETERS FOR USE IN BRIDGE SPECIFIC FRAGILITY METHOD

4.1 Design Parameters

The method of determining the bridge-specific fragility of a bridge design is based on incorporating the design aspects of the bridge into the method. The fragility methodology to be introduced in a later section requires design parameters as conditioning variables on the fragility equations and analysis. Thus, one need of this research is to find the design aspects which have the most effect on the responses of the different components of the two-span integral box girder bridge type. Certain details were identified as having a significant role in the design process as well as on the response of the bridge. This section will introduce these details, called design parameters, as well as the process used to determine whether these parameters in fact do affect the response of the two span integral box girder bridge type. The role of these parameters in the fragility methodology will be explained in a later section.

The bridge design parameters chosen correspond to characteristics of the geometry of a bridge were found to be important to monitor during the design process (Mackie & Stojadinović, 2005)(Caltrans, Seismic Design Criteria, 2010), significant in the evolution of seismic design of bridges (Sahs, Veletzos, Panagiutou, & Restrepo, 2008), as well as those suggested by the Caltrans team (Roblee, Yashinsky, & Mahan, 2011).The five design parameters chosen for research are longitudinal steel ratio of the columns, the volumetric ratio of transverse steel in the columns, the aspect ratio of the column height to column diameter, the ratio of superstructure depth to column diameter, and the ratio of span length to column height. All of these parameters have different

effects on the behavior and response of the bridge. Table 4 lists the design parameters used in this project and some of the effects on the behavior of a bridge. Illustrations of these characteristics are given in Figure 11. The validity of assuming these parameters have a significant impact on the response of the bridge was tested with a sensitivity study described in the next section.

Table 4: Description of design parameters used in this project.

Design Parameter	Symbol	Effect on Bridge Behavior
Longitudinal Steel Reinforcement Ratio of the Column	LS = ρ	A higher steel ratio stiffens and strengthens the column
Volumetric Ratio of Transverse Steel Reinforcement of the Column	VR = ρ_s	Determines the difference between unconfined and confined concrete strength, which determines the capacity of the component
Aspect Ratio – Column Height to Column Dimension Ratio	AR = H/D	Increasing this ratio makes the structure more flexible
Superstructure Depth to Column Dimension Ratio	DepthDiam = t/D	Increasing the depth makes the structure more stiff
Span length to column height ratio	SpanHt = L/H	Increasing the span length makes the structure more flexible

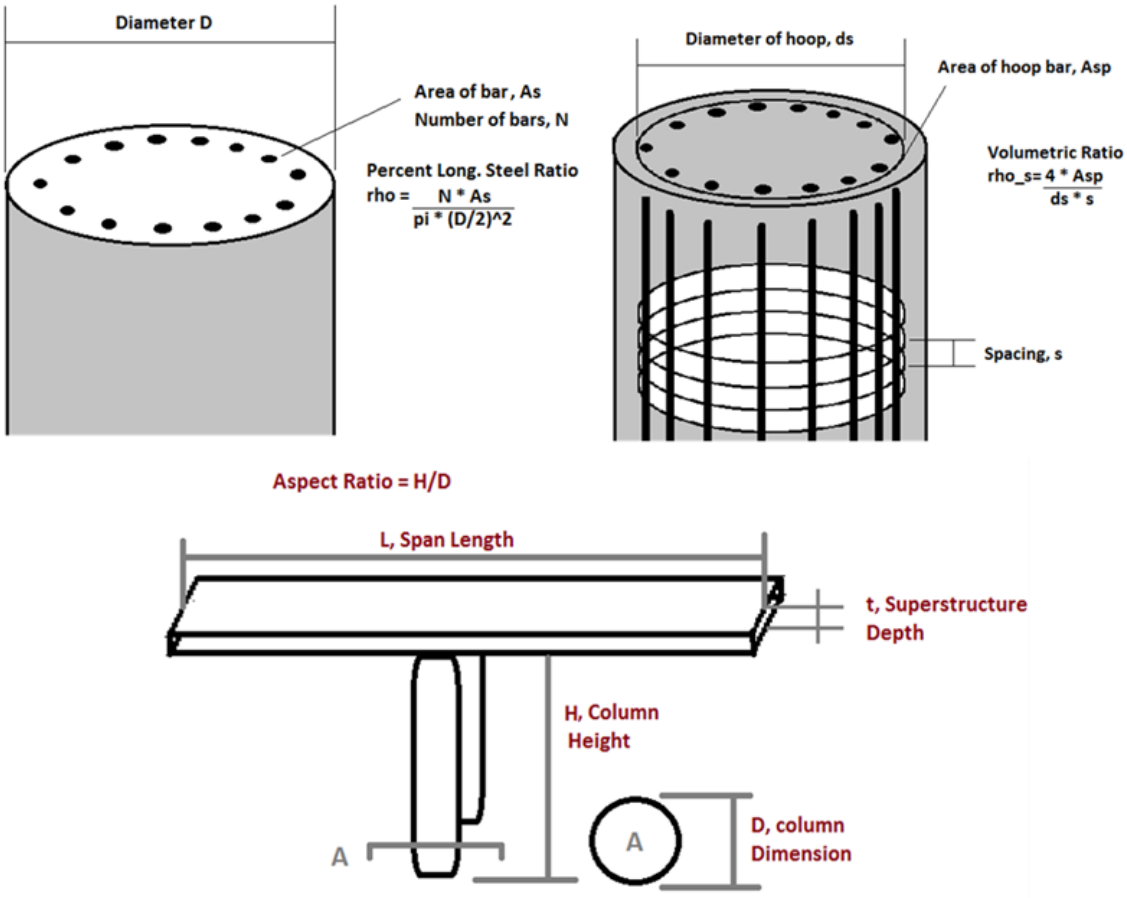

Figure 11: Illustration of design parameters.

From the bridge plan sample collected from the California state bridge inventory of this bridge type, information on the design parameters was gathered from each of the bridge plans. Histograms of the distributions of the parameters in the bridge plans are shown in Figure 12. The red brackets on the histograms indicate the cut off for the ranges to be used in the development of the bridge models, the process of which will be detailed later. The minimum and maximum values found in the sample of bridge plans, as well as the adjusted minimum and maximum values based on consideration of outliers in the data are given in Table 4. In constructing the demand model using an appropriate design of experiment (DOE), these values will be varied according to the DOE to create bridge

models that can be compared statistically. The creation of an appropriate DOE and construction of the demand model will be explained later. These ranges will also be used as upper and lower limits for the input parameters in the design tool, as the bridge models used to develop the tool were derived using these limits, so the tool would only be applicable for these ranges.

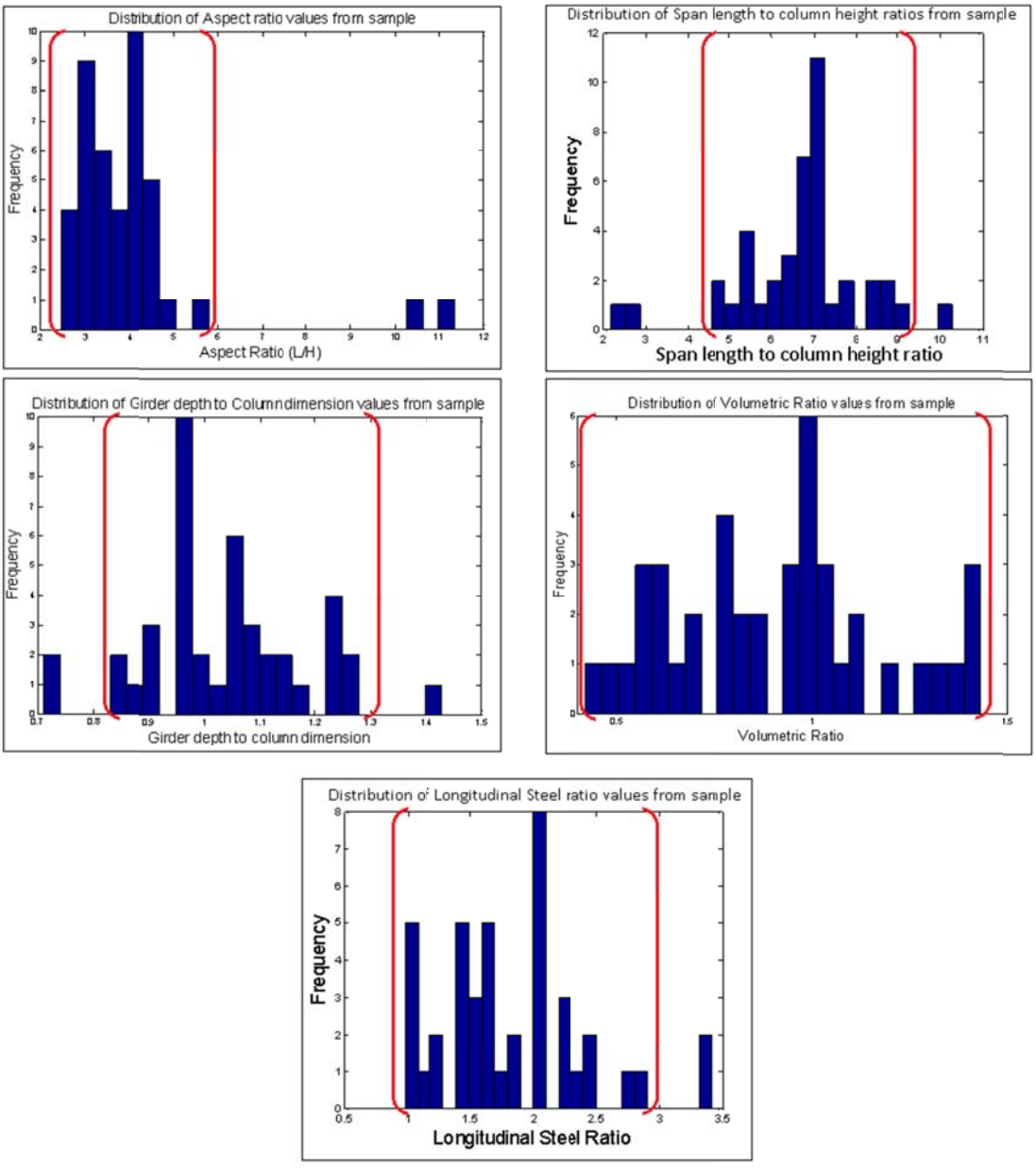

Figure 12: Histograms of the distributions of design parameters from bridge sample.

Table 5: Ranges of the design parameter values used in project

	AR	***LS***	***VR***	***SpanHt***	***DepthDiam***
Minimum	2.47	0.98%	0.42%	2.20	0.71
Maximum	11.35	3.41%	1.43%	10.29	1.43
Median	3.82	1.71%	0.93%	6.83	1.03
Adjusted Min*	**2.50**	**1.00%**	**0.50%**	**4.50**	**0.80**
Adjusted Max*	**6.00**	**3.00%**	**1.40%**	**9.50**	**1.30**

* Note: These adjusted values represent the actual ranges of the design parameters used in this research based on the limits shown in Figure 12.

4.2 Sensitivity Study of Design Parameters

A sensitivity study was completed to test the effects of varying the design parameters on the responses of key bridge components: column curvature ductility, longitudinal and transverse abutment movement and longitudinal and transverse bearing deformation. This investigation was a primary step finalizing the set of design parameters to be used in the bridge-specific fragility methodology. After the set of design parameters is defined, a multi-parameter fragility methodology can be implemented in order to produce individualized curves for a specific bridge design based on using the design parameters as conditioning variables in the fragility formulation. The five design parameters introduced earlier were varied in a statistical manner to create bridge models for analysis in order to quantify the effects of each parameter on the response of the bridge system and components.

The base bridge model from which all of the bridge models used in the study was built upon was based on median values of bridge characteristics, such as those listed in Table 1, excluding the defined design parameters. The base bridge is a two span integral concrete box girder bridge with zero skew or curve, two columns at the integral bent, and a seat-type abutment. Figure 5 depicted the plan and elevation views of a bridge similar to the base bridge from bridge plans.

The sensitivity study was designed as a confirmatory experiment, in which the factors investigated have been suggested to be significant in previous studies (Kutner, Nachtsheim, Neter, & Li, 2005). The factors in this case are the design parameters, and this experimental study will be used to confirm the importance of each factor in determining the response of different bridge components. A design of experiment (DOE) was developed in order to determine the effects of each individual factor, as well as interactions between them. A two-level fractional factorial design was chosen as the DOE of choice for this study. A two-level fractional factorial experiment looks at each factor at two levels, usually the upper and lower bound of the factor range, and instead of having a full factorial design of 2^k experiments, where k is the number of factors, a subset, or fraction, of that number of experiments is developed with little loss of information on the main effects of the factors (Kutner, Nachtsheim, Neter, & Li, 2005). Table 6 shows the schedule of factors that correspond to the values of the design parameters that will be used to create bridge models for this sensitivity study. A [-1] indicates the minimum value, and [1] indicates the maximum value. The upper and lower bounds given in Table 5 were used as the minimum and maximum values of each factor from the bridge sample.

Each of the bridge models developed for each run from the DOE described earlier was subjected to 30 ground motions chosen from a suite of 120 broadband earthquake ground motions from the Pacific Earthquake Engineering Research Center (PEER) Transportation Research Program ground motions compiled by Baker, et al. (Baker, Lin, Shahi, & Jayaram, 2011) . Further details of this ground motions suite, which is used in its entirety for the development of the design tool, will be discussed later. These 30 ground motions were chosen randomly from the 120 ground motions to ensure a variety of responses of the bridge models from each of the runs developed from the DOE. The peak ground acceleration (PGA) and spectral acceleration at 1 second values of these 30 chosen ground motions are shown in Figure 13. As is shown, the ground motion set

encompassed a wide range of ground motion intensity levels, ranging from less than 0.05g to 0.8g in terms of PGA.

Table 6: Design of experiment for sensitivity study

Run	LS	VR	AR	SpanHt	DepthDiam
1	1	-1	-1	1	1
2	-1	1	-1	1	1
3	-1	1	-1	-1	-1
4	1	-1	1	1	-1
5	-1	-1	1	-1	-1
6	1	1	-1	1	-1
7	-1	-1	1	1	1
8	1	1	1	-1	-1
9	-1	-1	-1	-1	1
10	1	-1	1	-1	1
11	1	1	1	1	1
12	1	-1	-1	-1	-1
13	-1	1	1	-1	1
14	-1	1	1	1	-1
15	-1	-1	-1	1	-1
16	1	1	-1	-1	1

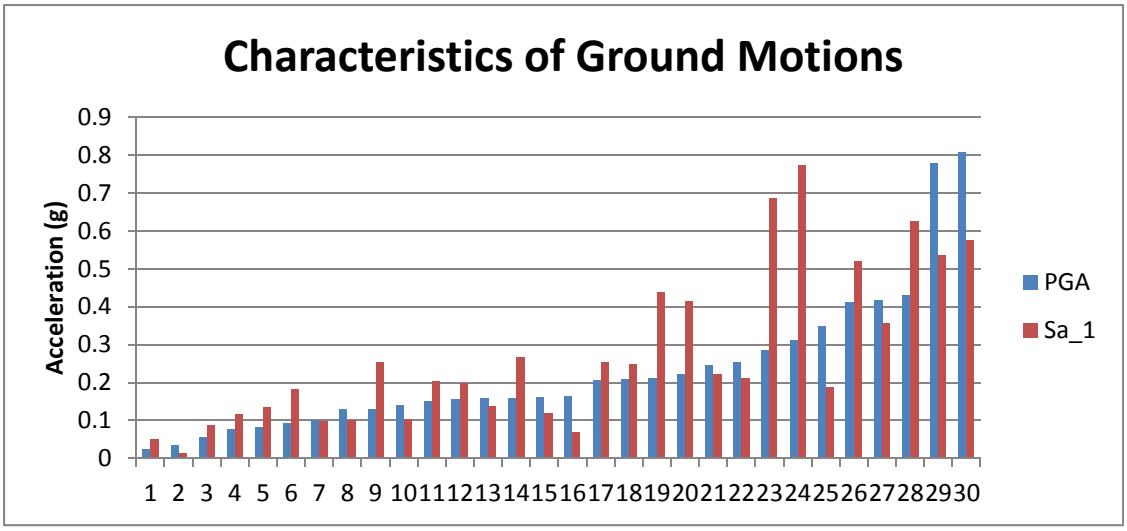

Figure 13: PGA and Sa_1 values of ground motions used in sensitivity study.

Finite element bridge models were created and analyzed in OpenSees (Mazzoni, McKenna, Scott, & Fenves, 2009). Figure 6 showed a typical layout of the nodes and elements that define the bridge model. These bridge models were analyzed using nonlinear time history analyses. Each model was subjected to two orthogonal ground motions at an incidence angle of zero input into the defined support nodes. Recorders defined in OpenSees recorded the deformation, displacement, force or stress specified at particular elements or nodes along the bridge in order to find the response of the bridge system after the analysis. These recorded responses serve as the data used to determine the effect of the design parameters on the response of the bridge.

4.3 Results of Sensitivity Study

After all of the analyses were run in OpenSees, the recorded responses of the different bridge parameters were extracted to be used to determine the effect of the different design parameters on the component responses. The different component responses were then regressed against the design parameters to determine the significance of the parameters on the responses. JMP software was used to conduct Analysis of Variance (ANOVA) tests on the data from the analyses, which are presented in this section (JMP the Statistical Discovery Software, 2010).

In conducting ANOVA tests, a hypothesis is considered and tested using the F-test (Kutner, Nachtsheim, Neter, & Li, 2005). In this case, the null hypothesis (H_0) is that the coefficient (β_1) of a regression relationship between a component response (Y) and a design parameter (X) (see Eqn. 2) is equal to zero, and therefore there is no regression relation between the response variable and the design parameter. The hypothesis tests and F statistic is computed per Eqn. 3 for a single variable regression (Kutner, Nachtsheim, Neter, & Li, 2005). MSR is the mean regression sum of squares, MSE is the mean squared error of the regression, and [n-2] represents the number of degrees of freedom in the relationship. For this study, α is assumed to be equal to 0.05, which is a typical value

used to test statistical significance. P-values are the probability of the calculated F statistic being greater than the (1- α)100 percentile of the F distribution.

$$Y = \beta_0 + \beta_1 * X \tag{2}$$

$$H_0 : \beta_1 = 0$$
$$H_a : \beta_1 \neq 0$$
$$F^* = MSR/MSE$$
$$\text{If } F^* \leq F(1-\alpha;\ 1,n-2), \text{ conclude } H_0$$
$$\text{If } F^* > F(1-\alpha;\ 1,n-2), \text{ conclude } H_a \tag{3}$$

Table 7 shows the p-values from the ANOVA analysis of six different bridge component responses for each design parameter. Statistical significance in an ANOVA test is determined by the value of the p-value; if the p-value is less than the predetermined α level, then it shows that the factor being tested has a statistically significant effect on the response quantity according to the test. In this case, the p-value is the probability that $F^* > F(1-\alpha;\ 1,n-2)$ as defined in Eqn. 2. As shown, every design parameter was found to be statistically significant in the prediction of one or more of the bridge component responses according to the ANOVA test and an α level of 0.05. The longitudinal steel ratio is significant in predicting column behavior, active and transverse abutment responses, and longitudinal bearing deformation. The transverse reinforcement ratio was found to be significant in predicting the passive and transverse abutment responses. The aspect ratio was significant for column behavior, active and passive abutment responses, and longitudinal bearing response. The span length to column height ratio was found to be significant in predicting the passive and transverse abutment responses, and longitudinal bearing response. The depth to diameter ratio was significant in the cases of column behavior and all abutment responses. As a result of this sensitivity study, it was determined that these five design parameters could be used in further research of developing bridge-specific fragility curves. The process of incorporating these parameters

into fragility analysis as well as using them to create bridge specific fragility curves will be detailed in the next sections.

Table 7: P-values of the design parameters from ANOVA analysis

Parameter	Column Curvature Ductility	Active Abutment Movement	Passive Abutment Movement	Transverse Abutment Movement	Longitudinal Bearing Deformation	Transverse Bearing Deformation
LS	**0.0018**	**0.0498**	0.2277	**0.0004**	**0.0283**	0.0605
VR	0.3149	0.3283	**0.0032**	0.0539	0.6281	0.7479
AR	**0.0001**	**0.0001**	**0.0001**	0.561	**0.0001**	0.2354
SpanHt	0.665	**0.0103**	**0.0001**	**0.0019**	**0.0063**	0.089
DepthDiam	**0.0426**	**0.0326**	**0.0001**	**0.0116**	0.9123	0.8416

CHAPTER 5

FRAGILITY ANALYSIS AND METHODS

5.1 Background of Fragility Analysis and Methods

Bridge seismic fragility curves are statistical functions that give the probability of exceeding a certain damage level or damage state as a function of a ground motion intensity measure. The fragility function can be written as $P[DS_i \mid IM=y\ ]$, where IM=y stands for a ground motion intensity measure taking a particular value, and DS_i is the exceedance of the damage state in question. Fragility curves are tools used to assess and mitigate the effects of earthquake ground motions on structures, and their popularity was motivated by the development of earthquake loss models (Calvi, Pinho, Magenes, Bommer, Restrepo-Velez, & and Crowley, 2006). Earthquake loss models were developed in response to the increasing losses in urban areas caused by earthquakes. One of the components of the loss model is the methodology to assess the vulnerability, or fragility, of a structure. The first seismic vulnerability assessment came in the 1970s in the form of damage probability matrices (DPM), developed using empirical methods that used past earthquake damage data. A DPM, shown in Table 8, displays the probability of a structure reaching or exceeding a damage state given a ground motion intensity, usually the Modified Mercalli Intensity (Cimellaro, Reinhorn, Bruneau, & and Rutenburg, 2006). Vulnerability curves, which came later, are very similar to DPMs. However they display the cumulative distribution of the probability of exceeding a damage state given a more continuous ground motion intensity measure, such as peak ground acceleration (Cimellaro, Reinhorn, Bruneau, & and Rutenburg, 2006)(Calvi, Pinho, Magenes, Bommer, Restrepo-Velez, & and Crowley, 2006). Many of the first fragility assessments were developed for nuclear power plant equipment and components because of the sensitivity of those structures to ground motions and the need for the contents to be

protected from damage (Bandyopadhyay & Hofmayer, 1985)(Bandyopadhyay & Hofmayer, 1986). Today, more research has been done to create additional fragility methodologies and analysis types and to analyze many different structures, including bridges.

Table 8: Damage Probability Matrix (Cimellaro, Reinhorn, Bruneau, & and Rutenburg, 2006)

Limit State	Modified Mercalli Intensity						
	VI	VII	VIII	IX	X	XI	XII
NONE	20.4						
SLIGHT	70.3	15.5					
LIGHT	9.3	84.5	88.4	28.9	1.4		
MODERATE			11.6	71.1	81.6	38.7	3.8
HEAVY					17.0	61.3	88.7
MAJOR							7.5
DESTROYED	--						

Applications of fragility curves include aiding in emergency response optimization, design support for performance-based engineering, planning support for seismic events, and policy support. The current damage states used in most fragility curves refer to the state or condition of a bridge following an earthquake event. States such as “Moderate” or “Complete” damage are an indication of the capacity that may be left in the bridge or bridge component. Figure 14 below depicts a fragility curve at the four HAZUS damage levels (FEMA, 2003). The particular damage states considered in this project will be discussed later in this chapter.

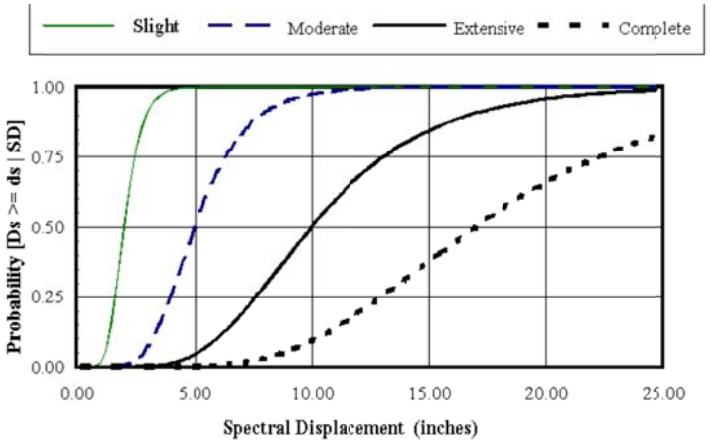

Figure 14: Fragility curves in HAZUS damage levels (FEMA, 2003).

There are four main approaches to developing fragility curves, which are based on the origins of the damage data used in the generation of the curve. Empirical fragility curves use observed damage data from past earthquakes to determine the probability of damage to a structure. Judgmental fragility curves use the opinions of experts to determine the damage an earthquake ground motion would cause to a structure at a certain damage level. Analytical fragility curves use simulations of structural models to develop damage distributions based on a comprehensive analysis of the structure. Hybrid fragility curves combine data from different sources to create damage states (Jeong & Elnashai, 2007).

5.2 Bridge Specific Fragility Framework

The fragility methodology used in this research project is a type of analytical fragility process rooted in a simulation based approach. Analytical bridge models will be analyzed with time history analyses using the Baker et al. ground motion suite (Baker, Lin, Shahi, & Jayaram, 2011), a suite of ground motions that is applicable to a range of sites and structural properties. Because this method uses bridge models and a suite of ground motions instead of damage data from past earthquake events, uncertainty in the results have to be considered and mitigated throughout the entire process. The risk due to

uncertainty must be mitigated and kept within acceptable levels, as all uncertainty is impossible to eliminate. For a structural system analyzed under earthquake loads, uncertainty comes from the demand and capacity of the analysis (Ji, Elnashai, & Kuchma, 2007). The uncertainties from the demand on a system can come from the ground excitation, which includes the soil conditions, load path of the motions, and the random motions generated from the source of the earthquake. The uncertainty from the capacity of the system can emanate from the material and geometric uncertainty, where the properties of the designed structure and materials are considered random for the built structure. Although the variability of the response of the system is much more susceptible to the ground motion variability than the material uncertainties (Kwon & Elnashai, 2006), variations in the bridge geometry and material properties will be included in the analyses. This inclusion will contribute to variability in the response in addition to the chosen ground motions suite. Once the analyses are done on the bridge models using the suite of ground motions, the responses of each bridge component are collected, and analysis on that data can be performed using the new fragility method of this report. A graphical overview of the typical analytical method is given in Figure 15. With regard to the new fragility method used in this report, some details about the fragility method will change, like the probabilistic seismic demand model, but the process is generally the same. A more detailed description of the fragility methodology will be detailed in subsequent sections.

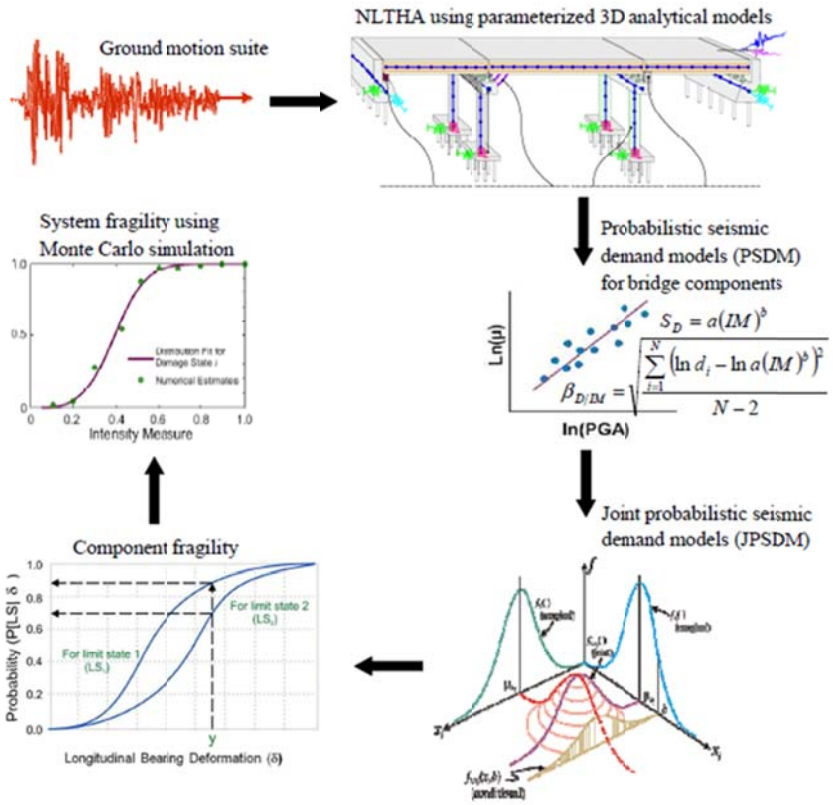

Figure 15: Illustration of the analytical fragility analysis method.

5.3 Limit States in Fragility Analysis

Damage states in fragility analysis are levels of damage that a bridge system or component might experience during seismic loading. Figure 16 shows levels of damage a bridge column might undergo based on field observations after an earthquake event (Shinozuka, Feng, Kim, Uzamwa, & Ueda, 2003). Also called limit states, damage states are an important part of the capacity model used to develop fragility curves. Often, limit states are defined as discrete threshold quantities of a component response that corresponds to a physical damage condition (Mackie & Stojadinović, 2005).

Damage State / Damage Mode	As	A	B	C	D
1. Bending Damage at ground level (This mode ultimately produces buckling of rebar, spalling and crushing of core concrete)	Damage through entire cross-section 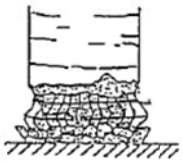	Damage mainly at two opposite sides 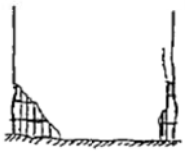	Damage mainly at one side 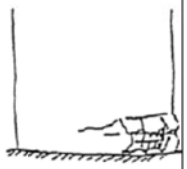	Light cracking and partial spalling 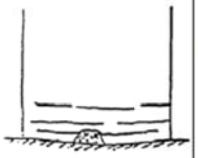	No Damage

Figure 16: Description of States of Damage for Hanshin Expressway Corporation's Bridge Columns (Shinozuka, Feng, Kim, Uzamwa, & Ueda, 2003)

The damage states used in fragility curves have traditionally been the following four levels: Slight, Moderate, Extensive, and Complete (Table 9)(Choi, Nielson, & DesRoches, 2004). The (N) damage level is usually not included in fragility analysis. These four categories apply to a particular component of the bridge being analyzed, such as the columns, footings, and abutments. Many fragility curves have focused on the response of one component, such as the drift of a column, to indicate the state of a bridge after an earthquake event. However, the responses of other major bridge components have emerged as significant elements in determining the fragility curve for the entire bridge (Nielson & DesRoches, 2007);(Padgett & DesRoches, 2008)(Shinozuka, Banerjee, & Kim, 2007). While including the effects of other component states on the bridge functionality is important, finding equivalent measures of loss due to damage between components is a challenge. For example, extensive damage in a column of a bridge may lead to a longer bridge closure and more repair costs than extensive damage in a bearing. This challenge is addressed later in this section with the discussion of Caltrans-aligned limit states.

Table 9: Damage States Commonly Used from Hazus (FEMA, 1997)

Damage States	Description
(N) – No Damage	No damage to a Bridge
(S) – Slight Damage	Minor cracking/spalling to abutment, cracks at hinges, minor spalling at column, or minor cracking to the deck
(M) – Moderate Damage	Moderate cracking and spalling at column, moderate settlement of approach, cracked shear keys or bent bolts at connection
(E) – Extensive Damage	Degraded column without collapse, some lost bearing support in connection, major settlement of approach
(C) - Complete Damage	Collapsed column, all bearing support lost in a connection, imminent deck collapse

To determine the damage level of a particular component, quantitative assessments may be in place for each component being inspected. For columns, it could be displacement or rotational ductility. For bearings, damage may be assessed by measuring the displacement of the bearing or deck from its original position. Often, the engineer must rely on his or her judgment to visually inspect the components and relate a damage level based on experience and the description above. Therefore, if a bridge were inspected by different engineers, the results of the inspection and corresponding damage states may vary. Quantitative damage states directly affect fragility analysis, as they are used as the basis of the capacity model. Uniform damage states that are used for fragility analysis, particularly for specific regions of the country where bridge types and hazard levels are similar, could allow for uniformity and more confidence in the use of the resulting fragility curves.

5.4 Caltrans-aligned Limit States

As the fragility methodology presented here involves multiple components, one objective of the project is to compile compatible limit states that were specific to Caltrans bridge inventory. Compatibility was needed in terms of similar damage and downtime consequences after an earthquake event. As this was not available in current literature, expert opinions from Caltrans design engineers and maintenance personnel combined

with experimental test data of components were used to develop Caltrans specific limit states (Roblee, et al., 2011). Individual component damage thresholds and a method to determine the overall bridge system state based on primary and secondary component damage states were developed. One of the goals of developing this new damage state definition was to coordinate what inspectors see in the field with what engineers see in their analysis. Figure 17 shows the component damage threshold (CDT) continuum. As is shown, every time a damage threshold is crossed, the component is expected to have a different level of visible damage, and thus a different repair strategy. Figure 18 describes the Caltrans-specific bridge limit state definition framework. The bridge damage states are closely tied with the ShakeCast inspection priority levels. This makes it easier to relate inspection criteria with engineering performance expectations. The chart also equates bridge damage states with traffic implications. Using the component continuum and bridge system damage states, the project team determined appropriate damage levels using engineering demand parameters that would be easily monitored during an analysis of a bridge model.

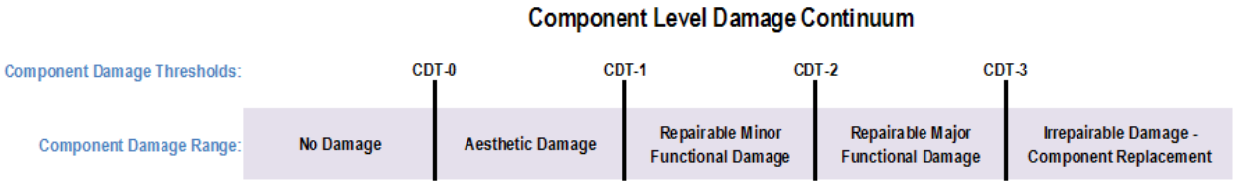

Figure 17: Caltrans component level damage continuum.

		BSST-0	BSST-1	BSST-2	BSST-3
ShakeCast Inspection Priority Levels	None[1]	Low	Medium	Medium-High	High
Bridge System States[2] ("Inspecting for possible ...")	BSS-0 No Bridge Damage	BSS-1 Slight Bridge Damage	BSS-2 Moderate Bridge Damage	BSS-3 Extensive Bridge Damage	BSS-4 Complete Bridge Damage
Component Damage Range[3]					
Primary Components[4]	Below CDT-0	CDT-0 to CDT-1	CDT-1 to CDT-2	CDT-2 to CDT-3	Above CDT-3
Secondary Components[5]	Below CDT-0	CDT-0 to CDT-2	Above CDT-2	na	na
Likely Immediate Post-Event Traffic State	Open to Normal Public Traffic - No Restrictions	Open to Normal Public Traffic - No Restrictions	Open to Limited Public Traffic - Speed/Weight/Lane Restrictions	Emergency Vehicles Only - Speed/Weight/Lane Restrictions	Closed (Until Shored/Braced) - Potential for Collapse
Traffic Operations Implications[6]					
Closure/Detour Needed?	Very Unlikely	Very Unlikely	Unlikely	Likely	Very Likely
Traffic Restrictions Needed?	Very Unlikely	Unlikely	Likely	Very Likely	Very Likely - Detour
Emergency Repairs Implications[6]					
Shoring/Bracing Needed?	Very Unlikely	Very Unlikely	Unlikely	Likely	Very Likely
Roadway Leveling Needed?	Very Unlikely	Unlikely	Likely	Very Likely	Very Likely - Detour

Figure 18: Caltrans bridge system damage states.

To relate bridge system performance with component performance, components are categorized into primary and secondary components. Primary components are those that create the risk of causing the bridge to collapse if they fail, indicated by surpassing the CDT-3 threshold. In conjunction with Caltrans engineers and bridge inspectors, two primary components were identified: columns and hinge openings (Roblee, et al., 2011). The failure of either of these components during an earthquake would likely lead to the collapse or inoperability of the bridge. Secondary components are defined as those components that affect the performance of the bridge following an earthquake event, but will not cause the bridge to collapse even at the highest component damage threshold. For this bridge type, that includes the displacement of the joint seals and the bearing displacement. The project team determined that bridges in the state inventory could have components with different properties based on the year that it was designed (Sahs, Veletzos, Panagiutou, & Restrepo, 2008). Thus, there are several performance groups for each component. For example, under the column component, the different performance groups include a brittle column, strength degrading column, and ductile column. As the focus in this research is on newly designed bridges, only the performance groups associated with the latest design standards are considered for the limit states. In Table 10, the primary and secondary components used for the capacity model for this bridge-specific project along with the engineering demand parameter (EDP) of the components used and the CDT values are listed.

Table 10: Primary and secondary component and corresponding limit states.

	EDP* for CDT's	CDT-0	CDT-1	CDT-2	CDT-3	Lognormal Dispersion
Primary Components						
Ductile Column	Curveature Ductility (μφ)	1	4	8	12	0.35
Hinge opening, >24" seat joint at abutment, small gap	Joint displ (in)	1	3	14	21	0.35
Secondary Components						
Sealed Joints, type B	Joint displ (in)	1	n/a	n/a	n/a	0.35
Elastomeric Bearings	Joint displ (in)	1	n/a	4	n/a	0.35

5.5 Ground Motion Suite Used in Fragility Analysis

In developing analytical fragility analysis, the importance of selecting the appropriate ground motions is paramount (Kwon & Elnashai, 2006). The characteristics of the input ground motion suite affects the outcome of fragility curves more than material variability or even limit state definition (Padgett & DesRoches, 2008). Therefore, significant consideration is needed when selecting ground motions. Having variety in the characteristics of ground motions, such as frequency content, phase, and duration, is important as the structural response of a bridge can differ even between ground motions that have similar peak ground acceleration or peak ground velocity values (Karim & Yamazaki, 2001). When analyzing bridges, it is also important to choose ground motions applicable to the site location in which the bridge may be designed.

For this project, Caltrans has chosen to adopt the Pacific Earthquake Engineering Research Center (PEER) Transportation Research Program ground motions developed by Baker, et al. (2011). Their work focused on providing a new selection procedure that allows for better matching of target response spectra quantities, as well as providing a standardized ground motion set that was applicable to many scenarios throughout California. These motions were not developed as structure-specific or site-specific, and

so are applicable to many research needs and can be tailored to fit individual user needs through pre-processing (i.e. scaling of motions) or post-processing (i.e. finding regression relationships between response of models and ground motion measure) of the ground motion characteristics (Baker, Lin, Shahi, & Jayaram, 2011). The suite is divided into 4 sets, which is shown in Table 11.

Each set has 40 unscaled ground motions selected from the PEER Next Generation Attenuation (NGA) project database (Chiou, Darragh, Gregor, & Silva, 2008) to match the terms of the set. All 160 ground motions will be used unscaled as well as scaled by a factor of 2 in the final analyses for this project, as variability in ground motion characteristics was determined to be needed to account for the unknown site locations of designed bridges (Roblee, Yashinsky, & Mahan, 2011). The total number of ground motions used in the analysis of the bride models was 320. Response spectra are shown for Sets 1a, 1b, and 2, and a histogram of peak ground velocities is shown for Set 3 in Figure 19 and Figure 20.

Table 11: Characteristics of ground motions in PEER ground motion suite.

Set 1a	Broad-band motions, Magnitude 7, R=10 km, Soil site (V_{s30} = 250 m/s)
Set 1b	Broad-band motions, Magnitude 6, R=25 km, Soil site (V_{s30} = 250 m/s)
Set 2	Broad-band motions, Magnitude 7, R=10 km, Rock site (V_{s30} = 760 m/s)
Set 3	Pulse-like motions (strong velocity pulses in strike-normal direction)

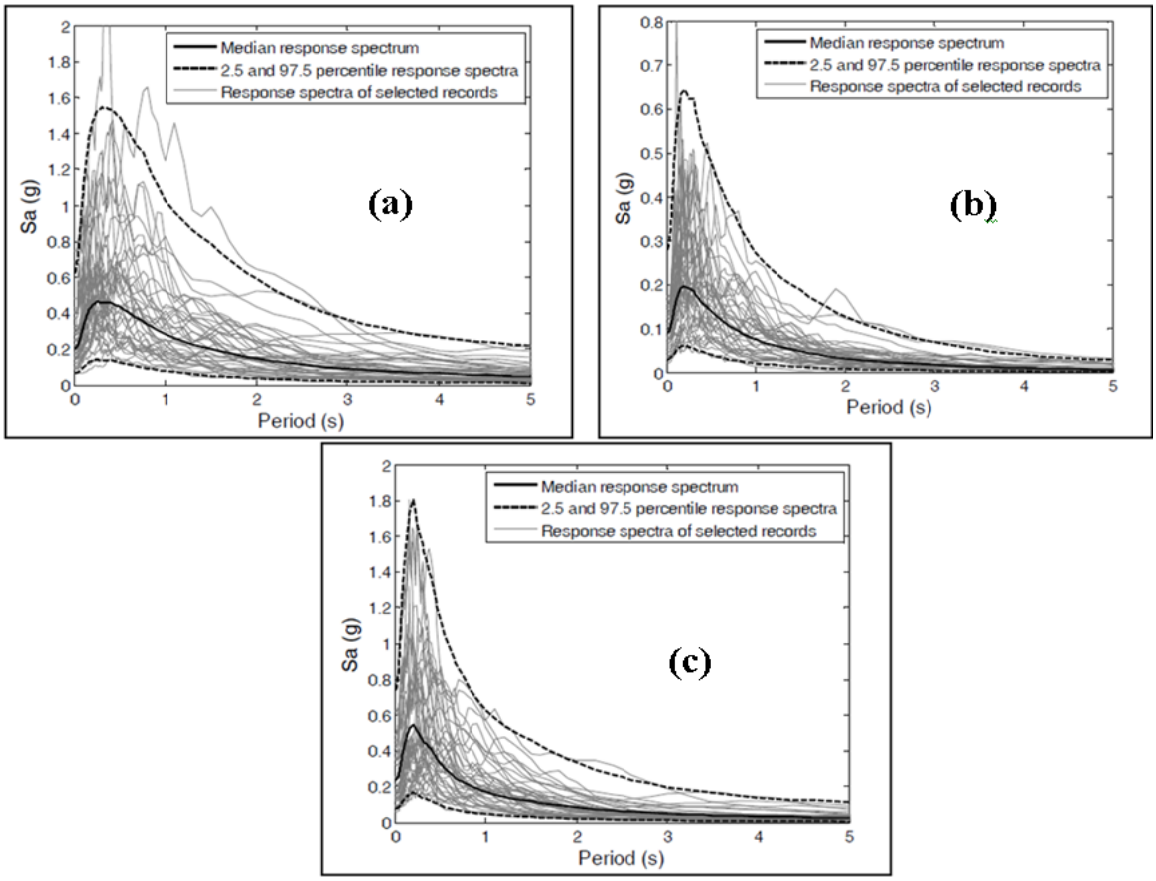

Figure 19: Response spectra for ground motions in sets (a)1a, (b) 1b, and (c) 2. **(Baker, Lin, Shahi, & Jayaram, 2011)**

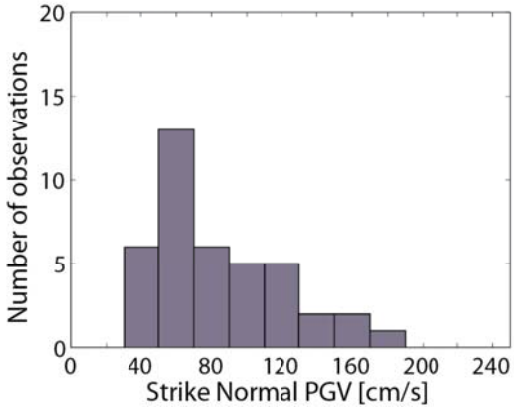

Figure 20: Peak ground velocities for ground motions in set 3 (Baker, Lin, Shahi, & Jayaram, 2011)

CHAPTER 6

BRIDGE SPECIFIC FRAGILITY AND DESIGN SUPPORT TOOL

One of the main outcomes of this Caltrans research project is the implementation of a design support tool that utilizes bridge-specific fragility analysis. This tool is meant to be used by Caltrans design engineers as a part of their final design check and an exploration on the effects of design parameters on the response of the bridge. With this tool, an engineer can determine if their design meets the criteria set by the SDC and criteria established for the particular project based on analytical fragility analysis. To develop this tool for applicability to specific bridges in consideration, a fragility method needed to be developed that could produce fragility curves that are specific to the design bridge, as opposed to fragility curves developed for a general class of bridges which is typical for regional risk assessment or loss estimation. Current methods of developing fragility curves involve creating probabilistic seismic demand models (PSDM) that establish a two-parameter lognormal relationship between a component response quantity and a ground motion intensity measure. In order to use that method for the bridge-specific needs of this tool, fragility curves would have to be developed for every possible configuration of the bridge type of this study. That would require a prohibitive amount of analyses; therefore, a different method of developing fragility must be used. More parameters relating to the specific bridge must be included in the PSDM of the new fragility method. In this chapter, such a demand model is presented to be used for this support tool, as well as the new method of developing fragility curves, which is an expansion of the method proposed by Ghosh, et al. (2012). Finally, the bridge specific design tool is detailed, and an example of the use of the tool is given.

6.1 Introduction to Metamodels

A metamodel is a "model of a model" (Simpson, Peplinski, Koch, & and Allen, 2001). It is a statistical technique used to replace computationally expensive simulations with an approximation to the analysis. The metamodel represents or approximates the true nature of a computer analysis by estimating the response due to certain input variables with a closed form solution (Towashiraporn, 2004) . In equations 4a, 4b, and 4c, the true relationship, the model of a model (metamodel), and the true model with an error term are presented, respectively. Metamodels can provide a better understanding of the relationship and faster analysis than the computer analyses. Concern regarding the lack of random error term in the equation because of the deterministic computer analysis has been expressed; thus the use of a metamodel has to account for that (Simpson, Peplinski, Koch, & and Allen, 2001).

$$y = f(x) \tag{4a}$$

$$\hat{y} = g(x) \tag{4b}$$

$$y = \hat{y} + \varepsilon \tag{4c}$$

There are three steps to developing a metamodel. First, an experimental design must be chosen, followed by selecting a model to fit the data produced. Finally, the technique of fitting the data to the model must be decided. Different combinations of each of these steps have led to many approximation techniques found in research. The chart in Figure 21 shows how different combinations of these three steps lead to established techniques.

The experimental design of the metamodel is very important to establish in order to make sure the set of computer experiments is efficient and will produce adequate data for the model. There are several experimental designs in place that are used for different scenarios. Types of designs include factorial designs, central composite designs, and space filling designs, among others. In Figure 22 and Figure 23, some of these designs

are illustrated to show how the data and parameters are chosen. Each design has some statistical background and theory behind choosing such a design. It is important to determine the needs of the end product in order to choose the best experimental design (Simpson, Peplinski, Koch, & and Allen, 2001). Before choosing a design, it is beneficial to do a pre-experimental plan, such as selecting a response variable and choosing the factors to input as variables, levels needs for each factor, and the range of the factors (Montgomery, 2009). Once these decisions are made, choosing a design becomes easier and can be aided by a statistical software program.

There are many models that can be used to fit the data after performing the experiments. The model choice will be tied to the design performed, as well as to the fitting of the model. Examples of different model choices include a polynomial model, network of neurons, and realizations of stochastic processes. Corresponding possible model fitting include least square regression, back propagation, and a best linear unbiased predictor, respectively (Simpson, Peplinski, Koch, & and Allen, 2001).

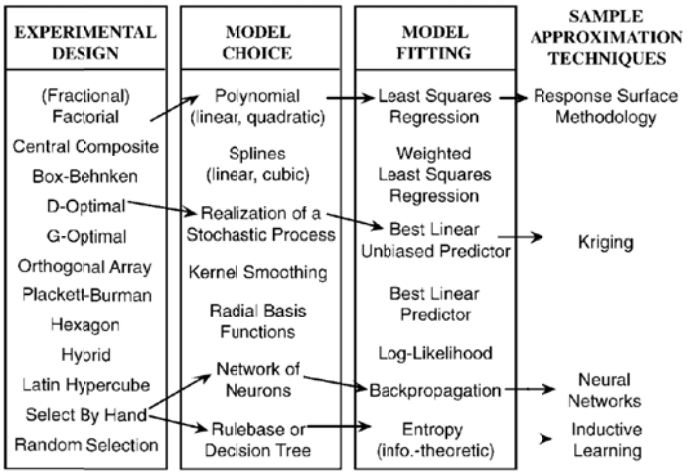

Figure 21: Different techniques for metamodels (Simpson, Peplinski, Koch, & and Allen, 2001)

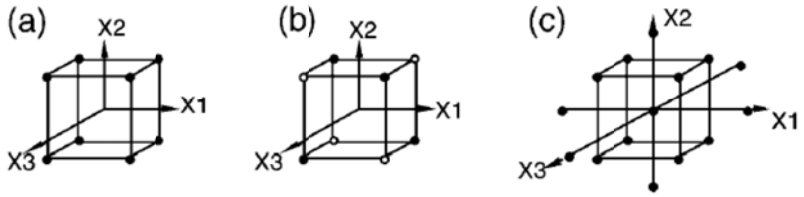

Figure 22: Basic three-factor designs. (a) 23 full factorial; (b) 23-1 fractional factorial; (c) composite design (Simpson, Peplinski, Koch, & and Allen, 2001)

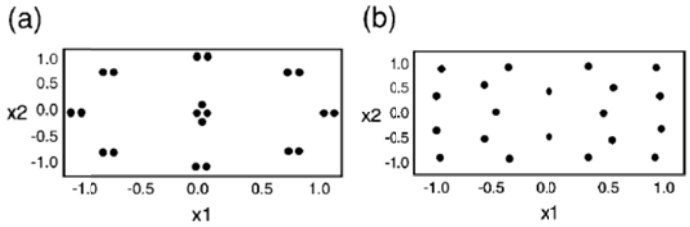

Figure 23: (a) 'Classical' and (b) 'Space filling' designs. (Simpson, Peplinski, Koch, & and Allen, 2001)

The combination of an experimental design, model choice, and model fitting results in a complete metamodel. The neural networks method can be accomplished by selecting data by hand as a design of experiments, choosing a network of neurons model and fitting the data with back propagation. This method is used mostly for deterministic functions. Kriging often entails a D-optimal design, a realization of stochastic processes and a best linear unbiased predictor fit. This method is mostly used with computer codes that are deterministic and don't have a measurement error. Response surface methodology usually combines a factorial design, polynomial model, and least squares regression (Simpson, Peplinski, Koch, & and Allen, 2001). RSM has a history of application in chemical and processing fields (Myers, Khuri, & Carter, 1989) as well as multiple engineering fields (Simpson, Peplinski, Koch, & and Allen, 2001). For this project, the response surface methodology will be used to develop a bridge specific PSDM.

6.2 Generation of Probabilistic Seismic Demand Model

The design support tool has been developed for this project where bridge specific curves will be created based on certain design parameters input. To accomplish this, we utilized the concepts of metamodels to develop a multiparameter fragility method. In this method, the response surface method (RSM) is used as the metamodel. RSM in general is a collection of tools in data analysis used to improve the knowledge of the effects of design variables on one or more response variables (Myers, Khuri, & Carter, 1989). It has been used in many statistical design of experiments (DOEs), including for the purpose of facilitating the analysis of fragility (Towashiraporn, 2004)(Ghosh, Padgett, & Dueñas-Osorio, 2012).

The first step in developing a metamodel is to choose a proper design of experiment (DOE) for the model. Several DOEs can be used in RSM, and all have different benefits. A common DOE used is the full factorial design, where the number of design points is determined by the factor levels desired and the number of factors considered (Simpson, Peplinski, Koch, & and Allen, 2001). The number of design points becomes prohibitively large as the number of factors increases. For an experiment with 5 factors and 3 factor levels, the number of design points required would be 3^5, or 243 design points, or in this case, 243 distinct bridge models. For this project, that number is too large, considering these models will be analyzed with 320 ground motions, requiring a total of over 75,000 analyses. Other DOEs to consider would be the fractional factorial design, central composite design, and Box-Behnken designs. Central composite designs (CCD) are basically two-level factorial designs that include center and star points (Simpson, Peplinski, Koch, & and Allen, 2001). Star points are where are factors are set at the mid levels except one, which can be set at the low or high α level. An illustration of this type of design is given in Figure 22b. CCDs are beneficial because they incorporate a small number of additional design points that allow estimation of a second order response surface model. This design type has the advantage of including three levels of a factor,

like a 3k factorial design, without the expensively large number of treatments (Kutner, Nachtsheim, Neter, & Li, 2005). For this project, a CCD was chosen for the DOE in this metamodel for the fragility method presented. The CCD used to create the bridge models is shown in Table 12. It is a two level fractional factorial design, like the one used for the sensitivity study of the design parameters, along with 2 center points, and 10 star points.

After the design of experiment has been chosen, the bridge models can be created for analysis. For each of the patterns in Table 12, 160 parameterized bridge models were realized with the design parameters as specified for that pattern. The creation of parameterized bridge models was introduced in an earlier section. These parameterized bridge models are then analyzed with the full suite of PEER ground motions (Baker, Lin, Shahi, & Jayaram, 2011) described earlier, unscaled and scaled for a total of 320 ground motions. Response quantities are then extracted from the analyses, such as the column and abutment responses, to be used to complete the response surfaces and create the multiparameter demand model.

Table 12: Design of Experiment for multiparameter demand model.

Run	Pattern	LS	VR	AR	SpanHt	DepthDiam
1	+−+++	1	-1	1	1	1
2	++−++	1	1	-1	1	1
3	000a0	0	0	0	-1	0
4	−++−−	-1	1	1	-1	-1
5	0000A	0	0	0	0	1
6	++−−−	1	1	-1	-1	-1
7	++++−	1	1	1	1	-1
8	−−−−−	-1	-1	-1	-1	-1
9	00000	0	0	0	0	0
10	+−−+−	1	-1	-1	1	-1
11	−−+−+	-1	-1	1	-1	1
12	+++−+	1	1	1	-1	1
13	0000a	0	0	0	0	-1
14	0A000	0	1	0	0	0
15	−++++	-1	1	1	1	1
16	000A0	0	0	0	1	0
17	−−−++	-1	-1	-1	1	1
18	+−−−+	1	-1	-1	-1	1
19	+−+−−	1	-1	1	-1	-1
20	−−++−	-1	-1	1	1	-1
21	−+−−+	-1	1	-1	-1	1
22	00000	0	0	0	0	0
23	00A00	0	0	1	0	0
24	a0000	-1	0	0	0	0
25	0a000	0	-1	0	0	0
26	00a00	0	0	-1	0	0
27	−+−+−	-1	1	-1	1	-1
28	A0000	1	0	0	0	0

The next steps in developing a metamodel are model choice and model fitting. The model choice for this project is a linear polynomial model. This model choice is common when developing response surfaces (Towashiraporn, 2004)(Ghosh, Padgett, & Dueñas-Osorio, 2012). The first order model to be used for this project is most often taken as shown in Eqn. 5. The fitting of the data will be accomplished with a least squares regression model.

$$Y = \beta_0 + \beta_1 X_1 + \beta_2 X_2 + ... + \beta_n X_n \tag{5}$$

Where X_1 … X_n are the different design variables and β_0 …β_n are the response coefficients used to estimate the response quantity Y. To determine these coefficients, the DOE data points are placed in a matrix, along with an intensity measure of choice from the ground motion suite, such as peak ground acceleration (PGA) or spectral acceleration. This makes up the X matrix of input variables. The Y vector would be comprised of response quantities of one component. To be more consistent with the traditional demand model shown in Eqn. 6a and to improve the model fit, the response quantities and ground motion intensity measures were transformed in the lognormal space before regressing the data. The other variables were not transformed. The final model on which the data was regressed is shown in Eqn. 7. This process will be done for each response quantity of interest, such as column response, abutment gap displacement, or bearing response. The input design variables X_i were introduced in an earlier section as the five design parameters of a bridge: longitudinal steel ratio, volumetric steel ratio, aspect ratio, span length to column height ratio, and deck depth to column diameter ratio.

$$\ln(S_d) = a + b * \ln(IM) \tag{6a}$$

$$S_d = a(IM)^b \tag{6b}$$

$$\ln(Y) = \beta_0 + \beta_1(\ln(PGA)) + \beta_2 X_1 + \beta_3 X_2 + \beta_4 X_3 + \beta_5 X_4 + \beta_6 X_5 \tag{7}$$

Eqn. 7 will be used as the PSDM of the fragility analysis. This multiparameter PSDM is similar to the traditional PSDM given in Eqn. 5a, developed by Cornell, et al (Cornell, Jalayer, Hamburger, & Foutch, 2002). The main difference is that the fragility of the response quantity will now be conditioned on the ground motion intensity measure as well as the other design variables, resulting in fragility curves developed specifically

for a bridge with the conditioning design variable quantities. This fragility can be expressed in the probability statement in Eqn. 8.

$$P[Fragility] = P[Demand > Capacity(LS_i) \mid IM, x_1, x_2, ..., x_n] \tag{8}$$

6.3 Logistic Regression and Fragility

The combination of the capacity and demand models will also differ from the traditional single variable fragility analysis. Generally, a closed form equation has been used to integrate the capacity and demand models in analytical fragility analysis at the component level. When these models follow a lognormal distribution, the fragility curve can be found with Eqn. 9 (Hwang, Liu, & Chiu, 2001), where S_d is the median value of the structural demand, S_c is the median value of the structural capacity, $\beta_{d|IM}$ is the logarithmic standard deviation of the demand, and β_c is the logarithmic standard deviation of the capacity. For this bridge specific fragility method, the capacity and demand models will be compared using Monte Carlo simulation and logistic regression. The chart in Figure 24 shows the steps to creating fragility curves with this method. If the probability of exceeding a damage level varies from 0 to 1 only, and is a never decreasing function, then any cumulative distribution function can be used to develop fragility curves (Koutsourelakis, 2010). In this method, a logistic distribution and regression, which has been used to find fragility surfaces in research before, is used instead of a lognormal distribution (Koutsourelakis, 2010)(Towashiraporn, 2004). This logistic regression provides the form of the cumulative distribution function that describes the parameterized bridge failure probability given multiple input parameters.

$$P[Demand > Capacity \mid IM] = \Phi\left(\frac{\ln\left(\frac{S_d}{S_c}\right)}{\sqrt{\beta_{d|IM}{}^2 + \beta_c{}^2}}\right) \tag{9}$$

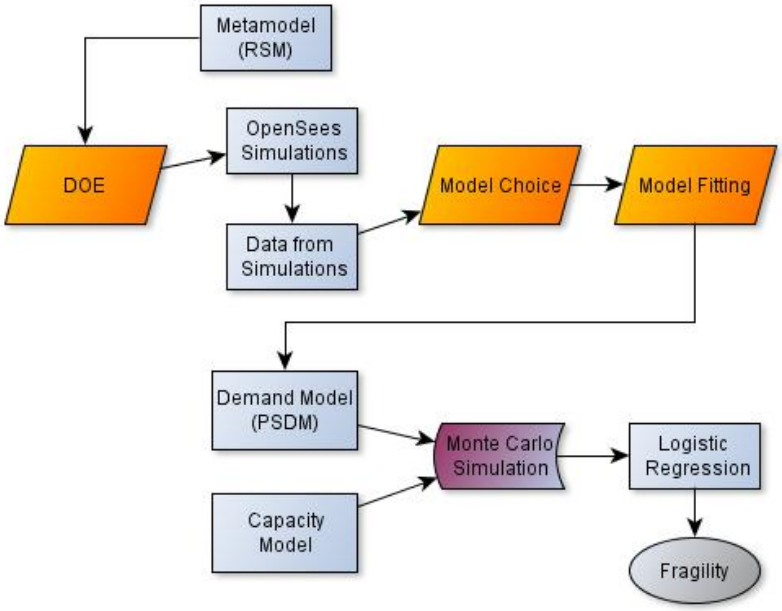

Figure 24: Steps to determining the fragility with new method.

Monte Carlo simulations were used to generate random samples from the distributions of the demand and capacity models in order to compare them and calculate the probabilities of failure for each component and limit state. The capacity model was described earlier as the limit states for primary and secondary components defined by engineering demand parameter values at four CDT levels and dispersion. The capacity models are described by a lognormal distribution. The demand model is the PSDM generated by the Response Surface Method detailed earlier. The design parameters in the demand models are randomly generated using uniform distributions. For each run in the Monte Carlo analysis, the realizations randomly simulated from the demand and capacity models are compared. The same demand model realizations were used to compare with each of the individual components capacity model realizations. The number [1] is assigned to a realization where the demand is greater than the capacity, and the number [0] is assigned when the capacity is greater than the demand. These binary results from the Monte Carlo simulation are assembled into vectors for each component. These result

vectors are then regressed against a matrix of the original design parameters using a logistic regression to find regression coefficients, α_i seen in Eqn. 10. This procedure will lead to the fragility of each bridge component, which can be calculated with the logistic regression formula in Eqn. 10, where the α_i values come from the Monte Carlo simulations and the x_i values are the design parameters to be defined by the specific bridge design. To find the fragility of the bridge system, a series approach will be used to combine the results of the components. The series approach specifies that for each simulation, if any of the components within a system fails, then the entire system has failed. So, for each run, the results from each component is compared, and if at least one of the components failed, the number [1] is assigned for the system, and if none of the components failed, then the number [0] is assigned to the system analysis. These new binary results are combined in a vector and regressed against the matrix of design parameters with a logistic regression to find a set of regression coefficients for the system fragility. Again, Eqn. 10 is used to define the probability of failure for the bridge system at each limit state. An illustration of this process is given in Appendix B.

$$P[Fragility] = p_f = \frac{e^{\alpha_0 + \alpha_1 x_1 + \ldots + \alpha_n x_n}}{1 + e^{\alpha_0 + \alpha_1 x_1 + \ldots + \alpha_n x_n}} \tag{10}$$

The results of the Monte Carlo simulation using the response surface metamodels and logistic regression are given in Appendix C. The results include the logistic regression coefficients of the probability of failure equation (Eqn. 10) for the primary and secondary components and bridge system. Those results will be used in the design support tool to produce bridge specific fragility curves. Eqn. 10, with the coefficients found in the Monte Carlo simulation included, becomes the fragility equation that is used to plot the fragility of the bridge and components, and directly correlates to the fragility equation shown in Eqn. 8. Substituting the design parameters in for the x_i in Eqn. 10, the probability of failure equation becomes Eqn. 11.

$$p_f = \frac{e^{\alpha_0+\alpha_1 \ln(PGA)+\alpha_2 LS+\alpha_3 VR+\alpha_4 AR+\alpha_5 SpanHt+\alpha_6 Depthdiam}}{1+e^{\alpha_0+\alpha_1 \ln(PGA)+\alpha_2 LS+\alpha_3 VR+\alpha_4 AR+\alpha_5 SpanHt+\alpha_6 Depthdiam}} \quad (11)$$

As the fragility will be based on more than one parameter, the result would be an n-dimensional fragility surface or cloud, generated by the points produced by the regression equation, instead of the traditional 2-d curve developed in current fragility methods. To graphically show the cloud in two or three dimensions, one would have to deterministically define all but one or two parameters and vary only one or two parameters of interest within a range and graph the 2-d fragility curve or 3-d fragility surface. The design tool does just that; it takes the bridge design inputs from the user as deterministic values, and varies the ground motion intensity measure in order to develop 2-d fragility curves. This fragility methodology was developed in order to create bridge-specific fragility analysis that would produce fragility curves in the most common form.

6.4 Design Tool Format and Example

The bridge specific design support tool is presented in a Microsoft Macro-enabled Excel worksheet. The spreadsheet utilizes Visual Basic Macros in order to produce the fragility curves, so the user would need to enable Macros content on their individual Excel programs. The design tool includes hidden and protected sheets in which the data from the logistic regressions for the fragility curves are placed in order to ensure the integrity of the analyses. The previous processes described earlier, generation of the PSDM and the logistic regression to obtain fragility information, were completed and verified before incorporating the results into the design tool. The only sheets that the user should be concerned with are the Information sheet and the sheet entitled “Bridge Specific Fragility – XXX”, where the XXX stands for whichever ground motion intensity measure the user chooses for the fragility analysis, such as PGA or spectral acceleration at 1 second (Sa_1). Separate worksheets would be provided for different ground motion

intensity measures, when available. The user only needs to input the design parameters, which were discussed earlier, into the sheets and click the appropriate buttons to generate the fragility curves of choice. There are optional input boxes where the user can input upper and lower bounds of the design parameters to see the effects of the parameters on the fragility. The outputs include system fragility curves, component fragility curves, estimated fundamental period of the bridge, and specific fragility points for a given hazard level. A screenshot of the input page is given in Figure 28.

The following is a short example detailing the use of the tool. When the tool is first opened, the user will be presented with an information sheet that details the process of using the tool, as well as contact information if there are issues or questions with the tool. The message is shown in Figure 27. The user should note a warning that may be displayed about enabling Macros content in Excel, and the user should choose to activate Macros for use of this tool. The next tab gives the limit states used for the creation of the fragility curves. These values were given in Table 10, and cannot be changed by the user.

The user will then move on to the input page to develop fragility curves. Figure 28 shows a snapshot of the input page, where the user would input the design parameters of his bridge. Input should only be placed in blue boxes. Red boxes will display output, and all other boxes should not be modified. In the figure, the inputs of the example bridge are shown. The example bridge chosen for analysis is California state bridge Willow Avenue Overcrossing, designed in 2002 and constructed in 2005. Figure 25 and Figure 26 show the elevation and typical section views of this bridge. This 2-column bridge has 1.64% longitudinal steel, 0.59% transverse steel per column, 18.1 foot columns with a 54 inch diameter, a 122.8 foot maximum span length, and 59 inch depth of the superstructure. In the optional input section, the effect of the longitudinal steel ratio on the performance of the bridge is investigated by providing lower and upper bounds for the steel ratio at 1.0% and 2.4%, and keeping the other parameters constant. The ratios of the bridge, which were described in the design parameter section of this report, are

calculated from the input variables within the tool and checked for compliance with the boundaries of this project.

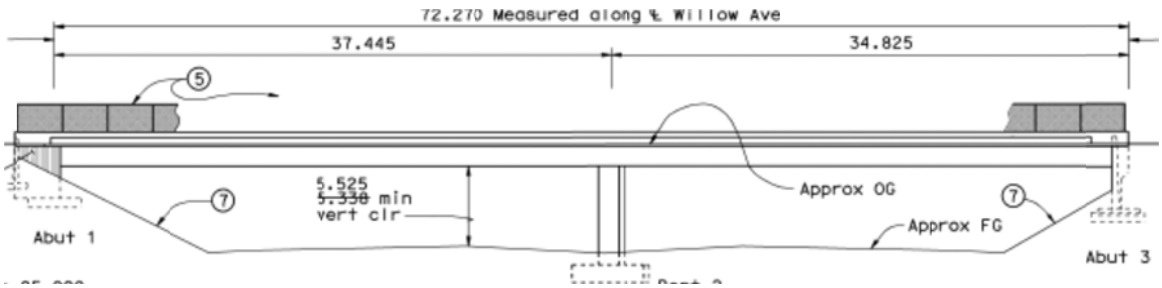

Figure 25: Elevation view of the Willow Avenue Overcrossing bridge.

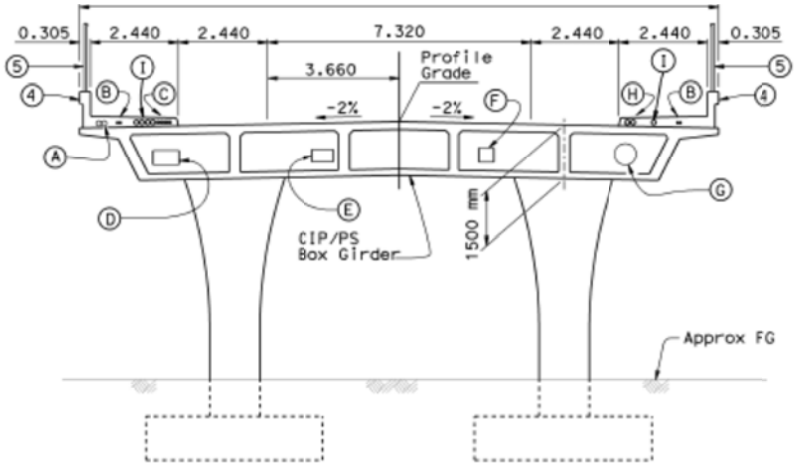

Figure 26: Typical Section of the Willow Avenue Overcrossing bridge.

An estimate of the fundamental period of the bridge is given in the tool, which is calculated with a linear regression formula as shown in Eqn. 12. The periods from the bridge models, calculated with an elastic analysis in OpenSees, were regressed against the design parameters described earlier with a least squares linear regression. The regression fit the data well, giving an R^2 value of 0.89. The resulting regression coefficients are used in the tool to provide an estimate of the fundamental period of the bridge design. The estimation is provided for the user's benefit, and is not used in the tool in any other capacity. Discussion of the fit of the regression used to estimate the fundamental period is given in Appendix E.

$$\hat{P}eriod = \beta_0 + \beta_1 * LS + \beta_2 * VR + \beta_3 * AR + \beta_4 * SpanHt + \beta_5 * DepthDiam \quad (12)$$

Once the design parameters are entered, fragility curves can be produced. Buttons on the input page link to VBA Macros commands that produce the fragility curves in separate sheets within the Excel file. Examples of the buttons are shown in Figure 29. Buttons that generate fragility curves with and without the upper and lower bounds are given for user flexibility. Once the button is pressed, the fragility curve is developed in a new chart sheet that is created in the tool. The user can view, copy, or manipulate the curve within the spreadsheet. If the user decides to change any of the design parameter inputs to produce the same type of fragility curve in order to see the effect of the change on the fragility, the original fragility curve window will be deleted and a new graph will be developed. The name of the sheet with the first fragility curve should be changed before developing a new curve in order to save and compare the fragility curves.

Welcome to the Bridge Specific Fragility Design Tool for Caltrans! This tool is in Beta mode and can only be used for 2 span integral concrete box girder bridges with 2, 3, or 4 columns and seat type abutments. If this is not your bridge, these results may not be accurate!
To begin, please start by inputting your design parameters, as listed. Input boxes are blue. Be sure to check your units! If you wish to include upper and lower bounds on your design parameters to determine the effect of the parameters on the fragility of your bridge, you may do so. Make sure to include bounds on all of the parameters. Even if you only want to see the effect of one design parameter, make sure to duplicate the design parameters for the bounds of the other parameters.
After inputting your design parameters, you will be able to choose different output for your bridge. There are buttons which will produce fragility curves for the system and component level of the bridge, an estimate of the fundamental period, as well as fragility information at specific hazard levels. Output boxes are in red. If you make any changes to any parameters and want to compare the fragility curves, be sure to save the curves before producing a new one.
If there are any issues with this design tool, please contact the developer, Jazalyn Dukes, at jdukes6@gatech.edu. Enjoy!

Figure 27: Introduction message for design support tool.

Figure 28: Input page for design support tool.

Figure 29: Buttons to produce fragility curves for column component.

The fragility curves based on the ground motion intensity measure, PGA, for the example bridge for the column components are given in Figure 30 and Figure 31. The fragility curves for the bridge system as well as the other primary and secondary components are given in Appendix D. The first figure shows the fragility curves for the four component damage threshold (CDT) values for the column component based on the design parameters of the design bridge. The colors of the curve correspond to the ShakeCast inspection priority levels as described earlier. The second figure includes the

fragility curves of the upper and lower bounds to show the effect of changing the design parameters, in this case the longitudinal steel ratio, on the fragility of the bridge. Table 13 shows the percent savings and gains made by choosing the upper or lower bounds of the longitudinal steel ratio. Based on the criteria for their specific bridge design project, the user can then decide which value of steel content works best for that particular project. The table shows that the user would increase the probability of the highest damage level (CDT-3) occurring by 128% if the lower longitudinal steel ratio was used instead of the original percent steel, and could reduce the probability of failure by around 62.7% if the amount of longitudinal steel was increased to 2.4% from 1.64% at a PGA of 0.5 g. The user can also find specific fragility points for any hazard level, as shown in Table 14, where LS-# correspond to appropriate CDT or BSST limit state. The user inputs the desired hazard level into the blue box and the different fragility points are displayed for the system level fragility as well as the component fragility information.

This procedure can continue with the other design parameters, by changing the bounds and design parameter inputs, to get the fragility information needed to gather useful performance based information on the user's bridge design to make more informed design decisions backed by probabilistic fragility analysis results.

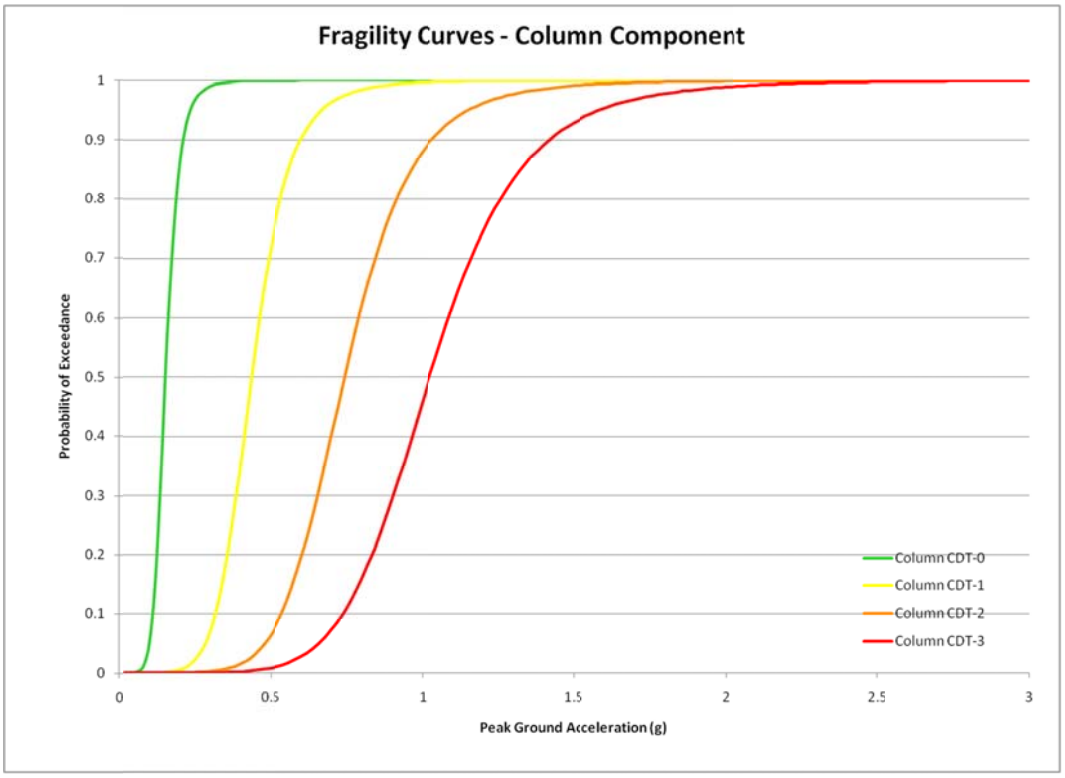

Figure 30: Bridge specific fragility curves for column components at CDT levels.

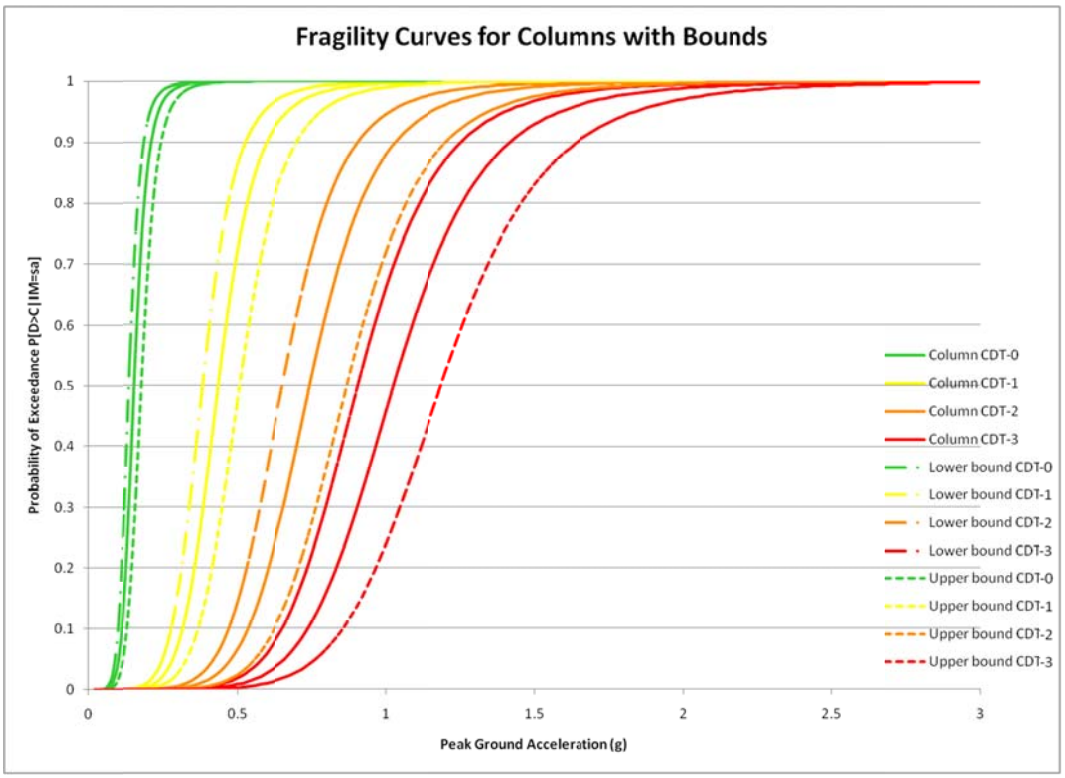

Figure 31: Bridge specific fragility curves for column components with upper and lower bounds.

Table 13: Comparison of fragility values at 0.5g of PGA at upper and lower bounds of the longitudinal steel content for the column component.

	Original (1.64%)	Lower bound (1.0%)	Percent Diff	Upper Bound (2.4%)	Percent Diff
CDT-0	1.000	1.000	0.0%	0.999	0.0%
CDT-1	0.719	0.861	19.8%	0.472	-34.4%
CDT-2	0.064	0.141	120.6%	0.024	-63.2%
CDT-3	0.008	0.018	128.0%	0.003	-62.7%

Table 14: Specific hazard level fragility information.

Peak Ground Acceleration (g)	0.5			
Probabilities of failure:	**LS-0**	**LS-1**	**LS-2**	**LS-3**
System	100.0%	97.8%	6.2%	0.7%
Column Component	100.0%	71.9%	6.4%	0.8%
Gap at Abutment Component	100.0%	88.4%	0.3%	0.0%
Joint Seal Component	100.0%	0.0%	0.0%	0.0%
Long Bearing Deformation	100.0%	60.8%	0.0%	0.0%
Trans Bearing Deformation	99.8%	26.4%	0.0%	0.0%

CHAPTER 7

CONCLUSION

The seismic bridge design process of California details the requirements of a bridge design that will result in a bridge that should be able to withstand the design hazard level without collapse. However, the process does not include a way to determine the expected performance of the bridge at the design hazard level or at other hazard levels. This project introduces a performance-based design tool into the Caltrans design process that will provide probabilistic fragility information that describes the performance of the bridge at different hazard levels as well as give insight to the effect that different design decisions have on the performance of a bridge. This tool is presented here for a common bridge type in California, a two span integral concrete box girder bridge.

In order to create a tool for this purpose, a new fragility method was created that incorporates bridge design details. Design details that were included in the new fragility method were those that, in research and experience, were found to have a significant effect on the response of the bridge during an earthquake. The significance of the effects of the design details, or design parameters, on the bridge responses was tested in a sensitivity study, and the results agreed with the assumption that the set of design parameters investigated were significant in affecting the response of certain bridge components.

One of the main components of the analytical fragility method that was modified for use in this project was the demand model. The traditional PSDM had to be modified to accommodate the design parameters as input variables, creating a multi-parameter demand model. The multi-parameter demand model facilitates the development of bridge specific fragility curves. Because the multi-parameter demand model uses specific bridge design details, the resulting fragility analysis can be specific to a bridge with those design

details. Applications of the demand model can extend to other bridge types, other design details, and other structures with appropriate modifications. The bridge specific fragility methodology can also have an extended use in Caltrans, as well as in other research areas.

The bridge specific design tool was created to be a supplemental analysis tool for the Caltrans bridge designer. The research behind the tool incorporated details from the Caltrans Seismic Design Criteria and other Caltrans design documents to create nonlinear finite element bridge models to analyze with a suite of ground motions pertaining to the California seismic hazards. The design tool makes use of the bridge-specific fragility methodology, which consists of the multi-parameter demand model, the capacity model developed for California bridges, and logistic regression to present bridge-specific fragility curves for the user. The design tool was created to be user friendly and easy to understand, with options for the user to extract only the information most useful to them. The user can get fragility information for the bridge system, as well as for individual primary and secondary components. There is an option to calculate an estimate of the fundamental period of the bridge and to get specific fragility points for any hazard level. This tool will be a useful and accessible way to generate probabilistic fragility information on new bridge designs as well as add a much needed performance-based design aspect into the Caltrans seismic design process.

The design tool can be expanded to all types of bridge classes in California, and also to other structures where applicable. The results of this research are part of a feasibility study into fragility methods and applications that may be expanded into full use by Caltrans in the future. If Caltrans design engineers find this tool useful, are comfortable with the way it works as a design check, and determines the fragility analysis to be accurate, then this method and tool will be developed for other bridge classes for expanded use in new seismic bridge design. There are other possibilities with this methodology and tool, such as for retrofit designs, use in retrofit planning, and use in

ShakeCast and other tools that required fragility analysis. This methodology and tool will be submitted and tested to determine the usefulness and possibilities of them, and based on preliminary results, the future looks bright.

REFERENCES

ATC. (1985). Earthquake Damage Evaluation Data for California. Applied Technology Council.

Baker, J., Lin, T., Shahi, S., & Jayaram, N. (2011). New Ground Motion Selection Procedures and Selected Motions for the PEER Transportation Research Program. Pacific Earthquake Engineering Research Center Report.

Bandyopadhyay, K., & Hofmayer, C. (1985). Component Fragilities: Data Collection, Analysis and Interpretation. Conference 13: Water Reactor Safety Research Information Meeting. Sponsored by the US Nuclear Regulatory Commission.

Bandyopadhyay, K., & Hofmayer, C. (1986). Synthesizing Seismic Fragility of Components by Use of Existing Data. Conference 14: Water Reactor Safety Information Meeting. Sponsored by the US Nuclear Regulatory Commission.

Caltrans. (2010). Seismic Design Criteria. California Department of Transporation.

Caltrans. (2006). Seismic Design Criteria, Version 1.4. California Department of Transportation.

Caltrans. (2010, July). Seismic Design Methodology. Memo To Designers 20-1 .

Calvi, G., Pinho, R., Magenes, G., Bommer, J., Restrepo-Velez, L., & and Crowley, H. (2006). Development Of Seismic Vulnerability Assessment Methodologies Over The Past 30 Years. ISET Journal of Earthuake Technology , Paper No. 472, Vol 43, No 3.

Chiou, B., Darragh, R., Gregor, N., & Silva, W. (2008). NGA Project Strong-Motion Database. Earthquake Spectra , 23 (1), 23-44.

Choi, E., Nielson, B., & DesRoches, R. (2004). Seismic Fragility of Typical Bridges in Moderate Seismic Zones. Engineering Structures 26 (2), 187-199 .

Cimellaro, G., Reinhorn, A., Bruneau, M., & and Rutenburg, A. (2006). Multi-Dimension Fragility of Structures: Formulation and Evaluation. University at Buffalo, The State University of New York, Buffalo, N.Y.

Cornell, A. C., Jalayer, F., Hamburger, R. O., & Foutch, D. A. (2002). Probabilistic basis for 2000 SAC Federal Emergency Management Agency steel moment frame guidelines. Journal of Structural Engineering, 128, 526-532 .

FEMA. (2006). FEMA 454: Designing for Earthquakes: A Manual for Architects. Washington, D.C.: U.S Department of Homeland Security.

FEMA. (1997). HAZUS 97: Technical Manual. Washington, D.C.: Federal Emergency Management Agency.

FEMA. (2003). Multi-hazard Loss Estimation Methodology: Earthquake Model. Technical Manual, HAZUS MR4.

Ghosh, J., Padgett, J. E., & Dueñas-Osorio, L. (2012). Comparative Assessment of Different Surrogate Modeling Strategies with Application to Aging Bridge Seismic Fragility Analysis. To Appear in the Proceedings of the 11th ASCE Joint Specialty Conference on Probabilistic Mechanics and Structural Reliability (PMC 2012), June 17-20, 2012. Notre Dame, Indiana.

Highway Bridges. (n.d.). Retrieved Jan 7, 2012, from http://nisee.berkeley.edu/northridge/highway_bridges.html

Hwang, H., Liu, J. B., & Chiu, Y.-H. (2001). Seismic Fragility Analysis of Highway Bridges. The University of Memphis, Center for Earthquake Research and Information. Mid-America Earthquake Center.

Jeong, S., & Elnashai, A. (2007). Probabilistic Fragility Analysis Parameterized by Fundamental Response Quantities. Engineering Structures 29, 1238-1251 .

Jeong, S.-H., & Elnashai, A. (2007). Probabilistic Fragility Analysis Parameterized by Fundamental Response Quantities. Engineering Structures 29 pp 1238-1251 .

Ji, J., Elnashai, A., & Kuchma, D. (2007). Seismic Fragility Assessment for Reinforced Concrete High-Rise Buildings. MAE Center Report 07-14.

JMP Software. (n.d.). Retrieved April 18, 2012, from www.jmp.com

JMP the Statistical Discovery Software. (2010). JMP Pro v9.0.2. Carry, NC.

Karim, K., & Yamazaki, F. (2001). Effect Of Earthquake Ground Motions On Fragility Curves Of Highway Bridge Piers Based On Numerical Simulation. Earthquake Engineering and Structural Dynamics 2001; 30:1839-1856 .

Koutsourelakis, P. (2010). Assessing Structural Vulnerability Against Earthquakes Using Multi-Dimensaional Fragility Surfaces: A Bayesian Framework. Probabilistic Engineering Mechanics 25:49-60 .

Kutner, M., Nachtsheim, C., Neter, J., & Li, W. (2005). Applied Linear Statistical Models (5th edition ed.). Boston: McGraw-Hill.

Kwon, O., & Elnashai, A. (2006). The effect of material and ground motion uncertainty on the seismic vulnerability curves of RC structure. Engineering Structures 28, 289-303 .

Kwon, O., & Elnashai, A. (2006). The effect of material and ground motion uncertainty on the seismic vulnerability curves of RC structure. Engineering Structures 28, 289-303.

Luco, N., Ellingwood, B. R., Hamburger, R. O., Hooper, J. D., Kimball, J. K., & Kircher, C. A. (2007). Risk-Targeted versus Current Seismic Design Maps for the Conterminous United States. SEAOC 2007 Convention Proceedings.

Mackie, K., & Stojadinović, B. (2005). Fragility Basis for California Highway Overpass Bridge Seismic Decision Making. Technical Report, PEER 2005/12.

Mander, J., Priestley, M., & Park, R. (1988). Theoretical Stress-Strain Model for Confined Concrete. Journal of Structural Engineering , 114 (No. 8).

Mazzoni, S., McKenna, F., Scott, M. H., & Fenves, G. L. (2009). Open System for Earthquake Engineering Simulation User Command-Language Manual. University of California, Berkeley. Pacific Earthquake Engineering Research Center.

Moehle, a., Fenves, G., Mayes, R., Priestley, N., Seible, F., Uang, C.-M., et al. (1995). Highway Bridges and Traffic Management. Earthquake Spectra , 11 (S2), 287-372.

Montgomery, D. (2009). Design and Analysis of Experiments. Hoboken, NJ: John Wiley & Sons.

Myers, R., Khuri, A., & Carter, J. W. (1989). Response Surface Methodology: 1966-1988. Technometric, Vol 31, No 2 .

Nielson, B., & Bowers, M. (2007). Seismic Bridge Fragilities for Post-design Verification. 1st US-Italy Seismic Bridge Workshop.

Nielson, B., & DesRoches, R. (2007). Seismic Fragility Methodology for Highway Bridges Using a Component Level Approach. Earthquake Engineering and Structural Dynamics, 36 (6), 823-839 .

Padgett, J. E., & DesRoches, R. (2008). Methodology for the Development of Fragility Curves for Retrofitted Bridges. Earthquake Engineering and Structural Dynamics 37 (8), 1157-1174 .

Roblee, C., Sahs, S., Mahan, M., Yashinsky, M., Setberg, H., Maintenance, C., et al. (2011, February). Caltrans-Aligned Limit States Discussion. (J. Dukes, K. Ramanathan, R. DesRoches, & J. Padgett, Interviewers)

Roblee, C., Yashinsky, M., & Mahan, M. (2011, October). Bridge Specific Fragility Discussion. (J. Dukes, R. DesRoches, J. Padgett, & K. Ramanathan, Interviewers)

Sahs, S., Veletzos, M., Panagiutou, M., & Restrepo, J. (2008). Visual Inspection & Capacity Assessment of Earthquake Damaged Reinforced Concrete Bridge Element: Integrated Research & Deployment Final Report. Report No CA08-0284 and SSRP-06/19 .

Setberg, H. (2011, February 18). Caltrans Seismic Design Process. (G. Tech, Interviewer)

Shamsabadi, A., Rollins, K., & Kapuskar, M. (2007, June). Nonlinear Soil-Abutment-Bridge Structure Interaction for Seismic Performance-Based Design. Journal of Geotechnical and Geoenvironmental Engineering .

Shinozuka, M., Banerjee, S., & Kim, S. (2007). Statistical and Mechanistic Fragility Analysis of Concrete Bridges. Technical Report, MCEER-07-0015.

Shinozuka, M., Feng, M., Kim, H., Uzamwa, T., & Ueda, T. (2003). Statistical Analysis of Fragility Curves. Technical Report, MCEER-03-0002.

Simpson, T., Peplinski, J., Koch, P., & and Allen, J. (2001). Metamodels for Computer-based Engineering Design: Survey and Recommendations. Engineering with Computers 17:129-150 .

Towashiraporn, P. (2004). Building Seismic Fragilities Using Response Surface Metamodels. Georgia Institute of Technology.

APPENDIX A

Bridge Seismic Design Flowcharts

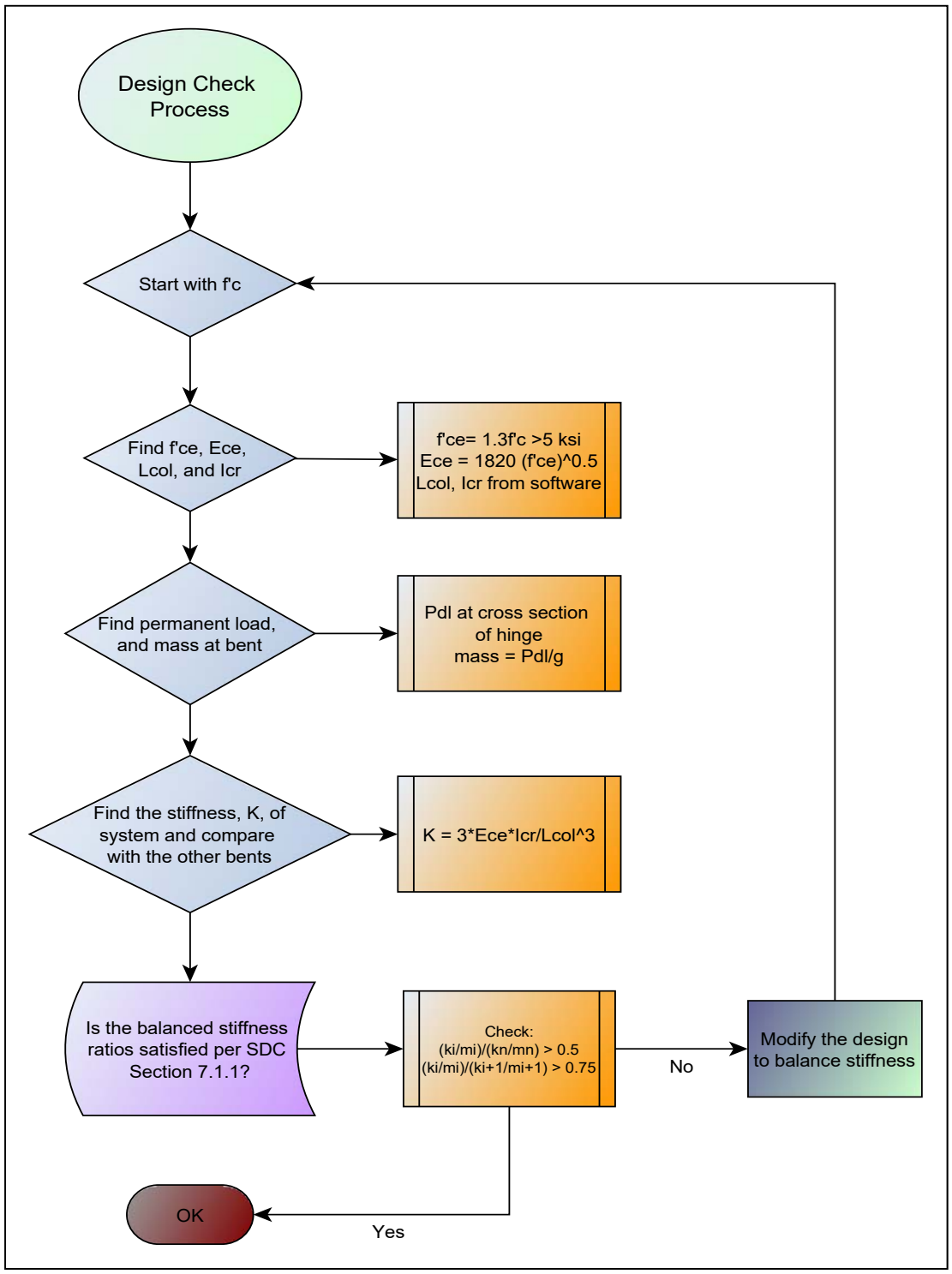

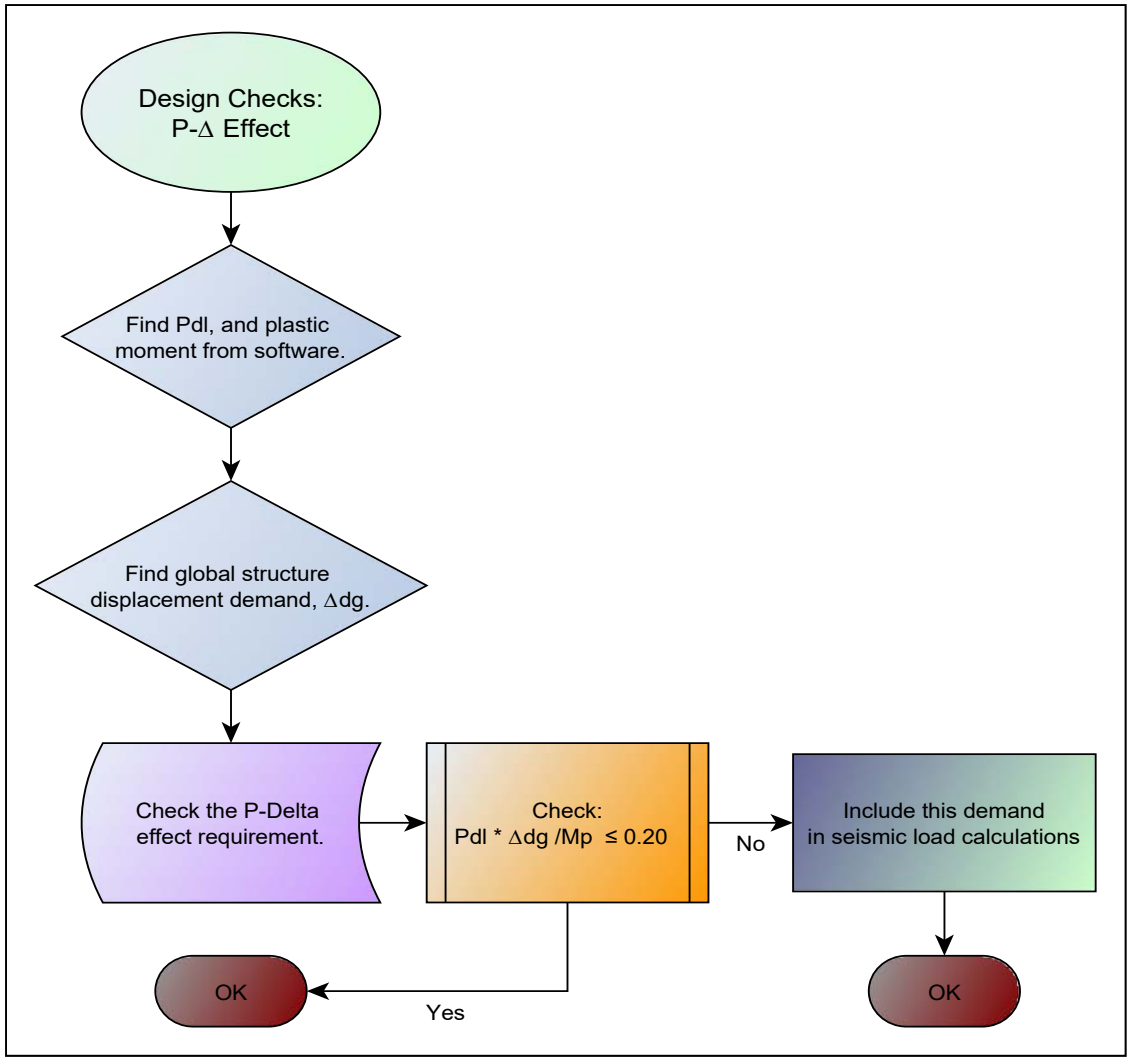
Design Checks:
P-Δ Effect
Find Pdl, and plastic moment from software.
Find global structure displacement demand, Δdg.
Check the P-Delta effect requirement.
Check:
Pdl * Δdg /Mp ≤ 0.20
No
Include this demand in seismic load calculations
OK
Yes
OK

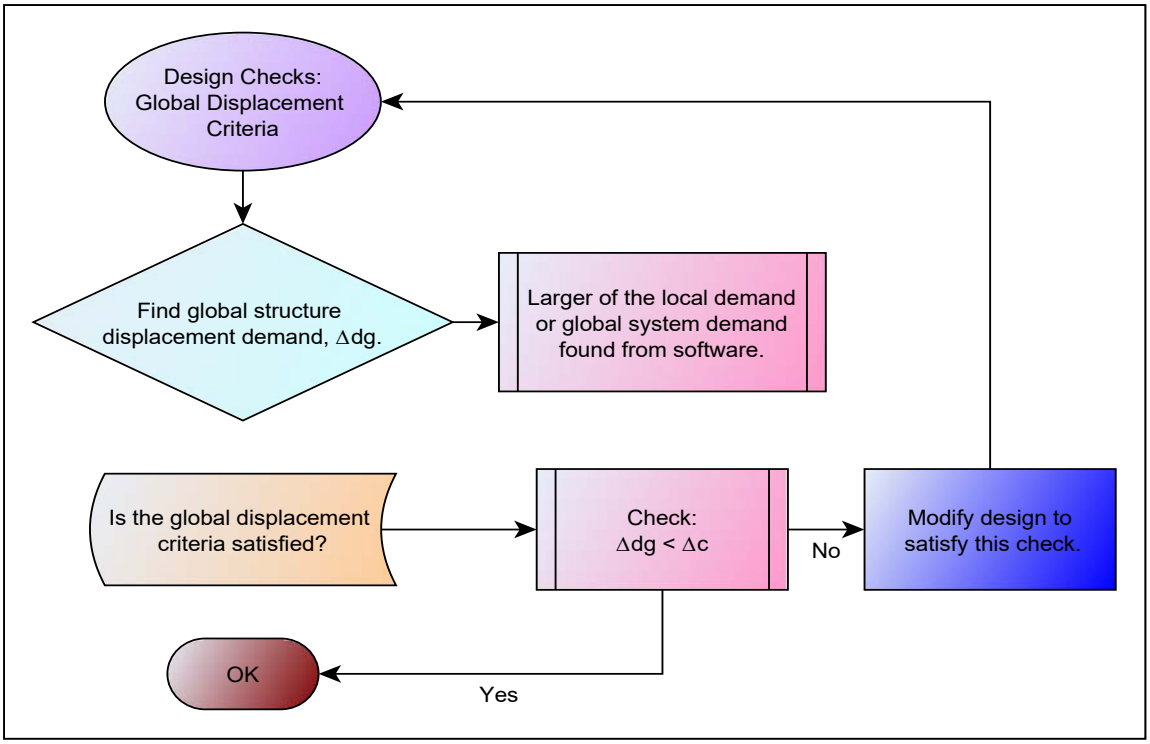
Design Checks:
Global Displacement
Criteria
Find global structure
displacement demand, Δdg.
Larger of the local demand
or global system demand
found from software.
Is the global displacement
criteria satisfied?
Check:
Δdg < Δc
No
Modify design to
satisfy this check.
OK
Yes

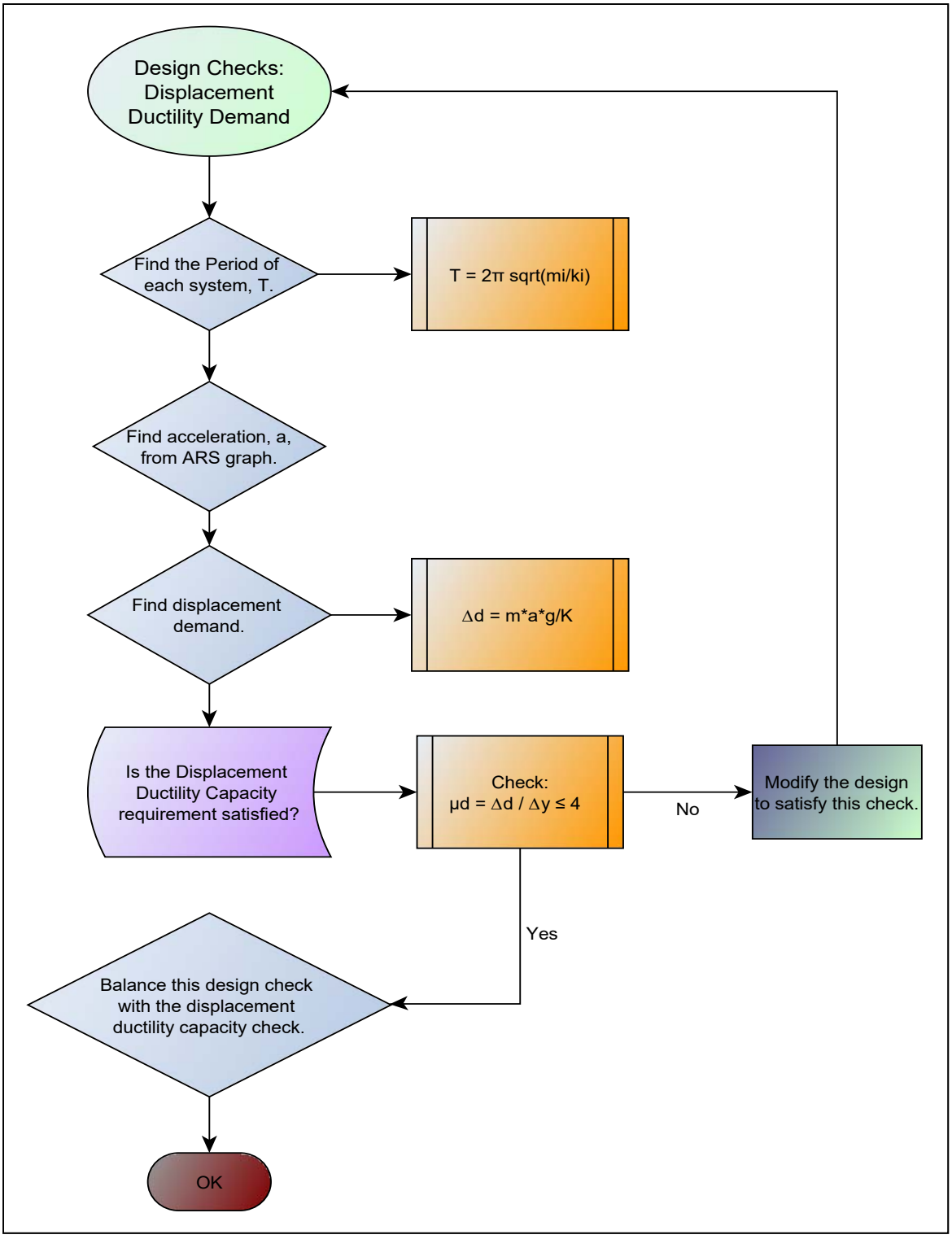
Design Checks: Displacement Ductility Demand
Find the Period of each system, T.
T = 2π sqrt(mi/ki)
Find acceleration, a, from ARS graph.
Find displacement demand.
Δd = m*a*g/K
Is the Displacement Ductility Capacity requirement satisfied?
Check: μd = Δd / Δy ≤ 4
No
Modify the design to satisfy this check.
Yes
Balance this design check with the displacement ductility capacity check.
OK

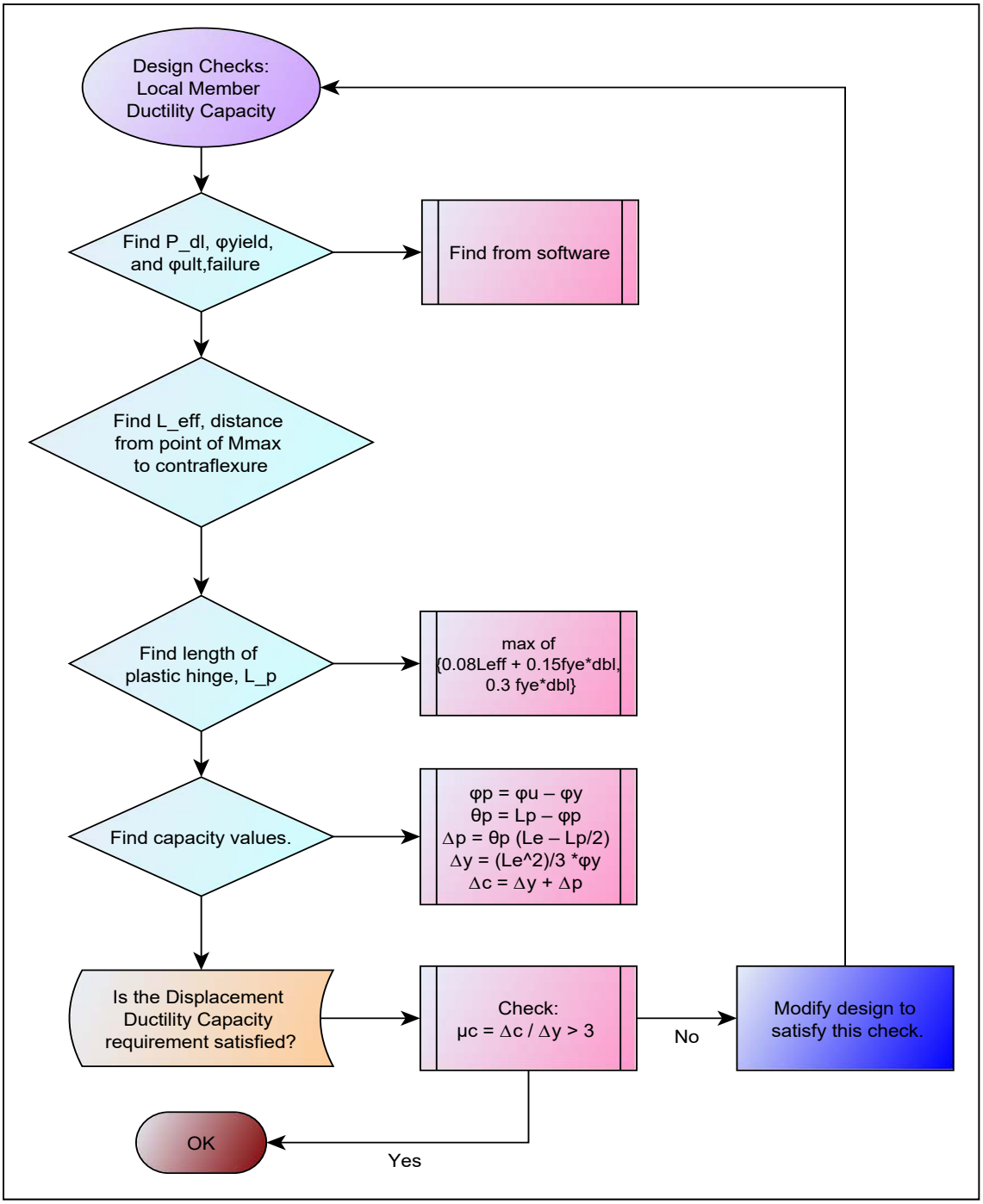
Design Checks:
Local Member
Ductility Capacity
Find P_dl, φyield,
and φult,failure
Find from software
Find L_eff, distance
from point of Mmax
to contraflexure
Find length of
plastic hinge, L_p
max of
{0.08Leff + 0.15fye*dbl,
0.3 fye*dbl}
Find capacity values.
φp = φu – φy
θp = Lp – φp
Δp = θp (Le – Lp/2)
Δy = (Le^2)/3 *φy
Δc = Δy + Δp
Is the Displacement
Ductility Capacity
requirement satisfied?
Check:
μc = Δc / Δy > 3
No
Modify design to
satisfy this check.
OK
Yes

APPENDIX B

Multiparameter Fragility Method Flowchart

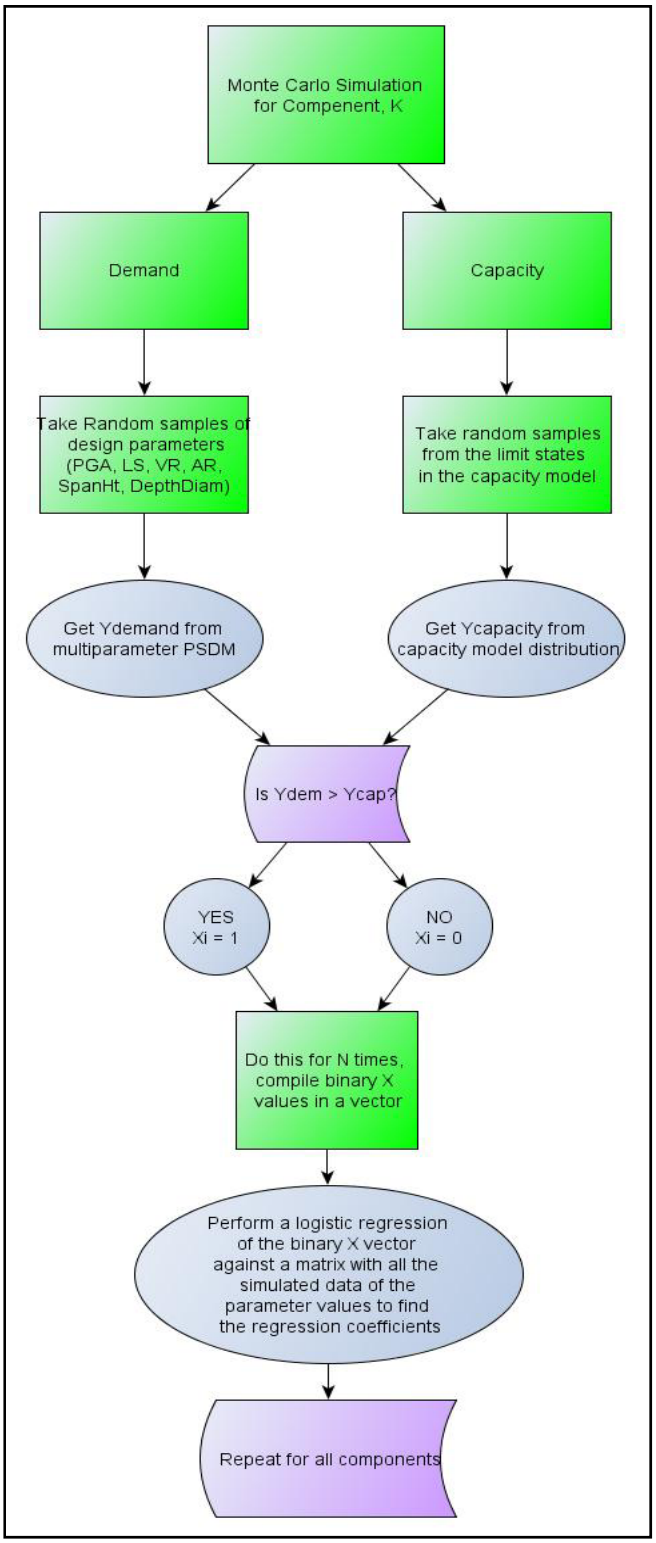

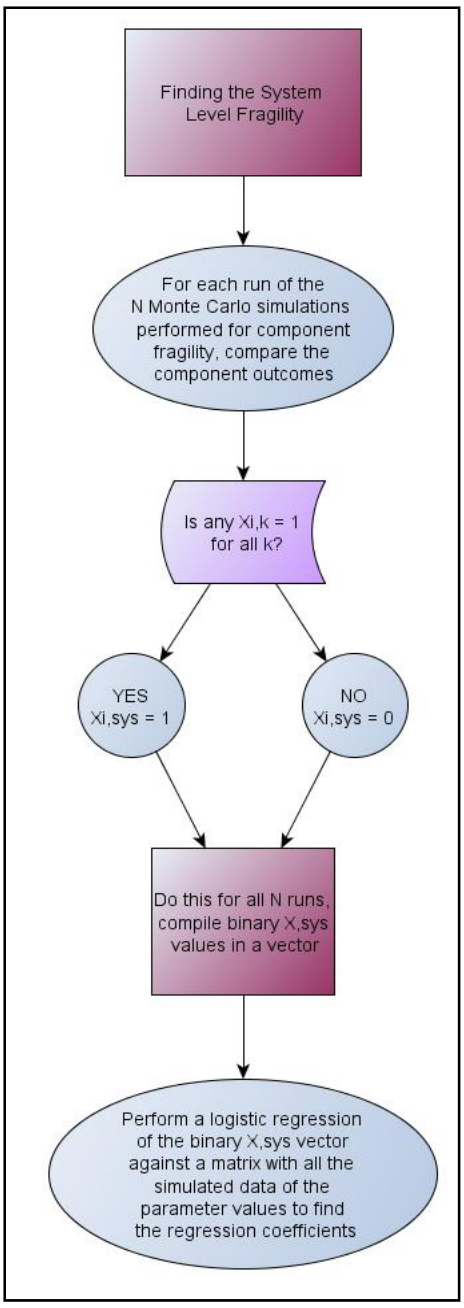
Finding the System Level Fragility
For each run of the N Monte Carlo simulations performed for component fragility, compare the component outcomes
Is any Xi,k = 1 for all k?
YES Xi,sys = 1
NO Xi,sys = 0
Do this for all N runs, compile binary X,sys values in a vector
Perform a logistic regression of the binary X,sys vector against a matrix with all the simulated data of the parameter values to find the regression coefficients

APPENDIX C

Logistic Regression Equation:

$$p_f = \frac{e^{\alpha_0+\alpha_1 \ln(Sa_1)+\alpha_2 LS+\alpha_3 VR+\alpha_4 AR+\alpha_5 SpanHt+\alpha_6 Depthdiam}}{1+e^{\alpha_0+\alpha_1 \ln(Sa_1)+\alpha_2 LS+\alpha_3 VR+\alpha_4 AR+\alpha_5 SpanHt+\alpha_6 Depthdiam}}$$

Table of Regression Coefficients for Spectral Acceleration at 1 second:

		Logistic Regression Equation Coefficients						
Component	Limit State	α0	α1	α2	α3	α4	α5	α6
System	BSS-1	12.84	5.63	-37.79	27.90	0.93	0.57	-1.08
	BSS-2	2.95	5.32	-54.66	46.26	0.73	0.49	-0.30
	BSS-3	1.60	5.18	-128.71	35.48	-0.46	0.30	1.22
	BSS-4	-0.09	4.94	-129.95	23.19	-0.52	0.28	1.26
Column	CDT-0	13.81	5.04	-141.97	20.28	-0.69	0.27	1.43
	CDT-1	6.22	5.16	-139.90	28.45	-0.64	0.30	1.29
	CDT-2	2.31	4.93	-133.87	33.00	-0.60	0.26	1.36
	CDT-3	0.37	4.78	-131.70	25.46	-0.60	0.26	1.30
Gap at Abutment	CDT-0	5.54	3.68	-24.76	8.04	0.80	0.41	-0.56
	CDT-1	-0.17	3.81	-34.18	10.91	0.83	0.40	-0.32
	CDT-2	-7.93	3.52	-27.93	19.35	0.75	0.36	-0.24
	CDT-3	-10.49	3.91	-32.31	3.81	0.80	0.39	-0.19
Long Brg Movement	CDT-0	6.24	3.92	-29.48	5.68	0.91	0.40	-0.81
	CDT-1	-1.78	3.71	-32.78	12.35	0.84	0.40	-0.39
	CDT-2	-102.57	0.00	0.00	0.00	0.00	0.00	0.00
	CDT-3	-102.57	0.00	0.00	0.00	0.00	0.00	0.00
Trans Brg Movement	CDT-0	7.87	3.89	16.52	134.68	0.04	0.25	-0.73
	CDT-1	0.37	3.81	19.70	120.87	0.07	0.25	-0.74
	CDT-2	-102.57	0.00	0.00	0.00	0.00	0.00	0.00
	CDT-3	-102.57	0.00	0.00	0.00	0.00	0.00	0.00
Joint Seals Movement	CDT-0	5.43	3.86	-19.67	1.61	0.86	0.41	-0.30
	CDT-1	-102.57	0.00	0.00	0.00	0.00	0.00	0.00
	CDT-2	-102.57	0.00	0.00	0.00	0.00	0.00	0.00
	CDT-3	-102.57	0.00	0.00	0.00	0.00	0.00	0.00

Table of Regression Coefficients for Peak Ground Acceleration:

		Logistic Regression Equation Coefficients						
Component	Limit State	α0	α1	α2	α3	α4	α5	α6
System	BSS-1	11.44	6.89	-14.51	77.15	0.75	0.52	-0.16
	BSS-2	3.40	6.80	-42.95	30.78	0.70	0.46	-0.26
	BSS-3	2.58	7.05	-133.15	21.54	-0.48	0.30	1.45
	BSS-4	0.72	6.98	-127.28	22.81	-0.53	0.30	1.13
Column	CDT-0	13.66	6.94	-133.88	54.57	-0.55	0.24	1.66
	CDT-1	6.87	6.88	-138.40	12.68	-0.62	0.29	1.44
	CDT-2	3.21	6.75	-137.09	21.62	-0.62	0.26	1.53
	CDT-3	1.20	6.74	-130.38	22.17	-0.63	0.27	1.21
Gap at Abutment	CDT-0	6.18	5.18	-26.19	8.78	0.83	0.43	-0.49
	CDT-1	0.53	5.13	-27.60	-4.82	0.83	0.39	-0.37
	CDT-2	-7.55	4.82	-27.31	13.95	0.77	0.38	-0.27
	CDT-3	-9.42	4.84	-24.45	14.78	0.76	0.38	-0.40
Long Brg Movement	CDT-0	5.88	5.06	-25.17	-5.34	0.77	0.46	-0.22
	CDT-1	-1.43	5.05	-27.38	18.30	0.80	0.42	-0.29
	CDT-2	-16.40	19.44	-328.59	-480.65	1.31	0.78	-16.67
	CDT-3	-102.57	0.00	0.00	0.00	0.00	0.00	0.00
Trans Brg Movement	CDT-0	6.42	4.33	31.78	143.64	0.09	0.20	-0.28
	CDT-1	-0.16	4.29	20.59	120.97	0.05	0.24	-0.66
	CDT-2	-102.57	0.00	0.00	0.00	0.00	0.00	0.00
	CDT-3	-102.57	0.00	0.00	0.00	0.00	0.00	0.00
Joint Seals Movement	CDT-0	5.75	5.00	-20.27	16.04	0.79	0.41	-0.36
	CDT-1	-38.20	15.93	-2.87	162.07	1.51	0.82	-1.17
	CDT-2	-360.28	278.43	12.00	581.65	6.40	0.70	1.53
	CDT-3	-102.57	0.00	0.00	0.00	0.00	0.00	0.00

APPENDIX D

Fragility Curves for example bridge for the Bridge System

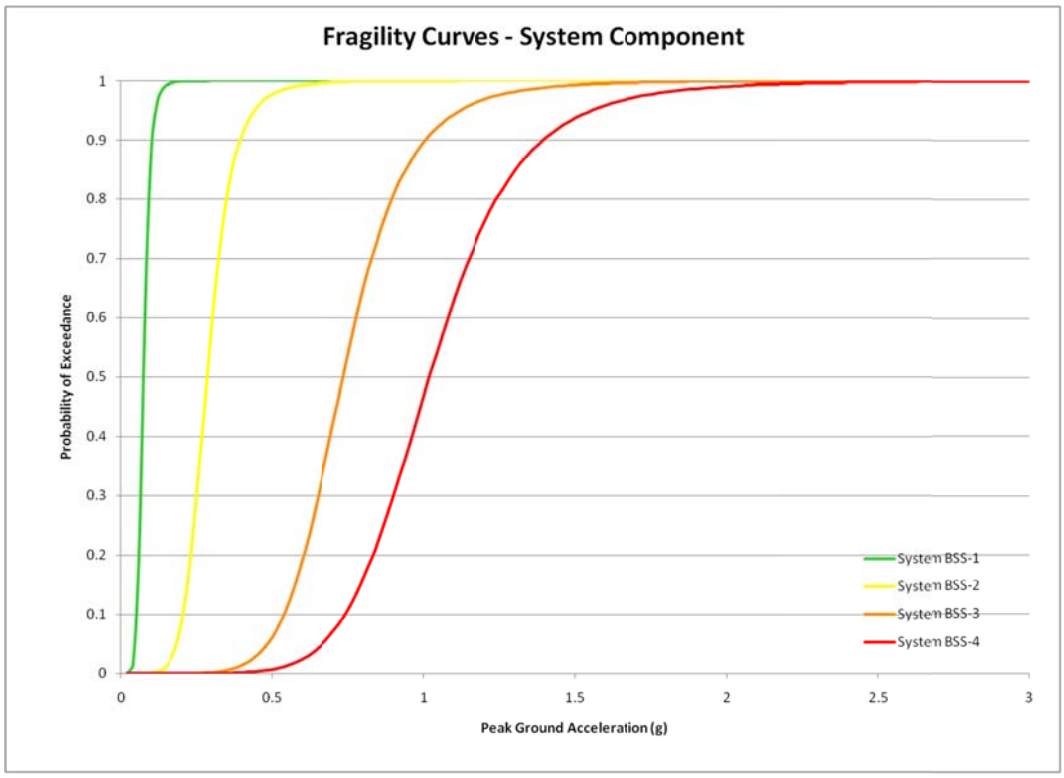

Fragility Curves for example bridge for the Bridge System with bounds

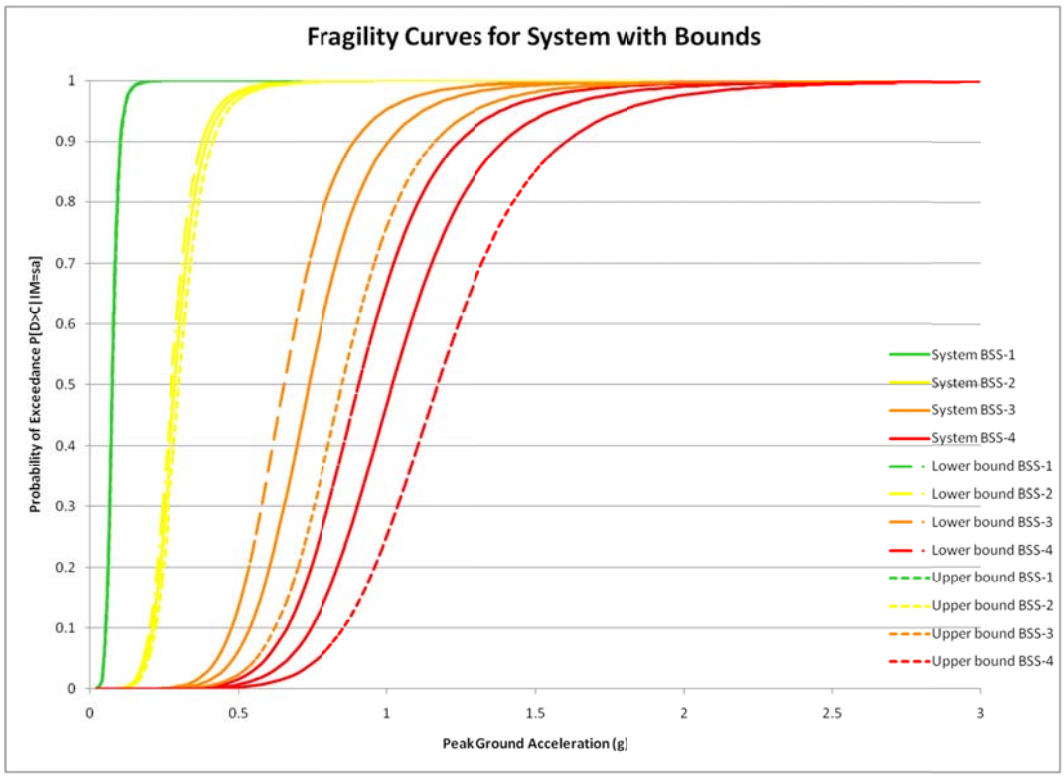

Fragility Curves for example bridge for the Abutment Gap Component

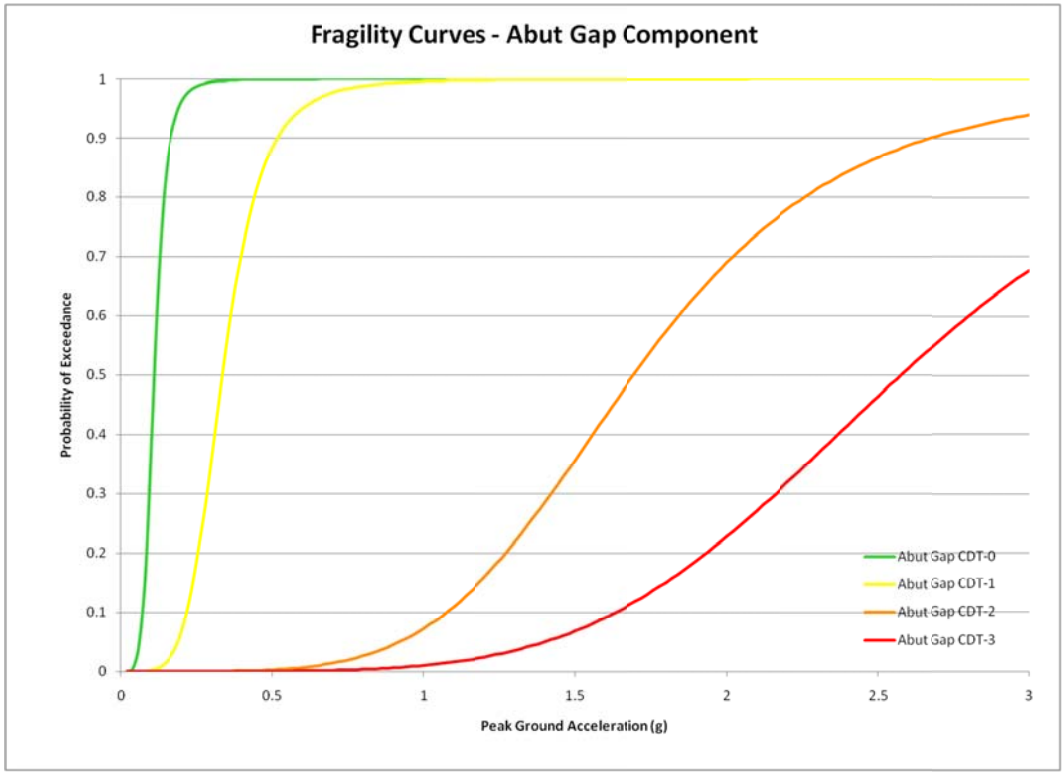

Fragility Curves for example bridge for the Abutment Gap Component with bounds

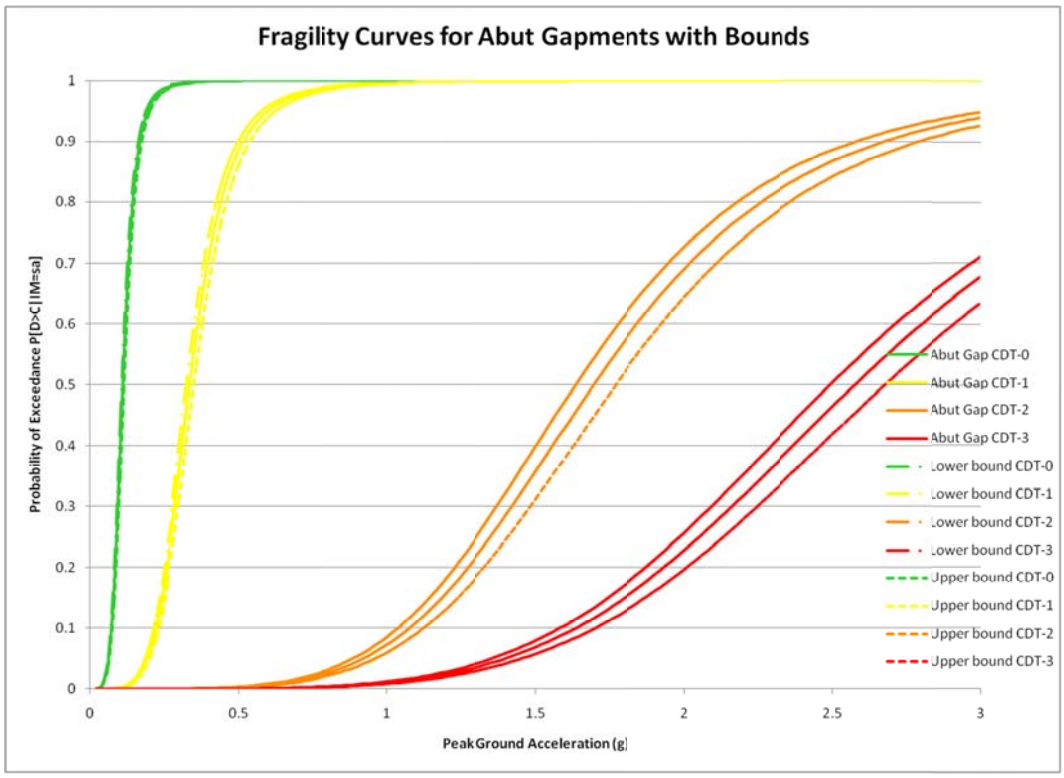

Fragility Curves for example bridge for the Transverse Bearing Component

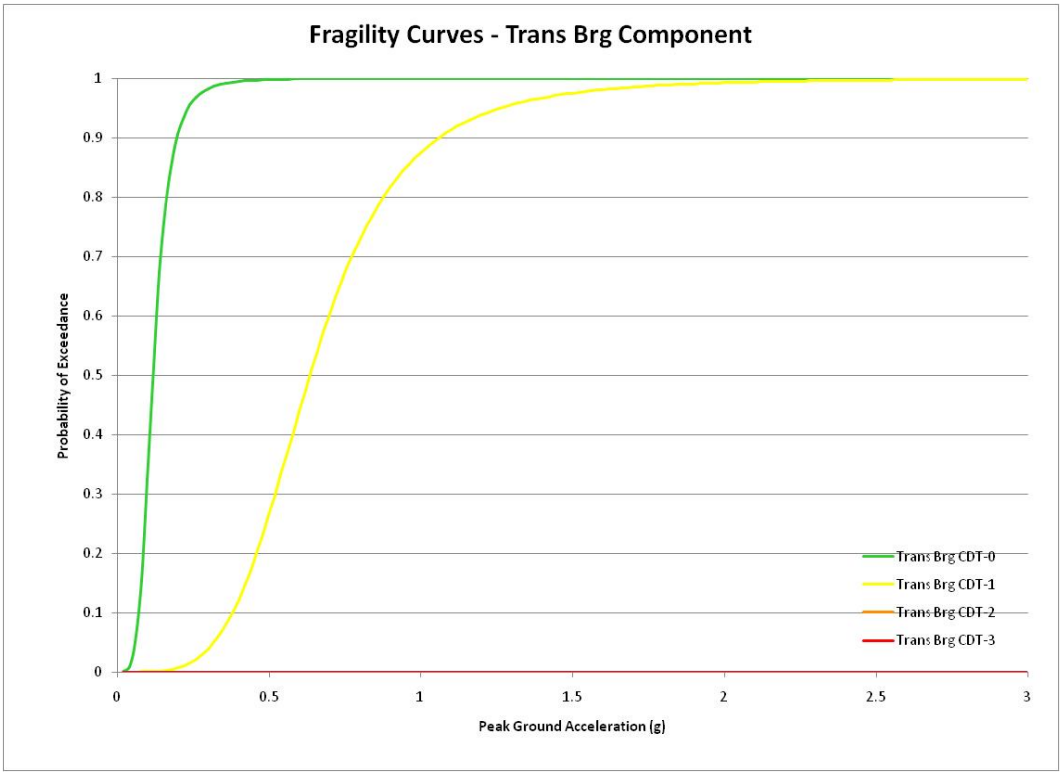

Fragility Curves for example bridge for the Transverse Bearing Component with bounds

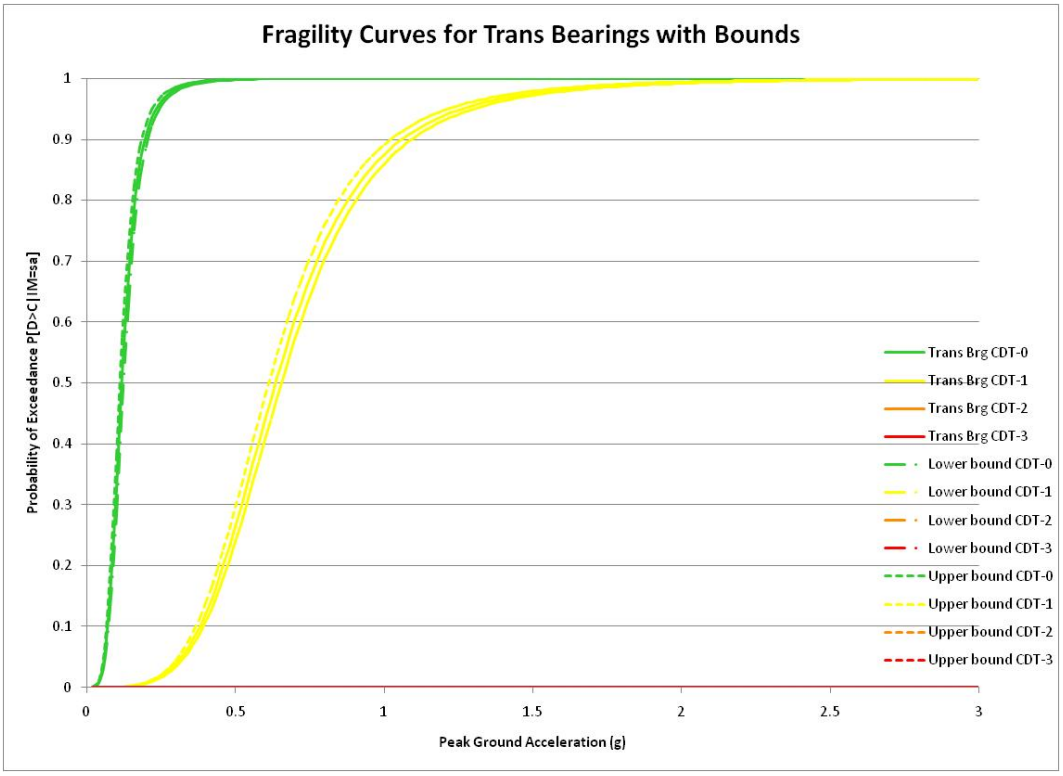

Fragility Curves for example bridge for the Longitudinal Bearing Component

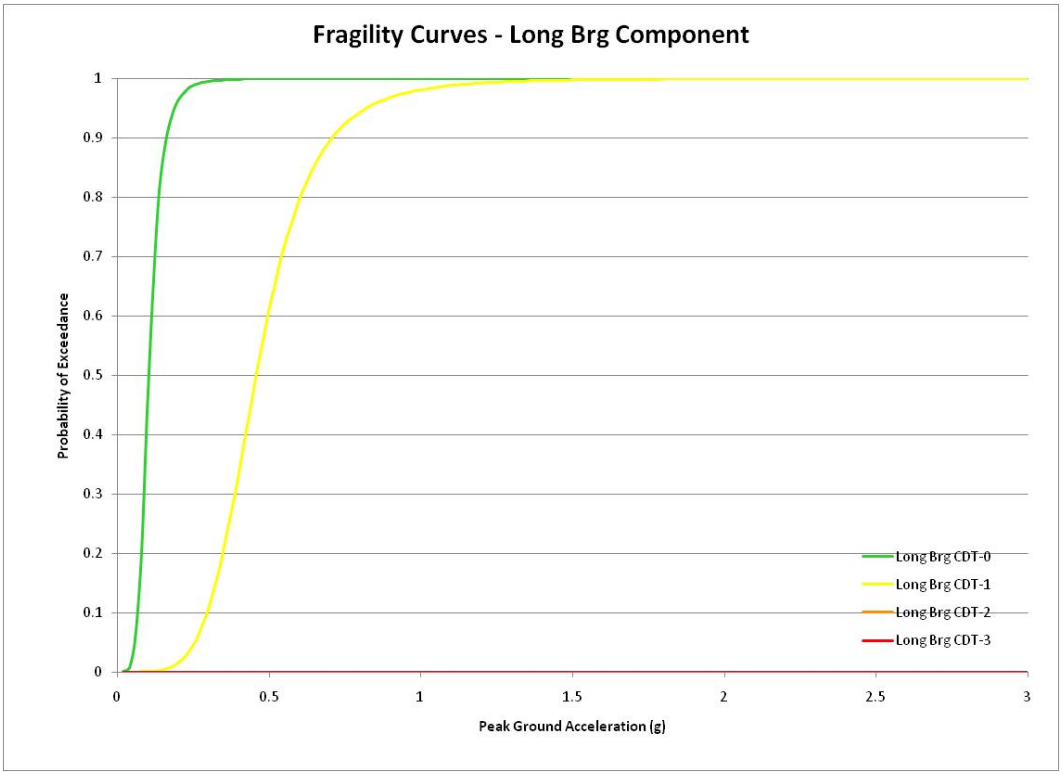

Fragility Curves for example bridge for the Longitudinal Bearing Component with bounds

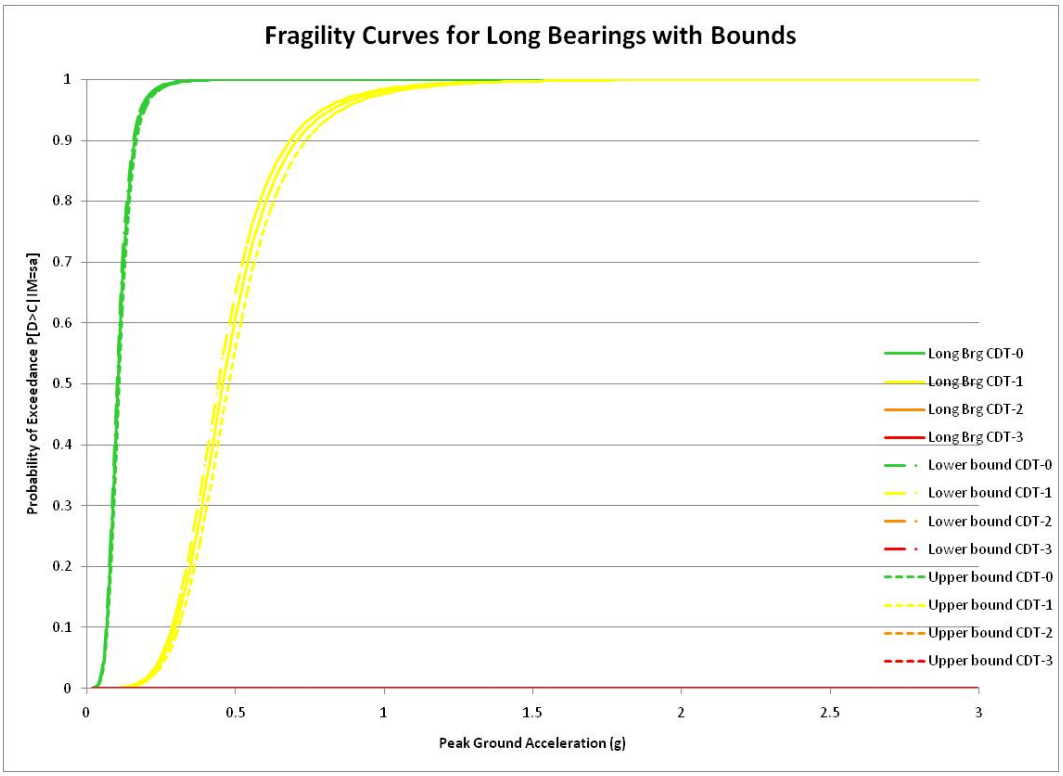

Fragility Curves for example bridge for the Joint Seals Component

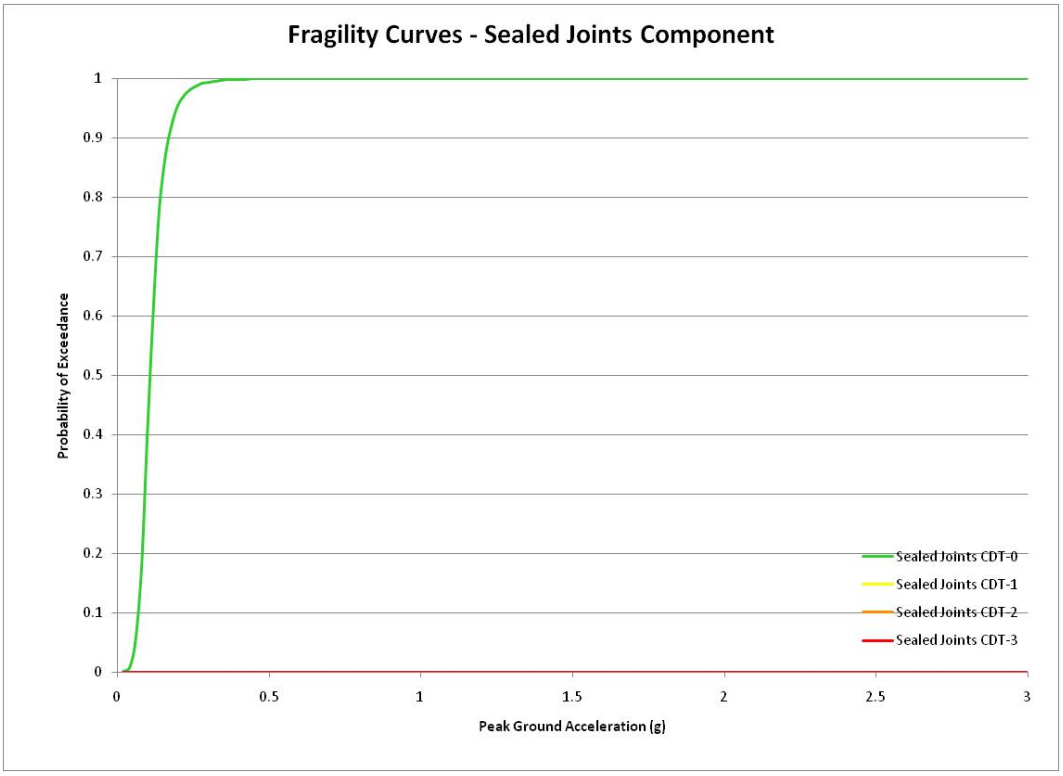

Fragility Curves for example bridge for the Joint Seals Component with bounds

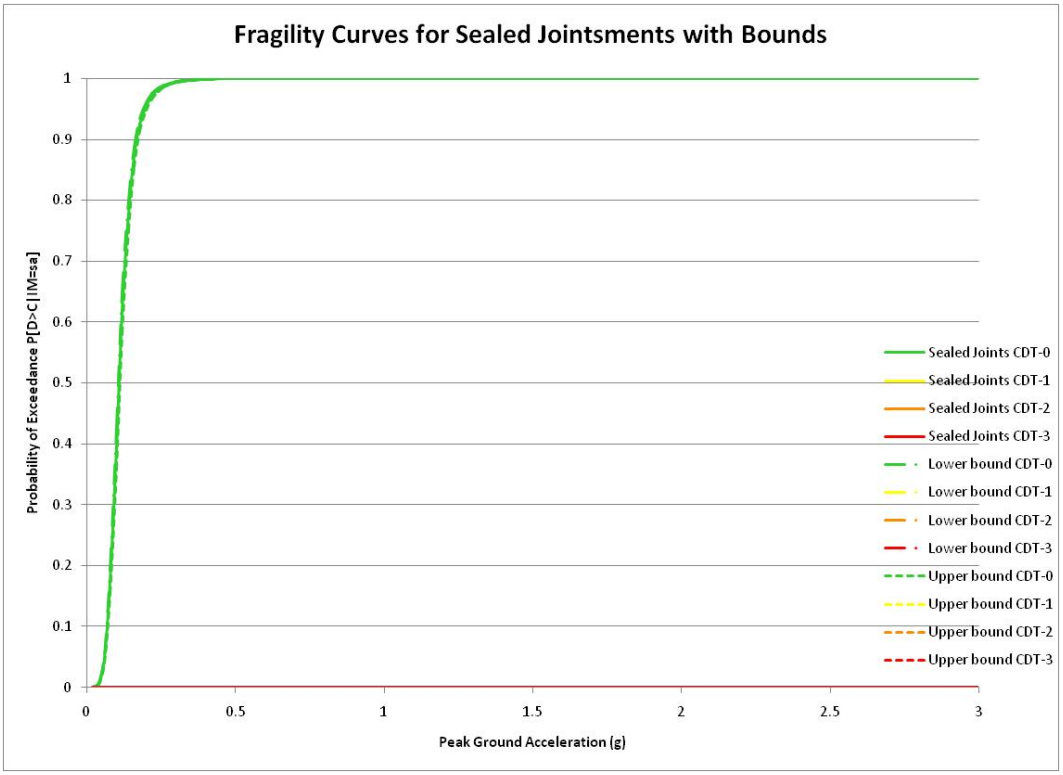

APPENDIX E

Regression Results and analysis

Fundamental Period Estimation:

Regression Equation and Results

$$\hat{P}eriod = \beta_0 + \beta_1 * LS + \beta_2 * VR + \beta_3 * AR + \beta_4 * SpanHt + \beta_5 * DepthDiam$$

The following are plots of the actual periods used in the regression estimation and the predicted periods with the regressions equation, as well as a plot of the residuals versus the predicted period values.

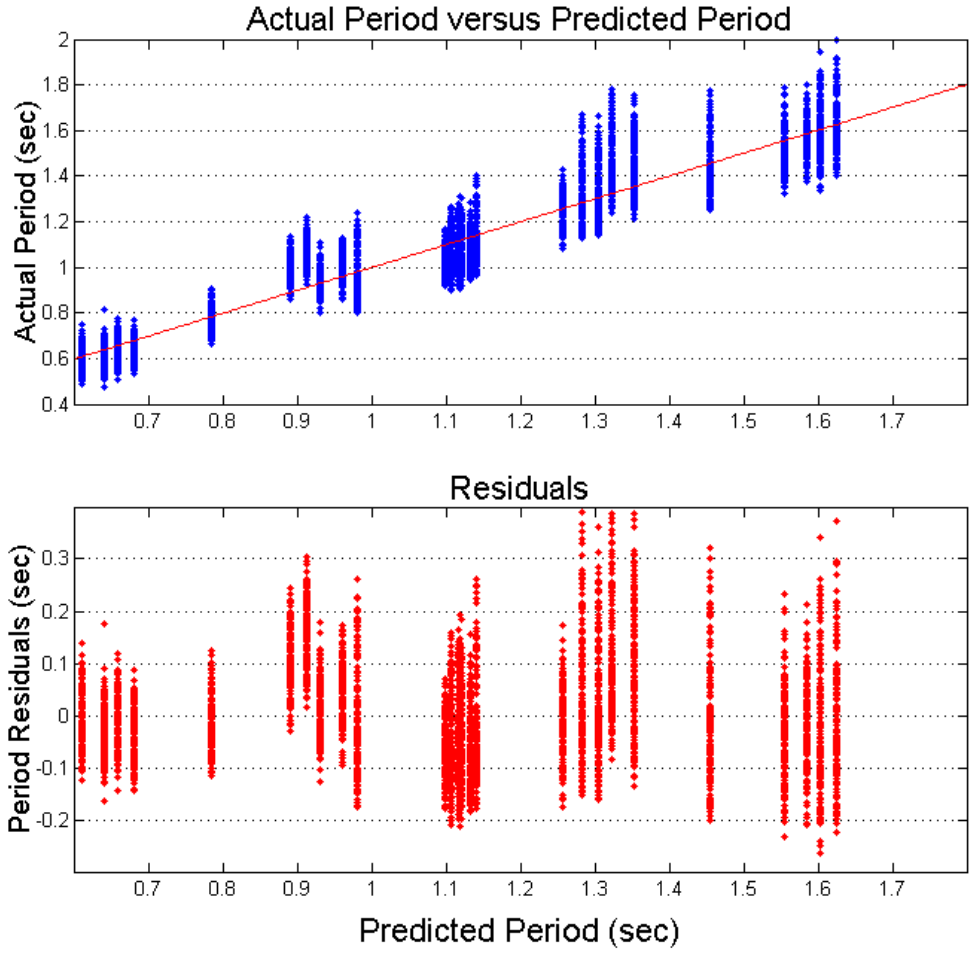

Discussion

The correlation between the predicted period value and the ones used in the regression estimation is 0.89, which strongly indicates a good model fit of the data. However, as is shown by the residual plot especially, there is a lot of scatter about the mean of the prediction equation, with residual up to 0.4 seconds, and up to 33% of the actual period value. This means this prediction equation may not give accurate estimations for the fundamental periods for all bridge designs. Possible reasons for the large errors could be the setup of the design of experiments, having only 28 base bridge models that differed according to the design parameters, the regression equation chosen was not the best fit, or more design parameters could be included to improve the fit. In future versions of the tool, these possible issues will be addressed in order to provide a much better fit for the estimation of the fundamental period of the bridge.

Feasibility Studies for Improving Caltrans' Bridge Fragility Relationships

Final Report

Part III

FINITE ELEMENT MODEL VALIDATION

Technical Report by Karthik N. Ramanathan, Jong-Su Jeon, Behzad Zakeri, Reginald DesRoches, and Jamie E. Padgett

FINITE ELEMENT MODEL VALIDATION

An important task in the current study was to test the efficacy of modeling assumptions and nonlinear dynamic analyses procedures in the vulnerability assessment of bridge classes in California. In order to do so, select bridges were modeled and the responses from the analytical finite element models were compared with recorded sensor data available through a wide network of sensors located on the bridges. The details of the modeling and validation procedure are presented in the attached technical paper which is currently under review.

SEISMIC RESPONSE PREDICTION AND MODELING CONSIDERATIONS FOR MULTISPAN CONTINUOUS CURVED AND SKEWED CONCRETE BOX-GIRDER BRIDGES

Karthik Ramanathan†*, Jong-Su Jeon†, Behzad Zakeri[£], Reginald DesRoches†, Jamie E. Padgett‡

†School of Civil and Environmental Engineering, Georgia Institute of Technology, 790 Atlantic Drive, Atlanta, GA 30332-0355
‡Department of Civil and Environmental Engineering, Rice University, 6100 Main Street, Houston, TX 77005-1827
[£]School of Civil Engineering, Iran University of Science and Technology, PO Box 16765-163, Narmak, Tehran 16846, Iran

*Corresponding author - Ph: (412) 736-8066, E-mail: karthik.ramanathan@gatech.edu

Abstract
This paper focuses on presenting modeling considerations and insight into the performance of typical straight, curved, and skewed box-girder bridges in California which form the bulk of the bridge inventory in the state. Three case study bridges are chosen: Meloland Road Overpass, Northwest Connector of Interstate 10/215 Interchange, and Painter Street Overpass, having straight, curved, and skewed superstructures, respectively. The efficacy of nonlinear dynamic analysis is established by comparing the response from analytical models to the recorded strong motion data. Finally insights are provided on the component behavioral characteristics and shift in vulnerability for each of the bridge types considered.

1. INTRODUCTION

The 1971 San Fernando, 1989 Loma Prieta, and 1994 Northridge earthquakes in California motivated significant research on the seismic response, analysis, and design of bridges. These earthquakes resulted in collapse or major damage to many bridges that were at least nominally

designed for seismic forces [Basoz and Kiremidjian, 1998; Priestley *et al.*, 1996]. Following the 1971 San Fernando earthquake, which exposed major deficiencies in bridges at that time; elastic bridge design philosophy was modified with a major focus on ductility and inelasticity and special attention to detailing aspects [Yashinsky and Ostrom, 2000]. The Loma Prieta and Northridge earthquakes furthered this approach when significant damage was observed in bridges constructed prior to 1971. A majority of the bridges constructed after 1971 performed exceptionally well demonstrating the superiority of the improved design and retrofitting philosophy.

Box-girder bridges constitute the bulk of the bridge inventory in California accounting for roughly 20% of the overall bridge inventory. These bridges experienced different levels of damage in the fore mentioned seismic events. Seventy six bridges were damaged during the Loma Prieta earthquake, and 233 in case of the Northridge event [Basoz and Kiremidjian, 1998]. The Loma Prieta earthquake demonstrated complete collapse of 48 bents of the Cypress viaduct built in 1957. Several other viaducts such as the Terminal Separation, Embarcadero, Central Viaduct, Southern Freeway Viaduct which were a part of the San Francisco Freeway System suffered extensive damage. The 1994 Northridge earthquake resulted in collapse of several bridges, all of which were multispan continuous concrete box-girder bridges. The vulnerability was attributed to the high skew, irregularities in the substructure stiffness, and inadequate seat widths [Fenves and Ellery, 1998]. Moehle et al. [1995] investigated the performance of the highway transportation system in the Los Angeles area during the 1994 Northridge earthquake. Partial and/or complete collapse of five reinforced and prestressed concrete box-girder bridges underlined the importance of understanding the seismic response of this class of bridges. As a result of the relative importance of the class of box-girder bridges and its abundance in the state inventory, it is imperative to accurately model and predict their response. Moreover, a better understanding of the effect of skew and curvature will result in the ability to better model these characteristics, and ultimately improve the capability of determining a number of principal effects of earthquakes such as traffic disruption, recovery cost and downtime as well as lead to robust design and retrofitting practices.

Advances in computing power together with a need for accurate response predictions greatly motivated the development and advancement of Finite Element (FE) Techniques. Description of the geometric domain, realistic representation of the boundary conditions, mass and damping, and imposed loading, forms the critical aspects of the technique. Global three dimensional bridge models have the unique capability of capturing the effects of complex geometries such as curves in plan and elevation, skewed orientations, and interaction between frames. However, the benefit of capturing the geometry accurately may be undermined due to errors arising from assuming uniformity or coherence in input seismic excitation at all supports, especially for long bridges. These estimates can be refined by imposing multi-support excitation in dynamic analysis. In most cases, earthquake scenarios cause damage at the member level and proper discretization of the total bridge system into smaller and sufficiently accurate subsystems such as frames, bents, bearings, abutments etc. is crucial.

Curved and skewed bridges suffered a lot of damage during the aforementioned seismic events in California. The presence of curves and skewed supports in the bridge superstructure results in complex vibration modes due to predominance of torsional with respect to the vertical axis of the

bridge. This out-of-phase motion may increase the deformation demand on several bridge components such as deck, column, abutments, and bearings. In particular, when these bridges with expansion joints at the abutments or intermediate hinges are subjected to varying levels of seismic excitations, additional hinge openings on the either side of deck due to the torsional effect may cause the potential for toppling of the bearing or potential unseating of the span. In addition, pounding between adjacent frames, occurring at the opposite side of the hinge opening, results in structural damage including concrete spalling at the hinges and create undesirable forces in the adjacent frames. Therefore, proper characterization of the force deformation response at the component level plays a major role in response prediction at the local member level and global bridge system level.

However, current bridge design specifications in the United States do not have any guidelines regarding performance assessment of curved and skewed concrete box-girder bridges subjected to earthquakes. Furthermore, very few studies focused on the behavior and modeling considerations of curved and skewed bridges and the relative shift in component vulnerability in these bridge types in comparison to straight and non-skewed bridges. The next section presents a concise literature survey on the modeling and behavioral aspects of curved and skewed bridges to date. This paper focuses on presenting modeling considerations and insight into the performance of typical straight, curved, and skewed box-girder bridges in California which form the bulk of the bridge inventory in the state. Three case study bridges are chosen for each of the fore mentioned types: Meloland Road Overpass, Northwest Connector of Interstate 10/215 Colton Interchange, and Painter Street Overpass, having straight, curved, and skewed superstructure geometries, respectively. The fundamental objective of this study is to provide detailed information about the FE modeling approach required to adequately capture the response of this bridge type and to determine the efficacy of nonlinear dynamic analysis to predict the response recorded in earthquakes. The responses from the generated FE models are compared with recorded strong motion data made available through a network of sensors instrumented on the case study bridges. A nonparametric evaluation technique is also employed to identify the bridge vibration periods using recorded sensor data. Finally insights are provided on the component behavioral characteristics and shift in seismic vulnerability among components for each of the bridge types considered with variable superstructure geometric configurations.

2. EARLY STUDIES ON PREDICTING BRIDGE RESPONSE TO SEISMIC EXCITATION

Ever since the 1971 San Fernando and 1989 Loma Prieta earthquakes, there has been an increased effort to understand the behavior of multispan bridges. These historic events lead to the establishment of a wide network of sensors on a large number of bridges in California by the Center for Engineering Strong Motion Data (CESMD) [Haddadi *et al.*, 2008].

Early studies on the seismic response prediction of bridges focused on the performance of the Meloland Road Overpass during the 1979 Imperial Valley earthquake. Several researchers [Douglas and Richardson, 1984; Douglas et al., 1990; Werner et al., 1987, 1993; Zhang and Makris, 2002] took advantage of the large amplitude response recorded during the 1979 Imperial Valley earthquake in validating and calibrating FE models. In addition, Werner et al. [1987,

1993], and Gates and Smith [1982] used system identification techniques to determine vibration properties of the bridge. Wilson and Tan [1990a, 1990b] proposed an analytical model composed of equivalent linear springs to represent the transverse and vertical stiffness of the abutment system and compared their responses with recorded sensor data pertaining to the 1979 Imperial Valley earthquake from the Meloland Road Overpass. The studies concluded that abutments and embankments had a major effect on the response of the bridge. Kwon and Elnashai [2008] used a multiplatform analysis including soil structure interaction and compared the response of the Meloland Road Overpass to the results from system identification techniques using recorded data on the bridge from the 1979 Imperial Valley earthquake.

Curved bridges exhibit complex behavior when subjected to seismic excitations. The presence of curves in the bridge superstructure gives rise to significant torsion about the vertical axis. This leads to coupled responses in the two horizontal directions, and thereby increasing the deformation demand on the bridge components. Fenves and DesRoches [1997] focused on the global response correlation using recorded sensor data with the analytical model for the Northwest Connector of Interstate (I) 10/215 Colton Interchange using Nonlinear Time History Analysis (NLTHA). The study employed elastic beam column models for most structural components except for the intermediate hinges. This could result in underestimating the column response if the columns experience nonlinear. Huang and Shakal [1995] provided a comprehensive interpretation of the recorded sensor data on the I10/215 Interchange bridge along with recommendations for bridge component modeling. Fenves and Ellery [1998] evaluated the earthquake response of the Separation and Overhead bridge at the Route 14 Interstate 5 interchange that partially collapsed during the 1994 Northridge earthquake. The analytical model represents intermediate hinge opening and closing, inelastic flexural response characterization of columns, restrainers, and abutments.

Akin to bridges curved in the superstructure, skewed bridges exhibit complex behavior and past earthquakes have demonstrated significant damage to bridges with higher skews as in the case of Foothill Boulevard Undercrossing and Interstate 5 Gavin Canyon Undercrossing damaged during the 1971 San Fernando and 1994 Northridge earthquakes, respectively [Schroeder, 2006]. Maroney et al. [1990] interpreted the dynamic response characteristics of the Painter Street Overcrossing by comparing the natural frequencies and mode shapes of different analytical models for six earthquakes events between 1980 and 1987. Sweet and Morrill [1993] used a nonlinear FE model to predict the response of the Painter Street Overcrossing in which special attention was given to the response of the embankment and foundations. Goel and Chopra [1997] calibrated the analytical model of the Painter Street Overcrossing using recorded sensor data to obtain refined values of embankment stiffness. McCallen and Romstad [1994] used the Painter Street Overcrossing as a case study to validate the stick modeling approach in estimating the seismic response of skewed bridges and compared it with detailed FE models. Zhang and Makris [2002] developed analytical FE models including soil structure interaction which was used in the response prediction of the Painter Street Overpass and showed good agreement. Fenves et al. [1992] obtained spectral estimates of vibration periods and compared the response obtained from a FE model with strong motion data recorded in the Dumbarton Bridge. The study revealed the sensitivity of earthquake response to assumptions about longitudinal constraints at the hinges. Although these studies did not focus on skew effects explicitly, they underscored the importance

of component modeling approaches when torsion dominates the overall response of the bridge which is predominant in skewed bridges.

The aim of this study is to provide detailed information about bridge component and system level modeling guidelines for box-girder bridges with three different superstructure plan layouts: straight, curved, and skewed. The approach chosen goes a long way in capturing the nonlinearity associated with bridge components, such as columns, bearings, abutments (soil-pile system), and pounding effects. A case study bridge is chosen depicting each case and the characteristics of the bridge are described and details are provided on the analytical modeling and validation procedure in the next section of the paper.

3. CASE STUDY BRIDGE DESCRIPTION – ANALYTICAL MODELING PROCEDURE

This section provides a detailed description of the three case study bridges along with information about the analytical modeling procedure.

3.1 Meloland Road Overpass

The Meloland Road Overpass is a two span reinforced concrete box-girder bridge built in 1971 located in Southern California. The bridge has two equal spans 104 ft in length and 34 ft wide supported on a single column bent 21 ft high integral with the superstructure that frames into diaphragm abutments at its ends. The bridge is instrumented with twenty six channels of accelerometers and the 1979 Imperial Valley earthquake is the strongest earthquake to strike the bridge with peak ground acceleration (PGA) values of 0.32g, 0.30g, and 0.23g in the longitudinal, transverse, and vertical directions, respectively.

Figure 1 shows the layout of the bridge along with details of the analytical modeling procedure. A three dimensional spine model of the bridge is created in the FE platform OpenSEES [McKenna *et al.*, 2010]. The deck and the columns are modeled using nonlinear beam column elements with fiber defined cross-sections and lumped masses. Fiber defined cross-sections help in capturing the spread of plasticity in the element and at the same time facilitates the specification of different properties for cover and core concrete to account for the effects of confinement and ductility. The model of Mander et al. [1988] was used to account for the enhanced compressive strength and ductility of core concrete due to confinement. The superstructure is characterized by three cross-sections in the longitudinal direction: rigid (solid) diaphragms at the top of the column and back wall in the abutments; three cell box-girder sections near the supports; and single cell box-girder sections in the central regions of the spans. Nonlinear translational springs are used to capture the response of the abutments in the longitudinal and transverse directions. The longitudinal abutment response is comprised of active and passive actions. Soil and piles contribute to the passive (compressive) resistance of the abutments while the active (tensile) resistance is assumed to be provided by the piles alone. The transverse response of the abutment is assumed to be characterized solely by the piles.

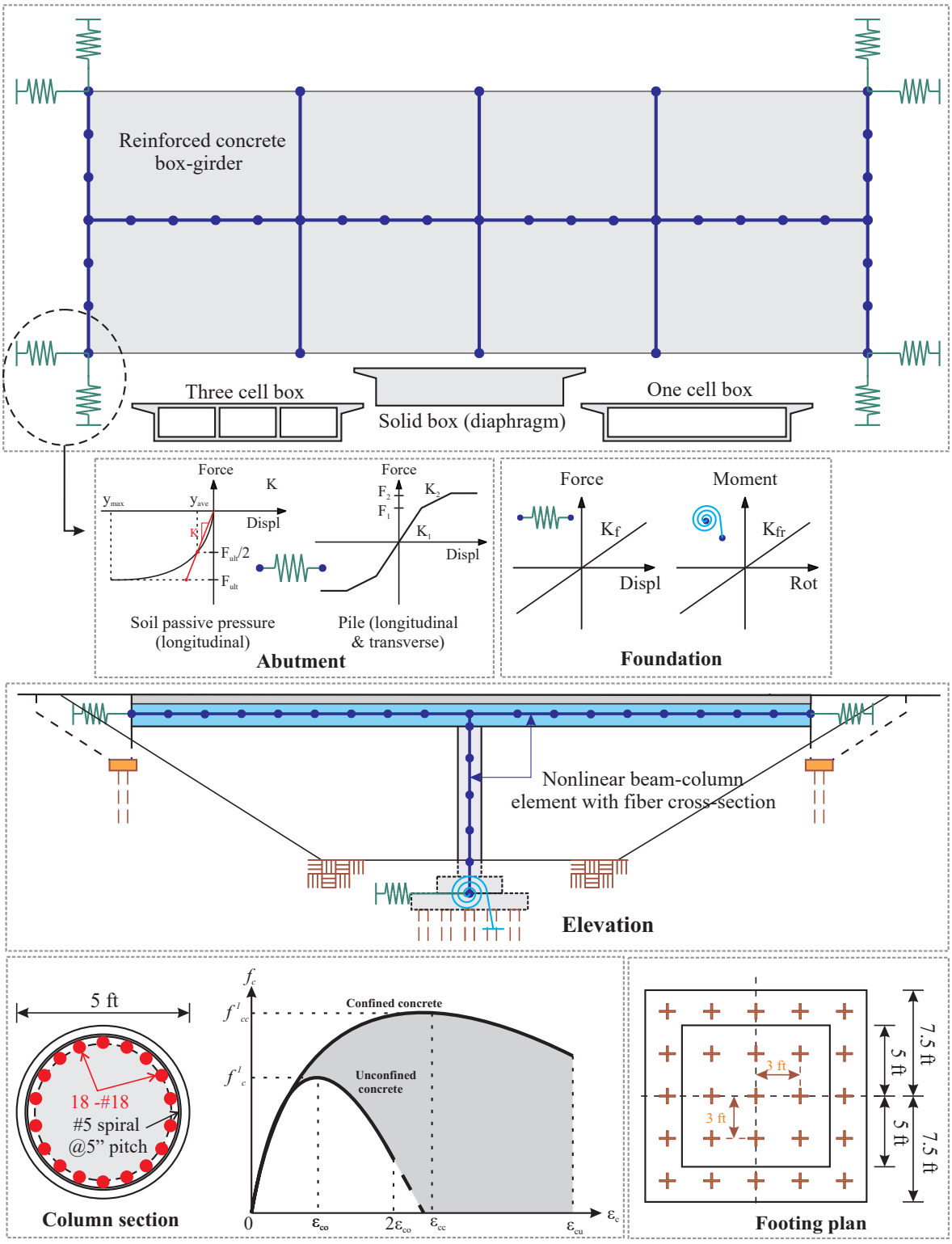

Figure 1: Details of the Meloland Road Overpass analytical modeling procedure

The hyperbolic soil model proposed by Shamsabadi *et al.* [2010] is used to capture the response of the abutment backwall soil in passive action. The model is based on experimental testing of

bridge abutments with typical backfills. The initial stiffness of the soil is assumed to be 116 kips/in and the ultimate passive resistance is 1.86 kips per inch width of the abutment back wall [Shamsabadi *et al.*, 2010]. Zero length springs characterized by nonlinear soil behavior are used to capture the response of the abutment soil. The response of piles was described by a trilinear force deformation curve stemming from the recommendations of Choi [2002] assuming a translational stiffness of 40 kips/in/pile based on the recommendations of Caltrans Seismic Design Criteria [Caltrans, 2010].

Lumped translational and rotational springs at the base of the column are used to capture the behavior of pile foundations. The composite behavior is evaluated based on geometry and pile group effects [Ma and Deng, 2000]. 15% Rayleigh damping in the first two modes was considered in this study following the recommendations of Zhang and Makris [2002].

3.2 Northwest Connector - I10/215 Colton Interchange

The Northwest Connector constructed in 1969 is a curved bridge which carries two lanes of traffic from eastbound I-10 to northbound I-215 at an interchange in Colton, California. The connector is a 2,540 ft long, curved, concrete box-girder bridge with sixteen spans supported on single column bents and diaphragm abutments. Beginning at Abutment 1, the alignment is composed of three segments: a curved segment 1,018 ft long and 1,200 ft radius, a curved segment 1,268 ft long and 1,300 ft radius, and a 254 ft straight segment ending at Abutment 17. The central portion of the bridge has a vertical curve of 900 ft radius with a maximum profile grade of 4.74%. The Northwest Connector was one of the first curved bridges to be instrumented by CESMD and has strong motion data recorded during the 1992 Landers earthquake.

The layout of the Northwest Connector is shown in Figure 2. The superstructure consists of five intermediate hinges (Hinge 3, Hinge 7, Hinge 9, Hinge 11, and Hinge 13) and six frames of conventional reinforced and prestressed concrete box-girders, which rest on elastomeric bearing pads at the bent caps. Both types of concrete box-girders are similar except for the web thickness of the interior cells. The as-built flared octagonal columns are 5.5 ft × 8.0 ft in dimension and the bent cap is 9.5 ft wide and 8 ft deep. The foundations for the column bents consist of a pile cap and reinforced concrete piles ranging from 21 ft to 50 ft in depth. At the diaphragm abutments, the box-girder is integral with a 13 ft high backwall and the tapered wing walls are 18 ft long. Abutments 1 and 17 have nine 72 ft long piles and seven 43 ft long piles, respectively. The five intermediate hinges have seat widths ranging from 32 to 36 in. Shear keys were used to inhibit the relative transverse displacement whose sides have a quarter inch joint filler. In 1991, the connector underwent column and footing retrofit along with replacement of the cable restrainers. The columns were retrofit using a half inch thick elliptical steel jacket, while the footings were strengthened by increasing their size, addition of steel jacket and provision of supplemental steel piles. The retrofitted bridge was considered for the analytical modeling procedure and FE model validation using the 1992 Landers earthquake since the strong motions were recorded on the retrofit bridge structure.

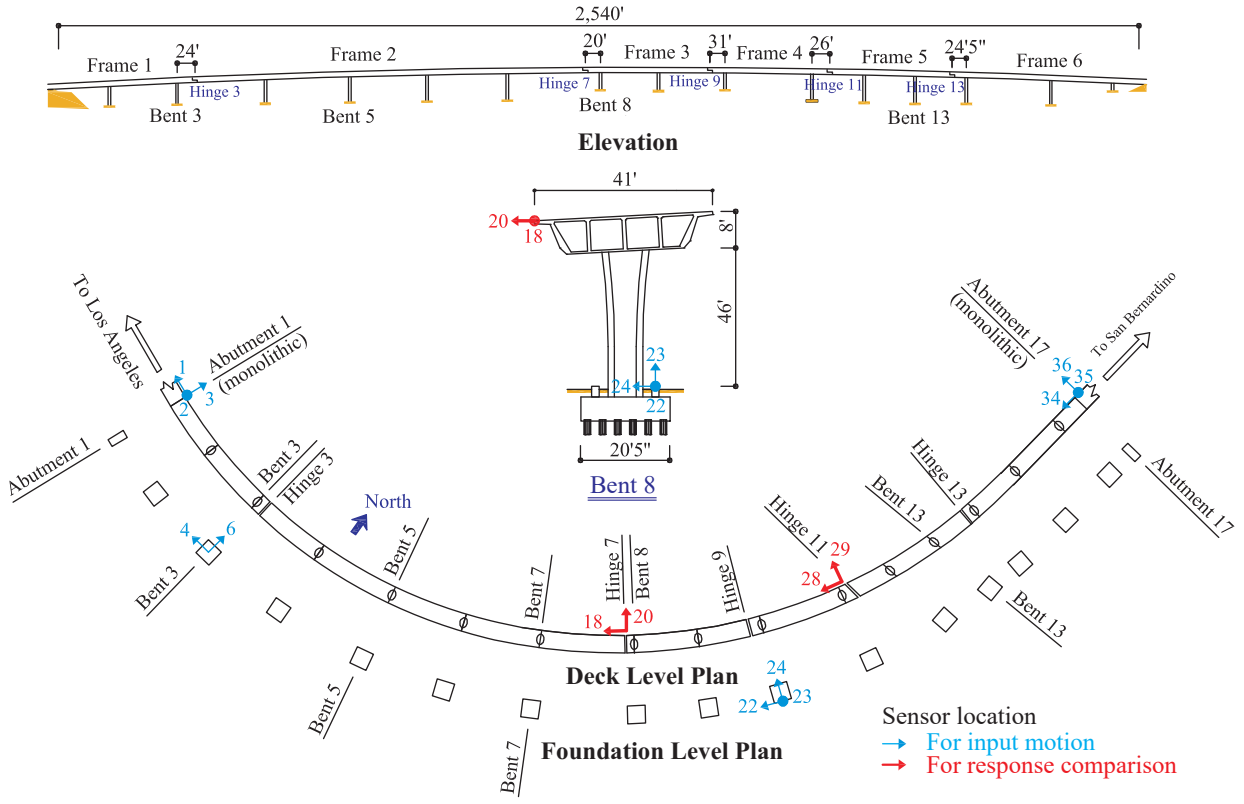

Figure 2: Layout and sensor locations for the Northwest Connector – Colton Interchange

Figure 3 shows the analytical modeling procedure of the Northwest Connector. As in the case of the Meloland Road Overpass, OpenSEES was chosen as the FE analysis platform. The superstructure is modeled as a spine with elastic beam column elements as it is expected to remain elastic during seismic events. The effective stiffness for reinforced (Frames 1, 3, 5, and 6) and prestressed (Frames 2 and 4) concrete box-girders are based on 75% of the gross stiffness to account for concrete cracking and the full gross stiffness [Caltrans, 2010]. The effective superstructure width is reduced near the bent caps following the recommendations of Priestley et al. [1996] and Caltrans [2010]. The transverse deck elements are modeled as rigid, massless beam elements to represent the diaphragm and intermediate hinges and account for the twisting of the box-girder. Buckle et al. [2006] emphasized the necessity to account for the rotational mass moment of inertia along the bridge axis for curved bridges. Henceforth, 40% of the energy equivalent mass is lumped at the ends of the transverse beam elements in the vertical direction, and the remainder of the mass is lumped at the centerline along the bridge axis.

The columns are modeled using displacement-based beam column elements with fiber sections and rigid links at the superstructure-column connections and the footing-column connections to transfer all of the moment. As in the previous case, the Mander model [1988] is used to account for the enhancement of compressive strength and ductility of core concrete. In addition, for retrofitted columns, the confinement due to elliptical steel jackets is accounted for based on

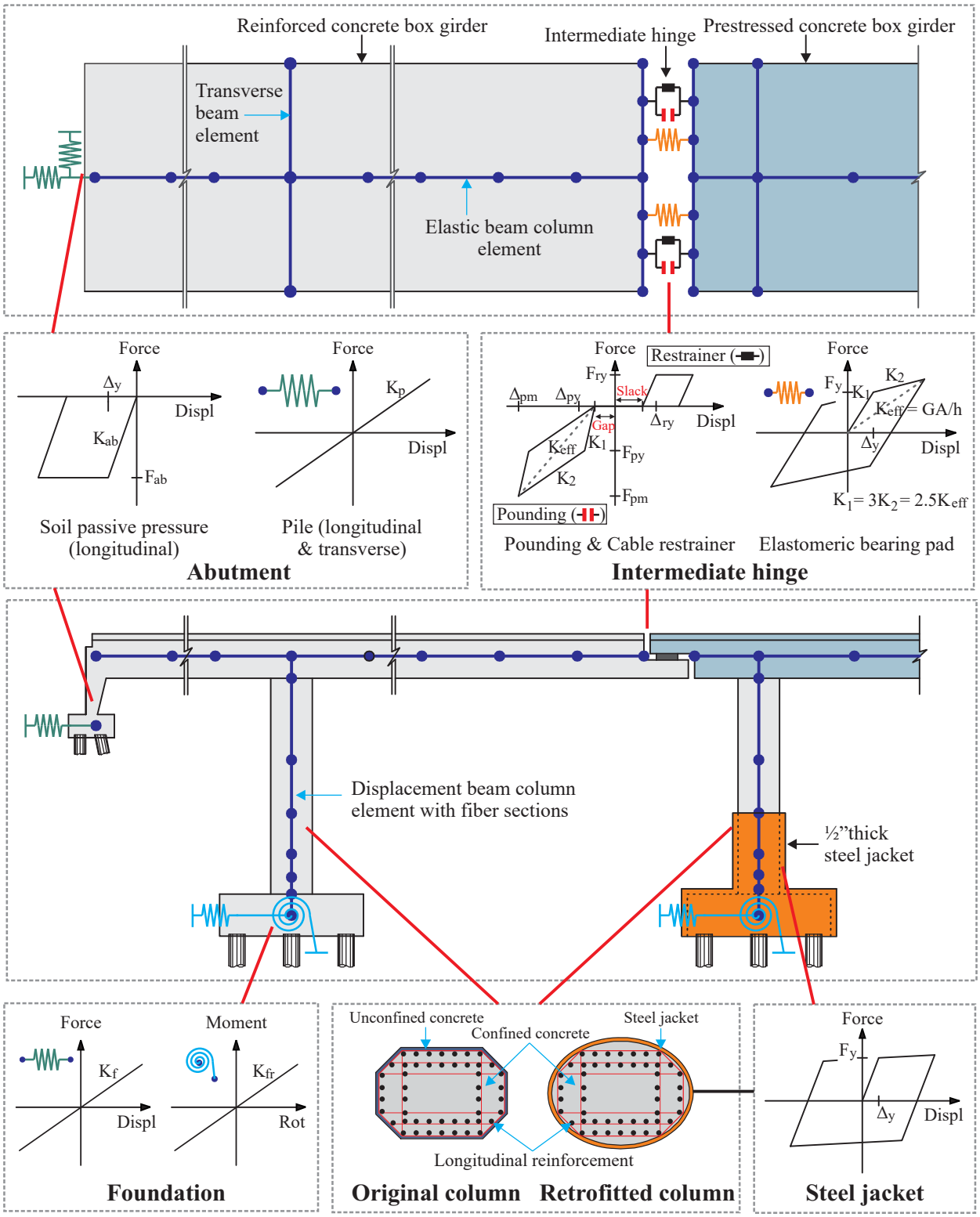

Figure 3: Details of the Northwest Connector – Colton Interchange analytical modeling procedure

the recommendations of Priestley et al. [1994] and the steel jacket is modeled using a hardening material. Furthermore, the torsional constant for columns was reduced by 80% following the

recommendations of Caltrans [2010]. Pile foundations are represented by altering the linear translational and rotational springs based on equations presented in Ma and Deng [2000]. The translational and vertical spring stiffnesses for the piles are considered as 40 kips/in [Caltrans, 2010] and 1,000 kips/in [Choi, 2002], respectively. The abutments are modeled using nonlinear translational springs characterized by bilinear behavior following the recommendations of Caltrans [2010]. In this case, the longitudinal behavior of the abutments is comprised of passive and active actions accounted for by the soil and piles and piles alone, respectively. The transverse abutment behavior is characterized by piles alone.

The intermediate hinge model consists of contact elements that consider the pounding effect between adjacent decks, cable restrainer with an initial slack and elastomeric bearing. The afore mentioned component behaviors are replicated by considering zero length nonlinear springs characterized by the respective component force deformation characteristics, as shown in Figure 3. The pounding element is defined based on the recommendations of Muthukumar and DesRoches [2006] and the restrainer is modeled as a nonlinear tension-only element with an initial slack. The stiffness of the cable restrainers is given by EA/L where E is the modulus of elasticity, A is total cross sectional area of the restrainer cables, and L is the length of the restrainers, with values of 10,000 ksi, 0.22 in^2, and 20 ft, respectively. The total yield force is based on an individual cable yield force of 39.1 kips. Elastomeric bearing pads with shear modulus of 150 psi are modeled using a bilinear element proposed by Naeim and Kelly [1999]. The hinge gaps and slack in the restrainer cables are the same as those adopted by Fenves and DesRoches [1997]. Since the gap between shear key and upper deck is only a quarter inch, the relative transverse displacement is constrained to be zero in the analytical model. Furthermore, the relative vertical displacement and twisting at the hinge is also constrained.

3.3 Painter Street Overpass

The Painter Street Overpass is located on Highway 101 in Rio Dell, California. The monolithic, cast-in-place skewed bridge built in 1976 consists of prestressed concrete box-girders supported on a two column bent framing into end diaphragm abutments. This bridge has two spans measuring 146 ft and 119 ft in length. The bridge has a 39° skew angle between the centerlines of bent and deck. The bridge columns are circular in cross section with 5 ft diameter and flare to a width of 9 ft at the top. While the east abutment is monolithic with the foundation, the west abutment is located on a bearing pad on top of the pile cap. Both the columns and abutments are founded on piles. A longitudinal shear key is located at a gap of 1 in at the right abutment and the transverse ones are located on either side of the abutment to prevent additional displacement of the bridge during seismic excitation. This expansion joint is filled with expanded polystyrene and protected with angle-shaped neoprene to prevent the entry of soil and water into the joint. The bridge was instrumented in 1977 with seventeen channels of accelerometers.

Global seismic behavior of a skewed bridge is affected by a number of factors, including the skew angle, column ductility, shear keys, and characteristics of the seismic source [Shamsabadi, 2007] among others. Figure 4 shows details of the analytical modeling procedure adopted for the Painter Street Overpass. As in the previous two case study bridges, the columns of the Painter Street Overpass are modeled using nonlinear beam column elements with fiber defined cross-section which accounts for the nonlinear behavior exhibited at the elemental and cross-sectional

levels, while the deck is modeled as a linear elastic section anticipating elastic response during seismic excitation.

Abutments tend to dominate the overall bridge response in the case of short and skewed bridges, and capturing their behavior is important [McCallen and Romstad, 1994]. Since the bridge abutments are monolithic with the deck, they are consequently modeled using vertical rigid elements. As in the case of the Meloland Road Overpass, the soil abutment interaction is modeled using the hyperbolic soil model proposed by Shamsabadi et al. [2010]. The model is based on experimental testing of bridge abutments with typical backfills [Stewart *et al.*, 2007; Romstad et al., 1995]. An average value of 2.1 kips/in/in is implemented as the initial stiffness for passive pressure with maximum deformation restricted to 10% of the back wall height in the hyperbolic force displacement curve purposed by Shamsabadi et al. [2010]. The hyperbolic curve is subsequently approximated by a multi-linear curve using parameters specified by Choi [2002]. Zero length elements characterized by this force deformation relationship are located at the top of the abutments in the longitudinal direction. The bridge has two wing walls at each end which significantly influence the seismic response of the bridge. As a result, the wing wall effectiveness and participation coefficient values equal to 2/3 and 3/3, respectively, are used following the recommendations of Maroney et al. [1994]. The passive response of the soil behind the wing walls are modeled in the same fashion as in the case of the abutment back wall. Zero length elements characterized by the force deformation response of the wing wall soil are assigned to the analytical model in the transverse direction. Pile elements are located in the longitudinal and transverse directions at the bottom of abutment rigid element. These elements are described by a trilinear force deformation curve stemming from the recommendations of Choi [2002] assuming a translational stiffness of 40 kips/in/pile based on the recommendations of Caltrans [2010].

As previously mentioned, the west abutment has one shear key in the longitudinal direction and two shear keys in the transverse direction at a 1 in gap. The force deformation response of the shear keys is modeled using a trilinear curve following the Caltrans - UCSD field experiments [Megally *et al.*, 2002]. The zero length elements capturing the response of the shear keys are assembled in series with pile elements and a gap element. In the longitudinal direction, the gap element is modeled using an initial stiffness equal to 15% of shear key stiffness. Further, the abutment rests on elastomeric bearing pads on top of the pile cap. The response of the bearing pads is modeled using a bilinear model governed by friction with an assumed value of coefficient of friction between concrete and the neoprene equal to 0.4. For the east abutment where the abutment and foundation are monolithic, a conservative approach is taken and the contribution of piles alone is considered in either direction.

The column foundation consists of 4 rows of 5 piles each, as shown in Figure 4. The foundation system is represented by a pair of translational springs in the longitudinal and transverse directions. The force deformation relationship of the springs is modeled using a bilinear relationship following the recommendations of Choi [2002]. The pile translational stiffness is assumed to be 40 kips/in/pile, similar to the case of the abutment piles. The rotational stiffness of the foundation is neglected since the columns are pinned to the pile cap.

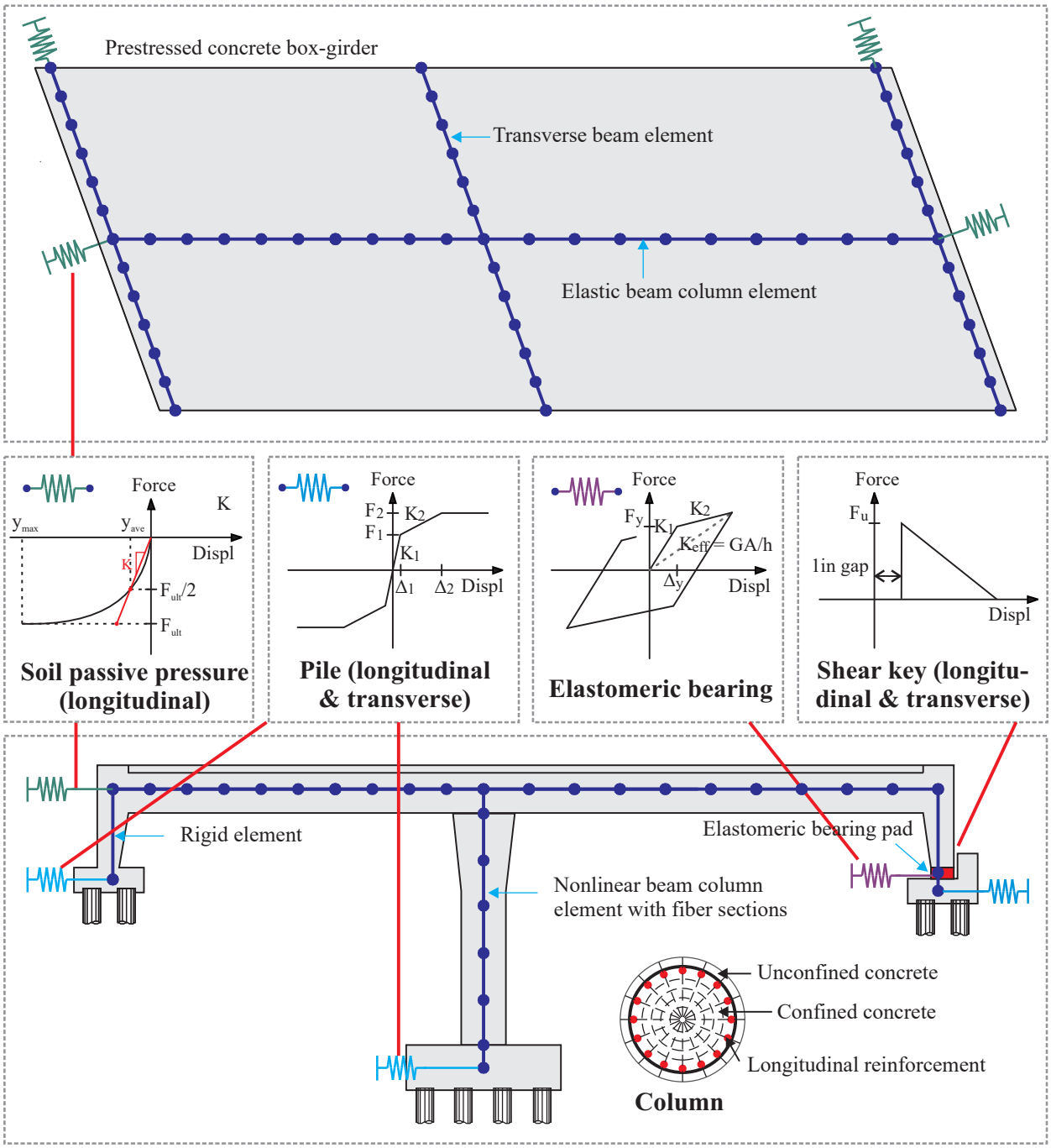

Figure 4: Details of the Painter Street Overpass analytical modeling procedure

4. FINITE ELEMENT MODEL VALIDATION

The aim of this study is to determine the efficacy of detailed nonlinear analytical modeling and dynamic analysis procedures to predict the response of box-girder bridges with complex geometries during earthquakes. This section presents the results of modal analysis for each of the case study bridges. Comparison between the results of NLTHA on the analytical bridge models and the recorded sensor data for certain scenario earthquakes that each bridge is subjected to are

also presented. The 1979 Imperial Valley earthquake is used in the case of the Meloland Road Overpass while the 1992 Landers earthquake is used in the case of the Northwest Connector. The 1992 Cape Mendocino/Petrolia earthquake is used for validating the Painter Street Overpass. Spectral analysis which is a non-parametric technique to determine the vibration periods using the sensor data is also performed to compare the respective values with those obtained using the analytical modeling.

4.1 Spectral Analysis

Spectral analysis is a qualitative non-parametric analysis technique that is used frequently to determine the vibration periods of structures. The technique involves the determination of transmissibility functions in order to aid in the determination of the modal periods of the bridge. Transmissibility functions [Ljung, 1987; Pandit, 1991] express the relationship between recorded input acceleration for a structure and the recorded output acceleration of the structure, as described in equation (1).

$$S_{yx}(\omega) = H(i\omega)S_{xx}(\omega) \qquad (1)$$
$$S_{yy}(\omega) = H(i\omega)S_{xy}(\omega)$$

In equation (1), ω is the frequency of vibration; $S_{xx}(\omega)$, $S_{yy}(\omega)$ denote the power spectral density (PSD) functions; $S_{xy}(\omega)$, $S_{yx}(\omega)$ denote the cross power spectral density (CPSD) functions; and $H(i\omega)$ is the transmissibility function. It must be noted that $S_{xy}(\omega)$ and $S_{yx}(\omega)$ are complex conjugates. Typically, the two estimates of the transmissibility function shown in equation (2) obtained by rearranging equation (1) slightly differ due to presence of noise and leakage associated with the discrete Fourier transform.

$$H_1(i\omega) = \frac{S_{yx}(\omega)}{S_{xx}(\omega)} \qquad (2)$$
$$H_2(i\omega) = \frac{S_{yy}(\omega)}{S_{xy}(\omega)}$$

The periodogram estimation technique [Oppenheim, 1989] is used to estimate the PSD and CPSD functions and the transmissibility function is derived as described in equation (2). The technique involves performing Fast Fourier Transform (FFT) of several overlapping segments of the signal. The periodogram is then computed as the average of the square of the FFT amplitudes over the segments and may therefore be visualized as a procedure to smoothen the Fourier spectrum of the recorded data. The absolute value or the magnitude of the transmissibility function, $H(i\omega)$ is called the transmissibility factor (TF) and the frequency at which the transmissibility factor is maximum is the fundamental frequency of vibration of the structure. The ratio of the imaginary and real components of $H(i\omega)$ gives the tangent of the phase angle between the input and output signals. The phase angle essentially varies between $-\pi$ and $+\pi$ radians.

Figures 5a and 5b show the plot of TF versus frequency for the Meloland Road Overpass and Painter Street Overpass, respectively while figures 5c and 5d show the plot of phase angle versus frequency. Clearly it is seen that the phase angles vary between -180 and +180 degrees for both the bridge types. Table 1 shows a comparison of the first two modal vibration periods obtained using the analytical model and spectral analysis. Also shown are results from some of the previous studies on these bridges. It is seen that in general there is a very good agreement between the results. Figures 6a thru 6c show the fundamental mode shapes for the case study bridges. The fundamental mode is in the transverse direction for the Meloland Road Overpass and the Northwest Connector while it involves a coupled longitudinal and transverse mode for the Painter Street Overpass.

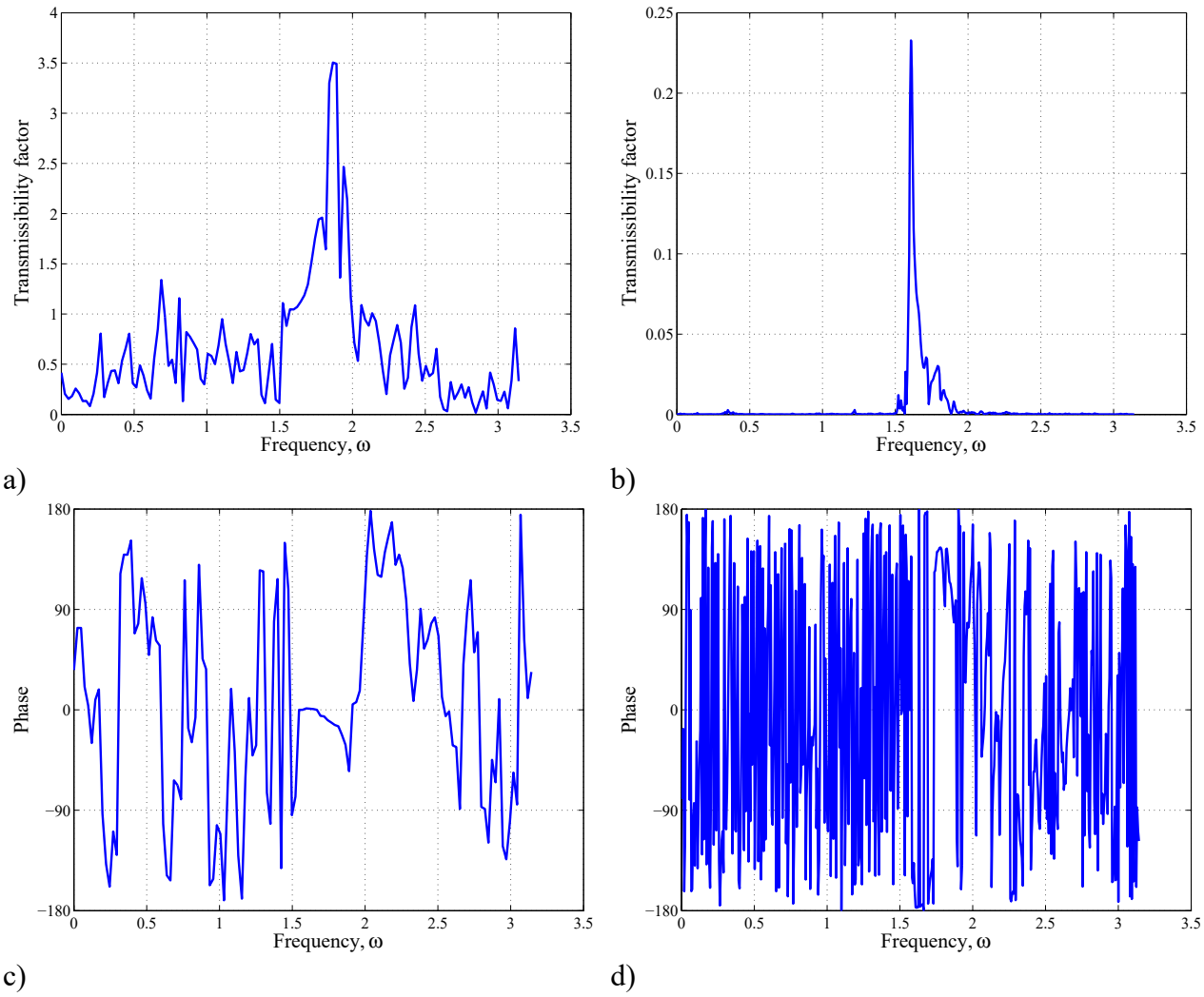

Figure 5: Plot of transmissibility factor versus frequency for a) Meloland Road Overpass and b) Painter Street Overpass; plot of phase angle versus frequency for c) Meloland Road Overpass and d) Painter Street Overpass.

Table 1: Comparison of modal vibration periods from spectral analysis and analytical model

Bridge	Analytical model		Spectral Analysis		Previous studies	Mode -1	Mode -2
	Mode-1	Mode-2	Mode-1	Mode-2			
Meloland Road Overpass	0.46	0.35	0.51	0.38	Zhang and Makris Kwon and Elnashai Werner et al.	0.49 0.32 0.39	0.35 0.31 -
Northwest Connector	1.58	1.44	1.56	1.30	Fenves and DesRoches Liu et al.	1.56 1.89	1.30 1.67
Painter Street Overpass	0.52	0.48	0.63	0.54	Zhang and Makris	0.56	0.44

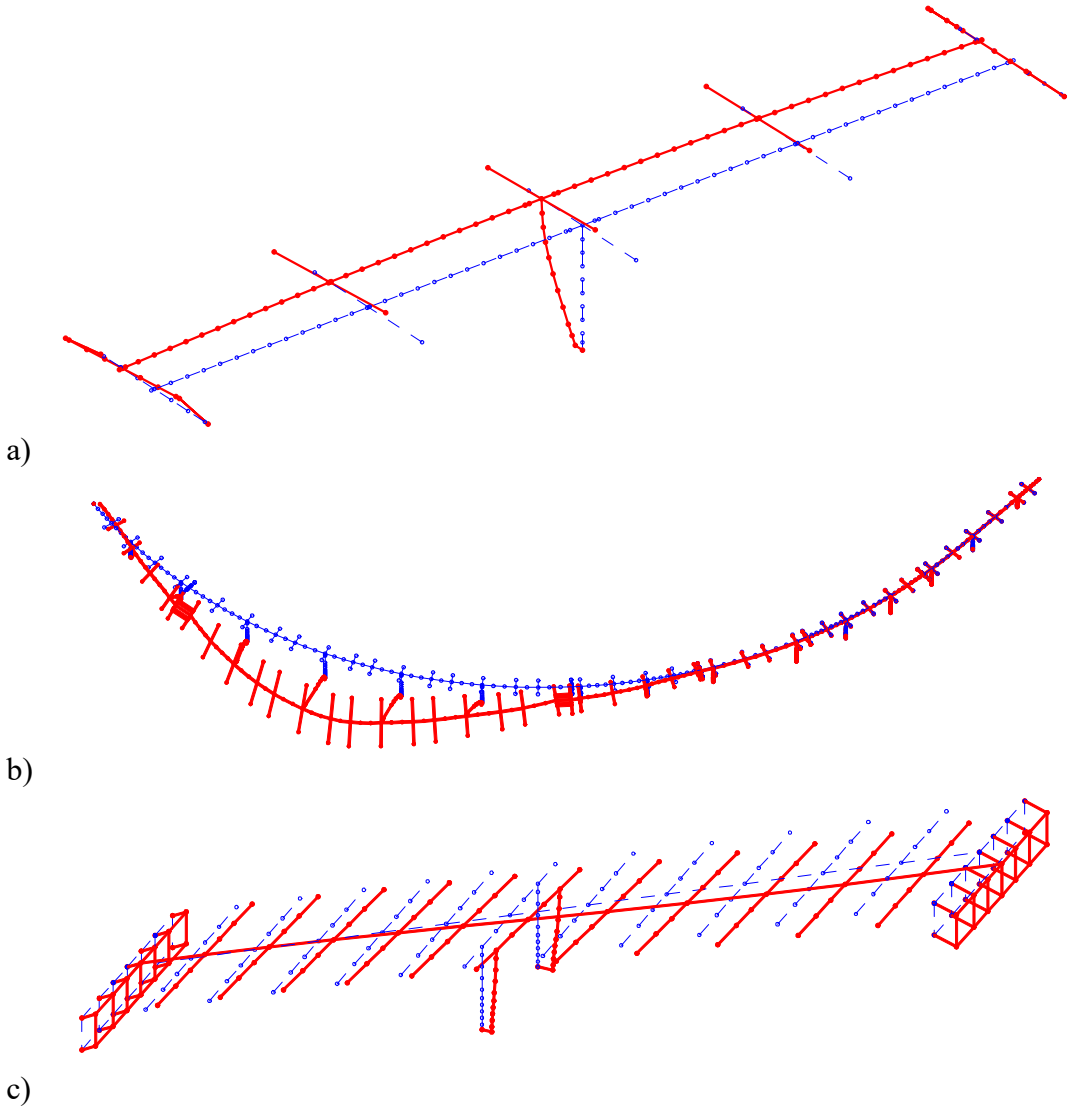

Figure 6: Fundamental mode shapes for a) Meloland Road Overpass, b) Northwest Connector, and c) Painter Street Overpass.

4.2 Response comparison – analytical model and recorded sensor data

Figures 7a and 7b show the sensor layout for the Meloland Road Overpass and Painter Street Overpass, respectively. The sensor layout for the Northwest Connector was already shown in Figure 2.

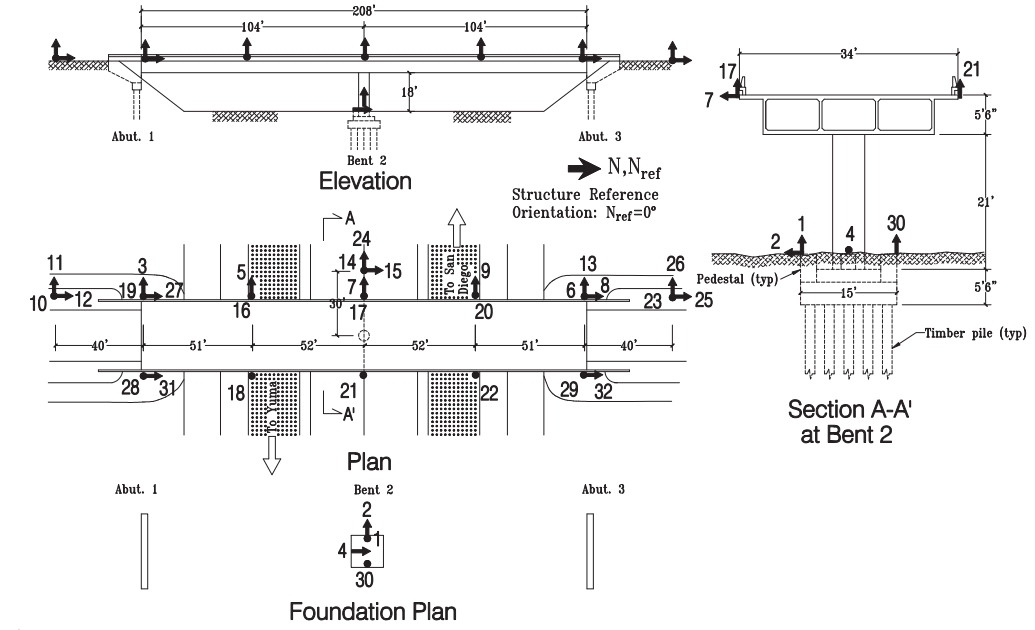

a)

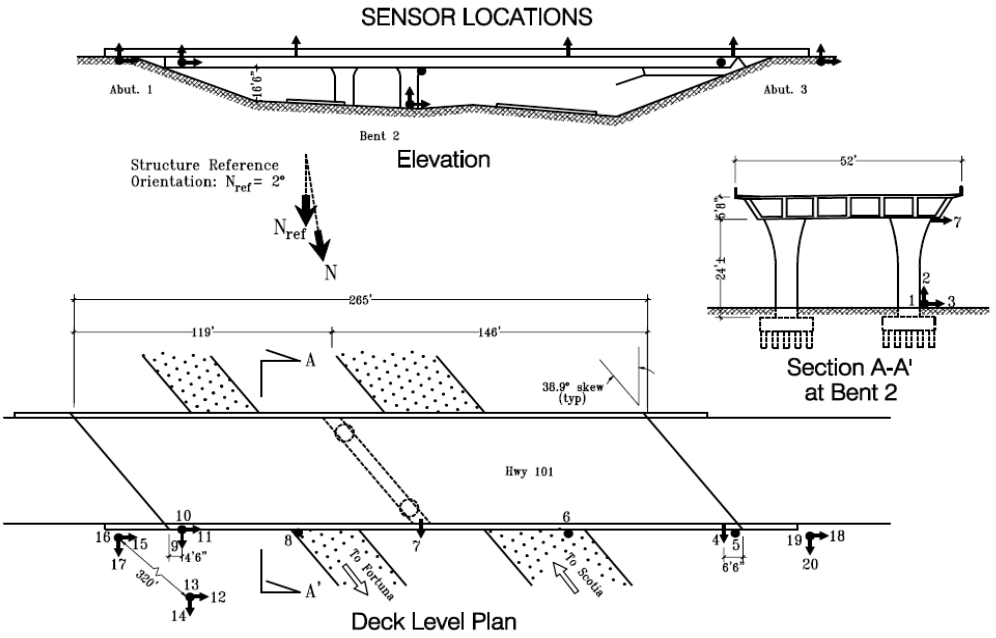

b)

Figure 7: Plan, elevation and sectional views of the a) Meloland Road Overpass and b) Painter Street Overpass, showing the sensor layout [Adapted from the Center for Engineering Strong Motion Data (CESMD)]

NLTHA was conducted on the analytical bridge models using the respective scenario bi-directional time histories recorded at the bridge sites. The longitudinal and transverse directions

of the Meloland Road Overpass are subjected to the 1979 Imperial Valley earthquake with PGA values of 0.31g and 0.29g, respectively. The 1992 Cape Mendocino/Petrolia earthquake is used in the case of the Painter Street Overpass and this is characterized with PGA values of 0.28g and 0.52g in the longitudinal and transverse directions, respectively. In the case of the Meloland and Painter Street Overpass, uniform excitation was imposed while in the case of the Northwest Connector, multi-support excitation was imposed. Multi-support excitation plays a very important role in the case of long span bridges where the probability of the input motion being coherent and synchronous at all supports is greatly reduced. It takes into account the spatial variability of ground motion records and random incoherence, difference in the local soil conditions, and wave propagation across the site [Fenves and DesRoches, 1994; Lupoi *et al.*, 2005; Crewe and Norman, 2006]. The ground motions were not recorded at the base of every column in the connector, and therefore the input motion for each column was based on the nearest recorded motion without interpolation. The 1992 Landers earthquake is used for analytical model validation of the Northwest Connector. Table 2 provides details about the ground motions and their locations used in the multi-support excitation analysis for the Northwest Connector.

Table 2: Details of the ground motions used in FEM validation of the Northwest Connector

Ground motion number	Location on bridge	Peak ground acceleration (g)		
		Longitudinal	Transverse	Vertical
1	Abutment 1	0.535	0.187	0.243
2	Bent 3	0.103	0.099	-
3	Bent 8	0.163	0.179	0.072
4	Abutment 17	0.322	0.139	0.102

Comparisons between the analytical model results and recorded real time sensor data for a few channels on the case study bridges are shown in Figures 8, 9, and 10. Figures 8a and 8b show the response comparison for abutments and deck in the transverse direction, respectively, for the Meloland Road Overpass. The response comparison shown in this figure corresponds to channels 3 and 7, respectively. The channels selected for the Northwest Connector: 20, 28, and 29, are all located close to the longitudinal center of the Connector and Figures 9a, 9b, and 9c show the response of the deck at hinges 7 and 11, respectively. In addition, Figures 10a, 10b, and 10c compare the displacement responses of the analytical results and recorded sensor data at Channels 4, 11, and 7, respectively. Channels 4 and 11 recording the response of the abutments in the transverse and longitudinal directions, respectively, were chosen for the Painter Street Overpass along with Channel 7, which show the transverse deck displacement. It can be seen that there is a very good agreement in all cases thereby demonstrating the accuracy and superiority of three dimensional modeling techniques.

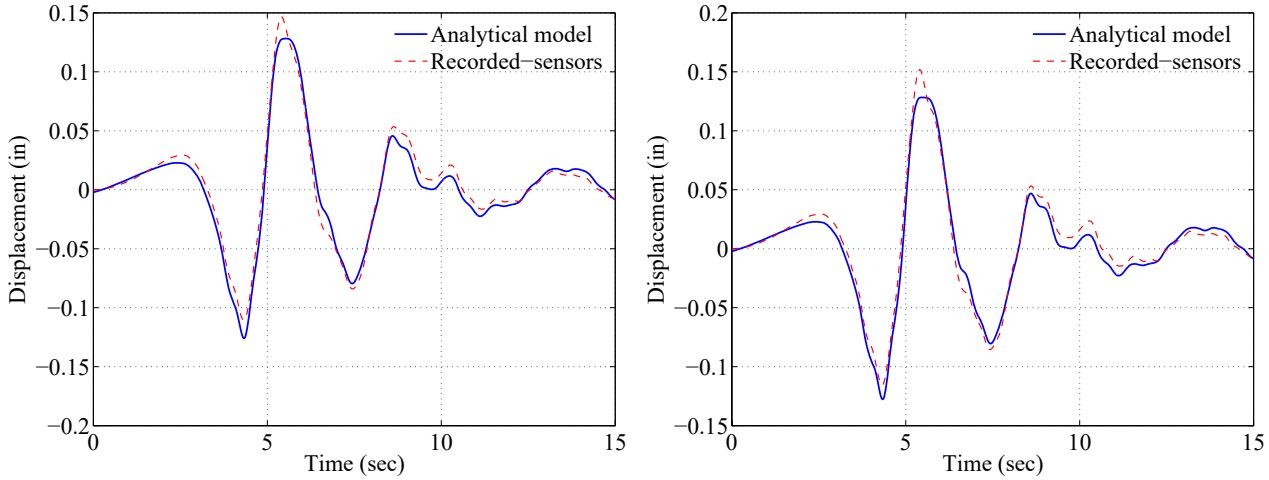

a) b)

Figure 8: Comparison of responses from the analytical model and sensor data for the Meloland Road Overpass: a) Channel 3 and b) Channel 7.

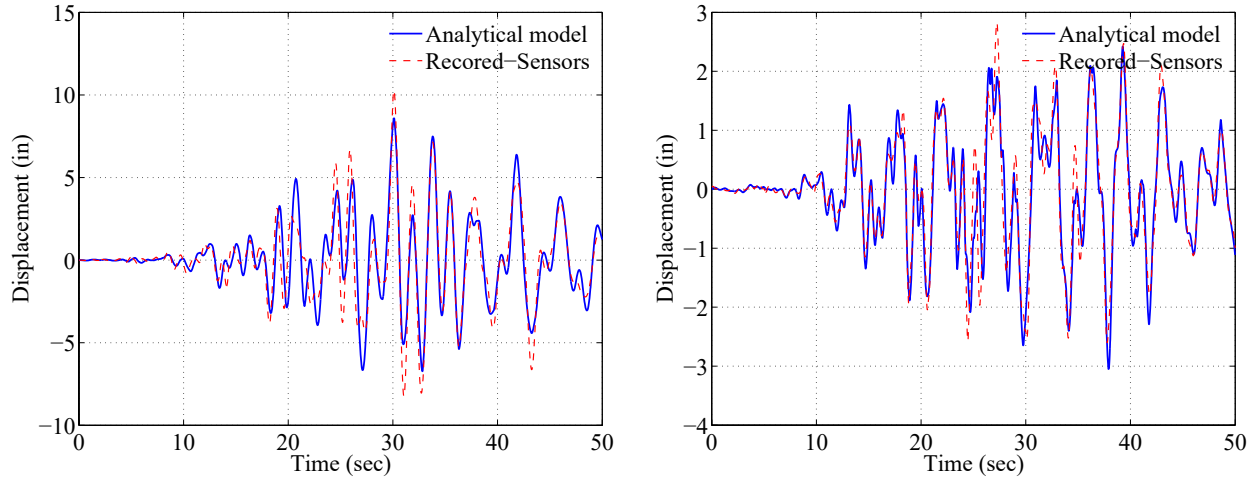

a) b)

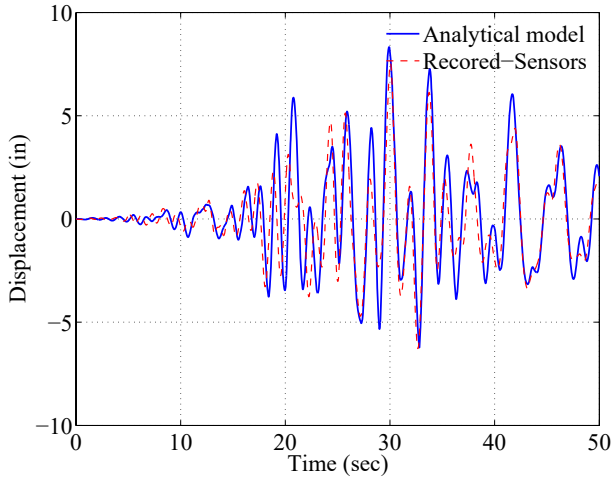

c)

Figure 9: Comparison of responses from the analytical model and sensor data for the Northwest Connector: a) Channel 20, b) Channel 28, and c) Channel 29.

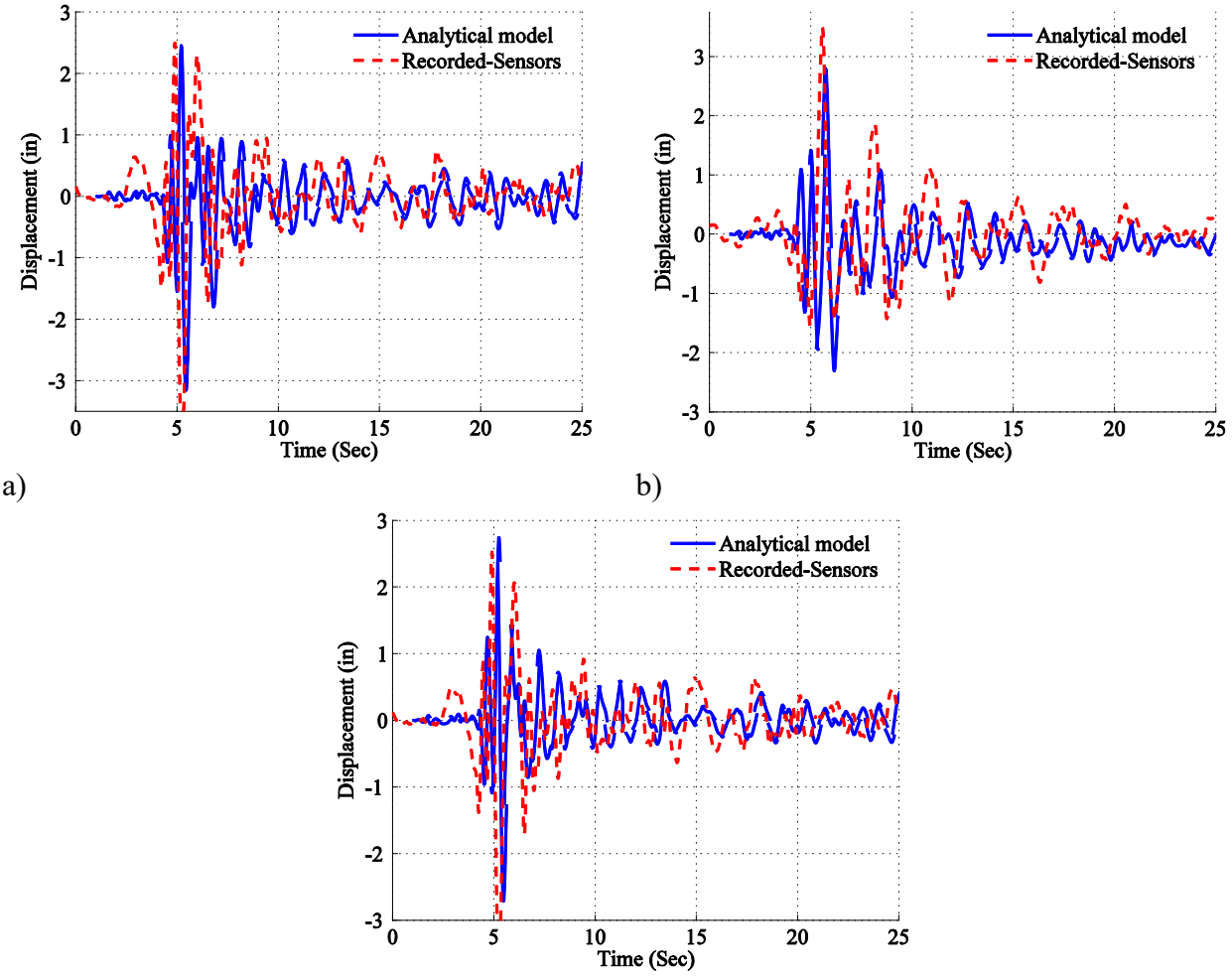

Figure 10: Comparison of responses from the analytical model and sensor data for the Painter Street Overpass: a) Channel 4, b) Channel 11, and c) Channel 7.

5. COMPONENT RESPONSES AND RELATIVE VULNERABILITY

This section provides some insights into the response of bridge components using deterministic analysis performed for the scenario earthquakes that each of the case study bridges were subjected to. The relative shift in vulnerability among bridge components is investigated by developing fragility curves for each of the case study bridges.

Figure 11a shows the response of the column of the Meloland Road Overpass in the transverse direction when subjected to the 1979 Imperial Valley earthquake. The maximum moment seen in the column is on the order of 22,000 kip-in resulting in a curvature of approximately 1.4×10^{-5} in^{-1}. Another potential way of assessing the response is by considering alternate metrics such as curvature ductility demand, defined as the ratio of the maximum curvature in the column cross-

section due to the imposed earthquake load to the curvature that causes first yield of the outermost reinforcing bar. The yield curvature of the column cross-section was determined based on a moment curvature analysis and found to be 7.75×10^{-5} in^{-1}. The transverse curvature ductility demand was found to be 0.18, which is less than one indicating that the column remains elastic. This is consistent with the observation during the earthquake where no damage was evident on the bridge column. Figure 11b shows the longitudinal response of the abutments when subjected to the same earthquake. It is evident that the abutment deforms 0.45 in in both active and passive directions and clearly the tensile response is a matter of concern since it could cause serious damage to the piles. This is expected in diaphragm type abutments where both active and passive actions tend to engage in contrary to seat type abutments where passive action is engaged to a greater extent due to pounding action between the deck and the abutment back wall. In the present case, active response of the abutment is critical when compared to the passive response since the horizontal resistance is offered solely by the piles when the abutment is pulled away from the backfill. Choi [2002] assumed the limit states for abutments in active action to occur at deformations of 0.15 in, 0.3 in, 1 in, and 2 in, for slight, moderate, extensive, and complete damage states, respectively. These correspond to half the first yield, first yield, ultimate and twice the ultimate deformation, respectively. In the present case, the active response of the abutment leads to moderate damage and is the same with the transverse response. As will be demonstrated later in the section, these two components tend to dominate the overall vulnerability of the Meloland Road Overpass at the system level.

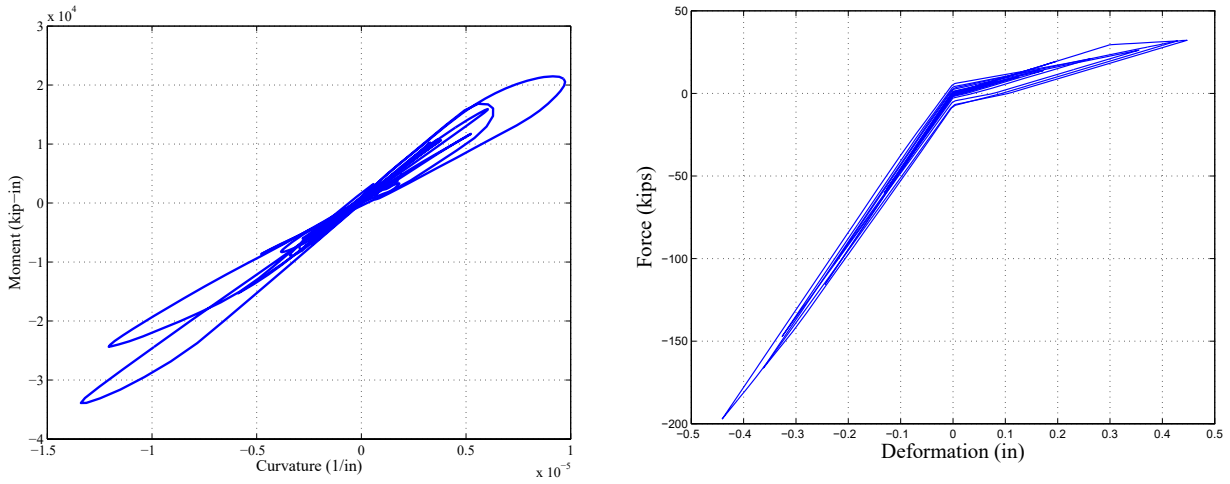

a) b)

Figure 11: a) Transverse column response and b) longitudinal abutment response in the Meloland Road Overpass subjected to the 1979 Imperial Valley earthquake.

Figure 12a illustrates the response of the column of the Northwest Connector in the transverse direction when subjected to the 1992 Landers earthquake. Bent 8 might be more vulnerable under seismic excitation in comparison to other bents due to a lack of retrofit and further its proximity to the longitudinal center of the bridge. This is demonstrated in the next section where the as-built columns tend to be a more vulnerable component at the bridge system level. The maximum moment seen in the column at Bent 8 is in the order of 290,000 kip-in resulting in a curvature of about 2.3×10^{-5} in^{-1}. The yield curvature of the column was found to be 6.4×10^{-5} in^{-1} using section analysis. As in the case of Meloland Road Overpass, the transverse curvature ductility demand was 0.36 which is less than one and therefore, the column remains elastic.

Fenves and DesRoches [1994] indicated that there was no evidence of damage to the column during the earthquake. Figure 12b shows the longitudinal response of Abutment 1 when subjected to the same earthquake. The abutment deforms 2.89 in and 1.17 in in the active and passive directions, respectively. As mentioned previously in the case of Meloland Road Overpass, the longitudinal response of abutments reemphasizes that the tensile (active) response is very important for bridges with diaphragm type abutments. In accordance with the limit states proposed by Choi [2002], the active response of Abutment 1 may lead to moderate damage. Intermediate hinges tend to be a vulnerable component because of the possibility of unseating due to its opening and closing during seismic excitation. Figure 12c indicates the response of hinge opening and closing including the effect of the cable restrainers at Hinge 3 during the same earthquake. The initial restrainer cable slack and the gap of expansion joint were assumed to be 0.5 in and 1.0 in, respectively, as proposed by Fenves and DesRoches [1994]. The maximum hinge opening and closing were found to be 2.43 in and 1.14 in, respectively. Post earthquake inspection indicated that the seat of Hinge 3 had three hairline cracks radiating from the reentrant corner of the seat. Although there was no observed damage to the cable restrainers, concrete spalling and reinforcing bar exposure on the inside edge of the deck near Hinge 3 were observed [Fenves and DesRoches, 1994]. The opening and closing movements of the hinge due to repeated loadings may lead to slight or moderate damage. The hysteretic response of elastomeric bearing pad at Hinge 3 is shown in Figure 10d. Unlike other components, the elastomeric bearing underwent inelastic response. The elastomeric bearing pad, 28 in×12 in×5.5 in in dimension, underwent a maximum deformation of 2.42 in. The yield displacement was assumed to be 10% of the thickness of the bearing pad as illustrated in Section 3.2 of the paper. The ratio of the maximum deformation to the yield displacement is about 4.4 and therefore the bearing might be subjected to moderate damage although this was not directly observed in the post earthquake inspection due to its location in the bridge. While the steel jacketing on the columns and footings made these components less vulnerable at the system level, the active component of abutment response, hinge opening and elastomeric bearing pads may have experienced moderate damage. As will be demonstrated later in the section, these three components tend to dominate the overall vulnerability of the Northwest Connector at the system level.

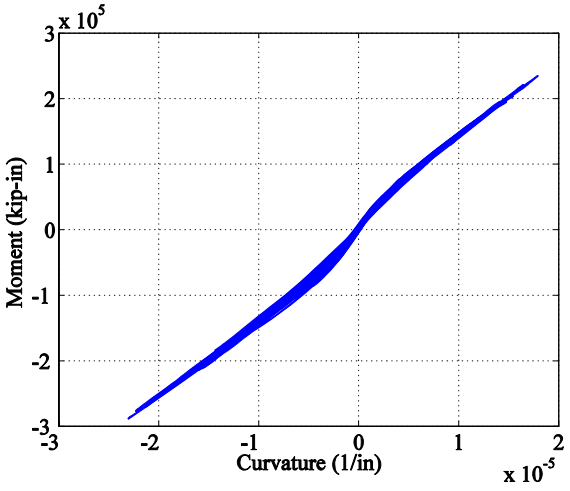

a)

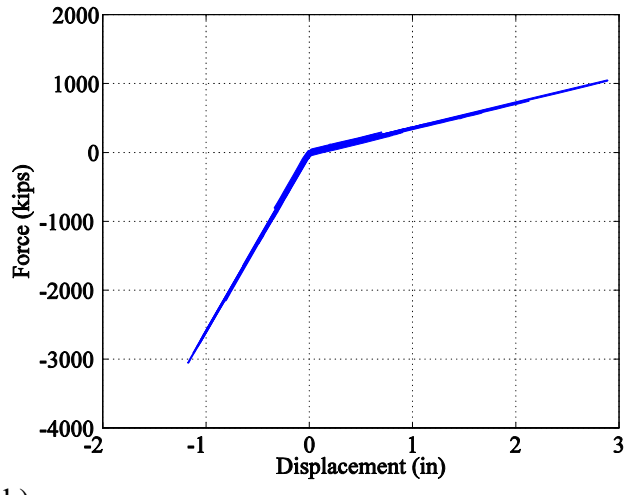

b)

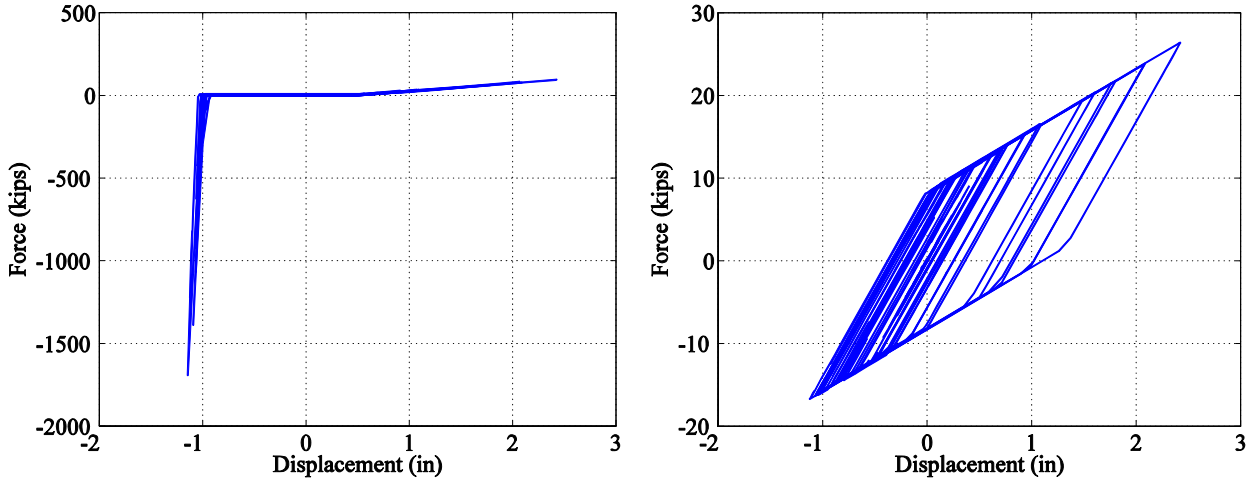

c) d)

Figure 12: a) Transverse column response at Bent 8, b) longitudinal abutment response at Abutment 1, c) hinge 3 opening and closure, and d) elastomeric bearing pad response at Hinge 3 in the Northwest Connector subjected to the 1992 Landers earthquake.

Figure 13a presents the column moment-curvature response of the Painter Street Overpass in the transverse direction when exited by the 1992 Cape Mendocino/Petrolia earthquake. It is clear from the figure that the maximum column curvature is 6×10^{-5} in^{-1} corresponding to a moment of 6.5×10^{4} kip-in. As in the previous case studies, the column yield curvature is found to be 8.7×10^{-5} in^{-1} from section analysis and this corresponds to a curvature ductility demand of 0.7. The column remains elastic under this excitation which is consistent with past bridge observation where no damage was evident on the bridge columns. The presence of skew typically leads to a complex coupled response of the bridge and this is evident in the case of the Painter Street Overpass where the abutments record comparable displacements in both longitudinal and transverse directions. As shown in Figures 13b and 13c, abutment 3 experiences displacements of 2.4 in and 3.3 in in the longitudinal and transverse directions, respectively. Additionally, these comparable displacements may be attributed to the fact that the deck and the abutments are monolithic. This is further demonstrated in case of abutment 1 which records an active displacement of 2.1 in, as shown in Figure 13d. In accordance with the limit states proposed by Choi [2002], the active response of abutment 1 may cause moderate damage to the abutment. Unlike the Meloland Road Overpass and the Northwest Connector, the Painter Street Overpass has wing walls in both east and west abutments and therefore the transverse capacity of the abutments is not dominated by the piles. Therefore, the same limit states are considered for both the longitudinal and transverse directions. Based on these limit states, abutment 3 experiences slight damage in the transverse direction. The bridge has shear keys in abutment 3 in both longitudinal and transverse directions. Figure 13e shows the transverse response of the shear key at abutment 3. Based on the response, it may be concluded that the shear key approaches its ultimate capacity and experiences a displacement of 2.7 in which corresponds to moderate damage. This is consistent with observations reported in the study by Shamsabadi *et al.* [2010]. Abutment 3 also has an elastomeric bearing pad on top of the pile cap, 15 in wide and 3 in thick. Based on the force deformation response of the bearing shown in Figure 13f, it is seen that the maximum bearing deformation is 2.75 in which translates to slight damage. Consistent with

these observations it is seen that the active response of the abutments and shear keys dominate the overall vulnerability of the bridge system. This will be demonstrated in the next section.

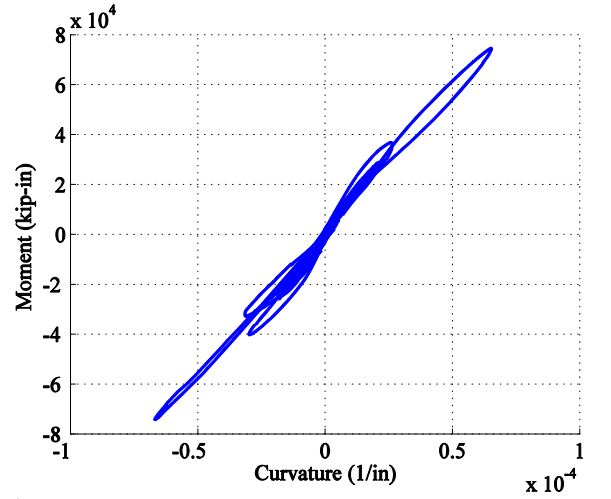

a)

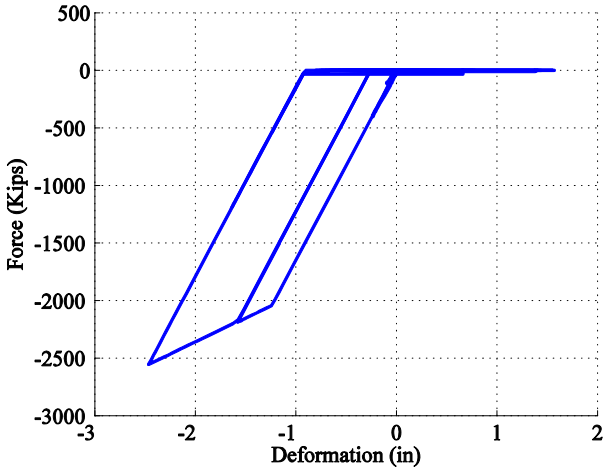

b)

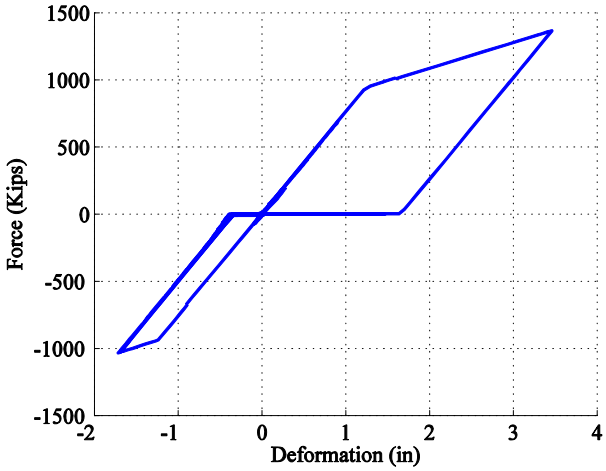

c)

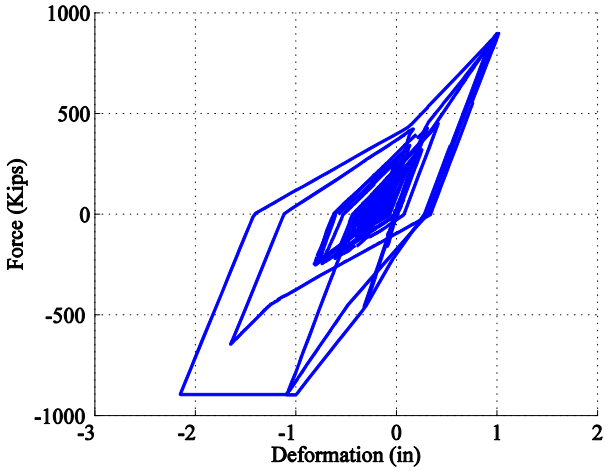

d)

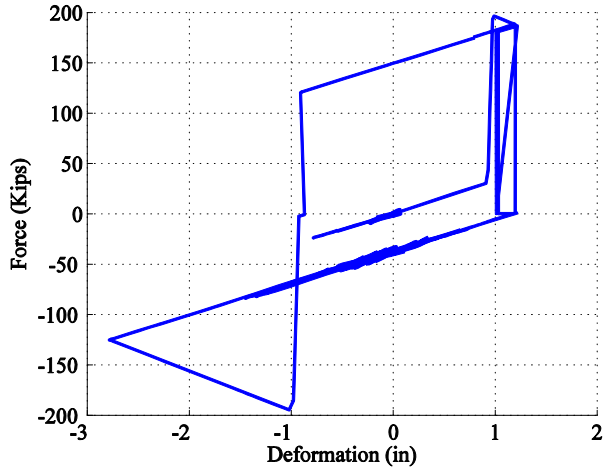

e)

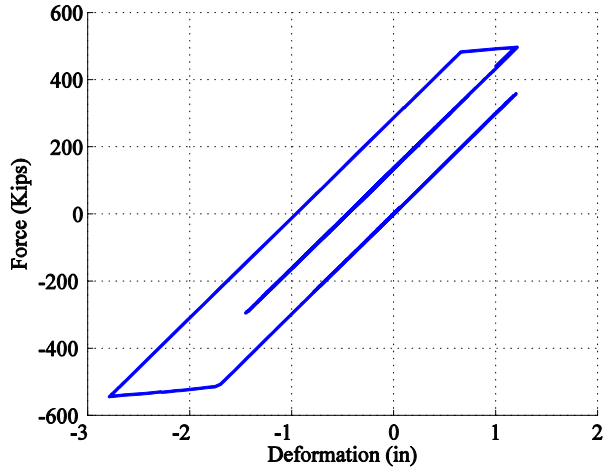

f)

Figure 13: a) Transverse column response, b) longitudinal, and c) transverse response of abutment 3, d) active response of abutment 1, e) transverse shear key response at abutment 3, and f) transverse elastomeric bearing pad response at abutment 3 in the Painter Street Overpass subjected to the 1992 Cape Mendocino/Petrolia earthquake.

5.1 Insights into the behavior of curved and skewed bridges

The aim of this section is to provide some insight into the performance of curved and skewed bridges by drawing from the component responses as discussed in the previous section. Curved bridge columns are subjected to multi-directional deformation with torsion due to the coupling of the longitudinal and transverse response thereby making them susceptible to complex flexural and shear failures. Further, there is likelihood for significant nonlinearity at the expansion joint associated with the slippage and pounding between the girders. The response might be different based on the intensity of the ground motion.

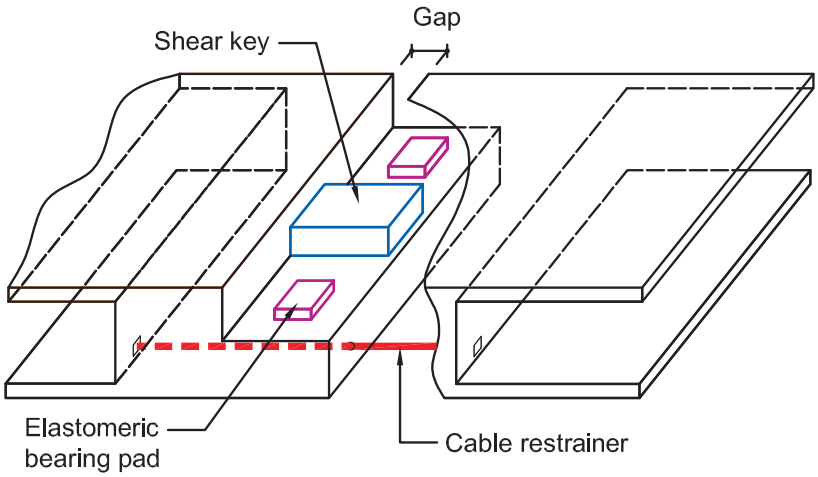

Figure 14: Typical bridge expansion joint

Figure 14 shows a schematic of a typical expansion joint in a curved bridge comprising of elastomeric bearing pads, shear key, and restrainers. The opening of the expansion joint is associated with the deformation of the elastomeric pads under shear thereby offering resistance to motion. This continues eventually leading to their slippage when the maximum friction force is mobilized. The restrainers engage to resist the opening of the joint when the relative joint displacement equals the initial slack and the resistance builds up linearly until the restrainer cables yield. The same happens during the closing of the joint except that the restrainer cables do not engage and pounding between the adjacent slabs and girders takes place when the joint completely closes. The response of the joint is unsymmetrical and the magnitude of joint opening and closure and the associated radially inward and outward motion of the bridge depends on the intensity of the ground motion. During small intensity earthquakes, it is likely that pounding between the girders will not take place since the relative displacement at the joint is below the initial joint gap. In this case, the elastomeric bearing pads and restrainers alone resist the joint separation and as such small or no displacement response may be expected in the radially outward direction of the bridge. On the other hand, during high intensity ground motions, significant pounding and yielding of the restrainer cables may be expected leading to increased

response in the radially outward direction of the bridge due to arching action between the abutments.

Similar to curved bridges, skewed bridges exhibit unique response to seismic excitations due to strut action which causes rotation of the superstructure due to pounding between the deck and the abutment. In multispan bridges, the stiffness of the bent may differ on either side of the skewed deck leading to differential transverse displacements thereby causing rotation of the superstructure and associated pounding.

The response predicted by linear analysis in which the expansion joint is idealized by a set of linear springs will significantly differ from that predicted by the analytical models in the present study which accounts for the effects of impact, slippage and yielding of the restrainer cables. Likewise, simplistic models neglecting the effect of pounding will not provide a good correlation with the actual response of the bridge subject to seismic excitations. It is imperative to correctly idealize the structural integrity of the bridge by accounting for nonlinear component effects to realistically predict the response of bridges with complex geometries.

5.2 Fragility and relative vulnerability

A common technique to compare the relative vulnerability among bridge components and account for uncertainty in the performance assessment is to derive fragility curves. Fragility curves serve as an excellent tool to study the effects of uncertainty propagated through the system and the probabilities of exceeding different user defined damage states. Further, the relative contribution of various bridge components to the overall system vulnerability can be assessed. This information is typically not available through deterministic analyses as illustrated in the previous section. Bridge system and component level fragility curves are developed for each of the case study bridges in accordance with the procedure adopted by Ramanathan et al. [2010, 2011]. Uncertainties are considered in the material properties: concrete compressive strength and reinforcing steel yield strength, in addition to the seismic hazard. A suite of one hundred recorded ground motions were used for generating the curves. Eighty recorded ground motions in California identified by previous researchers [Krawinkler *et al.*, 2003; Gupta and Krawinkler, 2000] were extracted from the Pacific Earthquake Engineering Research (PEER) Center's Strong Motion Database and used along with 20 ground motions pertinent to Los Angeles from the SAC project database (http://nisee.berkeley.edu/data/strong_motion/sacsteel/ground_motions.html). The 80 PEER ground motions have an even selection of recorded time histories from four bins that include combinations of low and high moment magnitudes, large and small epicentral distances. The magnitudes vary between 5.8 and 6.9 while the epicentral distances vary between 10.0 km and 60.0 km. The suite of twenty SAC ground motions for Los Angeles have ten pairs each with intensities of 2% and 10% probability of exceedence in 50 years, respectively. The bridge component engineering demand parameters (EDPs) considered and their prescriptive limit state values are shown in Table 3 and these are consistent with those found in Ramanathan et al. [2010, 2011]. As mentioned in the previous section, in the case of the Painter Street Overpass, the presence of wing walls and skew in the superstructure leads to a coupled response and hence the limit states for both passive and transverse response of the abutments are assumed to be the same, as listed in Table 3. The bearing limit states for the Painter Street Overpass are consistent

with those presented in Padgett and DesRoches [2008]. Shear strains of 100%, 150%, and 200% are assumed for slight through extensive limit states, corresponding to slight damage, yielding of steel shims, and severe bending of steel shims in the bearings of the Painter Street Overpass, respectively. Shear deformation dominates the limit states up to extensive damage while sliding in the bearings dictates the capacity thereon. The limit state for the complete damage state is defined as half of the bearing support length of 14 in in the present case.

Table 3: Bridge component limit states

Component	EDP	Units	Slight		Moderate		Extensive		Complete	
			S_c	β_c	S_c	β_c	S_c	β_c	S_c	β_c
Column (as-built)	Curvature ductility	N.A.	1.44	0.25	2.70	0.25	3.92	0.47	4.18	0.47
Column (retrofit)	Curvature ductility	N.A.	9.35	0.25	17.7	0.25	26.1	0.47	30.2	0.47
Abutment – passive	Displacement	in	1.45	0.25	5.75	0.25	7.87	0.47	7.87	0.47
Abutment – active	Displacement	in	0.40	0.25	1.50	0.25	3.00	0.47	7.87	0.47
Abutment – transverse	Displacement	in	0.40	0.25	1.50	0.25	3.00	0.47	7.87	0.47
Abutment–transverse (Painter)	Displacement	in	1.45	0.25	5.75	0.25	7.87	0.47	7.87	0.47
In-span hinge	Displacement	in	3.00	0.25	4.00	0.25	6.00	0.47	10.0	0.47
Elastomeric bearing pad	Displacement	in	1.14	0.25	4.10	0.25	5.35	0.47	7.35	0.47
Elastomeric bearing pad (Painter)	Displacement	in	3.00	0.25	4.50	0.25	6.00	0.47	10.6	0.47
Shear key	Displacement	in	1.00	0.25	3.00	0.25	6.00	0.47	14.0	0.47

Figure 15 shows the bridge system and component level fragility curves for the three case study bridges for a few representative damage states. In every case it is assumed that multiple components contribute to the overall vulnerability of the bridge system. Response of columns and abutments in the longitudinal (passive and active actions) and transverse directions are considered as components of interest in all the cases. Additionally, elastomeric bearing pads, in-span hinges and shear keys are considered in the case of the Northwest Connector and Painter Street Overpass. Figures 15a and 15b show the fragility curves at the bridge system and component level for the Meloland Road Overpass at the two intermediate damage states: moderate and extensive. It is seen that transverse and active response of the abutments dominates the overall vulnerability at the system level. This is consistent with the observations in the previous section when excessive demand was seen imposed on either of these responses. It should be noted that the bridge as a system is more fragile than any one of its components as a consequence of the underlying series assumption that was used in the system fragility formulation. The component fragility curves for the Northwest Connector at the higher damage states: extensive and complete, are shown in Figures 15c and 15d. The elastomeric bearings tend to be the most vulnerable component in this case followed by intermediate hinges and as-built columns, as discussed in the previous section. As in the case of the Meloland Road Overpass, the active abutment response dominates the system vulnerability in the case of Painter Street Overpass followed by the shear keys. This is depicted in Figures 15e and 15f.

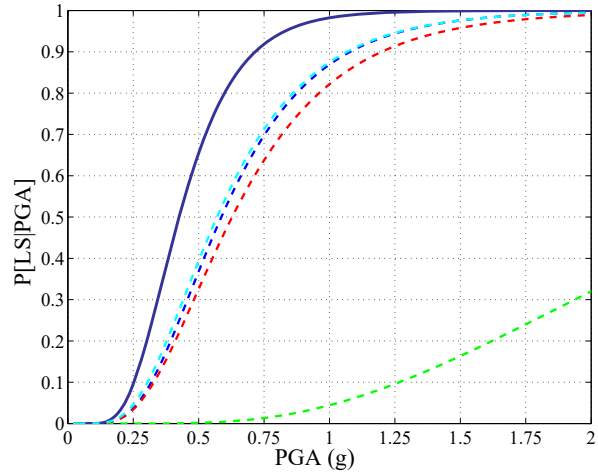
P[LS|PGA]
PGA (g)

a)

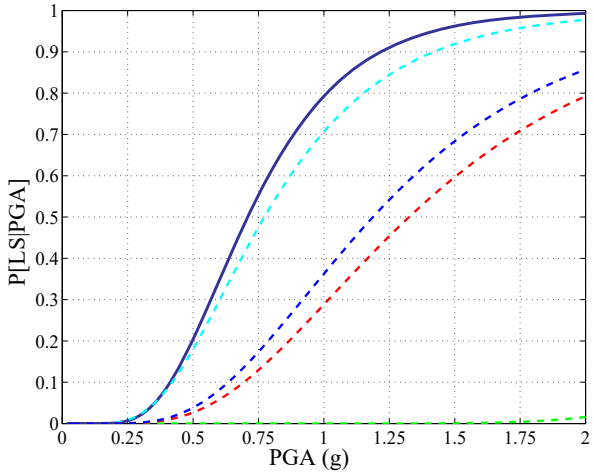
P[LS|PGA]
PGA (g)

b)

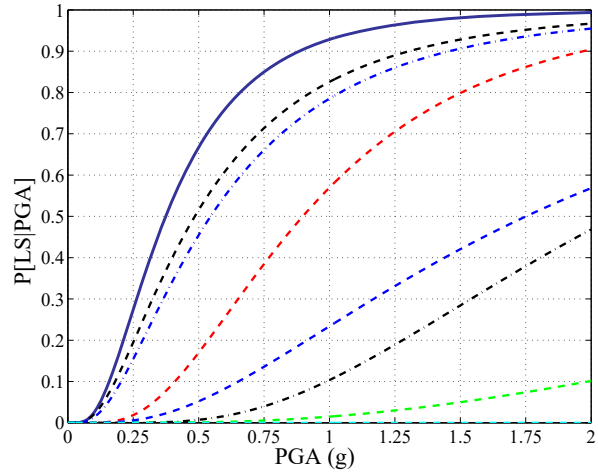
P[LS|PGA]
PGA (g)

c)

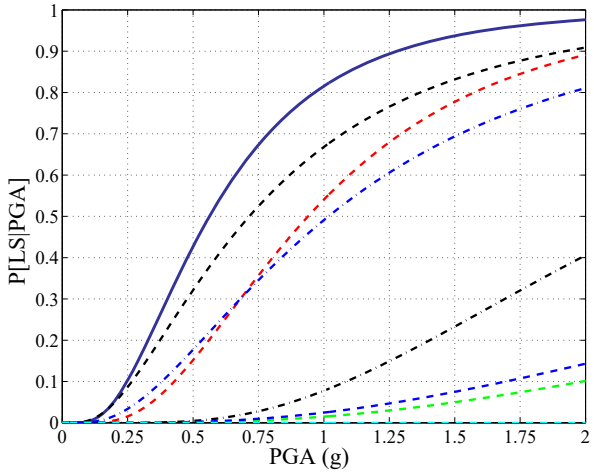
P[LS|PGA]
PGA (g)

d)

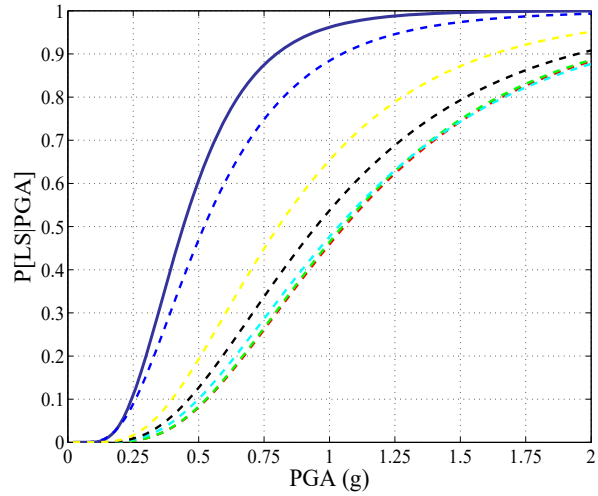
P[LS|PGA]
PGA (g)

e)

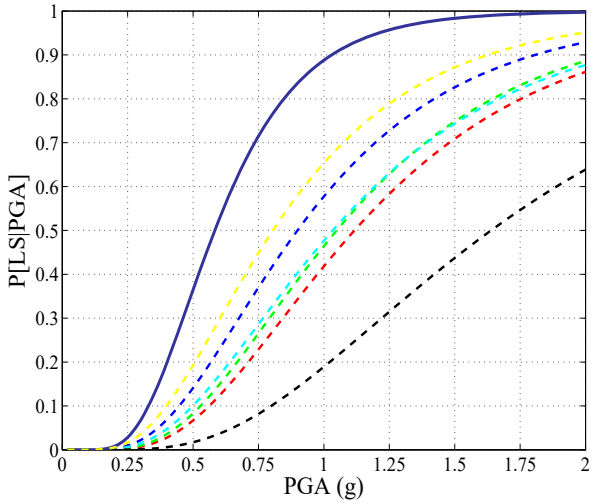
P[LS|PGA]
PGA (g)

f)

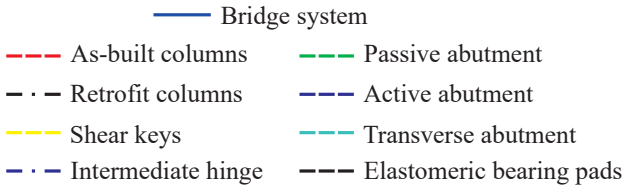

Figure 15: Bridge system and component level fragility curves for a) Meloland Road Overpass at moderate damage state, b) Meloland Road Overpass at extensive damage state, c) Northwest Connector at extensive damage state, d) Northwest Connector at complete damage state, e) Painter Street Overpass at extensive damage state, and f) Painter Street Overpass at complete damage state.

6. CONCLUSIONS

The fundamental focus of this paper is to present modeling considerations and insight into the performance of three instrumented multispan continuous concrete box-girder bridges in California. Meloland Road Overpass, Northwest Connector, and Painter Street Overpass are chosen as the case study bridges and detailed description is provided about the analytical modeling procedure, and key considerations for straight, curved, and skewed bridges. Three dimensional nonlinear finite element models are developed in each case and a detailed description is provided regarding the modeling considerations and associated assumptions. The responses from the analytical models are compared with recorded sensor data for scenario earthquakes specific to individual bridges made available through the Center for Engineering Strong Motion Data to test the robustness of the modeling and dynamic analysis procedures. Uniform support excitation was adopted in the case of the Meloland Road and Painter Street Overpasses while multi-support excitation was used in the case of the Northwest Connector to account for the random incoherence and spatial variability of ground motions due to its long bridge length. Spectral analysis is employed to identify fundamental frequencies from sensor data recorded during real time earthquakes and these are compared to the results from the modal analysis of analytical models. Component and system level fragility curves are developed to access the component vulnerabilities using a suite of one hundred ground motions that represent the seismic hazard in the region to provide additional insight into the uncertainty and probabilities of exceeding a few user defined bridge system level damage states.
The following are some of the conclusions drawn from the present study:

- The analytical models yield comparable responses to the sensor data available for the case study bridges. This reflects the efficacy of the modeling and analysis techniques.
- The fundamental mode is in the transverse direction for the Meloland Road Overpass and the Northwest Connector, while it is a coupled longitudinal and transverse mode for the Painter Street Overpass. The corresponding time periods are 0.46 sec, 1.58 sec, and 0.52 sec, respectively. There is a very good agreement between these results and those obtained by using Spectral Analysis.
- Response of abutments in active action and transverse direction was seen to be critical in the case of the Meloland Road Overpass. This is attributed to the presence of monolithic abutments in this bridge. Further, these components dominate the overall vulnerability of the bridge system as demonstrated by developing fragility curves. Analysis reveals potential slight to moderate damage to the abutments but this was not reported probably due to lack of access for inspection.

- In the case of the Northwest Connector, elastomeric bearing pads are found to be the most vulnerable components followed by the response of the intermediate hinges and as-built columns. This is consistent with past earthquake damage where hair line cracks radiating from the reentrant corner of the seat was observed. The analysis reveals moderate damage to the bearings, but this was not reported in the post-earthquake inspection potentially due to the location of the bearings in the bridge and difficulties associated with the inspection.
- Active response of the abutments and shear key response dominate the overall vulnerability of the Painter Street Overpass. The analysis reveals comparable abutment displacements in the longitudinal and transverse directions. This is attributed in part to the coupled response due to the presence of skew in the superstructure and being characterized by diaphragm type abutments.

REFERENCES

Basoz, N. and Kiremidjian, A. [1998] "Evaluation of Bridge Damage Data from the Loma Prieta and Northridge, California Earthquakes," Technical Report MCEER-98-0004, Multidisciplinary Center for Earthquake Research, University at Buffalo, New York.

Buckle, I. G., Friedland, I., Mander, J., Martin, G., Nutt, R. and Power, M. [2006] "Seismic retrofitting manual for highway structures: Part 1-bridges," Technical Report MCEER-06-SP10, Multidisciplinary Center for Earthquake Research, University at Buffalo, New York.

Caltrans [2010] "Seismic design criteria version 1.6," California Department of Transportation, Division of Engineering Services, Office of Structure Design. Sacramento, California.

Choi, E. [2002] "Seismic analysis and retrofit of Mid-America bridges," Ph.D. thesis, School of Civil and Environmental Engineering, Georgia Institute of Technology, Georgia.

Crewe A. J. and Norman J. A. P. [2006] "Experimental modeling of multiple support excitation of long span bridges," Fourth International Conference on Earthquake Engineering, Taipei, Taiwan, Paper No. 127.

Darragh, R. B. and Cao, T. Q. [1993] "Strong Motion Data from the Large California Earthquakes of 1992," SMIP 93, Sacramento, CA, pp. 13-26.

DesRoches, R. and Fenves, G. L. [1997] "Evaluation of recorded earthquake response of a curved highway bridge," Earthquake Spectra, 13(3), 363-386.

Douglas, B. M. and Richardson, J. [1984] "Maximum amplitude tests of a highway bridge," Proc. of the 8th World Conference on Earthquake Engineering, Earthquake Engineering Research Institute and International Association for Earthquake Engineering, San Francisco, CA.

Douglas, B. M. Maragakis, E. A., Vrontino, S. and Douglas, B. J. [1990] "Analytical studies of the static and dynamic response of the Meloland Road Overcrossing," Proc. of the Fourth US National Conference on Earthquake Engineering, Vol. 1, Palm Springs, California, pp. 987-996.

Fenves, G. L., Filippou, F. C. and Sze, D. T. [1992] "Response of the Dumbarton Bridge in the Loma Prieta earthquake", Report No. UCB/EERC-92/02, Earthquake Engineering Research Center, University of California, Berkeley, California.

Fenves, G. L. and DesRoches, R. [1994] "Response of the Northwest Connector in the Landers and Big Bear earthquakes," Report No. UCB/EERC-94/12, Earthquake Engineering Research Center, University of California, Berkeley, California.

Fenves, G. L. and Ellery, M. [1998] "Behavior and failure analysis of a multiple-frame highway bridge in the 1994 Northridge earthquake," Report No. PEER 98/08, Pacific Earthquake Research Center, University of California, Berkeley, California.

Gates, J. H. and Smith, M. J. [1982] "Verification of dynamic modeling method by prototype excitation," Report No. FHWA/CA/SD-82/07, California Department of Transportation, Office of Structures Design, Sacramento, California.

Goel, R. and Chopra, R. K. [1997] "Evaluation of bridge abutment capacity and stiffness during earthquakes," Earthquake Spectra, 13(1), 1-23.

Gupta, A. and Krawinkler, H. [2000] "Behavior of ductile SMRFs at various seismic hazard levels," Journal of Structural Engineering, 126(1), 98-107.

Haddadi, H., Shakal, A., Stephens, C., Savage, W., Huang, M., Leith, W., Parrish, J. and Borcherdt, R. [2008] "Center for Engineering Strong-Motion Data (CESMD)," Proc. of the 14th World Conference on Earthquake Engineering, Beijing, China.

Huang, M. J. and Shakal, A. F. [1995] "CSMIP strong-motion instrumentation and records from the I10/215 interchange bridge near San Bernardino," Earthquake Spectra, 11(2), 193-215.

Krawinkler, H., Medina, R. and Alavi, B., [2003] "Seismic drift and ductility demands and their dependence on ground motions," Engineering Structures, 25(5), 95-105.

Kwon, O. -S. and Elnashai, A. S. [2008] "Seismic analysis of Meloland Road Overcrossing using multiplatform simulation software including SSI," ASCE Journal of Structural Engineering, 134(4), 651-660.

Liu, W. D., Kartoum, A., Dhillon, S., Chen, X. and Imbsen, R. A. [1996] "Implications of the strong-motion records from a retrofitted curved bridge on seismic design and performance," SMIP96 Seminar on Seismological and Engineering Implications of Recent Strong-Motion Data, California Geological Survey, pp. 71-88.

Ljung, L. [1987] System Identification, Prentice-Hall, Englewood Cliffs, NJ.

Lupoi, A., Franchin, P., Pinto, P. E. and Monti, G. [2005] "Seismic design of bridges accounting for spatial variability of ground motion," Earthquake Engineering and Structural Dynamics, 34(4-5), 10-25.

McCallen, D. B. and Romstad, K. M. [1994] "Dynamic Analyses of a Skewed Short-Span, Box-Girder Overpass," Earthquake Spectra, 100(4), 729-755.

Ma, Y. and Deng, N. [2000] "Deep foundations," in Bridge Engineering Handbook, ed. W.-F. Chen and L. Duan, CRC Press LLC.

Mander, J. B., Priestley, M. J. N. and Park, R. [1988] "Theoretical stress-strain model for confined concrete," ASCE Journal of Structural Engineering, 114(8), 1804-1826.

Maroney, B., Romstad, K. and Chajes, M. [1990] "Interpretation of Rio Dell Freeway Response During Siz Recorded Earthquake Events," Proc. of the 4th US National Conference on Earthquake Engineering, Vol. 1, Palm Springs, CA, pp. 1007-1016.

Maroney, B., Kutter, B., Romstad, K., Chai, Y. H. and Vanderbilt, E. [1994] "Interpretation of large scale bridge abutment test results," Proc. of the Third Annual Seismic Research Workshop, Sacramento, California.

McKenna, F., Scott, M. H. and Fenves, G. L. [2010] "Nonlinear finite-element analysis software architecture using object composition," ASCE Journal of Computing in Civil Engineering, 24(1), 95-107.

Megally, S. H., Silva, P. F. and Seible, F. [2002] "Seismic response of sacrificial shear keys in bridge abutments," Report No. SSRP-200l/23, Dept. of Structural Engineering, University of California, San Diego, California.

Moehle J., Fenves, G., Mayes, R., Priestley, N., Seible, F., Uang, C. -M., Werner, S. and Aschheim, M. [1995] "Highway bridges and traffic management," Earthquake Spectra, 11(S2), 287-372.

Naeim, F., and Kelly, J. M. [1999] "Design of Seismic Isolated Structures: from Theory to Practice," John Wiley & Sons, Inc., New York.

Muthukumar, S. and DesRoches, R. [2006] "A Hertz contact model with non-linear damping for pounding simulation," Earthquake Engineering and Structural Dynamics, 35(7), 811-828.

Oppenheim, A. V. and Schafer, R. W. [1989] Discrete-Time Signal Processing, Prentice-Hall, Englewood Cliffs, NJ.

Padgett, J. E. and DesRoches, R. [2008] "Methodology for the development of analytical fragility curves for retroffited bridges," Earthquake Engineering and Structural Dynamics, 37(8), 1157-1174.

Pandit, S. M. [1991] Modal and Spectrum Analysis, John Wiley, New York, NY.

Priestley, M. J. N., Seible, F. and Calvi, G. M. [1996] "Seismic Design and Retrofit of Bridges", John Wiley & Sons, Inc., New York.

Priestley, M. J. N., Seible, F., Xiao, Y. and Verma, R. [1994] "Steel jacket retroffiting of reinforced concrete bridge columns for enhanced shear strength-Part 1: theoretical considerations and test design," ACI Structural Journal, 91(4), 394-404.

Ramanathan, K., DesRoches, R. and Padgett, J. E. [2010] "Analytical fragility curves for multispan continuous steel girder bridges in moderate seismic zones," Transportation Research Record: Journal of the Transportation Research Board, 2202(3), 173-182.

Ramanathan, K., DesRoches, R. and Padgett, J. E. [2011] "A Comparison of Pre- and Post-Seismic Design Considerations on Moderate Seismic Zones through the Fragility Assessment of Multispan Bridge Classes," Engineering Structures (In Review).

Romstad, K., Kutter, B., Maroney, B., Vanderbilt, E., Griggs, M., and Chai, Y. H. [1995] "Experimental measurements of bridge abutment behavior," Report No. UCD-STR-95-1, Department of Civil and Environmental Engineering, University of California, Davis.

Schroeder, B. L. [2006] “Seismic response assessment of skew highway bridges,’’ Master thesis, Civil Engineering Dept., University of Nevada, Reno, NV.
Shamsabadi, A. [2007] “Three-dimensional nonlinear seismic soil-abutment foundation structure analysis of skewed bridges,’’ Ph.D. thesis, Dept. of Civil Engineering, University of Southern California, Los Angeles, California.
Shamsabadi, A., Khalili-Tehrani, P., Stewart, J. P., and Taciroglu, E. [2010] “Validated simulation models for lateral response of bridge abutments with typical backfills,” ASCE Journal of Bridge Engineering, 15(3), 302-311.
Stewart, J. P., Taciroglu, E., Wallace, J. W., Ahlberg, E. R., Lemnitzer, A., Rha, C., Tehrani, P. K., Keowan, S., Nigbor, R. L., and Salamanca, A. [2007]_“Full scale cyclic testing of foundation support systems for highway bridges. Part II: Abutment backwalls,” Report No. UCLA-SGEL-2007/02, Structural and Geotechnical Engineering Laboratory, University of California, Los Angeles.
Sweet, J. and Morrill, K. B. [1993] “Nonlinear soil-structure interaction simulation of the Painter Street Overcrossing,” Proc. of the 2nd Annual CALTRANS Seismic Research Workshop, Sacramento, California.
Werner, S. D., Beck, J. L., and Levine, M. B. [1987] “Seismic response evaluation of Meloland Road Overpass using 1979 Imperial Valley earthquake records,” Earthquake Engineering and Structural Dynamics, 15(2), 249–274.
Werner, S. D., Beck, J. L., Katafygiotis, L., and Nisar, A. [1993] “Seismic analysis of Meloland Road Overcrossing using calibrated structural and foundation models,” Structural Engineering in Natural Hazards Mitigation, Irvine, California, pp. 367-372.
Wilson, J. C. and Tan, B. S. [1990a] “Bridge abutments: formulation of simple model for earthquake response analysis,” ASCE Journal of Engineering Mechanics, 116(8), 1828-1837.
Wilson, J. C. and Tan, B. S. [1990b] “Bridge abutments: assessing their influence on earthquake response of Meloland Road Overpass,” ASCE Journal of Engineering Mechanics, 116(8), 1838-1856.
Yashinsky, M. and Ostrom, T. [2000] “Caltrans’ New Seismic Design Criteria for Bridges,” Earthquake Spectra, 16(1), 285-307.
Zhang, J. and Makris, N. [2002] “Seismic response analysis of highway overcrossings including soil structure interaction.” Earthquake Engineering and Structural Dynamics, 31(11), 1967–1991.

Feasibility Studies for Improving Caltrans' Bridge Fragility Relationships

Final Report

Part IV

AMENDMENTS TO PART I TO ACCOMMODATE CALTRANS REVISIONS TO DAMAGE STATE DEFINITIONS

Supplemental Technical Report by Karthik N. Ramanathan

Part IV of this report contains revisions to the thesis presented in Part I. These revisions were requested by Caltrans after thesis defense, and are thereby reported separately. The revisions accommodate evolving damage state definitions where certain secondary components were reclassified to be general distress indicators (GDIs). Accordingly, the introductory portion of section 5.5, section 5.5.7 in Chapter 5, and Chapter 6 in entirety, are modified and presented in this part of the report. Also presented is a modified version of Appendix E in line with the changes in Chapters 5 and 6.

5.5 Component Capacity or Limit State Models

Seismic fragility involves the convolution of the demand and capacity models. The formulation of the demand models was explained in the previous section. Definition of the component capacities or limit states is not a trivial task and is a crucial step in the fragility formulation. The individual limit states are characterized by representative values for the median, S_C, and dispersion, β_C, (see equation (5.1)) for the component damage states distributions which are also assumed to be lognormal akin to the PSDMs. Discrete damage states are defined for each component corresponding to significant changes in its response and consequences to its own performance and performance of the bridge at the global or system level. Although the damage state definitions are discrete, the assumption is that a continuous range of damage exists between the discrete states to enable the closed-form computation of the component fragility curves. It is essential that the limit state definitions use the same metric as the EDP for the respective bridge components. Table 5.3 listed the bridge component EDPs that are used to monitor the response of specific components and assess their performance.

A significant contribution in the present study is that the damage state definitions for the components are derived in such a way that they align with the Caltrans design and operational experience. This will facilitate the evaluation of repair-related decision variables, repair cost and repair time, which are the end products in a typical risk assessment procedure. The major

challenge lies in being able to group components that have similar consequences at the system level in terms of functionality and repair consequences. A common question that could arise is: "Do the complete collapse of columns have the same effect on bridge functionality as the complete damage to a shear key or tearing of an elastomeric bearing pad?" In order to be able to address the aforementioned concerns, three classes of components are proposed viz., primary, secondary, and general distress indicators (GDIs). Primary components are defined as those that affect the vertical stability and load carrying capacity of the bridge. Extensive or complete damage to these components might lead to closure of the bridge. Columns and abutment seat belong to this category with regards to the bridge classes considered in this research. When looking at bridges with in-span hinges, which is out of the scope of the present study, the internal hinge is also considered as a primary component as excessive hinge opening (values exceeding the support seat length) could lead to unseating of the superstructure.

Secondary components may be defined as the ones that do not affect the vertical stability of the bridge. Failure of these components will not force closure of the bridge but might lead to restrictions on the travel speed and traffic conditions on the bridge. The fundamental distinction between secondary components and GDIs lies in the availability of a damage model to correlate the component level performance to the functionality consequence at the bridge system level. Damage models exist in the case of secondary components while they do not for the GDIs. Therefore, the GDIs will not be considered in the formulation of system fragility relationships and will serve as indicators of damage at the respective component level alone.

Table 5.6 lists the primary and secondary components along with the GDIs in the bridge classes considered in this study for both diaphragm and seat abutments.

Table 5.6: List of primary and secondary components in the bridge classes considered in this study

Seat Abutments	Diaphragm Abutments
Primary components	
Columns	Columns
Abutment seat	
Secondary Components	
Joint seal	Maximum deck displacement
Elastomeric bearing pads	Abutment active displacement
Restrainers	Joint seal*
Maximum deck displacement	Elastomeric bearing pads*
Abutment active displacement	Restrainers*
General Distress Indicators	
Bent foundation translation	Bent foundation rotation
Bent foundation rotation	Abutment active displacement
Abutment passive displacement	Abutment transverse displacement
Abutment active displacement	Shear key displacement*
Abutment transverse displacement	
Shear key displacement	

*These components are only present in the case of MSCC-IG bridges with diaphragm abutments

Tables 5.7 and 5.8 show the general description of the bridge system level damage states (BSST) and the component damage thresholds (CDT) for primary components, respectively. The bridge system level damage state descriptions, BSST-0 through BSST-3 are defined in Table 5.7 and are aimed at operational consequences in the aftermath of an earthquake. The CDT of primary components map directly to the BSSTs since the loss of a primary component affects the load carrying capacity and overall stability of the bridge system. In the case of secondary components, only two broad CDTs are defined, CDT-0 and CDT-1 and these map directly into BSST-0 and BSST-1, respectively. The damage state descriptions for CDT-0 and CDT-1 in the case of secondary components are shown in Table 5.9. The combinations of the Component Damage Thresholds (CDT) of primary and secondary components, detailed in Table 5.7, are aimed at achieving similar consequences in terms of bridge operations (repair and traffic implications) in the aftermath of an earthquake. As mentioned previously, due to the lack of damage models for the GDIs, these are not considered in the evaluation of system vulnerability estimates. As described in Table 5.7, the primary components: columns and abutment seat (the latter only in the case of seat abutments) directly map into the BSSTs and equally contribute to

the vulnerability across all damage states. On the other hand, the secondary components (detailed in Table 5.6) map into BSST-0 and BSST-1 since there complete failure will not have a similar consequence as that of the primary components. Both these tables are developed in close collaboration with Caltrans (Caltrans, 2010-2012) to ensure that the component mapping is in alignment with the inspection/maintenance closure decisions and the training guides for post-earthquake inspections (Sahs et al., 2008). The CDTs may be broadly defined as below:

- CDT–0 (Aesthetic damage) is a performance parameter threshold beyond which aesthetic damage of the component occurs. The associated repair is primarily aimed at restoring the aesthetics
- CDT–1 (Repairable minor functional damage) is a performance parameter threshold beyond which significant repairs are required to restore component functionality
- CDT–2 (Repairable major functional damage) is a performance parameter threshold beyond which extensive repairs are required to restore component functionality
- CDT–3 (Component replacement) is a performance parameter threshold beyond which component replacement is likely to be the most cost-effective means to restore component functionality

The CDT values can be described using a prescriptive (physics-based) approach, descriptive (judgmental-based) approach or by incorporating both (Padgett et al., 2007) using Bayesian updating principles. The prescriptive approach is based on the mechanics of the problem where a functional level is associated with component damage such as spalling of cover concrete in a column, buckling or rupture of the longitudinal column reinforcement etc. The descriptive approach is based on the functionality level of the components post disaster and is usually in terms of repair cost and downtime. In this study a combination of both techniques are used to define the threshold value.

Having broadly defined the CDTs for various components, the threshold values are determined based on experimental studies from the literature and based on extensive input from the Caltrans design and bridge maintenance groups. The subsequent sections provide these median values, S_C, for the CDTs along with visible signs of associated damage and repair

strategies. As mentioned before, the capacity distributions are assumed to be lognormal similar to the demand distributions. The uncertainty associated with the median values of the CDTs is prescribed in the form of a logarithmic standard deviation or dispersion, β_C. The assignment of dispersion is done in a subjective manner due to lack of enough information to quantify it and a dispersion value of 0.35 is adopted across the components and the respective damage states. This value is particularly a good estimate for columns and is consistent with the test results documented in the PEER column structural performance database (Berry and Eberhard, 2004).

Table 5.7: General description of bridge system level damage states along with component damage thresholds

Bridge system damage states	BSST-0 MINOR	BSST-1 MODERATE	BSST-2 EXTENSIVE	BSST-3 COMPLETE
ShakeCast Inspection Priority levels	Low	Medium	Medium-High	High
Likely Immediate Post-Event Traffic State	Open to normal public traffic – No Restrictions	Open to limited public traffic – speed/weight/lane restrictions	Emergency vehicles only – speed/weight/lane restrictions	Closed (until shored/braced) – potential for collapse
Traffic Operation Implications				
Is closure/detour needed?	Very unlikely	Unlikely	Likely	Very likely
Are traffic restrictions needed?	Unlikely	Likely	Very Likely	Very Likely - Detour
Emergency Repair Implications				
Is shoring/bracing needed?	Very unlikely	Unlikely	Likely	Very likely
Is roadway leveling needed?	Unlikely	Likely	Very Likely	Very Likely - Detour
Component Damage Threshold mapping				
Primary components	CDT-0 to 1	CDT-1 to 2	CDT-2 to 3	Above CDT-3
Secondary components	CDT-0	CDT-1	NA	NA

NA indicates that these CDTs are not defined for the secondary components

Table 5.8: Component level damage state descriptions – Component Damage Thresholds (CDT) for Primary Components

	CDT-0	CDT-1	CDT-2	CDT-3	
Component damage states	No damage	Aesthetic damage	Repairable minor functional damage	Repairable major functional damage	Component replacement

Table 5.9: Component level damage state descriptions – Component Damage Thresholds (CDT) for Secondary Components and General Distress Indicators (GDIs)

		CDT-0	**CDT-1**
Component damage states	No damage	Aesthetic damage/ Repairable minor functional damage	Repairable major functional damage/ Component replacement

5.5.7 Component Limit States Summary

Table 5.17: Summary of CDT values adopted in this study

Component	EDP	Units	Median values, S_C				β_C
			CDT-0	CDT-1	CDT-2	CDT-3	
Primary Components							
Columns							
Pre 1971	Curvature ductility	NA	0.8	0.9	1.0	1.2	0.35
1971-1990	Curvature ductility	NA	1.0	2.0	3.5	5.0	0.35
Post 1990	Curvature ductility	NA	1.0	4.0	8.0	12.0	0.35
Abutment seat							
AS1-S	Displacement	Inches	0.5	1.0	2.0	3.0	0.35
AS2-S	Displacement	Inches	1.0	3.0	6.0	9.0	0.35
AS3-S	Displacement	Inches	1.0	3.0	10.0	15.0	0.35
AS3-L	Displacement	Inches	2.0	6.0	10.0	15.0	0.35
AS4-S	Displacement	Inches	1.0	3.0	14.0	21.0	0.35
AS4-L	Displacement	Inches	2.0	6.0	14.0	21.0	0.35
Secondary Components							
Joint seal							
Type A	Displacement	Inches	0.5	NA	NA	NA	0.35
Type B	Displacement	Inches	1.0	NA	NA	NA	0.35
Strip	Displacement	Inches	2.0	5.0	NA	NA	0.35
Modular	Displacement	Inches	4.0	10.0	NA	NA	0.35
Bearings	Displacement	Inches	1.0	4.0	NA	NA	0.35
Restrainers	Displacement	Inches	1.5	4.0	NA	NA	0.35
Deck	Displacement	Inches	4.0	12.0	NA	NA	0.35
Abutments							
Active	Displacement	Inches	1.50	4.00	NA	NA	0.35
General Distress Indicators							
Bent foundation							
Translation	Displacement	Inches	1.00	4.00	NA	NA	0.35
Rotation	Rotation	Radian	1.50	6.00	NA	NA	0.35
Abutments							
Passive	Displacement	Inches	3.00	10.0	NA	NA	0.35
Transverse	Displacement	Inches	1.00	4.00	NA	NA	0.35
Shear keys	Displacement	Inches	1.5	5.0	NA	NA	0.35

The previous sections detailed the capacity models component wise along with details about the choice of the respective CDT values and typical repair strategies adopted. As stated previously, the capacity models are assumed to be lognormal characterized by a median value and dispersion. Table 5.17 provides a summary of the CDT values adopted for the bridge components.

CHAPTER 6

SYSTEM AND COMPONENT FRAGILITY CURVES

The end goal of seismic risk assessment of highway bridge infrastructure systems is the quantification of the expected damage in terms of metrics such as cost or time in the event of an earthquake. Estimates of vulnerabilities at the system and component level plays a significant role in assessing probable bridge losses to facilitate critical decision making pertinent to post earthquake safety, preparedness, mitigation and management. Fragility curves, which are conditional probability statements that express the probability of meeting or exceeding specific user defined damage states, play a significant role in risk assessment. Component and system level fragility relationships further help in the assignment of inspection priorities and assessing the post-earthquake serviceability condition of bridges and their components.

The previous chapters in addressed the different aspects of the fragility framework arriving at the formulation of probabilistic seismic demand models (PSDMs) and capacity models. Each of these is characterized by median values and dispersions completely describing a lognormal distribution, representing the component responses in the case of PSDMs, and the capacity (or resistance) for defined damage states in the case of the capacity models. The component fragility can be derived using a closed form solution described in equation (6.1), where, D and C denote demand and capacity, S_D and S_C denote the median values of demand and capacity and $\beta_{D|IM}$ and β_C denote the dispersions (logarithmic standard deviation) of the demand and capacity, respectively.

$$P[D > C \mid IM] = \Phi\left(\frac{\ln\left(S_D / S_C\right)}{\sqrt{\beta_{D|IM}{}^2 + \beta_C{}^2}}\right) \tag{6.1}$$

It must be noted that S_C and β_C are defined based on the limit state under consideration. As stated in the previous chapter, the components contributing to the vulnerability of the bridge

system are divided into primary and secondary components based on their influence on the stability and operational consequences in the aftermath of an earthquake (see Table 5.6 in Chapter 5). Due to the lack of a credible damage model for the general distress indicators, these are not considered to contribute to the vulnerability at the system level and hence are not included in the formulation of system fragility curves. Spectral acceleration at 1.0 sec, $S_a(1.0)$, was established as the optimal intensity measure (IM) in Chapter 5 and fragility curves will be developed and presented using this IM. Substituting the formulation for the median demand, S_D described in the PSDM formulation, and subsequent simplification, as illustrated in equation (6.2), leads to the formulation in (6.3) which is representative of the lognormal distribution describing the component fragilities with median, λ_c and dispersion, ζ_c. Component fragility curves provide valuable information about the most vulnerable component in the bridge system thereby prioritizing inspection and retrofit.

$$P[LS \mid IM] = \Phi\left(\frac{\ln\left(a\,IM^{\,b}\right) - \ln\left(S_C\right)}{\sqrt{\beta_{D|IM}{}^2 + \beta_C{}^2}}\right) = \Phi\left(\frac{\ln\left(IM\right) - \left(\frac{\ln\left(S_C\right) - \ln\left(a\right)}{b}\right)}{\frac{\sqrt{\beta_{D|IM}{}^2 + \beta_C{}^2}}{b}}\right) \tag{6.2}$$

$$P[LS \mid IM] = \Phi\left(\frac{\ln\left(IM\right) - \ln\left(\lambda_c\right)}{\zeta_c}\right) \tag{6.3}$$

The logical step following the determination of component fragilities is to integrate these to enable the macroscopic view of the vulnerability of the bridge system. Contrary to some of the previous studies (Nielson, 2005; Padgett, 2007; Ramanathan et al., 2010, 2012), the components in this study are combined in a way such that they are have equal consequences in terms of repair and traffic implications in the aftermath of an earthquake. Although the aforementioned studies tried to address the issue of consequence based system level damage states by adjusting the component capacities, the adjusted capacities did not correlate well to description of damage at the component level. On the contrary, in the present study, the component level damage states were defined in such a way that they were reflective of physical damage and the components

were them combined based on the influence of their respective damages on the system level repair and traffic consequences. This was detailed in Table 5.7 of Chapter 5, where the primary components directly mapped to the bridge system level thresholds (BSSTs) while the secondary components at most contributed to BSST-1.

Several techniques to develop system level fragility curves were presented in Chapter 2. In this study, the estimate of system fragility curves is facilitated through the development of joint probabilistic seismic demand model (JPSDM), recognizing that the demands on various components have some level of correlation. If $\underline{X} = (X_1, X_2, \ldots, X_n)$ represents the vector of demands, X_i, placed on the n components of the system, then the vector, $\underline{Y} = ln(\underline{X})$ represents the vector of component demands in the transformed lognormal space. Since the marginal component demands, X_i, are lognormally distributed, the transformed demands, Y_i, are normally distributed in the transformed space. The JPSDM is formulated in this space by assembling the vector of means, $\mu_{\underline{Y}}$ and the covariance matrix, $\sigma_{\underline{Y}}$. It must be noted that the covariance matrix, $\sigma_{\underline{Y}}$, considers the correlation coefficients between $ln(X_i)$ and not X_i. The correlation coefficients between the component demands are obtained by using the results of the NLTHA and the resulting covariance matrix is then assembled. A Monte Carlo simulation is then used to compare realizations of the demand (using the JPSDM defined by a conditional joint normal distribution in the transformed space) and component capacities to calculate the probability of system failure. It is important to note that correlation across the component capacities is not considered, although, a 100% correlation is assumed across damage states for a given component. Samples (10^6 in this case) are drawn from both the demand and capacity models and the probability of demand exceeding the capacity is evaluated for a particular IM value. The procedure is repeated for increasing values of the IM. Regression analysis is used to estimate the lognormal parameters, median and dispersion, which characterize the bridge system fragility. For a given system level damage state, the series system assumption is used to generate fragility curves. However, the number of components comprising the series system varies based on the BSST under consideration and is dictated by the mapping of component level damage states defined

previously. The mapping ensures the consistency of the series assumption in an attempt to achieve similar consequences in terms of repair and traffic implications at the system level.

The methodology presented in this section is used to develop system and component level fragility curves for the bridge classes and the respective seismic performance sub-bins (SPS) considered in this study. The nomenclature introduced in section 3.6 of Chapter 3 will be used to present the results. Finally, comparisons are also made with the fragilities in HAZUS-MH (2011) and insight is provided into the relative vulnerability of bridge classes and their seismic performance sub-bins, assess the effectiveness of seismic design philosophy currently adopted for the design of bridges, and guide future data collection that is presently absent in the NBI and the state databases.

6.1 Multispan Continuous Concrete Slab Bridges

Fragility curves are developed for MSCC-SL bridges with both seat and diaphragm abutments and the median values and dispersions are documented in Table 6.1. Since slab bridges employ integral pile columns which have seen no modifications in their geometry or reinforcing bar configuration over the decades, the fragilities reported in Table 6.1 are applicable across the design eras considered in this study. Table 6.1 also documents the average dispersion, ζ^*, which could be used as a single value of dispersion characterizing the fragility across all the four damage states. Appendix D documents the median and dispersion values for the component fragility curves for the bridge classes and SPS considered in this study.

Table 6.1: Multispan continuous slab bridge fragilities

Seismic performance sub-bin	BSST-0		BSST-1		BSST-2		BSST-3		
	λ	ζ	λ	ζ	λ	ζ	λ	ζ	ζ^*
MSCC-SL-P-S0	0.57	0.62	0.90	0.64	1.03	0.65	1.28	0.65	0.64
MSCC-SL-P-S1-S	0.09	0.43	0.16	0.46	0.29	0.49	0.39	0.49	0.46
MSCC-SL-P-S2-S	0.12	0.43	0.35	0.49	0.50	0.60	0.63	0.64	0.54
MSCC-SL-P-S3-S	0.12	0.42	0.35	0.49	0.54	0.68	0.65	0.71	0.57
MSCC-SL-P-S4-S	0.12	0.42	0.35	0.49	0.55	0.68	0.66	0.71	0.59

The plot of median values across damage states is shown in Figure 6.1. In the figure, BC stands for the bridge class which is MSCC-SL in the present case and EX denotes the applicability across all the design eras. A simple technique to compare differences in the fragility curves is to evaluate the relative change in the median value of the fragility curves. This facilitates the determination of the effect of certain attributes on the overall vulnerability of the bridge system. A positive change indicates a less vulnerable structure while a negative change indicates a more vulnerable structure. Figure 6.2 illustrates this using fragility curves for MSCC-SL-P-EX-S1 and MSCC-SL-P-EX-S4 for the BSST-3 damage state. The following inferences can be drawn:

- Diaphragm abutments (BC-P-EX-S0) are less vulnerable when compared to seat type abutments (BC-P-EX-SX) across the range of seat widths considered (S1 through S4). The percentage change in median values between diaphragm and seat abutments with largest seat width (S4) is 200%, 143%, 92% and 96% for BSST-0, -1, -2, and -3, respectively.
- The vulnerability of bridges reduces with an increase in the seat width. However, the median and dispersion values for MSCC-SL-P-EX-S2 through -S4 is very similar as seen in Figure 6.1 and documented in Table 6.1. The consistency in fragility parameters is due to the fact that the columns dominate the overall vulnerability across the damage states and as such increased seat width beyond 18 in (S2 category) does not contribute to the reduction in vulnerability. This is demonstrated in Figure 6.3 which shows a plot of system and component fragilities for MSCC-SL-P-EX-S1 and –S3 across all damage states. Clearly, in the case of MSCC-SL-P-EX-S1, the abutment seat is the most vulnerable component and the vulnerability of these is reduced when the seats are increased (S2 through S4) making columns the most vulnerable component in the latter cases. However, the present study shows relatively little impact on the system fragility if the seat width is increased beyond the 12 – 18 inch range but other components are not

improved such as the columns, as suggested by similar values of median and dispersion for the SPS with seats S2 through S4.

- Alternatively, it can be concluded that the most effective technique would be to focus on retrofitting the columns once the seat has been increased to at least the 12 – 18 inch (S2) range. The results suggest that the columns govern the overall vulnerability with seats increased to categories S2 through S4. It is not to be misconstrued that shorter seat widths are just as effective or that seats do not contribute to the vulnerability. Improvement in the performance of columns by retrofitting or replacement of the non-ductile columns with ductile ones, will demonstrate the impact of increasing the seat width potentially.
- This further reinforces the relatively fragile performance of the pile sections which are adopted as columns in the case of slab bridges and recommends for the improvement of the standard pile details to lead to betterment in their performance.
- The difference in vulnerabilities of slab bridges with diaphragm and seat abutments underscores the necessity to capture the type of abutment in a bridge which is not captured in the NBI. However, information about actual seat width is only of secondary interest. Coarse information on seats, such as short versus longer seats is sufficient to inform the system level vulnerability sufficiently accurate.

Table 6.2 provides details about the most vulnerable component across damage states in the SPS considered for this bridge class.

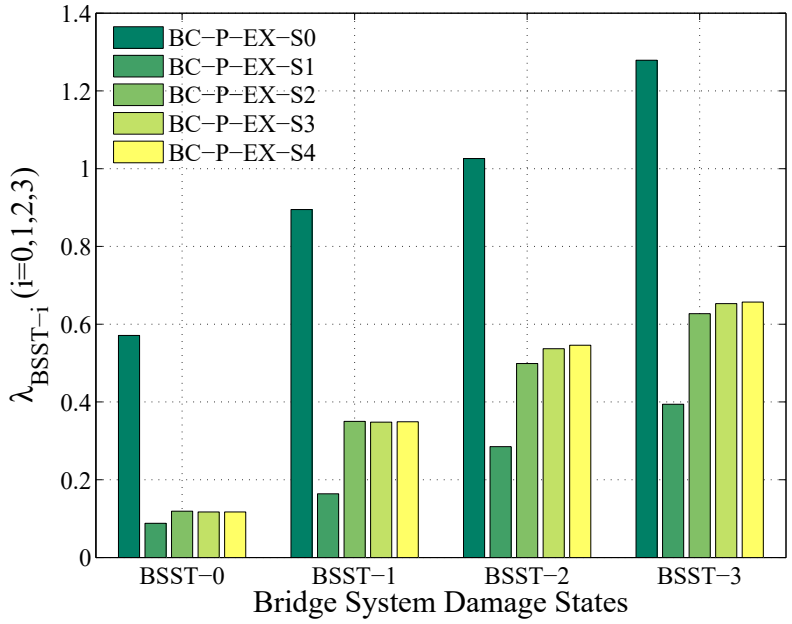

Figure 6.1: Plot of median values for MSCC-SL bridges across all damage states

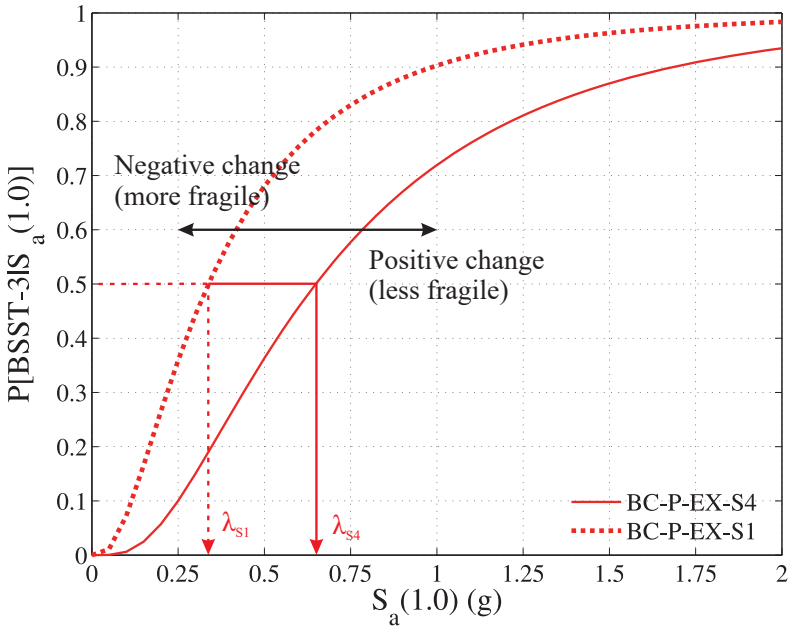

Figure 6.2: Illustration of change in median values and relative vulnerability

MSCC-SL-P-EX-S1 MSCC-SL-P-EX-S3

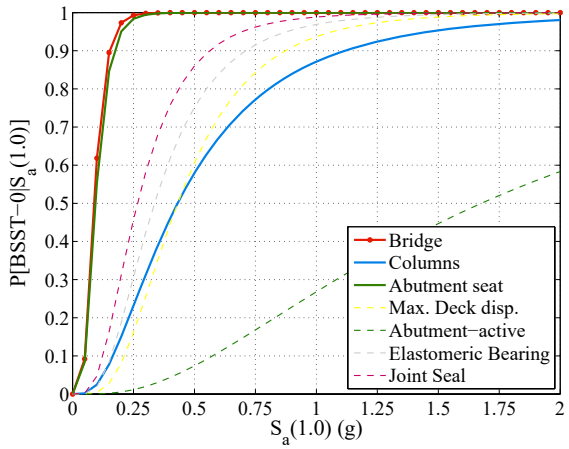
P[BSST−0|S_a(1.0)]
S_a(1.0) (g)
Bridge
Columns
Abutment seat
Max. Deck disp.
Abutment−active
Elastomeric Bearing
Joint Seal

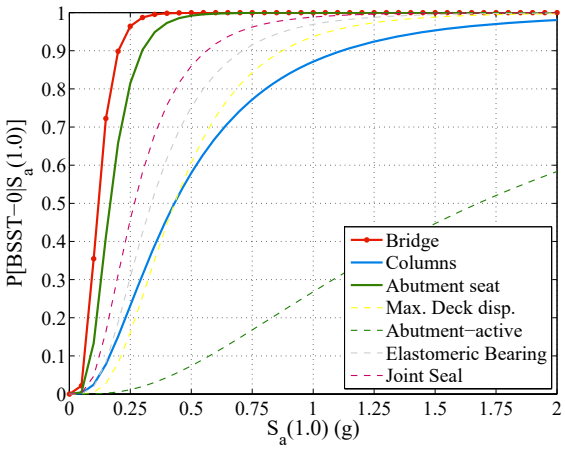
P[BSST−0|S_a(1.0)]
S_a(1.0) (g)
Bridge
Columns
Abutment seat
Max. Deck disp.
Abutment−active
Elastomeric Bearing
Joint Seal

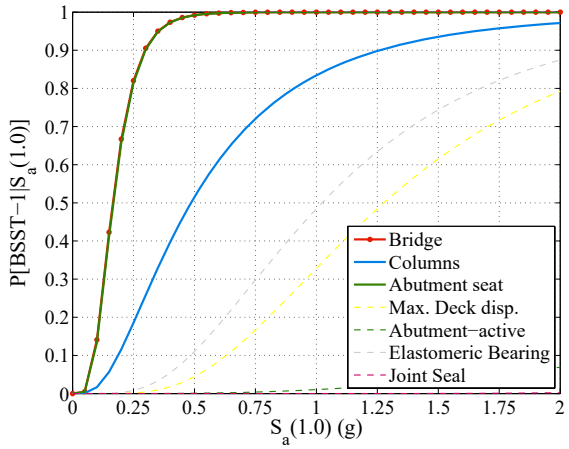
P[BSST−1|S_a(1.0)]
S_a(1.0) (g)
Bridge
Columns
Abutment seat
Max. Deck disp.
Abutment−active
Elastomeric Bearing
Joint Seal

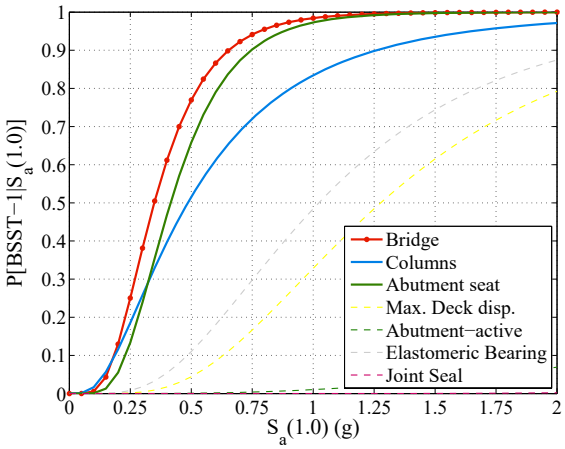
P[BSST−1|S_a(1.0)]
S_a(1.0) (g)
Bridge
Columns
Abutment seat
Max. Deck disp.
Abutment−active
Elastomeric Bearing
Joint Seal

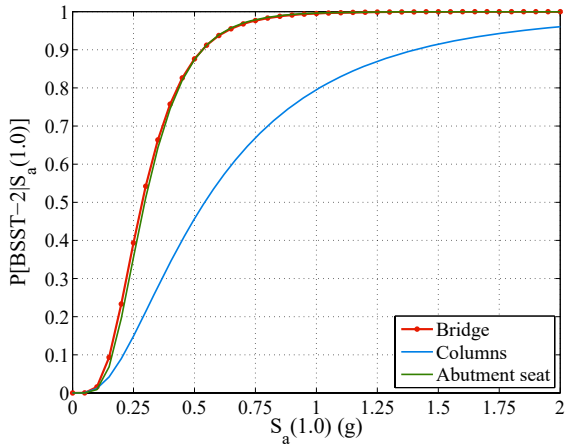
P[BSST−2|S_a(1.0)]
S_a(1.0) (g)
Bridge
Columns
Abutment seat

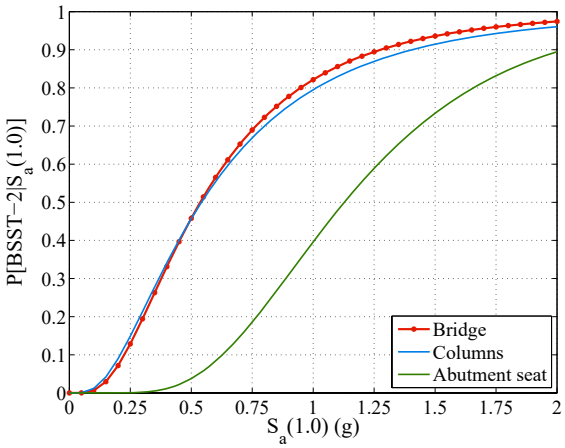
P[BSST−2|S_a(1.0)]
S_a(1.0) (g)
Bridge
Columns
Abutment seat

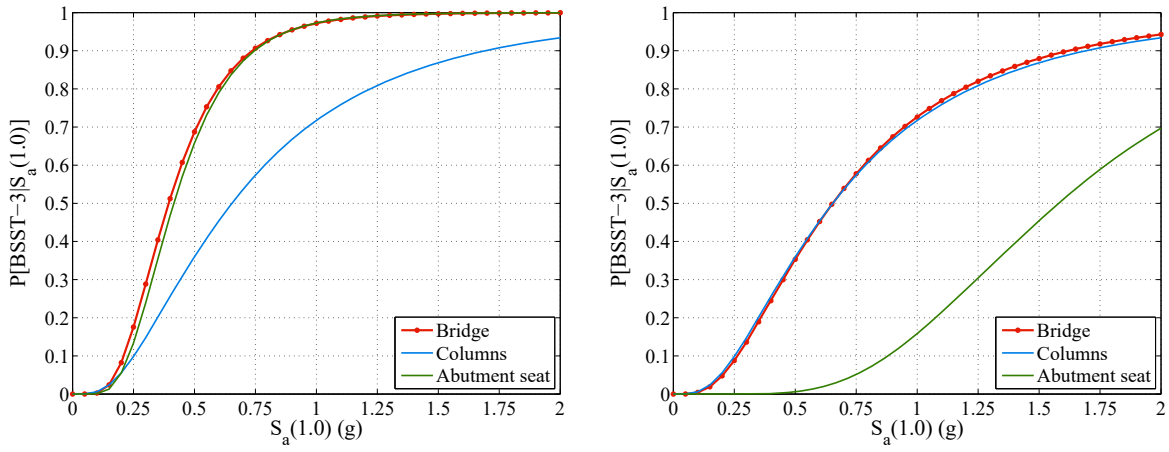

Figure 6.3: System and component level fragility curves for MSCC-SL bridges with seat type abutments and seat width class S1 and S3

Table 6.2: Details of the most vulnerable component across the SPS for MSCC-SL bridge class

Seismic performance sub-bin	BSST-0	BSST-1	BSST-2	BSST-3
MSCC-SL-P-EX-S0	Abut active	Columns	Columns	Columns
MSCC-SL-P-EX-S1	Abut seat	Abut seat	Abut seat	Abut seat
MSCC-SL-P-EX-S2	Abut seat	Abut seat	Columns	Columns
MSCC-SL-P-EX-S3	Abut seat	Abut seat	Columns	Columns
MSCC-SL-P-EX-S4	Abut seat	Abut seat	Columns	Columns

6.2 Multispan Continuous Concrete Single Frame Box-girder Bridges

Component and system level fragility curves are developed for MSCC-BG bridges with diaphragm and seat abutments, single and multi column bents across the three significant design eras considered in this study. Table 6.3 lists the median, λ, and dispersion, ζ, values for the SPS considered along with an average dispersion, ζ^*. Figure 6.4 shows a comparison of fragility curves for single (SCB) and multi column bents (MCB) in bridges with diaphragm abutments. A comparison of median fragilities for SCBs and MCBs with seat type abutments is shown in Figure 6.5. Based on these two figures and Table 6.3, inferences can be drawn based on the influence of the type of bent and abutment on the bridge fragility.

Table 6.3**:** Multispan continuous concrete box-girder bridge fragilities

Seismic performance sub-bin	BSST-0		BSST-1		BSST-2		BSST-3		
	λ	ζ	λ	ζ	λ	ζ	λ	ζ	ζ^*
Pre 1971 design era									
MSCC-BG-S-E1-S0	0.15	0.54	0.17	0.61	0.19	0.60	0.22	0.60	0.60
MSCC-BG-M-E1-S0	0.09	0.48	0.10	0.52	0.11	0.51	0.12	0.51	0.51
MSCC-BG-S-E1-S1	0.02	0.77	0.08	0.62	0.14	0.53	0.17	0.54	0.61
MSCC-BG-S-E1-S2	0.02	0.82	0.09	0.67	0.15	0.54	0.17	0.54	0.64
MSCC-BG-S-E1-S3	0.02	0.79	0.09	0.67	0.14	0.55	0.17	0.54	0.64
MSCC-BG-S-E1-S4	0.02	0.80	0.09	0.66	0.15	0.55	0.17	0.54	0.64
MSCC-BG-M-E1-S1	0.01	0.73	0.06	0.61	0.08	0.59	0.09	0.60	0.63
MSCC-BG-M-E1-S2	0.01	0.80	0.06	0.66	0.08	0.62	0.09	0.62	0.68
MSCC-BG-M-E1-S3	0.01	0.80	0.06	0.64	0.08	0.60	0.09	0.61	0.66
MSCC-BG-M-E1-S4	0.01	0.77	0.06	0.67	0.08	0.61	0.09	0.60	0.66
1971-1990 design era									
MSCC-BG-S-E2-S0	0.19	0.55	0.40	0.60	0.70	0.70	1.00	0.69	0.67
MSCC-BG-M-E2-S0	0.14	0.56	0.24	0.56	0.38	0.56	0.50	0.57	0.56
MSCC-BG-S-E2-S2	0.09	0.61	0.29	0.53	0.47	0.51	0.62	0.52	0.51
MSCC-BG-S-E2-S3	0.09	0.61	0.29	0.53	0.47	0.51	0.62	0.51	0.51
MSCC-BG-S-E2-S4	0.09	0.61	0.29	0.54	0.47	0.51	0.62	0.51	0.51
MSCC-BG-M-E2-S2	0.07	0.52	0.18	0.58	0.27	0.62	0.36	0.63	0.58
MSCC-BG-M-E2-S3	0.07	0.52	0.18	0.59	0.27	0.64	0.36	0.64	0.58
MSCC-BG-M-E2-S4	0.07	0.55	0.18	0.58	0.27	0.64	0.36	0.64	0.59
Post 1990 design era									
MSCC-BG-S-E3-S0	0.21	0.41	0.57	0.39	0.95	0.40	1.26	0.40	0.40
MSCC-BG-M-E3-S0	0.12	0.54	0.35	0.52	0.61	0.56	0.84	0.56	0.53
MSCC-BG-S-E3-S3	0.08	0.55	0.49	0.53	1.39	0.48	2.01	0.49	0.49
MSCC-BG-S-E3-S4	0.08	0.56	0.48	0.53	1.43	0.48	2.06	0.49	0.49
MSCC-BG-M-E3-S3	0.06	0.57	0.26	0.55	0.6	0.59	0.87	0.60	0.57
MSCC-BG-M-E3-S4	0.06	0.58	0.26	0.55	0.6	0.60	0.88	0.61	0.57

6.2.1 Trends based on Diaphragm Abutments

The following inferences can be drawn for SCBs and MCBs in bridges with diaphragm abutments across the three significant design eras considered in this study.

- The vulnerability of both SCBs and MCBs reduces with the evolution of the column design philosophy. Post 1990 era designed bridges with diaphragm abutments are much

less vulnerable when compared to their pre 1971 counterparts irrespective of the type of bent.

- In general, it is seen that SCBs are less vulnerable when compared to the MCBs. MCBs with diaphragm abutments are 46%, 50% and 34% more vulnerable in comparison to their SCB counterparts in the pre 1971, 1971-1990 and post 1990 design eras, respectively. Similar observations are seen in the case of seat abutments with MCBs, which are 47%, 42% and 57% more vulnerable than SCBs in the pre 1971, 1971-1990 and post 1990 design eras, respectively.
- The relative change in median values of post 1990 and 1971-1990 era SCBs with respect to their pre 1971 counterparts is 473% and 355% respectively, while the equivalent quantities in the case of MCBs is 592% and 317%, respectively – at the BSST-3 damage state. This indicates that the evolution of column design has a major impact in the reduction of vulnerability in MCBs when compared to SCBs although the former are more vulnerable when compared to the latter. The reduced vulnerability of SCBs when compared to MCBs may be attributed to a wide variety of reasons including the bridge geometry and dimensions, end conditions of the columns (pinned condition in the case of MCBs versus rotational restraint in the case of SCBs), to mention a few.
- Further the difference in vulnerabilities of SCBs and MCBs underscore the necessity to capture the type of bent in a bridge which is not available through the NBI.

Table 6.4 lists the most vulnerable component in MSCC-BG bridges with diaphragm abutments across the system damage states.

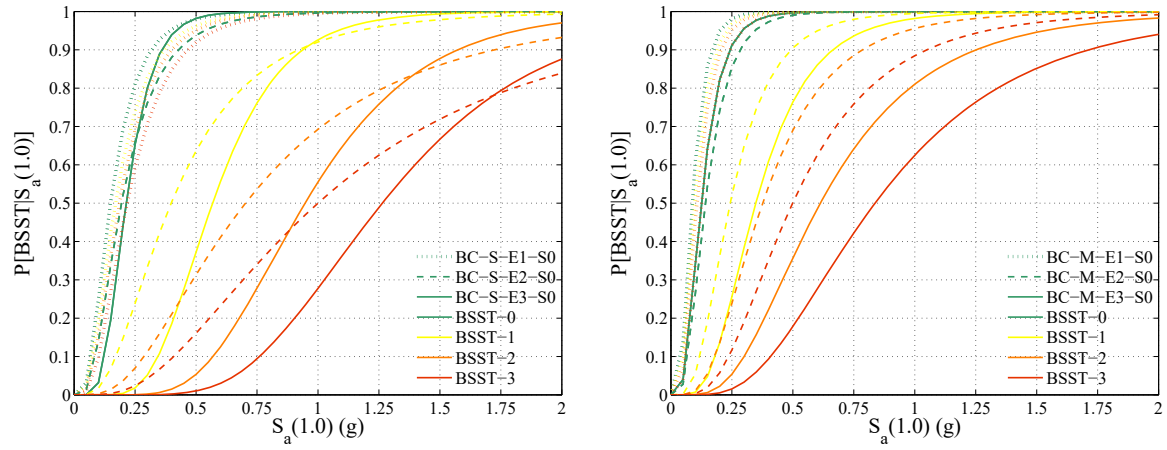

a) b)

Figure 6.4: Fragility curves for MSCC-BG bridges with diaphragm abutments across design eras having a) single column bents, and b) multi column bents

Table 6.4: Details of the most vulnerable component for MSCC-BG bridge class and diaphragm abutments

Seismic performance sub-bin	BSST-0	BSST-1	BSST-2	BSST-3
MSCC-BG-S-E1-S0	Columns	Columns	Columns	Columns
MSCC-BG-S-E2-S0	Columns	Columns	Columns	Columns
MSCC-BG-S-E3-S0	Columns	Columns	Columns	Columns
MSCC-BG-M-E1-S0	Columns	Columns	Columns	Columns
MSCC-BG-M-E2-S0	Columns	Columns	Columns	Columns
MSCC-BG-M-E3-S0	Columns	Columns	Columns	Columns

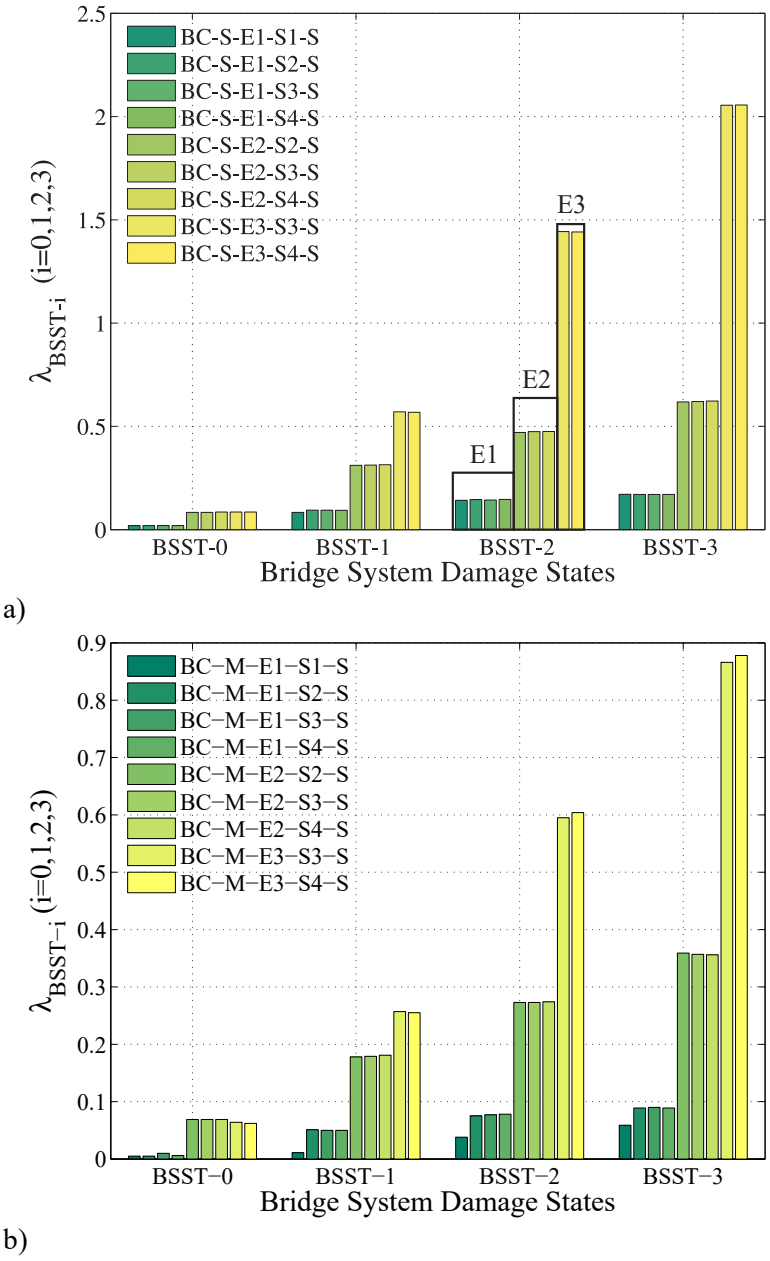

Figure 6.5: Plot of median values for MSCC-BG bridges with seat abutments across design eras for a) single column bents, b) multi column bents

6.2.2 Trends based on Seat Abutments

The following inferences can be drawn for SCBs and MCBs in bridges with seat type abutments across the three significant design eras considered in this study. It must be noted that bridges in the E1 era have all possible ranges of seat widths (S1 through S4), while those

designed in the 1971-1990 design era have only three possible ranges (S2 through S4). Bridges designed post 1990 fall under the S3 and S4 categories and this is depicted in Figure 6.5(a). Additionally, the same trend exists with respect to seat width availability per era in the case of MSCC-TG and MSCC-IG bridge classes which are discussed subsequently in this chapter.

- As in the case of diaphragm abutments, it is seen that the vulnerability of both SCBs (Figure 6.5(a)) and MCBs (Figure 6.5(b)) decreases with an evolution of column design philosophy.
- For a given design era, it is seen that the median fragilities remain consistently similar across the range of seat widths. This is due to the fact that columns govern the vulnerability in most cases and the details of the most vulnerable component are documented in Table 6.5. This serves as an indicator to prioritize the efforts leading to betterment in the performance of columns which will then help realize the true impact of increasing the seat widths.
- In any case, it is seen that there is a tremendous reduction in the vulnerability of post 1990 and 1971-1990 designed bridges with both SCBs and MCBs when compared to their respective pre 1971 counterparts.
- SCBs with seat type abutments are much less vulnerable when compared to MCBs with seat abutments. The median fragilities for post 1990 designed bridges with SCBs is found to be 2.06g in contrast to 0.88g for MCBs therefore making the MCBs 57% more vulnerable when compared to the SCBs. This once again underscores the necessity to capture the type of bent which is not captured by NBI to date.

Table 6.5: Details of the most vulnerable component for MSCC-BG bridge class and seat abutments

Seismic performance sub-bin	BSST-0	BSST-1	BSST-2	BSST-3
MSCC-BG-S-E1-S1	Abut seat	Abut seat	Abut seat	Abut seat
MSCC-BG-S-E1-S2	Joint seal	Abut seat	Columns	Columns
MSCC-BG-S-E1-S3	Joint seal	Abut seat	Columns	Columns
MSCC-BG-S-E1-S4	Joint seal	Abut seat	Columns	Columns
MSCC-BG-M-E1-S1	Joint seal	Abut seat	Abut seat	Abut seat
MSCC-BG-M-E1-S2	Joint seal	Abut seat	Columns	Columns
MSCC-BG-M-E1-S3	Joint seal	Abut seat	Columns	Columns
MSCC-BG-M-E1-S4	Joint seal	Abut seat	Columns	Columns
MSCC-BG-S-E2-S2	Joint seal	Columns	Columns	Columns
MSCC-BG-S-E2-S3	Joint seal	Columns	Columns	Columns
MSCC-BG-S-E2-S4	Joint seal	Columns	Columns	Columns
MSCC-BG-M-E2-S2	Joint seal	Columns	Columns	Columns
MSCC-BG-M-E2-S3	Joint seal	Columns	Columns	Columns
MSCC-BG-M-E2-S4	Joint seal	Columns	Columns	Columns
MSCC-BG-S-E3-S3	Joint seal	Abut seat	Columns	Columns
MSCC-BG-S-E3-S4	Joint seal	Abut seat	Columns	Columns
MSCC-BG-M-E3-S3	Joint seal	Columns	Columns	Columns
MSCC-BG-M-E3-S4	Joint seal	Columns	Columns	Columns

6.2.3 Trends based on the Design Era

Figure 6.6 shows a plot of median values based on design era. The following are some of the inferences that can be drawn:

- In general, irrespective of the type of bent or abutment, pre 1971 era bridges are highly vulnerable when compared to 1971-1990 and post 1990 era bridges.
- Across all the design eras, for a particular abutment type, it is seen that SCBs are much less vulnerable when compared to MCBs. The reduction in vulnerability of SCBs in comparison to MCBs is consistent for both seat and diaphragm abutments. As mentioned previously, this underscores the necessity to capture the type of bent in order to obtain reasonably good estimates of the overall vulnerability of the bridge system.
- Across the first two design eras, diaphragm abutments are much less vulnerable when compared to seat type abutments. The reduction in vulnerability of diaphragm type in

comparison to seat type is consistent for both SCBs and MCBs. The lower vulnerability of diaphragm abutments may be attributed to the complete engagement of the superstructure with the abutment and load transfer mechanisms. Further, in the case of seat abutments, the overall system fragility has an added contribution from the abutment seats in addition to the columns which is absent in the case of diaphragm abutments.

- However, in the post 1990 design era, the trend is reversed and seat abutments are seen to be less vulnerable when compared to diaphragm abutments. This may be attributed to the increased demands on the columns of the latter which is found to be the most vulnerable component.
- The differences in fragilities of diaphragm and seat abutments emphasize the necessity to capture the type of abutment in order to get a reasonable estimate of the overall bridge system fragility.

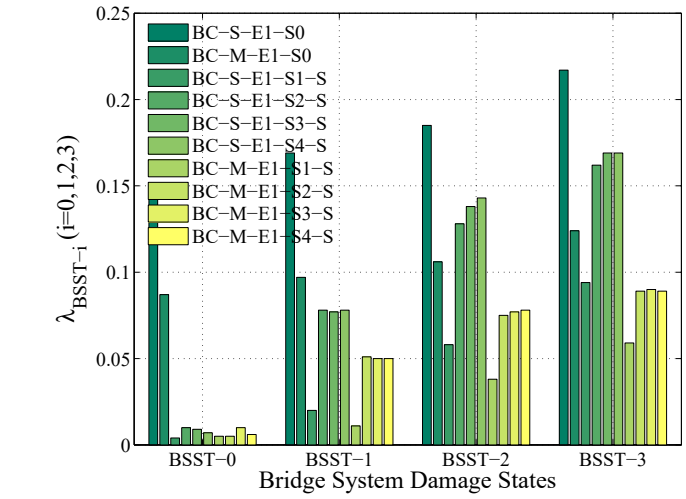

a)

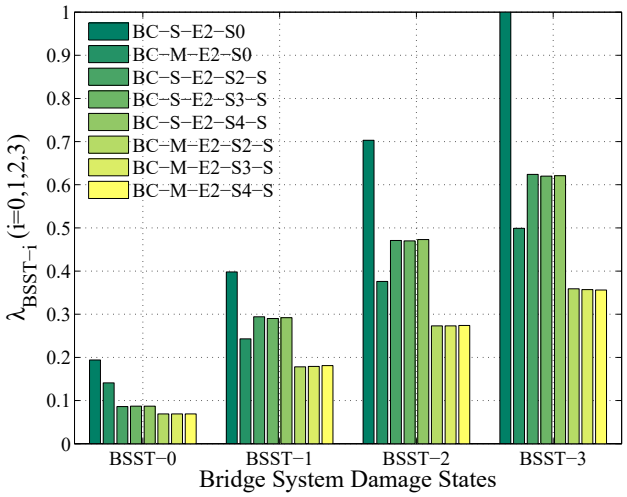

b)

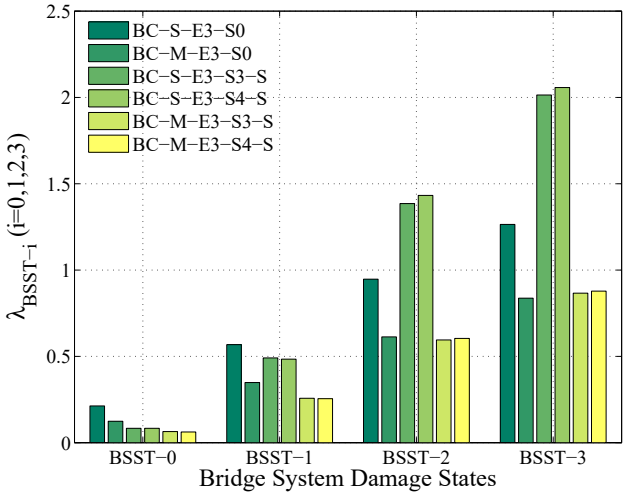

c)

Figure 6.6: Plot of median values of system fragility for a) pre 1971, b) 1971-1990, and c) post 1990 design era

6.2.4 Effect of Gap Size on the Fragility of Post 1990 MSCC-BG bridges

In order to determine the effect of the gap between the deck and abutment backwall on the vulnerability of the bridge system, fragility curves are developed for post 1990 MSCC-BG bridges with seat abutments using two ranges of gap sizes. NLTHA was conducted on two sets of 320 bridge models, the first set comprising of a small gap, denoted by S, between the deck and the abutment backwall which is considered as a uniform random variable between 0 and 1.5 in and a second set consisting of a larger gap, denoted by L, between the deck and the abutment backwall, also modeled as a uniform random number between 1.5 and 6.0 in. It must be noted that the gap size depends on the movement rating (MR) of the joint and further dictates the type of joint seal mechanism in place. Smaller gaps have Type A and B joint sealants while the larger ones have a joint seal assembly in place (either strip or modular type). Extensive details about the MR, gaps and joint seal types were provided in section 3.5.6 of Chapter 3. The comparison of gap sizes, therefore, takes into account the change in dynamic characteristics of the bridge as well as the contribution of joint seal components with different capacity definitions.

Figure 6.7 shows the comparison of median fragilities for post 1990 MSCC-BG bridges with small gap and larger gap, consisting of strip and modular joint seal assemblies. The median and dispersion values are reported in Table 6.6. The following inferences can be drawn by looking at Figure 6.7 and Table 6.6:

- The median values and dispersion for both strip and modular joint assemblies are similar across damage states for both SCBs and MCBs. This is due to the fact the joint seal does not dominate the vulnerability at the BSST-0 and -1 damage states for either case. This indicates that joints may be broadly classified based on the gap as small and large and significant additional effort is not required to further classify the gaps based on the seal mechanism.
- Bridges with large gaps and SCBs are less vulnerable when compared to small gaps. The reduced vulnerability of the abutment seat in the case of larger gaps may be attributed to the abutments not being engaged in this case. However, the trend is reversed in the case

of MCBs where bridges with small gaps are less vulnerable when compared to those with large gaps. In this case, the higher vulnerability of the larger gaps may be attributed to the contribution of piles, which attract a major proportion of the force in comparison to the backfill soil. This can further be understood by a quick inspection of the component fragility curves shown in Figure 6.8, which shows the system and component level fragility curves for MSCC-BG-S-E3-S4-L and MSCC-BG-M-E3-S4-L with modular joint assembly. It is evident that in the case of MCBs, the relative contribution of abutment seat to the overall system vulnerability is much higher when compared to that in the case of SCBs, and also MCBs with smaller gaps.

- The investigation of the effect of joint gap size or MR of the joint reinforces the need to capture this attribute in order to obtain reasonable estimates of the system vulnerability. Attributing similar fragilities to either joint gap size may lead to underestimation or overestimation of the vulnerability depending on the bent type in the bridge.
-

Strip joint seal assembly

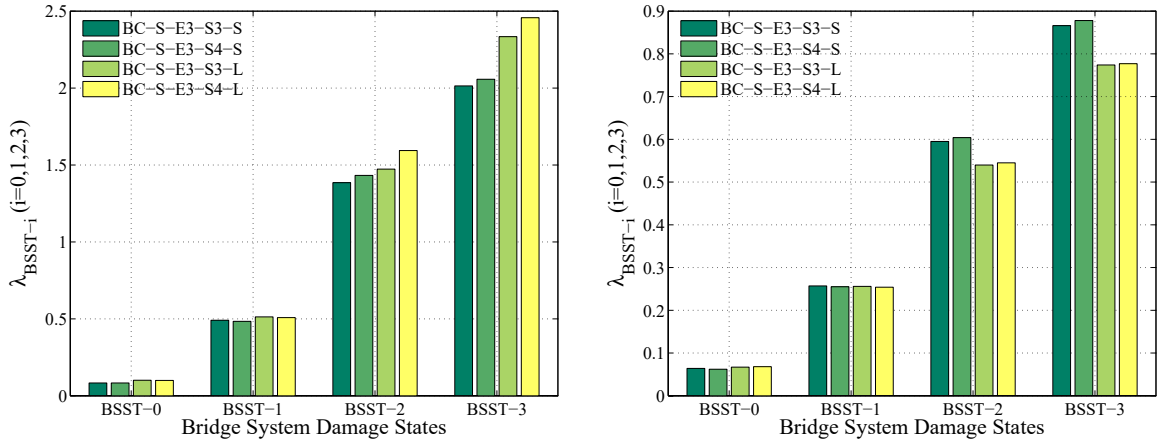

a) Single column bent b) Multi column bent

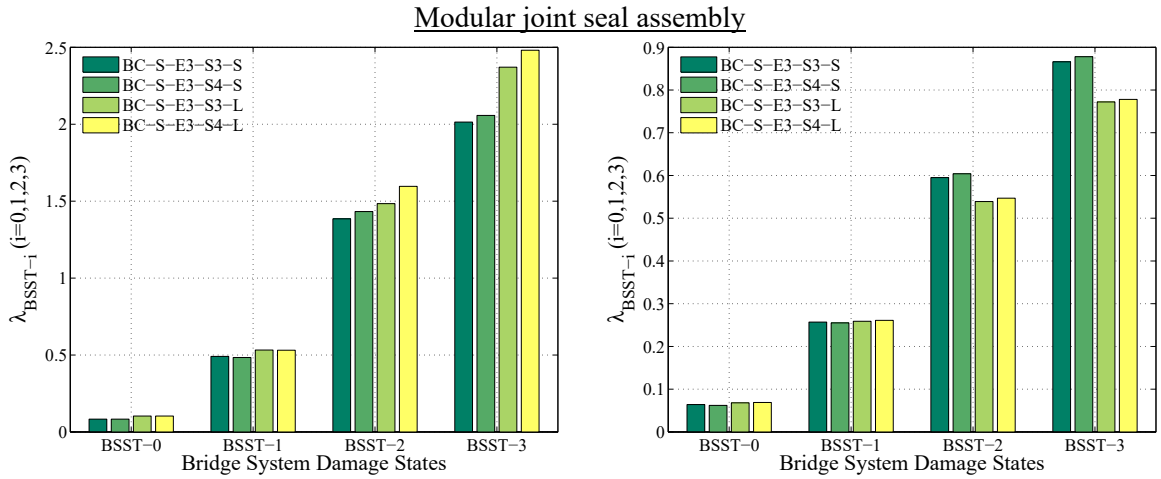

c) Single column bent d) Multi column bent

Figure 6.7: Comparison of median values for bridge fragility curves for post 1990 MSCC-BG bridges with small and large gaps installed with different joint seal units

Table 6.6: System fragilities for post 1990 designed MSCC-BG bridges with strip and modular joint seat assemblies

Seismic performance sub-bin	BSST-0		BSST-1		BSST-2		BSST-3		
	λ	ζ	λ	ζ	λ	ζ	λ	ζ	ζ^*
Strip assembly									
MSCC-BG-S-E3-S3-L	0.09	0.61	0.54	0.58	1.54	0.74	2.42	0.74	0.67
MSCC-BG-S-E3-S4-L	0.09	0.60	0.54	0.58	1.59	0.76	2.46	0.74	0.67
MSCC-BG-M-E3-S3-L	0.07	0.55	0.26	0.53	0.54	0.59	0.77	0.58	0.56
MSCC-BG-M-E3-S4-L	0.07	0.55	0.26	0.54	0.54	0.59	0.77	0.59	0.56
Modular assembly									
MSCC-BG-S-E3-S3-L	0.09	0.62	0.55	0.60	1.56	0.73	2.45	0.75	0.67
MSCC-BG-S-E3-S4-L	0.09	0.64	0.55	0.59	1.61	0.76	2.50	0.77	0.69
MSCC-BG-M-E3-S3-L	0.07	0.54	0.26	0.54	0.54	0.58	0.77	0.58	0.56
MSCC-BG-M-E3-S4-L	0.07	0.56	0.26	0.55	0.54	0.59	0.78	0.59	0.57

MSCC-BG-S-E3-S4-L

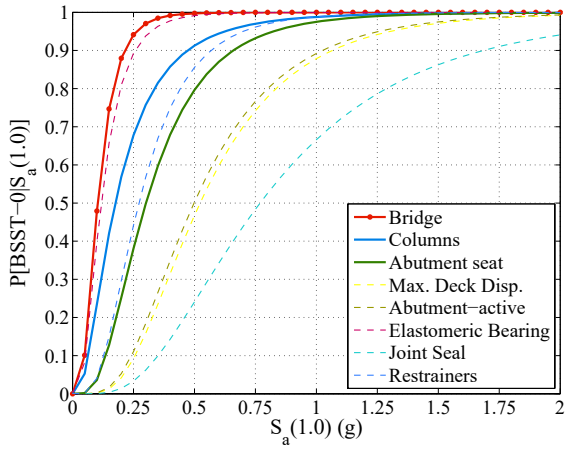

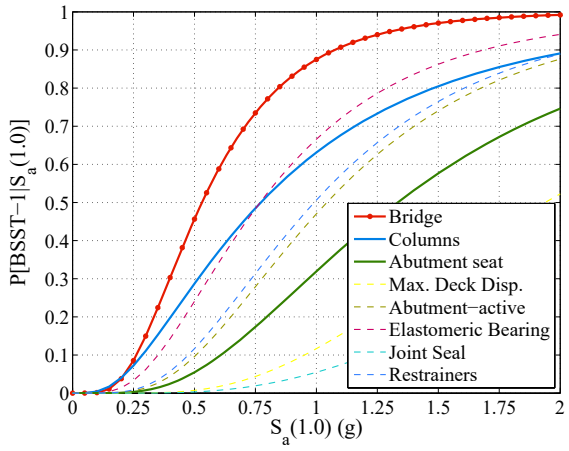

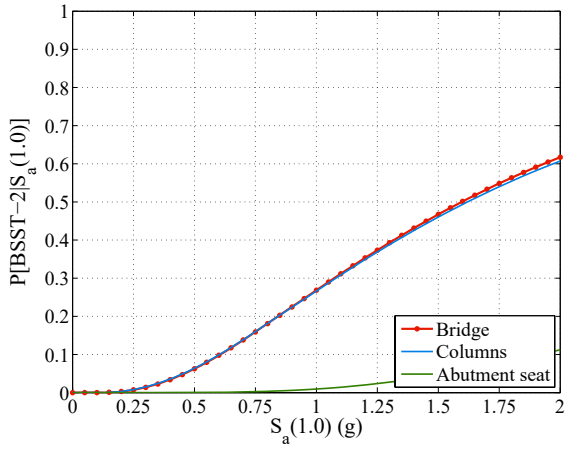

MSCC-BG-M-E3-S4-L

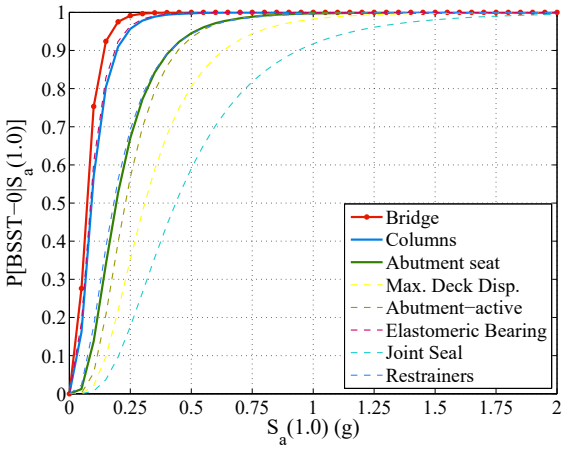

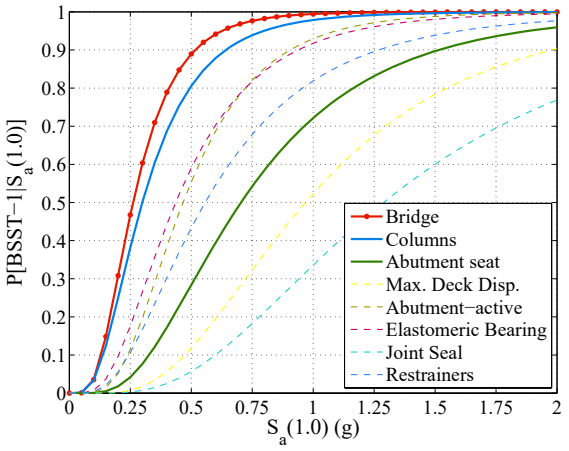

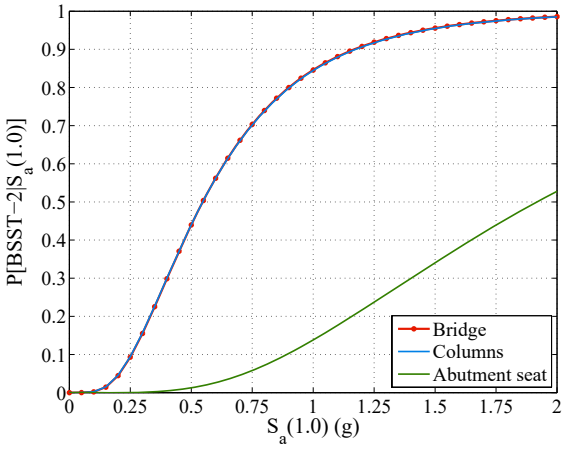

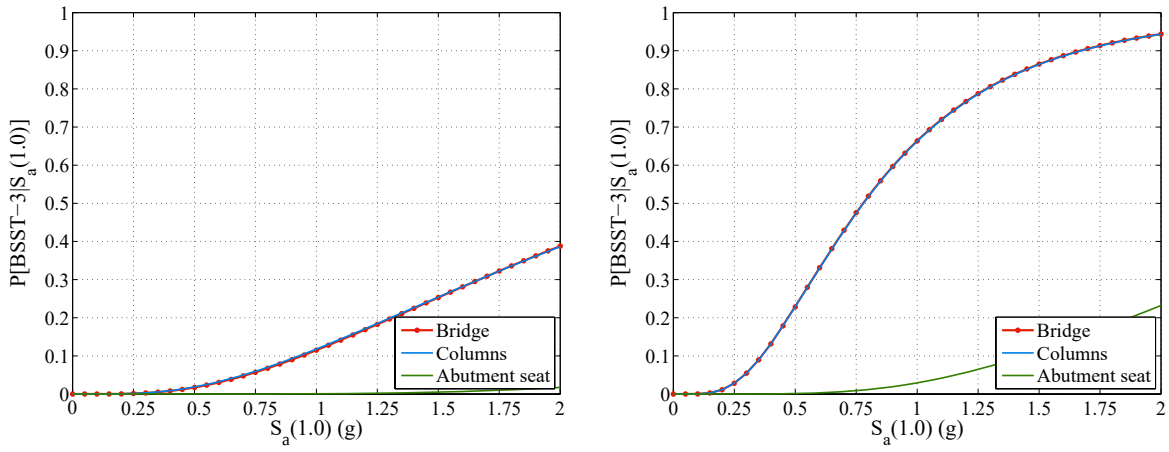

Figure 6.8: System and component level fragility curves for post 1990 MSCC-BG bridges with SCB and MCB equipped with modular joint seal assembly systems

6.3 Multispan Continuous Concrete Tee-girder Bridges

This section presents the results of fragility analysis of MSCC-TG bridges with MCB alone consisting of both integral pile columns (P) and traditional circular columns (M) with seat and diaphragm abutments. Table 6.7 lists the median, λ, and dispersion, ζ, values for the SPS considered along with an average dispersion, ζ^*. A comparison of median fragilities for integral pile columns and MCB in bridges with diaphragm and seat abutments is shown in Figure 6.9. Table 6.8 lists the most vulnerable component for the SPS considered in this bridge class.

Table 6.7**:** Multispan continuous concrete Tee-girder bridge fragilities

Seismic performance sub-bin	BSST-0		BSST-1		BSST-2		BSST-3		
	λ	ζ	λ	ζ	λ	ζ	λ	ζ	ζ^*
Pre 1971 design era									
MSCC-TG-P-E1-S0	0.46	0.52	0.78	0.65	0.88	0.68	1.07	0.67	0.63
MSCC-TG-M-E1-S0	0.27	0.56	0.31	0.57	0.36	0.58	0.45	0.58	0.57
MSCC-TG-P-E1-S1	0.06	0.37	0.12	0.41	0.20	0.42	0.27	0.44	0.41
MSCC-TG-P-E1-S2	0.08	0.36	0.23	0.43	0.31	0.51	0.37	0.53	0.45
MSCC-TG-P-E1-S3	0.08	0.35	0.24	0.43	0.32	0.55	0.38	0.56	0.47
MSCC-TG-P-E1-S4	0.08	0.37	0.23	0.43	0.32	0.57	0.38	0.58	0.49
MSCC-TG-M-E1-S1	0.07	0.50	0.14	0.54	0.23	0.56	0.31	0.56	0.54
MSCC-TG-M-E1-S2	0.10	0.50	0.24	0.58	0.27	0.62	0.34	0.64	0.59
MSCC-TG-M-E1-S3	0.10	0.50	0.24	0.59	0.27	0.63	0.34	0.64	0.59
MSCC-TG-M-E1-S4	0.10	0.51	0.24	0.58	0.28	0.65	0.35	0.65	0.60
1971-1990 design era									
MSCC-TG-P-E2-S0	0.45	0.47	0.76	0.57	0.86	0.60	1.04	0.60	0.56
MSCC-TG-M-E2-S0	0.47	0.52	1.07	0.57	1.99	0.58	2.95	0.61	0.57
MSCC-TG-P-E2-S2	0.09	0.55	0.28	0.60	0.38	0.68	0.46	0.70	0.63
MSCC-TG-P-E2-S3	0.09	0.56	0.28	0.60	0.39	0.72	0.46	0.73	0.65
MSCC-TG-P-E2-S4	0.09	0.56	0.28	0.59	0.39	0.73	0.46	0.73	0.65
MSCC-TG-M-E2-S2	0.12	0.47	0.41	0.47	0.78	0.49	1.12	0.49	0.48
MSCC-TG-M-E2-S3	0.12	0.46	0.41	0.47	1.07	0.52	1.52	0.52	0.49
MSCC-TG-M-E2-S4	0.12	0.46	0.41	0.47	1.19	0.56	1.69	0.56	0.51
Post 1990 design era									
MSCC-TG-P-E3-S0	0.42	0.46	0.74	0.56	0.86	0.62	1.03	0.62	0.57
MSCC-TG-M-E3-S0	0.48	0.47	1.93	0.49	5.12	0.59	99.00	0.00	0.52
MSCC-TG-P-E3-S3	0.07	0.40	0.26	0.44	0.44	0.55	0.55	0.58	0.49
MSCC-TG-P-E3-S4	0.07	0.40	0.26	0.43	0.44	0.58	0.54	0.60	0.50
MSCC-TG-M-E3-S3	0.11	0.44	0.39	0.46	1.20	0.48	1.70	0.48	0.46
MSCC-TG-M-E3-S4	0.11	0.46	0.39	0.45	1.55	0.47	2.23	0.47	0.46

Diaphragm Abutments

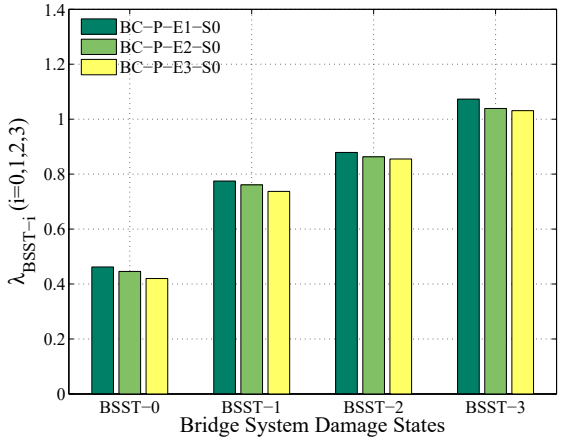

a) Integral pile column

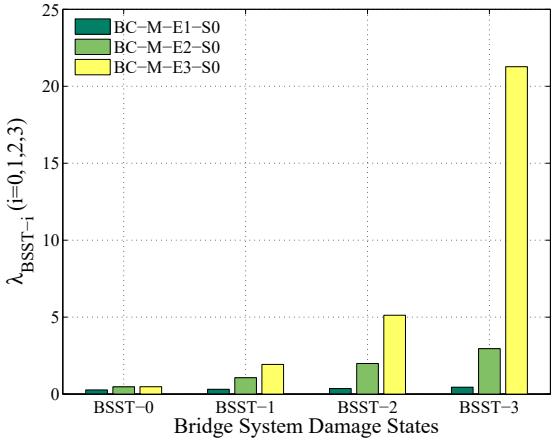

b) Regular multi column bents

Seat Abutments

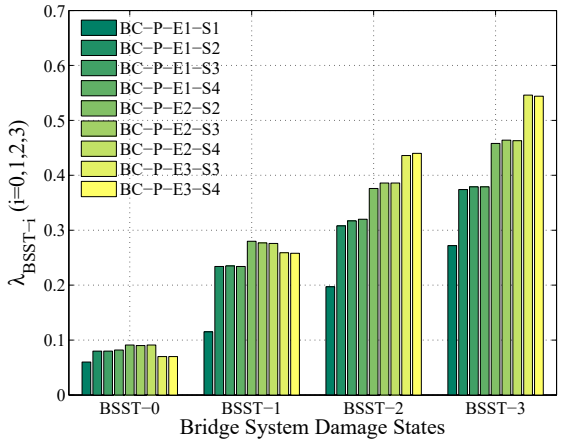

c) Integral pile column

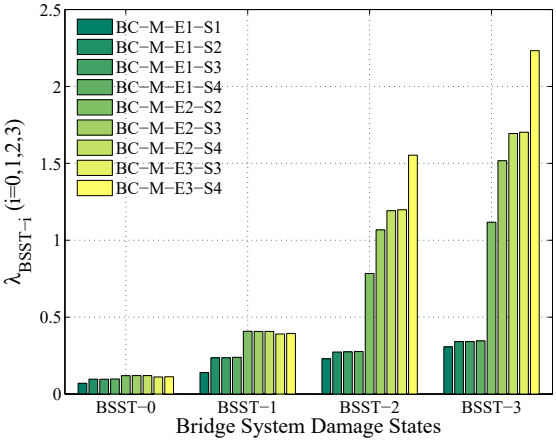

d) Regular multi column bents

Figure 6.9: Comparison of median values of system fragility for MSCC-TG bridge class

Table 6.8: List of the most vulnerable component across damage states for the SPS in MSCC-TG bridge class

Seismic performance sub-bin	BSST-0	BSST-1	BSST-2	BSST-3
Diaphragm Abutments				
MSCC-TG-P-E1-S0	Deck disp.	Columns	Columns	Columns
MSCC-TG-P-E2-S0	Deck disp.	Columns	Columns	Columns
MSCC-TG-P-E3-S0	Deck disp.	Columns	Columns	Columns
MSCC-TG-M-E1-S0	Columns	Columns	Columns	Columns
MSCC-TG-M-E2-S0	Columns	Columns	Columns	Columns
MSCC-TG-M-E3-S0	Columns	Columns	Columns	Columns
Seat Abutments				
MSCC-TG-P-E1-S1	Abut seat	Abut seat	Abut seat	Abut seat
MSCC-TG-P-E1-S2	Joint seal	Columns	Columns	Columns
MSCC-TG-P-E1-S3	Joint seal	Columns	Columns	Columns
MSCC-TG-P-E1-S4	Joint seal	Columns	Columns	Columns
MSCC-TG-M-E1-S1	Abut seat	Abut seat	Columns	Columns
MSCC-TG-M-E1-S2	Joint seal	Columns	Columns	Columns
MSCC-TG-M-E1-S3	Joint seal	Columns	Columns	Columns
MSCC-TG-M-E1-S4	Joint seal	Columns	Columns	Columns
MSCC-TG-P-E2-S2	Joint seal	Abut seat	Columns	Columns
MSCC-TG-P-E2-S3	Joint seal	Abut seat	Columns	Columns
MSCC-TG-P-E2-S4	Joint seal	Abut seat	Columns	Columns
MSCC-TG-M-E2-S2	Joint seal	Abut seat	Abut seat	Abut seat
MSCC-TG-M-E2-S3	Joint seal	Abut seat	Columns	Columns
MSCC-TG-M-E2-S4	Joint seal	Abut seat	Columns	Columns
MSCC-TG-P-E3-S3	Joint seal	Abut seat	Columns	Columns
MSCC-TG-P-E3-S4	Joint seal	Abut seat	Columns	Columns
MSCC-TG-M-E3-S3	Joint seal	Abut seat	Abut seat	Abut seat
MSCC-TG-M-E3-S4	Joint seal	Abut seat	Abut seat	Abut seat

6.3.1 Trends based on Diaphragm Abutments

The following are some of the conclusions and inferences that can be drawn for MSCC-TG bridges with diaphragm abutments:

- The median fragilities for integral pile columns are very similar across the design eras (Figure 6.9(a)). This is due to the fact that there has been no evolution in the standard pile details through the design eras unlike traditional MCBs with circular columns which saw a radical shift in the design philosophy from brittle to ductile behavior. This suggests that

a single set of fragilities may be employed for MSCC-TG with integral pile columns and diaphragm abutments irrespective of the time of construction of the bridge.

- Contrasting the case of integral pile columns, the vulnerability of traditional MCBs reduces with the progression of design eras, as expected (Figure 6.9(b)).
- Pre 1971 design era bridges with integral pile columns are less vulnerable when compared to bridges with traditional MCBs. This may be attributed to the slightly better confinement in the former (reinforced and prestressed piles) when compared to traditional circular columns with very little confinement and hence minimal ductility capacity, which is characteristic of this design era columns.
- On the other hand, traditional MCBs in the 1971-1990 and post 1990 era bridges are less vulnerable when compared to integral pile columns. This underscores the effectiveness of the shift in design philosophy towards energy dissipation in the latter design eras.
- The difference in vulnerability of integral pile columns versus traditional MCBs underscores the necessity to capture this attribute which is not done to date in the NBI.

6.3.2 Trends based on Seat Abutments

- Traditional MCBs with seat type abutments have a tremendous reduction in their vulnerability with the evolution of seat ranges and column design philosophy (Figure 6.9(d)). The enhanced ductility capacity of the modern day columns coupled with generous seat width makes these much less vulnerable when compared to the pre 1971 bridges.
- Bridges with integral pile columns do not see a major reduction in system vulnerability with the evolution of seat widths (Figure 6.9(c)). Although abutment seats are primary components along with columns, the benefit of a larger seat width is masked by the dominance of the brittle integral pile columns to the system vulnerability. Neglecting the subtle differences in the median fragilities, a single set of fragility curves can be used for

MSCC-TG-P across the design eras for all ranges of seat widths, thereby reducing the effort to capture these attributes.

- Integral pile columns and traditional MCBs have similar fragilities in the pre 1971 design era, although integral pile columns are slightly less vulnerable. This is due to similar response characteristics and limited ductility capacity of either of them.
- However, in the latter two design eras, traditional MCBs are far less vulnerable when compared to integral pile columns. As stated previously, this once again stresses the need to capture the type of column in the bridge to obtain reasonable estimates of the vulnerability.

6.3.3 Trends based on Design Era

The plot of median fragilities based on design era is shown in Figure 6.10. The observations can be summarized as below:

- Across design eras, it is observed that irrespective of the column type, diaphragm abutments are less vulnerable when compared to seat abutments.
- In the pre-1971 design era, integral pile columns are less vulnerable when compared to traditional MCBs due to slightly better confinement in the former when compared to the latter. In the case of seat abutments, it is seen that there is insignificant reduction in the vulnerability of the bridge system beyond the 12-18 inch seat range (S2) for both integral pile columns and traditional MCBs. This is indicated by the similar values of median fragilities for seat ranges S2 through S4 across all damage states. It can therefore be concluded that the most effective technique would be to focus on retrofitting the columns once the seat has been increased to at least the 12 – 18 inch (S2) range. The results suggest that the columns govern the overall vulnerability with seats increased to categories S2 through S4. This does not imply that shorter seat widths are just as effective or that seats do not contribute to the vulnerability. Improvement in the performance of

columns by retrofitting or replacement of the non-ductile columns with ductile ones, will demonstrate the impact of increasing the seat width potentially.

- In the 1971-1990 and post 1990 design eras, traditional MCBs are less vulnerable when compared to integral pile columns due to enhanced energy dissipation and ductile characteristics. Unlike the situation in the pre 1971 era bridges, the vulnerability of traditional MCBs is reduced with an increase in the seat width. This is due to the relatively larger contribution of the abutment seat to the overall vulnerability in the latter design eras when compared to the pre 1971 design era where columns dominate the vulnerability almost entirely. This is illustrated in Figure 6.11. Unlike the case of MSCC-BG and MSCC-SL bridges, where columns dominate the vulnerability with the provision of increased seat widths beyond a certain range, the situation is not the same in the case of MSCC-TG bridges, where the provision of increased seat widths (S1 through S4) leads to a reduction in vulnerability successively. This necessitates the need to capture not only the presence of seat abutments in this bridge class, but also specific information regarding the actual seat width range, in order to obtain reliable estimates of the vulnerability.
- The median fragilities across seat ranges (S2 through S4) is similar for bridges with integral pile columns in the 1971-1990 and post 1990 design eras. This once again serves as an indicator to target the retrofit prioritization efforts towards columns to see the potential benefit of increased seat widths and reduced bridge system vulnerability.
- The percentage reduction in vulnerability between diaphragm and seat abutments for integral pile columns and traditional MCBs not consistent across the design eras. Table 6.9 reports the percentage reduction in the vulnerability of diaphragm abutments in comparison to seat abutments for the two column types across the three design eras. Clearly it is seen that the trends are different for integral pile columns and traditional MCBs. This may be attributed to several factors such as change in the dynamic characteristics of the bridges, bridge geometry, end conditions of the column, relative vulnerability between bridge components, to mention a few.

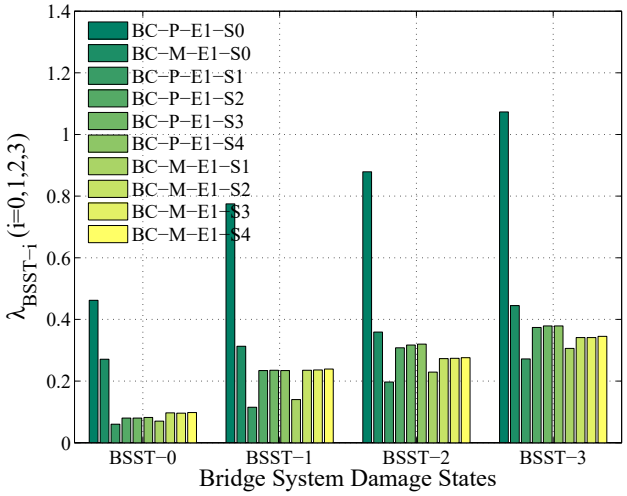

a)

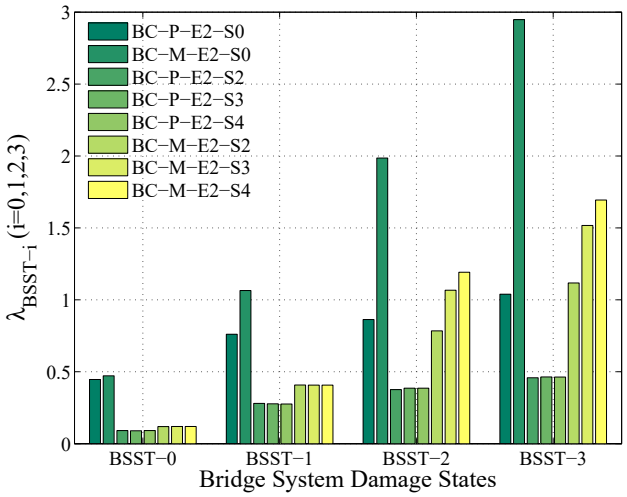

b)

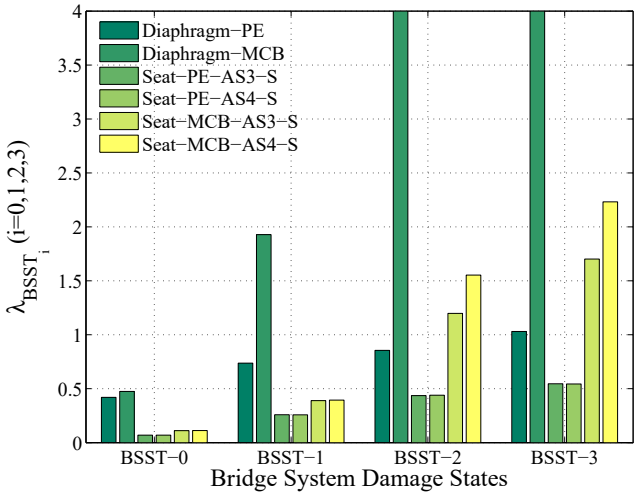

c)

Figure 6.10: Plot of median values of system fragility across damage states for MSCC-TG bridges designed a) pre 1971, b) 1971-1990, and c) post 1990

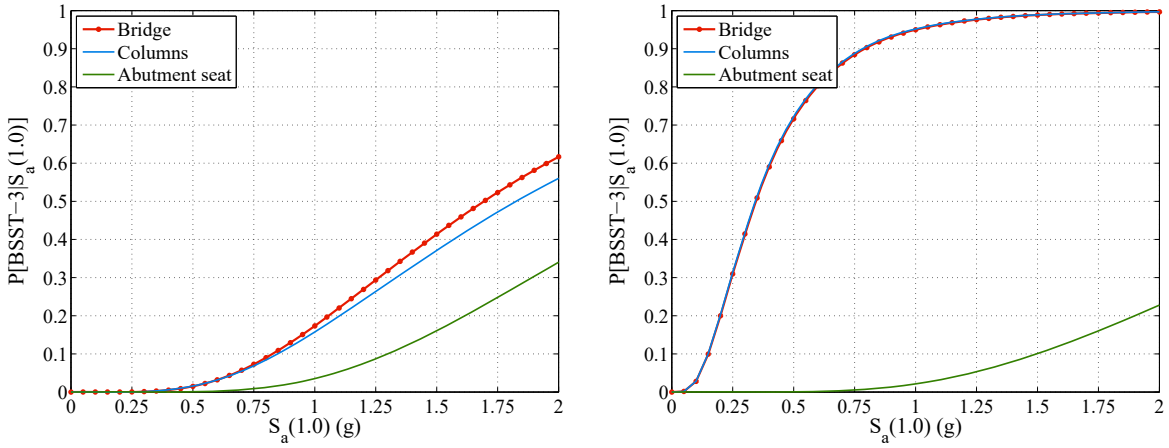

Figure 6.11: System and component fragility curves for a) MSCC-TG-M-E2-S4, and b) MSCC-TG-M-E1-S4

Table 6.9: Percentage reduction in vulnerability of diaphragm abutments with respect to seat abutments

Design era	Bent (column) type	
	Integral pile columns	Traditional MCBs
Pre 1971	182%	29%
1971-1990	121%	65%
Post 1990	93%	60%

6.4 Multispan Continuous Concrete I-girder Bridges

Component and system level fragility curves are developed for MSCC-IG bridges with diaphragm and seat abutments, single and multi-column bents across the three significant design eras considered in this study. Table 6.10 lists the median, λ, and dispersion, ζ, values for the SPS considered along with an average dispersion, ζ^*. The following sub-sections provide discussion about the observed trends based on a number of criteria.

Table 6.10: Multispan continuous concrete I-girder bridge fragilities

Seismic performance sub-bin	BSST-0		BSST-1		BSST-2		BSST-3		
	λ	ζ	λ	ζ	λ	ζ	λ	ζ	ζ^*
Pre 1971 design era									
MSCC-IG-S-E1-S0	0.12	0.56	0.33	0.58	0.47	0.76	0.54	0.76	0.67
MSCC-IG-M-E1-S0	0.09	0.59	0.22	0.63	0.27	0.71	0.32	0.71	0.66
MSCC-IG-S-E1-S1	0.04	0.45	0.09	0.50	0.16	0.51	0.24	0.50	0.49
MSCC-IG-S-E1-S2	0.06	0.46	0.22	0.47	0.39	0.50	0.51	0.51	0.48
MSCC-IG-S-E1-S3	0.06	0.44	0.22	0.48	0.47	0.52	0.56	0.54	0.50
MSCC-IG-S-E1-S4	0.06	0.47	0.22	0.48	0.48	0.55	0.57	0.56	0.51
MSCC-IG-M-E1-S1	0.04	0.46	0.08	0.51	0.15	0.49	0.20	0.49	0.49
MSCC-IG-M-E1-S2	0.05	0.46	0.17	0.50	0.21	0.53	0.25	0.55	0.51
MSCC-IG-M-E1-S3	0.05	0.46	0.17	0.49	0.21	0.56	0.25	0.56	0.52
MSCC-IG-M-E1-S4	0.05	0.47	0.17	0.48	0.21	0.56	0.25	0.56	0.52
1971-1990 design era									
MSCC-IG-S-E2-S0	0.10	0.61	0.25	0.61	0.68	0.92	0.88	0.91	0.76
MSCC-IG-M-E2-S0	0.11	0.53	0.36	0.52	0.77	0.59	1.03	0.59	0.56
MSCC-IG-S-E2-S2	0.04	0.52	0.15	0.54	0.31	0.56	0.46	0.56	0.54
MSCC-IG-S-E2-S3	0.04	0.51	0.15	0.54	0.50	0.55	0.73	0.55	0.54
MSCC-IG-S-E2-S4	0.04	0.52	0.16	0.54	0.68	0.56	0.98	0.57	0.55
MSCC-IG-M-E2-S2	0.06	0.43	0.21	0.44	0.42	0.45	0.61	0.45	0.44
MSCC-IG-M-E2-S3	0.06	0.42	0.21	0.44	0.58	0.46	0.83	0.47	0.45
MSCC-IG-M-E2-S4	0.06	0.42	0.21	0.44	0.66	0.49	0.93	0.50	0.46
Post 1990 design era									
MSCC-IG-S-E3-S0	0.05	0.84	0.19	0.81	2.25	1.03	3.33	1.06	0.93
MSCC-IG-M-E3-S0	0.10	0.56	0.37	0.56	1.58	0.64	2.24	0.64	0.60
MSCC-IG-S-E3-S3	0.02	0.72	0.11	0.72	0.56	0.74	0.93	0.74	0.73
MSCC-IG-S-E3-S4	0.02	0.75	0.11	0.72	0.85	0.74	1.41	0.74	0.74
MSCC-IG-M-E3-S3	0.06	0.42	0.23	0.43	0.73	0.46	1.05	0.46	0.44
MSCC-IG-M-E3-S4	0.06	0.42	0.23	0.44	0.95	0.45	1.37	0.45	0.44

6.4.1 Trends based on Diaphragm Abutments

The plot of median values of system fragility for MSCC-IG bridges with diaphragm abutments across the three design eras is shown in Figure 6.12. The trends observed in this case are very similar to those observed in the case of MSCC-BG bridge class and can be summarized as below.

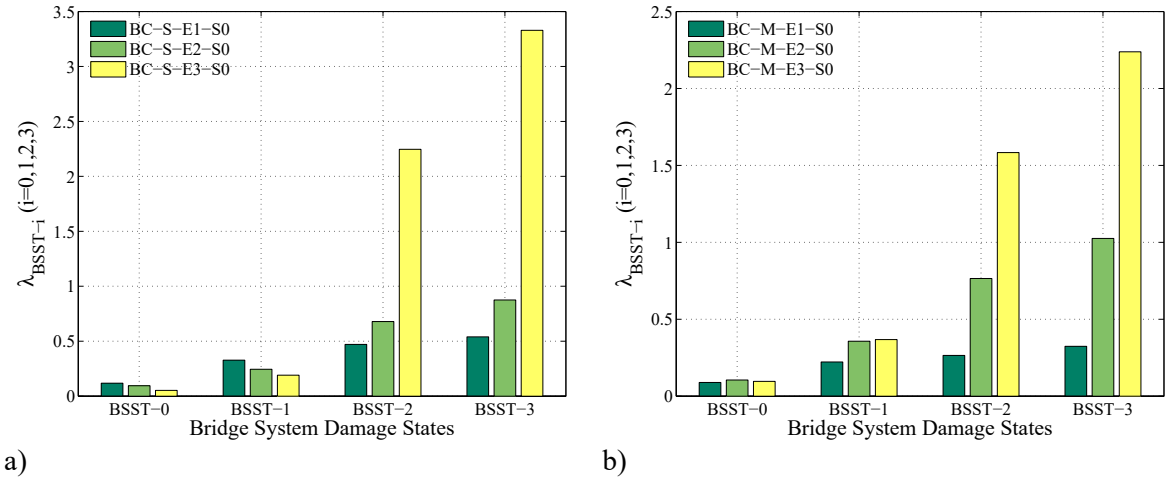

Figure 6.12: Plot of median fragilities for MSCC-IG with diaphragm abutments consisting of a) single column bents, b) multi column bents, across design eras

- The vulnerability of bridges decreases with the progression of the design era, which reinforces the effectiveness of the ductile design philosophy.
- SCBs are less vulnerable when compared to MCBs with diaphragm abutments. MSCC-IG bridges with diaphragm abutments and MCBs are 39%, 13% and 27% more vulnerable when compared to their SCB counterparts in the pre 1971, 1971-1990 and post 1990 design eras, respectively.
- This study recommends the need to capture the type of bent in the bridge owing to the differences in the median values and dispersions characterizing the system fragility due to this attribute.

6.4.2 Trends based on Seat Abutments

Figure 6.13 shows the comparison of median fragilities for I-girder bridge class with seat type abutments across the design eras considered in this study.

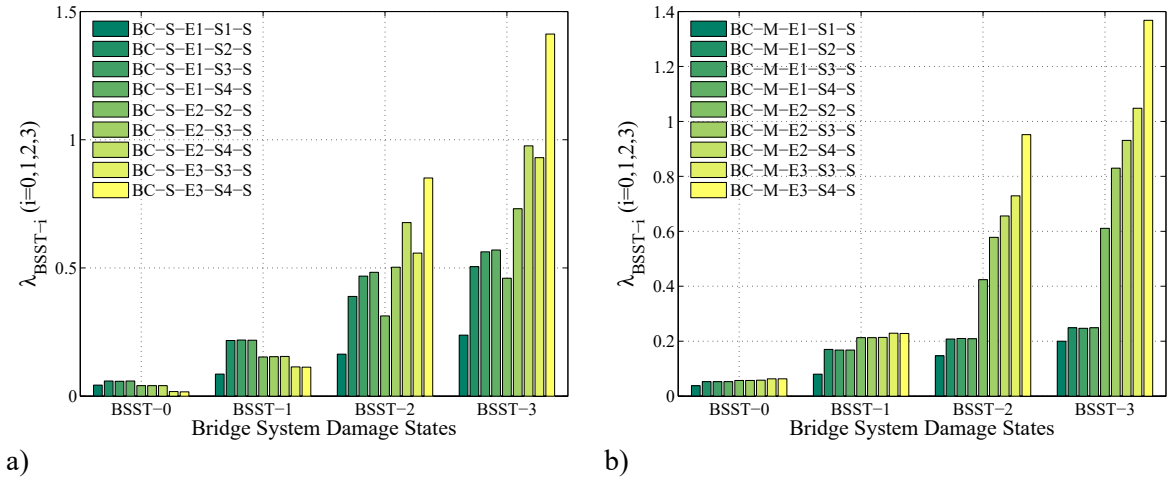

Figure 6.13: Plot of median fragilities for MSCC-IG with seat type abutments consisting of a) single column bents, b) multi column bents, across design eras

The important observations are summarized below.

- Akin to the case of diaphragm abutments, the vulnerability of bridges (both SCB and MCB) reduces across the design eras. However, in the case of seat abutments, it is seen that MCBs are less vulnerable when compared to the SCBs.
- In the pre 1971 design era it is seen that the median fragilities are similar for seat ranges S2 thru S4 and these are less vulnerable when compared to S1 as expected. This establishes the potential impact of increasing the seat widths beyond the S2 (12 – 18 in) range and focusing on modifying the response of columns in an attempt to reduce the overall vulnerability of the bridge system.
- However in the 1971-1990 and post 1990 design eras, there is a reduction in the vulnerability with the progression of seat ranges S2 through S4. This is due to the fact that the relative contribution of the abutment seat to the overall vulnerability is higher in these cases when compared to the situation in the pre 1971 designed bridges, where columns dominate the overall vulnerability.

- The results presented in this section underscore the importance of capturing attributes such as the bent type and type of abutment in order to obtain reliable estimates of the overall vulnerability of the bridge system.

Table 6.11 lists the most vulnerable component for the MSCC-IG bridge class and the different SPS associated with it.

Table 6.11: Details of the most vulnerable component for MSCC-IG bridge class

Seismic performance sub-bin	BSST-0	BSST-1	BSST-2	BSST-3
MSCC-IG-S-E1-S0	Bearings	Bearings	Columns	Columns
MSCC-IG-M-E1-S0	Bearings	Columns	Columns	Columns
MSCC-IG-S-E1-S1	Abut seat	Abut seat	Abut seat	Abut seat
MSCC-IG-S-E1-S2	Joint seal	Abut seat	Abut seat	Columns
MSCC-IG-S-E1-S3	Joint seal	Abut seat	Columns	Columns
MSCC-IG-S-E1-S4	Joint seal	Abut seat	Columns	Columns
MSCC-IG-M-E1-S1	Abut seat	Abut seat	Abut seat	Abut seat
MSCC-IG-M-E1-S2	Joint seal	Columns	Columns	Columns
MSCC-IG-M-E1-S3	Joint seal	Columns	Columns	Columns
MSCC-IG-M-E1-S4	Joint seal	Columns	Columns	Columns
MSCC-IG-S-E2-S0	Bearings	Bearings	Columns	Columns
MSCC-IG-M-E2-S0	Bearings	Bearings	Columns	Columns
MSCC-IG-S-E2-S2	Joint seal	Abut seat	Abut seat	Abut seat
MSCC-IG-S-E2-S3	Joint seal	Abut seat	Abut seat	Abut seat
MSCC-IG-S-E2-S4	Joint seal	Abut seat	Abut seat	Abut seat
MSCC-IG-M-E2-S2	Joint seal	Abut seat	Abut seat	Abut seat
MSCC-IG-M-E2-S3	Joint seal	Abut seat	Columns	Columns
MSCC-IG-M-E2-S4	Joint seal	Abut seat	Columns	Columns
MSCC-IG-S-E3-S0	Bearings	Bearings	Columns	Columns
MSCC-IG-M-E3-S0	Bearings	Bearings	Columns	Columns
MSCC-IG-S-E3-S3	Joint seal	Abut seat	Abut seat	Abut seat
MSCC-IG-S-E3-S4	Joint seal	Abut seat	Abut seat	Abut seat
MSCC-IG-M-E3-S3	Joint seal	Abut seat	Abut seat	Abut seat
MSCC-IG-M-E3-S4	Joint seal	Abut seat	Abut seat	Abut seat

6.4.3 Trends based on Design Era

The median values of system fragility curves for MSCC-IG bridges with SCBs and MCBs, seat and diaphragm abutments based on the design era are shown in Figure 6.14.

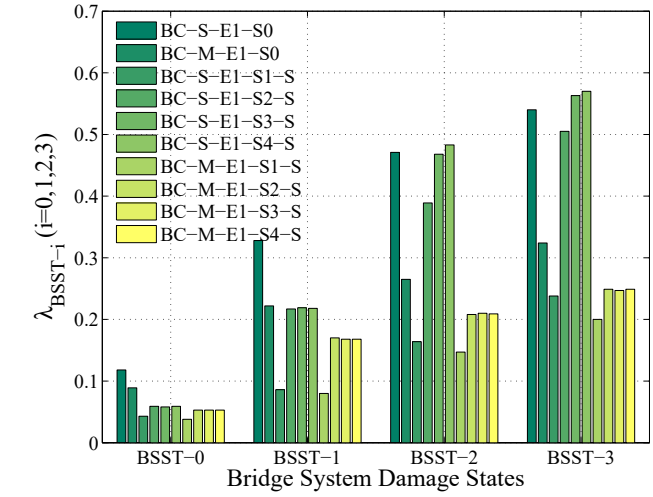

a)

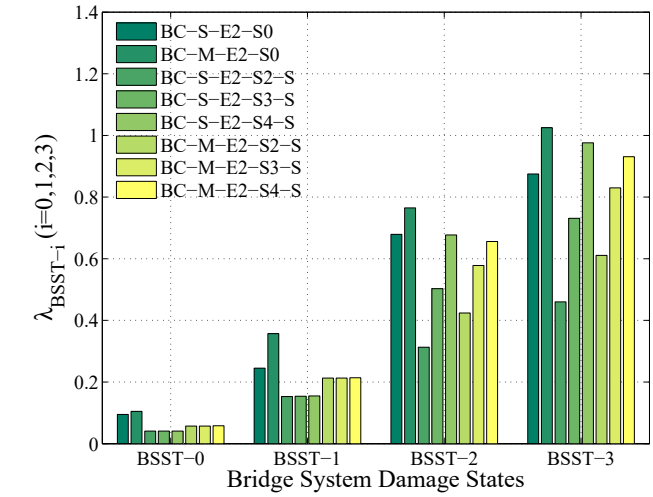

b)

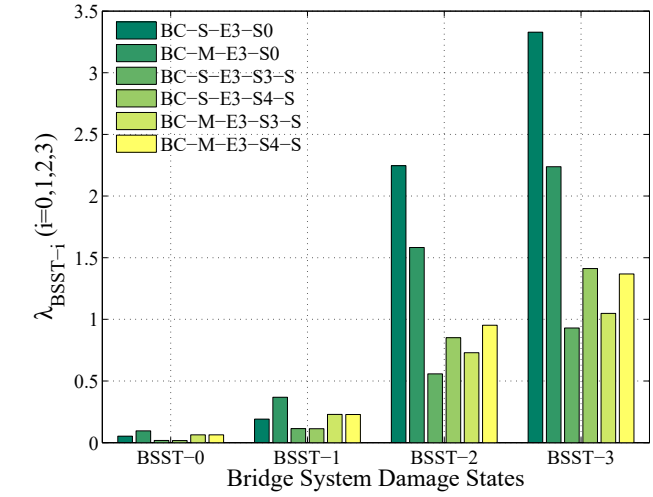

c)

Figure 6.14: Plot of median fragilities for MSCC-IG bridges designed in the a) pre 1971, b) 1971-1990, and c) post 1990 era

- Clearly, the vulnerability of the I-girder bridges reduces with the evolution of column design philosophy and seat widths moving from pre 1971 through 1971-1990 and post 1990 eras.
- MCBs and diaphragm abutments are less vulnerable when compared to MCBs and seat type abutments. However, the trend is quite complex in the case of SCBs where the seat abutments are less vulnerable when compared to diaphragm abutments in the pre 1971 and 1971-1990 design eras. However, SCBs and diaphragm abutments are less vulnerable when compared to SCBs and seat abutments in the post 1990 design era.

6.5 HAZUS Comparison

A detailed discussion about the assumptions, methodology and limitations of the HAZUS fragilities (HAZUS-MH, 2011) were discussed in Chapter 2. HAZUS fragilities were developed by synthesizing the information from the NBI alone unlike the present study where extensive data from bridge plans and in-house databases and the evolution of seismic design philosophy at the component level was used to supplement the information from NBI to obtain seismic performance sub-bins with similar characteristics. As was demonstrated in Chapter 5 and proceeding sections in this chapter, this led to significant variability in the median fragilities across design eras. Further, significant variation was seen with the SPS for the same design era. Despite the differences between the present study and HAZUS methodology, discussed previously, there are a couple of similarities. $S_a(1.0)$ is used as the intensity measure in both cases and so is the number of damage states characterizing the bridge system vulnerability. Although the vulnerability of bridges is governed by that of the columns alone in the case of HAZUS, the column damage state threshold values are chosen and the damage state descriptions are defined keeping in view the anticipated damage to the other bridge components and the HAZUS damage indicators are defined in Table 6.12.

Table 6.12: HAZUS damage state definitions (HAZUS-MH, 2011)

Damage state	Notation	Description
None	ds_1	None
Slight	ds_2	Minor spalling to the column requiring no more than cosmetic repair; minor cracking to the deck; minor cracking and spalling to the abutment; cracks in shear keys at the abutment
Moderate	ds_3	Moderate cracking (shear cracks) and spalling to the columns but is still structurally sound; moderate (< 2 in) movement of the abutment; extensive cracking and spalling of the shear keys; moderate settlement of the approach slab
Extensive	ds_4	Shear failure of the column causing strength degradation without collapse and columns is structurally unsafe; significant residual movement of superstructure-bent cap connection; vertical offset of the abutment; major settlement of the approach slab; shear key failure at the abutments
Complete	ds_5	Collapse of the column; loss of bearing support in the connection leading to unseating and imminent deck collapse; foundation failure leading to titling of the superstructure

The HAZUS median fragilities (λ_s, λ_m, λ_e, λ_c, corresponding to slight, moderate, extensive, and complete damage states, respectively) and dispersion (β_{ds}) are documented in Table 6.13. A single value of dispersion equal to 0.6 is prescribed across all the bridge classes. The equivalent bridge class notations between HAZUS and the present study are also noted to facilitate comparison. Figure 6.15 shows a plot of median values for MSCC-BG bridge class with single columns bents in the post 1990 design era and the HAZUS fragilities for illustrative purposes.

Table 6.13: Median values and dispersion for the HAZUS fragilities

Bridge class notation		Median fragilities				
Present study	HAZUS	λ_s	λ_m	λ_e	λ_c	β_{ds}
MSCC-BG-S-E1-SX	HWB8/HWB20	0.35	0.45	0.55	0.80	0.60
MSCC-BG-S-E2/3-SX	HWB9/HWB21	0.60	0.90	1.30	1.60	0.60
MSCC-TG-P/M-E1-SX MSCC-IG-S/M-E1-SX MSCC-BG-M-E1-SX MSCC-SL-P-EX-SX	HWB10/HWB22	0.60	0.90	1.10	1.50	0.60
MSCC-TG-P/M-E2/3-SX MSCC-IG-S/M-E2/3-SX MSCC-BG-M-E2/3-SX	HWB11/HWB23	0.90	0.90	1.10	1.50	0.60

Note: X stands for all possible combinations pertinent to the attribute under consideration

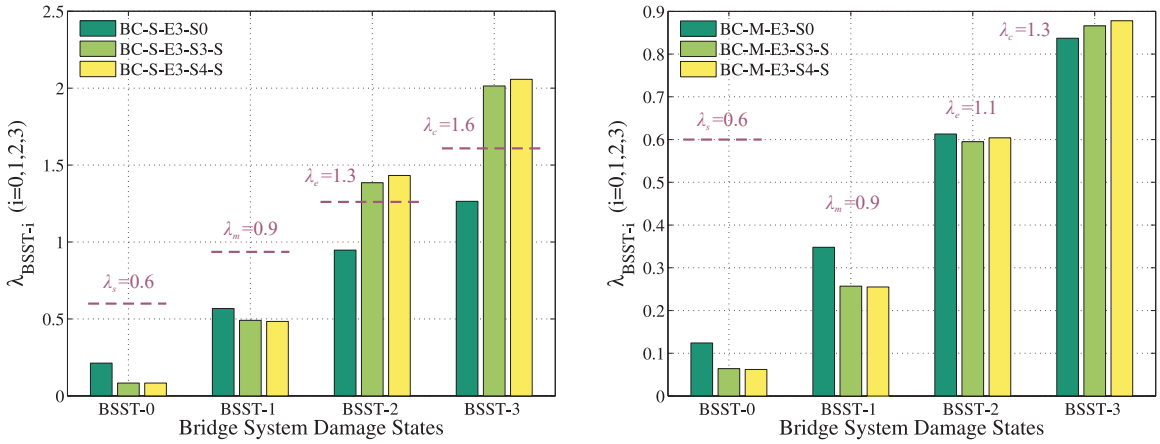

a) Single column bent b) Multi column bent

Figure 6.15: Comparison of median values of system fragility for MSCC-BG-S-E3 based on the present study and HAZUS

The following are some of the trends based on comparison:

- Bridges with diaphragm abutments are found to be more vulnerable than predicted by HAZUS, which does not distinguish this feature. The degree of vulnerability is higher for MCBs when compared to SCBs.
- Bridges with seat abutments and SCBs are more vulnerable relative to HAZUS at the BSST-0 and BSST-1 damage states while the trend reverses for the BSST-2 and -3 damage states where HAZUS predicts the bridge class to be more vulnerable.

- Bridges with seat abutments and MCBs are found to be more vulnerable than predicted by HAZUS.

The procedure of comparing the median values of the fragility at the system level is repeated for all of the bridge classes and the respective SPS across the design eras and the trends are summarized below. The percentage change in median values with respect to HAZUS is calculated in each case where a positive change in the median value indicates a less vulnerable bridge while a negative value indicates a more vulnerable bridge. These values are reported in Appendix E. In all cases, the bridges in this study are found to be more vulnerable than that predicted by HAZUS for the lower bridge system damage states, BSST-0 and BSST-1. This is mainly due to the contribution of the secondary components which account for the vulnerability at these lower damage states, which are perceived to necessitate repair.

- MSCC-BG bridges with SCBs and MCBs having both seat and diaphragm abutments in the pre 1971 and 1971-1990 design eras are more vulnerable than that predicted by HAZUS. The change in median values is very high for BSST-0 and -1 damage states when compared to the higher damage states in the bridge. In the post 1990 design era, MSCC-BG bridges with diaphragm abutments are more vulnerable than that predicted by HAZUS. The same is the case with MCBs and seat abutments. However, based on the results of this study, SCBs and seat abutments are less vulnerable than that predicted by HAZUS for the higher damage states BSST-2, and BSST-3. The dispersions obtained from the present study are close to the HAZUS values but are systematically lower for all the bridge classes considered in this study.
- The fragilities for MSCC-SL bridge class indicate that they are more vulnerable than those presented by HAZUS. The percentage change in the median values is as high as 50% for the higher bridge damage states. The average dispersion is about 0.7 which is roughly 17% higher than the HAZUS prescribed value.
- MSCC-TG bridges with integral pile columns and traditional MCBs in the pre 1971 design era are more vulnerable than that predicted by HAZUS. In the 1971-1990 and post

1990 design eras, traditional MCBs are less vulnerable than that predicted by HAZUS. However, the integral pile columns in the 1971-1990 and post 1990 design eras are much more vulnerable (about 60% lower median value of the fragilities) than that predicted by HAZUS. The dispersions for this bridge class are generally found to be lower than that predicted by HAZUS, particularly for the integral pile columns.

- The results from this study indicate that MSCC-IG bridges in the pre 1971 design era are more vulnerable than that predicted by HAZUS. However, the SCBs in the 1971-1990 and post 1990 are less vulnerable and the percentage change in median values is as high as 160% in the case of MSCC-IG-S-E3-S4. The MCBs in the 1971-1990 design era are more vulnerable than that predicted by HAZUS, however, the trend is reversed in the case of post 1990 design era MCBs. In short, the post 1990 bridge fragilities from this study reveal much lower vulnerability than that predicted by HAZUS. The dispersions calculated in this study are lower than that proposed in HAZUS in a majority of the SPS for this bridge class.

6.6 Closure

Bridge component and system level seismic fragility curves are generated and presented for four multispan continuous concrete bridge classes with several seismic performance sub-bins across three significant design eras considered in this study. The curves are generated using Monte Carlo simulation by comparing realizations of the joint probabilistic seismic demand models with realizations of the capacity models, discussed in the previous chapter.

The following are some of the significant findings of this chapter:

- The vulnerability of all the bridge classes reduced with the evolution of column and ductile design philosophy and seat widths across the design eras considered.
- MSCC-BG bridges are the most fragile in the pre 1971 design era in comparison to the other bridge classes considered in this study. The multi column bents (MCB) are more vulnerable when compared to the single column bents (SCB).

- In the 1971-1990 design era, MSCC-BG bridges with MCBs and diaphragm abutments are the most vulnerable bridges followed by their seat abutment counterparts. MSCC-IG bridges with diaphragm abutments are the most vulnerable considering SCBs.
- MSCC-TG bridges with integral pile columns and seat abutments are the most fragile among the modern day bridges followed by MSCC-BG bridges with MCBs and diaphragm abutments.
- Across bridge classes and design eras, in general it was seen that SCBs and diaphragm abutments are relatively less vulnerable when compared to MCBs and seat abutments, barring a few exceptions.
- Comparison with HAZUS fragilities revealed the wide disparity between the results of the present study and the values prescribed in HAZUS. The results from this study indicate that a majority of the SPS in the pre 1971 and 1971-1990 design eras are more vulnerable than that predicted by HAZUS. However, the SPS in modern day bridges are less vulnerable that predicted by HAZUS in a majority of cases. Discrepancies with HAZUS are likely due to the mechanical analyses technique used to define component response distributions, system reliability definition, capacity models or damage state definitions, to mention a few.

APPENDIX E

COMPARISON OF THE BRIDGE CLASS SYSTEM FRAGILITIES WITH HAZUS

Table E.1: Percentage change in the median values and dispersions of the bridge class fragilities with respect to HAZUS fragilities

Bridge class (CBC + SPS)	BSST median values, λ					% change in λ and ζ				
	0	1	2	3	ζ*	0	1	2	3	ζ*
HAZUS fragilities										
MSCC-BG-S-E1	0.35	0.45	0.55	0.80	0.60					
MSCC-BG-S-E2/E3	0.60	0.90	1.30	1.60	0.60					
MSCC-BG-M-E1	0.60	0.90	1.10	1.50	0.60					
MSCC-BG-M-E2/E3	0.90	0.90	1.10	1.50	0.60					
Current study										
MSCC-BG-S-E1-S0	0.15	0.17	0.19	0.22	0.6	-57	-62	-65	-73	0
MSCC-BG-M-E1-S0	0.09	0.10	0.11	0.12	0.51	-85	-89	-90	-92	-15
MSCC-BG-S-E1-S1	0.02	0.08	0.14	0.17	0.61	-94	-82	-75	-79	2
MSCC-BG-S-E1-S2	0.02	0.09	0.15	0.17	0.64	-94	-80	-73	-79	7
MSCC-BG-S-E1-S3	0.02	0.09	0.14	0.17	0.64	-94	-80	-75	-79	7
MSCC-BG-S-E1-S4	0.02	0.09	0.15	0.17	0.64	-94	-80	-73	-79	7
MSCC-BG-M-E1-S1	0.01	0.06	0.08	0.09	0.63	-98	-93	-93	-94	5
MSCC-BG-M-E1-S2	0.01	0.06	0.08	0.09	0.68	-98	-93	-93	-94	13
MSCC-BG-M-E1-S3	0.01	0.06	0.08	0.09	0.66	-98	-93	-93	-94	10
MSCC-BG-M-E1-S4	0.01	0.06	0.08	0.09	0.66	-98	-93	-93	-94	10
MSCC-BG-S-E2-S0	0.19	0.40	0.70	1.00	0.67	-68	-56	-46	-38	12
MSCC-BG-M-E2-S0	0.14	0.24	0.38	0.50	0.56	-84	-73	-65	-67	-7
MSCC-BG-S-E2-S2	0.09	0.29	0.47	0.62	0.51	-85	-68	-64	-61	-15
MSCC-BG-S-E2-S3	0.09	0.29	0.47	0.62	0.51	-85	-68	-64	-61	-15
MSCC-BG-S-E2-S4	0.09	0.29	0.47	0.62	0.51	-85	-68	-64	-61	-15
MSCC-BG-M-E2-S2	0.07	0.18	0.27	0.36	0.58	-92	-80	-75	-76	-3
MSCC-BG-M-E2-S3	0.07	0.18	0.27	0.36	0.58	-92	-80	-75	-76	-3
MSCC-BG-M-E2-S4	0.07	0.18	0.27	0.36	0.59	-92	-80	-75	-76	-2
MSCC-BG-S-E3-S0	0.21	0.57	0.95	1.26	0.4	-65	-37	-27	-21	-33
MSCC-BG-M-E3-S0	0.12	0.35	0.61	0.84	0.53	-87	-61	-45	-44	-12
MSCC-BG-S-E3-S3	0.08	0.49	1.39	2.01	0.49	-87	-46	7	26	-18

MSCC-BG-S-E3-S4	0.08	0.48	1.43	2.06	0.49	-87	-47	10	29	-18
MSCC-BG-M-E3-S3	0.06	0.26	0.6	0.87	0.57	-93	-71	-45	-42	-5
MSCC-BG-M-E3-S4	0.06	0.26	0.6	0.88	0.57	-93	-71	-45	-41	-5
HAZUS fragilities										
MSCC-SL	0.60	0.90	1.10	1.50	0.60					
Current study										
MSCC-SL-P-S0	0.57	0.90	1.03	1.28	0.64	-5	-1	-7	-15	6
MSCC-SL-P-S1-S	0.09	0.16	0.29	0.39	0.46	-85	-82	-74	-74	-23
MSCC-SL-P-S2-S	0.12	0.35	0.50	0.63	0.54	-80	-61	-55	-58	-10
MSCC-SL-P-S3-S	0.12	0.35	0.54	0.65	0.57	-81	-61	-51	-56	-4
MSCC-SL-P-S4-S	0.12	0.35	0.55	0.66	0.59	-81	-61	-50	-56	-1
HAZUS fragilities										
MSCC-TG-S/M-E1	0.60	0.90	1.10	1.50	0.60					
MSCC-TG-S/M-E2/E3	0.90	0.90	1.10	1.50	0.60					
Current study										
MSCC-TG-P-E1-S0	0.46	0.78	0.88	1.07	0.63	-23	-13	-20	-29	5
MSCC-TG-M-E1-S0	0.27	0.31	0.36	0.45	0.57	-55	-66	-67	-70	-5
MSCC-TG-P-E1-S1	0.06	0.12	0.2	0.27	0.41	-90	-87	-82	-82	-32
MSCC-TG-P-E1-S2	0.08	0.23	0.31	0.37	0.45	-87	-74	-72	-75	-25
MSCC-TG-P-E1-S3	0.08	0.24	0.32	0.38	0.47	-87	-73	-71	-75	-22
MSCC-TG-P-E1-S4	0.08	0.23	0.32	0.38	0.49	-87	-74	-71	-75	-18
MSCC-TG-M-E1-S1	0.07	0.14	0.23	0.31	0.54	-88	-84	-79	-79	-10
MSCC-TG-M-E1-S2	0.10	0.24	0.27	0.34	0.59	-83	-73	-75	-77	-2
MSCC-TG-M-E1-S3	0.10	0.24	0.27	0.34	0.59	-83	-73	-75	-77	-2
MSCC-TG-M-E1-S4	0.10	0.24	0.28	0.35	0.6	-83	-73	-75	-77	0
MSCC-TG-P-E2-S0	0.45	0.76	0.86	1.04	0.56	-50	-16	-22	-31	-7
MSCC-TG-M-E2-S0	0.47	1.07	1.99	2.95	0.57	-48	19	81	97	-5
MSCC-TG-P-E2-S2	0.09	0.28	0.38	0.46	0.63	-90	-69	-65	-69	5
MSCC-TG-P-E2-S3	0.09	0.28	0.39	0.46	0.65	-90	-69	-65	-69	8
MSCC-TG-P-E2-S4	0.09	0.28	0.39	0.46	0.65	-90	-69	-65	-69	8
MSCC-TG-M-E2-S2	0.12	0.41	0.78	1.12	0.48	-87	-54	-29	-25	-20
MSCC-TG-M-E2-S3	0.12	0.41	1.07	1.52	0.49	-87	-54	-3	1	-18
MSCC-TG-M-E2-S4	0.12	0.41	1.19	1.69	0.51	-87	-54	8	13	-15
MSCC-TG-P-E3-S0	0.42	0.74	0.86	1.03	0.57	-53	-18	-22	-31	-5
MSCC-TG-M-E3-S0	0.48	1.93	5.12	99	0.52	-47	114	365	999	-13
MSCC-TG-P-E3-S3	0.07	0.26	0.44	0.55	0.49	-92	-71	-60	-63	-18
MSCC-TG-P-E3-S4	0.07	0.26	0.44	0.54	0.5	-92	-71	-60	-64	-17

MSCC-TG-M-E3-S3	0.11	0.39	1.2	1.7	0.46	-88	-57	9	13	-23
MSCC-TG-M-E3-S4	0.11	0.39	1.55	2.23	0.46	-88	-57	41	49	-23
HAZUS fragilities										
MSCC-IG-S/M-E1	0.60	0.90	1.10	1.50	0.60					
MSCC-IG-S/M-E2/E3	0.90	0.90	1.10	1.50	0.60					
Current study										
MSCC-BG-S-E1-S0	0.12	0.33	0.47	0.54	0.66	-81	-64	-57	-64	11
MSCC-BG-M-E1-S0	0.09	0.22	0.27	0.33	0.66	-85	-75	-76	-78	9
MSCC-BG-S-E1-S1	0.05	0.16	0.37	0.52	0.55	-91	-82	-66	-66	-9
MSCC-BG-S-E1-S2	0.07	0.29	0.49	0.57	0.52	-88	-68	-56	-62	-13
MSCC-BG-S-E1-S3	0.07	0.29	0.49	0.57	0.53	-88	-68	-56	-62	-12
MSCC-BG-S-E1-S4	0.07	0.29	0.49	0.57	0.53	-88	-68	-56	-62	-12
MSCC-BG-M-E1-S1	0.06	0.13	0.19	0.23	0.47	-90	-86	-83	-84	-21
MSCC-BG-M-E1-S2	0.07	0.18	0.21	0.25	0.51	-88	-80	-81	-83	-15
MSCC-BG-M-E1-S3	0.07	0.18	0.21	0.25	0.52	-88	-80	-81	-83	-14
MSCC-BG-M-E1-S4	0.07	0.18	0.21	0.25	0.52	-88	-80	-81	-84	-14
MSCC-BG-S-E2-S0	0.09	0.24	0.68	0.88	0.75	-90	-73	-38	-41	25
MSCC-BG-M-E2-S0	0.11	0.35	0.76	1.02	0.55	-88	-61	-31	-32	-9
MSCC-BG-S-E2-S2	0.06	0.21	1.00	1.49	0.57	-94	-76	-9	-1	-6
MSCC-BG-S-E2-S3	0.06	0.21	1.20	1.68	0.60	-94	-76	9	12	-1
MSCC-BG-S-E2-S4	0.06	0.22	1.24	1.72	0.60	-94	-76	13	14	1
MSCC-BG-M-E2-S2	0.08	0.26	0.56	0.80	0.43	-92	-71	-49	-47	-28
MSCC-BG-M-E2-S3	0.08	0.26	0.67	0.95	0.44	-92	-71	-39	-37	-26
MSCC-BG-M-E2-S4	0.08	0.26	0.69	0.98	0.47	-92	-71	-37	-34	-22
MSCC-BG-S-E3-S0	0.05	0.19	2.15	3.05	0.88	-94	-79	95	103	47
MSCC-BG-M-E3-S0	0.10	0.37	1.59	2.24	0.59	-89	-59	44	49	-1
MSCC-BG-S-E3-S3	0.03	0.18	2.76	3.41	0.66	-97	-80	151	127	10
MSCC-BG-S-E3-S4	0.03	0.18	3.59	3.87	0.75	-97	-80	227	158	25
MSCC-BG-M-E3-S3	0.08	0.28	1.00	1.44	0.41	-91	-69	-9	-4	-32
MSCC-BG-M-E3-S4	0.08	0.28	1.25	1.80	0.41	-91	-69	14	20	-32

The entities shaded in red indicate more vulnerability with respect to HAZUS (negative change in median fragilities) while those shaded in green indicate less vulnerability with respect to HAZUS (positive change in median fragilities).
The entry 999 indicates fields corresponding to median fragilities of 99

Feasibility Studies for Improving Caltrans' Bridge Fragility Relationships

Final Report

Part V

ADDITIONAL DISCUSSION OF PHASE-1 FINDINGS AND IMPACT ON FUTURE RESEARCH

Supplemental Technical Report by Reginald DesRoches and Jamie E. Padgett

V.1 Introduction

This research forms the initial foundation of a multi-phase research initiative sponsored by Caltrans aimed at systematic development of next generation fragility relationships tailored for the state bridge inventory with the intention of replacing currently employed HAZUS fragilities in the ShakeCast earthquake-damage alerting system. The newly developed fragility relationships are intended to ultimately be used in assigning inspection priorities at the component and system level to aid in post-earthquake response. The fundamental contribution of the present study is the sub-binning of bridge classes considering the evolution in seismic design philosophy along with capturing the variability in several bridge attributes such as the columns, abutments, seats, bent type, foundation systems, and superstructure-to-substructure connectivity which had not been previously done. This leads to the creation of improved bridge classes that are consistent with the Caltrans inventory and reflective of the design and detailing characteristics prevalent in three design eras separated by the historic 1971 San Fernando and 1989 Loma Prieta earthquakes.

The fragility relationships developed in this study are the first iteration, exploring the feasibility and impact of characterizing and modeling distinct sub-bins, as well as offering insights into refinements needed in future research phases. Sections 6.1 through 6.4 and 6.6 in Chapter 6 provided an assessment of the relative vulnerability of different bridge classes and sub-bins while Section 6.5 in Chapter 6 showed a comparison to HAZUS fragilities. Several key observations arise regarding the resulting phase-one fragility curves that may be somewhat surprising, which include differences in the bridge vulnerability suggested by the newly derived fragility curves relative to HAZUS. The major summary of differences with HAZUS fragilities are listed below:

- Across bridge classes and design eras, it was revealed that single column bents (SCBs) and diaphragm abutments are the least vulnerable. This is contrary to the findings in HAZUS where bridges conventionally (non-seismically) designed and

multi column bents (MCBs) are documented to be less vulnerable. However, the trend is consistent with seismically designed bridge classes where SCBs are documented to be less vulnerable.

- The results from this study indicate that a majority of the seismic performance sub-bins in the pre 1971 and 1971-1990 design eras are more vulnerable than that predicted by HAZUS. The discrepancy in median values is 3-4 times in some cases.

- The fragility curve values are extremely sensitive to the limit state values that are chosen, reinforcing the importance of selecting limit state values that are appropriate for the bridge details used in California construction.

Although it is not completely appropriate to compare the results of the present study with those presented in the commonly used risk assessment package, HAZUS-MH (2011) due to the range of differences in methodology, bridge design and detailing attributes, and treatment of uncertainty, it is important to recognize and understand the differences that exist between the results presented in this study, and those in HAZUS. Moreover, it is important to understand what assumptions lead to the differences between these two studies. This report is devoted to exploring reasons for some of these differences along with providing areas deserving future research. First, the differences in vulnerability predicted by HAZUS and this study are evaluated in section V.2 primarily through an assessment of the key effect limit states play in the fragility results, including comparisons with other research in the literature and directly with HAZUS results. Second, the reasons behind the relative vulnerability revealed for single and multi-column bent bridges are explored in section V.3 through additional deterministic and probabilistic analyses. Lastly, given the iterative nature of this study, refinements needed and recommendations for future research are provided in section V.4.

V.2 Investigation into Discrepancies in Results

As stated previously, two strategies are adopted to investigate the differences in results obtained from the current study and those presented in HAZUS-MH. First, a survey of literature is done and the CDT values adopted by several researchers' are obtained and compared with those used in the current study. Fragility curves are redeveloped using the CDT values adopted by other researchers' and comparison limit (CL) CDTs are proposed which around the average value of CDTs adopted by researchers'. The fragility curves obtained in the current study using the original and CL CDTs are then compared to the fragility curves presented in HAZUS and those developed by other researchers' and the likely reasons for the discrepancies are then detailed.

V.2.1 Comparison of Limit State Criteria

In this section, we show that the prescriptive limit state values (CDTs) have a significant impact on the fragility curves at the component and system level. As a first step, the limit state values adopted by different researchers are used in the fragility formulation and integrated with the demand models developed in this study, which were derived through refined finite element modeling of Caltrans bridge sub-bins and rigorous uncertainty treatment. A majority of the previous research studies considered the bridge system to be characterized by the vulnerability of columns alone (even in the case of seat abutments) and hence the column CDTs proposed by several researchers are considered in the fragility formulation. Further this serves well since the columns dominate the vulnerability in many cases, as documented in Chapter 6 of Part I. Table 1 summarizes the CDTs adopted by several researchers in the literature along with the values adopted in the current study (GT-CT). As detailed in section 5.5 of Chapter 5, the prescriptive values of component CDTs in the present study stemmed predominantly based on the input from the Caltrans design engineers and maintenance professionals. As noted in Table 1, the

limit state values from other researchers exceed those used in this study by as much as a factor of 27.

Curvature ductility, μ_φ, is the engineering demand parameter (EDP) used in the current study. In cases where other demand parameters are used, these values are converted to curvature ductility to allow for a direct comparison. In most cases, the dispersions of the component limit states were not mentioned in the references, and the logarithmic standard deviation of 0.35 adopted in the current study was also used for the other cases when comparisons are made in applying the limit states of other researchers. Appendix V.A describes the EDPs adopted by others researchers, details of the bridges considered, along with their threshold values and demonstrate the conversion to μ_φ for ease of comparison to the present study.

Table 1: Column damage threshold values adopted by various researchers in terms of equivalent curvature ductility, μ_φ

Researcher	Notation	Researcher's Demand Parameter	Equivalent Curvature Ductility			
			CDT-0	CDT-1	CDT-2	CDT-3
GaTech-Caltrans†		Curvature ductility, μ_φ				
	GT-CT-B	Brittle – Pre 1971	0.80	0.90	1.00	1.20
	GT-CT-SD	Strength degrading – 1971-1990	1.00	2.00	3.50	5.00
	GT-CT-D	Ductile – Post 1990	1.00	4.00	8.00	12.00
Mackie & Stojadinovic*	MS	Displacement ductility, μ_Δ				
		Class I	1.00	3.23	18.75	20.95
		Class II	1.00	2.80	15.28	17.05
Kwon & Elnashai*	KE	Top displacement	1.00	--	3.04	18.00
Banerjee & Shinozuka*	BS	Rotational ductility, μ_θ	3.90	7.11	12.44	17.80
Kim & Shinozuka*	KS	Displacement ductility, μ_Δ				
		Bridge I	1.83	5.43	10.14	21.22
		Bridge II	2.54	7.92	14.83	32.51
Comparison Limit‡	CL	Curvature ductility, μ_φ	1.00	3.00	8.00	20.00

*Details of the conversion of different EDPs to curvature ductility, μ_φ, is described in the Appendix of this document

†GT-CT is used to denote the CDTs used in the current study developed in collaboration with Caltrans design engineers and maintenance personnel

‡Comparison limit for CDTs is specified as an approximate average of the CDTs as adopted by other researchers in literature. Note that this applies only to the post 1990 design era since the studies by other researchers in literature considered bridges designed post 1990

Table 2 details the results of fragility analyses by considering the GT-CT and several other CDTs from the literature for the multispan continuous concrete box-girder (MSCC-BG) bridge class in the Pre 1971 (E1), 1971-1990 (E2) and Post 1990 (E3) design eras and different seismic performance sub-bins (SPS). The first column in the table indicates the bridge class (BC) and the seismic performance sub-bin (SPS) under consideration. The second column provides information about the "modified" CDTs used in the fragility formulation. Note that these are different from the CDTs used in the generation of fragility curves presented in Sections 1 and 4 of this report. The third column GT-CT, provides the median values corresponding to the BSST-3 state using the original GT-CT CDT values. These median values are consistent with those presented in Sections 1 and 4 of this report. The fourth column presents the median fragilities by using the modified CDT values. It must be noted that the differences in the median fragilities reported in columns 3 and 4 are just due to the differences in the CDT threshold values. These are generated by using the exact same demand analyses and replacing the GT-CT limit states with the modified CDT values under consideration. The last column presents the median fragilities reported by other researchers' wherever applicable.

To facilitate comparison, the median fragilities corresponding to BSST-3 alone are reported in Table 2. Also shown in Table 2 are median fragilities reported by other researchers wherever applicable. Comprehensive tables showing median value comparisons across BSSTs using the CDTs proposed by the researchers (see Table 1) is shown in Appendix V.A. Details about the bridge class (BC) and SPS codes are presented in Tables 3.8 and 3.9 in Chapter 3 of Section 1 and these are presented below.

Table 2: The effect of limit states on the median and dispersion of system fragilities for MSCC-BG bridge class and comparison with fragilities reported by other researchers'

BC+SPS	CDT values		BSST-3 median fragility†				
	GT-CT	CDT considered	GT-CT	CDT considered	Other Researchers*		
Pre 1971 (E1) design era							
MSCC-BG-S-E1-S0	1.2	5.0	0.22	0.80	NF		
MSCC-BG-S-E1-S4-S	1.2	5.0	0.17	0.60	NF		
MSCC-BG-M-E1-S0	1.2	5.0	0.12	0.40	NF		
MSCC-BG-M-E1-S4-S	1.2	5.0	0.09	0.27	NF		
1971-1990 (E2) design era							
MSCC-BG-S-E2-S0	5.0	12.0	1.00	2.36	NF		
MSCC-BG-S-E2-S4-S	5.0	12.0	0.62	1.20	NF		
MSCC-BG-M-E2-S0	5.0	12.0	0.49	0.96	NF		
MSCC-BG-M-E2-S4-S	5.0	12.0	0.36	0.68	NF		
Post 1990 (E3) design era							
					KE	**BS**	**KS**
MSCC-BG-S-E3-S0	12.0	20.0	1.26	1.81	-	-	-
MSCC-BG-S-E3-S4-S	12.0	20.0	2.06	3.57	-	1.43	1.47
MSCC-BG-M-E3-S0	12.0	20.0	0.83	1.24	-	-	-
MSCC-BG-M-E3-S4-S	12.0	20.0	0.88	1.43	0.59	-	-

*The entry NF stands for Not Found

KE – Kwon and Elnashai (2010), BS –Banerjee and Shinozuka (2007), KS – Kim and Shinozuka (2004)

†The values reported in the column is the median value of the system fragility at the BSST-3 damage state. The median fragilities reported in the GT-CT column are the ones reported in Sections 1 and 4 of this report. These are obtained by convolving the demand models with the CDTs listed in the GT-CT column. Similarly, the median fragilities in the CDT considered column are obtained by convolving the demand models with the CDTs listed in the CDT considered column.

Table 3: Conventional bridge class codes (BC) adopted in the present study

Spans	Continuity	Material	Superstructure	Bent type	Nomenclature
Multi (MS)	Continuous (C)	Concrete (C)	Box-Girder (BG)	Multi column bent (M)	MSCC-BG-M
				Single column bent (S)	MSCC-BG-S
Multi (MS)	Continuous (C)	Concrete (C)	Slab (SL)	Pile extensions (P)	MSCC-SL-P
Multi (MS)	Continuous (C)	Concrete (C)	T-Girder (TG)	Multi column bent (M)	MSCC-TG-M
				Pile extensions (P)	MSCC-TG-P
Multi (MS)	Continuous (C)	Concrete (C)	I-Girder (IG)	Multi column bent (M)	MSCC-IG-M
				Single column bent (S)	MSCC-IG-S

Table 4: Seismic performance sub-bins (SPS) in each bridge class

Design era	Abutment type	Seat width class	Gap size	Nomenclature
Pre 1971 (E1)	Diaphragm	NA (S0)	NA	E1-S0
	Seat	4 – 12 in (S1)	Small (S)	E1-S1-S
		12 – 18 in (S2)	Small (S)	E1-S2-S
		18 – 24 in (S3)	Small (S)	E1-S3-S
			Large (L)	E1-S3-L
		> 24 in (S4)	Small (S)	E1-S4-S
			Large (L)	E1-S4-L
1971 – 1990 (E2)	Diaphragm	NA (S0)	NA	E2-S0
	Seat	12 – 18 in (S2)	Small (S)	E2-S2-S
		18 – 24 in (S3)	Small (S)	E2-S3-S
			Large (L)	E2-S3-L
		> 24 in (S4)	Small (S)	E2-S4-S
			Large (L)	E2-S4-L
Post 1990 (E3)	Diaphragm	NA (S0)	NA	E3-S0
	Seat	18 – 24 in (S3)	Small (S)	E3-S3-S
			Large (L)	E3-S3-L
		> 24 in (S4)	Small (S)	E3-S4-S
			Large (L)	E3-S4-L

V.2.2 Comparison with HAZUS Fragilities

Unlike the CDT values reported in Table 1 adopted by other researchers, information regarding the CDT values adopted in HAZUS is not available. The information provided in HAZUS about CDTs is limited to qualitative description of the visible damage in bridge components at the damage states defined in the report. In this section, the median fragilities characterizing the system fragility for the BSST-3 damage state using the GT-CT and other damage state values (similar to the details in Table 2) are compared with those found in HAZUS, and the details are presented in Table 5.

Table 5: Comparison of median fragilities at BSST-3 from the current study with those in HAZUS

BC+SPS	CDT values		BSST-3 median fragility		
	GT-CT	CDT considered	GT-CT	CDT considered	HAZUS
Pre 1971 (E1) design era					
MSCC-BG-S-E1-S0	1.2	5.0	0.22	0.80	0.80
MSCC-BG-S-E1-S4-S	1.2	5.0	0.17	0.60	0.80
MSCC-BG-M-E1-S0	1.2	5.0	0.12	0.40	1.50
MSCC-BG-M-E1-S4-S	1.2	5.0	0.09	0.27	1.50
1971-1990 (E2) design era					
MSCC-BG-S-E2-S0	5.0	12.0	1.00	2.36	1.60
MSCC-BG-S-E2-S4-S	5.0	12.0	0.62	1.20	1.60
MSCC-BG-M-E2-S0	5.0	12.0	0.49	0.96	1.50
MSCC-BG-M-E2-S4-S	5.0	12.0	0.36	0.68	1.50
Post 1990 (E3) design era					
MSCC-BG-S-E3-S0	12.0	20.0	1.26	1.81	1.60
MSCC-BG-S-E3-S4-S	12.0	20.0	2.06	3.57	1.60
MSCC-BG-M-E3-S0	12.0	20.0	0.83	1.24	1.50
MSCC-BG-M-E3-S4-S	12.0	20.0	0.88	1.43	1.50

It is suggested that the discrepancies with HAZUS are primarily due to the structural modeling and analysis techniques used in the demand analysis, system reliability definition, and capacity models or damage state definitions. The HAZUS fragilities were developed for bridge classes based on a limited number of parameters available in the NBI, damage states based on limited sets of field damage observations and simplified two dimensional analysis techniques. Bridge classes, defined beyond the parameters listed in the NBI, were extended taking into account seismic design, number of spans (single versus multiple), span continuity (continuous versus simply supported), and bent type (single versus multi). Particularly, separate fragilities are assigned based on seismic design and this is taken into account in terms of a spectrum modification factor, strength reduction factor due to cyclic motion, drift limits and the longitudinal reinforcement ratio (HAZUS, 2011). However, details are absent regarding the attributes of conventional (or non-seismically designed) versus seismically designed bridges which makes it difficult, particularly in the pre 1971 and 1971-1990 design eras to facilitate

comparison. In any case, the analyses used in the generation of HAZUS fragilities did not consider the variability of the bridge class geometrical attributes such as the variation of number of spans, span length, deck width, column height, at the least. These fragilities included limited uncertainty characterized by material properties such as concrete compressive strength and reinforcing steel yield strength. Additional and specific information for bridges pertinent to a region might be difficult to obtain and hence the curves were developed with the intention that the information out of NBI is all that is required for seismic evaluation of bridge classes.

Another significant drawback of the NBI based fragility relationships employed in HAZUS is that these curves were derived assuming that the vulnerability of the bridge is characterized by the vulnerability of the columns alone. However, the unseating potential of the bridge deck at the seat abutments or the bents, tearing of the elastomeric bearing pads, and collapse of the shear keys adds to the vulnerability of the bridge system and will need significant repairs in the aftermath of an earthquake. Unfortunately, these components are not accounted for the in the formulation of the HAZUS fragilities. Further, there is a mismatch between the damage state definitions used in fragility analysis and overall bridge functionality following a seismic event. This hampers the decision making needs by agencies like the California Department of Transportation (Caltrans) with regards to emergency response and management. Attempts have subsequently been made to account for some differences in California bridge design by incorporating design specific parameters such as span length, span-to-column height ratio, column-to-superstructure dimension ratio, reinforcement nominal yield strength, concrete nominal strength, longitudinal and transverse reinforcement ratio, deck thickness, foundation soil dry unit weight and angle of internal friction (Mackie and Stojadinovic, 2005). These attempts, however, were mainly focused on deriving structure specific fragility relationships or fragility curves applicable for a smaller subset of

bridges such as single frame multispan continuous box-girder bridges with a single column bent (Mackie and Stojadinovic, 2005).

V.2.3 General Conclusions – CDT Aspects

The following are some of the inferences that can be drawn based on the results presented in the Tables 2 and 5.

- An important aspect that was seen is that the CDTs have a significant impact on the resulting fragility of the bridge system. By devoting careful attention to deriving CDTs that are consistent with experimental datasets and damage observed in the field during post-earthquake inspection and reconnaissance, system fragilities that are less vulnerable than that portrayed in the current study can be obtained.
- As shown in Tables 2 and 5, when strength degrading column CDTs (GT-CT-SD) are used in the fragility formulation of Pre 1971 designed bridge classes instead of the brittle column CDTs, there is a better agreement between the median fragilities (shown in column 4 of the tables) with those presented in HAZUS. Similar observations are seen in the case of the 1971-1990 designed bridge classes where a better agreement is seen between the results of the present study and the HAZUS medians when ductile column CDTs (GT-CT-D) are used instead of the strength degrading column CDTs, as shown in Table 5.
- As stated previously, the comparison level (CL) CDTs are established as an average of the CDTs proposed by several researchers', listed in Table 1. These are strictly applicable for comparison in the post 1990 (E3) design era alone. As seen in Table 2, the results obtained in this study using the GT-CT and CL CDT values yields system fragilities that are less vulnerable when compared to those presented by Kwon and Elnashai (2010) for MCBs; and Banerjee and Shinozuka (2007) and Kim and Shinozuka (2004) for SCBs. Also, it is important to note that

the median fragilities reported by Kwon and Elnashai for MSCC-BG bridges with MCBs is far more vulnerable than that predicted by HAZUS and the GT-CT.

- Unlike HAZUS, the current study demonstrates that SCBs are less vulnerable when compared to MCBs irrespective of the design era under consideration. HAZUS predicts that seismically designed SCBs are less vulnerable when compared to MCBs while the trend is reverse in the case of non-seismic design. This is particularly interesting since both SCBs and MCBs undergo similar evolutions in seismic design philosophy across the design eras considered in this study. Furthermore, this evolution in design was validated based on an extensive review of bridge plans pertinent to other types across the design eras. It is anticipated that the column end boundary condition plays a significant role in the relative vulnerability.

As demonstrated in this section, it is evident that component CDTs have a significant impact on the system fragilities. The CDTs adopted by GT-Caltrans are extremely conservative in comparison to other researchers. Adoption of the CDT values available in literature within the proposed fragility formulation of the current research leads to median fragilities more comparable to those found in HAZUS, thereby necessitating further research on prescribing component CDTs. Since the results of this study show significant differences in the demand models and fragility across the three design eras and bridge sub-classes (not considered explicitly in HAZUS or other studies) it is recommended that the fragility formulation and sub-binning be maintained with refined CDTs.

V.3 Deterministic Validation of Discrepancies in Single and Multi Column Bents

This section is devoted to examining the relative vulnerability of single (SCB) and multi column bents (MCBs). As mentioned previously, the current research indicated that SCBs are less vulnerable in comparison to MCBs, which is contrary to the findings in

HAZUS where multi column bents (MCBs) are documented to be less vulnerable for conventional bridge classes. The trend of SCBs being less vulnerable in comparison to MCBs is consistent with the HAZUS findings for seismically designed bridge classes.

In order to examine their relative vulnerability, deterministic analyses are conducted on a common geometry to provide insight on the performance of bridge components in bridges with SCBs and MCBs. Further, fragility analysis is conducted with only uncertainty in ground motions (or seismic hazard) to explore the impact of single versus multi column bents on the overall vulnerability. It must be noted that in the original study for bridge classes, the fragility formulation incorporates the variation in several geometric and material properties (details of which are provided in Chapter 5 of Part I) along with the uncertainty in seismic hazard, and the aim of the present section is twofold: isolate the effect of number of columns per bent on the fragility of bridge systems and investigate the effect of column end boundary condition.

V.3.1 Effect of Number of Columns in the Bent

In order to isolate the effect of number of columns in the bent and geometric effects in general, deterministic analyses were performed on post 1990 designed MSCC-BG bridge models and diaphragm abutments with all the material attributes set to their median values, specific values of geometric parameters described henceforth, except the number of columns per bent. The spans measure 120.1 ft and the bridge is 43.75 ft wide. The width of the top and bottom flange in the superstructure box-girder is 7.75 in and 7 in, respectively and the thickness of the box separation wall is 12 in. The box-girder has an overall depth of 57.6 in. The details of the single (SCB) and multi column bents (MCBs) are reported in the table below. The diaphragm abutment consists of a 6 ft. tall backwall with Class 70 precast prestressed concrete piles at spacing of 7 ft. on center. Further details of the deterministic bridge models are presented in Table 6.

Table 6: Column details and curvature ductility demand in the deterministic bridge models with variable number of columns per bent

Bent type	Number of columns	Column diameter (ft)	Longitudinal reinforcement	Transverse reinforcement	Yield curvature (in^{-1})	Curvature ductility demand, μ_φ
SCB	1	7	58 #11	#4 @ 3 in o.c.	3.43×10^{-5}	4.23
MCB	2	5	42 #11	#4 @ 3 in o.c.	3.85×10^{-5}	5.19
MCB	3	4	26 #11	#4 @ 3 in o.c.	4.49×10^{-5}	5.01
MCB	4	4	26 #11	#4 @ 3 in o.c.	4.49×10^{-5}	4.54
MCB	5	4	26 #11	#4 @ 3 in o.c.	4.49×10^{-5}	4.34

In all cases, the deterministic responses are illustrated using a single ground motion from the suite of ground motions developed for the PEER Transportation Systems Research Program (Baker et al., 2011). The chosen ground motion pertains to a rock site with an average shear wave velocity of 2180 ft/sec and is characterized by a moment magnitude of 7.62 and hypocentral distance of 16.27 km. The ground motion time histories for the fault normal and fault parallel components are shown in Figure 1. Also shown as an inset in the figure is the response spectrum corresponding to the two orthogonal components.

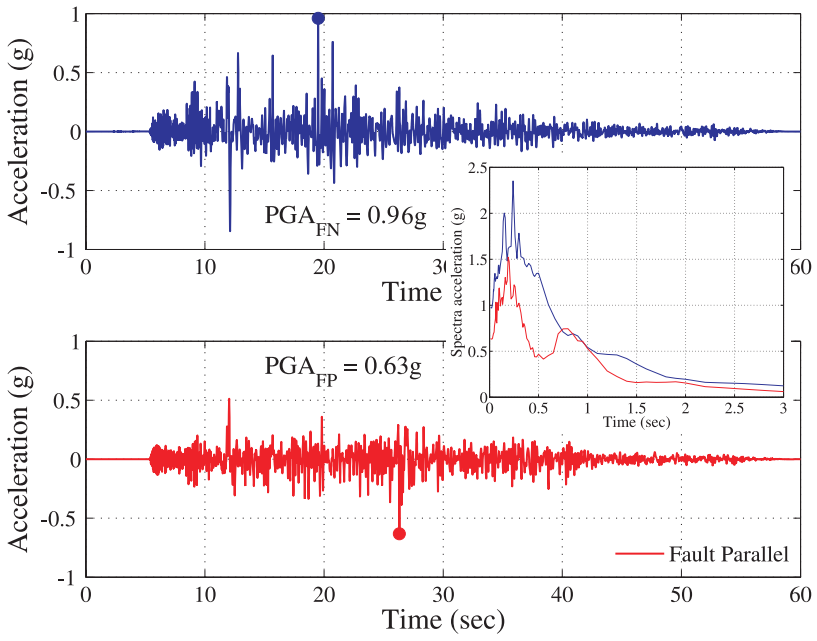

Figure 1: Fault normal and fault parallel components of ground motion used in deterministic analyses

The first and second mode time periods of the deterministic bridge models are reported in Table 7. In all cases, the first mode is in the longitudinal direction while the second mode is in the transverse direction except in the case of bridge model with five columns in the bent where the mode shapes are reversed. The modal periods vary as a function of the number of columns per bent and the boundary conditions at the base of the column. SCBs are stiffer in comparison to MCBs, in general. Further, in the case of MCBs with different number of columns per bent, the vibration periods are different, thereby leading to differences in the dynamic response of bridges with different number of columns per bent.

Table 7: First and second mode time periods of deterministic bridge models

Bent type	Number of columns	First mode (sec)	Second mode (sec)
SCB	1	0.74	0.71
MCB	2	0.81	0.76
MCB	3	0.86	0.83
MCB	4	0.82	0.77
MCB	5	0.78	0.55

The component responses for the columns, abutment backfill soil, longitudinal and transverse pile response, longitudinal and transverse deck displacement are shown in the Figure 2.

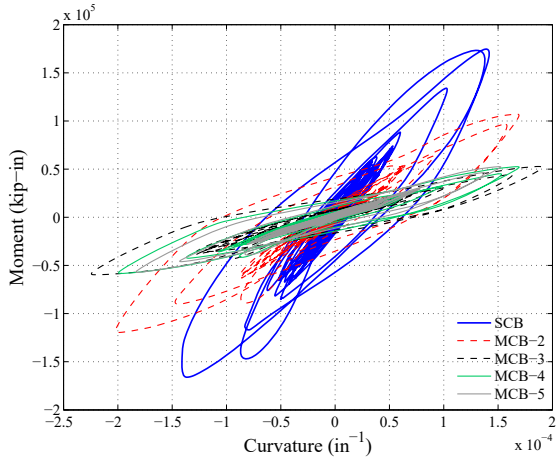

a) Column moment curvature response

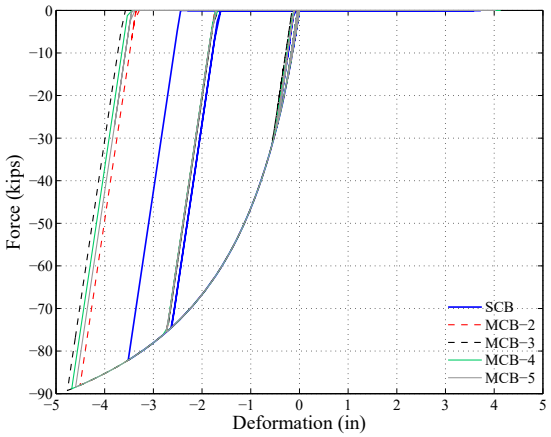

b) Passive abutment backfill soil response

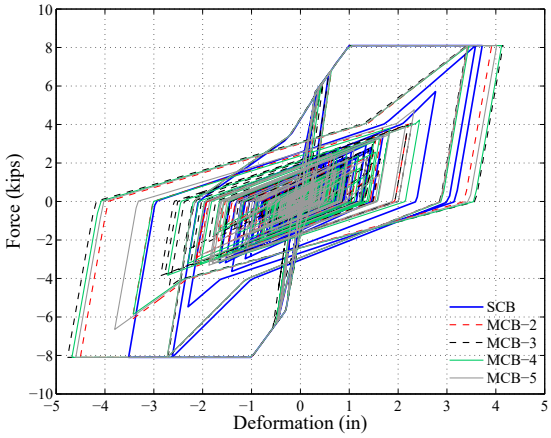

c) Abutment pile longitudinal response

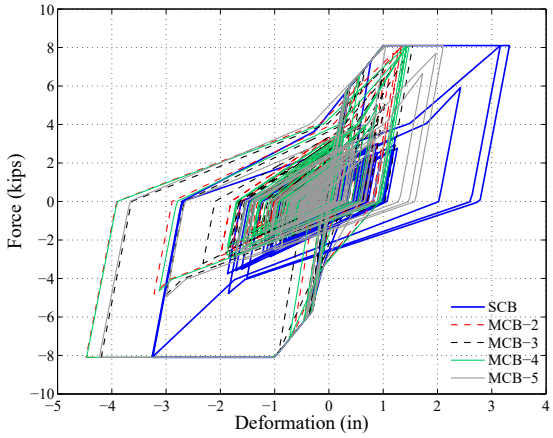

d) Abutment pile transverse response

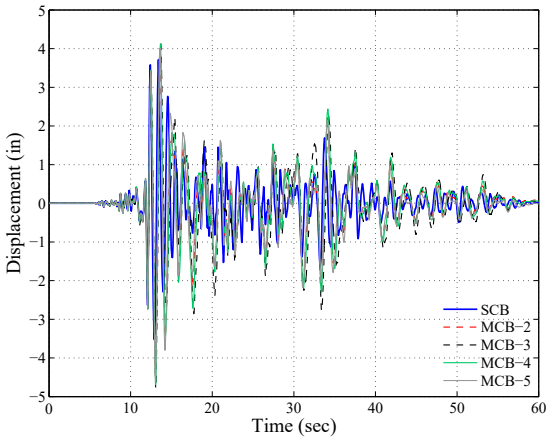

e) Longitudinal deck response

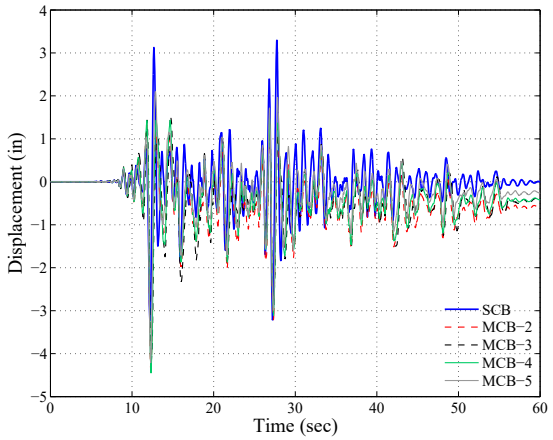

f) Transverse deck response

Figure 2: Component response comparison in deterministic bridge models with variable number of columns per bent

The following are some of the key observations from the deterministic bridge responses:

- As documented in Table 6, the columns in MCBs experience more nonlinearity in comparison to the columns in SCBs. SCBs are seen to be stiffer in comparison to MCBs thereby attracting more force and relatively lower levels of displacement or ductility in comparison to their MCB counterparts. Since columns tend to be the most vulnerable component in the bridge system, intuitively it can be expected that MCBs will be more vulnerable than SCBs.
- The passive abutment displacement is higher for MCBs (4.8 in) in comparison to SCBs (3.5 in). Similar trends are observed in the case of active and passive response of piles. Both these response measures are seen to be higher in the case of MCBs when compared to SCBs. The passive and active displacement of the piles is 4.8 in and 4.1 in, respectively in the case of MCBs in comparison to 3.5 in and 3.5 in for the respective measures in the case of SCBs.
- The longitudinal and transverse deck displacement is also seen to be higher for the MCBs when compared to SCBs. The transverse deck response in the case of MCBs reveals the presence of residual displacements thereby signifying nonlinearity in the substructure. Residual displacements in SCBs are negligible when compared to MCBs and this is yet another indicator for the increased vulnerability of MCBs in comparison to SCBs.

Deterministic analyses of bridges with similar geometry and material properties and variable number of columns per bent reveal that all the components (columns, abutments, foundations) in bridges with MCBs experience higher demands and are more vulnerable in comparison to their counterparts in bridges with SCBs. However, it must be noted that these observations are based on a single ground motion and the component responses might change as the seismic hazard changes. A complete probabilistic evaluation will allow for the characterization of component responses and will allow for drawing significant conclusions about the relative contribution of the number of columns

per bent to the overall system level performance, which is detailed in the forthcoming section.

V.3.1.1 Probabilistic Seismic Demand Models (PSDMs) and Fragility Curves

Using the same deterministic models described previously and the suite of 160 unscaled Baker ground motions, probabilistic seismic demand models (PSDMs) and fragility curves are developed using nonlinear time history analyses (NLTHA). One hundred and sixty NLTHA simulations are performed for the deterministic bridge model with SCB using the suite of 160 unscaled ground motions. In the case of MCBs, the deterministic bridge models with two, three, four and five columns per bent are randomly paired with the 160 unscaled ground motions and NLTHA is performed in each case.

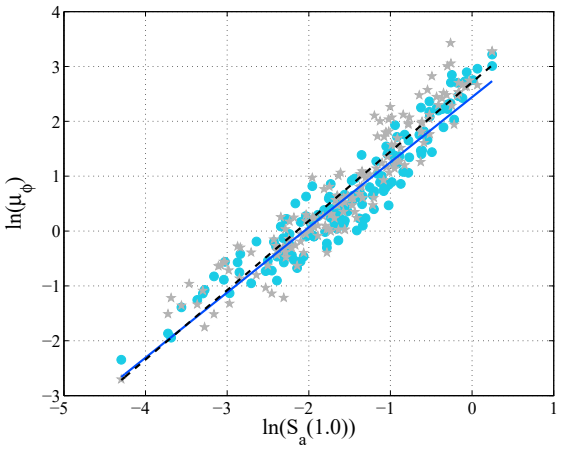

a) Column curvature ductility

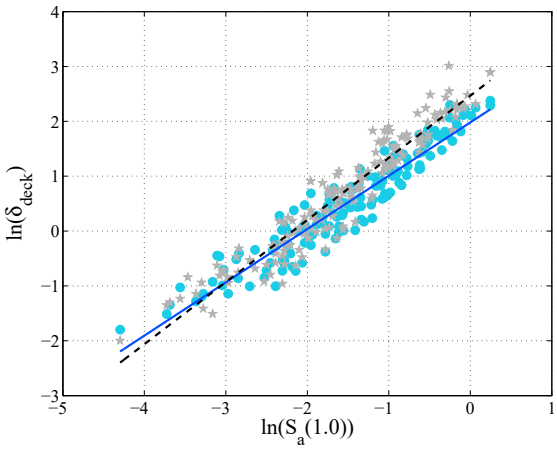

b) Maximum deck displacement

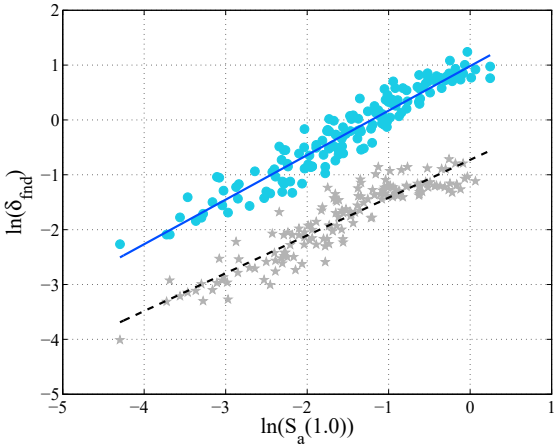

c) Foundation translation

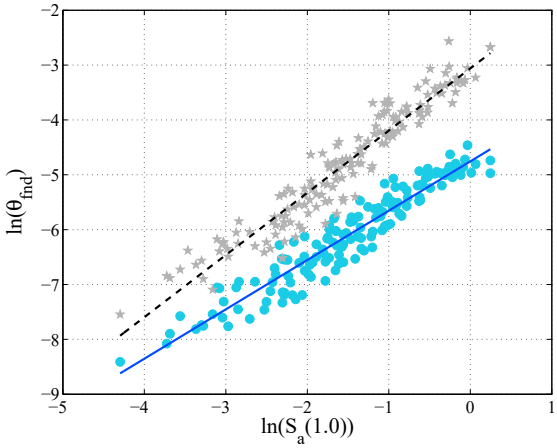

d) Foundation rotation

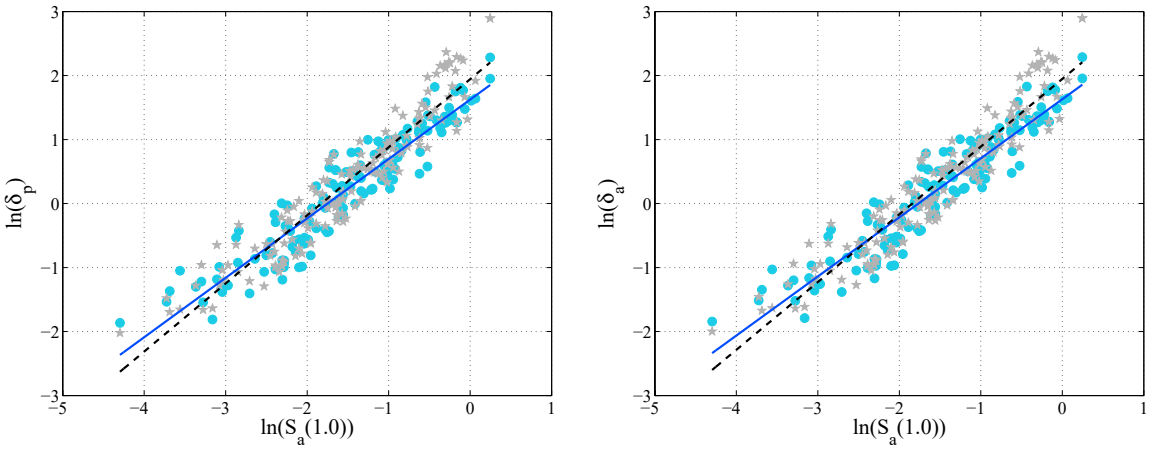

e) Passive abutment displacement f) Active abutment displacement

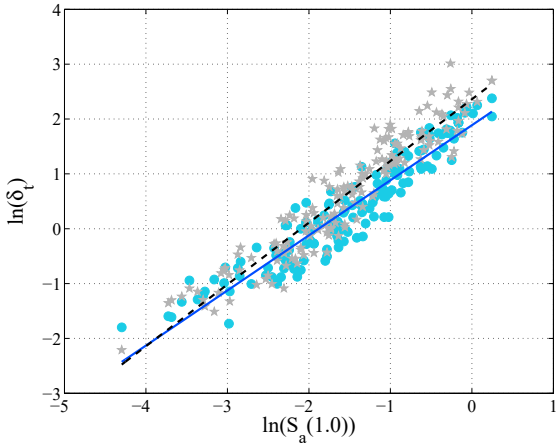

g) Transverse abutment displacement

Figure 3: Bridge components PSDMs
Single column bents are plotted in blue and **multi column bents in black**

Consistent with the observations in the previous section based on deterministic analysis, the PSDMs developed based on the NLTHA results using the suite of ground motions, reveal the increased demands across all components in bridges with MCBs in comparison with bridges with SCBs, as shown in Figure 3. This is evident from the steeper slopes exhibited by the component demand models in bridges with MCBs when compared to those in bridges with SCBs.

Using the PSDMs and the GT-CT limit states, system fragility curves are derived using the procedure described in Chapter 6 of Section 1. The median fragilities and dispersion for bridges with SCB and MCBs are documented in the Table 8. Consistent

with the PSDMs, the fragility analyses reveals that bridges with SCBs are less vulnerable characterized by higher median fragilities when compared to bridges with MCBs with lower median fragilities. This is consistent with the results presented in Chapter 6 in Sections 1 and 4 for bridge classes. The dynamic behavior of the MCBs relative to SCBs as described above and subsequent demands placed on key bridge components is the attributing factor to the difference in fragility.

Table 8: Median and dispersion values of system fragility for deterministic bridge models

Seismic performance sub-bin	BSST-0		BSST-1		BSST-2		BSST-3		
	λ	ζ	λ	ζ	λ	ζ	λ	ζ	ζ^*
MSCC-BG-S-E3-S0	0.13	0.41	0.40	0.41	0.74	0.42	1.04	0.42	0.41
MSCC-BG-M-E3-S0	0.12	0.40	0.34	0.40	0.61	0.42	0.84	0.42	0.41

Another important inference that can be drawn by comparing the median fragilities reported in Tables 2, 5 and 8 is the significant effect of bridge geometric characteristics on the median fragility of SCBs. The median fragility of SCBs reduces by 17% when the variability in geometric characteristics is not considered. Further, the difference between the median fragilities of SCBs and MCBs reduces when variability in geometric characteristics is not considered. However, it is seen that geometric characteristics do not influence the median fragilities in the case of MCBs. Therefore, the column end boundary condition is suggested to contribute to the increased vulnerability of bridges with MCBs and the role of this is seen in the next section. Table 9 shows variation in some of the bridge geometric features for bridges with SCBs and MCBs that were used in the generation of fragility relationships documented in Sections 1 and 4. There is significant variation in geometric attributes such as bridge width, superstructure box girder details which are contributing to the differences in the vulnerability. Appendix A in Section 1 presents significant details about bridge geometric attributes and their ranges.

Table 9: Geometric attributes for post 1990 MSCC-BG bridge class with single and multi-column bents

Attribute	Number of columns per bent				
	1	2	3	4	5
Superstructure					
Number of spans	2	2	2	2	2
Span length (ft)	90.0 – 180.0	90.0 – 180.0	90.0 – 180.0	90.0 – 180.0	90.0 – 180.0
Deck width (ft)					
Minimum	25	40	60	80	100
Maximum	40	60	80	100	130
Number of boxes	3	5	7	9	11, 15
Columns					
Diameter (ft)	7	5	4	4	4
Long. reinf. ratio (%)	1.0 – 3.5	1.0 – 3.5	1.0 – 3.5	1.0 – 3.5	1.0 – 3.5
Tran. reinf. ratio (%)	0.4 – 1.7	0.4 – 1.7	0.4 – 1.7	0.4 – 1.7	0.4 – 1.7

V.3.3 Investigation of Column End Boundary Condition

In order to understand the effect of column end boundary condition (pinned condition in MCBs versus close to fixity in SCB) on the component responses, the deterministic bridge models with multi column bents (2, 3, 4, 5 columns per bent) described in the previous section (Table 6) are modified and a rotational restraint is introduced at the base of the columns similar to the case of SCBs. Table 10 reports the first and second mode time periods for the deterministic bridges with the restrained and pinned boundary condition. As seen in the table, the bridges with restrained column ends have a reduction in the modal time periods indicating a stiffer structure in comparison to the case when the column ends are pinned. This affects the dynamics and force transfer among bridge components in comparison to the case where the columns are pinned to the pile cap.

Table 10: Comparison of first and second mode time periods of multi column bents with pinned and rotationally restrained column ends

Number of columns	Pinned base		Restrained base	
	First mode (sec)	Second mode (sec)	First mode (sec)	Second mode (sec)
2	0.81	0.76	0.62	0.50
3	0.86	0.83	0.66	0.51
4	0.82	0.77	0.64	0.60
5	0.78	0.55	0.55	0.47

Time history analysis is performed using the ground motion shown in Figure 1, and the comparison of component responses for the case where the column end is pinned versus restrained are presented in Figure 4. In all the cases, it is seen that the response of the bridge components with restrained boundary conditions is smaller than the respective case with pinned boundary condition. This leads to the inference that the components experience less vulnerability in the case with restrained boundary conditions.

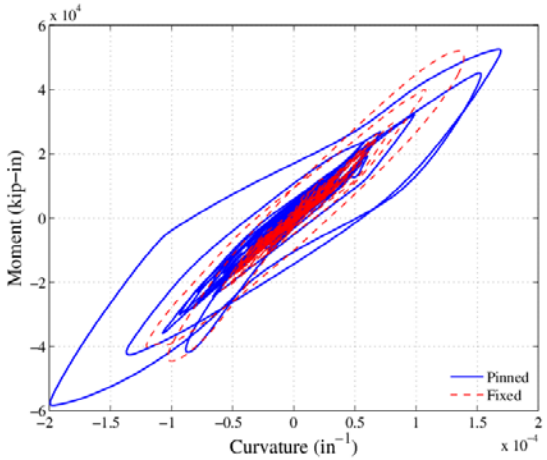

a) Column moment curvature response for 4 columns per bent

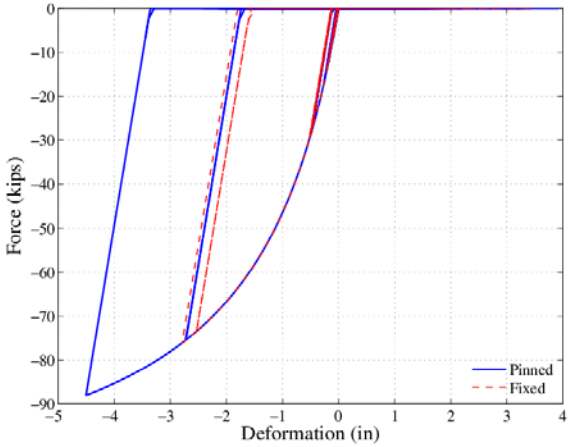

b) Passive abutment backfill soil response for 2 columns per bent

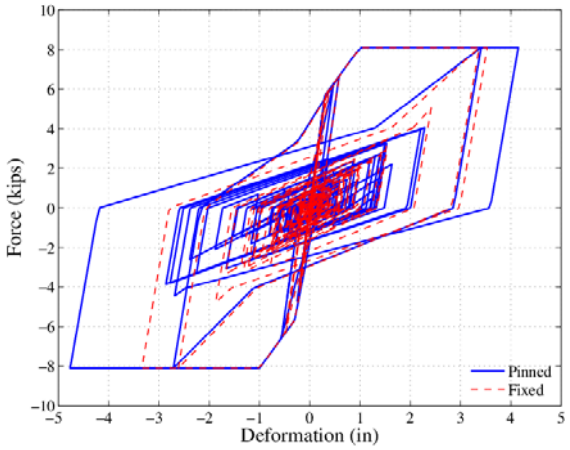

c) Abutment pile longitudinal response for 3 columns per bent

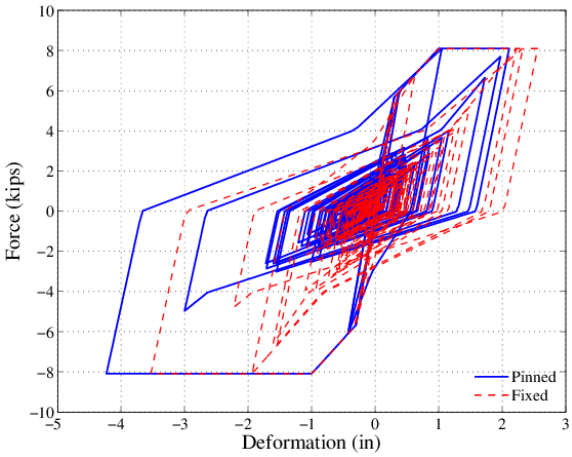

d) Abutment pile transverse response for 5 columns per bent

Figure 4: Comparison of component responses in deterministic bridge models with multi column bents characterized by pinned and restrained column end boundary conditions

Although PSDMs and fragility curves are not developed in this case to investigate the propagation of the effect of the column end boundary condition on the system fragility, based on the deterministic analyses, it can be concluded that the restrained boundary condition leads to smaller displacement demand on the bridge components in comparison to the case of pinned boundary condition. This will lead to a bridge system with lower vulnerability when columns in a bridge with MCB are restrained instead of pinned. This demonstrates that the column end boundary condition has a substantial impact on the vulnerability of bridges with MCBs and deserves further research.

V.4 Recommendations for Future Work

As an initial phase of the development of next generation fragility curves, this study has provided extensive modeling and characterization of the Caltrans bridge inventory and sub-bins, range of design and detailing characteristics and alignment with design eras, and probabilistic modeling based on refined nonlinear dynamic analysis. Furthermore, this chapter has provided preliminary insights into the differences in the study results and those currently adopted (HAZUS), and other researchers. There are

several potential areas which deserve attention based on the results of the present study. Further investigation of such items can be considered in future refinement of the fragility models for adoption into ShakeCast. These are highlighted below:

- As demonstrated in this study, there is a wide disparity with the bridge class fragilities documented in HAZUS. The lack of documentation of the underlying assumptions involved in the generation of HAZUS fragilities particularly inhibits direct comparisons. Studies must be devoted to investigate various aspects involved in the generation of HAZUS fragilities such as the fundamental assumptions involved in their formulation, modeling and analyses considerations, prescriptive values of column CDTs used in the fragility formulation, to mention a few.
- It was apparent that a wide range of values have been used for the limit states for columns in past studies, and that the CDTs adopted have a significant impact on the resulting fragilities. Additional work is needed to develop limit states that are most appropriate for the bridge classes that are common in the California bridge inventory. Although priority is given to columns, other component CDTs should also be reviewed in future research phases.
- This study revealed significant differences in the vulnerabilities of single versus multi column bents and diaphragm versus seat abutments, which in some cases might seem counter-intuitive. Preliminary investigations in this study reveal that the relative high stiffness of bridges with single column bents and difference in the column boundary conditions in single versus multi column bents plays a significant role in the dynamic characteristics and the associated vulnerability of the bridge system. Future studies are needed to validate and explain key results and sources for discrepancies including the investigation into the column end conditions and the associated foundation spring stiffnesses.

- In the current study, the general distress indicators were separated from the secondary components due to the unavailability of representative damage models to correlate their damage to system level performance. There is a need to develop damage models across these components and consider their contribution to the overall system performance as in the case of primary and secondary components. Further refinement of the damage models and damage threshold values of all components is needed based on an extensive survey of literature and Caltrans expertise similar to what was done for the columns in the earlier sections of this report.
- This study did not consider aspects such as the effect of number of spans, skew, superstructure curvature, liquefaction damage, explicit modeling of foundations considering soil structure interaction, contribution of approach slab settlement on bridge functionality and closure consequences, effect of soil in the transverse response of abutments, to mention a few. The aforementioned details should be included in future studies.

APPENDIX V.A

Curvature ductility, μ_φ, is chosen as the engineering demand parameter (EDP) to describe the response of columns in the present study. However, different researchers use different EDPs and corresponding prescriptive CDT values to signify different levels of damage and these need to be converted in terms of μ_φ to be used to generate the median fragilities reported in Tables V.A.6, V.A.7, and V.A.8, details of which are presented in this Appendix.

V.1 Relationship between EDPs and curvature ductility, μ_φ

V.1.1 Relationship Between Curvature Ductility and Displacement Ductility

$$\mu_\Delta = 1 + 3(\mu_\varphi - 1)\frac{L_p}{L}\left(1 - 0.5\frac{L_p}{L}\right) \tag{V.1}$$

In the above equation, μ_Δ is the displacement ductility, μ_φ is the curvature ductility, L_p is the length of the plastic hinge and L is column height. The length of the plastic hinge is calculated in accordance with equation 7.25, §7.6.2(a), Caltrans SDC (2010). Note that L, L_p are in units of inches and f_{ye} is expressed in ksi.

$$L_p = 0.08L + 0.022 f_{ye} d_{bl} \tag{V.2}$$

For 60 ksi longitudinal reinforcement (f_{ye} = 60 ksi), equation (V.2) simplifies to:

$$L_p = 0.08L + 9d_{bl} \tag{V.3}$$

V.1.2 Relationship between Curvature Ductility and Rotational Ductility

$$\mu_\theta = 6\frac{L_p}{L}(\mu_\varphi - 1) \tag{V.3}$$

In the above equation, μ_θ is the rotational ductility, μ_φ is the curvature ductility, L_p is the length of the plastic hinge and L is column height.

V.2 Component Damage Threshold (CDT) Values Adopted by Other Researchers

V.2.1 Mackie and Stojadinovic

Ref: Mackie, K. R., Wong, J.-M., Stojadinovic, B. (2007). *Integrated Probabilistic Performance-Based Evaluation of Benchmark Reinforced Concrete Bridges*, PEER Report No. 2007/09, Pacific Earthquake Engineering Research Center, University of California, Berkeley, CA.

The study looked at a sub-class of post 1990 designed MSCC-BG bridges with single column bents with seat type abutments. Two classes of columns – Class I (4', 5', 6', 7' diameter circular columns – 50 feet tall) and Class II (6', 7', 8' diameter circular columns – 22 feet tall) were considered and displacement ductility was the chosen EDP.

Table V.A.1: CDTs adopted by Mackie and Stodinovic (2007)

EDP	CDT-0	CDT-1	CDT-2	CDT-3
Displacement ductility, μ_Δ	0.23	1.64	6.09	6.72
Curvature ductility, μ_φ				
Class I	1.00	3.23	18.75	20.95
Class II	1.00	2.80	15.28	17.05

V.2.2 Kwon and Elnashai

Ref: Kwon, O.-S., Elnashai, A. S. (2010). *Fragility analysis of a highway over-crossing bridge with consideration of soil-structure interactions*, Structure and Infrastructure Engineering, 6(1-2), pp: 159-178.

An as-built post 1990 MSCC-BG bridges with multi column bents with seat type abutments were considered in this study. The columns are 24 in in diameter and are 17.5 feet tall and reinforced with 8 #7 longitudinal reinforcing bars (f_y = 60 ksi).

Approximate yield curvature of the column cross-section,

$$\varphi_y = 2.25\frac{\varepsilon_y}{D} = 2.25\frac{60/29000}{24} = 1.94\times10^{-4}\ in^{-1}$$

Yield displacement, $\Delta_y = \dfrac{\varphi_y L^2}{3} = \dfrac{1.94\times10^{-4}(17.5\times12)^2}{3} = 2.86\,in$

Plastic hinge length, $L_p = 0.08L + 9d_{bl} = 25.8\,in$

Kwon and Elnashai used the column top displacement to quantify damage in bridge columns and the CDT values are tabulated in Table V.A.2.

Table V.A.2: CDTs adopted by Kwon and Elnashai (2010)

EDP	CDT-1	CDT-2	CDT-3
Top displacement (in)	2.86	4.88	19.69
Displacement ductility	1.00	1.70	6.87
Curvature ductility	1.00	3.04	18.00

V.2.3 Banerjee and Shinozuka

Ref: Banerjee, S., Shinozuka, M. (2007). *Nonlinear Static Procedure for Seismic Vulnerability Assessment of Bridges*, Computer-Aided Civil and Infrastructure Engineering, 22, pp: 293-305.

This study considered an as-built post 1990 MSCC-BG bridge with single column bents and seat type abutments. The columns are 96 in in diameter and 69 feet tall.

Approximate yield curvature of the column cross-section,

$$\varphi_y = 2.25\frac{\varepsilon_y}{D} = 2.25\frac{60/29000}{96} = 4.93\times10^{-5}\ in^{-1}$$

Plastic hinge length, $L_p = 0.08L + 9d_{bl} = 75.14\,in$

Banerjee and Shinozuka used rotational ductility to quantify damage in bridge columns and these are indicated in Table V.A.3 below.

Table V.A.3: CDTs adopted by Banerjee and Shinozuka (2007)

EDP	CDT-0	CDT-1	CDT-2	CDT-3
Rotational ductility	1.58	3.33	6.24	9.16
Curvature ductility	3.90	7.11	12.44	17.80

V.2.4 Kim and Shinozuka

Ref: Kim, S.-H., Shinozuka, M. (2004). *Development of fragility curves of bridges retrofitted by column jacketing*, Probabilistic Engineering Mechanics, 19, pp: 105-112.

This study considered two as-built post 1990 MSCC-BG bridges with single column bents and seat type abutments, details of which are provided in Table V.A.4.

Table V.A.4: Details of the columns – Kim and Shinozuka (2004)

	Col. Dia (in)	Col. Ht (in)	φ_y (in^{-1})	L_p (in)	L_p/L
Bridge I	31.50	185.04	1.48E-04	23.80	0.13
Bridge II	94.49	826.77	4.93E-05	75.14	0.09

Kim and Shinozuka (2004) used displacement ductility as the engineering demand parameter and the values adopted as documented in the Table V.A.5.

Table V.A.5: CDTs adopted by Kim and Shinozuka (2004)

	CDT-0	CDT-1	CDT-2	CDT-3
Bridge I				
Displacement ductility	1.3	2.6	4.3	8.3
Curvature ductility	1.83	5.43	10.14	21.22
Bridge II				
Displacement ductility	1.4	2.8	4.6	9.2
Curvature ductility	2.54	7.92	14.83	32.51

V.2.4 Basoz and Kiremidjian

Ref: Basoz, N., Kiremidjian, A. S. (1997). *Evaluation of Bridge Damage Data from the Loma Prieta and Northridge CA Earthquakes*, Report No. MCEER-98-0004, MCEER, University at Buffalo, The State University of New York, Buffalo, NY.

Most of the bridges damaged in previous historic seismic events (1989 Loma Prieta and 1994 Northridge CA earthquakes) were concrete bridges. About one-third of these bridges belonged to the 1971-1990 design era. In the work by Basoz and Kiremidjian (1997), the bridge types were aggregated due to difficulty in obtaining substantial number of damaged bridges belonging to a particular class. For instance, all

multispan continuous bridges with diaphragm abutments and MCBs were aggregated irrespective of the superstructure type. Further, there was no distinction made regarding the material type (concrete, steel, timber, masonry).

The empirical fragility curves suffer from certain drawbacks associated with the subjective nature of the bridge inspector in assigning damage states, uncertainty pertinent to the actual intensity felt by each bridge at the location depending on the shaking map used in their evaluation. For instance, the USGS shake map indicates a maximum PGA value of 1.55g experienced during the Northridge earthquake at a bridge site while the Woodward-Clyde Federal Services (WCFS) reports a maximum PGA value of 0.66g and the difference is significant and makes it difficult to build confidence in the empirical fragility functions.

V.3 Comparison of Median Fragilities across Bridge System Level Damage States Using Different Values for CDTs

This section provides median fragilities across all the system level damage states (BSSTs) for multispan continuous concrete box-girder bridges across the three design eras and various seismic performance sub-bins. Unlike Tables 2 and 3, where comparisons were presented only for the BSST-3 system state using GT-CT and few representative CDT values (for instance, CL), the fragilities reported in Tables V.A.6 through V.A.8 are developed using the CDTs adopted by various researchers' (documented in Table 1) to facilitate comparison on an equal footing.

Table V.A.6: Effect of limit states on the median and dispersion of system fragilities for pre 1971 MSCC-BG bridge class

BC+SPS	CDT considered		Fragility parameters				
			λ_0	λ_1	λ_2	λ_3	ζ
MSCC-BG-S-E1-S0							
GT-CT	GT-CT-B		0.15	0.17	0.18	0.22	0.60
	GT-CT-SD		0.18	0.35	0.58	0.81	0.59
HAZUS			0.35	0.45	0.55	0.80	0.60
MSCC-BG-S-E1-SX							
GT-CT	GT-CT-B						
		BC-E1-S1-S	0.02	0.08	0.14	0.17	0.54
		BC-E1-S2-S	0.02	0.09	0.15	0.17	0.64
		BC-E1-S3-S	0.02	0.09	0.14	0.17	0.64
		BC-E1-S4-S	0.02	0.09	0.15	0.17	0.64
	GT-CT-SD						
		BC-E1-S1-S	0.02	0.09	0.32	0.42	0.53
		BC-E1-S2-S	0.02	0.10	0.41	0.60	0.59
		BC-E1-S3-S	0.02	0.10	0.41	0.60	0.59
		BC-E1-S4-S	0.02	0.10	0.41	0.60	0.59
GT-CT Vulnerability of columns alone	GT-CT-B		0.12	0.13	0.15	0.18	0.54
	GT-CT-SD		0.14	0.27	0.44	0.61	0.53
HAZUS			0.35	0.45	0.55	0.80	0.60
MSCC-BG-M-E1-S0							
	GT-CT-B		0.08	0.10	0.11	0.12	0.51
	GT-CT-SD		0.11	0.19	0.30	0.40	0.51
HAZUS			0.60	0.90	1.10	1.50	0.60
MSCC-BG-M-E1-SX							
GT-CT	GT-CT-B						
		BC-E1-S1-S	0.01	0.06	0.08	0.09	0.63
		BC-E1-S2-S	0.01	0.06	0.08	0.09	0.68
		BC-E1-S3-S	0.01	0.06	0.08	0.09	0.66
		BC-E1-S4-S	0.01	0.06	0.08	0.09	0.66
	GT-CT-SD						
		BC-E1-S1-S	0.01	0.04	0.09	0.15	0.64
		BC-E1-S2-S	0.01	0.06	0.15	0.22	0.71
		BC-E1-S3-S	0.01	0.06	0.21	0.27	0.73
		BC-E1-S4-S	0.01	0.06	0.21	0.27	0.73
GT-CT Vulnerability of columns alone	GT-CT-B		0.06	0.07	0.08	0.09	0.60
	GT-CT-SD		0.08	0.14	0.21	0.27	0.59
HAZUS			0.60	0.90	1.10	1.50	0.60

Note: The values in **dark brown** are the ones obtained using the CDTs used in the current study titled GT- Caltrans and the values in **blue** are the ones prescribed in HAZUS.

Table V.A.7: Effect of limit states on the median and dispersion of system fragilities for 1971-1990 MSCC-BG bridge class

BC+SPS	Notes (description)	Fragility parameters				
		λ_0	λ_1	λ_2	λ_3	Z
MSCC-BG-M-E2-S0						
GT-Caltrans	Strength degrading – 1971-1990	0.14	0.25	0.38	0.49	0.57
	Ductile – Post 1990	0.14	0.39	0.71	0.96	0.55
	Average of ductile and strength degrading	0.14	0.33	0.55	0.75	0.57
HAZUS		0.90	0.90	1.10	1.50	0.60
MSCC-BG-M-E2-SX						
GT-Caltrans	Strength degrading – 1971-1990					
Vulnerability of both	BC-E2-S2-S	0.07	0.18	0.28	0.36	0.59
columns and seats	BC-E2-S3-S	0.07	0.18	0.28	0.36	0.59
are considered	BC-E2-S4-S	0.07	0.18	0.28	0.36	0.59
	Ductile – Post 1990					
	BC-E2-S2-S	0.07	0.26	0.48	0.66	0.57
	BC-E2-S3-S	0.07	0.26	0.50	0.68	0.57
	BC-E2-S4-S	0.07	0.26	0.50	0.68	0.57
GT-Caltrans	Strength degrading – 1971-1990	0.11	0.18	0.28	0.36	0.61
Vulnerability of	Ductile – Post1990	0.11	0.30	0.50	0.68	0.61
columns alone						
HAZUS		0.90	0.90	1.10	1.50	0.60
Basoz & Kiremidjian	WCFS Shake Map†	0.39	0.43	0.63	0.82	0.28
(MSCC-BG-M-E2-SX)	USGS Shake Map†	0.73	0.85	1.66	3.18	0.55

Note: The values in **dark brown** are the ones obtained using the CDTs used in the current study titled GT- Caltrans and the values in **blue** are the ones prescribed in HAZUS.

†Refer to section V.2.4 in Appendix V.A for details on the Shake Map

Table V.A.8: Effect of limit states on the median and dispersion of system fragilities for post 1990 MSCC-BG bridge class

BC+SPS	Bent type	Notes (description)	Fragility parameters				
			λ_0	λ_1	λ_2	λ_3	ζ
~~MSCC-BG-E3-S0~~							
GT-Caltrans	SCB	Ductile – Post 1990	0.21	0.57	0.95	1.26	0.40
GT-Caltrans	MCB	Ductile – Post 1990	0.10	0.32	0.61	0.83	0.54
HAZUS	SCB		0.60	0.90	1.30	1.60	0.60
HAZUS	MCB		0.90	0.90	1.10	1.50	0.60
MSCC-BG-E3-SX							
GT-Caltrans	SCB	Ductile – Post 1990					
		BC-E3-S3-S	0.09	0.57	1.44	2.06	0.51
		BC-E3-S4-S	0.09	0.57	1.44	2.06	0.51
	MCB	Ductile – Post 1990					
		BC-E3-S3-S	0.06	0.26	0.59	0.87	0.58
		BC-E3-S4-S	0.06	0.26	0.61	0.88	0.59
HAZUS	SCB		0.60	0.90	1.30	1.60	0.60
HAZUS	MCB		0.90	0.90	1.10	1.50	0.60
Mackie & Stojadinovic	SCB	See Table 1 for CDTs					
(MSCC-BG-S-E3-SX)		BC-E3-S3-S	0.08	0.47	2.35	3.06	0.50
Using Mackie's CDTs		BC-E3-S4-S	0.08	0.47	2.77	3.57	0.51
in this study	MCB	BC-E3-S3-S	0.06	0.24	1.07	1.36	0.56
		BC-E3-S4-S	0.06	0.24	1.21	1.43	0.57
Kwon & Elnashai	MCB	See Table 1 for CDTs					
(MSCC-BG-M-E3-SX)		BC-E3-S3-S	0.06	0.26	0.82	1.21	0.56
Using Kwon's CDTs in this study		BC-E3-S4-S	0.06	0.26	0.86	1.26	0.57
Kwon & Elnashai	MCB	Median fragilities		**0.22**	**0.42**	**0.59**	**0.59**
Banerjee & Shinozuka	SCB	See Table 1 for CDTs					
(MSCC-BG-S-E3-SX)		BC-E3-S3-S	0.08	0.51	1.88	2.73	0.50
Using Banerjee's CDTs		BC-E3-S4-S	0.08	0.51	2.05	2.86	0.49
in this study	MCB	BC-E3-S3-S	0.07	0.30	0.84	1.20	0.56
		BC-E3-S4-S	0.07	0.30	0.88	1.24	0.57
Banerjee & Shinozuka	SCB	Median fragilities	**0.40**	**0.71**	**1.15**	**1.43**	**1.25**
Kim & Shinozuka	SCB	Median fragilities	**0.44**	**0.65**	**0.86**	**1.47**	**0.96**
Deterministic fragility	SCB	MSCC-BG-S-E3-S0	0.13	0.40	0.74	1.04	0.41
GT-Caltrans	MCB	MSCC-BG-M-E3-S0	0.12	0.34	0.61	0.84	0.41

Note: The values in **dark brown** are the ones obtained using the CDTs used in the current study titled GT- Caltrans and the values in **blue** are the ones prescribed in HAZUS. The ones in **purple** are from researchers in the field.